ЖУРНАЛ
ЭКСПЕРИМЕНТАЛЬНОЙ И ТЕОРЕТИЧЕСКОЙ
ФИЗИКИ
АКАДЕМИЯ НАУК СССР

SOVIET PHYSICS

JETP

VOLUME 2 **NUMBER 3**

A Translation

of the

Journal of Experimental and Theoretical Physics

of the

Academy of Sciences of the USSR

MAY, 1956

Published by the

AMERICAN INSTITUTE OF PHYSICS
INCORPORATED

SOVIET PHYSICS
JETP

A translation of the Journal of Experimental and Theoretical Physics of the USSR.

A publication of the

AMERICAN INSTITUTE OF PHYSICS

Governing Board

Frederick Seitz, *Chairman*
Allen V. Astin
Robert F. Bacher
H. A. Bethe
J. W. Buchta
S. A. Goudsmit
Deane B. Judd
Hugh S. Knowles
W. H. Markwood, Jr.
William F. Meggers
Philip M. Morse
Brian O'Brien
Harry F. Olson
R. F. Paton
Eric Rodgers
Ralph A. Sawyer
William Shockley
H. D. Smyth
J. H. Van Vleck
Mark W. Zemansky

Administrative Staff

Henry A. Barton,
Director
George B. Pegram,
Treasurer
Wallace Waterfall,
Executive Secretary
Theodore Vorburger,
Advertising Manager
Ruth F. Bryans,
Publication Manager
Edith I. Neftel,
Circulation Manager
Kathryn Setze,
Assistant Treasurer
Melvin Loos,
Consultant on Printing

American Institute of Physics Advisory Board on Russian Translations

Elmer Hutchisson, *Chairman*
Dwight Gray, Morton Hamermesh, Vladimir Rojansky,
Victor Weisskopf

Editor of Soviet Physics
Robert T. Beyer, Department of Physics, Brown University,
Providence, R.I.

Soviet Physics is a bi-monthly journal published by the American Institute of Physics for the purpose of making available in English reports of current Soviet research in physics as contained in the Journal of Experimental and Theoretical Physics of the Academy of Sciences of USSR. The page size of Soviet Physics will be 7⅞″ x 10½″, the same as other Institute journals.

Transliteration of the names of Russian authors follows the system employed by the Library of Congress.

This translating and publishing project was undertaken by the Institute in the conviction that dissemination of the results of researchs everywhere in the world is invaluable to the advancement of science. The National Science Foundation of the United States encouraged the project initially and is supporting it in large part by a grant.

The American Institute of Physics and its translators propose to translate faithfully all the material in the Journal of EXPERIMENTAL & THEORETICAL PHYSICS OF THE USSR appearing after January 1, 1955. The views expressed in the translated material, therefore, are intended to be those expressed by the original authors, and not those of the translators nor of the American Institute of Physics.

One volume is published annually. Volume 1 (1955) contains three issues. Subsequent volumes, beginning with January 1956, will contain six issues.

Subscription Prices:

Per year (6 issues)	
United States and Canada	$30.00
Elsewhere	32.00
1st Volume (3 issues)	
United States and Canada	$15.00
Elsewhere	16.00
Back Numbers	
Single copies	$ 6.00

Subscriptions should be addressed to the American Institute of Physics, 57 East 55 Street, New York 22, New York.

Copyright by American Institute of Physics 1956

SOVIET PHYSICS

JETP

SOVIET PHYSICS JETP VOLUME 2, NUMBER 3 MAY, 1956

Temperature Dependence of the Elastic Constants of Monocrystals of Sodium Chloride and Silver Chloride

A. V. STEPANOV AND I. M. EIDUS
Leningrad Physico-Technical Institute, Academy of Sciences, USSR

(Submitted to JETP editor March 26, 1953)
J. Exper. Theoret. Phys. USSR **29**, 669-675 (November, 1955)

Results are reported of the measurement of the elastic constants of single crystals of sodium chloride and silver chloride in the temperature range from room temperature to the melting point.

1. THE present research is the extension of earlier work[1-4], in which the properties of halide compounds of silver and thallium were investigated. In it we report the results of the determination of the elastic constants of single crystals of silver chloride and sodium chloride at temperatures ranging from room temperature to the melting temperature.

The method of measuring the constants is as follows[5-7]. A long rod of amorphous quartz is attached to a piezoquartz. To the rod in turn there is attached the sample to be investigated (such a system we call a triple oscillator in the following). Mechanical vibration of the oscillator is produced by applying a variable electrical potential to the piezoquartz crystal. By an investigation of the condition for resonance of the triple oscillator we could determine the eigenfrequency of the sample under investigation, and the elastic constants were calculated from this frequency. At a temperature of 577°C. the piezoquartz loses its piezoelectric property (transition $\alpha \rightarrow \beta$ quartz). In view of this fact, the piezoquartz and the specimen were separated in high temperature experiments by a sufficiently long rod of fused quartz (or similar material), so that the piezoquartz could be at room temperature while the specimen was at an arbitrary high temperature.

The oscillator consisting of the piezoquartz and the specimen is called a double oscillator. Measurements with the use of a double oscillator are possible only at temperatures below 577 °C.

The reactive impedance between the electrodes of the piezoquartz contains a part which depends on the amplitude of the mechanical vibration. This amplitude is given by the expression

$$a = \frac{V_0 F(y_1, y_2, y_3)}{\Delta}; \tag{1}$$

here V_0 is the amplitude of the applied voltage;

$$y_i = \pi \frac{\nu_0}{\nu_1}\left[1 + \frac{1}{2}\pi^2\mu_i^2\left(\frac{I_i}{\rho_i l_i^2}\right)\left(1 - \frac{\nu^2_0}{\nu_i^2}\right)\right], \tag{2}$$

where ν_i are the characteristic frequencies, μ_i the Poisson's ratios, l_i the lengths, I_i the moments of inertia of the cross section relative to the axis of symmetry, ρ_i the densities, ν_0 the characteristic frequency of the triple oscillator. $F(y_1, y_2, y_3)$ is a function practically independent of ν_0 in a sufficiently wide frequency range in the neighborhood of ν_0. In what follows we denote the various

---

[1] A. V. Stepanov, Z. Phys. Sowjetunion **6**, 313 (1934).

[2] A. V. Stepanov, Z. Phys. Sowjetunion **8**, 25 (1935).

[3] A. V. Stepanov, Zh. Tekhn. Fiz. **19**, 205 (1949).

[4] B. M. Krasnov and A. V. Stepanov, J. Exper. Theoret. Phys. USSR **25**, 98 (1953).

[5] L. Hunter and S. Siegel, Phys. Rev **61**, 84 (1942).

[6] F. C. Rose, Phys. Rev. **49**, 50 (1936).

[7] M. Durand, Phys. Rev. **50**, 449 (1936).

parts by $i = 0$ for the composite oscillator: $i = 1$ for the specimen; $i = 2$ for the piezoquartz; $i = 3$ for the amorphous rod;

$$\Delta = \frac{m_1 \operatorname{tg} y_1}{y_1} + \frac{m_2 \operatorname{tg} y_2}{y_2} + \frac{m_3 \operatorname{tg} y_3}{y_3} - \frac{m_1 m_2}{m_3} \frac{y_3}{y_1 y_2} \operatorname{tg} y_1 \operatorname{tg} y_2 \operatorname{tg} y_3. \tag{3}$$

The characteristic frequencies ν_i are given by the expression

$$\nu_i = n \left(\frac{M^{1/2}}{2\rho_i^{1/2} l_i} \right) \left(1 - \frac{\pi^2 n^2 \mu_i^2 I_i}{2 l_i^2 \rho_i} \right), \tag{4}$$

where n is an integer (the number of the harmonic), M is Young's modulus or the shear modulus in a direction parallel to the axis of the specimen. The term

$$\frac{\pi^2 n^2 \mu^2 I_i}{2 l_i^2 \rho_i} \tag{5}$$

of Eq. (4) takes into account the lateral deformation of the specimen.

In the measurements described below, Eq. (5) enters as a small correction in the calculation of the dimensions of all arrangements of the triple oscillator. Because of the size of experimental errors, we have neglected terms of the form (5) in all our calculations. The calculation of the characteristic frequencies in Eq. (4) is then based on the expression

$$\nu_i = \frac{n}{2 l_i} \sqrt{\frac{M}{\rho_i}}. \tag{6}$$

It follows from Eq. (1) that the condition for resonance (i.e., coincidence of the electrical vibration frequency and the frequency of the characteristic mechanical vibration of the composite oscillator, ν_0) is defined by the relation

$$\frac{m_1 \operatorname{tg} y_1}{y_1} + \frac{m_2 \operatorname{tg} y_2}{y_2} + \frac{m_3 \operatorname{tg} y_3}{y_3} - \frac{m_1 m_2}{m_3} \frac{y_3}{y_1 y_2} \operatorname{tg} y_1 \operatorname{tg} y_2 \operatorname{tg} y_3 = 0. \tag{7}$$

If ν_0, ν_1, ν_2 and ν_3 are sufficiently close to each other, then

$$\frac{\operatorname{tg} y_1}{y_1} = \frac{1}{\nu_0} \left[\frac{m_2}{m_1} (\nu_2 - \nu_0) + \frac{m_3}{m_1} (\nu_3 - \nu_0) \right], \tag{8}$$

or, if we denote the right hand side of Eq. (8) by a,

$$\operatorname{tg} \pi \frac{\nu_0}{\nu_1} = a \pi \frac{\nu_0}{\nu_1}\,{}^{*} \tag{9}$$

The dependence of ν_0/ν_1 on a is found graphically.

The determination of the modulus at high temperatures is made by means of Eq. (6), in which a correction is made for the thermal expansion. The correction is made both for the length l and the density ρ, after which Eq. (6) takes the form

$$M = \frac{4 l^2 \rho \nu_1^2}{n^2 \left(1 + \frac{\Delta l}{l} \right)}, \tag{11}$$

where $\Delta l/l$ is the relative extension of the specimen in the temperature interval from room temperature to the temperature of measurement.

The temperature dependence of the frequency ν_1 of the quartz rod was taken into account in the calculation of the frequency of the specimen ν_3.

The formulas were developed for the case in which the specimen, piezoquartz and quartz rod all have cylindrical shape, and are valid for longitudinal vibrations of cylindrical and rectangular specimens and for torsional vibrations of cylindrical specimens. For the case of torsional vibrations of specimens of rectangular cross section, the formulas differ only by a factor in front of the term $1 - \frac{\nu_0^2}{\nu_i^2}$ in Eq. (2) **, but the order of magnitude of this multiplier remains the same. The origin of this factor is similar to that of the remaining term in Eq. (4).

All measurements of torsional vibrations were carried out on specimens of rectangular cross section.

Calculation of the shear modulus was made from Eq. (11), with a correction for the fact that the cross section does not remain plane in the torsion of a specimen of rectangular cross section[2].

In this case we can use the formula which is valid for isotropic material provided that the axis of torsion of the crystalline specimen has a sym-

---

* If $\nu_0 = \nu_1 = \nu_2 = \nu_3$, the approximate relation

$$\nu_1 = \nu_0 + \frac{m_2}{m_1} (\nu_0 - \nu_2) + \frac{m_3}{m_1} (\nu_0 - \nu_3) \tag{10}$$

is satisfied.

** This term is generally absent for torsional vibrations of cylindrical specimens. See reference 6.

metry higher than third order. This condition was satisfied in our measurements, since the measurements (of torsional vibrations) were carried out on specimens which were oriented along the axis of a cube [100]. With the correction term added, Eq. (11) has the form

$$G_{[100]} = \frac{4,77\, l_0^2 \nu_1^2 \rho}{n^2}. \qquad (13)$$

Here G_{100} is the shear modulus for a specimen whose axis coincides with the [100] direction[+].

Two types of oscillators were employed in the research: a double oscillator for the measurements at room temperature, and a triple for measurements at elevated temperatures. Some of the oscillators were used for longitudinal vibrations, some for torsional.

The piezoquartz for the longitudinal vibrations were in the form of bars of square cross section 3 × 3 mm², length 27 mm (frequency ~ 100 kc), cut along the mechanical axis. Silver electrodes were attached to the faces perpendicular to the electric axis. The piezoquartz for the torsional vibrations were in the form of cylinders of diameter 3 mm, length 27 mm (frequency ~ 75 kc), whose axes coincided with the electric axis. Electrodes were attached to the generating cylinder, which was perpendicular to the bisector of the angle between the optical and mechanical axes.

The length of the quartz rod was ~ 500 mm, and was so adjusted that the frequency of the system: piezo-quartz rod was equal, within 0.5%, to that of the piezoquartz alone.

The specimens of sodium chloride and silver chloride examined were either square (3 × 3 mm²) or circular ($d \approx 3$ mm) in cross section. The length of the specimen ranged from 10 to 20 mm.

Electrical vibrations were produced by a standard signal generator. This generator was frequency calibrated to within 0.05%. An EO-4 oscilloscope, inserted in the diagonal of the bridge fed by the standard signal generator, served as an indicator of resonance. The piezoquartz formed one arm of this bridge; another arm was a variable capacitance, which was so adjusted that the bridge was in equilibrium in the absence of resonance.

Measurement of the frequency of the triple oscillator was carried on during slow heating of a furnace. The time required for these measurements was small in comparison with the time necessary for a measurable change in the temperature of the oscillator. From this point of view, the measurements during the heating process were justified. Only in experiments at temperatures close to the melting point of the crystal under measurement were the measurements carried out in the steady state.

Cementing of the parts of the oscillator was one of the most critical operations. The cementing spot had to be very strong, heat resistant, and thin, in order that it present no obstacles to the measurement. For cementing, we used a mixture of water glass and $CaCO_3$ in the form of a thin powder. In the case of temperature measurement with NaCl four days drying were allowed; for AgCl, two days drying. The cementing mixture did not have to be very thick. The cementing was carried out in a special arrangement which guaranteed the matching and pressing together of all the cemented parts.

The quartz rods were cemented to the piezoquartz; then the quartz rod was shortened until the frequency of the entire system was within 0.5% of the frequency of the piezoquartz[‡].

The frequency of the quartz rod ν_3 enters into the calculated formula (9) for the determination of the frequency ν_1 of the specimen. For this

---

[+] As is known[8],

$$\nu_n = \frac{u}{2l}\sqrt{\frac{N_s}{I_p \rho}}, \qquad (12)$$

where N_s is the static torsional coefficient I_p is the polar moment of inertia of the cross section of the specimen. For a specimen of square cross section with side a, $I_p = a^4/6$, $N_s = \propto a^4 G$, $\propto = 0.14$, G = shear modulus. Substituting the values of I_p and N_s in Eq. (13).

[8] W. Cady, *Piezoelectricity.*

[‡] In this case the frequency of the quartz rod was close to the frequency of the piezoquartz, since the mass of the quartz rod was appreciably greater that that of the piezoquartz, and therefore the frequency of the system piezoquartz + rod was close to that of the quartz rod than to the frequency of the piezoquartz. Let ν_2 be the frequency of the piezoquartz, ν_0' the frequency of the system piezoquartz + rod, ν_3 the frequency of the quartz rod. Then, from Eq. (1), which is written for the double oscillator,

$$\nu_3 = \nu_0' + \frac{m_2}{m_3}(\nu_0' - \nu_2), \qquad (14)$$

where m_2 is the mass of the piezoquartz, m_3 the mass of the quartz rod.

TABLE I

Sodium Chloride

t °C	s_{11}, $10^{-12}\frac{cm^3}{dyne}$	s_{44}, $10^{-12}\frac{cm^3}{dyne}$	s_{12}, $10^{-12}\frac{cm^3}{dyne}$	$\varkappa$, $10^{-12}\frac{cm^3}{dyne}$
20	2.28	7.60	—0.26	4.40
100	2.52	7.82	—0.51	4.50
150	2.67	7.94	—0.61	4.35
200	2.81	8.14	—0.71	4.16
250	2.98	8.34	—0.81	4.10
300	3.16	8.46	—0.89	4.14
350	3.36	8.70	—1.00	4.10
400	3.58	8.84	—1.06	4.37
450	3.82	9.08	—1.11	4.50
500	4.08	9.34	—1.21	4.98
550	4.36	9.52	—1.24	5.64
600	4.70	9.70	—1.35	6.00
650	5.10	10.00	—1.46	6.54
700	5.55	10.20	—1.55	7.35
750	6.10	10.40	—1.58	8.82
780	6.58	10.50	—1.73	9.36
790	6.67	10.62	—1.78	9.33
800	6.75	10.62	—1.71	9.99
804	6.85	10.62	—1.76	9.99

TABLE II

Silver Chloride

t °C	s_{11}, $10^{-12}\frac{cm^3}{dyne}$	s_{44}, $10^{-12}\frac{cm^3}{dyne}$	s_{12}, $10^{-12}\frac{cm^3}{dyne}$	$\varkappa$, $10^{-12}\frac{cm^3}{dyne}$
20	3.15	16.25	—1.08	3.00
100	3.79	16.50	—1.21	4.10
125	4.13	16.60	—1.33	4.40
150	4.41	16.70	—1.40	4.83
175	4.69	16.80	—1.45	5.36
200	4.88	17.00	—1.43	5.75
225	5.05	17.20	—1.43	6.57
250	4.21	17.35	—1.39	7.30
275	5.40	17.60	—1.20	9.00
300	5.52	18.25	—1.05	10.30
325	5.65	19.05	—0.97	11.10
350	5.78	19.80	—0.88	12.10
375	5.92	20.07	—0.70	12.80
400	6.06	22.20	—0.76	13.60
425	6.29	23.80	—0.95	13.50
435	6.41	24.50	—0.90	13.80
445	6.58	25.30	—1.23	12.35
450	6.71	25.80	—1.41	11.90
455	6.90	26.20	—1.48	11.80

reason, the temperature dependence of the frequency of the quartz rod (without the specimen) was first measured in the same position in the furnace as in the subsequent measurements with the specimen. The dependence of the frequency of the double oscillator: piezoquartz + quartz rod $\nu_0'(T)$, was recorded and the temperature dependence of the frequency ν_3 of the quartz rod was determined.

The frequency of the quartz rod changed very slightly with change in temperature. Measurements were carried out for all oscillators used in the research[++]

After the preliminary investigation of the system piezoquartz + quartz rod, the specimen under investigation was attached. The necessary length of the specimen was chosen earlier on the double oscillator at room temperature (the specimen was attached directly to the piezoquartz). The dependence of the frequency of the system ν_0, on the length of specimen l was determined. The length of the specimen was then changed by abrasion or by cutting, and the specimen length l_0 was selected for which the frequency of the specimen, ν_1, was equal to the frequency of the piezoquartz, ν_2. Usually a specimen of length somewhat different from l_0 was attached to the system piezoquartz + quartz rod. As a result, the whole cycle of temperature measurements could be carried out on the specimen without cutting it.

Measurements of the cross section of the specimens was obtained to within 0.01 mm. The lengths of the specimens were measured by a comparator with accuracy to within 0.03 mm. The accuracy of the determination of the orientation of the crystals was within 1° (in the case of pitting of specimens by cleavage it was higher). The value of the resonance frequency was measured on the generator scale to within 0.05%. The temperature in the furnace was measured with a platinum platinum-rhodium thermocouple by the compensation method. Measurements were accurate to within 1 °C.

The temperature gradient in the oven in the part where the specimen was located was about 0.3 degrees /cm.

Density data for sodium chloride, silver chloride and quartz were taken from tables of physical constants.

The coefficients of expansion and their temperature dependence (i.e., the values of $\Delta l/l$ in Eq. (11) for crystals of sodium chloride and silver chloride were taken from references 9, 10. The frequency of the piezoquartz in a temperature interval from 20° to 35°C remained constant within the limits of accuracy of the apparatus. The accuracy of the measurement of the elastic moduli at room temperature was of the order of 1% with the double oscillator. The accuracy of measurement of the elastic moduli at high temperatures with the triple oscillator was within 10% for silver chloride and 5% for sodium chloride.

3. Measurements were made of the temperature dependence of the eigenfrequency of the samples of sodium chloride and silver chloride in the interval from room temperature to the melting temperature with the aid of triple oscillators.

The measurements were made in the case of longitudinal vibrations with specimens oriented along the directions [100] and [110], and for torsional vibrations with specimens oriented in the [100] direction. For crystals of sodium chloride and silver chloride, the temperature dependence of Young's modulus was measured in the [100] and [110] directions ($E_{[100]}$ and $E_{[110]}$) and the shear modulus was measured in the [100] direction in the temperature interval from room temperature to the melting point. All specimens had square cross sections in these experiments. Measurements of $E_{[100]}$ and $G_{[100]}$ for sodium chloride were obtained in two steps, with cutting of the specimen. In all other cases the measurements were made without cutting of the sample.

The constants s_{11}, s_{44} and s_{12} were computed from known relations[11] on the basis of the data obtained. The results are shown in Tables I and II. The values of the compressibility $\varkappa$, computed from the data for S_{ik}, are also given in the tables.

The results in Table I show that our data for

[++] The resonant frequencies of the system piezoquartz + quartz rod were close to one another. This is explained by the fact that the resonance frequencies of the quartz rod were close to one another (because of high number of the harmonic), and since the mass of the quartz rod underwent a transition from one harmonic to another, the frequency of the whole system underwent a small change

$$\nu_0' = \frac{\nu_3 m_3 + \nu_2 m_2}{m_3 + m_2}, \qquad (15)$$

where $\nu_3 m_3$ is the principal term $m_3 \gg m_2$.

[9] P. G. Strelkov, A. K. Val'ter and V. P. Gachkovskii, J. Exper. Theoret. Phys. USSR 7, 519 (1937).

[10] P. G. Strelkov, V. P. Gachkovskii, J. Exper. Theoret. Phys. USSR 1, 231, 243 (1931).

[11] W. Voigt, *Lehrbuch der Kristallphysik*, Teubner, 1910.

sodium chloride are in agreement, within experimental errors, with the results of other authors[5,12]. The measurements for silver chloride at room temperature are in agreement with those of Arenberg[13].

As is seen from Table II, a significant decrease in the compressibility of silver chloride was observed at temperatures close to the melting point.

A detailed investigation was carried out for sodium chloride[5]. In our measurements we did not observe such an effect for sodium chloride, evidently because of the insufficient accuracy of the method.

It is also evident from the results that the Cauchy relation $\frac{c_{11}}{c_{44}} = 1$ is satisfied approximately for sodium chloride crystals in the temperature interval investigated. In the case of silver chloride the ratio c_{11}/c_{44} is a function of the temperature and is approximately unity only for temperatures close to the melting point. From this it follows that the Cauchy condition is not universal, and can be satisfied only in a limited temperature range.

In conclusion, we consider it our duty to express our gratitude to E. M. Evstaf'ev for a series of valued instructions on the method of investigation, and to A. L. Shakh-Budagov for criticism of the results and for the great help during the course of the work.

---

[12] A. E. Briukhanov, J. Exper. Theoret. Phys. USSR 9, 722 (1939).

[13] D. L. Arenberg, J. Appl. Phys. 21, 941 (1950).

Translated by R. T. Beyer
252

SOVIET PHYSICS JETP VOLUME 2, NUMBER 3 MAY, 1956

The Theory of the Hall Effect in Ionic Semiconductors

M. I. KLINGER
Chernovitskii State University

(Submitted to JETP editor June 8, 1954)
J. Exper. Theoret. Phys. USSR 29, 439-448 (October, 1955)

The Hall coefficient is calculated for ionic semiconductors. The interaction of the electron with the polarizing vibrations of the crystal is considered both in the adiabatic approximation and the weak coupling case.

1. INTRODUCTION

THE calculation of the Hall coefficient R is usually carried out by means of the solution of the kinetic equation. However, as is pointed out in references 1 and 2, the quantization of the energy spectrum of the current carriers in crossed electric and magnetic fields $E \perp H$ remains unstudied.

The problem of the present research was the calculation of the Hall coefficient for an ionic semicomductor by the method of stationary states[2], which allows a consideration of the quantization of the energy spectrum by the fields $E \perp H (E \| OX, H \| OZ)$.

The following expression is obtained in Appendix II for the Hall coefficient R:

$$R = -j_y E_x (j_y^2 + j_x^2)^{-1} H^{-1}, \tag{1}$$

where j_y, j_x are the currents, in an unbounded gyrotropic layer, along the axes OY and OX. As noted in Appendix II, $|j_y| > |j_x|$ usually, since the current j_x is proportional to a small parameter which characterizes the weak coupling of the current carrier with the phonons which scatter it. Therefore,

$$R \approx -\frac{1}{j_y}\frac{E}{H}. \tag{2}$$

To compute the current j_y we need a concrete model of the semiconductor under consideration. For example, for the simplest solid, in which the current carrier is an electron with effective mass μ[2],

$$j_y^{\pm} = \mp e N_{\pm} \gamma, \tag{3}$$

where $N_{\pm}$ is the number of current carriers [in semiconductors $N_{\pm}$ is a function of the temperature $N_{\pm} = N_{\pm}(T)$]: $\gamma = -cE/H = -\bar{v}_y$ is the mean y component of the velocity [the upper sign in (3) refers to holes, the lower to electrons].

Therefore, in this model, we obtain from Eqs. (2) and (3), for $|j_y^{\pm}| > |j_x^{\pm}|$:

$$R_{+} \approx \pm 1 / N_{\pm} ec. \tag{4}$$

In the presence of combined conduction,

$$R = -\frac{j_y^+ + j_y^-}{(j_y^+ + j_y^-)^2 + (j_x^+ + j_x^-)^2}\frac{E}{H} \tag{5}$$

$$= -\frac{c}{eH}\frac{N_- - N_+}{\left[(N_- - N_+)^2 \frac{c^2}{H^2} + (N_+ \tilde{u}_+ + N_- \tilde{u}_-)^2\right]},$$

where $\tilde{u}_-$, $\tilde{u}_+$ are the mobilities of the electrons and the holes.

The case of small $|N_- - N_+|$, i.e., semiconductors with a small amount of impurities, requires a special investigation, because, as follows from Eq. (5), it turns out that $|j_y^+ + j_y^-| < |j_x^+ + j_x^-|$ in this case, even for $|j_y^{\pm}| \gg |j_x^{\pm}|$.

2. THE HALL EFFECT IN IONIC SEMICONDUCTORS WITH WEAK COUPLING

We now consider the Hall effect in an ionic semiconductor in which the coupling between the electron and the optical vibrations is small.

As is given in reference 2, the operator of the y component of the velocity is defined by the relation

$$\hat{v}_y = \frac{1}{\mu}(P_y + \mu\omega_0 x - \Sigma \hbar f_y \xi_f^+ \xi_f), \tag{6}$$

where $P_y = p_y + \Sigma \hbar f_y \xi_f^+ \xi_f$ is the component of the operator of the total momentum of the system; ξ_f^+, ξ_f are the operators of emission and absorption of the optical vibrations; $\omega_0 = eH/\mu c$. Carrying out a canonical transformation of Eq. (6)[2,3]

$$\xi_f \rightarrow \zeta_f = \xi_f - \alpha_f,$$

---

[1] S. Titeica, Ann. Physik 22, 129 (1935).

[2] M. I. Klinger, J. Exper. Theoret. Phys. USSR 26, 159 (1954).

[3] S. B. Tiablikov, J. Exper. Theoret. Phys. USSR 21, 16 (1951).

where

$$\alpha_f = -A_f\left(\hbar\omega + \frac{\hbar^2 f^2}{2\mu} + \hbar\gamma f_y - \frac{\hbar}{\mu} P_z f_z\right)^{-1},$$

$$A_f = \frac{1}{|\mathbf{f}|}\sqrt{\frac{2\pi\hbar\omega c' e^2}{V}},$$

$$c' = \frac{1}{n_1^2} - \frac{1}{\varepsilon_1},$$

ω is the limiting frequency of the optical branch, we obtain the following expression for the y component of the velocity of the current carrier:

$$\hat{v}_y = \frac{1}{\mu}\{P_y + \mu\omega_0 x - \Sigma\hbar f_y|\alpha_f|^2 - \Sigma\hbar f_y(\alpha_f\zeta_f + \alpha_f^+\zeta_f^+)\}. \tag{7}$$

Averaging $\hat{v}_y$ over the unperturbed state of the system, we get the following expression for $\overline{v}_y$ ($\alpha_f = \alpha_f^+$):

$$\overline{v}_y = \frac{1}{\mu}\{P_y + \mu\omega_0 x_0 - \Sigma\hbar f_y \alpha_f^2\}, \tag{8}$$

or, after making the substitution[2] $x_0 = -\frac{P_y}{\mu\omega_0} - \frac{eE}{\mu\omega_0^2}$,

$$\overline{v}_y = -\gamma + J_y, \tag{9}$$

where

$$J_y = -\frac{2\pi\hbar\omega c' e^2}{V\mu}\sum \hbar f_y / f^2 \left(\hbar\omega + \frac{\hbar^2 f^2}{2\mu} + \hbar\gamma f_y - \frac{\hbar}{\mu} P_z f_z\right)^2.$$

We calculate J_y for the special cases (1) $\hbar\omega > \mu\gamma^2/2$ and (2) $\hbar\omega < \frac{1}{2}\mu\gamma^2$.

1) $\hbar\omega > \frac{1}{2}\mu\gamma^2$.

We change Eq. (9) from a summation to an integration and limit ourselves, in the expansion of J_y in powers of γ and P_z, to terms of order γ and P_z^2 (for $P_z^2 < 2\mu\,|\hbar\omega - \frac{1}{2}\mu\gamma^2|$); we get

$$J_y = -(\gamma/\mu)(J_1' + J_1'' P_z^2), \tag{10}$$

where

$$J_1' \approx \frac{\varepsilon_0^2\mu}{48\pi}\sqrt{\frac{\mu}{m}}, \quad J_1'' \approx \frac{\varepsilon_0^2}{160\hbar\omega\pi}\sqrt{\frac{\mu}{m}}.$$

$\varepsilon_0 = \left(\frac{2\pi c' e^2 \hbar\omega}{(\hbar\omega - \mu\gamma^2/2)^2}\sqrt{\frac{2m\,|\hbar\omega - \mu\gamma^2/2|}{\hbar^2}}\right) \ll 1$ is the small parameter in the theory of weak coupling[2,3].

2) $\hbar\omega < \frac{1}{2}\mu\gamma^2$.

In this case, in the transition in J_y from a summation to an integration, we must obtain the integral in the form of a principal value; this amounts to a neglect of the finiteness of the lifetime of the stationary state considered in the given approximation[2,3]. For the calculation we express J_y in the following form:

$$J_y = -\frac{\hbar\omega c' e^2}{(2\pi)^2\mu}\int \frac{(\hbar F_y - \mu\gamma)(dF)}{\left(F^2 - \frac{2\mu}{\hbar}\gamma F_y + \frac{\gamma^2\mu^2}{\hbar^2} + \frac{P_z^2}{\hbar^2} + \frac{2}{\hbar}P_z F_z\right)\left(A + \frac{\hbar^2 F^2}{2\mu}\right)^2}, \tag{11}$$

where

$$A = \hbar\omega - \frac{\mu\gamma^2}{2} - \frac{P_z^2}{2\mu} < 0.$$

By means of an expansion of the integral in powers of γ and P_z, we obtain

$$J_y = -\frac{\gamma}{\mu}(J_2' + J_2'' P_z^2), \tag{12}$$

where

$$J_2' = -\frac{4}{3}\mu\varepsilon^2\left(\frac{\hbar\omega}{\mu\gamma^2}\right)^{3/2}, \quad J_2'' = -28\frac{\varepsilon^2}{\hbar\omega}\left(\frac{\hbar\omega}{\mu\gamma^2}\right)^{5/2}.$$

Substituting the expressions for J_y from Eqs. (10) and (12) in Eq. (9), we get

1) $\hbar\omega > \mu\gamma^2/2$;

$$\overline{v}_y \approx -\gamma\left(1 - \frac{\varepsilon_0^2}{48\pi}\sqrt{\frac{\mu}{m}} + \frac{\varepsilon_0^2}{160\mu\hbar\omega}\sqrt{\frac{\mu}{m}}P_z^2\right); \tag{13}$$

2) $\hbar\omega < \mu\gamma^2/2$;

$$\overline{v}_y \approx -\gamma\left[1 + \frac{4\varepsilon^2}{3}\left(\frac{\hbar\omega}{\mu\gamma^2}\right)^{3/2} + \frac{28\varepsilon^2}{\mu\hbar\omega}\left(\frac{\hbar\omega}{\mu\gamma^2}\right)^{5/2}P_z^2\right]. \tag{14}$$

It follows from Eqs. (13) and (14) that in this model $\overline{v}_y$ depends on the state (on P_z); therefore, in the calculation of the macro-current $j_y = -eN\langle\overline{v}_y\rangle$ (the symbol $\langle\ \rangle$ denotes the statistical average of $\overline{v}_y$ over the states), we must compute $\langle P_z^2\rangle$. As is shown in Appendix I, the equilibrium distribution function over P_z for the carriers has the following form in the weak coupling case[*]

---

[*] A misprint appears in the expression for T_1 in our earlier paper [reference 1, Eq. (4.5)].

(for

$$T_1 \lesssim T \leqslant \frac{\hbar\omega}{k}, \qquad T_1 = \frac{\hbar\omega}{2k}\ln 2 - \left[\left(\frac{\hbar\omega}{2k}\ln 2\right)^2 - 4\frac{\hbar a_0^2}{k^2\mu^2}|P_z|^3\right]^{1/2}\Big):$$

$$f(P_z) = (2\pi\mu_e' kT)^{-1/2}\exp\left(-\frac{P_z^2}{2\mu_e' kT}\right), \qquad (15)$$

where μ_e' is the effective mass of the quasiparticles moving along OZ. We obtain the expression for μ' from the expression for μ_e^2 by substituting $\bar{n}_0 = \left[\exp\left(\frac{\hbar\omega_0}{kT}\right) - 1\right]^{-1}$ for n_0 (see Appendix I).

Restricting ourselves to the case $T_1 \lesssim T \lesssim \hbar\omega/k$ and assuming that $<P_z^2> = \mu_e'^{\pm} kT$, we obtain the following expression for

$$j_y = -eN\langle\bar{v}_y\rangle = j_y^0 + j_y' \quad [j_y^{0\pm} = \mp ecN(E/H)]:$$

1) $\hbar\omega > {}^1/_2\,\mu\gamma^2$:

$$j_y'^{\pm} \approx \mp ecN_\pm \frac{E}{H}\left(\frac{\varepsilon_0^2}{48\pi}\sqrt{\frac{\mu}{m}} - \frac{kT}{160\pi\hbar\omega}\varepsilon_0^2\sqrt{\frac{\mu}{m}}\frac{\mu_e'^{\pm}}{\mu_+}\right) \qquad (16)$$

2) $\hbar\omega < {}^1/_2\,\mu\gamma^2$:

$$j_y'^{\pm} \approx \mp ecN_\pm \frac{E}{H}\left[\frac{4\varepsilon^2}{3}\left(\frac{\hbar\omega}{\mu_\pm\gamma^2}\right)^{3/2} + \frac{28\,kT}{\hbar\omega}\varepsilon^2\left(\frac{\hbar\omega}{\mu_\pm\gamma^2}\right)^{5/2}\frac{\mu_e'^{\pm}}{\mu_{e\pm}}\right]. \qquad (17)$$

If we substitute j_y from Eqs. (16) and (17) in (2), we get in the two cases:

1) $\hbar\omega > {}^1/_2\,\mu\gamma^2$, $|j_y| > |j_x|$:

$$R_\pm \approx \pm\frac{1}{N_\pm ec}\left[1 - \frac{\varepsilon_0^2}{2\pi}\left(\frac{1}{24} - \frac{1}{80}\frac{kT}{\hbar\omega}\frac{\mu_e'^{\pm}}{\mu_\pm}\right)\right]; \qquad (18)$$

2) $\hbar\omega < {}^1/_2\,\mu\gamma^2$:

$$R_\pm \approx \pm\frac{1}{N_\pm ec}\left[1 - \varepsilon^2\left(\frac{4}{3}\left(\frac{\hbar\omega}{\mu_\pm\gamma^2}\right)^{3/2} - \frac{28\,kT}{\hbar\omega}\left(\frac{\hbar\omega}{\mu_\pm\gamma^2}\right)^{5/2}\frac{\mu_e'^{\pm}}{\mu_\pm}\right)\right]. \qquad (19)$$

It follows from these equations that:

1) $N_\pm R_\pm$ depends on T and on $\gamma = cE/H$.

2) $R_\pm$ is determined by different expressions in the two cases $\hbar\omega > \mu\gamma^2/2$ and $\hbar\omega < \mu\gamma^2/2$.

We now return to the consideration of a semiconductor with combined conduction. If $N_- \gg N_+$ or $N_+ \gg N_-$, or

$$|j_y^+ + j_y^-| > |j_x^+ + j_x^-| \text{ and } |j_y^{0+} + j_y^{0-}| > |j_y'^+ + j_y'^-|,$$

then

$$R \approx -1/ec(N_- - N_+). \qquad (20)$$

We take the case of a semiconductor without impurity ($N_- = N_+$).

In this case the expression which defines R depends on the ratio of the two quantities $|j_y'^+ + j_y'^-|$ and $|j_x^+ + j_x^-|$, since $j_y^{0+} + j_y^{0-} = 0$.

For $|j_x^+ + j_x^-| > |j_y'^+ + j_y'^-|$, $N_+ = N_- = N$.

$$R \approx \frac{ecN}{H^2(\sigma_+(H) + \sigma_-(H))^2}\frac{\varepsilon_0^2}{2\pi}\left(\frac{1}{24} - \frac{kT}{80\,\hbar\omega}\right) \times \left(\sqrt{\frac{\mu_+}{m}} - \sqrt{\frac{\mu_-}{m}}\right) \text{ for } \hbar\omega > \frac{\mu\gamma^2}{2}, \qquad (21)$$

where $\sigma_+(H)$ and $\sigma_-(H)$ are the conductivities of the hole and electron currents in the magnetic field.

In this case R is defined by the relation of the effective mass $\mu_\pm$ and the conductivities $\sigma_+(H)$ and $\sigma_-(H)$: for large H ($\hbar\omega_0 > kT$), $j_x^\pm(H)$ changes as $\exp(-\hbar\omega_0/2kT)$ with increase in H, and $R \sim \exp(\hbar\omega_0/2kT)$.

In the other case, $|j_x^+ + j_x^-| < |j_y'^+ + j_y'^-|$, $N_- = N_+ = N$,

$$R = \frac{1}{ecN}\frac{2\pi}{\varepsilon_0^2}\left\{\left(\frac{1}{24} - \frac{kT}{80\hbar\omega}\right) \times \left(\sqrt{\frac{\mu_+}{m}} - \sqrt{\frac{\mu_-}{m}}\right)\right\}^{-1}. \qquad (22)$$

Here R (in the approximation used) depends weakly on H for $\hbar\omega > \frac{1}{2}\mu\gamma^2$.

Thus in the case of a semiconductor without impurities ($N_- = N_+$) the Hall coefficient R has the following form:

1) for $\hbar\omega_0 > kT$, and with increasing magnetic field, R varies as $\sim \exp\{\hbar\omega_0/2kT\}$ up to the point where the current $|j_x^+ + j_x^-| \sim$

$\exp\{-\hbar\omega_0/2kT\}$ is no longer less than the current $|j_y^{\prime +} + j_y^{\prime -}|$ for a certain $H = H_0$.

2) For $H > H_0$ and $\hbar\omega > \frac{1}{2}\mu\gamma^2$, R depends weakly on H ($\mu_e^{\prime\pm}$, $\mu_\pm$ depend weakly on H).

3) R depends on T fundamentally as $N(T) \sim \exp(\Phi_{\mathrm{chem}}/kT)$ (we can show that all the results obtained are valid for $|\Phi_{\mathrm{chem}}| > \hbar\omega_0/2$).

For semiconductors with composite conductivity and an excess of one type of carrier, R is determined by Eq. (20). The same equation follows from kinetic theory[4]. However, while it is valid in our case for $|j_y^+ + j_y^-| > |j_x^+ + j_x^-|$, in the kinetic theory it holds for $|j_x^+| > |j_y^+|$ and $|j_x^-| > |j_y^-|$, i.e., for $|j_x^+| + |j_x^-| > |j_y^+| + |j_y^-|$.

3. HALL EFFECT IN A POLARIZED SEMICONDUCTOR

We make use of the results of reference 5 and the calculation of the Hall coefficient by the method of stationary states for polarized semiconductors. As before, we must find an expression for $\hat{v}_y$. In this case we separate the translational $\hat{v}_y^{(1)}$ and fluctuating $\hat{v}_y^{(2)}$ parts:

$$\hat{v}_y = (\hat{v}_y^{(1)} + \hat{v}_y^{(2)}), \tag{23}$$

$$\hat{v}_y^{(1)} = \frac{\hbar}{i\mu}\frac{\partial}{\partial\lambda_2} + \omega_0\lambda_1, \quad \hat{v}_y^{(2)} = \omega_0 q_1,$$

where $\mathbf{r} = \mathbf{q} + \vec{\lambda}$, $\mathbf{q}(q_1 q_2 q_3)$ represents the translational part[5,6] of the coordinates of the electron and $\vec{\lambda}$ its fluctuating part.

In zeroth approximation[5] the states of the system are characterized by the wave functions

$$\Psi^0 = \exp\{(i/\hbar)(P_y q_2 + P_z q_3)\} \tag{24}$$

$$\times\ H_n(q_1 - q_{10})\,\psi_N(\vec{\lambda})\prod_f \Theta_f(n_f),$$

where $q_1^0 = -eE/\mu\omega_0^2$, n is the quantum number of the "magnetic" oscillator, N is the quantum number of the fluctuating motion in the polarization potential hole of the polaron, in accord with the ground state of the polaron, $\mathbf{P}$ is the total momentum of the polaron. Here $\mathcal{H}_1 = \omega_0 q_1(p_{\lambda_2} + \mu\omega_0\lambda_1)$ [reference 5, Eq. (4)] is considered as a perturbation, since $(\mathcal{H}_1)_{nn'} \sim (q_1)_{nn'} \sim \sqrt{\hbar/\mu_{xx}\omega_0} \sim \epsilon \ll 1$[5].

With the help of Eq. (24), we average $\hat{v}_y$ and obtain*

$$\bar{v}_y = \omega_0(\bar{q}_1 + \bar{\lambda}_1) = \omega_0 q_1^0 + \omega_0\bar{\lambda}_1 \tag{25}$$

$$= -\gamma + \omega_0(\lambda_1)_{NN},$$

where

$$(\lambda_1)_{NN} = \int \Psi_N^* \lambda_1 \Psi_N (d\lambda).$$

As is seen from references 5 and 7, the quantities $(\lambda_1)_{NN}$ for the weakly perturbed states N of the discrete spectrum of the polaron whose potential well coincides with the ground state Ψ_0, are almost one and the same (in order of magnitude).

The states of the more perturbed part of the spectrum are not generally taken into account in the calculation of $\langle(\lambda_1)_{NN}\rangle$, since the corresponding Boltzmann factors are much smaller[8]. Therefore, we make the approximation

$$\langle(\lambda_1)_{NN}\rangle \approx (\lambda_1)_{00} = 2\pi\alpha_2 R_{10}^{21}, \tag{27}$$

where $R_{10}^{21} = \int\psi_{1s}(\lambda)\,\lambda_1\,\psi_{2p}(\lambda)(d\lambda)$. It was shown in reference 5 that α_2 is coupled with the polarization of the polaron Γ_0 in its ground state: $\alpha_2 R_{10}^{21} = -(\Gamma_0/2e)E$. Consequently, we get from Eqs. (25) and (27):

$$\bar{j_y} = -eN\langle\bar{v}_y\rangle = eN_-\gamma(1 - \nu_- r_0^- H^2), \tag{28}$$

where

$$\nu_- = \Gamma_0^-/2e^2, \quad r_0^- = e^2/\mu_- c^2.$$

(For the holes,

$$j_y^+ = -eN\gamma(1 - \nu_+ r_0^+ H^2),$$

where $\nu_+ = \Gamma_0^+/2e^2$, $r_0^+ = e^2/\mu_+ c^2$.)

The calculation in reference 5 of the spectrum of the polaron in crossed fields $E \perp H$ was carried out only for such E and H which produce slight changes in the polaron well$[H < H_k = (\frac{2}{\chi_0} | J[\Psi_0])^{1/2}$, reference 5, Eq. (17)]. It is easy to see in such a case that, from Eq. (28) the polarization part of the current is $|\Delta j_y^{\pm}| = eN_+ \gamma \nu_{\pm} r_0^+ H^2 < |j_y^{0\pm}| = eN_{\pm}\gamma$. In accord with Eqs. (20) and (28), for $|j_y| > |j_x|$,

---

[4] B. N. Davydov and I. M. Shmushkevich, Uspekhi Fiz. Nauk 24, 21 (1940).

[5] M. I. Klinger, J. Exper. Theoret. Phys. USSR 26, 168 (1954).

[6] S. V. Tiablikov, J. Exper. Theoret. Phys. USSR 18, 377 (1948).

* In the calculation of $\bar{v}_y$ in the following approximations, we must take a more accurate wavefunction.

[7] S. I. Pekar and M. F. Deigen, J. Exper. Theoret. Phys. USSR 18, 481 (1948); Iu. S. Perlin, J. Exper. Theoret. Phys. USSR 20, 274 (1950).

[8] S. I. Pekar, *Investigation of the electronic theory of crystals*, GTTI, 1951.

$$R_{\pm} \approx -\frac{1}{j_y^{\pm}}\frac{E}{H} = -\frac{1}{N_{\pm}ec(1-\nu_{\pm}r_0^{\pm}H^2)}. \quad (29)$$

In the case of polaron semiconductors with composite conductivity there can be two cases which we consider separately.

1) $|j_y^+ + j_y^-| > |j_x^+ + j_x^-|$:

$$R \approx -\frac{1}{ec}[N_- - N_+ - (\nu_- N_- r_0^- - \nu_+ N_+ r_0^+) H^2]^{-1}. \quad (30)$$

We note that for $H < \tilde{u}_{\pm}/\nu_{\pm}cr_0^+$ ($\tilde{u}_{\pm}$ is the mobility of the current carrier in the field $H \perp E$), i.e., for $|\Delta j_y^{\pm}| < |j_x^+| = eN_{\pm}\tilde{\mu}_{\pm}E$, Eq. (30) is valid if $|N_- - N_+| > (H/c)|N\tilde{u}_- + N_+\tilde{u}_+|$. If $H_k > H \gtrsim \tilde{u}_{\pm}/\nu_{\pm}cr_0^{\pm}$, i.e., $|\Delta j_y^{\pm}| > |j_x^{\pm}|$, then Eq. (30) is valid even for $N_- = N_+ = N$. In that case,

$$R \approx -1/NecH^2(\nu_- r_0^- - \nu_+ r_0^+). \quad (31)$$

For $N_- = N_+$ the sign of R is determined by the ratio of the effect mass of the electron μ_- and of the hole μ_+, since

$$\nu_- r_0^- - \nu_+ r_0^+ = B\frac{e^2}{mc^2}\left[\left(\frac{\mu_-}{m}\right)^2 - \left(\frac{\mu_+}{m}\right)^2\right],$$

where B is a constant which is different for different materials.

2) For $H \lessdot \tilde{u}_+/\nu_{\pm}cr_0^{\mp}$ and

$|N_- - N_+| < (H/c)|N_-\tilde{u}_- + N_+\tilde{u}_+|$,

$|j_y^+ + j_y^-| < |j_x^+ + j_x^-|$, and R is determined from the formula

$$R \approx -\frac{c}{H^2}\frac{[N_- - N_+ - H^2(\nu_- N_- r_0^- - \nu_+ N_+ r_0^+)]}{e(N_+\tilde{u}_+ + N_-\tilde{u}_-)^2}, \quad (32)$$

or, for $N_- = N_+ = N$,

$$R = -\frac{c(\nu_- r_0^- - \nu_+ r_0^+)}{eN(\tilde{u}_+(H) + \tilde{u}_-(H))^2}. \quad (33)$$

CONCLUSION

In the present paper the Hall coefficient has been calculated for ionic semiconductors, considered both in the weak coupling approximation and in the adiabatic approximation. The method of stationary states was used, i.e., the calculation was carried out without use of the kinetic equation. The difference between our equations and those following from kinetic theory are most marked for $N_- = N_+$, i. e., in particular, in the case of a semiconductor without impurity. For example, in in this case, for a polaron semiconductor, R is determined by the ratio of the polarizabilities of the electron and hole polarons.

APPENDIX I

We find the equilibrium distribution in P_z - $f(P_z)$ with the aid of a Gibbs grand ensemble; if the energy of the system is given by the expression $E_c = E_c(P_z, P_y, n_0, n_f)$, then

$$f(P_z) = \sum_{P_y, n_0, n_f} \exp\left(-\frac{E_c}{kT}\right) \times \left\{\sum_{P_z, P_y, n_0, n_f} \exp\left(-\frac{E_c}{kT}\right)\right\}^{-1}. \quad (I.1)$$

If we substitute in (I.1) the equation for E_c, computed in reference 2 with accuracy to ϵ^2 [Eq. (2.5)], we obtain (keeping the notation of reference 2):

$$f(P_z) = D\exp\left(-\frac{P_z^2}{2\mu_1 kT}\right)\overline{W}_1\overline{W}_2, \quad (I.2)$$

where

$$\overline{W}_1 = \sum_{\ldots n_f \ldots} \exp\left\{-\frac{1}{kT}\left[\Sigma\mathscr{E}'(f)n_f + \frac{\hbar^2}{2\mu}\Sigma f_{1z}f_{2z}n_{f_1}n_{f_2} + \varepsilon^2\Sigma\alpha_2(f)n_f + \varepsilon^2 P_z^2\Sigma C_2(f)n_f\right]\right\};$$

$$\overline{W}_2 = \sum_{n_0}\exp\left\{-\frac{n_0}{kT}[\hbar\omega_0 + \varepsilon^2 C_1 P_z^2 + \varepsilon^2\alpha_1]\right\}; \quad (I.3)$$

$$\mu_1 = \mu\,(1 + 2\mu\varepsilon^2 C_3)^{-1}; \quad D = \exp\left\{-\frac{\hbar\omega_0}{2kT}\right\}$$

$$\times \left[\sum_{P_y,\,P_z,\,n_0,\,n_f} \exp\left(-\frac{E_c}{kT}\right)\right]^{-1}.$$

The quantities α_1, $\alpha_2(f)$; C_1, $C_2(f)$, C_3 are obtained by an expansion of ΔE in reference 5 [Eq. (2.5)] in powers of P_z (with accuracy to P_z^2):

$$\Delta_2 E = \varepsilon^2 \Sigma \alpha_2(f)\, n_f + \varepsilon^2 P_z^2 \Sigma C_2(f)\, n_f, \qquad \text{(I.4)}$$

$$\Delta_1 E = (\Delta_1 E)_{P_z=0} + \varepsilon^2 C_3 P_z^2,$$

$$\Delta_3 E = \varepsilon^2 n_0 \alpha_1 + \varepsilon^2 n_0 C_1 P_z^2.$$

We return to the calculation of $\overline{W}_1$; inasmuch as $\epsilon \ll 1$, we can decompose $\overline{W}_1$ in powers of ϵ:

$$\overline{W}_1 = Z_\Gamma\left(1 + P_z^2\frac{\overline{W}_1'}{Z_\Gamma} + \frac{\overline{W}_1''}{Z_\Gamma}\right), \qquad \text{(I.5)}$$

where

$$Z_\Gamma = \sum_{\dots n_f \dots}\left\{-\frac{1}{kT}\left[\Sigma \mathcal{E}'(f)\, n_f + \frac{\hbar^2}{2\mu}\Sigma f_{1z} f_{2z} n_{f_1} n_{f_2}\right]\right\}$$

is the statistical sum of the system of quasi-particles $\mathcal{E}'(f)$.

$$\frac{\overline{W}_1'}{Z_\Gamma} = -\frac{\varepsilon^2}{kT}\Sigma C_2(f)\, \overline{n}_f; \quad \frac{\overline{W}_1''}{Z_\Gamma} = -\frac{\varepsilon^2}{kT}\Sigma \alpha_2(f)\, \overline{n}_f, \qquad \text{(I.6)}$$

since, by definition,

$$\overline{n}_f = \frac{1}{Z_\Gamma}\sum_{\dots n_f \dots} n_f \exp\left\{-\frac{1}{kT}\left[\Sigma \mathcal{E}'(f)\, n_f + \frac{\hbar^2}{2\mu}\Sigma f_{1z} f_{2z} n_{f_1} n_{f_2}\right]\right\}$$

is the equilibrium value of the occupation number n_f, computed in reference 5. Consequently,

$$\overline{W}_1 = Z_\Gamma \exp\left\{-\frac{\varepsilon^2}{kT}\left[P_z^2 \Sigma C_2(f)\, \overline{n}_f + \Sigma \alpha_2(f)\, \overline{n}_f\right]\right\}.$$

By analogy,

$$\overline{W}_2 = (1 - e^{-\hbar\omega_0/kT})^{-1} \exp\left\{-\frac{\varepsilon^2 \overline{n}_0}{kT}(P_z^2 C_1 + \alpha_1)\right\}. \qquad \text{(I.7)}$$

Here we introduce the equilibrium number of oscillator quanta $\overline{n}_0 = [\exp\frac{\hbar\omega_0}{kT} - 1]^{-1}$. Then it follows from Eqs. (I.1)-(I.7) that

$$f(P_z) = D_1 Z_\Gamma \exp\left(-\frac{P_z^2}{2\mu_e' kT}\right), \qquad \text{(I.8)}$$

where

$$D_1 = D\,(1 - e^{-\hbar\omega_0/kT})^{-1}\exp\left\{-\frac{\varepsilon^2}{kT}\left(\alpha_1 \overline{n}_0 + \Sigma\alpha_2(f)\, \overline{n}_f\right)\right\};$$

$$\mu_e' = \mu\,\{1 + 2\mu\varepsilon^2(C_1\overline{n}_0 + \Sigma C_2(f)\, \overline{n}_f + C_3)\}^{-1}$$

(μ_e' differs from the μ_e in reference 5 by the fact that n_0 is replaced by $\overline{n}_0$).

Making use of the expressions for $\overline{n}_f(T)$, computed in reference 5 [Eqs. (4.5), (4.6)], we calculate Z_Γ:

$$Z_\Gamma = \exp\left[-\frac{\pi^2 k^2 T^2}{12\hbar a_0^2\, |P_z - a_z|}\right] \text{ for } 0 < T < T_1,$$

$$Z_\Gamma = \exp\left[-\frac{\pi^2 k^{5/3} \mu^{1/3} T^{5/3}}{10\hbar\,(\omega a_0 \ln 2)^{1/3}}\right] \text{ for } T_1 < T \leqslant \frac{\hbar\omega}{k},$$

where $a_z = \Sigma\hbar f_z \overline{n}_f(T)$.

Consequently, for $0 < T < T_1$,

$$f(P_z) = D_1 \exp\left[-\frac{P_z^2}{2\mu_e' kT} - \frac{\pi^2 kT}{12\hbar a_0^2\, |P_z - a_z|}\right] \qquad \text{(I.9)}$$

and for $T_1 < T \lesssim \hbar\,\omega/k$,

$$f(P_z) = (2\pi\mu_e' kT)^{-1/2}\exp\{-P_z^2/2\mu_e' kT\}. \qquad \text{(I.10)}$$

APPENDIX II

In the method of stationary states, we initially calculate the currents j_x, j_y in an infinite gyrotropic medium (taking into account the quantization of the spectrum of the system in the crossed fields $E \perp H$), and then these j_x, j_y are substituted in the expression which connects the currents j_x, j_y with the Hall coefficient R and the resistance in a transverse magnetic field, ρ. In this case, we introduce the tensors of electrical conductivity σ_{ik} and electrical resistance ρ_{ik} in a gyrotropic medium ($i, k = 1, 2$) and employ the local ratios of the fields E_x, E_y and the currents j_x, j_y, applying them initially to the case of a crystal bounded along OY ($j_y = 0$), in order to establish the connection of ρ and R with ρ_{ik} and σ_{ik}; then we consider the case of an unbounded gyrotropic crystal ($E_y = 0$), to connect R and ρ with the currents j_x and j_y computed with account of the quantization of the energy of the system in the field $E \perp H$. This can be done since the relations

$$E_i = \sum_{k=1}^{2} \rho_{ik} j_k \text{ and } j_i = \sum_{k=1}^{2} \sigma_{ik} E_k \quad (i,\ k = 1.2)$$

are local relations.

As is shown below, the ordinary expressions for ρ and R ($\rho = j_1 E_1 / j_1^2 + j_2^2$), $R = -j_2 E_1 / (j_1^2 + j_2^2)$ are obtained only if the Onsager relations are satisfied: $\sigma_{12}(H) = +\sigma_{21}(-H)$, $\rho_{12}(H) = \rho_{21}(-H)$. There are cases for which the Onsager relations are not satisfied, e.g., if σ_{12} and σ_{21} (and also ρ_{21}, ρ_{12}) depend not only on H but also on the external field E_1 (the local relation between j_i and E_i remains valid as before). In such a case, because of the axial symmetry of the system in the field H, $\rho_{11} = \rho_{22} \equiv \rho$, $\sigma_{11} = \sigma_{22} \equiv \sigma$, but $\rho_{12} \equiv \rho' \neq -\rho_{21}$ and $\sigma_{12} = \sigma' \neq -\sigma_{21}$. In Sec. 2 of this paper we considered such a case ($\hbar\omega < \frac{1}{2}\mu\gamma^2$).

We can set $\rho_{21} = -\rho' + \overline{\rho}$, $\sigma_{21} = -\sigma' + \overline{\sigma}$, where $\overline{\rho} = \rho_{12} + \rho_{21}$, $\overline{\sigma} = \sigma_{12} + \sigma_{21}$.

Then

$$E_1 = \rho j_1 + \rho' j_2,\ E_2 = (-\rho' + \overline{\rho}) j_1 + \rho j_2; \quad \text{(II.1)}$$

$$j_1 = \sigma E_1 + \sigma' E_2,\ j_2 = (-\sigma' + \overline{\sigma})\ E_1 + \sigma E_2 \quad \text{(II.2)}$$

We first return to the conclusion of the expression for R: for $j_2 = 0$, $E_2 = +(-\rho' + \overline{\rho}) j_1 = RHj_1$, i.e., $RH = -\rho' + \overline{\rho}$.

It follows from (II.2) that

$$RH = -\rho' + \overline{\rho} = \frac{\sigma' - \overline{\sigma}}{\sigma^2 + (\sigma' - \sigma)^2 + \sigma'\overline{\sigma}}, \quad \text{(II.3)}$$

but for $E_2 = 0$ it follows from (II.2) that

$$\sigma = j_1 / E_1, \quad \sigma' - \overline{\sigma} = -j_2 / E_1. \quad \text{(II.4)}$$

Therefore, (II.3) reduces to the form

$$R = -\frac{j_2 E_1}{H} \{j_1^2 + j_2^2 - \overline{\sigma} j_2 E_1 + \overline{\sigma}^2 E_1^2\}^{-1} \quad \text{(II.5)}$$

This is the general formula for R.

If $\overline{\sigma} = \epsilon^2 \overline{\sigma}_0$ (as is the case in the present work for $\hbar\omega < \frac{1}{2}\mu\gamma^2$) with accuracy to $\epsilon^2 \ll 1$ we obtain inclusively [for $|j_2| > |j_1|$ $R_\pm \approx R_0^\pm \equiv \pm(N_\pm ec)^{-1}$ with accuracy to ϵ^4]:

$$R \approx -\frac{j_2 E_1}{H(j_1^2 + j_2^2)} \left(1 + \epsilon^2 \frac{\overline{\sigma}_0 j_2 E_1}{j_1^2 + j_2^2}\right). \quad \text{(II.6)}$$

Consequently, for $|j_1| < |j_2| = |j_2^0 + \epsilon^2 j_2'|$

$$R \approx -E_1 / j_2^0 H = R_0. \quad \text{(II.7)}$$

For $|j_1| > |j_2|$

$$R \approx -(E_1 j_2^0 / j_1^2 H) - \epsilon^2 E_1 j_2' / j_1'. \quad \text{(II.8)}$$

We begin consideration of the expression for the resistance in a transverse magnetic field $H \perp E_1$. It follows from Eqs. (II.1) and (II.2) that

$$\rho = \frac{\sigma}{\sigma^2 + (\sigma' - \overline{\sigma})^2 + \sigma'\overline{\sigma}} \quad \text{(II.9)}$$

$$= \frac{j_1 E_1}{j_1^2 + j_2^2} \left(1 - \frac{\overline{\sigma} j_2 E_1 - \overline{\sigma}^2 E_1^2}{j_1^2 + j_2^2}\right)^{-1}$$

If $\overline{\sigma} \sim \epsilon^2 \ll 1$, we obtain (with accuracy to ϵ^2 inclusively):

for $|j_2| > |j_1|$:

$$\rho \approx \rho^0 \left(1 + \epsilon^2 \frac{\overline{\sigma}_0 E_1}{j_2}\right),$$

for $|j_1| > |j_2|$:

$$\rho \approx \rho^0 \left(1 + \epsilon^2 \frac{\overline{\sigma}_0 j_2 E_1}{j_1^2}\right),$$

whence

$$\rho^0 = j_1 E_1 / (j_1^2 + j_2^2).$$

It should be noted that if the Onsager relations are satisfied and $\overline{p} = \overline{\sigma} = 0$, then, in correspondence to the above,

$$R = -j_y E_x (j_x^2 + j_y^2)^{-1}, \quad \rho = j_x E_x (j_x^2 + j_y^2)^{-1}.$$

In conclusion, I take this opportunity to express my gratitude to Professor A. G. Samoilovich for suggesting the work, for his valued advice and constant interest.

Translated by R. T. Beyer
223

SOVIET PHYSICS JETP VOLUME 2, NUMBER 3 MAY, 1956

The Double-Configurational Approximation in the Case of Carbon-like Atoms

A. B. BOLOTIN, I. B. LEVINSON AND L. I. LEVIN
Vilna State University

(Submitted to JETP editor May 29, 1954)
J. Exper. Theoret. Phys. USSR **29**, 449-453 (October, 1955)

Parametric values of analytical one-electron wave functions are presented for C, N^+, O^{++}, $F^{3+}$and Ne^{4+} in the configurations $1s^2 2s^2 2p^2$, $1s^2 2s\, 2p^3$ and $1s^2 2p^4$. Corrections to the energy in the double-configurational approximation for the fundamental configurations of the above atoms were determined in the double-configurational approximation $1s^2 2s^2 2p^2 - 1s^2 2p^4$. The theoretical values obtained for the energy are compared with experimental data. The total dipole strengths and the probabilities of the transitions $1s^2 2s 2p^3 - 1s^2 2s^2 2p^2$ were determined in both the single- and double-configurational approximations.

INTRODUCTION

A poly-configurational approximation for beryllium and boron-like atoms and its effect on quantities in the theory of transitions were investigated in the work of reference 1 by means of analytical one-electron wave functions. The present work is devoted to the study of carbon-like atoms by means of the above wave functions.

A poly-configurational approach for the case of the carbon atom was studied in detail in reference 2, using wave functions of a self-consistent field without quantum exchange. From this work it follows that in the case of the fundamental configuration of carbon-like atoms, the poly-configurational approximation reduces in practice to the double-configurational $1s^2 2s^2 2p^2 - 1s^2 2p^4$. Furthermore, the manner of consideration proposed in part 2 of reference 3 leads to the conclusion that as long as we use one-electron wave functions determined in the single-configurational approximation, then in the case of the configuration $1s^2 2s 2p^3$ the poly-configurational approach reduces to the single-configurational approximation. Therefore, in the investigation of quantities in transition theory for the configuration $1s^2 2s^2 2p^2$ we use a double-configurational approach and for $1s^2 2s 2p^3$ a single-configurational approach.

2. PARAMETERS OF THE ONE-ELECTRON WAVE FUNCTIONS

The expressions for the wave functions and all the notations used in reference 1 are retained in the present work. The parameters η, a, b and c were found by a graphical method from the condition of minimum total energy in the single-configurational approximation. The numerical values of these parameters and the total energy for the configurations $1s^2 2s^2 2p^2$, $1s^2 2s 2p^3$ and $1s^2 2p^4$ are presented in Table I for the atoms C, N^+, O^{++}, F^{3+} and Ne^{4+}. Experimental data for the total energy, compiled with the aid of reference 4, are also included in the Table.

By means of the data in Table I, values were determined for the correction to the energy of the fundamental configuration in the double-configurational approximation $1s^2 2s^2 2p^2 - 1s^2 2p^4$, and for the constant a_{12}; the absolute value of the latter is the weight of the configuration $1s^2 2p^4$ relative to $1s^2 2s^2 2p^2$. The results are entered in Table II.

3. THE TOTAL DIPOLE STRENGTH AND THE TRANSITION PROBABILITY IN THE DOUBLE-CONFIGURATIONAL APPROXIMATION

For the total dipole strength in the double-configurational approach we obtain the following expression:

$$S(SL', SL) = \frac{\alpha}{1+a_{12}^2}[N(r2s,\ 2p)_{13} + a_{12}\beta N(r2s,\ 2p)_{32}]^2, \quad (1)$$

---

[1] A. B. Bolotin and A. P. Iutsis, J. Exper. Theoret. Phys. USSR **24**, 537 (1953).

[2] A. P. Iutsis, J. Exper. Theoret. Phys. USSR **19**, 565 (1949).

[3] A. P. Iutsis and V. I. Kavetskis, J. Exper. Theoret. Phys. USSR **21**, 1139 (1951).

[4] C. E. Moore, Atomic Energy Levels, Nat. Bur. Stand. Cir. 467, Washington (1949).

TABLE I *

Values of the parameters in the wave functions for the configurations $1s^22s^22p^2$, $1s^22s2p^3$, $1s^22p^4$ of the carbon-like atoms C, N$^+$, O^{++}, F^{3+}, Ne^{4+} (energies in atomic units).

Configuration	a	ηa	b	ηb	$2\eta c$	2η	$E_{\text{theor.}}$	$E_{\text{exper.}}$
$1s^22s^22p^2$								
^3P	3.61	5.70	2.25	5.14	3.10	3.16	− 37.600	−37.855
	3.34	6.71	2.90	5.83	4.14	4.02	− 53.765	−54.072
	3.15	7.72	2.73	6.62	5.29	4.90	− 72.940	−73.317
	3.00	8.72	2.60	7.55	6.28	5.81	− 95.120	—
	2.90	9.72	2.50	8.38	7.30	6.70	−120.285	—
^1D	3.60	5.69	3.20	5.06	3.10	3.16	− 37.530	−37.809
	3.37	6.71	2.97	5.97	4.14	3.98	− 53.685	−54.005
	3.16	7.71	2.75	6.71	5.22	4.88	− 72.835	−73.225
	3.01	8.72	2.62	7.59	6.20	5.79	− 94.985	—
	2.95	9.72	2.50	8.35	7.21	6.68	−120.140	—
^1S	3.60	5.69	3.18	5.02	3.10	3.16	− 37.435	−37.757
	3.39	6.71	2.99	5.92	4.12	3.96	− 53.555	−53.926
	3.18	7.71	2.80	6.79	5.20	4.85	− 72.675	−73.120
	3.03	8.72	2.65	7.63	6.16	5.76	− 94.790	—
	2.92	9.72	2.55	8.49	7.13	6.66	−119.900	—
$1s^22s2p^3$								
^1P	3.52	5.68	3.20	5.15	3.03	3.22	− 36.995	−37.309
	3.25	6.65	2.93	5.99	4.17	4.09	− 52.980	−53.315
	3.07	7.64	2.72	6.77	5.13	4.98	− 71.985	−72.358
	2.93	8.64	2.55	7.52	6.14	5.90	− 93.985	—
	2.80	9.63	2.45	8.43	7.22	6.88	−119.010	—
^1D	3.53	5.68	3.23	5.20	3.06	3.22	− 37.065	−37.409
	3.30	6.66	2.87	5.80	4.08	4.04	− 53.065	−53.418
	3.07	7.64	2.75	6.84	5.18	4.98	− 71.950	−72.465
	2.93	8.62	2.60	7.65	6.29	5.88	− 94.115	—
	2.81	9.60	2.55	8.71	7.31	6.83	−119.155	—
^3P	3.42	5.67	2.90	4.81	3.12	3.32	− 37.245	−37.512
	3.12	6.65	2.75	5.86	4.09	4.26	− 53.295	−53.577
	2.97	7.64	2.65	6.81	5.19	5.14	− 72.370	−72.668
	2.87	8.64	2.55	7.68	6.20	6.02	− 94.425	—
	2.77	9.64	2.50	8.70	7.17	6.96	−119.505	—
^3D	3.45	5.67	3.15	5.18	3.13	3.29	− 37.305	−37.563
	3.22	6.62	3.00	6.22	4.14	4.14	− 53.380	−53.655
	3.05	7.65	2.70	6.78	5.17	5.02	− 72.470	−72.770
	2.89	8.64	2.55	7.62	6.22	5.98	− 94.555	—
	2.77	9.64	2.40	8.35	7.24	6.96	−119.660	—
^3S	3.55	5.69	3.22	5.16	3.01	3.20	− 37.045	−37.373
	3.35	6.69	3.00	5.99	4.07	3.99	− 53.050	−53.368
	3.18	7.68	2.78	6.71	5.17	4.83	− 72.070	−72.419
	3.03	8.68	2.60	7.45	6.19	5.73	− 94.105	—
	2.88	9.66	2.50	8.39	7.24	6.71	− 119.135	—
^5S	3.48	5.66	3.14	5.10	3.12	3.25	− 37.030	−37.702
	3.25	6.64	2.95	6.03	4.17	4.09	− 53.050	−53.860
	3.05	7.63	2.82	7.05	5.25	5.00	− 72.085	−73.042
	2.97	8.62	2.72	7.90	6.27	5.80	− 94.105	—
	2.90	9.61	2.67	8.85	7.29	6.63	−119.140	—
$1s^22p^4$								
^3P	3.59	5.67	—	—	3.00	—	− 36.820	—
	3.30	6.67	—	—	4.04	—	− 52.735	—
	3.05	7.67	—	—	5.08	—	− 71.660	−72.024
	2.89	8.66	—	—	6.10	—	− 93.595	—
	2.80	9.66	—	—	7.10	—	−118.535	—

TABLE I (*continued*)

Configuration	a	ηa	b	ηb	$2\eta c$	2η	$E_{\text{theor.}}$	$E_{\text{exper.}}$
^1D	3.59	5.67	—	—	3.00	—	— 36.760	—
	3.30	6.67	—	—	4.04	—	— 52.650	—
	3.05	7.66	—	—	5.08	—	— 71.555	—71.958
	2.89	8.65	—	—	6.10	—	— 93.470	—
	2.78	9.64	—	—	7.14	—	—118.390	—
^1S	3.59	5.67	—	—	3.00	—	— 36.660	—
	3.20	6.67	—	—	4.04	—	— 52.520	—
	3.05	7.66	—	—	5.08	—	— 71.400	—71.753
	2.89	8.64	—	—	6.10	—	— 93.275	—
	2.78	9.63	—	—	7.14	—	—118.165	—

---

* Precision of the parameter values ± 0.02, and of the energy ± 0.005.

TABLE II

Corrections to the energy in the double-configurational approximation for the investigated configurations, values of the constant a_{12} and of the non-diagonal element of the energy.

Entity	C	N$^+$	O^{++}	F^{3+}	Ne^{4+}
			^3P		
ΔE^1	—0.018	—0.023	—0.027	—0.031	—0.035
E_{12}	0.118	0.153	0.186	0.218	0.249
a_{12}	—0.15	—0.15	—0.14	—0.14	—0.14
			^1D		
ΔE^1	—0.018	—0.022	—0.026	—0.030	—0.034
E_{12}	0.120	0.153	0.185	0.217	0.248
a_{12}	—0.15	—0.14	—0.14	—0.14	—0.13
			^1S		
ΔE^1	—0.068	—0.084	—0.100	—0.116	—0.131
E_{12}	0.240	0.305	0.372	0.434	0.495
a_{12}	—0.28	—0.28	—0.27	—0.27	—0.26

wherein

	$^1P - {}^1S$	$^1P - {}^1D$	$^1D - {}^1D$
α	4	5	15
β	+1	—1	+1

	$^3P - {}^3P$	$^3D - {}^3P$	$^3S - {}^3P$
α	9	15	12
β	—1	+1	+1

The integrals $N(nl, nl)_{13}$ and $N(nl, nl)_{32}$ are equal to unity within the limits of error and are omitted in Eq. (1). To obtain Eq. (1) it is convenient to use the methods applied in references 5 and 6. Formula (4.3) of reference 1 was used for the determination of transition probabilities. The values of the total dipole strength and probability of transitions determined with the use of the

---

[5] G. Racah, Phys. Rev. 62, 438 (1942).

[6] G. Racah, Phys. Rev. 63, 367 (1943).

TABLE III

Values of the total dipole strength and transition probability for carbon-like atoms. (The transition probability is in units of 10^8 per second, all other quantities are in atomic units).

Entity	C	N^+	O^{2+}	F^{3+}	Ne^{4+}	
$N(r2s, 2p)_{13}$	1.64	1.25	1.00	0.842	0.712	^3S—^3P
$N(r2s, 2p)_{32}$	1.63	1.26	1.02	0.855	0.732	
$S(^3S, {}^3P)$ a	10.8	6.25	4.00	2.84	2.07	
b	7.62	4.40	2.88	2.04	1.49	
$W(^3S, {}^3P)$ a	130	160	190	210	220	
b	100	125	145	165	175	
$N(r2s, 2p)_{13}$	1.61	1.25	1.00	0.841	0.725	^3P—^3P
$N(r2s, 2p)_{32}$	1.59	1.22	0.995	0.838	0.722	
$S(^3P, {}^3P)$ a	7.78	4.69	3.00	2.12	1.58	
b	10.2	6.02	3.82	2.70	2.01	
$W(^3P, {}^3P)$ a	8.20	11.5	14.0	16.5	17.5	
b	12.5	17.0	21.0	24.0	25.5	
$N(r2s, 2p)_{13}$	1.60	1.24	1.00	0.839	0.719	^3D—^3P
$N(r2s, 2p)_{32}$	1.60	1.24	1.00	0.840	0.723	
$S(^3D, {}^3P)$ a	12.9	7.69	5.02	3.52	2.58	
b	9.11	5.43	3.63	2.55	1.87	
$W(^3D, {}^3P)$ a	4.70	6.20	7.35	8.90	9.00	
b	3.95	5.20	6.30	7.30	7.70	
$N(r2s, 2p)_{13}$	1.64	1.24	1.02	0.848	0.725	^1P—^1S
$N(r2s, 2p)_{32}$	1.62	1.25	1.01	0.845	0.723	
$S(^1P, {}^1S)$ a	3.59	2.05	1.39	0.959	0.701	
b	1.74	0.979	0.694	0.478	0.360	
$W(^1P, {}^1S)$ a	21.5	27.5	32.5	34.5	35.0	
b	16.0	20.5	24.5	26.5	27.0	
$N(r2s, 2p)_{13}$	1.64	1.24	1.01	0.847	0.725	^1P—^1D
$N(r2s, 2p)_{32}$	1.62	1.25	1.01	0.845	0.723	
$S(^1P, {}^1D)$ a	4.48	2.56	1.70	1.20	0.876	
b	5.78	3.27	2.17	1.52	1.11	
$W(^1P, {}^1D)$ a	48.5	63.0	74.0	85.0	89.5	
b	69.5	88.5	103	115	120	
$N(r2s, 2p)_{13}$	1.63	1.26	1.00	0.833	0.719	^1D—^1D
$N(r2s, 2p)_{32}$	1.62	1.26	1.00	0.845	0.723	
$S(^1D, {}^1D)$ a	13.3	7.88	5.00	3.47	2.53	
b	9.40	5.70	3.62	2.50	1.90	
$W(^1D, {}^1D)$ a	58.0	73.0	86.5	97.5	105	
b	46.0	58.0	69.0	78.0	83.5	

Note: *a* – denotes the single-configurational approximation; *b* – the double-configurational.

parameters in Table I and of the quantities in Table II are represented in Table III.

4. CONCLUSIONS

From Table II it is seen that the correction to the energy in the double-configurational approach in the case of carbon-like atoms increases in absolute value with increase in nuclear charge, while decreasing percentagewise. In the cases of C and O^{++}, the correction to the energy in the double-configurational approximation and the constant a_{12} agree with the results of references 7 and 8.

The results in Table III show that the total dipole strength in the double-configurational approximation is increased 1.3-2.0 times or decreased in the same amount, depending on the sign of β in (1). The transition probabilities ${}^3S$ - ${}^3P$, ${}^3D$ - ${}^3P$, ${}^1P$ - ${}^1S$, ${}^1D$ - ${}^1D$ are reduced by 1.2-1.3 times, while the transition probabilities ${}^3P$ - ${}^3P$, ${}^1D$ - ${}^1D$ are increased by 1.4 -1.5 times.

In the case of carbon-like atoms the total dipole strengths of the transitions ${}^3S$ - ${}^3P$, ${}^3P$ - ${}^3P$, ${}^3D$ - ${}^3P$ have the ratios 12:9:15 in the single-configurational approximation and 8.5:11:10 in the double-configurational, while for the transitions ${}^1P$ - ${}^1S$, ${}^1P$ - ${}^1D$, ${}^1D$ - ${}^1D$ the ratios are 4:5:15 and 2:6:11 in the single- and double-configurational approximations, respectively.

The authors consider it their pleasant duty to express deep thanks to Prof. A. P. Iutsis for his suggestion of the topic and his constant attention to the work.

Translated by R. L. Eisner
224

---

[7] A. Iutsis, Proc. Roy. Soc. (London) **A173**, 59 (1939)

[8] D. R. Hartree, W. Hartree and B. Swirles, Phil. Trans. Roy. Soc. **A238**, 229 (1939)

SOVIET PHYSICS JETP VOLUME 2, NUMBER 3 MAY, 1956

Investigation of the Isotopic Constitution of Lithium

K. ORDZHONIKIDZE AND V. SHIUTTSE

(Submitted to JETP editor July 2, 1954)
J. Exper. Theoret. Phys. USSR 29, 479-485 (October, 1955)

Investigations of the separation effects of the isotopes of lithium have been carried out by evaporation of lithium ions from a tungsten surface and by ionization of molecular beams of lithium compounds by an electron beam. In the first case two processes of ionic emission have been discovered: the first process occurs at low anode temperatures with a separation coefficient greater than for free evaporation; the second process takes place at high anode temperatures without separation of the isotopes and provides a simple and accurate method of measuring the relative abundance of the isotopes of lithium. The relative abundance of the lithium isotopes Li^7/Li^6 was found to be 12.47 ±0.02. A small separation effect of unexplained origin has been found to take place during ionization of the lithium compounds by the electron beam. By means of the method developed by the authors, the relative abundances of the lithium isotopes have been measured for several minerals.

PREVIOUS results of relative abundance measurements of lithium isotopes with mass numbers 6 and 7 show considerable spread caused by the impossibility of computing with sufficient accuracy the separation property of the ion source. Because of this, the values quoted by various authors for the relative abundance of the lithium isotopes Li^7/Li^6 range from 5 to 37. Considering the difficulty of introducing reliable corrections in the relative abundance measurements of lithium isotopes, excellent agreement may be said to exist between the early measurements of Brewer[1] and later measurements of Hintenberger[2], Inghram, Hess and Hayden[3], White and Cameron[4] and Hibbs[5]. In the published investigations of the isotopic constitution of lithium, the lithium ions were obtained by thermionic emission from hot surfaces (glass melt, Kuntzman anode, platinum surface). Ionization was also produced in a molecular vapor of lithium compounds LiCl and LiI by an electron beam.

We have measured the relative abundance of lithium isotopes utilizing various methods for ion production and making use of two-mass spectrometers built by us (predecessors of mass-spectrometers MC - 1, MC - 2 and others).

A magnetic sector field is used in the mass-spectrometers with a 60° angle of deflection and 16° 18′ beam entry and exit angles. Thereby second order geometrical aberrations in the image are reduced to zero[6,7]. The introduction of higher order focussing could increase somewhat the resolving power of the instrument, but a better reason for correcting aberrations is given next. During the course of a series of experiments an insulating layer was often formed in the ion source and on the entrance slit, somewhat deflecting the beam from its original direction, thereby worsening the image and thus the resolving power of the instrument. In the case of a field with corrected aberrations, the position of the focus and the width of resolution do not depend on small variations in the direction of the beam; thus the resolving power and the line shape depend much less upon working conditions at the ion source.

The radius of the average ionic trajectory is 200 mm; correspondingly the dispersion in the plane of the receiver, perpendicular to the beam, is 1.33 mm for a 1% mass difference. The resolving power of the mass-spectrometers that we have used is $m/\Delta m = 1000$ for a 0.1 mm wide exit slit of the ion source and 0.1 mm wide entry slit in front of the ion collector. During the course of our experiments we have used as an ion source a source of Bleakney[9] construction employed in reference 8 for gaseous ionization, or a hot anode of a form proposed by Koch[10]. A description of the latter appears below.

The ion source and the analyzer tube are pumped out by separate mercury-diffusion pumps which can pump 7 l/sec through a metallic trap. The tube of the mass-spectrometer is made of copper with steel end flanges and provided with metallic (copper or aluminum sheet) gaskets[11]. Electrical connections to the electrodes of the ion emitter and receiver were soldered in Kovar, so that the entire tube could be heated to 400°C and outgassed. The gaskets appear completely reliable and in some of our instruments were heated hundreds of times without need to change or tighten the bolts. We reached a final vacuum definitely below 10^{-8} mm of mercury (measured with an ionization manometer tube LM-2, by reading its ion current in the mass-spectrometer itself, and applying the proper correction for an ionization manometer at lowest pressures).

---

[1] A. K. Brewer, J. Chem. Phys. 4, 350 (1936).

[2] H. Hintenberger, Naturwiss. 34, 52 (1947).

[3] M. G. Inghram, D. C. Hess and R. J. Hayden, *Plutonium Project Report* ANL 4012, p.7 (July 1947) as quoted by G. T. Seaborg and I. Perlman, Revs. Mod. Phys 20, 585 (1948).

[4] J. R. White and A. E. Cameron, Phys. Rev. 74, 991 (1948).

[5] R. F. Hibbs, Natl. Bur. St., Circular 499, Supplement 1 (1951).

[6] H. Hintenberger, Z. Naturforsch 3a, 125 (1948).

[7] L. Kerwin, Rev. Sci. Instr. 20, 36 (1949); L. Kerwin and C. Geoffrion, Rev. Sci. Instr. 20, 381 (1949).

[8] A. O. Nier, Rev. Sci. Instr. 11, 212 (1940); 18, 398 (1947).

[9] W. Bleakney, Phys. Rev. 40, 496 (1932).

[10] J. Koch, Z. Physik 100, 685 (1936).

The ion source is fed by the usual electronically stabilized system. The ion accelerating potential measures 2500 V and is maintained constant. During adjustment only the magnetic field varies. The ion currents are measured with one or, when using two receivers, with two constant current amplifiers with 100% feed-back; moreover when using two amplifiers, the ratio of the ion currents could be immediately determined on a decimal voltage divider.

1. EVAPORATION OF LITHIUM IONS FROM A TUNGSTEN SURFACE

In order to obtain more reliable data about the evaporation process of lithium ions and a correct value for the relative abundance of the isotopes, we decided to study the emission process of lithium ions from the beginning of ionic emission until exhaustion of the ion source. For a hot anode we used an anode of early Koch[10] design but of simpler construction. The anode consists of a ribbon of tantalum pressed into the shape of a groove and filled with 15 mg of fine tungsten powder. This anode is carefully evacuated for several hours at a temperature of 2200°C in a special apparatus after which no trace of alkaline ion emission can be detected. During the heating process the tungsten powder is baked into a hard porous body into which the lithium salt is introduced in the form of water or alcohol solution. With the help of such an anode in the mass-spectrometer, a constant ionic current can be obtained easily and repeatedly in high vacuum. The anode is heated by a constant current from a battery. During measurements the battery is charged by a rectifier; the current through the rectifier is kept equal to the anode heating current thereby providing a constant heating current and ensuring exact measurements up to anode temperatures of 2000°C. The ion current is registered by means of a self-recording apparatus. In order to record the ion current of the lithium isotopes as a function of time, an automatically repeating recording was set up with automatic switching of the sensitivity of the recording apparatus. The method worked out for recording the ion currents of lithium isotopes is of special importance, when carrying out an isotopic analysis of small quantities of material with quickly falling ionic currents. Measurements were carried out with different quantities of LiCl (5×10^{-9}, 3×10^{-8}, 2×10^{-7} and 10^{-6} gm) as shown on the figure.

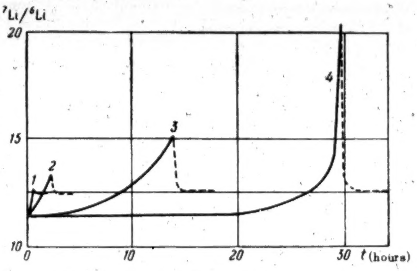

Relative abundance of lithium isotopes as a function of time during evaporation of lithium ions from the surface of tungsten powder. Original quantity of LiCl: 1 - 5×10^{-9}; 2 - 3×10^{-8}; 3 - 2×10^{-7}; 4- 10^{-6} gm.

---

[11] W. Paul, Z. Physik **124**, 244 (1948).

At the beginning, the value of the ratio Li^7/Li^6 is found to be 11.42 ± 0.02 for all quantities of lithium chloride. The smaller was this quantity the faster the ratio Li^7/Li^6 grew, and the larger was this quantity the larger this ratio became; in the case of 10^{-6}g, the ratio Li^7/Li^6 grew in 30 hours to 20.60.

While the measurements were carried out the ionic current remained constant with the anode temperature increasing gradually from 800 to 1200°C. The first process of evaporation of lithium ions during which the ratio Li^7/Li^6 increases in time takes place within this temperature interval. Upon further increase in temperature the ion current falls sharply and becomes unstable. An increase of anode temperature to 1500°C does not produce a visible increase in ion current. It is therefore impossible to obatin an exact value for the ratio Li^7/Li^6 in the temperature interval 1200-1500°C. This interval is indicated on the figure by dotted lines. There is a strong impression that the material under investigation has completely disappeared.

However, upon further increase in temperature a constant ion current is observed again, and maintains itself with gradual increase in temperature to 2000°C. During this process the value of the ratio Li^7/Li^6 does not change in time and remains constant upon further increase in anode temperature until exhaustion of the anode, which takes place around 1800-2000°C. Measurement of the value of the ratio during this process yields 12.48 ± 0.02.

Thus, two entirely separate processes take place during evaporation of lithium ions. During the occurrence of the first process the value of the abundance ratio of the lithium isotopes increases with time; the duration of the first process depends upon the starting quantity of lithium. During the second process the ratio Li^7/Li^6 remains constant. Since we have followed the whole evaporation process of lithium ions by means of the automatically recording potentiometer, we can compute the total ionic charge $\int i\,dt$ produced during the time T, the life of the anode. Then the ratio

$$\int_0^T i_1 dt \Big/ \int_0^T i_2 dt,$$

where i_1 is the total current of Li^7 and i_2 is the total current of Li^6, must equal the natural ratio of the lithium isotopes, independently of the isotope effect observed during the first process of evaporation of lithium ions. The use of this method for computing the relative abundance of lithium isotopes yields the value 12.47 ± 0.02. Hence the value of the relative abundance of lithium isotopes obtained during the second process coincides with the true value of this ratio within limits of experimental errors.

The two processes of evaporation of lithium ions can be explained as follows. In the mass spectra, we can only observe the ions of metallic lithium; this means that dissociation of the salt takes place during the first heating of the anode. The free chlorine easily combines with tungsten and volatilizes into the vacuum. Lithium is mainly adsorbed in the form of ions and neutral atoms by the grains of the baked tungsten and a small part of lithium dissolves into the tungsten forming an alloy.

At lower anode temperatures, i.e., during the first process, ionic emission depends upon the adsorption of lithium ions by the tungsten surface. The growth of the measured ratio Li^7/Li^6 is explained by the gradual enrichment of the residue in the anode with heavier isotope, called isotope effect in free evaporation. If the evaporation of the lithium ions proceeds ideally, then the initial value of the ratio multiplied by the square root of the ratio of the masses must give the true value of the abundance ratio, in other words one must obtain a separation coefficient equal to $\sqrt{7.018/6.017} = 1.080$. The results of our measurements give for the separation coefficient the value $12.47/11.42 = 1.092 \pm 0.002$. The value thus obtained is greater than the separation coefficient predicted by the kinetic theory of gases. This means that during the first process a small effect is present in addition to the free evaporation and which further enhances the evaporation of Li^6 ions. This effect may be due to a difference in the elastic properties of the vapors of the lithium isotopes. During the first process the lithium adsorbed by the grains of tungsten is used up after a while, the ion current falls and becomes unstable. The end of stable ion emission makes it possible to reach considerably higher anode temperatures. From this moment on the second process of evaporation of lithium ions begins. In this case the ionic emission depends upon that part of the lithium which formed an alloy with the tungsten at the beginning of the heating of the anode. The relative abundance of lithium isotopes in this alloy remains normal since this part of the lithium is not exchanged with the lithium adsorbed by the grains of tungsten; it begins to evaporate with normal isotopic abundance at sufficiently high temperature, starting when the solubility of lithium in tungsten decreases with increasing temperature. The lithium which is freed upon dissolution of the alloy is vaporized and does not remain; therefore no separation effect is observed and the measured value of the abundance ration of the isotopes remains constant and is the true value.

2. THE IONIZATION OF LITHIUM COMPOUNDS WITH THE HELP OF ELECTRON BEAMS

For ideal evaporation from a surface, one might expect that the number of molecules evaporating from the surface which contain the lighter isotope is $\sqrt{M_2/M_1}$ times greater than the number of molecules containing the heavier isotope, where M_1 and M_2 are the molecular masses of the respective compounds. Because of this, the isotopic concentration within a given unit volume of atomic beam does not vary since as we just saw $\sqrt{M_2/M_1}$ more light molecules flow into this unit and similarly $\sqrt{M_2/M_1}$ more light molecules flow out of it.

It should therefore be very simple to measure the relative abundance of isotopes at the start of the evaporation process of any lithium compound or even lithium itself. In order to verify this, we prepared from lithium carbonate (supplied by the Shering-Kal'baum Co.) after additional purification by repeated recrystallization, the compounds LiF, LiCl, LiBr and LiI; moreover observations of the reaction yield made it possible to conclude that no chemical separation of isotopes had taken place. A small quantity of the compound contained in a small electrically heated platinum crucible is introduced into the ion source from which it can reach by evaporation the ionization region. The ratio Li^7/Li^6 arising upon dissociation of the halogen ions LiF^+, $LiCl^+$, $LiBr^+$ and LiI^+ is measured every time. There is superimposed upon the Li^7Cl^{37} ions a small intensity beam of CO_2^+ ions with the same mass number 44, and which cannot be corrected for; small amounts of Rb^{85} and Rb^{87} ions are also superimposed upon the Li^6Br^{79} and Li^6Br^{81} ions; one can however correct for these without serious error from the known abundance ratio of Rb. The results of these measurements reveal that within experimental accuracy (0.2%) the ratio Li^7/Li^6 is the same for all ions and equals 12.43 ±0.03. In order to settle the question of reliability of our results we measured at the same time the relative isotopic abundance of Cl and Br, for if the relative isotopic abundance of lithium varies during evaporation of the lithium halides, that of chlorine and bromine must vary in the same way. Indeed we discovered for both elements a small difference outside experimental errors, from the values we found on the very same apparatus for large quantities of the compounds in gaseous form.

	Cl^{35}/Cl^{37}	Br^{81}/Br^{79}
Evaporation of lithium compounds	0.3251	0.979
Gaseous compounds	0.3263	0.984

This difference, the reason for which we have not found, gives reasons to conjecture that the computed ratio for Li^7/Li^6 may be similarly too low. Since the difference in question is so small we can recompute the value of the ratio Li^7/Li^6 proportionally to the change in relative isotopic abundance of Cl and Br.

We find in that case

$$Li^7/Li^6 = 12.43\ \frac{0.3263}{0.3251} = 12.48 \text{ and}$$

$$Li^7/Li^6 = 12.43\ \frac{0.984}{0.979} = 12.49$$

When a few milligrams of easily vaporized salt of LiCl, LiBr, LiI are placed in the anode box and the box is heated externally, a constant ion current is produced. To obtain irreproachable data, one should use only Li^+ ions, for the presence of large quantities of heated metal of high mass number gives rise to a great many difficulties. The material vaporizing from the inner walls of the anode box recondenses on the inner walls except for a small quantity which escapes through the slit. Hence, there is no free evaporation, but a balance is established at the wall between evaporation and condensation. We found for the Li^+ ions that the ratio $Li^7/Li^6 = 12.47 \pm 0.03$, and thereby have confirmed the value computed from the first measurements.

Thus, the relative abundance of lithium isotopes obtained from ionization of LiCl and LiBr by an electron beam agrees within experimental error with the value obtained from emission of lithium ions from a hot tungsten surface.

The results of measurements of relative abundance of lithium isotopes obtained from different methods and applied to the same preparation of Li_2CO_3 supplied by Shering-Kal'baum are as follows:

Ratio of integrals of currents of lithium isotopes	12.47 ±0.02
During occurrence of the second process	12.48 ±0.02

Recomputed value:

$$12.43\,\frac{0.3263}{0.3251} = 12.48 \pm 0{,}02$$

$$12.43\,\frac{0.984}{0.978} = 12.49 \pm 0.02$$

During evaporation from anode walls 12.48 ± 0.03

Average 12.48 ± 0.02

Comparison of our average value for the relative abundance of lithium isotopes with values obtained by other authors,

12.53,[1]

12.4 ± 0.2,[2]

12.53 ± ?,[3]

12.7 ± 0.07,[4]

12.46 ± ?[5]

shows good agreement with the result of Hibbs[5].

Based on the results of investigations of lithium ions emission from a hot tungsten surface there emerges a simple method for obtaining the relative isotopic abundance of lithium. This method makes use of the second process of emissions of lithium ions. During this process, measurement of the ration Li^7/Li^6 gives the relative isotopic abundance of the material under investigation. During the occurrence of the second process of emission of lithium ions a stable ion current is obtained in the anode temperature interval 1600 - 2000°C; with as little as 10^{-9} gm of lithium, this process permits a determination of the relative isotopic abundance with an accuracy of 0.2%.

3. RESULTS OF MEASUREMENTS OF RELATIVE ABUNDANCE OF LITHIUM ISOTOPES IN SEVERAL MINERALS

Making use of the method worked out, the relative abundance of lithium isotopes was measured in four typical minerals bearing lithium, and in one mineral in which lithium occurs as an accidental compound in small concentration. The results that were obtained are presented in the table. There appears to be excellent agreement between the results of measurements on the four minerals and on the industrial compound; at the same time the lithium found with a concentration of 1.7×10^{-6} in pitchblend shows within experimental error a noticeable difference in isotopic ratio.

The impoverishment of the lithium isotope of mass number six found in pitchblend may be explained by the effect of neutrons appearing in the ore as a result of spontaneous uranium fission and (α, n) reactions. Calculations show that the decrease in pitchblend of the isotope Li^6 does not depend upon the effect of α-particles, but upon the action of neutrons in the reaction

$$Li^6(n, \alpha)\,H^3.$$

Mineral	Source	Li^7/Li^6
Lepidolite	Village of Shrosha, Upper Imeretia Georgian SSR	12.49 ± 0.02
Zinnwaldite	Ergerbirge Zinnwald, Germany	12.48 ± 0.02
Spodumene	Kalbinski mountains Kazakh SSR	12.48 ± 0.03
Petalite	Kalbinski mountains Kazakh SSR	12.49 ± 0.02
Pitchblend	Erzgebirge Jachimov, Czechoslovakia	12.83 ± 0.04
Mean value of Li_2CO_3	From all measurements on lithium obtained from Shering-Kal'baum	12.48 ± 0.02

Note added in proof.- In 1955 M. Higatsberger [Acta Phys. Austria 9, 179 (1955)] published the results of his measurements on the relative isotopic abundance of lithium as 11.56 ± 0.04. This value measured at the beginning of the process of ionic evaporation compares with the value obtained by Brewer for the starting value of the ratio Li^7/Li^6, 11.60. Higatsberger, like Brewer, conjectures that the evaporation of lithium ions has the character of a free evaporation, and applies a correction for the isotope effect, 11.56 × 1.080= 12.48, and computes the ratio Li^7/Li^6 to be 12.48. Higatsberger in common with other authors has not studied the process of emission of lithium ions, and apparently makes the hypothesis of free evaporation of lithium ions on the basis of Brewer's work.

In our work we first study the complete process of evaporation of lithium ions from a hot anode surface. By means of our method and without requiring any correction, the relative isotopic abundance of lithium, Li^7/Li^6, is found to be 12.47 ±0.02. The new value that we find for the separation coefficient, 1.092 ±0.002, shows that Higatsberger's correction to the ratio Li^7/Li^6 is not correct.

Translated by M. A. Melkanoff
228

7

SOVIET PHYSICS JETP VOLUME 2, NUMBER 3 MAY, 1956

An Investigation of the Isotopic Constitution of Boron

V. Shiuttse

(Submitted to JETP editor July 2, 1954)
J. Exper. Theoret. Phys. USSR 29, 486-489 (October, 1955)

When conducting a mass-spectrometer measurement of the isotopic constitution of boron (the compounds of boron were ionized with an electron beam), an effect was observed which depended upon the isotopic distribution. The resulting investigation of this effect showed that during the evaporation of the boron compounds from the platinum oven, vapors of the heavy isotope appeared preferentially, which is an effect opposite to that which should be observed during and ideal evaporation. It was found that in the preparation of gaseous and solid boron compounds a similar separation of the isotopes occurs with the same sign for the separation coefficient. The influence of the indicated distribution effect on the accuracy of the determination of the isotopic constitution of boron was investigated.

In the work of Inghram[1] on the relative concentrations of the two isotopes of boron with masses 10 and 11, the value $^{11}B/^{10}B = 4.31_1 \pm 0.017$ was quoted. Recently, Osberghaus[2] has repeated the measurement using a commercial product, with six different compounds of boron, and has obtained the value $^{11}B/^{10}B = 4.11 \pm 0.04$. In reference 3, where compounds different from those employed by Osberghaus were used, the values $^{11}B/^{10}B = 4.269$ to 4.420 were obtained. On the basis of these results one can draw the conclusion that the diversity of the experimental data for the ratio $^{11}B/^{10}B$ obtained in the various experiments is due not only to the actual different isotopic constitution of the various samples with different origins, but also to systematic errors. One must assume that the preparation of the compounds resulted in changes in the isotopic constitution of the boron, and that for this reason it is necessary to apply special methods. For the solution of this problem it is necessary to conduct experiments with various compounds of boron. The measurements were taken by the same method with two spectrometers that are described by the author and Ordzhonikidze[4].

Our measurements utilized a series of boron compounds with different origins: compounds of amorphous boron (Kalbaum), boron hydroxide $B(OH)_3$, boron sesquioxide B_2O_3 and potassium-borofluoride KBF_4 (Glavkhimreaktiv). The BCL_3 was prepared from amorphous boron by chlorination, and the oxides of boron were taken from a wet stream of oxygen over $B(OH)_3$. The $Na_2B_4O_7$ was also obtained from amorphous boron by fusion with sodium in a stream of oxygen. During the manufacture of these substances special attention was paid to letting the reactions be as close to 100% complete as possible. This was done to minimize the possibility of chemical separation of the isotopes. The BF_3 was obtained from potassium borofluoride either by heating in vacuo or by reaction with dry sulfuric acid.

TABLE I

Type of Ions	$^{11}B/^{10}B$
B^+	4.103 ± 0.001
BCl^+	4.105 ± 0.005
BCl_2^+	4.106 ± 0.002

The two gaseous compounds were investigated first. Using BCl_3, the ratio $^{11}B/^{10}B$ was measured for different ions. The results are shown in Table I. The measurements of the $^{11}B/^{10}B$ ratio for BCl^+ ions were somewhat less accurate because it was necessary to correct for the presence of $^{13}C^{16}O_2^+$ and $^{12}C^{16}O^{18}O^+$ lines by measuring the intensity of $^{12}C^{16}O_2^+$. A small systematic change in the relative amounts of the two isotopes can be attributed to a discrimination between two masses in the ion source with ions of different masses being ejected differently, an effect which decreases with increase in the mass being measured. In our measurements such a discrimination could be caused by the magnetic fields of the ion source (for our mass-spectrometer $H \sim 150$ oersteds, for a constant accelerating potential of – 2500 volts). The measured value of the ratio $^{11}B/^{10}B$ using B^+ and BCl_2^+ ions does not change when either the electron energy is changed between 30 and 150 ev or the reservoir pressure is change by factors of 150-200. This eliminates the possibility that the measured isotope ratio could be affected by the formation of an extraneous ion layer on the line of mass 10. Lines due to the ions $^{20}Ne^{++}$ and FH^{++} could be superimposed on the boron line of mass 10. However, Ne was absent from the apparatus and the presence of FH^{++} was excluded by the use of chlorinated boron compounds.

---

[1] M. G. Inghram, Phys. Rev, **70**, 119, 653 (1946).

[2] O. Osberghaus, Z. Physik **128**, 366 (1950).

[3] H. G. Thode, J. Macnamara, F. P. Lossing and C. R Callins, J. Amer. Chem. Soc. **70**, 3008 (1948).

[4] K. Ordzhonikidze and V. Shiuttse, J. Exper. Theoret. Phys. USSR **29**, 479 (1955); Soviet Phys. **2**, 392 (1956).

Due to the possibility of isotope separation in the accelerating region of the ion source, we should choose as the more reliable value of $^{11}B/^{10}B$ the value obtained with the largest mass, i. e. for BCl_2^+. Here $^{11}B/^{10}B = 4.106 \pm 0.002$, which agrees very well with the value given in reference 2.

TABLE II

Type of Ions	$^{11}B/^{10}B$
B^+	4.305 ± 0.002
BF^+	4.306 ± 0.005
BF_2^+	4.302 ± 0.03

The results of measurements with BF_3, obtained from KBF_4 (Glavkhimreaktiv), are shown in Table II. Measurements with BF^+ ions have to be corrected for the COH^+ line, and hence are less accurate. Ions from Si^+ to SiF_3^+ were not observed, since glass was never used in the apparatus. Our measurements are remarkably close to the results in reference 1. Hence, the results shown in Table II coincide exactly with those of (1), while the results of Table I agree equally well with reference 2. The results of Tables I and II differ, however, by an amount almost 34 times as large as the sum of the experimental errors. The superposition of the HF^{++} line would have shifted the tesult in just the opposite direction. The same comment applies to the horon-hydrogen compounds, which, in the BCl_3 case should, at the same time, have changed the relative amounts of the chlorine isotopes, and which, in the BF_3 case, should have given a new line. However, this type of interference was not observed. Osberghaus[2] states in his paper that in his measurements with BCl_3 he often observed large changes in the isotopic constitution (up to 8%) without finding any explanation for this phenomenon. In view of this result, he regards the measurements with BF_3 as more accurate. However, we did not observe changes in the isotopic abundance of boron if in the measurements we used BCl_3 and BF_3 compounds prepared by methods which give a 100% yield. But if we purposely produced fractionation by thermal dissociation, then we got unexpectedly high values for the isotope ratio, as shown by the following experiment. Into a quartz or nickel tube we put a small amount of KBF_4 or $NaBF_4$, which gave rise to BF_3 at a pressure of 1 atmosphere in the system used for storage and preparation of samples for the mass-spectrometer. The KBF_4 and $NaBF_4$ were not entirely dissociated at once, but in steps, giving 10 fractions at about 1 atmosphere each. The isotope ratio was measured in all the 10 fractions. The results are shown in the graph of Fig. 1.

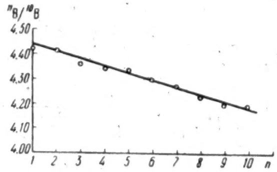

FIG. 1. Dependence of isotopic constitution of B in BF_3 on the number of the fraction.

As is evident from the figure, there is a significant amount of isotope separation, $^{11}KBF_4$ dissociating initially more than $^{10}KBF_4$, in contradiction to what one expects from kinetic considerations. From this it follows that if, when samples are prepared, 100% yield is not guaranteed, (which is difficult to do with boron), then significant, systematic and hard to control errors can creep in. In order to have full confidence in our results, in addition to measurements with gaseous compounds of boron, we also sublimated solid boron compounds in the ion source. The sesquioxide B_2O_3 and dry borax $Na_2B_4O_7$ were placed in a platinum crucible and evaporated. The isotopic constitution of boron was measured using B^+ ions. The results were corrected, if accuracy so required, for the discrimination effect of about 0.8%. The results of these measurements are shown in Table III. The measurements on $Na_2B_4O_7$ and especially on B_2O_3 are less accurate because we could not keep the ion currents sufficiently constant. Nevertheless, the measurements confirm our previous result and clearly show that the isotopic constitution of both types of boron varies by almost 5%.

TABLE III

Substance	Compound Measured	$^{11}B/^{10}B$
a) Boron (Kal'baum)	BCl_3	4.106 ± 0.002
" "	B_2O_3	4.11 ± 0.01
" "	$Na_2B_4O_7$	4.108 ± 0.007
b) Boron (Glavkhimreaktiv)	BF_3	4.308 ± 0.003
" "	B_2O_3	4.30 ± 0.01
" "	$Na_2B_4O_7$	4.305 ± 0.005
c) Mixture of 56% a) and 44% b)	$Na_2B_4O_7$	4.183
d) by computation	—	4.189

It should be noted that these results are confirmed by observations on the halides of lithium, described in reference 4, where the same systematic changes in isotopic constitution occur upon evaporation. It is impossible to draw conclusions directly from the measurements, because the boron measurements are much less accurate than the lithium ones. We cannot say here how big the separation coefficient is, but the very fact of separation upon evaporation is shown by the following experiment. In an ideal evaporation the residue should gradually be enriched in the heavy isotope. This process is governed by Raoult's law for ideal distillation, with the condition that the vapors of both isotopes have the same pressure. In the previous work this ideal case was shown to hold for the evaporation of Li^+ ions from a tungsten surface. When LiCl is evaporated the heavy isotope enrichment in the residue becomes observable only when the residue is almost gone, and then the ion currents become unstable, so that it is not possible to make good measurements. In 2 out of 30 experiments it was possible to get a change in the ratio of $^{11}B/^{10}B$ as the B_2O_3 was sublimated. One of these cases is shown in Fig. 2. As before, the curve is opposite to what one would expect theoretically. This means that when B_2O_3 (or $Na_2B_4O_7$) is ideally sublimated more molecules with ^{11}B go into the gaseous phase than molecules

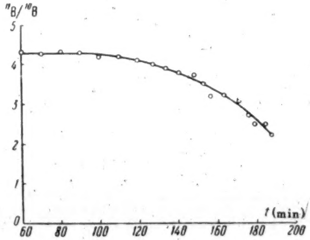

FIG. 2. Dependence on time of the isotopic constitution of B in the evaporation of B_2O_3.

TABLE IV

Substance	Source	$^{11}B/^{10}B$
Amorphous boron	Kal'baum	4.106
Crystalline boron	Shering-Kal'baum	4.100
Boric oxide	" "	4.112
Boron carbide	?	4.238
Borax	Glavkhimreaktiv	4.232
Boric oxide	"	4.240
" "	"	4.308
" "	"	4.241
" "	"	4.461

with ^{10}B. We should note that when BF_3 or BCl_3 were fractionated, the backwards effect was again observed[5].

The results of measurements on a number of technical compounds of boron which were available to us are shown in Table IV.

From the above it is evident that the agreement between the original measurements of Osberghaus and Inghram was fortuitous. It appears that there are systematic differences in the value of $^{11}B/^{10}B$ between boron samples from Central Asia (Glavkhimreaktiv) and boron samples of presumably Italian origin (Kalbaum). The Italian boron has an isotope ratio of about 4.10 ±0.02, while the central Asiatic boron has 4.25 ±0.05. The differences obtained between the various other boron KBF_4 samples are presumably due to various subsidiary chemical reactions leading to an enrichment of the heavy isotope. Experiments in separating out boron from various minerals, with the purpose of avoiding isotope separation, have so far not been successful. For these reasons we must consider the measurements of Osberghaus as unsatisfactory, while the measurements of Thode and Macnamara are probably high due to various subsidiary separation effects.

A significant part of the measurements described in this paper were made by K. Kupriianov and L. Chernov, to whom the author expresses his gratitude.

---

[5] M. Greene and G. R. Martin, Trans. Farad. Soc. 48, 416 (1952).

Translated by G. E. Schrank
229

SOVIET PHYSICS JETP VOLUME 2, NUMBER 3 MAY, 1956

The Behavior of Helium II in the Neighborhood of a Heat Radiating Surface

E. L. ANDRONIKASHVILI AND G. G. MIRSKAIA
Institute of Physics, Academy of Sciences, Georgian SSR
Institute for Physical Problems, Academy of Sciences, USSR

(Submitted to JETP editor June 5, 1954)
J. Exper. Theoret. Phys. USSR **29**, 490-494 (October, 1955)

Investigations have been made on the magnitudes of temperature discontinuities arising in the surface layer of He II in contact with a solid wall that is supplied with heat.

1 HELIUM II has practically infinite thermal conductivity and the thermal resistance within its volume is equal to zero. This means that the temperature is uniform at all interior points. However, in sufficiently small capillaries and slits a measurable temperature gradient appears, thanks to the thermo-mechanical effect. This gradient is associated with the flow of the normal component.

The basic features of the peculiar mechanism of heat transfer in He II find their explanation in researches based on Landau's theory of superfluidity.[1] However, up to now, there are several factors which lack a theoretical explanation. Among the unexplained phenomena is the presence of maximum thermal conductivity, observed by many authors in the temperature range 1.8-2.05° K[2]. In this connection, the temperature gradient along a capillary with constant thermal stress undergoes a minimum in the same temperature interval. Also unexplained is the presence of a significant thermal resistance, discovered by Kapitza[3], at the boundary between liquid He II and a solid surface which is emitting heat.

Recently, in a work by Khalatnikov[4], an explanation has been given of the fact of the presence of a thermal resistance near a heat radiating wall in contact with He II. In the work, which represents a significant step forward, it is shown that at a sufficient distance from the λ-point, heat is radiated in He II principally at the expense of the vibrations of the heated surface. For such a mechanism, Khalatnikov obtained the expression

$$\Delta T = w / aT^3, \tag{1}$$

where ΔT is the temperature difference between the heat radiating solid surface and the liquid He II in contact with it, w is the density of heat flow, T is the absolute temperature and a is some constant. It is evident from Eq. (1) that at constant thermal stress, the temperature difference ΔT decreases monotonically with increase of the temperature of the He II.

It is of interest to compare the results of this theory with experimental data available to us that we had obtained in 1948.

2. Experiments on the investigation of the behavior of He II near a heat emitting wall were set up in the following way: a constantan wire K and a copper wire Cu (diameter of each, 100 μ) were stretched parallel to one another on the glass frame R (Fig. 1). Each wire was held on the frame with the aid of a spring P. Both wires were coated with a layer of lacquer which provided electrical insulation. The constantan and copper were connected in series with a battery. Hence, the magnetic field on their surfaces was always the same. The constantan wire also served as a heater. On the copper and constantan were wound the wires B_i and B_k of phosphor bronze, diameter 40 μ. These served as resistance thermometers. One of them was intended to measure the temperature near the heater, the other as a control thermometer which was balanced with the first by means of a potentiometric arrangement.

The leads of the bronze thermometers were connected in parallel, so that the measuring currents in them could be chosen so that the decrease in the voltage on the two thermometers was the same. The connection of the current and voltage leads of the thermometers to the potentiometer is clear from Fig. 1.

Because of the very nature of the arrangement of the thermometer relative to the constantan heater in our experiments, we measured not the actual

---

[1] L. D. Landau, J. Exper. Theoret. Phys. USSR **11**, 592 (1941); **14**, 112 (1944).

[2] W. H. Keesom, A. P. Keesom and B. F. Saris, Physica 5, 281 (1938); W. H. Keesom and B. F. Saris, Physica **7**, 241 (1940); J. Allen, R. Peierls and M. Zaki Uddin, Nature **140**, 62 (1937).

[3] P. L. Kapitza, J. Exper. Theoret. Phys. USSR **11**, 1 (1941).

[4] I. M. Khalatnikov, J. Exper. Theoret. Phys. USSR **22**, 687 (1952).

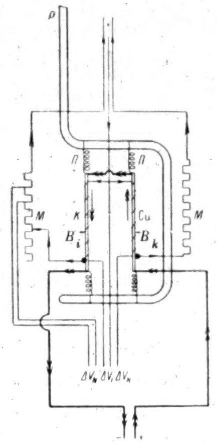

FIG. 1. Arrangement of the heater K, the copper conductor Cu and bronze thermometers B_i and B_k. The direction of the electric current through the current leads of the thermometers is shown by arrows. The directions of the electric current through the constantan heater and the copper wire are shown by the double arrows. R = glass frame, P = spring, M = plug in resistor box, ΔV_N = potential drop across standard resistance, ΔV_i, that on bronze thermometer B_i, ΔV_k, that on control bronze thermometer B_k; ΔV_N, ΔV_i, ΔV_k are connected to the potentiometer by appropriate leads.

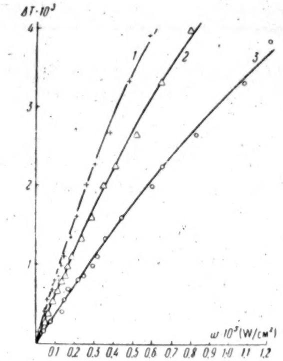

FIG. 2. Dependence on thermal flux of the drop in temperature near the heater. *1.* 1.60_5^{0} K; *2.* 1.69_6° K; *3.* 1.89_1° K.

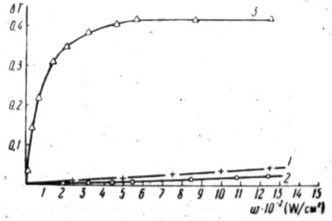

FIG. 3. Dependence on thermal flux at 8 atmospheres of the temperature drop near the heater. *1.* 1.63° K (He II); *2.* 2.045° K (He II); *3.* 2.175° K (He I).

rise in temperature of the heater above the temperature of the heating bath, but only the lower limit of the original temperature difference. It is therefore impossible to compare the results of Khalatnikov's theory directly with our experimental measurements. However, some general regularities, whose character does not depend on the particular form of the experiment, allow comparison.

3. The results of the measurement on the fall in temperature that takes place in the He II near the heated surface as a function of the thermal flux are shown in Fig. 2. It is evident from the graph that the dependence of ΔT on w--the heat flux--is by no means linear. It corresponds to the theoretical dependence only for relatively small flux.

Measurements carried out at a pressure of 8 atmospheres (Fig. 3) show that the thermal resistance under these conditions is changed by a factor of 10-20 relative to the thermal resistance observed at the saturated vapor pressure. It should also be noted that the dependence $\Delta T = f(w)$, obtained at $p = 8$ atm only begins to deviate from linearity at heatings that are at least 500 times larger than is observed in the case of saturated vapor pressure.

It can be seen from Fig. 3 that the character of the dependence $\Delta T = f(w)$ for He I is completely different from the character of the corresponding dependence obtained for He II*.

---

* Apparatus for the investigation of the properties of liquid helium under high pressures was put at our disposal by V. P. Peshkov and K. N. Zinov'ev, to whom we acknowledge our gratitude.

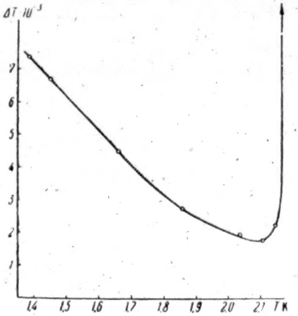

FIG. 4. Dependence on temperature of the thermal resistance for constant thermal flux at the heater.

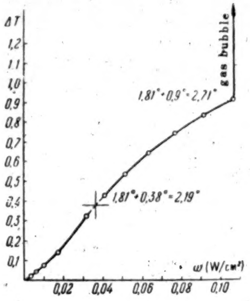

FIG. 5. Dependence of the thermal resistance on the thermal flux for the case of a capillary placed in a slit.

Investigation of the dependence $\Delta T = f(T)$ for constant heat flux w (in our case, $w = 0.836 \times 10^{-3}$ watt/cm^2) showed the presence of a minimum thermal resistance (maximum thermal conduction) at a temperature of 2.1° K. This minimum of the thermal resistance was not predicted by the theories which are limited to the treatment of the phenomenon only under the condition of being sufficiently far from the λ-point.

The experimental curve $\Delta T = f(T)$ which we obtained in the temperature interval from 1.6 to 2.1° K is satisfactorily fitted (Fig. 4) by the function

$$\Delta T = \text{const}/T^4. \quad (2)$$

In this case the experimental points lie on the curve of Eq. (2) with an accuracy to within ±2%. For temperatures below 1.6° K, the experimental curve (in agreement with theory) is better fitted by the equation

$$\Delta T = \text{const}/T^3. \quad (1')$$

Since the value of the coefficient a in Eq. (1) was computed by Khalatnikov only for platinum, comparison of the computed values from experiment and theory is not possible.

4. Consideration of the curve of Fig. 4 shows that, close to the λ-point (temperature of the helium bath at 2.17° K), the resistance of the phosphor bronze increases sharply. This corresponds to a temperature which appreciably exceeds the λ-point. This indicates that, at a bath temperature of 2.17° K, a heat flux of 8.36×10^{-4} watt/cm^2 is quite sufficient to produce superheating by 0.016 °, which results in the transition through the λ-point, and in the production of a stable gas bubble.

The problem then arises as to the superheating which can be achieved in a layer of the He II which is adjacent to the heater.

Investigation of this phenomenon was carried out by means of a glass capillary, on whose surface a thin layer of platinum was applied by cathode sputtering. The film had a resistance of 780 ohms and served as a heater. The external diameter of the capillary was 0.317 mm, the diameter of the internal opening, 0.140 mm. In other experiments, a constantan wire, which had been coated on the outside of a capillary of approximately the same dimensions, served as a heater. To eliminate the effect of the magnetic field of the current in the constantan heater on the reading of the bronze thermometer, the constantan was wound in bifilar fashion with a copper wire of the same diameter.

The platinum capillary of the capillary with constantan heater was clamped between two plane parallel plates. A resistance thermometer was stretched across the capillary. Thus assembled, the apparatus was submerged in the He II. At the time of the experiment, the power W at the heater, and the corresponding rise in resistance ΔR were measured.

As in the much earlier experiments of Strelkov[5], visual observation was carried on through a slit made of plane parallel glasses, which enabled us to fix precisely the moment of the origin of the gas bubble, and also to determine the maximum possible heating of the liquid helium near the capillary.

---

[5] P. G. Strelkov, J. Exper. Theoret. Phys. USSR **10**, 1225 (1940).

5. The heat flux through 1 cm^2 of transverse cross section of the slit is plotted along the abscissa in Fig. 5:

$$w = W / dl, \tag{3}$$

where d and l are the diameter and length of the capillary.

It is evident from the curve at 1.81° K that the gas bubble arises at temperatures which greatly exceed the λ-temperature. Thus, the superheatings which are obtained in He II in contact with a sufficiently powerful heater, can reach enormous size, of the order of 1° and beyond. Moreover, in irradiation by a heater of large heat flux, the heater, as can be seen from the curve of Fig. 5, is surrounded (even at rather low temperatures) by a thin layer of He I, rather than by He II.

The character of the dependence $\Delta T = f(w)$ for small values of w in the case of a capillary clamped between two parallel surfaces is completely determined by the law of heat transmission through a slit[6], in which grad T is taken with the heat flow, with viscosity, temperature and other quantities determined by the state of He II.

The heat flux for which the gas bubble arises varies considerably in dependence on the depth of the submerged apparatus beneath the surface of the liquid helium.

It should be noted that, at a temperature of 1.8° K, with heating to 2.186° K of a thin layer of He II which surrounds the capillary, we communicate to the normal and superfluid components relative velocities of the order of 20-30 cm/sec. Of course, these velocities are known to lie in the critical region.

Along with the experiments just described, we have set up experiments for the purpose of establishing the presence of a temperature discontinuity on the boundary of the He II and a solid wall emanating cold. However, such discontinuities have not been obtained.

CONCLUSIONS

1. The behavior of He II near a heat radiating solid surface has been investigated. It is shown that under these conditions a significant thermal resistance arises in a thin layer of He II.

2. The dependence of the temperature drop on the heat flux has been found. For a heater freely in contact with He II, this dependence is linear only for small heat fluxes.

3. The thermal resistance near a heat radiating surface is significantly decreased at elevated pressures.

4. It is established that superheating reaching 1° is possible in the neighborhood of a heat emitting surface in He II. For large heat fluxes, such superheatings are possible even at the temperature of a helium bath lying much lower than the λ-point. These lead to the formation of a thin layer of He I around the heater. Meanwhile, even at a very slight distance from the surface of the heater it has not been possible to find any sort of temperature gradient in the He II.

Translated by R. T. Beyer
230

---

[6] E. L. Andronikashvili, J. Exper. Theoret. Phys. USSR 19, 535 (1949).

SOVIET PHYSICS JETP VOLUME 2, NUMBER 3 MAY, 1956

Secondary Electron Emission in Thin Layers of Be II

I. M. Bronshtein and T. A. Smorodina
Leningrad State Teachers' Institute

(Submitted to JETP editor June 14, 1954)
J. Exper. Theoret. Phys. USSR **29**, 495-499 (October, 1955)

A study was made of the change in the coefficient of secondary electron emission σ and the distribution of secondary electrons according to energies in the deposition of thin layers of Be on a silver backing. It was established that, in the deposition of thin layers ($\Theta \sim 1$) of Be on Ni and Ag, the maxima of the curves of the distribution of secondary electrons from Ni and Ag are displaced in the direction of the smaller energies of the secondary electrons.

---

1. SECONDARY emission properties of thin layers of Be, deposited on a nickel target, were described in a previous paper[1], henceforward cited as I. In order to verify the results obtained and to determine the effect exerted by the backing on the secondary-emission properties of the layers of Be, we have studied in this work the change in σ and the distribution of the secondary electrons with respect to energies in the adsorption of Be on a silver target. For Ag $\sigma_{max} = 1.56$ at $E_p = 800$ ev, for Be – 0.6 at $E_p = 200$ ev, so that $\sigma_{Ag} - \sigma_{Be} > \sigma_{Ni} - \sigma_{Be}$ and therefore, the required condition $\sigma_p \gg \sigma_s$[1,2] in this case is fulfilled better than in investigation I for the vapor of Ni – Be.

2. The experimental procedure has been described previously[1,3]. Using the apparatus shown in Fig. 1 it was possible to obtain molecular beams of Be and Ag. The calibration of the silver gun was carried out by a method similar to the calibration of the beryllium gun. At a constant intensity of incandescence of the molecular gun, the speed of the deposition of a monatomic layer ($\Theta = 1$) on the backing is equal to 44 seconds.

The experiment was carried out in the following manner. In order to verify the accuracy of the performance of the apparatus we have first obtained the curves $\sigma = f(E_p)$ and $d\sigma/dE_s = f(E_s)$ for the backing (Ni). After this a thick layer of silver was deposited on the Ni and the curves $\sigma = f(E_p)$ and $d\sigma/dE_s = f(E_s)$ for Ag were obtained. Moreover, the constancy of emission with respect to time was being checked near the operating beryllium gun. Then layers of beryllium of different thickness ($\Theta = 0.9$; 2; 3; 5; 8; 16; 22; 28; 45; 55; 70; 85; 104; 130 etc.) were deposited on the target and the curves $\sigma = f(E_p)$ and $d\sigma/dE_s = f(E_s)$ were obtained.

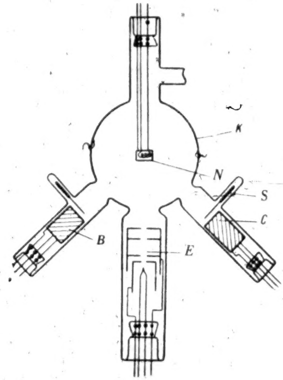

FIG. 1. The apparatus in which was studied the secondary electron emission of thin layers of beryllium deposited on a silver backing; *E* - electron gun; *B* - beryllium molecular gun; *C* - silver molecular gun; *S* - screen; *N* - nickel target; *K*- collector of secondary electrons – a glass sphere the inner surface of which is coated with a layer of nickel.

As in investigation I, the results of the measurements were repeatedly reproduced and they did not depend on the fact whether the layer of Be of a given thickness was obtained at once by using a single portion, or in steps by using smaller portions.

3. The results of measurements of the dependence of σ on E_p for various Θ are shown in Fig. 2. From Fig. 2 it is evident that in this case, as in the case of the adsorption of Be on Ni, with an increase in Θ, σ decreases monotonically and approaches the value of σ_{Be} for all values of E_p. Curve 14 already corresponds to the emission of pure Be ($\sigma_{max} = 0.58$ at $E_p = 200$ ev).

---

[1] I. M. Bronshtein and T. A. Smorodina, J. Exper. Theoret. Phys. USSR 27, 215 (1954).

[2] A. E. Kadyshev, J. Exper. Theoret. Phys. USSR 15, 651 (1945).

[3] I, M, Bronshtein, Zh. Tekh. Fiz.13, 176 (1943).

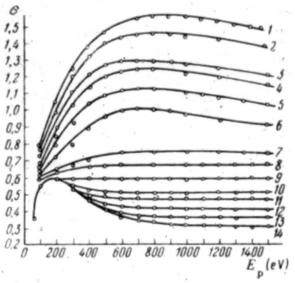

FIG. 2. The curves of the dependence of σ on E_p for various values of Θ. *1* - $\Theta = 0$; emitter – pure silver; *2* - $\Theta = 0.9$; *3* - $\Theta = 2$; *4* - $\Theta = 3$; *5* - $\Theta = 5$; *6* - $\Theta = 8$; *7* - $\Theta = 16$; *8* - $\Theta = 22$; *9* - $\Theta = 28$; *10* - $\Theta = 45$; *11* - $\Theta = 55$; *12* - $\Theta = 70$; *13* - $\Theta = 85$; *14* - $\Theta \geq 104$ atomic layers.

From Fig. 2 is derived the dependence of σ on Θ for various values of E_p, which is shown in Fig. 3. The curves of Fig. 3 indicate that σ for a given value of E_p, beginning with some value of Θ, ceases to vary. To this value of Θ corresponds, apparently, the limiting maximum depth from which at a given E_p secondary electrons can be emitted – the depth of yield d of secondary electrons.

The dependence of d on E_p, shown in Fig. 4, indicates that in the region of E_p from 100 to 600 ev there exists a linear relationship between the depth of yield d of the secondaries and the energy E_p of the primary electrons, and in the region $E_p > 600$ ev d is found to be a constant values (~ 23 mμ) independent of the energy of the primary electrons.

In Figs. 5 and 6 the curves are shown of the dependence of σ on the stopping potential on the collector in the adsorption of Be on Ni and Ag.

The energy distribution curves of the secondary electrons were obtained by differentiating the stopping curves drawn on a large scale. The distribution curves for the adsorption of Be on Ni are shown in Fig. 7. Curve 1 corresponds to pure nickel; its maximum is located at $E_s = 3.2$ ev. The value $\Theta = 0.6$ corresponds to curve 2; its maximum had been displaced to the left, in the direction of lower energies, and it is located at $E_s = 2$ ev. The maximum of curve 3($\Theta = 1.3$) is located even further to the left, at $E_s = 1.3$ ev. The value $\Theta = 4$ corresponds to curve 4; its maximum, the same as the maxima of the other curves for which $\Theta \geq 2$, is located further to the right ($E_s = 2$ ev). This curve coincides with the curve of distribution of the secondary electrons for a massive layer of Be ($\Theta > 100$). The curves of distribution obtained during the adsorption of Be on Ag are shown in Fig. 8. Curve 1 pertains to Ag; its maximum is located at 2.3 ev. At $\Theta = 0.9$ (curve 2) the maximum of the curve had been displaced to the left in the direction of lower energies and is located at 1.3 ev. At $\Theta = 2$ (curve 3) the distribution curve coincides with that for a thick layer of Ag.

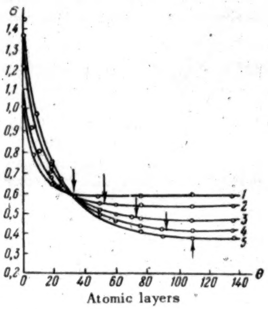

FIG. 3. The curves of the dependence of σ on Θ during the adsorption of Be on Ag. Curve *1* corresponds to $E_p = 200$; *2* - $E_p = 300$; *3* - $E_p = 400$; *4* - $E_p = 500$; *5* - $E_p = 600$ ev; the rate of the establishment of emission, corresponding to a massive layer of Be, is a function of the energy of the primary electrons. The arrows in Fig. 3 indicate the values of Θ beginning with which the coefficient of the secondary electron emission of the emitter ceases to vary.

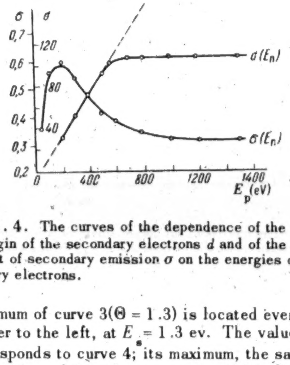

FIG. 4. The curves of the dependence of the depth of origin of the secondary electrons d and of the coefficient of secondary emission σ on the energies of the primary electrons.

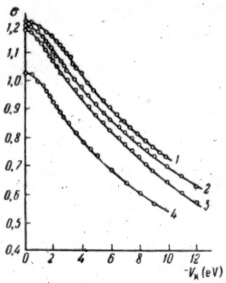

FIG. 5. The curves of the dependence of σ on the stopping potential ($-V_k$) during the adsorption of Be on Ni. 1 - $\Theta = 0$ (pure Ni); 2 - $\Theta = 0.6$; 3 - $\Theta = 1.3$; 4 - $\Theta = 4$. All curves are obtained at $E_p = 300$ ev.

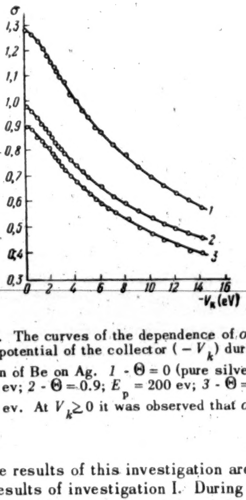

FIG. 6. The curves of the dependence of σ on the stopping potential of the collector ($-V_k$) during the adsorption of Be on Ag. 1 - $\Theta = 0$ (pure silver); $E_p = 300$ ev; 2 - $\Theta = 0.9$; $E_p = 200$ ev; 3 - $\Theta = 2$, $E_p = 200$ ev. At $V_k \geq 0$ it was observed that σ is constant.

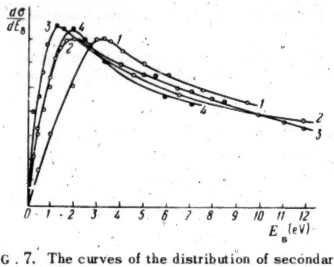

FIG. 7. The curves of the distribution of secondary electrons with respect to energies during the adsorption of Be on Ni. Curve 1 corresponds to pure nickel; 2 - $\Theta = 0.6$; 3 . $\Theta = 1.3$; 4 - $\Theta = 4$ atomic layers. All curves were obtained at $E_p = 300$ ev.

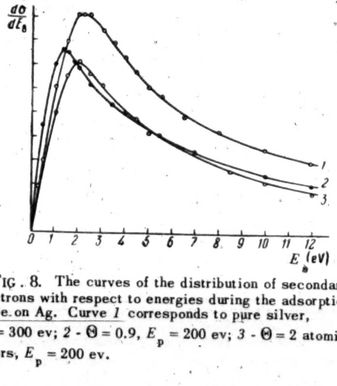

FIG. 8. The curves of the distribution of secondary electrons with respect to energies during the adsorption of Be on Ag. Curve 1 corresponds to pure silver, $E_p = 300$ ev; 2 - $\Theta = 0.9$, $E_p = 200$ ev; 3 - $\Theta = 2$ atomic layers, $E_p = 200$ ev.

4. The results of this investigation are similar to the results of investigation I. During the adsorption of Be atoms ($\varphi = 3.9$ ev) on the surface of Ag ($\varphi = 4.4$ ev) the yield performance of the target at $\Theta \sim 2-3$ should decrease to the value φ_{Be}. It is possible that at $\Theta \sim 1$ the yield performance of the emitter is $\varphi < \varphi_{Be}$. Nevertheless, as is shown by the data in Fig. 2, the coefficient of the secondary emission of the target for all energies of E_p of the primary electrons monotonically decreases from the value σ_{Ag} to the value σ_{Be} as Θ increases. This indicates, apparently, that small changes in the yield performance produce no effect on the change in the values of the coefficient σ. This is understandable, since the secondary electrons possess considerable energies; therefore, small changes in the performance of the yield will produce practically no change in the value of σ.

As regards the energy distribution of the secondary electrons it is essentially dependent on the yield performance of the emitter. As was shown by Kadyshevich[4], upon changing the yield performance of the target, the maximum of the distribution curve should at first (when φ decreases) be displaced in the direction of the lower energies, and then (when φ increases) it will again shift in the direction of the higher energies. This was observed experimentally[3] in the study of the secondary emission of thin films of Ag on Ni.

---

[4] A. E. Kadyshevich, J. Exper. Theoret. Phys. USSR 15, 600 (1945).

We have also obtained a similar result for the adsorption of Be on Ni and Ag. Although the method of differentiating the stopping curves, which we have used, is not very precise, still from the curves of Figs. 7 and 8 one may draw the conclusion that the energy distribution of secondary electrons is dependent on the change in the performance of the yield of the target.

The position of the maximum of the distribution curve for Be, which we have obtained by the method of the stopping field, agrees well with the position of the maximum of the distribution curve obtained in investigation[5] by the method of magnetic analysis. This fact, as well as the invariable and good reproducibility of the results, permits the assumption that the positions of the maxima of the distribution curves of the secondary electrons, which we have determined by the method of the stopping field, are correct. Nevertheless, it stands to reason that in the future it will be necessary to study the distribution of the velocities of the secondary electrons by another method, which will not depend on the differentiation of curves, and measure simultaneously the changes in the performance of the yield.

The distribution curves are found to be independent of the energies of the primary electrons over the entire interval of E_p investigated.

As in investigation I, during the adsorption of Be on Ag in the region $E_p = 200 - 600$ ev there exists a linear dependence of the depth of yield of secondary electrons d on the energy of the primary electrons[6,7]. From Fig. 4 it is evident that the maximum of the secondary emission corresponds to a thickness of the Be layer $d \sim 7\mathrm{m}\mu$. The maximum emission is attained at $E_p = 200$ ev. With an increase in the energy of the primary electrons their path increases, and together with this there is an increase in the depth of origin and in the yield of secondary electrons but the emission decreases. Beginning with $E_p = 600$ ev the depth of yield d of secondary electrons ceases to depend on the energy of the primary electrons. Moreover, it is obvious that the path of the primary electrons exceeds 100 atomic layers, but secondary electrons, originated at such depths, owing to elastic and inelastic losses are unable to escape. The secondary emission current in this region of energies of primary electrons is ensured by those electrons which were produced at depths $d \leq 100$ atomic layers.

---

[5] R. Kollath, Ann. Physik **39**, 59 (1941).

[6] A. Ia. Viatskin, J. Exper. Theoret. Phys. USSR **20**, 547 (1950)

[7] A. J. Dekker and A. van der Ziel, Phys. Rev. **86**, 755 (1952)

Translated by E. Rabkin
231

Secondary Electron Emission in Thin Layers of Silver

I. M. BRONSHTEIN AND T. A. SMORODIN
Leningrad State Teachers' Institute

(Submitted to JETP editor July 14, 1954)
J. Exper. Theoret. Phys. USSR **29**, 500-506 (October, 1955)

The effects of the underlying surface on the emission depth of the secondary electrons are examined for the experimental method which uses deposits of the investigated metal on a metal base. A real emission depth d of secondary electrons from silver is determined. It is shown that in the region of 100-600 ev the emission depth depends linearly on the energy of the primary electrons. It is established that, for adsorption of approximately monatomic layers of silver on nickel and beryllium, displacements of the maxima of the energy distribution curves of the secondary electrons take place for increasing thickness. The maximum of the curve for Ag on Ni is displaced to the left and that for Ag on Be to the right. This facts points to an influence of the work function of the base on the energy distribution function of the secondary electrons.

1. INTRODUCTION

SEVERAL papers have been devoted to the investigation of secondary emission from thin layers of silver and to the determination of the effective emission depth of the secondary electrons from silver. In several cases[1,2] silver was deposited on oxidized aluminum and dielectric surfaces such as mica[2] and glass[3]. At other times metals such as platinum[4] and nickel[5] were used. Even though in all of these experimental determinations of the emission depth of secondary electrons the wedgelike silver layer was deposited by the same technique on the base, the obtained values of the emission depth turned out to be very different from each other. Furthermore, the dependence of the emission depth on the energy of the primary electrons has a different character for the wedge method than for our work: in our case[2] a linear dependence of the emission depth d on the energy of the primary electrons E_p was found, while in the second case[3] this dependence was absent.

It should be noted in connection with these facts that the conductivity of thin metallic layers adsorbed on dielectric surfaces depends very substantially on the thickness of the metallic layer. For thicknesses less than 8 mμ the conductivity of the metallic layers is extraordinarily small. Such layers are closer in their properties to semiconductors and dielectrics than to metals[6]. Only at thicknesses of about 50 mμ does the conductivity of the layers become approximately equal to the conductivity of a massive specimen. Therefore, a doubt arises as to the feasibility of obtaining the correct values of the coefficients for secondary electron emission from thin metallic layers deposited on dielectric surfaces. Indeed, as shown by Haas and Scott[7], the resistance of a silver layer approximately 20 mμ thick is still very large (about 10^8 times larger than the normal value). Under such conditions the coefficient of of secondary electron emission of a layer should be approximately equal to the coefficient of secondary emission for a free electron, i.e., unity.

Experimental investigation proved the latter conclusion to be correct. Instead of a metallic target a glass base was placed onto the apparatus described previously[5]. The sides of the glass base were covered with thick layers of silver that served as electrodes. The layer of silver on which the experiments were carried out was about 18 mμ thick and was obtained by 2 minutes of evaporation from a red-hot tungsten filament. The measurements showed that the coefficient of secondary electron emission of this silver layer was practically equal to unity through the entire energy range of 50 - 1500 ev of primary electrons. The resistance of the layer was about $10^{10}\,\Omega$.

It was shown previously[8,9] that the correct

---

[1] I. F. Pesiatskii, Zh. Tekhn. Fiz. **9**, 188 (1939).

[2] M. M. Vudynskii Dokl. Akad. Nauk SSSR **82**, 705 (1952).

[3] N. D. Morgulis and N. D. Nakhodkin, Dokl. Akad. Nauk SSSR **94**, 1029 (1954).

[4] A. E. Hastings, Phys. Rev. **57**, 695 (1940).

[5] I. M. Bronshtein, Zh. Tekhn. Fiz. **13**, 176 (1943).

[6] I. D. Konozenko, Uspekhi Fiz. Nauk **52**, 561 (1954).

[7] G. Haas and N. Scott, J. Phys. Radium **11**, 394 (1950).

[8] A. E. Kadyshevich, J. Exper. Theoret. Phys. USSR **15**, 651 (1945).

[9] I. M. Bronshtein and T. A. Smorodin, J. Exper. Theoret. Phys. USSR **27**, 215 (1954).

Emitter	σ_{max}	$E_{p\ max}$(ev)	φ (ev)
Ag	1.56	800	4.4
Ni	1.27	500	5.0
26-atomic layer of Be on Ni	0.61	300—1500	3.9

values of the effective depth of the secondary electron emission may be obtained only if the coefficient of secondary emission σ_1 of the metallic layer differs greatly from the coefficient σ_b of the base. This basic condition was not satisfied in any of the cited experiments and generally the effect of the base was not taken into account. This fact apparently explains the differences in values of the effective emission depth obtained by various authors.

It was found earlier[10] that it is possible to exclude entirely the effect of the base and determine the real emission depth of secondary electrons by depositing layers of one metal on various bases which have increasing or decreasing values of σ_b. The present work is devoted to an investigation of this question; the role of the base is explained and a real emission depth of secondary electrons from Ag is determined. Thin layers of Ag were deposited on Ni, Be and on a Be layer 26 atoms thick adsorbed on Ni. In the table above the values of σ_{max}, $E_{p\ max}$ and the work functions of the emitters are given.

As is apparent from the table, σ_{max} for Ag differs from σ_{max} for Ni by 0.3 and from σ_{max} of Be by unity. Also, Ag is electropositive relative to Ni and electronegative relative to Be. This circumstance allows us to clarify the influence of the difference between the work functions of the base and the metallic layer on the regularity of the change in the secondary emission.

Techniques and methods used in the present experiments were described previously[5,9,10]. As criteria of the accuracy of the apparatus and purity of the experimental conditions the following curves were used for Ni, Ag and Be: $\sigma = f(E_p)$ and $\frac{d\sigma}{dE_{sec}} = f(E_{sec})$ where E_{sec} is the energy of the secondary electrons. The results of the measurements were repeatedly reproducible with a great degree of accuracy.

2. RESULTS OF THE MEASUREMNTS

Figures 1 - 3 present the curves of the dependence of σ on E_p for silver atoms adsorbed on Ni, Be and 26 atomic layer of Be on Ni. In Fig. 4 analogous results are shown as obtained by one of the authors[5] for adsorption of silver on irreversibly altered nickel surface with $\sigma_{max} = 1.43$.

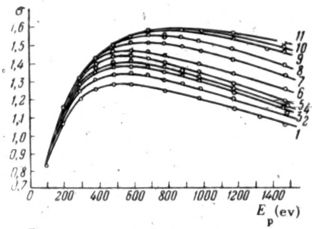

FIG. 1. Curves $\sigma = f(E_p)$ for adsorption of atoms of Ag on Ni. *1* - Ni ($\Theta = 0$, $\sigma_{max} = 1.27$); *2* - $\Theta = 0.7$; *3* - $\Theta = 1.4$; *4* - $\Theta = 2$; *5* - $\Theta = 4$; *6* - $\Theta = 7$; *7* - $\Theta = 14$; *8* - $\Theta = 24$; *9* - $\Theta = 42$; *10* - $\Theta = 56$; *11* - $\Theta \geq 70$ atomic layers ($\sim$ 20 mμ).

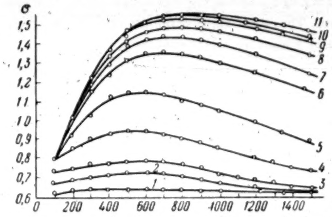

FIG. 2. Curves $\sigma = f(E_p)$ for adsorption of atoms of Ag on 26-atomic layer of Be on Ni. *1* - curve of dependence of σ on E_p for the nickel base with beryllium layer approximately 6 mμ thick; *2* - $\Theta = 0.7$; *3* - $\Theta = 2$; *4* - $\Theta = 4$; *5* - $\Theta = 8$; *6* - $\Theta = 21$; *7* - $\Theta = 28$; *8* - $\Theta = 42$; *9* - $\Theta = 56$; *10* - $\Theta = 70$; *11* - $\Theta \geq 84$ atomic layers ($\sim$ 24 mμ).

---

[10] I. M. Bronshtein and T. A. Smorodinov, J. Exper. Theoret. Phys. USSR 27, 495 (1954).

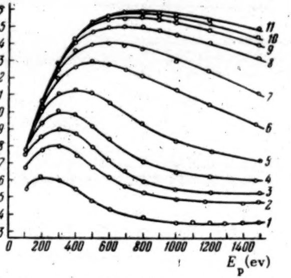

FIG. 3. Curves $\sigma = f(E_p)$ for adsorption of Ag on Be. 1 - Be ($\Theta = 0$); 2 - $\Theta = 1$; 3 - $\Theta = 2$; 4 - $\Theta = 4$; 5 - $\Theta = 8$; 6 - $\Theta = 17$; 7 - $\Theta = 28$; 8 - $\Theta = 49$; 9 - $\Theta = 70$; 10 - $\Theta = 84$; 11 - $\Theta \geq 98$ atomic layers (~ 30 mμ).

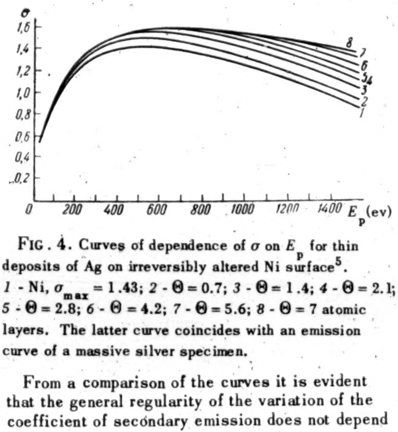

FIG. 4. Curves of dependence of σ on E_p for thin deposits of Ag on irreversibly altered Ni surface[5]. 1 - Ni, $\sigma_{max} = 1.43$; 2 - $\Theta = 0.7$; 3 - $\Theta = 1.4$; 4 - $\Theta = 2.1$; 5 - $\Theta = 2.8$; 6 - $\Theta = 4.2$; 7 - $\Theta = 5.6$; 8 - $\Theta = 7$ atomic layers. The latter curve coincides with an emission curve of a massive silver specimen.

From a comparison of the curves it is evident that the general regularity of the variation of the coefficient of secondary emission does not depend on the properties of the base. In adsorption of Ag on various surfaces the coefficient of secondary emission increased monotonically for all values of E_p to the value of σ for a massive specimen of Ag. The major change in σ (~ 80%) occurs within the first 20 - 30 atomic layers.

A comparison of the curves in Figs. 1-4 shows that in spite of the fact that α_{Ag} is greater than φ_{Be} and smaller than φ_{Ni}, there is no additional regularity of change of σ, directly connected with a change in the work function of the base in the adsorption on it of the first layers of Ag.

The curves in Figs. 5-7 show a dependence of σ on Θ (where Θ is the number of deposited atomic layers of Ag) for various E_p. The arrows point to these values of Θ at which σ attains maximum. To these values of Θ correspond the values for the maximum depth d of emission of secondary electrons at a given energy E_p.

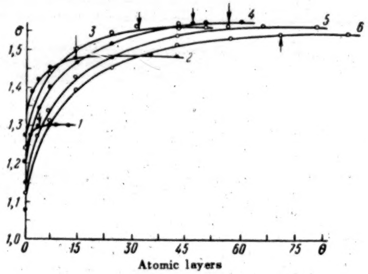

FIG. 5. Curves of dependence of σ on Θ for adsorption of Ag on Ni for various E_p. 1 - $E_p = 300$; 2 - $E_p = 500$; 3 - $E_p = 700$; 4 - $E_p = 900$; 5 - $E_p = 1100$; 6 - $E_p = 1200$ ev.

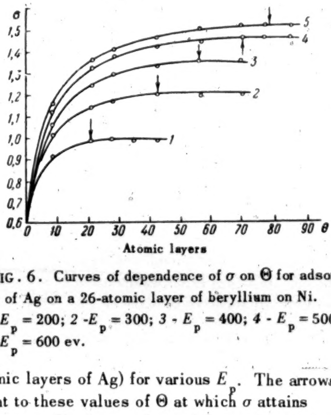

FIG. 6. Curves of dependence of σ on Θ for adsorption of Ag on a 26-atomic layer of beryllium on Ni. 1 - $E_p = 200$; 2 - $E_p = 300$; 3 - $E_p = 400$; 4 - $E_p = 500$; 5 - $E_p = 600$ ev.

Figures 8 - 11 present the curves of entrapment $\sigma = f(-V_k)$ and of $\frac{d\sigma}{dE_{sec}}$ obtained by differentiation of these curves to show the energy distribution of the secondary electrons. The curves in Figs. 10-11 show that for the adsorption of Ag on Ni($\Theta \sim 1$) the maximum of the energy distribution curve shifts first to the left (to lower energies) by 1.8 ev, then with increasing Θ to the right by 0.8 ev and remains unchanged for any Θ thereafter. As an example a curve for $\Theta = 7$ is shown in Fig.

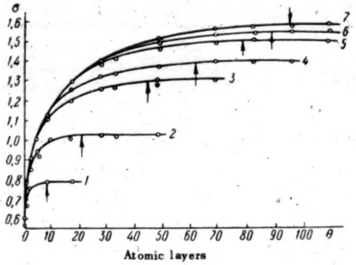

FIG. 7. Curves of dependence of σ on Θ for adsorption of Ag on Be. 1 - $E_p = 100$; 2 - $E_p = 200$; 3 - $E_p = 300$; 4 - $E_p = 400$; 5 - $E_p = 500$; 6 - $E_p = 600$; 7 - $E_p = 700$ ev.

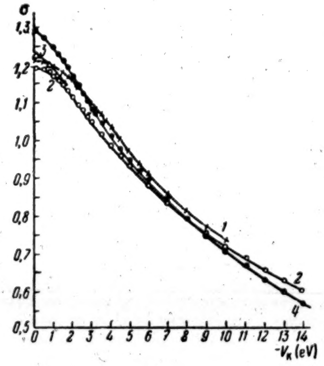

FIG. 8. Curves of dependence of σ on retarding potential of the collecting electrode (-V_k) for adsorption of Ag on Ni. 1 - Ni ($\Theta = 0$, $E_p = 300$ ev); 2 - $\Theta = 0.7$; $E_p = 250$ ev; 3 - $\Theta = 1.4$; $E_p = 250$ ev; 4 - $\Theta = 7$; $E_p = 300$ ev. For $V_k \geq 0$, σ was observed to be constant.

10. For adsorption of Ag and Be one observes a different picture: for $\Theta = 1$ the maximum shifts to higher energies by 0.8 ev, then at $\Theta = 2$ it shifts to lower energies and thereafter its position remains unchanged and coincides with the position of the maximum of the distribution curve for thick layers of Ag.

The energy distribution curves of the secondary electrons were obtained for various energies of primary electrons. The character of the distribution curves and also the regularity observed with variation of Θ do not depend on the velocities of the primary electrons.

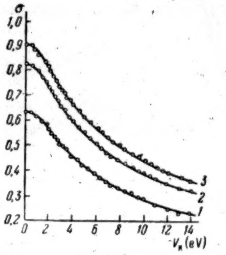

FIG. 9. Curves of dependence of σ on the retarding potential of the collecting electrode (-V_k) for adsorption of Ag on Be. 1 - Be; 2 - $\Theta = 1$; 3 - $\Theta = 2$. All curves were obtained with $E_p = 300$ ev. For $V_k \geq 0$, σ was again observed to be constant.

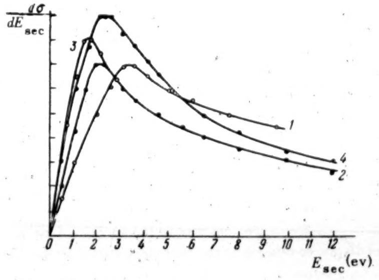

FIG. 10. The variation of the energy distribution curves of secondary electrons for adsorption of atoms of Ag on Ni. 1 - Ni, $E_p = 300$ ev; 2 - $\Theta = 0.7$, $E_p = 250$ ev; 3 - $\Theta = 1.4$, $E_p = 250$ ev; 4 - $\Theta = 7$, $E_p = 300$ ev.

3. EVALUATION OF RESULTS

The curves of Figs. 1 - 7 convincingly demonstrate that it is necessary to take into account the effect of the base in the determination of the effective emission depth of the secondary electrons. However, the role of the base may be eliminated in the final calculations, if the layers of the investigated metal are deposited on various bases whose σ values differ by various amounts from the σ values of the metallic layer. To every base and

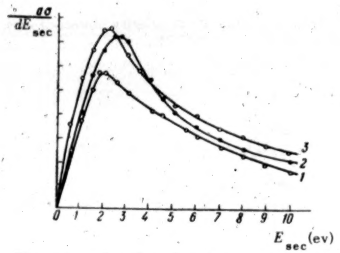

FIG. 11. The variation of the energy distribution curves of secondary electrons for adsorption of atoms of Ag on Be. *1* - Be; *2* - $\Theta = 1$; *3* - $\Theta = 2$. All curves were obtained with $E_p = 300$ ev.

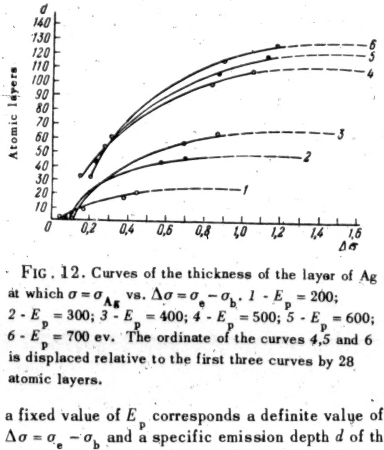

FIG. 12. Curves of the thickness of the layer of Ag at which $\sigma = \sigma_{Ag}$ vs. $\Delta\sigma = \sigma_e - \sigma_b$. *1* - $E_p = 200$; *2* - $E_p = 300$; *3* - $E_p = 400$; *4* - $E_p = 500$; *5* - $E_p = 600$; *6* - $E_p = 700$ ev. The ordinate of the curves 4,5 and 6 is displaced relative to the first three curves by 28 atomic layers.

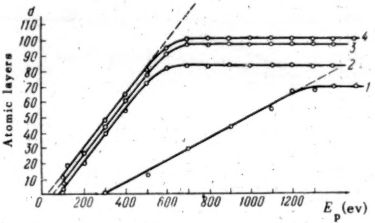

FIG. 13. The dependence of the emission depth of the secondary electrons from silver on the energy of the primary electrons and on the base on which the silver atoms are adsorbed. *1* - Ni base; *2*- base of approximately 6 mμ thick layer of Be adsorbed on Ni; *3* - Be base; *4* - the real emission depth of secondary electrons from silver as a function of the energy of primary electrons E_p. The effect of the base is eliminated.

a fixed value of E_p corresponds a definite value of $\Delta\sigma = \sigma_e - \sigma_b$ and a specific emission depth d of the secondary electrons. Our results show that $d = f(\Delta\sigma)$. It is evident that the real value of d will correspond to $\Delta\sigma = \sigma_e$.

In Fig. 12 a series of curves obtained in the present work shows the dependence of the emission depth of the secondary electrons on $\Delta\sigma = \sigma_e - \sigma_b$. From these curves the real emission depth of secondary electrons may be found by extrapolation to $\Delta\sigma = \sigma_1$ for a given value of E_p. The emission depth d corresponding to the latter value of $\Delta\sigma$ will be the real emission depth of the secondary electrons.

The dependence of the real emission depth of the secondary electrons on the energy of the primary electrons is shown in Fig. 13. There the curves $d = f(E_p)$ are presented for the cases of adsorption of Ag on Ni, Be and on 26 atomic layer of Be on Ni.

It is evident that the values of d_{real} and d_{exp} obtained for adsorption of Ag on thick layer of Be, and their dependence on E_p almost coincide. Therefore, it may be assumed that the effect of the base practically does not appear for the pair Ag - Be. Using the Be base, we may then determine the real emission depth of the secondary electrons from Ag and its dependence on E_p by depositing on Be base layers of Ag of increasing thickness.

As far as a nickel base is concerned, the corresponding curve of Fig. 13 shows that its effect on the determination of the emission depth of secondary electrons from Ag is by no means negligible: d_{real} and d_{exp} obtained by adsorption of Ag on Ni and their dependence on E_p differ greatly from each other.

The emission depth d appears to be linearly dependent on E_p for energies up to $E_p = 600$ ev. Consequently, it is again possible to form the conclusion that the penetration of primary electrons is linearly proportional to their energies in the region 100 - 600 ev[11,12]. It is not possible to say anything about the penetration of the primary electrons of energies above 600 ev since the secondary electrons freed by them are often formed in depths

---

[11] A. Ia. Viatskii, J. Exper. Theoret. Phys. USSR **20**, 547 (1950).

[12] A. J. Dekker and A. van der Ziel, Phys. Rev. **86**, 755 (1952).

from which they cannot escape due to elastic and inelastic collisions.

The changes in the work function due to adsorption of Ag on Be apparently are not manifested by changes in σ, since in both cases σ increases linearly with the thickness of the Ag layer. At the same time the energy distribution of the secondary electrons depends on the change in the emitter work function on agreement with the work of Kadyshevich[13]. In spite of the fact that the method of differentiating the curves of entrapment used in the present work is not satisfactorily accurate, the position of the maximum of the energy distribution curve obtained by the method of the retarding potential agrees well with the position of the same maximum obtained by Kollath[14] directly by means of magnetic analysis. This fact and also the good reproducibility of the results lead us to the conclusion that the other curves for various Θ obtained by our method of spherical condensers are also correct. As Figs. 10 - 11 show, the position of the maximum of the energy distribution curve of secondary electrons shifts to lower energies when electropositive atoms are adsorbed (for Ag on Ni at $\Theta \sim 1$ by 1.8 ev) and to higher energies when electronegative atoms are adsorbed (for Ag on Be at $\Theta \sim 1$ by 0.8 ev). This effect should apparently increase with an increase in the difference between the work functions of the adsorbed metal and the base, and with an increase in the separations of the maxima of their distribution curves.

To explain more fully the role of the work function in secondary emission it will be necessary to obtain the energy distribution curves by a method which yields directly the energy distribution of the secondary electrons and which allows simultaneous measurement by some means of the change in the work function of the base with a change in Θ.

Translated by M. J. Stevenson
232

---

[13] A. E. Kadyshevich, J. Exper. Theoret. Phys. USSR 15, 600 (1945).

[14] R. Kollath, Ann. d. Phys. 39, 59 (1941).

SOVIET PHYSICS JETP VOLUME 2, NUMBER 3 MAY, 1956

Direct Measurement of the Total Light of Rapidly Decaying Processes of Luminescence

N. A. TOLSTOI AND I. A. LITVINENKO

(Submitted to JETP editor June 13, 1954)
J. Exper. Theoret. Phys. USSR 29, 507-515 (October, 1955)

A new, objective method is proposed for the direct measurement of L_p and L_z for rapidly proceeding luminescent processes.

The relationship of the area above the curve of fluorescent rise L_p to the area under the curve of fluorescent decay L_z can serve as the criterion for the selection of one or another theory of phosphorescence, since the various theories, generally speaking, predict different magnitudes for L_p/L_z. The measurement of L_p/L_z for a quenched ZnS-Cu phosphor indicates the inapplicability of a theory based on a bimolecular mechanism of luminescence and a monomolecular mechanism of decay.

1. INTRODUCTION

AS experience in the study of the kinetics of the processes of luminescence[1,2] shows, the relaxation curves for luminescence, with the exception of a small number of "favorable" cases, cannot, as a rule, be described to any extent by simple analytic laws*.

The complexity of the laws of relaxation in crystalline phosphors makes the task of qualitative integration of the relaxation curves extremely difficult. In this connection it is expedient in a number of instances to make the object of the investigation not the relaxation curves themselves, but rather several simpler quantities, which are in the final analysis connected with the form of the relaxation curves. Thus, for example, the method of electrical differentiation[4] makes it possible to measure the slope of the luminescent decay curve or the curve of the drop in photoconductivity at an instant of time directly following the instant of departure of the system from the stationary state. The measurement of this slope results in a number, characterizing "the departure of the system from the stationary condition". Utilization of this method makes it possible to draw important conclusions as to the nature of the luminescence of crystalline phosphors and the nature of photoconductivity.

It is possible to indicate another magnitude, expressed by a single number, which is closely related to the form of the relaxation curve—specifically, the integral of the luminescent decay curve

$$L_z = \int_0^\infty I_z(t)\,dt,$$

and also the magnitude

$$L_p = \int_0^\infty (I_{\text{stat}} - I_p(t))\,dt.$$

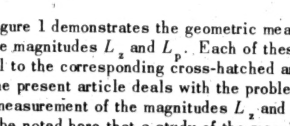

FIG. 1. Geometric significance of the magnitudes L_p and L_z.

Figure 1 demonstrates the geometric meaning of the magnitudes L_z and L_p. Each of these is equal to the corresponding cross-hatched area.

The present article deals with the problem of the measurement of the magnitudes L_z and L_p. It may be noted here that a study of the magnitude L_z, corresponding to prolonged processes of phosphorescence (minutes, hours), was carried out as long as half a centruy ago by means of the graphic integration of decay curves, recorded point by point with the aid of a stop watch. The measurement of L_z and also of L_p for the initial stages of relaxation (from 10^{-5} to 10^{-1} sec) has never been made by anyone up to the present time.

---

* In this article we shall deal only with "rapid" processes of luminescent rise and decay (10^{-1} to 10^{-5} sec), i.e., with luminophors, the relaxation curves of which can be studied by the Tau-meter method[3].

[1] V. S. Arkhangelskaia, A. M. Bonch-Bruevich, N. A. Tolstoi and P. P. Feofilov, J. Exper. Theoret. Phys. USSR 21, 290 (1951).

[2] N. A. Tolstoi and P. P. Feofilov, Izv. Akad. Nauk SSSR, Ser. Fiz. 16, 59 (1952).

[3] N. A. Tolstoi and P. P. Feofilov, Uspekhi Fiz. Nauk 41, 44 (1950).

[4] N. A. Tolstoi, Izv. Akad. Nauk SSSR, Ser. Fiz. 15, 690 (1951).

2. THE RELATIONSHIPS OF THE MAGNITUDES L_p AND L_z FOR SEVERAL CASES

a) Let us imagine a luminophor in which no decay exists, i.e., in which every excited electron returns to the unexcited condition by emitting one quantum of luminescence. Then, hypothesizing that each quantum of excited light excites one electron, it is possible to write the most general kinetic equation

$$dn/dt = -I(n) + E, \tag{1}$$

where n is the number of excited electrons, I is the number of emissive transitions per second and E is the number of quanta of excitational light absorbed in one second by the luminophor. The solution of (1) results in curves of fluorescent decay and rise, $I_z(t)$ and $I_p(t)$, which depend parametrically on E. We will consider that E = constant or that $E = 0$, i.e., we will examine, as usual, "square wave" excitation. Then

$$I_z(0) = E,\ I_z(\infty) = 0,\ I_p(0) = 0,\ I_p(\infty) = E$$

and

$$\int_0^{n_\infty} dn = \int_0^\infty (E - I_p(t))\, dt = L_p,$$

$$-\int_{n_\infty}^{0} dn = \int_0^\infty I_z(t)\, dt = L_z,$$

From whence

$$L_p = L_z. \tag{2}$$

In this case L_p has the significance of the total stored light, and L_z the total light emitted during the decay process. Since no hypothesis has been made with regard to the form of the function $I(n)$, it is clear that Eq. (2) is valid for any kinetics satisfying Eq. (1), in particular, for monomolecular, pseudomonomolecular and bimolecular kinetics.

b) If there is inactive absorption, i.e., if not every quantum of excitational light excites an electron (output < 1, but no decay), Eq. (2) remains as before.

c) If there is decay after recombination, then Eq. (2) remains valid.

d) If there is decay before recombination and the kinetics of luminescence are monomolecular ($I = \alpha n$),

$$dn/dt = -\alpha n - \beta n + \gamma E,$$

then Eq. (2) is valid.

e) If there is decay before recombination and the kinetics of luminescence are bimolecular ($I = \alpha n^2$),

$$dn/dt = -\alpha n^2 - \beta n + \gamma E,$$

then in the limiting case of very rapid decay ($\beta n \gg \alpha n^2$)

$$I = \frac{\gamma^2 E^2}{\beta^2}(1 - e^{-\beta t})^2 \qquad \text{(rise)},$$

$$I = \frac{\gamma^2 E^2}{\beta^2} e^{-2\beta t} \qquad \text{(decay)}$$

and $L_p = 3L_z$.

Since in the other limiting case (vanishingly small decay) $L_p = L_z$, then the intermediate cases lie within the limits

$$L_z \leqslant L_p \leqslant 3L_z.$$

f) If there is no decay, but an extinguishing action takes place on the part of the exciting light, then

$$L_p < L_z.$$

The foregoing examples are adequate to convince one that the ratio L_p/L_z can serve as one of the criteria for judging the applicability of one or another mechanism for the interpretation of the kinetics of luminescent rise or decay*. The selection of concrete models, of course, results in a quantitative value for the magnitude L_p/L_z, which can be checked by experiment.

3. L-METER

The task described in the introduction is, from the point of view of methodology, related to the measurement of the area above the luminescence rise curve L_p and the area under the luminescence decay curve L_z (Fig. 1) by electronic means. Since the rise and decay curves under study represent electrical signals which do not possess a constant component due to the method by which they are obtained (passage through a circuit having dividing capacitors--seeFig. 2, *a*) the integral of these curves on the whole is equal to zero. The artificial introduction of a constant component corresponding to the zero reading at complete decay (Fig. 2, *b*) permits us to obtain the integral of the decay curve. However, it is obtained simultaneously and inseparably with the integral under the rise curve which does not interest us. It is obvious that in order to perform our task it is necessary to change the investigated signal in such a manner as to remove from the signal--in the one case, the rise curve (Fig. 2, *c*), and in the other case, the decay curve (Fig. 2, *d*). In the first case the integral will be positive and proportional to L_z, and in the second case, negative and proportional to L_D.

---

* A more-detailed analysis of the connection between the magnitude L_p/L_z and the character of the kinetics will be given in a later publication.

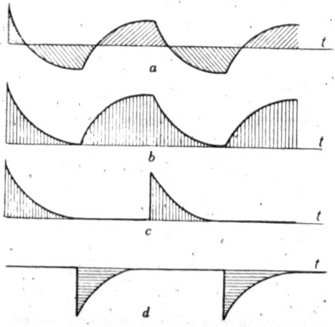

FIG. 2. *a*. Signal after passing through a divider circuit; *b*. The same signal with the addition of a constant component producing a zero reading corresponding to complete decay; *c*. Rise curve eliminated, zero reading is at complete decay; *d*. Decay curve eliminated, zero reading is at complete rise.

If the aforementioned transformation of the signal (the displacement of the zero line and the elimination of one or another half of the curves) is accomplished, then it is possible to solve the given problem by integration of the signals with the aid of any electrical measuring instrument which possesses sufficient inertia (the natural period of the instrument should be much greater than the period of repetition of the signals) and which will respond to the average value of the voltage or current (for example, a needle-indicating magneto-electric microammeter). The basic method with the aid of which we obtain the desired transformation of the signal consists in the application of synchronized detection. The signal controlling the operation of the synchronized detector is in the final analysis a rectangular light pulse (square wave) synchronized with the square wave of light which excites luminescence in the luminophor being investigated.

4. OPTICAL SETUP

The schematic for obtaining square waves of light and transforming the luminescence relaxation curves into corresponding electrical signals fully conforms to the schematic of the Tau-meter[3] which is based on the mechanical modulation of light, with the sole difference that in our setup there is no functional analysis. Since the Tau-meter has been described in detail in the works of Tolstoi and Feofilov, we will only briefly touch upon the optical portions of the method.

As can be seen from Fig. 3, the excitational light from a mercury arc lamp L_1 is focused on a narrow slit S_1 near which the light beam is interrupted by the rotating disc *D*, which is equipped with projections. The square pulse of light thus obtained excites a sample of the luminophor *O*. The luminescence of the latter is detected by a photoelectric multiplier *FEU*-1, which is equipped with a cathode follower *CF*-1. K_1, K_2 and K_3 are condensing lenses; F_1 and F_2 are crossed polarizers. The second light source L_2 produces synchronous square waves of light which are detected by *FEU*-2 and repeated by *CF*-2. Thus, at the output of *CF*-1,relaxation curves are obtained which are the subject of investigation, and at the output of *CF*-2 electrical square waves occur which control the process of synchronous detection. The steepness of the wave fronts of the square pulses in such a setup can be carried to 10^{-5} sec. The repetition frequency of the square waves is 10-200 pulses/sec.

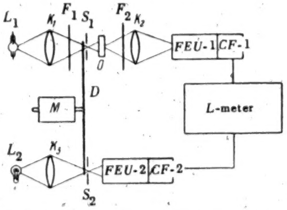

FIG. 3. Schematic of the optical setup.

5. SYNCHRONOUS DETECTOR

The operation of the synchrounos detector (*SD*) is apparent from an examination of the schematic represented in Fig. 4. A duo-triode 6N8 (let us call it a synchronous signal detector) has two inputs 1 and 2, upon which are imposed, respectively, the square waves and the relaxation signals under investigation. Both halves of the tube have a common cathode resistance. The left-hand triode is a cathode follower; the right-hand triode is an amplifier with a cathode-anode load (i.e., with negative feedback). When the voltage on the grid of the left-hand triode is negative, the right-hand triode amplifies the signal and its plate voltage reproduces, let us say, the decay curve (inverted, of course, as a result of the usual phase reversal in an amplifier stage with a plate load). When the voltage on the grid of the left-hand triode is positive and sufficiently large, a strong current flows in the cathode resistor, and the voltage drop across the resistor cuts off the right-hand triode completely. Instead of the "rise curve", a constant voltage appears at the plate of the right-hand triode which is equal to the B-plus voltage shown in the schematic. On the whole, the plate voltage of the right-hand triode has the appearance shown in Fig. 5, *a*. The rise curves have been eliminated, but in their place have appeared rectangular "projections". A second, completely analogous duo-triode (synchronous square wave detector) is used to eliminate these projections. Square waves of small, regulated amplitude are imposed on the grid of the right-hand triode, and controlling square waves of sufficiently large amplitude are imposed on the grid of the left-hand triode. At the plate of the right-hand triode, square waves are obtained with an upper voltage limit equal to the B-plus voltage (Fig. 5, *b*) and with an amplitude of ΔV, which (with the aid of potentiometer A_3, see Fig. 8) is set equal to the ΔV in Fig. 5, *a*. (For the method of matching these voltages, see text following.) The difference between the two signals will then give a pure decay curve computed from a zero base, and a pure zero line in place of the rise curve. (The "zero" in our instance will be the constant B-plus volt-

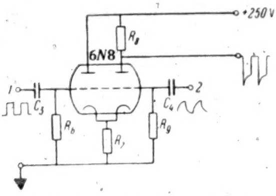

FIG. 4. Schematic of synchronous detector (for the values of R and C, see the subscript to Fig. 8).

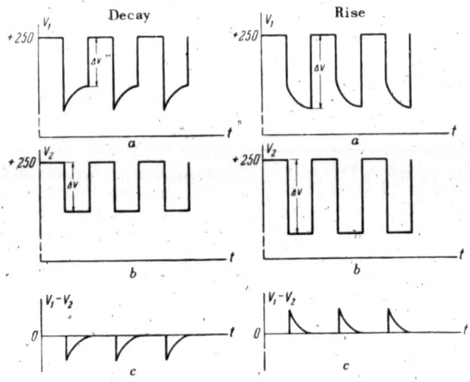

FIG. 5. *a*. Voltage at the plate of the right-hand triode of the synchronous signal detector; *b*. Voltage at the plate of the right-hand triode of the synchronous square wave detector; *c*. Difference in the signals at the plates of the right-hand triodes of the synchronous signal detector and the synchronous square wave detector.

age.) The same figure shows the analogous treatment of the signal for obtaining a pure rise curve, which does not need further explanation.

If the signals at the plates of the right-hand triodes of the synchronous signal detector and the synchronous square wave detector are sufficiently strong, and if a microammeter connecting these anodes (in the form of a bridge) has a sufficiently high resistance, then the reading of the microammeter will be proportional to the area of the relaxation curve in which we are interested.

As we already stated, the square waves at the plate of the right-hand triode of the synchronous square wave detector are so adjusted that their amplitude ΔV exactly "fills" the rectangular projection in the investigated relaxation curves, which are obtained as a result of the elimination of the undesirable halves of the processes in the synchronous signal detector. Obviously, it is necessary to be able to control the correctness of this adjustment. To achieve this aim, a pulse shaper (*KFK*) is utilized. The schematic of the *KFK* unit is presented in Fig. 6, *a*. Signals from the synchronous signal detector (input *1*) and the synchronous square wave detector (input *2*) are impressed on the grids of the corresponding cathode followers, which are assembled in the single envelope of the duo-triode 6*N*8. An oscilloscope which is connected between the cathode outputs of the two followers reproduces the shape of the curve to be integrated. Regulation of the amplitude of the square wave "filler" projections can be attained by "compensation" (Fig. 6, *b*). If compensation is attained, integration of the curve will give the correct result being sought.

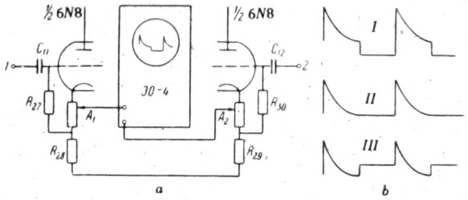

FIG. 6. *a*. Schematic of pulse shaper (*KFK*); *b*. Shape of the curves on the oscilloscope screen (for the values of *R* and *C*, see the subscript to Fig. 8): *I*, Insufficiently compensated; *II*, Compensated; *III*, Over-compensated.

Since there is no *a priori* guarantee that the operation of the two cathode followers will be identical, potentiometers A_1 and A_2 have been introduced in the circuit of the *KFK* unit (Fig. 6, *a*), by regulation of which complete symmetry of the circuit is attained. It is necessary, however, to have some means of assuring ourselves that this symmetry is actually attained, i.e., that the *KFK* unit is itself working properly. To accomplish this, a pulse shaper control is employed. Instead of the relaxation curve being studied, square

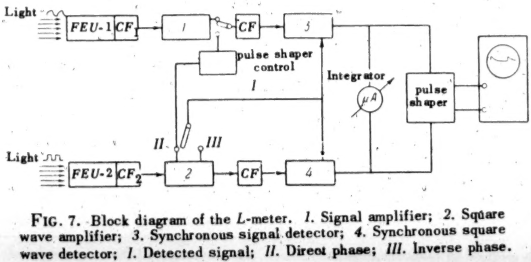

FIG. 7. Block diagram of the *L*-meter. *1*. Signal amplifier; *2*. Square wave amplifier; *3*. Synchronous signal detector; *4*. Synchronous square wave detector; *I*. Detected signal; *II*. Direct phase; *III*. Inverse phase.

control waves are imposed on the synchronous signal detector. It is clear that L_p and L_z for the square waves are equal to zero. Then, by regulation of the amplitude of these square control waves (potentiometer A_4, Fig. 8) or by regulation of the amplitude of the square waves obtained from the output of the synchronous square wave detector, we can attain a condition in which the integrating unit will produce a zero reading. This obviously corresponds to a condition in which the voltage is always equal to zero and there are no "projections" between the output plates of the synchronous signal detector and the synchronous square wave detector. Then by regulation of potentiometers A_1 and A_2 in the *KFK* unit, we attain a condition in which a straight line without any "projections" is obtained on the oscilloscope screen. After this operation, the *KFK* unit may be considered adjusted, and the *L*-meter is ready for use.

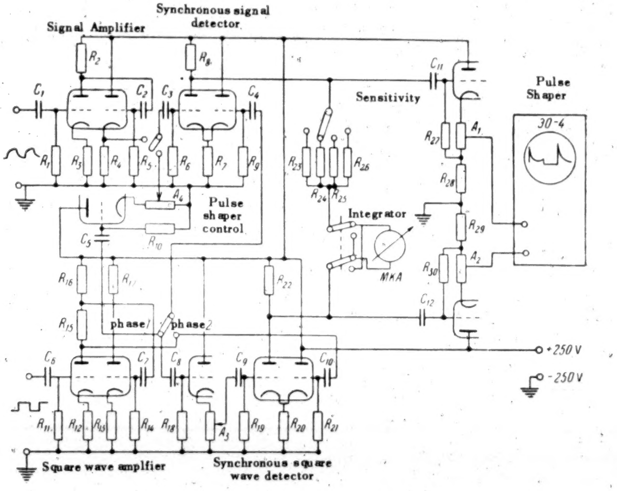
Synchronous signal detector
Signal Amplifier
R_2
R_8
C_1
C_2
C_3
C_4
C_{11}
Sensitivity
Pulse Shaper
30-4
R_1
R_3
R_4
R_5
R_6
R_7
R_9
R_{23}
R_{26}
R_{27}
A_1
R_{28}
R_{24}
R_{25}
A_4
Pulse shaper control
Integrator
C_5
R_{10}
R_{29}
MKA
A_2
R_{30}
R_{16}
R_{17}
R_{22}
C_{12}
R_{15}
phase 1
phase 2
+250 V
-250 V
C_6
C_7
C_8
C_9
C_{10}
R_{11}
R_{12}
R_{13}
R_{14}
R_{18}
A_3
R_{19}
R_{20}
R_{21}
Square wave amplfier
Synchronous square wave detector

FIG. 8. Circuit diagram of the *L*-meter. All tubes are 6*N*8. *MKA* - microammeter with a shadow-type indicator; *EO*-4 - cathodic oscilloscope.

$C_1, C_2, \ldots, C_{14} = 4\ \mu F$. $R_1 = 0.5$ MΩ; $R_2 = 2.5$ kΩ; $R_3 = 1$ kΩ; $R_4 = 5$ kΩ; $R_5 = 0.5$ MΩ; $R_6 = 0.5$ MΩ; $R_7 = 4.7$ kΩ; $R_8 = 6$ kΩ; $R_9 = 0.5$ MΩ; $R_{10} = 0.5$ MΩ; $R_{11} = 0.5$ MΩ; $R_{12} = 2$ kΩ; $R_{13} = 2$ kΩ; $R_{14} = 0.5$ MΩ; $R_{15} = 0.6$ kΩ; $R_{16} = 1$ kΩ; $R_{17} = 3$ kΩ; $R_{18} = 0.5$ MΩ $R_{19} = 0.5$ MΩ; $R_{20} = 4.7$ kΩ; $R_{21} = 0.5$ MΩ; $R_{22} = 6$ kΩ; $R_{23} = 50$ kΩ; $R_{24} = 0.2$ MΩ; $R_{25} = 0.5$ MΩ; $R_{26} = 1$ MΩ; $R_{27} = 0.5$ MΩ; $R_{28} = 4$ kΩ; $R_{29} = 4$ kΩ; $R_{30} = 0.5$ MΩ. $A_1, A_2 = 1$ kΩ; $A_3 = 5$ kΩ; $A_4 = 5$ kΩ

Figure 7 shows the block diagram of the *L*-meter, and Fig. 8 shows its circuit diagram. Note that the square wave amplifier is equipped with two outputs from which are derived the square waves controlling the operation of the two synchronous detectors. The square waves at these outputs are oppositely phased (phase *1* and phase *2*, Fig. 8). When one of these phases is utilized, the rise curves are eliminated, and the *L*-meter integrates the decay curves; when the other phase is utilized, the decay curves are eliminated and we obtain the areas above the rise curves.

6. CHARACTERISTIC CURVE OF THE *L*-METER

For the adjustment and testing of the *L*-meter, calibrated exponents of the form $V = V_0(1 - e^{-t/T})$

("rise") and $V = V_0 e^{-t/\tau}$ ("decay"), obtained as a result of the charging of capacitor C through the resistor R by square waves from a special square wave generator, were imposed on the input of the L - meter in place of the actual pulses to be investigated. Since we knew the values of V_0 and $\tau = RC$ beforehand, we could determine the areas L_p and L_z of our calibrated exponents and compare them with the areas L_p and L_z measured on the L-meter, and thus judge the accuracy of its operation. The areas L_p and L_z for the exponent are obviously equal.

$$L_p = -\tau V_0; \quad L_z = \tau V_0. \tag{3}$$

Thus the reading of the L-meter must pe proportional to both V_0 and τ. Measurements showed that the dependence of the average current through the integrating unit on the magnitude τ and the dependence of the average current through the integrating unit on the magnitude V_0 (at $\tau = 1.2 \times 10^{-4}$ sec) for both the "decay" curve and the "rise" curve are strictly linear (deviation from linearity less than 1%). The linearity of the characteristic curve of the L-meter is based on the linearity of all its stages; the frame of reference of this linearity is, of course, the limited range of input voltages employed in the L-meter. As a result of the control measurements, we determined that with input voltages which do not exceed 3 v the L-meter retains its linear characteristics. Since the amplitude of the pulses derived from the photoelectric multiplier does not exceed this value as a rule, and for the most part is ordinarily much lower, this input range is entirely satisfactory.

The readings of the integrating unit, aside from their linear dependence on V_0 and τ, must be directly proportional to the repetition frequency of the relaxation curves. For example, in studying the L_p and L_z of luminophors with the aid of the optical unit described in unit 4, the readings of the integrator will be proportional to the speed of revolution of the disc D, which modulates the light*. Measurements have shown that the dependence of the strength of the current through the integrator on the speed of revolution of the disc is linear within the limits of accuracy of the measurement. The signals here were luminescence relaxation curves for uranyl potassium sulphate (exponents with $\tau \approx 2 \times 10^{-4}$ sec).

The accuracy of operation of the L-meter thus depends on the repetition frequency of the signals, on their amplitude and on their speed of relaxation. In practice, it is possible to measure L_p and L_z for curves equivalent (in area) to exponents with $\tau > 10^{-5}$ sec. As τ is increased, the accuracy is increased; however, curves with too large a τ ($\gg 10^{-1}$ sec) will be distorted as a result of "low-frequency pile-up", introduced by the divider circuits.

The operation of the L-meter was tested on a series of luminophors with exponential relaxation (ruby, uranyl salts) and with well-known τ values. The relationship of L_z and the relationship of L_p for these substances (at the induced brightness of luminescence) coincided well with the relationships of their τ's. However, measurements of L_p and L_z alone are of no slight interest for non-exponential relaxation curves. The present work does not have systematic measurements of this sort as its aim; however, as an important illustration, we present the results of measurements of the magnitude L_p/L_z for the phosphor ZnS-Cu (with a concentration of copper equal to 1%) at various temperatures.

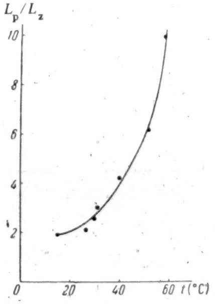

FIG. 9. Dependence of the ratio L_p/L_z on temperature for the phosphor ZnS-Cu (concentration of copper 10^{-2} g/g).

The phosphor was placed in a transparent oven, the internal temperature of which was measured by a thermocouple. Excitation was produced by the mercury line $\lambda = 365$ mμ. Figure 9 presents the graph of the dependence of L_p/L_z on temperature. As can be seen, the ratio L_p/L_z even at room temperature is equal to two (this conforms to the fact that the given phosphor is noticeably quenched at room temperature); this ratio rises rapidly with temperature, attaining a value equal to 10 at a temperature of approximately 60° C.

---

* The constancy of the speed of revolution is controlled in our optical setup with the aid of a stroboscope using a neon lamp fed by a 50 cycle voltage.

From the considerations developed in Sec. 2, we became convinced of the fact that in the quenching of a phosphor with a bimolecular recombination mechanism, the ratio L_p/L_z must not exceed a value equal to three. The obvious nonfulfillment of this condition (Fig. 9) signifies the invalidity of the application of the usual bimolecular schematic to phosphors of the ZnS-Cu type, even under conditions of strong quenching when the mechanism of their recombination has indubitably been freed of complications to a very considerable degree. Note that the great difference between L_p and L_z ($L_p \gg L_z$) is generally typical for quenched phosphors of the sulphide type. It is significant that even the introduction of the concept of the dependence of the probability of quenching on the intensity of the excitational light[5] (the quenching action of excitational light) is unable to produce the result $L_p/L_z \gg 3$, since in the case

$$\beta = \beta_T + \beta_0 E$$

(where β is the total probability of quenching, β_T is the probability of purely thermal quenching, β_0 is the probability of optical quenching and E is the intensity of the excitational light) the ratio L_p/L_z assumes a value of < 3.

$$L_p = 3I_0/(\beta_T + \beta_0 E); \qquad L_z = I_0/\beta_T;$$

$$L_p/L_z = 3\frac{\beta_T}{\beta_T + \beta_0 E} < 3.$$

---

[5] N. A. Tolstoi, Dokl. Akad. Nauk SSSR 95, 249 (1954).

Translated by A. Certner
233

SOVIET PHYSICS JETP VOLUME 2, NUMBER 3 MAY, 1956

Observation of Electroconductive Convection in Electrolytes

G. A. Ostroumov
Moscow State University

(Submitted to JETP editor June 2, 1954)
J. Exper. Theoret. Phys. USSR **29**, 529-532 (October, 1955)

Several series of experiments of a qualitative character were carried out to clarify spontaneous movement in distilled water, the electroconductivity of which in some places is increased by the addition of a dyed electrolyte. The experiments substantiated the assumed properties of the phenomenon, in particular, it was possible to produce a model of the phenomenon of corona discharge from a point. Fluctuating characteristics were noted.

1. INTRODUCTION

PREVIOUSLY[1] it was shown theoretically that there exists the possibility of the appearance of spontaneous motion in a moving medium in an electric field under the condition that the medium is heterogeneous with respect to specific resistance or conductivity. This possibility is dependent on the appearance in the medium of the volume force

$$\frac{\mathbf{D}}{4\pi}(\mathbf{E}\,\nabla \ln \rho),$$

directed along the line of the electric induction (compare reference 2). Here **E** denotes the strength of the electric field at a given point of the medium, **D** is the vector of electric induction and ρ is the specific resistance.

If this force is substituted into the hydrodynamic equation of Navier-Stokes, then one could conclude the following. During slow motions of the medium, when

$$\gamma\frac{v^2}{l} < \mu\frac{v}{l^2}, \qquad \text{i.e.} \qquad \mathrm{Re} \equiv \frac{vl\gamma}{\mu} < 1,$$

the velocity of motion v can be evaluated thus:

$$\mu\frac{v}{l^2} \approx \frac{\varepsilon}{4\pi}\frac{E^2}{\rho}\frac{\Delta\rho}{l}$$

or

$$v \approx \frac{1}{4\pi}\frac{\varepsilon}{\mu}\,l\Delta\rho P.$$

Here the general constants are collected in the first factor; in the second factor the constants characterizing the properties of the medium: the dielectric constant ϵ and the dynamic viscosity μ; the third factor characterizes the flow: its linear dimensions l and the difference in the specific resistances $\Delta\rho$; the fourth factor gives the specific force produced by the electric current per unit volume of the medium $P \equiv E^2/\rho$; γ denotes the mechanical density of the medium. As is evident, the velocity of such a movement is proportional to the force, to the difference in the specific resistances encountered in the medium, and also to its dielectric constant.

For fast movements (Re > 1) we obtain

$$\gamma\frac{v^2}{l} \approx \frac{\varepsilon}{4\pi}\frac{E^2}{\rho}\frac{\Delta\rho}{l}$$

or

$$v^2 \approx \frac{1}{4\pi}\frac{\varepsilon}{\gamma}\Delta\rho P.$$

It is evident that in this case the square of the velocity is proportional to the force and to the difference in the specific resistances.

Thus for the observation of electroconductive convection it is necessary to select a medium with a fairly high specific resistance, otherwise the force produced will mask the phenomenon with thermal effects. The direction of the current does not play any part.

2. APPARATUS

For the observation of electroconductive convection an apparatus was used which is shown schematically in Fig. 1. The bent glass tube, having a diameter of 5/7 mm and extending into a capillary, connects two vessels. Of these the vessel *A*, with dimensions of 50 × 50 × 25 mm, is filled with distilled water and contains two electrodes: + and –. The vessel *B* contains a solution of potassium permanganate, the concentration of which is such that even in the capillary it appears opaque. The vessel *B* can be moved in a vertical direction by means of a micrometer screw, so that the solution in vessel *B* can be established at a level considerably higher than the level of the water in vessel *A*. By this method it is possible to regulate the force of the jet of the solution flowing out from vessel *B* through the capillary into vessel *A*. A mirror photographic apparatus records on film the picture observed through a light filter.

---

[1] G. A. Ostroumov, Zh. Tekh. Fiz. **24**, 1915 (1954).

[2] J. A. Stratton, *Electromagnetic Theory*, p. 222, problem 31.

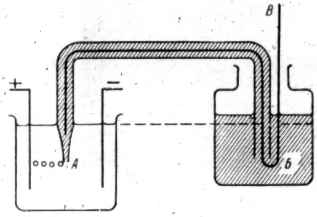

FIG. 1. Schematic diagram of the apparatus.

3. FIRST SERIES OF EXPERIMENTS

One would expect [3] that the anions would be pulled out from the flowing out jet by the force of the electric field, so that we would see in the water a pinkish band directed towards the anode, as is indicated in Fig. 1 by a dotted line (compare reference 4). One would also expect to see a similar colorless jet of potassium cations in the direction of the cathode. But thus far we have not succeeded in obtaining such an effect in pure water, irrespective of how the force of the efflux jet and the electrode voltage were regulated. On the contrary, it was always necessary to deal with an electroconductive effect which can be described as follows. When the jet of the solution flows out into the water in the absence of a field, it appears as a thin, somewhat velvety, pile-like, cylindrical rod, with a characteristic cup-like figure at its end in the initial stages. Later this figure submerges to the bottom, and the jet flows over the bottom in a uniform layer. In the presence of an electric field, the jet flattens out fan-like along the lines of force in the field. The outside contour of this fan forms a fairly well-defined curve, resembling an exponential curve. The fan spreads out symmetrically in the directions of both electrodes, and its form is independent of the direction (sign) of the field. In addition, by applying to the electrodes an alternating field of commercial frequency, one can observe exactly the same stages and forms of the jet as at a d-c voltage of either direction.

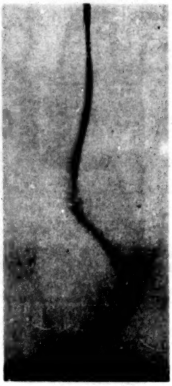

FIG. 2. Breaks in the jet of the electrolyte in an electric field of moderate intensity; electrodes on the right and on the left. Scale 2:1.

When the intensity of the jet is low, then the fan-like, flattened out jet reduces to zero at its lower section and is lost in the water. With the strengthening of the jet the intensity of its coloration is increased at all heights, so that the behavior of the lower section of the flattened out jet is clearly visible. At the same time it becomes apparent that the degree of flattening of the jet decreases; it now deviates more slowly from the cylindrical form. The velocity of its submergence increases.

With an increase in the applied voltage the degree of deviation of the jet from the cylindrical form increases: the jet broadens, undergoing a number of characteristic changes. The successive stages of these changes are shown in the photographs 2-5. With an increase in voltage it is as though a jet of average intensity breaks up in a few places at first (Fig. 2). Upon an increase in the voltage, the number and intensity of the breaks increases; moreover, threadlike whiskers branch out towards the electrodes from each bend (Fig. 3). Upon a further increase in the voltage, the velocity of the movement of sections of the jet towards the opposite electrodes increases; this produces a turbulence in the liquid at a sufficient intensity of the jet (Fig. 4). A weak jet at sufficiently high voltages splits up into two threads directed

---

[3] V. G. Levich, *Physico-chemical Hydrodynamics*, Acad. Sciences Publishing House, 1952, p. 191.

[4] K. A. Putilov, *Course of Physics*, Uchpedgiz, 1937, p. 495, Fig. 426.

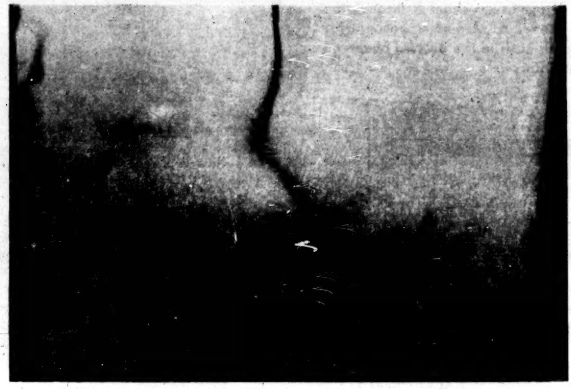

FIG. 3. Breaks in the jet in a strong electric field. Scale 2:1.

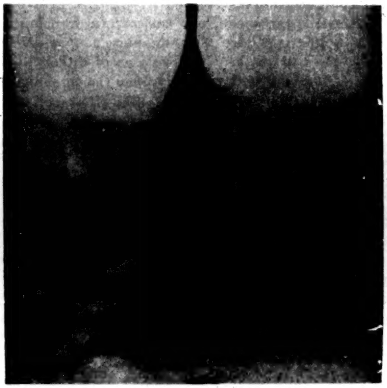

FIG. 4. Turbulent electroconductive convection. Scale 2:1.

towards the opposite electrodes (Fig. 5). Sometimes there are observed ripples or folds in the body of the flattened out jet. This appears in the lower and the peripheral sections of the flattened out jet and often spreads out over almost the entire area.

It is essential to carry out the experiments each time using fresh distilled water. If the water is contaminated by the electrolyte of the previous experiment, or if we use tap water instead of distilled water, the experiment is greatly complicated, with a decrease in its reproducibility and, as one would expect, production of parasitic thermal effects.

Thus, the concentrated sections of the solution in a medium of high resistance are in reality attracted to the electrodes, following the force lines of the electric field. Such an attraction produces

FIG. 5. Splitting of the jet in a very strong electric field. Scale 2:1.

hydrodynamic phenomena in the surrounding medium. These experiments demonstrate that electroconductive convection is possible and that it can be easily realized by mixing electrolytes with distilled water.

FIG. 6. Electroconductive convection at the outlet of the capillary; one electrode inside the capillary, the other at the right and at the left. Scale 4:1.

4. SECOND SERIES OF EXPERIMENTS

In other cases in which a similar situation is produced, for example, in non-uniformly ionized gases, this type of convection is also possible. To explain the character of the phenomenon under conditions resembling the conditions of point corona discharge, a second series of experiments was carried out. Both electrodes (the + and −) in the vessel *A* were joined together, forming one electrode. The second electrode was represented by the copper wire *B* (Fig. 1), introduced into the capillary through the wider section of the tube. Thus, within the weakly electroconductive distilled water the potassium permanganate solution produces a hydrodynamically movable electrode of high conductivity. As in the previous apparatus, we were unable to detect any phenomena of the dissociation of the anions of the permanganic acid and of the cations of the potassium. But the phenomenon of electroconductive convection revealed itself in a new light.

In the presence of an electric field a turbulence is produced in the outlet opening of the capillary. A great number of rays, replacing each other, emerge vigorously in various directions from the solution, and it appears as though the end of the capillary is boiling (Fig. 6).

Similar experiments showed that neither a drop nor a jet of an electroconductive solution in distilled water appeared at the flat electrodes. The haphazard and chaotic character of the deformations of such electrodes, obtained in the presence of an electric field, as well as the visible velvetiness or "pile-like appearance" of the jet of the solution which flows out into the water necessitates a more thorough investigation of the actual state of conditions.

5. THIRD SERIES OF EXPERIMENTS

A small quantity of mercury was poured into a high prismatic vessel with dimensions of 30 × 30 × 90 mm so arranged as to produce a strictly horizontal bottom, which served as the lower electrode. The end of a wire, which was insulated along the rest of its extension was submerged in the mercury. Distilled water was poured into the vessel up to the top, and just under its upper surface a second flat electrode was located, which served as the upper electrode. Several crystals of potassium permanganate were placed carefully on the surface of the mercury. After 3-4 hours the crystals dissolved, forming a layer of concentrated dyed solution on the surface of the mercury with a thickness of 10-15 mm. Above this was pure water. We thus obtained a flat condenser with an imperfect double-layer dielectric.

A careful examination of the solution layer showed that it did not possess any regular laminations. The surface of the solution appeared velvety or pile-like. This property should be assigned to two factors: first to the fluctuations in the density of the solution, and second to the presence of an absorption band in the visible region of the spectrum. The combined effect of these two

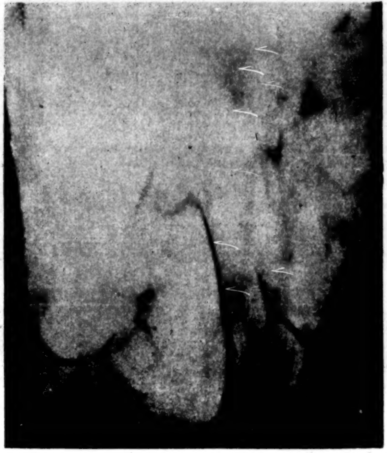

FIG. 7. Electroconductive convection in the body of a movable imperfect double-layer dielectric between the horizontal plates of a flat condenser. Scale 5:2.

factors provides the conditions for the sharp distortion of the coherence of the visible light rays and gives the surface of the solution a characteristic rough appearance.

One would expect that having set up a voltage between the electrodes we could amplify the lifting force which is produced on the movable electrode in the almost nonconducting water by the layer of the concentrated solution. The resulting hydrodynamic instability would lead to the condition that this solution would begin to be attracted to the upper electrode, moving along one side of the vessel; to replace it pure water would descend in an anti-symmetric convection flow along the other side of the vessel. Numerous experiments did not even once substantiate these expectations. In reality it was found that the applied voltage of the order of 200 v pulls out only individual thin threads from the surface of the solution. These threads are located at random, and are often far from vertical (Fig. 7). The development of these thread-like rays causes the solution to mix with the water, and when its concentration in the vessel approaches a certain (not very high) value (hardly noticeable pink coloring), the phenomenon ceases.

Thus, the results of the second and third series of experiments showed that the microscopic hydrodynamic process under conditions of electroconductive convection may be strongly dependent on the specific molecular conditions, in particular, on the fluctuations in the electroconductivity, determined by the fluctuations in the concentration (during the diffusion of the solution). The experiments on the whole qualitatively substantiated the theoretically predicted properties of electro-conductive convection.

Translated by E. Rabkin
235

SOVIET PHYSICS JETP VOLUME 2, NUMBER 3 MAY, 1956

Fission of Heavy Nuclei by Slow π^- Mesons*

N. A. PERFILOV AND N. S. IVANOVA
Radium Institute, Academy of Sciences, USSR

(Submitted to JETP editor March 19, 1955)
J. Exper. Theoret. Phys. USSR **29**, 551-558 (November, 1955)

Experimental data are given showing that on capture of slow π^- mesons by nuclei of U, Pb and W, fission of these nuclei occurs. Of the three nuclei studied, the fission probability is greatest for uranium, for which more than 300 cases of fission by slow π^- mesons were found. The distribution in range of the fission fragments and the existence of cases of fission with emission of fast charged particles (principally protons) show that in the end result the capture of a slow π^- meson by a nucleus is similar to the action on it of a particle with high ($\sim$ 100 mev) energy.

1. INTRODUCTION

WITH the production of π^+ and π^- mesons under laboratory conditions great scientific interest was aroused in investigating the character of the interaction of these new particles with nuclei. In the capture of π^- mesons by elements of low and medium atomic weight (observations in photo-emulsions) the nucleus emits various kinds of particles: protons, neutrons, α-particles and deuterons. The number of tracks of charged particles observed in the stars from the disintegration of nuclei by π^- mesons reaches 5 or 6. These data indicate a strong excitation of the nuclei on capture of π^- mesons.

On capture of π^- mesons by heavy nuclei it was expected that fission would occur and that it would be possible to arrive at some conclusions as to the mechanism of the interaction of mesons with nuclei from the character of the distribution in the range of the fragments, and a comparison with the data on the fission of nuclei by other particles.

In the present paper results are given of experiments on the interaction of slow π^- mesons principally with uranium nuclei. For Pb and W, only photographs are given; these show the possibility of fission of these nuclei on capture of slow π^- mesons.

2. OBSERVATION OF FISSION OF U, Pb AND W NUCLEI

Thick emulsion photographic plates with uranium, lead and tungsten introduced into the emulsion in a special holder were irradiated by π^- mesons. Mesons of a definite energy, which had been separated by a magnetic field, were moderated before entering into the emulsion in a wedge-shaped filter to such energies that the majority ended their path in the emulsion.

The photographic plates were impregnated with the substance to be studied by boiling water solutions of salts of the above elements in suitable concentration. For impregnation with uranium we used the salt $UO_2Na(C_2H_3O_2)_3$. This salt can be used in water solution up to a concentration of 4% without noticeable effect on the sensitivity of the emulsion. For impregnation with lead and tungsten the plates were bathed in water solutions of lead acetate and sodium tungstenate at concentrations of 2 and 12%, respectively. After 30 minutes bathing, there remains in the emulsion about 0.3 and 2 mg/cm^2 of the salts of Pb and W, respectively (determined by weighing the dry plates before and after bathing). The quantity of uranium was determined from a count of the number of disintegrations (number of α-particles) in a definite time interval (from the moment of impregnating with uranium to the moment of developing the plates). The measured number of α-

---

* The experiments which form the basis of the report were begun in January, 1950, and extended over 2½ years. The results of the investigation were published in references 1-5. The first reference, in which the documentary photographs are given showing the fission of U and W nuclei, received its final form in March, 1950. The most important results of all the reports were selected for publication in the present paper.

Independently of us and at almost the same time, the fission of the uranium nucleus by slow π^- mesons was observed by Belovitskii and Frank (Report Phys. Inst., Acad. Sci., USSR).

[1] N. A. Perfilov and N. S. Ivanova, Otchet RIAN (Report of Radium Inst.), Acad. Sci., USSR, March, 1950.

[2] N. A. Perfilov and N. S. Ivanova, Otchet RIAN (Report of Radium Inst.), Acad. Sci., USSR, October, 1950.

[3] N. S. Ivanova and N. A. Perfilov, Otchet RIAN (Report of Radium Inst.), Acad. Sci., USSR, June, 1951.

[4] D. V. Viktorov, N. S. Ivanova and N. A. Perfilov, Otchet RIAN (Report of Radium Inst.), Acad. Sci., USSR, January, 1952.

[5] N. S. Ivanova and N. A. Perfilov, Otchet RIAN (Report of Radium Inst.), Acad. Sci., USSR, June, 1952.

particles per unit volume permitted a calculation of the number of uranium nuclei introduced into this volume, since it is known[6] that 1 mg of the natural mixture of uranium emits 1500 α-particles per minute.

After irradiation with mesons and developing, the plates were examined under the microscope. In the observation the following were noted: a) disintegrations with formation of stars, b) fission events. Fission events were recognized as being those in which traces of multiply charged particles of the type of fission fragments were observed diverging in approximately opposite directions at the end of a meson track.

In the first experiments we observed a very small number of fission events in lead and tungsten. Only three cases were observed in lead (Fig. 1, photomicrograph 2), but they may be considered reliable, since the fact of fission was later established in a neighboring element, namely, bismuth. As for the tungsten nucleus (Fig. 1, microphotograph 3) it appeared subsequently that the fission probability of this element is very small for slow π^- mesons.

For uranium, quite a large number of fission events were found; from their examination it was possible to make a number of deductions and to draw some conclusion as to the mechanism of the interaction of this nucleus with slow π^- mesons.

3. DISTRIBUTION IN RANGE OF THE FISSION PRODUCTS OF THE URANIUM NUCLEUS

In all we observed 356 fissions of uranium nuclei from capture of slow π^- mesons. Of these the greater part (87%) were events with emission at the place of absorption of the π^- meson of two heavy fragments in almost opposite directions (Fig. 1, photomicrograph 4). In addition to the fissions in which only two heavy fragments were visible, fissions of uranium nuclei were observed accompanied by the emission of a light charged particle (Fig. 1, photomicrograph 1). Thirty-five such cases were found, or 10% of the total*.

In what follows we shall designate as double fissions those in which tracks of two heavy particles are observed. If, however, along with the fragments, tracks of light charged particles are observed, we shall provisionally call these events "complex fissions".

The considerable number of fissions found makes it possible to get a certain amount of statistical regularity.

As is well known, one of the essential characteristics of the fission process is the distribution of individual fragments in range (from the point of fission to the end of the track). For all our cases the tracks of every fragment could be measured individually, since the center of fission can be well determined from the end of the track of the slow π^- meson.

The distribution in range of the individual fragments is presented in Fig. 2. for double fissions, and in Fig. 3 for complex fissions. Both curves are similar within the limits of error.

The most essential fact to be noticed in these curves is the existence of one sharply defined maximum, indicating a considerable percentage of fissions into approximately equal masses. The same phenomenon, as is well known, is observed in the fission of heavy nuclei by high energy particles (> 70 mev) as distinguished from the fission of uranium by slow neutrons, where the fission is principally into fragments of unequal mass. In the distribution in range, this asymmetry of fission is expressed in the appearance of a saddle-shaped curve for the individual fragments.

Figures 4 and 5 show the distributions of the total range of the two fragments in each fission event for double and complex fissions of uranium nuclei. Both curves with one broad maximum correspond to the type of the similar curve for the fission of uranium by slow neutrons.

The mean total range of the two fragments for double fission is equal to 27.3 μ, which agrees sufficiently well with the mean total tange (in the same emulsion) for fission by slow neutrons (24 μ). This shows, as is to be expected, that the energy released from the rest mass of the π^- meson is not realized in the form of kinetic energy of the fragments.

The mean total range of the heavy fragments from complex fission is somewhat less (21.7 μ). However, this difference lies within the limits of error, which is fairly large in view of the small statistical accuracy of the curve (Fig. 5).

4. NATURE, ENERGY AND ANGULAR DISTRIBUTION OF THE LIGHT CHARGED PARTICLES EMITTED FROM FISSION OF URANIUM NUCLEI BY SLOW π^- MESONS

To explain the process of the fission of uranium by slow π^- mesons it is essential to know the properties of the light charged particles accompanying the fission. Under the conditions of our experiment, two methods can be employed for estimating the mass and energy of these particles.

---

* In addition to these, one fission event was found with emission of a light charged particle from the end of the fragment.

[6] C. A. Kienberger, Phys. Rev. 76, 1561 (1949).

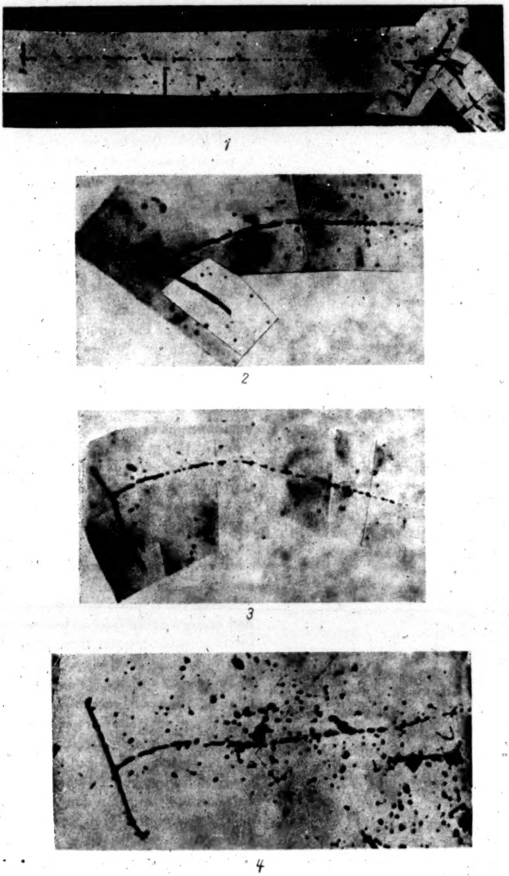

FIG. 1. Photomicrograph *1:* Fission of the uranium nucleus on capture of a slow π^- meson with emission of a proton; Photomicrograph *2*: Fission of the Pb nucleus on capture of a slow π^- meson; Photomicrograph *3*: Fission of the W nucleus on capture of a slow π^- meson; Photomicrograph *4*: Fission of the uranium nucleus on capture of a slow π^- meson.

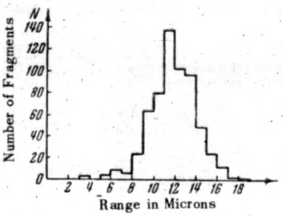

FIG. 2. Distribution in range of the individual fragments from double fission of the uranium nucleus by slow π^- mesons.

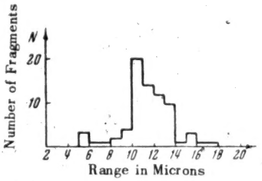

FIG. 3. Distribution in range of the individual fragments from complex fission of the uranium nucleus by slow π^- mesons.

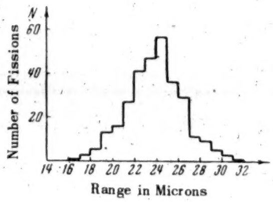

FIG. 4. Distribution of the total range of the two fragments from double fission of the uranium nucleus by slow π^- mesons.

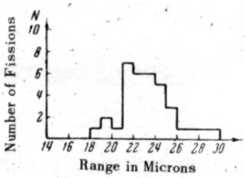

FIG. 5. Distribution of the total range of the two fragments from complex fission of the uranium nucleus by slow π^- mesons.

a) For particles finishing their track in the emulsion--by a grain count as a function of the residual range.

b) For particles which leave the emulsion, but have a sufficiently long track--by measuring the mean scattering angle and the grain density at corresponding parts of the track.

It was possible to study only two particles by the first method, since only two tracks out of 35 observed ended in the emulsion, which had a considerable range. The rest left the emulsion. One of the particles had a range of 3800 μ, the other, of 480 μ.

The determination of mass from a grain count as a function of the residual range R is possible, as is well known, if there exists an analogous curve of N as a function of R for particles of known mass. Such particles in our case were the π^- mesons, which have a long track and stay in the emulsion. The curve for these was taken as the mean of the grain count of ten π^- mesons. The mass of the particles being studied, determined by this method from the dependence of log N on log R, was found to be equal to the mass of the proton within the limits of experimental error. The energy of these protons, determined from the whole range in the emulsion, is 30 and 9.3 mev, respectively.

Using the second method, an estimate of mass and energy could be carried out for eight particles (with a range greater than 350 μ)[*]. These particles were also shown to be protons.

The results of the measurements are given in Fig. 6. In this Figure the solid lines give the derivative dN/dR of the grain density as a function of the mean scattering angle $\bar{\alpha}$ for protons and π^- mesons. For calibration of the protons, in order to be sure of the absence of regression in determining the grain density, tracks of particles ending in the emulsion were selected from a number of stars formed by π^- mesons. The mass of these particles, equal to the proton mass, was determined by a grain count as a function of the residual range. For orientation, the analogous curve of dN/dR for high energy α-particles is

---

[*] Graduate student D. V. Viktorov took part in the mass determination by the method of scattering.

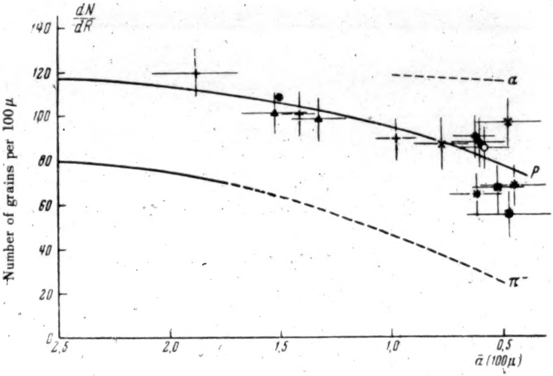

FIG. 6. Dependence of grain density in the track on mean scattering angle for p, π^- and α; +, case *1*; ▲, case *2*; O, case *3*; ■, case *4*; ●, case *5* (stops in emulsion-proton); ×, case *6*; *, case *7*; ◆, case *8*.

shown dotted in the same Figure**.

The experimental points for the particles being studied are also given in Fig. 6. Some tracks, in view of their length, can be divided into several parts (2-3). For this reason we have two or three points designated by identical symbols for one and the same track.

From Fig. 6, it is seen that all the experimental points are grouped fairly well around the proton curve, which gives a basis for considering these particles to be protons.

As a check, a particle (whose track stopped in the emulsion) was selected from the group of particles studied by the method of scattering, whose mass and energy had already been determined by the first method. We see that the point for this curve, designated ●, fits the proton curve well. The energy, estimated from the mean scattering angle, and equal to 9.9 mev, agrees within experimental error with the energy determined termined from the residual range (9.3 mev).

Our data do not make it possible to distinguish protons from deuterons, but the probability of appearance of the latter should not be large in such processes.

Twenty-one additional particles could be identified as protons from the low grain density in the residual tracks on the basis of a comparison of the curves of density vs. range for protons and alpha particles. Only 5 particles with a high grain density could be considered alpha particles (photomicrograph, Fig. 7). Consequently, it is possible to say that the light charged particles emitted in the fission of uranium by π^- mesons are principally protons. It is well known that the light charged particles, which in rare cases (~ 1/100) accompany the fission of uranium by slow neutrons, are always alpha particles.

The energy of the protons emitted in fission could be estimated in 17 cases. The histogram of the energy distribution of the particles is given in Fig. 8. The spectrum shows a relatively large number of fast protons with energy > 20 mev.

The distribution in angle of the emitted protons, relative to the line of ejection of the heavy fragments, is shown in Fig. 9, and is nearly isotropic. This isotropic distribution emphasizes even more strongly the difference in character between fission by π^- mesons and fission by slow neutrons. The latter case is characterized by the emission of alpha particles in a direction perpendicular to the line of emission of the fragments.

In conclusion, we would like to note one more special case in which the track of a charged

---

** The data for the construction of the curve were taken from reference 7, combining the curves for protons and π^- mesons with our curves.

[7] P. H. Fowler, Phil. Mag. **41**, 169 (1950).

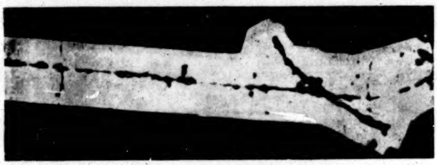

FIG. 7. Fission of the uranium nucleus on capture of a π^- meson with emission of an α-particle.

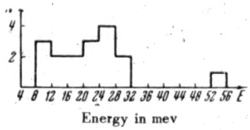

FIG. 8. Distribution in energy of the protons emitted in fission of the uranium nucleus by slow π^- mesons.

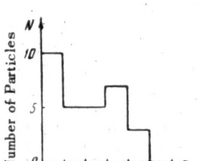

FIG. 9. Angular distribution of the light particles accompanying fission of the uranium nucleus by slow π^- mesons.

particle starts from the end of a heavy fragment (photomicrograph, Fig. 10). The track of this particle ends in the emulsion. The relatively high density and its small change with range, give some reason to believe that this is an alpha particle. We have only one such event. Unless this is a chance superposition, the observed phenomenon may be explained as an alpha decay after a preceeding beta decay.

5. FISSION PROBABILITY OF THE URANIUM NUCLEUS FOR SLOW π^- MESONS

The value P_F of the probability of fission of the uranium nucleus on capture of a π^- meson can be found from our experimental data according to the relation:

$$P = P_U P_F \tag{1}$$

where $P = N_F/N_\pi$ is the observed ratio of the number of fissions, N_F, to the number of π^- mesons, N_π, stopped in the same volume of emulsion; P_U is the probability of meson capture by a uranium nucleus in the emulsion and P_F is the probability of fission of the uranium nucleus after having captured the π^- meson.

The probability P_U can be evaluated from a relation proposed by Fermi[8], that the probability of capture of a slow π^- meson in the orbit of a nucleus is proportional to the Z of the nucleus:

$$P_U = \frac{N_U Z_U}{\sum N_i Z_i + N_U Z_U}, \tag{2}$$

where N_U is the number of uranium nuclei per unit volume of emulsion; Z_U is the atomic number of uranium; N_i and Z_i are the number of nuclei per unit volume and the atomic number of the elements entering into the composition of the emulsion. The probability P_U can be calculated if N_U is known, i.e., if the number of uranium nuclei introduced, and the composition of the emulsion are known. The value of N_U, the number of uranium nuclei per cm^2 of an emulsion $100\,\mu$ in thickness, determined (as decribed above) from the number of alpha decays, was $(3.6 \pm 0.3) \times 10^{17}$ for our plates. The value of N_π, the mean number of mesons stopped per cm^2 of a $100\,\mu$ thick emulsion, was found equal to 3260 ± 400 in our experiment. The comparatively large error in the determination of the mean number of mesons stopped per cm^2 is explained by the variation in current from one end of the plate to the other. The current of mesons being stopped is distributed uniformly along the thickness of the layer of emulsion. The value of N_F, the mean number of fissions from π^- mesons per cm^2 of $100\,\mu$ thick emulsion, was equal in our case to 9.1 ± 1. The composition of the Ilford C-3 emulsion is known.

---

[8] E. Fermi and E. Teller, Phys. Rev. **72**, 399 (1947).

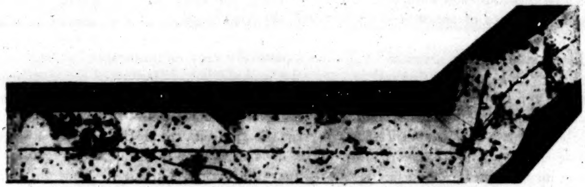

FIG. 10. Fission of the uranium nucleus with emission of an α-particle from the end of a fission fragment.

Using the above data, we can calculate a value for the fission probability by π^- mesons:

$$P_F = 0.87 \pm 0.27,$$

i.e., we get a probability near unity, from which it follows that almost every uranium nucleus, which captures a π^- meson, undergoes fission.

It should be said that the probability calculations given above were made under the assumption that the uranium nuclei are mixed uniformly with all the elements forming the emulsion. In a recent report[9], the probability of fission of the uranium nucleus by π^- mesons, evaluated by this same method, has a somewhat different value, equal to 0.37 ±0.13. However, this value was obtained on the basis of a relatively small number of events. In addition, the authors of this report felt that the uranium nuclei might not be distributed uniformly throughout the emulsion, that is, that all the uranium might be in the gelatine, without penetrating the crystals of AgBr. In this case the fission probability from the data of reference 9 becomes 0.18 ±0.06.

The question of the distribution of the uranium nuclei through the elements forming the emulsion was solved experimentally by Lozhkin and Shamov[10]. They showed that in an emulsion immersed in a water solution of a uranium salt, as used in our experiments, all the uranium nuclei are located in the gelatine, and none are observed in the crystals. We can take account of this nonuniformity of distribution of the uranium nuclei among the elements forming the emulsion in calculating the fission probability. For this it is necessary in calculating P_U, the probability of capture of a meson by the uranium nuclei, to consider the latter distributed in the gelatine and for N_π to take the number of mesons stopped in the gelatine only (which constitutes 39% of the total number of stopped mesons[11]).

Then for the fission probability we get the value

$$P_F = 0.42 \pm 0.15,$$

that is, of all the uranium nuclei which interact with slow π^- mesons, only ~ 40% experience fission. For the rest it is necessary to assume that they lose their excitation by boiling off particles.

On the other hand, the assumption can be made that the probability of fission of a uranium nucleus which has received a considerable excitation by interaction with a π^- meson is nevertheless near unity. Then it can be said that the formula we took, according to which the capture probability of a π^- meson is proportional to the Z of the element, does not entirely correspond with reality. Hence, taking $P_F = 1$, our experimental data give a formula proportional to Z^a, where $a = 2/3$.

CONCLUSIONS

1. On capture of slow π^- mesons by nuclei of elements at the upper end of the periodic table, there is a definite probability of fission. For uranium the fission probability is not greatly different from unity.

2. For uranium nuclei, the distribution in range of the individual fission fragments from interaction with slow π^- mesons gives one sharply defined

---

[9] W. John and W. F. Fry, Phys. Rev. 91, 1234 (1953).

[10] O. V. Lozhkin and V. P. Shamov, Otchet RIAN (Report of Radium Inst.), Acad. Sci., USSR, January, 1954.

[11] S. Tamor, Phys. Rev. 77, 412 (1950).

maximum, which shows a considerable number of cases of fission into fragments of approximately equal mass.

3. Along with the fissions of the uranium nucleus which are binary in nature, giving only two heavy particles, in ten cases out of a hundred the fission is accompanied by the emission of light charged particles. A special investigation of the nature of these light particles has shown them to be protons in an overwhelming majority. Their angular distribution, measured from the line of ejection of the fragments, is isotropic. These data show the marked difference between the fission process on capture of π^- mesons and the fissions caused by slow neutrons, and correspond more nearly with the fission of uranium nuclei by fast particles.

4. The sum total of the facts adduced does not contradict the following conception of the mechanism of the process. A slow π^- meson, captured in one of the Bohr meson orbits of a uranium atom, interacts with a pair of nuclear particles (np) or (pp), to which it transfers the energy of its rest mass and charge. As a result, two fast particles are produced, with energies of about 70 mev each[12]. Fast particles of this energy, passing through the nucleus, can knock out one or two nucleons by collision and then escape (if they have enough energy), leaving the nucleus in a strongly excited state. The excited uranium nucleus then loses the energy of excitation by boiling off nucleons, undergoing fission at some stage of the excitation.

If the probability of fission of the uranium nucleus on capture of a π^- meson is equal to unity, then, in our view, it follows that at some (possibly very considerable) energy of excitation, the probability of fission of the uranium nucleus and the probability of the nucleus boiling off a neutron are comparable to one another. A value for the fission probability less than unity apparently means that in a number of cases all the energy of excitation may be lost only by boiling off nucleons.

Starting with the above proposed mechanism of the interaction it is possible to explain double fission as fission with emission of neutrons (primary or secondary), and the difference between this and complex fission consists merely in the fact that in the latter, primary or secondary protons are emitted along with the neutrons. The large number of protons with energies > 20 mev that accompany fission indicates in our view that a considerable part of the protons observed in fission must be charged to knock-out and not to boiling.

The nearly isotropic angular distribution of the emitted protons, which was observed, follows naturally from the above.

The authors are grateful to M. G. Meshcheriakov and the staff of co-workers in his laboratory for their cooperation in carrying out the work on the study of the interaction of slow π^- mesons with nuclei.

The authors recall with gratitude the late Prof. P. I. Lukirski, who showed a constant interest in this work.

---

[12] H. Morinage and W. F. Fry, Nuovo Cim. **10**, 308 (1953).

Translated by C. V. Larrick
239

SOVIET PHYSICS JETP VOLUME 2, NUMBER 3 MAY, 1956

On the Correlation Method for the Determination of the Absolute Yield of Nuclear Reactions

V. I. GOL'DANSKII AND M. I. PODGORETSKII
P. N. Lebedev Physical Institute, Academy of Sciences, USSR

(Submitted to JETP editor June 17, 1954)
J. Exper. Theoret. Phys. USSR **29**, 559-571 (November, 1955)

An examination has been made of the statistical method of investigating nuclear transformations and of determining their absolute yield and mechanism. The method is based on measurement of the magnitude of the correlation function between the observed transformations of various types. The correlation function and its dispersion have been calculated (in the absence and in the presence of background), and the question of the accuracy of the method has been examined. The well-known method of coincidences is a special case of the correlation method, which is also applicable for longer time intervals between related transformations at high radiation intensities.

1. INTRODUCTION

ONE of the important methods of experimental physics of the last few years has been the method of coincidences, based on the recording (by means of special circuits) of nuclear particles emitted in an individual nuclear transformation or in several successive transformations separated by very short time intervals. Coincidence circuits are used both in those cases when an angular correlation exists between the recorded particles, and also in the absence of such a correlation. In particular, the recording of the coincidences permits one to determine the absolute number of such transformations independently of the efficiency with which they are recorded. An example of such a kind is afforded by the well-known method of $\beta\gamma$ and $\gamma\gamma$ coincidences[1] which may be illustrated by the following very simple case.

If in the course of the radioactive decay of an atom of a given isotope (for example, $\mathrm{Al}^{28}\xrightarrow[\beta^-]{}\mathrm{Si}^{28*}\xrightarrow[\gamma]{}\mathrm{Si}^{28}$) one β-particle and one γ-quantum are emitted, then, if M individual disintegrations occur in the course of the experiment in the absence of background, the β-counter will record

$$M_\beta = g_\beta M \qquad \beta\text{-particles,} \tag{1}$$

while the γ-counter will record

$$M_\gamma = g_\gamma M \qquad \gamma\text{-quanta} \tag{2}$$

and the coincidence circuit will record

$$M_{\beta\gamma} = g_\beta g_\gamma M + \frac{2\tau}{T} g_\beta g_\gamma (1-g_\beta) \times (1-g_\gamma) M^2 \quad \text{coincidences.} \tag{3}$$

Here g_β and g_γ are unknown efficiencies of recording, and τ is the resolving time of the coincidence circuit. The first term in Eq. (3) characterizes the recording of true counts, the second term characterizes the recording of chance coincidences determined by the disintegration being investigated. In a practical application of the method of $\beta\gamma$ and $\gamma\gamma$ coincidences the quantity τ is usually chosen to be so small that the second term in Eq. (3) is negligible, and

$$M_{\beta\gamma} \approx g_\beta g_\gamma M. \tag{4}$$

From Eqs. (1)-(3) it follows that the true number of individual radioactive disintegrations may be determined from

$$M = M_\beta M_\gamma / M_{\beta\gamma}. \tag{5}$$

Knowing the value of M, one can then determine the efficiencies of recording the disintegrations, and also the cross section of the nuclear reaction leading to the formation of the given isotope if the flux of the activating radiation is known (or, conversely, one can determine the flux of the activating radiation from the known cross section of the nuclear reaction).

The recording of coincidences is also utilized, as is well known, for the investigation of the mechanism of nuclear disintegration. A number of appropriate examples is given by Mitchell[1]. The above illustrates sufficiently clearly the possibilities of the method of coincidences because of which it has received wide acceptance.

---

[1] A. C. G. Mitchell, Rev. Mod. Phys. 20, 296 (1948).

Let us now turn to a description of the essence of the method of correlations in which, instead of measuring the number of coincidences, one should measure the correlation function between the counts of the various radiations being recorded. This method can yield exactly the same results as the method of coincidences and represents an alternative experimental possibility of obtaining quantities which are presently determined by means of coincidence circuits.

However, it is important to note that in the method of correlation the time interval between successive disintegrations may be in principle arbitrarily large. Its allowable magnitude is determined only by practical considerations, and may be as large as one second. This circumstance provides the main advantage of the method of correlations which allows it to be used even in those cases when the method of coincidences is quite inapplicable because of the overloading of the coincidence circuit.

2. GENERAL BASIC ASSUMPTIONS. DEFINITION OF THE CORRELATION FUNCTION AND THE CORRELATION COEFFICIENT. THE THEORY OF THE METHOD.

Let us consider the chain of daughter products $B, C, D, \ldots L$, the first of which is formed either by the decay of a radioactive substance A, the amount of which practically does not change during the experiment, or as a result of a nuclear reaction occurring when a target is irradiated externally by particles of some kind. Then the probability $P_{bc\ldots l}$ of finding at some instant of time t, $n_b, n_c, n_d \ldots n_l$ atoms, respectively, of the various types is determined by the many-dimensional Poisson law:

$$P_{bc\ldots l}=\frac{e^{-\overline{B}}\overline{B}^{n_b}}{n_b!}\,\frac{e^{-\overline{C}}\overline{C}^{n_c}}{n_c!}\cdots\frac{e^{-\overline{L}}\overline{L}^{n_l}}{n_l!}, \tag{6}$$

where $\overline{l}$ is the mean number determined by the laws of radioactive decay of atoms of the kind l which exists at the time t for a given intensity of the primary radiation.

From (6) follow the relations between the dispersions and the mean values of the products:

$$D\left(\sum_{l=B}^{l=L} n_l\right)=\sum_{l=B}^{l=L} D(n_l), \tag{7}$$

$$\overline{\prod_{l=B\ldots L}}(n_l)=\prod_{l=B\ldots L}(\overline{n}_l), \tag{8}$$

where n_i is the number of atoms which are found at the given instant of time in the state i.

The many-dimensional Poisson distribution in this case follows physically from the complete statistical independence of the decay of the individual atoms; each of the atoms may be found at the time t in some one definite state independently of the behavior of the others, and in virtue of the lack of limitation on the total number of atoms of the original substance, the presence of a certain number of atoms in one state does not impose any restrictions on the possible quantities of atoms in other states. The complete statistical independence of the decay of individual atoms which makes it possible to apply Eqs. (6) to (8) is realized, in particualr, in an equilibrium radioactive mixture.

Let us now turn to the relations between the disintegrations of various kinds observed in such mixtures. Let us denote by m_i the actual number of disintegrations of the ith type during a certain time interval, and by r_i the recorded number of such disintegrations, with

$$r_i=g_i\overline{m_i}, \tag{9}$$

where g_i is the efficiency of recording the disintegrations of the ith kind. Evidently each of the quantities m_i and r_i is distributed in accordance with the one-dimensional Poisson law, but relations of the type (7) and (8) are no longer applicable, for here the events are no longer independent--the same atom may, during the course of the experiment, undergo disintegrations of the ith, $(i+1)$th, $\ldots$ kth type. In this case

$$D(m_l+m_k)=D(m_l)+D(m_k)+2(\overline{m_lm_k}-\overline{m_l}\cdot\overline{m_k}), \tag{10}$$

$$D(r_l+r_k)=D(r_l)+D(r_k)+2(\overline{r_lr_k}-\overline{r_l\cdot r_k}). \tag{10'}$$

The last terms in (10) and (10′)--the so-called correlation functions--play a determining role in the proposed method. Thus the problem arises of the calculation of the correlation functions

$$\Phi_{lk}=\overline{r_lr_k}-\overline{r}_l\cdot\overline{r}_k \tag{11}$$

or of the correlation coefficient

$$R_{lk} = \frac{\overline{r_l r_k} - \overline{r}_l \cdot \overline{r}_k}{\sqrt{D(r_l) D(r_k)}} = \frac{\overline{r_l r_k} - \overline{r}_l \cdot \overline{r}_k}{\sqrt{\overline{r}_l \overline{r}_k}} \,. \qquad (12)$$

Because of its importance for the following let us begin with an examination of the case when $g_l = g_k = 1$ which is seldom met with in practice, but which demonstrates the principle most clearly.

It is evident that the correlation functions and the correlation coefficients are essentially different in the cases when the radiation of the lth and kth type (i.e., the disintegrations of the lth and kth type) occur independently of one another, or when, on the contrary, radiation of one type (for example of the lth type, or the lth disintegration) is necessarily accompanied at the same instant or later by radiation of another kind (for example, of the kth kind, i.e., by the kth disintegration).

If the emissions of the lth and the kth radiation are independent of one another (for example, in the parallel disintegration in a radioactive chain), naturally

$$\Phi_{lk} = R_{lk} = 0. \qquad (13)$$

A different situation will exist in the case of related disintegrations. Let us suppose for the sake of simplicity that the length of the chosen time interval t for the measurement greatly exceeds the mean time interval between the related disintegrations of the lth and kth type (in the case of a chain of radioactive transformations).

$$\sum_{i=l+1}^{k} \frac{1}{\lambda_i t} \ll 1. \qquad (14)$$

Then each disintegration of the lth type is necessarily accompanied by a disintegration of the kth type, and conversely, i.e., $\overline{m}_l = \overline{m}_k = m$. It then follows that

$$\Phi_{lk} = \overline{m_l m_k} - \overline{m}_l \overline{m}_k = \overline{m^2} - (\overline{m})^2 = \overline{m} \neq 0, \qquad (15)$$

$$R_{lk} = \frac{\overline{m}}{D(m)} = 1, \qquad (16)$$

which could have been written down immediately since we are dealing with completely correlated random variables.

Thus it is evident that the measurement of the correlation coefficient allows one to distinguish between the cases of mutually unrelated and related disintegrations. The related disintegrations may be either simultaneous, or separated by considerable intervals of time. However, for the sake of generality of treatment, we shall consider in the following the case of two related disintegrations, the lth disintegration (emission of particles of the lth type) preceeding in time the kth disintegration (emission of particles of the kth type). Let us now examine the case when g_l and g_k differ from unity. If the lth and the kth disintegrations are independent, then evidently Eq. (13) remains valid. However, if these disintegrations are related, then among the r_l disintegrations of the lth type recorded in the time interval under consideration there will be registered ${}_kr_l$ such disintegrations which also give rise to disintegrations of the kth type within the same interval (irrespectively of whether these disintegrations are recorded or not) and r_l' such disintegrations which are not followed by disintegrations of the kth type.

In its turn the number r_k of recorded disintegrations of the kth type may be divided into ${}_lr_k$--the number of disintegrations of the kth type originating from the disintegrations of the lth type (irrespectively of whether they were recorded or not) which occurred in the same time interval, and r_k'--the number of disintegrations of the kth type which were not preceded by a disintegration of the lth type within the given time interval. If one denotes by ${}_km_l$ not merely the recorded but the total number of disintegrations of the lth type in the given time interval which were followed by disintegrations of the kth type, and by ${}_lm_k$ the total number of disintegrations of the kth type within the given interval which were preceded by disintegrations of the lth type, then it is evident that

$${}_km_l = {}_lm_k = m_{kl}, \qquad (17)$$

$$\overline{{}_kr_l} = g_l \overline{m}_{kl}, \qquad (18)$$

$$\overline{{}_lr_k} = g_k \overline{m}_{kl}. \qquad (18')$$

In the expressions

$$r_l = {}_kr_l + r_l' \qquad (19)$$

and

$$r_k = {}_lr_k + r_k', \qquad (19')$$

only the terms ${}_kr_l$ and ${}_lr_k$ are mutually dependent, while all the others are independent of one another.

From all the above we obtain

$$\Phi_{lk} = \overline{r_l r_k} - \overline{r}_l \overline{r}_k = \overline{{}_kr_l\,{}_lr_k} - \overline{{}_kr_l}\,\overline{{}_lr_k} = \qquad (20)$$
$$= g_l g_k \overline{m^2_{kl}} - g_l g_k (\overline{m}_{kl})^2 = g_l g_k \overline{m}_{kl},$$

since for the quantity m_{kl} we have

$$D(m_{kl}) = \overline{m}_{kl}. \tag{21}$$

In what follows below we shall take the length of the time interval t such that Eq. (14) is satisfied, and then in the absence of branching between disintegrations of the lth and kth type

$$\overline{m}_{kl} = \overline{m}_l = \overline{m}_k = \overline{m}, \tag{22}$$

from which we obtain for the correlation function and the correlation coefficient

$$\Phi_{lk} = g_l g_k \overline{m}, \tag{23}$$

$$R_{lk} = g_l g_k \overline{m} / \sqrt{g_l \overline{m}\, g_k \overline{m}} = \sqrt{g_l g_k}. \tag{24}$$

We note that the expressions for the correlation function and for the number of true coincidences in a given time interval are the same. It may be easily shown that the corresponding expressions are analogous also in the presence of an angular correlation of the radiations.

Thus, if, instead of determining the numbers of disintegrations M_l and M_k that have taken place in the course of the whole experiment, and the number of coincidences M_{lk}, we determine the average number of disintegrations $\overline{r}_l$ and $\overline{r}_k$ recorded during one interval, and the correlation function Φ_{lk}, we can solve all the problems which can be solved by the method of coincidences; in particular we can determine the absolute number $\overline{m}$ of disintegrations during one interval from the relation

$$\overline{m} = \overline{r}_l \overline{r}_k / \Phi_{lk}, \tag{5'}$$

wholly analogus to Eq. (5). This constitutes the essence of the correlation method.

In examining the practical applicability of the correlation method two questions arise. First of all we must determine the accuracy with which the correlation coefficient can be measured. If g_l and g_k are small, then the question of the accuracy of determination of R_{lk} becomes particularly important, for the quantity R_{lk}, in accordance with Eq. (24), cannot differ appreciably from $R_{lk} = 0$ which corresponds to the case of two mutually independent processes. The second important question is the elucidation of the role which the background plays in measurements using the correlation method. Therefore, let us turn now to the examination of the accuracy of the correlation method both in the absence and in the presence of background.

3. DISPERSION OF THE CORRELATION FUNCTION. COMPARISON OF THE CORRELATION METHOD WITH THE METHOD OF COINCIDENCES.

In accordance with the definition (11) of the correlation function its value obtained as a result of measurements in N intervals is:

$$\Phi_{lk} = \frac{\sum_{i=1}^{N} r_{l_i} r_{k_i}}{N} - \frac{\sum_{i=1}^{N} r_{l_i}}{N} \frac{\sum_{i=1}^{N} r_{k_i}}{N}. \tag{25}$$

It is evident that

$$\overline{\Phi}_{lk} = \frac{\overline{\sum r_{l_i} r_{k_i}}}{N} - \frac{\overline{\sum r_{l_i} \sum r_{k_i}}}{N^2}, \tag{26}$$

$$\overline{\Phi^2_{lk}} = \frac{\overline{\left(\sum r_{l_i} r_{k_i}\right)^2}}{N^2}. \tag{27}$$

$$- 2 \frac{\overline{\sum r_{l_i} r_{k_i} \sum r_{l_i} \sum r_{k_i}}}{N^3} + \frac{\overline{\left(\sum r_{l_i} \sum r_{k_i}\right)^2}}{N^4}$$

(here and in the following, in writing the summation signs we shall omit the summation index $i = 1, \ldots N$). For further calculations we shall need the following equations

$$\overline{\sum r_{l_i} r_{k_i}} = N \overline{r_l r_k}; \tag{28}$$

$$\overline{\sum r_{l_i} \sum r_{k_i}} = N \overline{r_l r_k} + N(N-1)(\overline{r}_l \overline{r}_k;) \tag{29}$$

$$\overline{\left(\sum r_{l_i} r_{k_i}\right)^2} = N \overline{r_l^2 r_k^2} + N(N-1)(\overline{r_l r_k})^2; \tag{30}$$

$$\begin{aligned} \overline{\sum r_{l_i} r_{k_i} \sum r_{l_i} \sum r_{k_i}} &= N \overline{r_l^2 r_k^2} \\ &+ N(N-1)[\overline{r}_l \overline{r_l r_k^2} + \overline{r}_k \overline{r_k r_l^2} + (\overline{r_l r_k})^2] \\ &+ N(N-1)(N-2)\, \overline{r}_l\, \overline{r}_k\, \overline{r_l r_k}; \end{aligned} \tag{31}$$

$$\begin{aligned} \overline{\left(\sum r_{l_i} \sum r_{k_i}\right)^2} &= N \overline{r_l^2 r_k^2} + N(N-1) \overline{r_l^2}\, \overline{r_k^2} \\ &+ 2N(N-1)[\overline{r}_l\, \overline{r_l r_k^2} + \overline{r}_k \overline{r_k r_l^2} + (\overline{r_l r_k})^2] \\ &+ N(N-1)(N-2)(N-3)(\overline{r}_l)^2(\overline{r}_k)^2 \\ &+ N(N-1)(N-2)[\overline{r_l^2}\, (\overline{r}_k)^2 \\ &+ \overline{r_k^2}\, (\overline{r}_l)^2 + 4\overline{r}_l\, \overline{r}_k\, \overline{r_l r_k}]. \end{aligned} \tag{32}$$

Equations (28)-(32) are considerably simplified if the disintegrations of the lth and kth type are independent, for in that case,

$$\overline{r_l^2 r_k^2} = \overline{r_l^2}\,\overline{r_k^2}; \tag{33}$$

$$\overline{r_l}\,\overline{r_l r_k^2} = (\overline{r_l})^2\,\overline{r_k^2}; \tag{33'}$$

$$\overline{r_k}\,\overline{r_k r_l^2} = (\overline{r_k})^2\,\overline{r_l^2}; \tag{33''}$$

and

$$\overline{(r_l r_k)^2} = (\overline{r_l})^2\,(\overline{r_k})^2. \tag{33'''}$$

In this case $\overline{\Phi}_{lk} = 0$, and

$$\overline{\Phi_{lk}^2} = \frac{N-1}{N}\,[\overline{r_l^2}\,\overline{r_k^2} - (\overline{r_l})^2\,\overline{r_k^2} - (\overline{r_k})^2\,\overline{r_l^2} \tag{34}$$

$$+ (\overline{r_l})^2\,(\overline{r_k})^2] = \frac{N-1}{N^2}\,\overline{r_l}\,\overline{r_k}.$$

Thus the dispersion of the correlation function in the case of independence of disintegrations of the lth and kth type is given by

$$D_{\text{indep}}\,(\Phi_{lk}) = \overline{\Phi_{lk}^2} = \frac{N-1}{N^2}\,\overline{r_l}\,\overline{r_k} \tag{35}$$

$$= \frac{N-1}{N^2}\,g_l g_k\,(\overline{m})^2.$$

In the case of related disintegrations (we shall assume here that there is no branching between these disintegrations) it follows from (22), (26), (28) and (29) that the average value of the correlation function is equal to

$$\overline{\Phi}_{lk} = \frac{N-1}{N}\,(\overline{r_l r_k} - \overline{r_l}\,\overline{r_k}) = \frac{N-1}{N}\,g_l g_k \overline{m}. \tag{36}$$

For $N \to \infty$ we obtain the "theoretical" mean value $g_l g_k \overline{m}$. For the determination of the mean square value $\overline{\Phi_{lk}^2}$ we must obtain the values $\overline{r_l r_k^2}$, $\overline{r_l^2 r_k}$ and $\overline{r_l^2 r_k^2}$. We shall explain the method of obtaining these quantities by using $r_l r_k^2$ as an example, and by noting first of all that for the determination of the correlation function we are interested only in those disintegrations of the lth type which are followed by disintegrations of the kth type in the given interval, and only in those disintegrations of the kth type which are preceded in the given interval by disintegrations of the lth type. In satisfying condition (14) we can consider, neglecting distortions near the boundary of the interval, that each disintegration of the lth type necessarily leads to a disintegration of the kth type in the same interval. Let the values of r at a time t at the end of the interval be, respectively, r_l and r_k. Let us add an infinitesimal time dt at the beginning of the interval. Then we shall have the probability adt, where a is the equilibrium activity of all the members of the series, that during this infinitesimal time a disintegration of the type l will take place necessarily followed by a disintegration of the type k within the interval, while $1-adt$ gives us the probability that a disintegration of the type l will not occur. Therefore,

$$\overline{r_l r_k^2}\,(t+dt) = \overline{r_l r_k^2}\,(t) + \frac{d\,\overline{r_l r_k^2}}{dt}\,dt \tag{37}$$

$$= (1 - adt)\,\overline{r_l r_k^2} + adt\,\{g_l g_k\,\overline{(r_l+1)(r_k+1)^2}$$

$$+ g_l(1-g_k)\,\overline{(r_l+1)\,r_k^2} + g_k\,(1-g_l)\,\overline{r_l(r_k+1)^2}$$

$$+ (1-g_l)\,(1-g_k)\,\overline{r_l r_k^2}\}.$$

From this it follows that

$$\frac{d\overline{r_l r_k^2}}{dt} = 2ag_k\overline{r_l r_k} + ag_l\overline{r_k^2} \tag{38}$$

$$+ ag_k\overline{r_l} + 2ag_l g_k\overline{r_k} + ag_l g_k.$$

Similarly

$$\frac{d\overline{r_k r_l^2}}{dt} = 2ag_l\overline{r_l r_k} + ag_k\overline{r_l^2} \tag{39}$$

$$+ ag_l\overline{r_k} + 2ag_l g_k\overline{r_l} + ag_l g_k,$$

$$\frac{d\overline{r_l^2 r_k^2}}{dt} = 2ag_k\overline{r_k r_l^2} + 2ag_l\overline{r_l r_k^2} \tag{40}$$

$$+ ag_k\overline{r_l^2} + ag_l\overline{r^2}_k + 4ag_l g_k\overline{r_l r_k} +$$

$$+ 2ag_l g_k\overline{r_l} + 2ag_l g_k\overline{r_k} + ag_l g_k.$$

Integration of Eqs. (38)-(40) gives

$$\overline{r_l r_k^2} = g_k^2 g_l\,(\overline{m})^3 + 2g_k^2 g_l\,(\overline{m})^2 \tag{41}$$

$$+ g_l g_k\,(\overline{m})^2 + g_l g_k \overline{m},$$

$$\overline{r_k r_l^2} = g_l^2 g_k\,(\overline{m})^3 + 2g_l^2 g_k\,(\overline{m})^2 \tag{42}$$

$$+ g_l g_k\,(\overline{m})^2 + g_l g_k \overline{m},$$

$$\overline{r_l^2 r_k^2} = g_l^2 g_k^2\,(\overline{m})^4 + 4g_l^2 g_k^2\,(\overline{m})^3 + \tag{43}$$

$$+ g_l^2 g_k (\bar{m})^3 + g_l g_k^2 (\bar{m})^3$$

$$+ 2g_l^2 g_k^2 (\bar{m})^2 + 2g_l^2 g_k (\bar{m})^2$$

$$+ 2g_l g_k^2 (\bar{m})^2 + g_l g_k (\bar{m})^2 + g_l g_k \bar{m}.$$

We can now turn to the direct calculation of the mean square of the correlation function which gives

$$\overline{\Phi_{lk}^2} = \frac{N-1}{N} g_l^2 g_k^2 (\bar{m})^2 \tag{44}$$

$$+ \frac{N-1}{N^2} g_l g_k (\bar{m})^2 + \frac{(N-1)^2}{N^3} g_l g_k \bar{m}.$$

The dispersion of the correlation function is given by

$$D(\Phi_{lk}) = \overline{\Phi_{lk}^2} - (\bar{\Phi}_{lk})^2 \tag{45}$$

$$= \frac{N-1}{N^2}\left[1 + g_l g_k + \frac{N-1}{N\bar{m}}\right] g_l g_k (\bar{m})^2,$$

where N is the number of intervals in which readings are taken, $\bar{m}$ is the mean value of disintegration of each kind during one interval. The relative error in determining Φ_{lk} is

$$\delta(\Phi_{lk}) = \sqrt{D(\Phi_{lk})}/\bar{\Phi}_{lk} \tag{46}$$

$$= \sqrt{\frac{1}{N-1} + \frac{1}{g_l g_k N \bar{m}} + \frac{1}{g_l g_k (N-1)}}.$$

If $\bar{m} \gg 1$ and $N \gg 1$, then

$$\delta(\Phi_{lk}) \approx \sqrt{\frac{1 + g_l g_k}{g_l g_k N}}. \tag{46'}$$

If, on the other hand, $\bar{m} \ll 1$, then

$$\delta(\Phi_{lk}) \approx \frac{1}{\sqrt{g_l g_k N \bar{m}}} = \frac{1}{\sqrt{g_l g_k M}}, \tag{46''}$$

where M is the total number of disintegrations of each kind during the experiment.

We may compare the expressions which characterize the general content and the accuracy of the correlation method and the method of coincidences. The effective length of one interval of measurement in the method of coincidences is obviously equal to 2τ. The mean number of coincidences during one interval S_{lk} in the case of $g_l \ll 1$ and $g_k \ll 1$, which is the most interesting one practically, is equal to

$$S_{lk} = g_l g_k \bar{m} + g_l g_k (\bar{m})^2 = \Phi_{lk} + \bar{r}_l \bar{r}_k. \tag{47}$$

It is evident that for $\bar{m} \ll 1$, when the chance coincidences are negligible,

$$S_{lk} = \Phi_{lk}. \tag{47'}$$

The relative error in the determination of the correlation function is given in this case (for $N \gg 1$) by the relation (46''), i.e., it is equal to the relative error in counting the number of true coincidences in the course of the whole experiment.

Thus for $m \to 0$ and $N \to \infty$, the correlation method is identical with the method of coincidences. This circumstance has a clear physical significance. Indeed, for $\bar{m} \ll 1$ *a fortiori* $\bar{r}_l \ll 1$ and $\bar{r}_k \ll 1$, and hence $\Phi_{lk} = \overline{r_l r_k} - \bar{r}_l \bar{r}_k \approx \overline{r_l r_k}$. The quantity $\overline{r_l r_k}$ is either zero if one of the r is zero, of unity if $r_l = r_k = 1$. But in the first instance the coincidence circuit would not record a coincidence; it would record a coincidence in the second instance. This shows that the two methods are identical if the counters are not heavily loaded. Of course we are discussing the equivalence of the methods only in principle, and not in practice, even in the region $\bar{m} \ll 1$.

If $\bar{m}_l \gtrsim 1$, i.e., if the chance coincidences cannot be neglected, then in the method of coincidences the second term in Eq. (47) is measured or calculated by one means or another, i.e., in fact the correlation function is determined indirectly. However, with a further increase of $\bar{m}$ when $\bar{m} \gtrsim 1/\sqrt{g_l g_k}$, i.e., $S_{lk} \gtrsim 1$, the method of coincidences can no longer be used because of the large number of counts being lost. In the correlation method no limitations exist in principle for large values of $\bar{m}$. This means that for a given intensity of the primary radiation a one may increase the length of the interval t during which measurements are made, i.e., one can investigate related processes separated by long time intervals. The possibility of such investigations is limited only by the total length of the experiment and by the desired accuracy of results, which increases with increasing number of intervals in accordance with Eq. (46).

As has already been shown, the minimal error of the correlation method for a given duration of the whole experiment [retaining condition (14)], is attained for $\bar{m} \to 0$ and $N \to \infty$, and is determined by (46''). As the number of intervals is decreased (and, correspondingly, $\overline{m}$ is increased), the relative error of the correlation method for $g_l g_k \ll 1$ increases in accordance with

$$\delta = \delta_{\min} \sqrt{1 + \overline{m}}. \tag{48}$$

Thus, for a given duration of the experiment, the accuracy of the method begins to diminish appreciably only for $\overline{m} \gg 1$, when the method of coincidences begins to become completely unusable. By increasing the duration of the experiment, one can also achieve in this region any desired degree of accuracy in the determination of the correlation function. However, it should be noted (this was not emphasized in our short preliminary communication[2]) that if the intensity of radiation a can be decreased so that, for a given large t, the condition $\overline{m} \ll [g_l g_k]^{1/2}$ is satisfied, then measurements by means of coincidence circuits become possible and, for the same duration of the experiment, give the same accuracy as the correlation method. Let us now turn to a comparison of the effect of background in both methods.

4. THE ROLE OF BACKGROUND IN THE CORRELATION METHOD. COMPARISON WITH THE ROLE OF BACKGROUND IN THE METHOD OF COINCIDENCES

In the presence of background the total number of counts recorded by each counter in a certain time interval will be given by

$$r_l = r'_l + r''_l, \tag{49}$$

$$r_k = r'_k + r''_k. \tag{49$'$}$$

where r'_l and r'_k are the counts associated with the process being investigated, and r''_l and r''_k are the background counts statistically independent of the former. It follows from Eq. (49) that

$$\overline{r_l} = \overline{r'_l} + \overline{r''_l}, \tag{50}$$

$$\overline{r_k} = \overline{r'_k} + \overline{r''_k}, \tag{50$'$}$$

and also that

$$D(r_l) = D(r'_l) + D(r''_l) \tag{51}$$

and

$$D(r_k) = D(r'_k) + D(r''_k). \tag{51$'$}$$

Insofar as $\overline{r''_l}$ and $\overline{r''_k}$ may usually be measured separately, the quantities r'_l and r'_k which we require may be determined easily. The correlation function is given by

$$\Phi_{lk} = \overline{r_l r_k} - \overline{r_l}\,\overline{r_k} \tag{52}$$

$$= (\overline{r'_l r'_k} - \overline{r'_l} \cdot \overline{r'_k}) + (\overline{r''_l r''_k} - \overline{r''_l} \cdot \overline{r''_k}).$$

If the background counts of the two counters are statistically independent, as is most frequently the case, then the second term in Eq. (52) is equal to zero, and the correlation function in which we are interested is identical with the one measured directly. In the opposite case (if, for example, both counters may be set off by the same particle) it is necessary to subtract from the measured correlation function the correlation function of background counts which is obtained by a separate experiment.

Thus the presence of background does not introduce any noticeable complications with respect to the speed of counting or the mean value of the correlation function. The presence of background, however, may increase the fluctuations of all the measured quantities, thus reducing the accuracy of measurement. The effect of background on the accuracy of measuring r'_l and r'_k is easily taken into account. Let us examine the more complicated question of the effect of background on the accuracy of measurement of the correlation function assuming that the background counts of the two counters are mutually independent. Using equations analogous to Eqs. (26)-(32), we obtain for the dispersion of the correlation function in the presence of background the expression

$$D(\Phi_{lk}) = \frac{N-1}{N^2}\Big[1 + g_l g_k + \frac{N-1}{N\overline{m}} \tag{53}$$

$$+ \alpha_k + \alpha_l + \alpha_k \alpha_l\Big] g_l g_k (\overline{m})^2,$$

where α_l and α_k are the ratios of the background to the desired counts of the lth and kth counters. The relative error in the determination of Φ_{lk} is given by

$$\delta(\Phi_{lk}) = \sqrt{\frac{1}{N-1} + \frac{1}{g_l g_k N \overline{m}} + \frac{1}{(N-1) g_l g_k}[1 + \alpha_l + \alpha_k + \alpha_l \alpha_k]}. \tag{54}$$

---

[2] V. I. Gol'danskii and M.I. Podgoretskii, Dokl. Akad. Nauk SSSR **100**, 237 (1955).

While in the method of correlations the background merely increases the fluctuations without changing the average value of the correlation function, in the method of coincidences the background also affects the mean value of S_{lk} which, in accordance with Eq. (47), becomes equal to

$$S_{lk} = g_l g_k \overline{m} + g_l g_k (\overline{m})^2 \times [1 + \alpha_l + \alpha_k + \alpha_l \alpha_k]. \qquad (55)$$

Thus in the presence of background for $\overline{m} \geq (1 + \alpha_l + \alpha_k + \alpha_l \alpha_k)^{-1}$ chance coincidences have already become important, while for $\overline{m} > [g_l g_k \times (1 + \alpha_l + \alpha_k + \alpha_l \alpha_k)]^{-1/2}$ the method of coincidences becomes inapplicable in practice because of missed counts. It is evident that in the correlation method, as before, $\delta_{\min}(\Phi_{lk})$ for $\overline{m} \to 0$, $N \to \infty$ is determined by Eq. (46″), and for arbitrary $\overline{m}$,

$$\delta(\Phi_{lk}) = \delta_{\min}(\Phi_{lk}) \times \sqrt{1 + \overline{m}\,(1 + \alpha_l + \alpha_k + \alpha_l \alpha_k)}. \qquad (56)$$

Consequently, in the presence of background, and for $\overline{m}\,[1 + \alpha_l + \alpha_k + \alpha_l \alpha_k] \gg 1$, i.e., in the region in which the method of coincidences is no longer applicable, the error of the correlation method increases not faster than $\sqrt{\overline{m}}$.

For a very high background count ($\alpha_l \gg 1$, $\alpha_k \gg 1$) we obtain from Eqs. (46″) and (56),

$$\delta^2(\Phi_{lk}) \approx \alpha_l \alpha_k / g_l g_k N. \qquad (57)$$

Consequently, for the required number of intervals of measurement, which is determined by the condition $\delta(\Phi_{lk}) \ll 1$, we have

$$\sqrt{N} \gg \sqrt{\alpha_l \alpha_k / g_l g_k}, \qquad (58)$$

and if we are dealing with the region in which $\overline{m} \gtrsim 1/\alpha_l \alpha_k$, then we obtain for the required total number of disintegrations in the course of the whole experiment

$$\sqrt{N\overline{m}} = \sqrt{M} \gg 1/\sqrt{g_l g_k}. \qquad (59)$$

Let us now turn to an examination of concrete examples of possible applications of the correlation method.

5. EXAMPLES OF POSSIBLE APPLICATIONS OF THE CORRELATION METHOD

It has already been mentioned above that, in principle, the correlation method can be used to solve all those problems which are solved by the method of coincidences. Therefore, we shall not examine in detail those examples for which both methods are applicable. Let us just note briefly that above we were everywhere comparing the correlation method with that variant of the method of coincidences in which g_l and g_k are unknown, and for the determination of M it is necessary to record not only the number of coincidences but also the number of counts in the individual channels.

Frequently, however, this is not necessary, and only the number of coincidences is recorded. In such cases the method of correlations may become inapplicable, because in this method the counts in individual channels must be determined, and because of the presence of background they may be so large as to become difficult to record. Therefore, it may become necessary to reduce the intensity of radiation a when the correlation method is used, i.e., to increase the length of time of taking measurements in using the correlation method in comparison with the method of coincidences, and the correlation method may turn out to be the less advantageous one.

Let us now turn to typical problems, the solution of which at high intensities is possible by means of the correlation method, but impossible by the method of coincidences.

a) *Determination of cross sections of nuclear reactions.*

If, when the target A is bombarded by particles a, a nuclear reaction c takes place with the emission of particles b and the formation of a radioactive isotope B: $A + a \to b + B$, then, from observing the correlation between the emission of particles b at the instant of formation of B and the subsequent radioactive disintegration of B, one can determine the rate of formation of B under equilibrium conditions, and consequently, for a known flux of particles the cross section of the nuclear reaction which leads to the formation of B (one can of course also formulate this question in the opposite direction). Example:

$$\mathrm{Be}^9 + n \to \alpha + \mathrm{He}^6 \xrightarrow[\beta^-]{0.82\ \mathrm{sec}} \mathrm{Li}^6 \quad (\alpha\beta \text{ correlation}).$$

It is clear that at high intensities the method of coincidences is not applicable to the solution of this and many similar problems. Indeed, for long resolving times the circuit will be missing counts almost continuously, and for short resolving times Δt, the efficiency of recording would be reduced by a factor of order $\Delta t/\tau$, where τ is the mean lifetime of the isotope formed.

In such cases the only way of obtaining by the coincidence method the same accuracy and the same duration of the experiment as in the correlation method is to reduce the intensity of radiation (without increasing the original ratio of background to desired counts). However, this does not turn out to be possible in all cases, and coincidence circuits with resolving times greater than $10^{-4} - 10^{-3}$ sec usually cannot be used because of missing counts.

The correlation method permits one to determine the cross section of the indicated reaction on the basis of the determination of the correlation function for the α and β counters for some one arbitrary relative orientation of the two counters. For processes separated by large time intervals angular correlation is generally absent. Therefore, the cross section of the reaction under consideration is determined independently of the angular distribution of the α-particles, and it therefore becomes unnecessary to measure the angular distribution in this problem. Any competing reactions accompanied by the emission of α-particles [for example, $Be^9(n, 2n)2He^4$] are of no importance for the determination of the cross section.

Another example of the same kind is the reaction

$$T^3(t\gamma)He^6 \xrightarrow[\beta^-]{0{,}82\ \text{sec}} Li^6.$$

By studying the $\gamma\beta$ correlation for one arbitrary relative orientation of the two counters it is possible to determine the cross section of this reaction without knowing either the efficiency of the γ-counter or the cross sections of competing reactions.

b) *Identification of the products of nuclear reactions.*

If when the target A is bombarded by some given particles several nuclear reactions can take place:

$$\begin{array}{l} \qquad\quad b + B \\ \qquad\nearrow \\ A + a \rightarrow b' + B' \\ \qquad\searrow \\ \qquad\quad b'' + B'' \end{array}$$

with the formation of different radioactive isotopes then by a suitable choice of various operating conditions of the counters one can determine with which particular radioactive decay one or another type of secondary particles b is correlated, i.e., one can ascribe definite radioactive properties to definite isotopes.

Example:

$$\begin{array}{l} \qquad\quad d + He^6 \xrightarrow[\beta^-]{0{,}82\ \text{sec}} Li^6 \quad (E_{\beta}\ \text{up to}\ 3.7\ \text{mev}) \\ \qquad\nearrow \\ Li^7 + n \\ \qquad\searrow \\ \qquad\quad \gamma + Li^8 \xrightarrow[\beta^-]{0{,}88\ \text{sec}} 2He^4 \quad (E_{\beta}\ \text{up to}\ 12\ \text{mev}) \end{array}$$

It is evident that, for example, by varying the thickness of filters in front of the counters or the characteristics of the counters (we do not examine these possibilities in detail, because the same is done also in the method of coincidences, as is described, for example, in reference 1, one may select the more penetrating β-particles or distinguish between γ and d and to identify the resulting isotopes by this means. Still another possibility of separating effects produced by different isotopes is connected with the variation of the length t of the intervals of measurement which leads to a violation of condition (14).

c) *Determination of half-lives of decay.*

The correlation function for disintegrations of the lth and kth kind in an equilibrium radioactive mixture is defined by the general relation (20). Up till now we used assumption (14) because for intervals of length much greater than the half-lives of decay of all the substances formed between the lth and kth disintegrations the correlation is the most marked. However, assumption (14) is by no means compulsory. In the general case, for example, if the lth and kth decays are adjacent we obtain from Eq. (20) and from the laws of radioactive decay

$$\Phi_{lk} = g_l g_k\left[at - \frac{a}{\lambda_k}(1 - e^{-\lambda_k t})\right] = \Phi_{lk}(t), \quad (60)$$

where $at = \overline{m}$, and λ_k is the decay constant for the disintegration of the kth type.

It is evident that if we know $\Phi(t)$ for at least two values of interval length we can determine the half-life of the kth member of the radioactive family without knowing the quantity of the kth or of the other substances, or the half-lives of the other substances, and independently of a, g_l and g_k.

Knowing λ_l, we can then determine in a way analogous to what was done before the quantities a, g_l and g_k, and also the equilibrium number of atoms of the kth type. Indeed

$$\frac{\Phi_{lk}(t_1)}{\Phi_{lk}(t_2)} = (\lambda_k t_1 - 1 + e^{-\lambda_k t_1})/(\lambda_k t_2 - 1 + e^{-\lambda_k t_2}). \tag{61}$$

It is evident from (61) that the determination of λ_k must be carried out in such a way that at least one of the values of t utilized is of order $1/\lambda_k$, since for $\lambda_k t \ll 1$ the correlation functions approach zero, while for $\lambda_k t \gg 1$ they approach the constant value utilized in all the above calculations. The determination of the half-lives of decay by the correlation method may be carried out, naturally, not only for adjacent decays, but for arbitrarily related decays (including those separated by branchings of the chain), but the corresponding relations will be more complicated than (61).

The number of examples could be easily multiplied, but we have set ourselves for the present merely the problem of the general illustration of the possibilities of the method. For the same reason we shall not here dwell on the different variants of the correlation method which can differ appreciably from the one described above.

6. CONCLUSIONS

1. The determination of the correlation function between the recorded number of decays of the lth and the kth type:

$$\Phi_{lk} = \overline{r_l r_k} - \overline{r_l} \cdot \overline{r_k}.$$

permits one to find the absolute yield of nuclear transformations.

2. The mean value of the correlation function of consecutive related disintegrations in the absence of branching in between and with the length of the interval during which measurements are taken considerably larger than the mean time interval between these disintegrations is equal to $\overline{\Phi}_{lk} = \frac{N-1}{N} g_l g_k \overline{m}$ and does not depend on the background. The relative error in the determination of $\overline{\Phi}_{lk}$ in the general case (in the presence of background) is equal to

$$\delta(\Phi_{lk}) = \sqrt{\frac{1}{N-1} + \frac{1}{g_l g_k N \overline{m}} + \frac{1}{(N-1) g_l g_k}(1+\alpha_l)(1+\alpha_k)}.$$

3. For a given duration of the measurement interval t the accuracy of the correlation method is the same as the accuracy of the method of coincidences. However, for $\overline{m} > [g_l g_k (1+\alpha_l) \times (1+\alpha_k)]^{-1/2}$ the method of coincidences can no longer be used because of missed counts, while the correlation method continues to be usable.

4. The applicability of the correlation method for large $\overline{m}$ is particularly important for the study of nuclear transformations the individual stages of which are separated by relatively great time-intervals (of the order of $10^{-3} - 1$ sec).

Translated by G. M. Volkoff
240

SOVIET PHYSICS JETP VOLUME 2, NUMBER 3 MAY, 1956

Theory of Strong Coupling for Meson Fields. III

B. T. Geilikman
Moscow State Teachers' Institute

(Submitted to JETP editor July 12, 1954)
J. Exper. Theoret. Phys. USSR **29**, 572-584 (November, 1955)

Examination is made of the pseudoscalar meson field which interacts with moving nucleons in the strong coupling approximation. A theory is developed which takes into account the polarization of the nucleonic vacuum.

1. IN earlier works[2,3] we investigated the meson field which interacts with infinitely massive nucleons at rest. We now consider this problem for moving nucleons with finite mass.

The Hamiltonian (1) and (29) in reference 1, for nucleons at rest,

$$H=\frac{1}{2}\int\sum_{\alpha=1}^{3}\Big[\Pi_\alpha^2+c^2(\nabla\Phi_\alpha)^2+c^2\varkappa^2\Phi_\alpha^2 \qquad (1)$$

$$-2\sqrt{4\pi}\,gc\sum_{i}^{n}O_\alpha(\mathbf{r}-\mathbf{r}_i)\,\Phi_\alpha\Big]d\mathbf{r}$$

$[O_{\alpha i}=\tau_\alpha\vec{\sigma}_i\ \nabla U(\mathbf{r}-\mathbf{r}_i)$ in the case of a pseudoscalar field $]$ is obtained from the exact Hamiltonian, which has the following form for a pseudoscalar charged field:

$$H=\sum_{i}^{n}[c(\vec{\alpha}_i,\mathbf{p}_i)+\beta_i mc^2] \qquad (2)$$

$$+\frac{1}{2}\int\sum_{\alpha}^{3}\Big[\Pi_\alpha^2+c^2(\nabla\Phi_\alpha)^2+c^2\varkappa^2\Phi_\alpha^2$$

$$-2c\sqrt{4\pi}\sum_{i}^{n}(G_{\alpha i}\Phi_\alpha$$

$$+F_{\alpha i}\Pi_\alpha)+4\pi c^2\sum_{ij}^{n,n}F_{\alpha i}F_{\alpha j}\Big]d\mathbf{r};$$

$$G_{\alpha j}=-i\beta_j\gamma_{5j}\tau_{\alpha j}g_{ps}U(\mathbf{r}-\mathbf{r}_j)$$

$$+\frac{g_{pv}}{\varkappa}\tau_{\alpha j}(\vec{\sigma}_j,\nabla U(\mathbf{r}-\mathbf{r}_j));$$

$$F_{\alpha j}=\frac{g_{pv}}{\varkappa c}\gamma_{5j}\tau_{\alpha j}U(\mathbf{r}-\mathbf{r}_j);$$

$2\pi c^2\int\sum_{\alpha,i,j}F_{\alpha i}F_{\alpha j}\,d\mathbf{r}$ are the so-called contact terms[3]. The Hamiltonian (1) is obtained from (2) with the help of a transition to the nonrelativistic approximation (i.e., a neglect of terms of order E/nmc^2) in comparison with those entering into (1), and then with neglect of the kinetic energy of the nucleons. Neglect of the kinetic energy of the nucleons in the zeroth approximation corresponds to expansion in powers of μ/m, as it does in molecular theory. The motion of the nucleons can easily be taken into account by means of adiabatic perturbation theory, analogous to the theory which applies to molecules[4].

However, if we take into consideration in the Hamiltonian (1) the subsequent terms in the expansion of (2) in powers of (E/nmc^2), then, as was shown in reference 4, these terms give the following correction for φ_α^0 in the case of a single nucleon:

$$\delta\varphi_\alpha^0=h\left(1+\frac{g_{ps}^2}{mc^2}\int hU\,d\mathbf{r}\right. \qquad (3)$$

$$\left.-B\langle\vec{\tau}\rangle^2\int hU\,d\mathbf{r}\right)^{-1}\left\{\left[B\langle\vec{\tau}\rangle^2-\frac{g_{ps}^2}{mc^2}\right]\right.$$

$$\times\int f_\alpha U\,d\mathbf{r}-\langle\tau_\alpha\rangle B\sum_\beta\langle\tau_\beta\rangle\int f_\beta U\ d\mathbf{r}$$

$$\left.\times\ \left(1+\frac{g_{ps}^2}{mc^2}\int hU\,d\mathbf{r}\right)^{-1}\right\};$$

$$f_\alpha=(g/c\sqrt{4\pi})\int\langle O_\alpha(\mathbf{r}')\rangle G(\mathbf{r},\mathbf{r}')\,d\mathbf{r}';$$

$$h=\int U(\mathbf{r}')G(\mathbf{r},\mathbf{r}')\,d\mathbf{r}';\qquad \langle\tau_\alpha\rangle=\frac{(\psi_{\lambda\lambda}^{0*},\tau_\alpha\psi_{\lambda\lambda}^0)}{(\psi_{\lambda\lambda}^{0*},\psi_{\lambda\lambda}^0)};$$

$$B=4\pi\left(\frac{g_{ps}g_{pv}}{m\varkappa c^3}\right)^2\int U^2\,d\mathbf{r}\left(1+\frac{4\pi g_{pv}^2}{m\varkappa^2c^2}\int U^2\,d\mathbf{r}\right)^{1};$$

---

[1] T. Geilikman, J. Exper. Theoret. Phys. USSR **29**, 417 (1955); Soviet Phys. **2**, 509 (1956).

[2] B. T. Geilikman, J. Exper. Theoret. Phys. USSR **29**, 430 (1955).

[3] N. Kemmer, Proc. Roy. Soc. (London) **166A**, 127 (1938).

[4] B. T. Geilikman, Dokl. Akad. Nauk SSSR **91**, 39 (1953).

Equation (3) keeps terms of order $g^2(amc^2)^{-1}$ in comparison with φ^0_α for $m = \infty$ (a = nuclear "radius"). The correction for the energy E^0_λ is of the same order of magnitude (i.e., it is of order E/mc^2). If we assume that the eigenvalue of the energy of the nucleon in the meson field amounts to only a small part of its rest energy, then $g^2/a \sim mc^2$ and $g^2/\kappa^2a^3 \sim mc^2$ (for gradient coupling); if $a \to 0$, then the passage of m to infinity must be removed by renormalization. In this case the usual transition from the exact Hamiltonian to the nonrelativistic approximation and then to nucleons at rest (1) is invalid. For two or more nucleons, the condition for the applicability of the non-relativistic approximation $(E^0_\lambda - E^0_{\lambda'})/mc^2 \ll 1$ is not satisfied in the case of small separation of the nucleons, even for $\delta\varphi^0_\alpha = 0$, i.e., without taking into account the subsequent terms in (E/nmc^2). Indeed, it was shown in reference 2 that the distance between two levels $E^0_{33} - E^0_{11}$ for a system of two nucleons is equal to $2K$, i.e., $\sim g^2/a$ for $r \sim a$ (nongradient coupling) and (g^2/κ^2a^3) (gradient coupling). Thus, $E^0_{33} - E^0_{11}$ is of order mc^2 if $g^2/a \sim mc^2(g^2/\kappa^2a^3 \sim mc^2)$. Therefore, if $mc^2 \sim g^2/a(mc^2 \sim g^2/\kappa^2a^3)$ we must consider the Hamiltonian (2) directly. In this case, only the solution of (2) for the nonrelativistic case $v \ll c$ makes sense, so long as the nucleons are assumed to be extended.

For pseudoscalar coupling the energy of interaction of the nucleons with the field depends not only on Φ_α but also on the momenta Π_α. Therefore, $\dot{\Phi}_\alpha = \frac{i}{\hbar}[H, \Phi_\alpha] \neq \Pi_\alpha$. As was shown in reference 1, the zeroth approximation corresponds to a neglect of the kinetic energy of the field, but since $\Pi_\alpha \neq 0$ for $\dot{\Phi}_\alpha = 0$, then $\Pi_\alpha \neq$ for the zero field also (potential momentum). We assume that $\Phi_\alpha = \varphi^0_\alpha + \varphi_\alpha$; $\Pi_\alpha = \pi^0_\alpha + \pi_\alpha$. The Hamiltonian of zeroth approximation is then

$$H^0 = \sum_i^n [c(\vec{\alpha}_i, \mathbf{p}_i) + \beta_i mc^2]$$
$$+ \frac{1}{2}\int \sum_\alpha \Big[(\pi^0_\alpha)^2 + c^2\varphi^0_\alpha(\varkappa^2 - \Delta)\varphi^0_\alpha$$
$$- 4c\sqrt{\pi}\sum_i^n (G_{\alpha i}\varphi^0_\alpha + F_{\alpha i}\pi^0_\alpha) + 4\pi c^2 \sum_{i,j}^{n,n} F_{\alpha i}F_{\alpha j}\Big] d\mathbf{r}$$

The eigenfunctions of $H^0\psi^0_n$ depend on the coordinates $\mathbf{r}_1, \ldots, \mathbf{r}_n$, and on the spin variables $s_1, \ldots, s_n$. The perturbation is

$$H' = H - H^0 = H^{(1)} + H^{(2)};$$
$$H^{(1)} = \int \sum_\alpha \Big\{ c^2 \Big[(\varkappa^2 - \Delta)\varphi^0_\alpha$$
$$- \sqrt{4\pi}/c \sum_i^n G_{\alpha i}\Big]\varphi_\alpha$$
$$+ \Big[\pi^0_\alpha - c\sqrt{4\pi}\sum_i^n F_{\alpha i}\Big]\pi_\alpha\Big\} d\mathbf{r};$$
$$H^{(2)} = \frac{1}{2}\int \sum_\alpha [\pi^2_\alpha + c^2\varphi_\alpha(\varkappa^2 - \Delta)\varphi_\alpha]\, d\mathbf{r}.$$

The equation for φ^0_α and π^0_α must be found from the condition

$$H^{(1)}_{nn} = \int (\psi^{0*}_n, H^{(1)}\psi^0_n) \prod_i^n d\mathbf{r}_i = 0.$$

as was shown previously in reference 1 [see Eq. (12)]. This condition will be satisfied if φ^0_α and π^0_α obey the equations[4,5]:

$$(\varkappa^2 - \Delta)\varphi^0_\alpha = \frac{\sqrt{4\pi}}{c}\sum_i^n \langle G_{\alpha i}\rangle^s_{nn}; \tag{4}$$
$$\pi^0_\alpha = c\sqrt{4\pi}\sum_i^n \langle F_{\alpha i}\rangle^s_{nn}.$$

Here

$$\langle G_{\alpha i}\rangle^s_{nn}$$
$$= \frac{(\psi^{0*}_n(\mathbf{r}_1, \ldots, \mathbf{r}_n, s_1, \ldots, s_n),\ G_{\alpha i}\psi^0_n(\mathbf{r}_1, \ldots, s_n))}{(\psi^{0*}_n, \psi^0_n)}$$

is the mean value of $G_{\alpha i}$ over the variables of ordinary and isotopic spin of the nucleons. Equations (4) are the natural generalizations of the equations for the zero field in the case of nucleons at rest (reference 1). We substitute the solution of Eq. (4) in the expressions for H^0 and $H^{(1)}$:

---

[5] B. T. Geilikman, Dokl. Akad. Nauk SSSR **91**, 225 (1953).

$$H^0 = \sum_i^n [c(\vec{\alpha}_i, \mathbf{p}_i) + \beta_i mc^2]$$

$$+ \frac{1}{2} \sum_{\alpha, l, j}^{3, n, n} \int [\langle G_{\alpha i}(\mathbf{r}')\rangle_{nn}^s$$

$$-2G_{\alpha i}(\mathbf{r}')] \langle G_{\alpha l}(\mathbf{r})\rangle_{nn}^s G(\mathbf{r}, \mathbf{r}')\, d\mathbf{r}\, d\mathbf{r}'$$

$$+ 2\pi c^2 \sum_{\alpha, i, j}^{3, n, n} \int [(\langle F_{\alpha j}\rangle_{nn}^s$$

$$- 2F_{\alpha i}) \langle F_{\alpha j}\rangle_{nn}^s + F_{\alpha i} F_{\alpha j}]\, d\mathbf{r}; \tag{5}$$

$$G(\mathbf{r}, \mathbf{r}') = \frac{e^{-\varkappa|\mathbf{r}-\mathbf{r}'|}}{|\mathbf{r}-\mathbf{r}'|}; \tag{6}$$

$$H^{(1)} = c\sqrt{4\pi} \sum_{\alpha, i}^{3, n} \int [(\langle G_{\alpha i}\rangle_{nn}^s - G_{\alpha i})\varphi_\alpha$$

$$+ (\langle F_{\alpha i}\rangle_{nn}^s - F_{\alpha i})\pi_\alpha]\, d\mathbf{r}.$$

If the eigenfunctions ψ_n^0 and eigenvalues E_n^0 of the nonlinear equation $H^0\psi_n^0 = E_n^0\psi_n^0$ are found, it is possible to form the Hamiltonians H_n^0 from H^0 by substituting in $\langle F_{\alpha i}\rangle_{nn}^S$ and $\langle G_{\alpha i}\rangle_{nn}^S$ the function $\psi_n^0(\mathbf{r}_1, \ldots, s_n)$ in explicit form. The eigenfunctions ψ_{nl}^0 of the equation $H_n^0\psi_{nl}^0 = E_{nl}^0\psi_{nl}^0$ form a complete orthogonal set. We now seek the total function for the Hamiltonian (2) in the form

$$\Psi_n = \sum_l [\chi_n^0(\varphi_\alpha)\delta_{nl} + \chi'_{nl}(\varphi_\alpha)]\,\psi_{nl}^0(\mathbf{r}_1, \ldots s_n).$$

Assuming that $\varphi \ll \varphi^0$, $\chi'_{nl} \ll \chi_n^0$, we can develop the theory of perturbations as in reference 1, Sec. 2 (only now the spectrum of the unperturbed Hamiltonian is continuous or quasi-discrete if a finite volume V is considered). In this case we obtain an equation for χ_n^0 (in the absence of degeneracy for E_{nn}^0: $E_{nl}^0 \neq E_{nn}^0$ of $l \neq n$; the degenerate case will be considered below):

$$(H_{n2} + H'_{n3} + H''_{n3})\chi_n^0 = E'_n\chi_n^0; \tag{7}$$

$$E'_n = E_n - E_{nn}^0;$$

$$H_{n2} = H'_{nn} + \sum_{l \neq n} H_{nl}^{(1)} H_{ln}^{(1)} (E_{nn}^0 - E_{nl}^0)^{-1};$$

$$H'_{n3} = \sum_l H_{nl}^{(1)} H_{ln}^{(1)} [(E_{nn}^0 - E_{nl}^0 + E'_n)^{-1}$$

$$- (E_{nn}^0 - E_{nl}^0)^{-1}];$$

$$H''_{n3} = \sum_l \sum_m H_{nl}^{(1)} H_{lm}^{(1)} H_{mn}^{(1)} (E_{nn}^0 - E_{nl}^0)^{-1}$$

$$\times \quad (E_{nn}^0 - E_{nm}^0)^{-1};$$

$$H'_{lm} = \int (\psi_{nl}^{0*}, H'\psi_{nm}^0) \prod_i^n d\mathbf{r}_i;$$

$$H'_{nn} = H_{nn}^{(2)}, \text{ так как } H_{nn}^{(1)} = 0.$$

If we generalize the usual method of reducing to the sum of squares a Hamiltonian which is quadratic in momenta p_S and coordinates q_S (see reference 6) to the case of π_α and φ_α which depend on the continuous index $\mathbf{r}$, we can show that H_{n2} takes the form:

$$H_{n2} = \frac{1}{2}\sum_k (p_k^2 + \omega_k^2 q_k^2)$$

after the canonical transformation:

$$\pi_\alpha =$$

$$\sum_k \left[\pi_{k\alpha}^+(\mathbf{r})(q_k - ip_k/\omega_k) + \frac{1}{2}\pi_{k\alpha}^-(\mathbf{r})(p_k - i\omega_k q_k)\right];$$

$$\varphi_\alpha =$$

$$\sum_k \left[\varphi_{k\alpha}^+(\mathbf{r})(q_k - ip_k/\omega_k) + \frac{1}{2}\varphi_{k\alpha}^-(\mathbf{r})(p_k - i\omega_k q_k)\right];$$

Here $\pi_{k\alpha}^+$, $\varphi_{k\alpha}^+$ are the solutions of the field equations

$$\dot{\varphi}_\alpha \doteq -i\omega\varphi_\alpha$$

$$= \frac{i}{\hbar}[H_{n2}, \varphi_\alpha] \text{ and } -i\omega\pi_\alpha = \frac{i}{\hbar}[H_{n2}, \pi_\alpha],$$

---

[6] E. T. Whittaker, *Analytical Dynamics*.

which correspond to the frequency $+\omega_k$, and $\pi^-_{k\alpha}$, $\varphi^-_{k\alpha}$ to the frequency $-\omega_k$.

Inasmuch as $H^{(2)}$ for $m \neq \infty$ coincides with $H^{(2)}$ for $m = \infty$, the frequencies $\omega_k = c\sqrt{\kappa^2 + k^2}$ as before, and do not depend on φ^0_α. Since the field $\varphi^0_\alpha \sim g^1$ and $\varphi_\alpha \sim g^0$, as was the case for $m = \infty$, the nonlinearity of the field of real mesons φ_α remains of the order g^{-2}.

The conditions of applicability of the perturbation theory $\varphi \ll \varphi^0$, $\chi'_{nl} \ll \chi^0_n$ have the same form as in the case of nucleons at rest, since the estimates of φ and φ^0 ($\pi^0 = \kappa c\, \varphi^0$) remain unchanged: $g^2/\hbar c \gg 1$ and $g^2/\hbar c \gg \kappa^2 a^2$ (in the absence of mesons).

2. The solution of the zeroth order approximation of the equation with the Hamiltonian (5) presents the greatest difficulty in the case of moving nucleons. Equation (5) is then a nonlinear differential equation, and not an algebraic equation as was the case for nucleons at rest. The problem is simplified in the case of a single nucleon. There the solution has the form: $\psi^0(\mathbf{r}, s) = [u^0 \times (s)\, e^{i\,\mathbf{k}\cdot\mathbf{r}}$ [$u^0(s)$ is a factor which depends on the spin variable s]. Substituting $u^0(s)e^{i\,\mathbf{k}\cdot\mathbf{r}}$ in Eq. (5), we get an algebraic equation for the eight component function $u^0(s)$:

$$\Big\{\hbar c\,(\vec{\alpha},\ \mathbf{k}) + \beta mc^2 + \frac{1}{2}\sum_\alpha \int [|G_\alpha(\mathbf{r}')|_{\lambda\lambda} - 2G_\alpha(\mathbf{r}')]\,|G_\alpha(\mathbf{r})|_{\lambda\lambda} G(\mathbf{r},\ \mathbf{r}')\,d\mathbf{r}\,d\mathbf{r}' + 2\pi c^2 \sum_\alpha \int [(|F_\alpha|_{\lambda\lambda} - 2F_\alpha)\,|F_\alpha|_{\lambda\lambda} + F^2_\alpha]\,d\mathbf{r}\Big\}\,u^0_\mu = E^0_\mu u^0_\mu. \tag{8}$$

An analogous equation is obtained in the case of a scalar field with scalar coupling:

$$\Big[\hbar c\,(\vec{\alpha},\ \mathbf{k}) + \beta mc^2 + \frac{g^2}{2}\sum_\alpha \int [|\tau_\alpha\beta|_{\lambda\lambda} - 2\tau_\alpha\beta]\,|\tau_\alpha\beta|_{\lambda\lambda} U(\mathbf{r})\,U(\mathbf{r}')\,G(\mathbf{r},\ \mathbf{r}')\,d\mathbf{r}\,d\mathbf{r}'\Big] \times u^0_\mu = E^0_\mu u^0_\mu.$$

As an example we take the solution of the equation for u^0_μ with a neutral field:

$$[c\,(\vec{\alpha},\ \mathbf{p}) + \beta mc^2 + (J_s\xi^2/2) - \beta J_s\xi]\,u^0_\mu = E^0_\mu u^0_\mu;$$

$$J_s = g^2 \int U(\mathbf{r})\,U(\mathbf{r}')\,G(\mathbf{r},\mathbf{r}')\,d\mathbf{r}\,d\mathbf{r}';$$

$$\xi = |\beta|_{\lambda\lambda};\quad \mathbf{p} = \hbar\mathbf{k}.$$

If we equate the determinant of this set of four equations to zero, we get:

$$\left[\left(mc - \frac{J_s\xi}{c}\right)^2 + p^2 - \left(\frac{E^0}{c} - \frac{J_s\xi^2}{2c}\right)^2\right]^2 = 0;$$

$$E^0 = \frac{J_s\xi^2}{2} \mp c\sqrt{\left(mc - \frac{J_s\xi}{c}\right)^2 + p^2}.$$

We see that both the level with $E^0 > 0$ and the level with $E^0 < 0$ are doubly degenerate. The same degeneracy is obtained for a pseudoscalar field with pseudoscalar coupling. Because of the degeneracy, we cannot use Eq. (4), since the expression $\langle G_\alpha\rangle^S_{nn}$ remains indeterminate in the case of the two functions ψ^0_{n1} and ψ^0_{n2}. With degeneracy, therefore, it is more appropriate to use the first, and not the second, variant of the adiabatic perturbation theory (see reference 1, Sec. 2). In such a case

$$H^0 = c\,(\vec{\alpha},\ \mathbf{p}) + \beta mc^2 + \frac{1}{2}\sum_\alpha^3 \int [c^2\Phi_\alpha(\varkappa^2 - \Delta)\,\Phi_\alpha - 4c\sqrt{\pi}G_\alpha\Phi_\alpha]\,d\mathbf{r};$$

$$H' = \frac{1}{2}\sum_\alpha^3 \int \Pi^2_\alpha d\mathbf{r};$$

for the scalar field $G_\alpha = \beta\tau_\alpha gU(\mathbf{r} - \mathbf{r}_1)$. (For pseudovector and mixed coupling, the degeneracy is absent; see below.) The ψ functions of zeroth approximation depend upon Φ_α:

$$H^0\psi^0_{\mu\mathbf{k}}(\mathbf{r},\ s,\ \Phi_\alpha) = E^0_{\mu\mathbf{k}}(\Phi_\alpha)\,\psi^0_{\mu\mathbf{k}}(\mathbf{r},\ s,\ \Phi_\alpha).$$

We seek the total Ψ function of the system in the form[1]:

$$\Psi_{\lambda\mathbf{k}} = \sum_{\mu,\ \mathbf{k}'} \chi_{\mu\mathbf{k}'}(\Phi_\alpha)\,u^0_{\mu\mathbf{k}'}(s,\ \Phi_\alpha)\,e^{i\,(\mathbf{k}',\ \mathbf{r})}.$$

If the degeneracy is twofold (as was the case for neutral field with nongradient coupling), then for $\mathbf{k}' = \mathbf{k}$, $E^0_{1\mathbf{k}}(\varphi^0) = E^0_{2\mathbf{k}}(\varphi^0)$. In the first approximation in the sum over $\mathbf{k}'$ and μ, there remain only two components with $\mathbf{k}' = \mathbf{k}$ and $\mu = 1$ and $\mu = 2$. If we substitute in the equation

$$H\Psi = E\Psi,\quad \Psi = (\chi^0_{1\mathbf{k}}u^0_{1\mathbf{k}} + \chi^0_{2\mathbf{k}}u^0_{2\mathbf{k}})\,e^{i\,(\mathbf{k},\ \mathbf{r})},$$

we get two equations for $\chi^0_{1\mathbf{k}}$ and $\chi^0_{2\mathbf{k}}$ (below,

$\chi_\lambda^0 \equiv \chi_{\lambda\mathbf{k}'}^0\, V^{-1} \int E_{1\mathbf{k}}^0 d\mathbf{r}_1 = V^{-1} \int E_{2\mathbf{k}}^0 d\mathbf{r}_1 \equiv E^0(\Phi)$, $u_{\lambda\mathbf{k}}^0 \equiv u_\lambda^0$):

$$\left[\frac{1}{2}\int \Pi^2 d\mathbf{r} + E^0(\Phi)\right]\chi_1^0 + f_{11}(\Pi,\ \Phi)\chi_1^0 + f_{12}(\Pi,\ \Phi)\chi_2^0 = E\chi_1^0; \tag{9}$$

$$\left[\frac{1}{2}\int \Pi^2 d\mathbf{r} + E^0(\Phi)\right]\chi_2^0 + f_{21}(\Pi,\ \Phi)\chi_1^0 + f_{22}(\Pi,\ \Phi)\chi_2^0 = E\chi_2^0;$$

Here

$$f_{\mu\lambda}(\Pi,\ \Phi) = \frac{1}{2}\left(u_\mu^{0*},\ \left[\int \Pi^2, d\mathbf{r},\quad u_\lambda^0\right]\right);$$

$$([A,\ B] = AB - BA).$$

We can now introduce the 2×2 Pauli matrices σ_x, σ_y, σ_z and the two component function $\chi^0 = \frac{\chi_1^0}{\chi_2^{0}}$. Then the set (9) is written in the form

$$H_1\chi^0 = E\chi^0;\ H_1 = \frac{1}{2}\int \Pi^2 d\mathbf{r} + E^0(\Phi) + (\vec{\sigma},\ \mathbf{a}(\Phi,\ \Pi)) + b(\Phi,\ \Pi); \tag{10}$$

$$a_x = \frac{1}{2}(f_{12} + f_{21});$$

$$a_y = \frac{i}{2}(f_{12} - f_{21});\ a_z = \frac{1}{2}(f_{11} - f_{22});$$

$$b = \frac{1}{2}(f_{11} + f_{22}).$$

We calculate

$$\varepsilon = \left[\int \Pi^2 d\mathbf{r},\ u_\lambda^0(\Phi)\right] = \int (\Pi[\Pi,\ u_\lambda^0(\Phi)] + [\Pi,\ u_\lambda^0(\Phi)]\Pi)\, d\mathbf{r};$$

$[\Pi,\ u_\lambda^0(\Phi)] = g_\lambda(\Phi)$ = functional of Φ. Therefore

$$\varepsilon = \int ([\Pi,\ g_\lambda] + 2g_\lambda\Pi)\, d\mathbf{r} = \int (h_\lambda(\Phi) + 2g_\lambda(\Phi)\Pi)\, d\mathbf{r};$$

$$f_{\mu\lambda} = \frac{1}{2}\int [(u_\mu^{0*},\ h_\lambda) + 2(u_\mu^{0*},\ g_\lambda)\Pi]\, d\mathbf{r}.$$

Thus b and a_x, a_y, a_z are linear functionals of Π.

Equation (10) can be solved by the usual method. We set $\Phi = \varphi^0 + \varphi$, $\Pi = \pi^0 + \pi$ and expand H_1 in a power series in φ, π: $H_1 = \sum_{k=0} H_1^{(k)}$, limiting ourselves to the quadratic terms. The equations for φ^0 and π^0 are found from the conditions[1]: $\langle H_1^{(1)}\rangle = 0$; they have the form:

$$\delta E / \delta\varphi^0 = \delta\langle H_1^0\rangle / \delta\varphi^0 = 0;\quad \delta\langle H_1^0\rangle / \delta\pi^0 = 0.$$

In first approximation for Eq. (10) we write $\chi^0 = \psi^0(q,\ \varphi^0,\ \pi^0)\chi^0(\varphi)$, we obtain an equation for the two component function $\chi^0(q)$ (q is the spin variable $\vec{\sigma}$; $q = q_1, q_2$):

$$\left[\frac{1}{2}\int (\pi^0)^2 d\mathbf{r} + E^0(\varphi^0) + (\vec{\sigma},\ a(\varphi^0,\ \pi^0)) + b(\varphi^0,\ \pi^0)\right]\psi_\nu^0(q) = E_{0\nu}^0\psi_\nu^0(q) \tag{11}$$

and the equation for $\chi^0(\varphi)$ is

$$\left[H_1^{(2)} + \sum_\rho^2 |H_1^{(1)}|_{\nu\rho}\, |H_1^{(1)}|_{\rho\nu}\, (E_{0\nu}^0 - E_{0\rho}^0)^{-1}\right]\chi^0(\varphi) = E_\nu'\chi^0(\varphi);$$

$$|H_1^{(1)}|_{\nu\rho} = (\psi_\nu^{0*}(q),\ H_1^{(1)}\psi_\rho^0(q)).$$

It is evident that the degeneracy is removed because of the terms in Eq. (11) which contain $\vec{\sigma}$, and we obtain $E_{01}^0 \neq E_{02}^0$ for a given $\mathbf{k}$.

For χ_{nl}' with $l \neq n$, i.e., $\mathbf{k}' \neq \mathbf{k}$ or $\mu = 3, 4$ for $\mathbf{k}' = \mathbf{k}$, we can make use of the usual equation (see reference 1, Sec. 2). The appropriate solution of Eq. (10) will be given in another work.

In the case of fourfold, rather than twofold, degeneracy, a set of four equations for $\chi_{1\mathbf{k}}^0$, $\chi_{2\mathbf{k}}^0$, $\chi_{3\mathbf{k}}^0$, $\chi_{4\mathbf{k}}^0$ can be written with the help of 4×4 Dirac matrices. The method outlined above, with the introduction of the matrices $\vec{\sigma}$ can also be employed in molecular theory in the case of degeneracy of the electronic level for arbitrary values of the nuclear radius vectors R_i.

We now consider the solution of Eq. (8) for the pseudoscalar neutral field with pseudovector coupling (degeneracy is not present in this case):

$$\left[c(\vec{\alpha},\ \mathbf{p}) + \beta mc^2 + \frac{J_p(\vec{\eta})^2}{2} + \frac{J(1+\zeta^2)}{2} - J_p(\vec{\eta},\ \vec{\sigma}) - J\zeta\gamma_5\right]u_\mu^0 = E_\mu^0 u_\mu^0; \tag{12}$$

$$\vec{\eta} = |\vec{\sigma}|_{\lambda\lambda};\ \zeta = |\gamma_5|_{\lambda\lambda};$$

$$J_p = \frac{g_{pv}^2}{\varkappa^2}\int \frac{\partial^2 G(\mathbf{r},\ \mathbf{r}')}{\partial x\, \partial x'} U(\mathbf{r})\, U(\mathbf{r}')\, d\mathbf{r}\, d\mathbf{r}';$$

$$J = \frac{4\pi g_{pv}^2}{\varkappa^2}\int U^2(\mathbf{r})\, d\mathbf{r}'.$$

If we set the determinant of the system (12) to zero, and assume that the z axis is directed along the vector **p**, we obtain

$$[(p_0+b_z)^2-\gamma^2]\,[(p_0-b_z)^2-\gamma^2]$$
$$+\,2\,(p^2+\delta^2)\,(p_0^2-\gamma^2-b_z^2)$$
$$-\,2\,(b^2-b_z^2)\,(p_0^2+\gamma^2-b_z^2+\delta^2-p^2)$$
$$+\,(b^2-b_z^2)^2+(p^2-\delta^2)^2$$
$$+\,8pb_z\delta\gamma=0;\quad p_0=mc;$$
$$\mathbf{b}=-\frac{J_p\vec{\eta}}{c};\quad \delta=-\frac{J\zeta}{c};$$
$$\gamma=\left(E-\frac{J}{2}-\frac{J\zeta^2}{2}-\frac{J_p(\vec{\eta})^2}{2}\right)\Big/\,c.$$

For $\mathbf{p}=0$, the system (12) divides into two systems of two equations, if we assume that the axis $\bar{z}$ is parallel to **b** (see reference 2, Sec. 1).

1) For $\lambda=1$ and $\lambda=2$: $u^0_{\mu 2}=u^0_{\mu 4}=0$; $\eta_{\bar{z}}=+1$; $\zeta=0$ for $\lambda=1$

$$E^0_{11}=\frac{J-J_p}{2}+mc^2;$$

$$\text{for}\quad \lambda=2\quad E^0_{22}=\frac{J-J_p}{2}-mc^2.$$

2) For $\lambda=3$ and $\lambda=4$: $u^0_{\mu 1}=u^0_{\mu 3}=0$; $\eta_{\bar{z}}=-1$; $\zeta=0$;

$$\text{for}\quad \lambda=3\quad E^0_{33}=\frac{J-J_p}{2}+mc^2;$$

$$\text{for}\quad \lambda=4\quad E^0_{44}=\frac{J-J_p}{2}-mc^2.$$

The vector **b** is oriented in arbitrary fashion for $\mathbf{p}=0$. For $\mathbf{p}\neq 0$, the energy E^0 and u^0_μ can be found by means of a Lorentz transformation. Also, for $\mathbf{p}\neq 0$, $\mathbf{b}\,\|\,\mathbf{p}$ and $\zeta\neq 0$.

If the "nonmeson" mass of the nucleon is small in comparison with the "meson" mass: $mc^2\ll J$, we can effect a transition in Eq. (2) for a single nucleon to the nonrelativistic approximation, assuming that $E=\text{const}+J+E'$ and $E'\ll J$ ($cp\ll J$, $mc^2\ll J$). But there is no necessity for this, since, as we have seen, it is possible to solve Eq. (8), which corresponds to the relativistic Hamiltonian (2), and then assume $p\ll J/c$.

For two and more nucleons, the transition to the nonrelativistic approximation ($E'\ll J$) and then to the case of nucleons at rest, is possible for large separations $|\mathbf{r}_i-\mathbf{r}_j|\gg a$; for small separations $|\mathbf{r}_i-\mathbf{r}_j|\sim a$, such a transition is not possible in principle, as was shown above. Thus, in this case the concept of a static potential of interaction loses its meaning. The general form of the energy of zeroth approximation can be found by taking the mean value of H^0 (5) (in terms of the eigenfunctions ψ^0_{nm}):

$$E^0_{nn}=\sum_i^n[c\,|\,(\vec{\alpha}_i,\ \mathbf{p}_i)\,|_{nn}+|\,\beta_i\,|_{nn}mc^2]$$
$$-\sum_{\alpha,\,i,\,j}^{3,\,n,\,n}\left\{\frac{1}{2}\int|\,G_{\alpha i}(\mathbf{r})\,|_{nn}\,|\,G_{\alpha j}(\mathbf{r}')\,|_{nn}G(\mathbf{r},\,\mathbf{r}')\,d\mathbf{r}\,d\mathbf{r}'\right.$$
$$\left.+\,2\pi c^2\int(|\,F_{\alpha i}\,|_{nn}\,|\,F_{\alpha j}\,|_{nn}-|\,F_{\alpha i}F_{\alpha j}\,|_{nn})\,d\mathbf{r}\right\}.$$

Here, in addition to an interaction with effective radius κ^{-1} (due to terms which contain $F_{\alpha_i}F_{\alpha_j}$, we also get forces between nucleons with a radius of action $\sim a$ [this is seen directly from Eq. (4)].

3. Up to the present, we have been assuming the nucleons to be extended, and have not considered the presence of a nucleonic vacuum which, as is known, leads to an additional interaction of nucleons among themselves, of mesons among themselves and of nucleons with mesons.

A systematic consideration of the vacuum is possible only in a relativistically invariant theory, i.e., for the transition from extended nucleons to point nucleons. Therefore, in the following we shall assume that the transition to the limit $a\to 0$ [$U(\mathbf{r}-\mathbf{r}_i)\to\delta(\mathbf{r}-\mathbf{r}_i)$] is carried out. In this case, the eigenvalue of the energy of the nucleon which enters into the energy of zeroth approximation is divergent, and there arises the problem of renormalization, which will be considered elsewhere. It must be observed that a transition to zero nuclear radii, without consideration of the vacuum, gives reasonable results in the case of nongradient coupling. Actually, as was shown in reference 2, Eq. (9), for an infinitely extended nucleon interacting with the scalar field, the scattering cross section of the meson with the nucleon is, at $a=0$, $d\sigma=(\kappa^2+k^2)^{-1}d\Omega$; in the case of gradient coupling, the cross section tends to zero as a approaches zero in the limit. However, it is necessary to take account of the nucleonic vacuum in a systematic relativistic theory, in addition to the transition to point nucleons.

The effect of the vacuum, without application of second quantization to the nucleons was estimated in reference 5. It is more convenient to make use of the method of second quantization.

In this case the Hamiltonian has the form (in charge symmetric form; see reference 7):

$$H = \int \psi^+ (c(\vec{\alpha}, \mathbf{p}) + \beta mc^2)\psi \, d\mathbf{r} \tag{13}$$

$$+ \frac{1}{2}\int \sum_{\alpha}^{3} \Big\{ \Pi_\alpha^2 + c^2 (\nabla\Phi_\alpha)^2 + c^2 \varkappa^2 \Phi_\alpha^2$$

$$- 2c\sqrt{\pi}\int [\bar{\psi}(\mathbf{r}'),$$

$$\beta (G_\alpha \Phi_\alpha(\mathbf{r}) + F_\alpha \Pi_\alpha(\mathbf{r}))\psi(\mathbf{r}')] \, d\mathbf{r}',$$

$$+ c^2\pi \Big(\int [\bar{\psi}(\mathbf{r}'), \beta F_\alpha \psi(\mathbf{r}')] \, d\mathbf{r}'\Big)^2 \Big\} \, d\mathbf{r},$$

$U(\mathbf{r} - \mathbf{r}')$ enters in G_α and F_α [see Eq. (2)]:

$$\bar{\psi} = \psi^+\beta; \quad \psi(\mathbf{r})\psi^+(\mathbf{r}') + \psi^+(\mathbf{r}')\psi(\mathbf{r}) = \delta(\mathbf{r} - \mathbf{r}').$$

The Hamiltonian (13) is obtained from the Hamiltonian (2) in the usual way by a transition from the method of configuration space to the method of second quantization. The Ψ function of the state now depends on the occupation number.

We assume, as earlier, that $\Phi_\alpha = \varphi_\alpha^0 + \varphi_\alpha$; $\Pi_\alpha = \pi_\alpha^0 + \pi_\alpha$. Then $H = H^0 + H^{(1)} + H^{(2)}$:

$$H^0 = H_f^0 + \int \psi^+ (c(\vec{\alpha}, \mathbf{p}) + \beta mc^2)\psi \, d\mathbf{r} \tag{14}$$

$$- c\sqrt{\pi}\int \sum_{\alpha}^{3} [\bar{\psi}(\mathbf{r}'),$$

$$\beta (G_\alpha \varphi_\alpha^0(\mathbf{r}) + F_\alpha \pi_\alpha^0(\mathbf{r}))\psi(\mathbf{r}')] \, d\mathbf{r} \, d\mathbf{r}';$$

$$H_f^0 = \frac{1}{2}\int \sum_{\alpha} \Big\{ (\pi_\alpha^0)^2 + c^2 (\nabla\varphi_\alpha^0)^2 + c^2\varkappa^2 (\varphi_\alpha^0)^2$$

$$+ \pi c^2 \Big(\int [\bar{\psi}(\mathbf{r}'), \beta F_\alpha \psi(\mathbf{r}')] \, d\mathbf{r}'\Big)^2 \Big\} \, d\mathbf{r};$$

$$H^{(1)} = \int \sum_{\alpha} \Big\{ \pi_\alpha^0 \pi_\alpha + c^2 \varphi_\alpha (\varkappa^2 - \Delta)\varphi_\alpha^0$$

$$- c\sqrt{\pi}\int [\bar{\psi}(\mathbf{r}'), \beta(G_\alpha \varphi_\alpha + F_\alpha \pi_\alpha)\psi(\mathbf{r}')] \, d\mathbf{r}' \Big\} \, d\mathbf{r};$$

$$H^{(2)} = {}^1/_2 \int \sum_{\alpha} [\pi_\alpha^2 + c^2 \varphi_\alpha (\varkappa^2 - \Delta)\varphi_\alpha] \, d\mathbf{r}.$$

As was shown in Sec. 1, and in reference 1, Eq. (12), the zero field φ_α^0, π_α^0 must be found from the condition $\langle H^{(1)} \rangle = 0$ (if degeneracy is absent; see above), i.e., in case of Eq. (13):

$$(\varkappa^2 - \Delta)\varphi_\alpha^0 = (\sqrt{\pi}/c)\int \langle [\bar{\psi}', \beta G_\alpha \psi'] \rangle \, d\mathbf{r}'; \tag{15}$$

$$\pi_\alpha^0 = c\sqrt{\pi}\int \langle [\bar{\psi}', \beta F_\alpha \psi'] \rangle \, d\mathbf{r}';$$

$$\psi' = \psi(\mathbf{r}');$$

Here $\langle [\bar{\psi}, \beta G_\alpha \psi] \rangle$ is the mean value (diagonal matrix element) of $[\bar{\psi}, \beta G_\alpha \psi]$ as a function of the state, which depends on the occupation number. It is not difficult to show that the condition $\langle H^{(1)} \rangle = 0$ will be satisfied in this case also, if the averaging in the equations for φ_α^0, π_α^0 is carried out only over the spin variables:

$$(\varkappa^2 - \Delta)\varphi_\alpha^0 = (\sqrt{\pi}/c)\int ([\bar{\psi}', \beta G_\alpha \psi'])^s \, d\mathbf{r}'; \tag{16}$$

$$\pi_\alpha^0 = c\sqrt{\pi}\int ([\bar{\psi}', \beta F_\alpha \psi'])^s \, d\mathbf{r}'.$$

If ψ_m and ϵ_m are eigenfunctions and eigenvalues of the equation

$$\Big[c(\vec{\alpha}, \mathbf{p}) + \beta mc^2 - c\sqrt{\pi}\int \langle [\bar{\psi}', \beta(G_\alpha \varphi_\alpha^0 \tag{17}$$

$$+ F_\alpha \pi_\alpha^0)\psi'] \rangle \, d\mathbf{r}' \Big] \psi_m = \varepsilon_m \psi_m$$

with φ_α^0 and π_α^0 from Eq. (15), then, substituting the expansion $\psi = \sum_m (a_m \psi_m^{(+)} + b_m^+ \psi_m^{(-)})$ in H^0 (14) (see reference 7), we evidently obtain:

$$H^0 = \sum_m (a_m^+ a_m \varepsilon_m - b_m b_m^+ \varepsilon_m).$$

Here we find from Eq. (15)

$$(\varkappa^2 - \Delta)\varphi_\alpha^0 = (j_\alpha)_{\mathrm{vac}} \tag{18}$$

$$+ \frac{\sqrt{4\pi}}{c} \sum_m \Big\{ n_m^+ \int (\bar{\psi}_m^{(+)\prime} \beta G_\alpha \psi_m^{(+)\prime}) \, d\mathbf{r}'$$

$$+ n_m^- \int (\bar{\psi}_m^{(-)\prime} \beta G_\alpha \psi_m^{(-)\prime}) \, d\mathbf{r}' \Big\}$$

(with an analogous equation for π_α^0): $n_m^+ = a_m^+ a_m$; $n_m^- = b_m^+ b_m$. The mean value of the current in the vacuum $(j_\alpha)_{\mathrm{vac}}$, as is known, is given by[8]

$$(j_\alpha)_{\mathrm{vac}} = \frac{\sqrt{\pi}}{c} \, \mathrm{sp} \langle [\bar{\psi}, \beta G_\alpha \psi] \rangle_{\mathrm{vac}};$$

In the equation for $(j_\alpha)_{\mathrm{vac}}$ we have undergone a transition from $U(\mathbf{r} - \mathbf{r}')$ to the δ-function $\delta(\mathbf{r} - \mathbf{r}')$, since such a transition, as is well

---

[7] A. I. Akhiezer and V. B. Berestetskii, *Quantum Electrodynamics*, GTTI, 1953, pp. 150, 130, 442, 126.

[8] J. Schwinger, Phys. Rev. 82, 664 (1952).

known, does not lead to additional divergences (sp denotes the diagonal sum over the spin indices $G_\alpha = U(\mathbf{r}-\mathbf{r}')\overline{G}_\alpha$).

Since $<[\overline{\psi}, \beta G_\alpha \psi]>^S$ has a complicated form if the method of second quantization is used, then it is expedient in the case of Eq. (16) to return to the method of configuration space:

$$(\kappa^2 - \Delta)\varphi_\alpha^0 = (j_\alpha)_{\mathrm{vac}} + \frac{\sqrt{4\pi}}{c}\sum_i^n <G_{\alpha i}>^S \tag{19}$$

(and analogous equation for π_α^0):

$(j_\alpha)_{\mathrm{vac}}$ has the same form as in (18), and $<G_{\alpha i}>^S$ as in (4).

It is not difficult to show that the interaction of the nucleons (and anti-nucleons) in Eq. (18) is substituted for the self-consistent field, in contrast to Eqs. (16) and (19). This is explained by the fact that the operators ψ^+, ψ, as well as the spin operators τ_α, α_k, β enter into H^0. Therefore, the averaging in the equations for φ_α^0, π_α^0 in the case of Eq. (15) is carried out not only over the spin variables, but also over the occupation numbers. In Eqs. (16) and (19), the averaging is carried out only over the spin variables; they entirely correspond to Eqs. (4). If the system consists of a large number of nucleons (for example, the nucleons in the nucleus), it is expedient to use Eqs. (15) for φ_α^0, π_α^0. In this case, however, we must add the usual condition for the applicability of the self-consistent field to the condition of applicability of strong coupling, given in Sec. 1 and in reference 1. In our problem we can obtain this condition by comparing the correction for the Ψ-functions with the Ψ-functions of zero approximation.

The perturbation theory for second quantization of the Hamiltonian $H = H^{(0)} + H^{(1)} + H^{(2)}$ is entirely similar to the perturbation theory developed in Sec. 1 and in reference 1. Expressing the complete Ψ-function of the system in terms of the eigenfunctions of the Hamiltonian H^0:

$$\Psi_n = \sum_l [\chi_n^0(\varphi_\alpha)\delta_{nl} + \chi'_{nl}(\varphi_\alpha)]\,\Psi_{nl}^0(n_m),$$

we obtain an equation for χ_n^0 which is similar to Eq. (7). It is evident that the anharmonicity of the field of real mesons φ_α is connected with the presence of the vacuum as well as with the absence of the vacuum, and appears only in the second approximation $1/g^2$. Consequently, the anharmonicity of φ_α is small in the case of strong coupling just as in the case of weak coupling[5].

We consider the zeroth approximation of perturbation theory for one nucleon which is located at a positive level. In this case the field φ_α^0, π_α^0 is defined by the Eqs. (19).

The eigenfunctions of the Hamiltonian H^0 can easily be found, since Eq. (17) for the function ψ_m, by which we can expand the second quantized functions ψ and ψ^+, depends on the operators **p**, **r** and the spin operators τ_α, α_k, β just as Eqs. (5) and (8) in the absence of the vacuum. Therefore, diagonalization of (17) and the spin variables is obtained in the same way as the diagonalization of Eq. (8) in Sec. 1, and the solution has the form $u_\mu e^{i\mathbf{k}\cdot\mathbf{r}}$. However, inasmuch as the equation for the field φ_α^0, π_α^0, because of the term with $(j_\alpha)_{\mathrm{vac}}$ have some other form than in the absence of the vacuum, then the integrals analogous to J_S and J_p are also proportional to g^2; hence they will diverge for $a \to 0$ differently than was shown in reference 1, where the vacuum was not considered. If we introduce the corresponding integrals in the form of numerical parameters, ignoring the character of their divergence, then it is not difficult to carry out calculations in the first and second approximation of perturbation theory, i.e., to compute the scattering cross section of the mesons with nucleons and the interaction of the mesons among themselves. This problem will be considered in another work. It should be noted that the greatest difficulty is presented by the calculation of the interaction forces between nucleons (in zeroth approximation of perturbation theory). In order to estimate the internuclear forces, we must solve Eq. (19) for $n \neq 1$ and find the form of the function $\varphi_\alpha^0(\mathbf{r})$.

We now return to Eq. (19) for a single nucleon. The average current in the vacuum can be expressed by the Green's function of the Dirac equation[8]

$$G(x, x') = i(c\hbar)^{-1}\langle T(\psi(x)\overline{\psi}(x'))\rangle;\qquad x = \{\mathbf{r}, ct\};$$

T is the symbol of the T-product[7]:

$$[c\gamma p + mc^2 - c\sqrt{4\pi}\,\beta(\bar{G}_\alpha\Phi_\alpha + \bar{F}_\alpha \Pi_\alpha)]\,G(x, x') = \delta(x - x'); \tag{20}$$

$$\mathrm{sp}\,\frac{1}{2}\langle[\bar{\psi},\ \beta\bar{G}_\alpha\psi]\rangle_{\mathrm{vac}} = ic\hbar\,\mathrm{sp}\,[\beta\bar{G}_\alpha G(x, x')]_{x'\to x};$$

$$\gamma p = \sum^{4}\gamma_k p_k;$$

$$\gamma_k = \beta\alpha_k;\ \gamma_4 = i\beta;$$

$$p_4 = -\ \frac{\hbar}{c}\frac{\partial}{\partial t}.$$

Schwinger[8] has pointed out the method for the computation of the mean current in the vacuum, i.e., the Green's function of the Dirac equation without application of the theory of perturbation for the case of a constant electromagnetic field. This method was used by Malenka[9] in the case of a constant neutral meson field with pseudoscalar coupling in the presence of a given current. We now attempt to take into account the change of the field Φ_α in space. By way of an example, we consider a charged field with pseudoscalar coupling. In this case the equation $\delta H_1/\delta\varphi^0_\alpha = 0$ (see Sec. 1) for φ^0_α has the same form as Eq. (19), but the current of the nucleon $j_{\alpha n}$, in view of the presence of degeneracy, will not equal $\frac{2\sqrt{\pi}}{c}<G_\alpha>^S$. We first find $G(x, x')$:

$$G(x, x') = c^{-1}(\gamma p + mc + ig'\gamma_5\sum\tau_\alpha\Phi_\alpha)^{-1}\delta(x - x')$$

$$= c^{-1}(mc - \gamma p - ig'\gamma_5\sum\tau_\alpha\Phi_\alpha)(m^2c^2 + p^2 + \hbar g'\gamma_5\sum\gamma_k\tau_\alpha\partial_k\Phi_\alpha + (g')^2\sum\Phi^2_\alpha)^{-1}\delta(x - x');$$

$$\partial_k\Phi_\alpha \equiv \frac{\partial\Phi_\alpha}{\partial x_k};\qquad g' = g\sqrt{4\pi};\quad \gamma_5^2 = 1.$$

Expanding $\hbar\gamma_5 g'\Sigma\gamma_k\tau_\alpha\partial_k\Phi_\alpha(m^2c^2 + p^2 + (g')^2 \times\Sigma\Phi^2_\alpha)^{-1}$ in a power series and noting that $(AB)^{-1} = B^{-1}A^{-1}$, we find

$$G(x, x') = c^{-1}(mc - \gamma p - ig'\gamma_5\Sigma\tau_\alpha\Phi_\alpha)\sum_{n=0}^{\infty}(a^{-1}b)^n a^{-1}\delta(x - x'); \tag{21}$$

$$a = m^2c^2 + p^2 + (g')^2\Sigma\Phi^2_\alpha;$$

$$b = -\hbar g'\gamma_5\sum\gamma_k\tau_\alpha\partial_k\Phi_\alpha;$$

$$j_\alpha(x, x') = i\hbar\sqrt{4\pi}\,\mathrm{sp}\,[\bar{\beta}G_\alpha G(x, x')] \tag{22}$$

$$= \frac{g'\hbar}{c}\,\mathrm{sp}\Big[\gamma_5\tau_\alpha(mc - \gamma p - ig'\gamma_5\Sigma\tau_\beta\Phi_\beta)\sum_n(a^{-1}b)^n a^{-1}\delta(x - x')\Big].$$

In the calculation of the spur in Eq. (22), after multiplication by $\gamma_5\tau_\alpha$ all terms of the row are zero, after multiplication by $\tau_\alpha\tau_\beta$, the terms of the row with odd n are zero, and after multiplication by $\tau_\alpha\gamma_5\gamma_k$ the terms with even n are zero. Therefore, we get from Eq. (22):

$$j_\alpha(x, x') = \frac{8}{i}\frac{(g')^2\hbar}{c}\Big[\Phi_\alpha + i\hbar\sum_k p_k(m^2c^2 + p^2 + \sum(g')^2\Phi^2_\alpha)^{-1}\partial_k\Phi_\alpha\Big] \times\Big[p^2 + m^2c^2 + (g')^2\sum\Phi^2_\beta + \hbar^2(g')^2\sum_{k,\beta}\partial_k\Phi_\beta(p^2 + m^2c^2 + (g')^2\sum\Phi^2_\beta)^{-1}\partial_k\Phi_\beta\Big]^{-1} \times\ \delta(x - x'). \tag{23}$$

If the field Φ_α is changed slowly, then:

---

[9] B. Malenka, Phys. Rev. 85, 686 (1952).

$$j_\alpha(x,x') \simeq f_0 a^{-1} + f_1 a^{-1} + f_0 a^{-1} \delta a^{-1}; \tag{24}$$

$$f_0 = -i\,8\,(g')^2\,\hbar c^{-1}\Phi_\alpha;$$

$$f_1 = 8\,(g')^2 \hbar^2 c^{-1} \Sigma\, p_k\, a^{-1}\,\partial_k \Phi_\alpha;$$

$$\delta = -\hbar^2 (g')^2 \sum_{k,\beta} \partial_k \Phi_\beta\, a^{-1}\, \partial_k \Phi_\beta.$$

Using the identity

$$A^{-1} = \frac{1}{2i}\int_0^\infty (e^{iAs} - e^{-iAs})\,ds$$

(see, for example, reference 7), it is possible to write Eq. (23) in the following form:

$$j_\alpha(x,x') = \frac{8(g')^2\hbar}{ic}\Big\{\Phi_\alpha + i\hbar\,\Sigma\, p_k \int_0^\infty \sin\,[(p^2 + m^2c^2 + (g')^2 \sum_\beta \Phi_\beta^2)\,u]\,du\,\partial_k\Phi_\alpha\Big\}\int_0^\infty \sin\Big\{\Big[p^2 + m^2c^2 + (g')^2\sum_\beta \Phi_\beta^2 + \hbar^2 (g')^2 \sum_{k,\beta}\partial_k\,\Phi_\beta \int_0^\infty \sin\Big(\Big(p^2 + m^2c^2 + (g')^2\sum_\beta \Phi_\beta^2\Big)\,v\Big)\,dv\,\partial_k\,\Phi_\beta\Big]\,s\Big\}\,ds\,\delta\,(x - x').$$

If A and B are noncommutating operators, then we have, with accuracy to terms of first order in $\epsilon = AB - BA$[10]:

$$e^{A+B} \approx e^A e^B + e^A e^B \varepsilon/2. \tag{25}$$

For a slowly changing field, we can consider $[p^2, \Sigma\Phi_\beta^2]$ to be a small quantity. Then, using Eq. (25), and expressing $\delta(x - x')$ in the form of a Fourier integral, we obtain the zeroth term in Eq. (24), corresponding to a constant field Φ_α:

$$j_\alpha^0(x,x') = -\frac{4(g')^2\hbar\Phi_\alpha}{c\,(2\pi)^4}\int_0^\infty [\exp\{is\,(m^2c^2 + (g')^2\,\Sigma\Phi_\beta^2\}\,e^{isp^2} - \exp\{is\,(m^2c^2 + (g')^2\Sigma\Phi_\beta^2)\}\,e^{-isp^2}]\,ds \int_{-\infty}^\infty \exp \times \Big\{i\sum^4 k_i\,(x_i - x_i')\Big\}\,d^4k.$$

Evidently,

$$\exp(is\hat{p}^2)\exp\Big(i\sum^4 k_i\,(x_i - x_i')\Big) = \exp\Big[-i\hbar^2\Big(\sum_i^3 k_i^2 - k_4^2\Big)s + i\sum^4 k_i(x_i - x_i')\Big].$$

Integrating over d^4k, we find:

$$j_\alpha^0(x,x') = \frac{(g')^2}{c\hbar^3}\frac{\Phi_\alpha}{2\pi^2}\int_0^\infty \sin\Big\{\Big[m^2c^2 + (g')^2\,\Sigma\,\Phi_\beta^2 + \frac{i}{4s\hbar^2}\Big((\mathbf{r} - \mathbf{r}')^2 - c^2(t - t')^2\Big)\Big]\,s\Big\}\frac{ds}{s^2};$$

$$(j_\alpha(x))_{\text{vac}} = j_\alpha(x,x')_{x=x'}.$$

For $x = x'$, the integral over s is easily computed with the help of differentiation with respect to the parameter (the small quantity s_0 must be substituted for the lower limit);

$$j_\alpha^0(x) = \frac{(g')^2\Phi_\alpha}{2c\hbar^3\pi^2}\Big(m^2c^2 + (g')^2\sum_\beta \Phi_\beta^2\Big)\Big[1 - \gamma - \ln\Big(s_0\,(m^2c^2 + (g')^2\sum_\beta \Phi_\beta^2)\Big)\Big]; \tag{26}$$

$$\gamma = 1{,}78.$$

In the case of the field φ_α^0 we must assume $\Phi_\alpha = \varphi_\alpha^0$ in Eq. (26). We see that a logarithmic divergence appears in Eq. (26). The other terms in Eq. (24) can be computed in a similar manner. If we limit ourselves to second derivatives of φ_α^0 (which are necessary for the renormalization of the meson mass), then only in the first member of Eq. (24) -- $f_0 a^{-1}$ -- must one consider the second component of Eq. (25) in the expression for a^{-1}; in the remaining members of Eq. (24), one must keep only the first component of Eq. (25). This method of obtaining the mean current in a vacuum can easily be applied to the case of pseudovector coupling, when φ_α^0, π_α^0 are defined by Eqs. (19). In the same manner, we find the Green's function $G^0(x, x')$ which corresponds to the constant field Π_α, Φ_α:

---

[10] R. Peierls, Z. Physik **80**, 763 (1933).

$$G^0(x, x') = \frac{1}{(2\pi)^4 c}(mc - \gamma p + f\beta\gamma_5 \Sigma \tau_\beta \Pi_\beta)\int\limits_0^\infty \sin$$

$$\times\left[\left(m^2c^2 + f^2\Sigma\Pi_\beta^2 + \frac{i}{4s\hbar^2}(x - x')^2\right)s\right]\frac{ds}{s^2};$$

$$f = g\sqrt{4\pi}/(\varkappa c).$$

We can then find the mean current in the vacuum for the momentum $\Pi_\alpha - g_\alpha$:

$$g_\alpha(x) \equiv c\sqrt{\pi}\,\mathrm{sp}\,\langle[\bar{\psi}, \beta\bar{F}_\alpha\psi]\rangle_{\mathrm{vac}} \tag{27}$$

$$= \frac{f^2 c\Pi_\alpha}{2\pi^2\hbar^3}(m^2c^2 + f^2\Sigma\Pi_\beta^2)$$

$$\times[1 - \gamma - \ln(s_0(m^2c^2 + f^2\Sigma\Pi_\beta^2))].$$

Close to the nucleon, it is not possible to consider the field φ_α^0, π_α^0 to be changing slowly. Therefore, for the investigation of the behavior of φ_α^0, π_α^0 in the neighborhood of $\mathbf{r}_1$($\mathbf{r} - \mathbf{r}_1 \to 0$), it is appropriate in the exact equation for $j_\alpha(x, x')$ (23) and $g_\alpha(x, x')$ or for $G(x, x')$ (21) to substitute the solution of the equation of the field (19) (or $\delta H_1/\delta\varphi_\alpha^0 = \delta H_1/\delta\pi_\alpha^0 = 0$; see above) in the form of a functional of $j_\alpha(x)$ and $g_\alpha(x)$.

For the computation and later renormalization of the mass of the nucleon, the equations for π_α^0 and φ_α^0 must be solved. Renormalization of the meson charge of the nucleon can be carried out[8,9] on the basis of the expressions for $j_\alpha(x)$ and $g_\alpha(x)$.

Translated by R. T. Beyer
241

SOVIET PHYSICS JETP VOLUME 2, NUMBER 3 MAY, 1956

Existence of Quantum Stationary States of Point Nucleons Which Interact with the Meson Field

S. I. PEKAR
Physics Institute of the Ukraine SSR Academy of Sciences

(Submitted to JETP editor May 22, 1954)
(J. Exper. Theoret. Phys. USSR **29**, 599-604 (November, 1955)

Investigation is carried out of the problem of the existence of stationary quantum states of a system consisting of point nucleons which interact with a field of neutral and charged mesons. Various types of interaction operators between the nucleon and the meson-field are considered. With the motion of the nucleons treated non-relativistically, the absence of stationary states is proved for the case when the interaction is of a pseudo-vector character. The proof involves none of the approximations employed, for example, in the weak or strong coupling method.

1. INTRODUCTION

A variant of the meson theory of nuclear forces most popular at the present time is based on the assumption that π - mesons are describable in terms of pseudo-scalars and that their interaction with nucleons has a pseudo-vector character. It is known that this theory based on the weak coupling approximation for the nucleons in the meson field, leads to the conclusion that in the g^2 approximation the interaction potential of two nucleons separated by a small distance r is proportional to $1/r^3$; this is why no stationary states are obtained in the deuteron problem. Thus, even if we ignore the infinite self-energies of the interaction between the nucleons and the meson field, the system has no stationary quantum states. Tamm proved[1] that the same difficulty is encountered when the motion of the nucleons is treated relativistically, and also if several other approximations of the theory, for example, the quasi-static point of view, are not made.

When the next approximation of the weak coupling theory, of the order of g^4, was computed, new terms[2] of an order of magnitude that is higher than the previous terms of the g^2 approximation appeared in the interaction potential for two nucleons. In particular, if the distance of separation is small, the new terms are proportional to $1/r^6$, corresponding to a repulsion, and predominate over the terms of the earlier approximation; the $-1/r^3$ difficulty is therefore eliminated.

The fact that going to the next approximation alters even the qualitative nature of the theoretical result is very unfavorable to the weak coupling approximation. The question of the existence of stationary states of the system remains open, for it is not at all excluded that high approximations may show that at small values of r the interaction potential for two nucleons is an alternating series of increasing powers in $1/r$. This means formally that the existence of the stationary states depends on whether the last term in this series is positive or negative. In essence this means that for small values of r the potential cannot be represented by this series, and it may be that introducing a quasi-static potential is in general meaningless. This article therefore treats the question of the existence of stationary quantum states of nucleons in a meson field without resorting to the weak coupling approximation, and also without introducing quasi-static potentials for the nucleon interaction.

We shall express the Hamiltonian of the meson field without sources in the conventional form:

$$\hat{H}_0 = \frac{1}{2}\sum_{\alpha=1}^{3}\int\left[\frac{\pi_\alpha^2}{c^2} + (\nabla\varphi_\alpha)^2 + \mu^2\varphi_\alpha^2\right]d\tau. \tag{1}$$

Here all the φ_α and π_α terms are real: φ_1 and φ_2 are the fields of the charged mesons, and φ_3 is the field of the neutral mesons; π_α are fields that are canonically conjugate to φ_α. The masses of the positive, negative, and neutral mesons are assumed to be the same, and equal to m_π, with $\mu = m_\pi c/\hbar$.

Introducing a complete set of functions

$$\chi_{\vec{\varkappa}}(\mathbf{r}) = \sqrt{\frac{2}{L^3}}\begin{cases}\cos\vec{\varkappa}\mathbf{r} & \text{for } \varkappa_x \leqslant 0,\\ \sin\vec{\varkappa}\mathbf{r} & \text{for } \varkappa_x > 0,\end{cases} \tag{2}$$

which are orthonormalized in the volume L^3, it is possible to expand φ_α and π_α in Fourier series:

$$\varphi_\alpha = \sum_{\vec{\varkappa}}\varphi_{\alpha\vec{\varkappa}}\,\chi_{\vec{\varkappa}}(\mathbf{r}), \tag{3}$$

---

[1] I. E. Tamm, Journ. of Phys. USSR **9**, 449 (1945).

[2] K. Nakabayasi and I. Sato, Phys. Rev. **88**, 144 (1952).

$$\pi_\alpha = \sum_{\vec{\varkappa}} \pi_{\alpha\vec{\varkappa}} \chi_{\vec{\varkappa}}(\mathbf{r}). \tag{4}$$

Then, assuming

$$\omega_{\vec{\varkappa}} = c\sqrt{\mu^2 + \vec{\varkappa}^2}\,(\omega_{\vec{\varkappa}} > 0) \tag{5}$$

and introducing the dimensionless canonically conjugate quantities

$$q_{\alpha\vec{\varkappa}} = \varphi_{\alpha\vec{\varkappa}} \frac{1}{c}\sqrt{\omega_{\vec{\varkappa}}/\hbar}, \tag{6}$$

$$g_{\alpha\vec{\varkappa}} = \pi_{\alpha\vec{\varkappa}}(1/c\sqrt{\hbar\omega_{\vec{\varkappa}}}),$$

the Hamiltonian of the meson field can be rewritten as:

$$\hat{H}_0 = \frac{1}{2}\sum_{\alpha\vec{\varkappa}} \hbar\omega_{\vec{\varkappa}}[q^2_{\alpha\vec{\varkappa}} + g^2_{\alpha\vec{\varkappa}}]. \tag{7}$$

Instead of considering $q_{\alpha\vec{\varkappa}}$ and $g_{\alpha\vec{\varkappa}}$ as operators that obey the known commutation rules, we shall take $q_{\alpha\vec{\varkappa}}$ to be the independent variable, and represent the operators $g_{\alpha\vec{\varkappa}}$ in the following form:

$$g_{\alpha\vec{\varkappa}} = -i\partial/\partial q_{\alpha\vec{\varkappa}}. \tag{8}$$

As a result we obtain

$$\hat{H}_0 = \frac{1}{2}\sum_{\alpha\vec{\varkappa}} \hbar\omega_{\vec{\varkappa}}[q^2_{\alpha\vec{\varkappa}} - (\partial^2/\partial q^2_{\alpha\vec{\varkappa}})]. \tag{9}$$

The non-relativistic Hamiltonian of the ith nucleon in the absence of a meson field will have the following form:

$$K_i = -\frac{\hbar^2}{2m}\Delta_i. \tag{10}$$

The masses of the proton and of the neutron are assumed to be the same and equal to m.

The interaction between the ith nucleon and the meson field is chosen to be of the following form:

$$\hat{H}'_i = -\sqrt{4\pi}\sum_{\alpha=1} g_\alpha \tau_{\alpha i}\{\hat{A}_i\varphi_\alpha(\mathbf{r}_i), \hat{L}_i\}, \tag{11}$$

$$\{\hat{A}_i\varphi_\alpha, \hat{L}_i\} \equiv \sum_\beta (\hat{A}_{\beta i}\varphi_\alpha)\hat{L}_{\beta i}, \tag{12}$$

where g_α are constants, $\tau_{\alpha i}$ are the usual "isotopic spin" operators, r_i are the nucleon coordinates, and $\hat{A}_{\beta i}$ is an operator acting on $\varphi_\alpha(\mathbf{r}_i)$. It is assumed that operators $B_{\beta i}$ conjugate to $A_{\beta i}$ exist and satisfy the following relationship

$$\int f(\mathbf{r}_i)\hat{A}_{\beta i}\chi(\mathbf{r}_i)\,d\tau_i = \int \chi(\mathbf{r}_i)\hat{B}_{\beta i}f(\mathbf{r}_i)\,d\tau_i \tag{13}$$

for arbitrary quadratically-integrable f and χ. The operator $L_{\beta i}$ acts only on the spatial and spin coordinates of the nucleon, but not on its charge degree of freedom. Thus $\hat{L}_{\beta i}$ commutes with $\tau_{\alpha i}$.

We assume that operators B_β and L_β are homogeneous, that is, they satisfy the following relationships

$$\hat{B}_\beta(k\mathbf{r}) = k^n\hat{B}_\beta(\mathbf{r}), \tag{14}$$

$$\hat{L}_\beta(k\mathbf{r}) = k^m\hat{L}_\beta(\mathbf{r}), \tag{15}$$

where k, n, and m are constants. The generally known forms of interaction, namely scalar, pseudoscalar, and pseudo-vector, are particular cases of (11) and possess propoerties (14) and (15). In case of a mixture of meson fields having different types of interaction $\hat{H}'_1$, the values of n and m in relationships (14) and (15) can be different for each type of interaction.

2. INVESTIGATION OF THE EXISTENCE OF STATIONARY STATES IN THE NON-RELATIVISTIC TREATMENT OF NUCLEON MOTION

The energy operator of the system has the following form:

$$\hat{H}(r, q) \equiv \hat{H}(\ldots r_i \ldots, \ldots q_{\alpha\vec{\varkappa}} \ldots)$$

$$= \hat{H}_0(q) + \hat{K}(r) + \hat{H}'(q, r),$$

$$\hat{K} = \sum_{i=1}^{A}\hat{K}_i(\mathbf{r}_i);\ \hat{H}' = \sum_{i=1}^{A}\hat{H}'_i(q, \mathbf{r}_i). \tag{16}$$

If the system has a stationary state, the lowest eigenvalue of operator (16) (the ground energy level) should have a finite value. According to the general assumptions of the quantum mechanics, the average energy value of any arbitrary state of the system $\Psi(\ldots\mathbf{r}_i\ldots q_{\alpha\vec{\varkappa}}\ldots)$ is not less than the lowest energy level W_0:

$$\overline{H} \equiv \int \Psi^*\hat{H}\Psi\,dr\,dq \geqslant W_0, \tag{17}$$

$$dr = \prod_{i=1}^{A} dx_i\,dy_i\,dz_i,\ dq = \prod_{\alpha\vec{\varkappa}} dq_{\alpha\vec{\varkappa}},$$

W_0 is the absolute minimum of the integral in the left half of (17), provided that $\Psi(\ldots\mathbf{r}_i\ldots q_{\alpha\vec{\varkappa}}\ldots)$ is chosen from among the admissible functions, i.e., normalized, continuous, with continuous first derivatives, finite, and single-valued. Were the system to contain only a single nucleon, Ψ would be a four-component function, for two values assume the spin index and two values assume the nuclear-charge index. If the system contains A nucleons, Ψ has 4^A components. Treating Ψ as a multi-dimensional vector, we can regard expressions such as $\Psi^*\Psi$ and $\Psi^*\hat{H}\Psi$ as being scalar products (sum of the products of the components that have equal indices).

Let us assume the following wave function for the system

$$\Psi(r, q) = \psi(\mathbf{r}_1 \dots \mathbf{r}_A) \tag{18}$$

$$\times \exp\left\{-\frac{1}{2}\sum_{\alpha\vec{\varkappa}}\left[(q_{\alpha\vec{\varkappa}} - q^0_{\alpha\vec{\varkappa}})^2 + \frac{1}{2}\ln\pi\right]\right\},$$

where $\psi(\mathbf{r}_1 \dots \mathbf{r}_A)$ is a certain quadratically-integrable function in the coordinate space $x_1, y_1, z_1 \dots x_A, y_A, z_A$ of the nucleons.

Let $q^0_{\alpha\vec{\varkappa}}$ be, in accordance with equations (6) and (3), the dimensionless Fourier coefficients of a certain constant prescribed meson field

$$\varphi^0_\alpha(\mathbf{r}) = \int \frac{\eta_\alpha[\psi, \mathbf{r}'] \exp\{-\mu|\mathbf{r} - \mathbf{r}'|\}}{|\mathbf{r} - \mathbf{r}'|}\, d\tau', \tag{19}$$

where

$$\eta_\alpha[\psi, \mathbf{r}] = \sum_{i=1}^{A} \eta_{i\alpha}[\psi, \mathbf{r}], \tag{20}$$

$$\eta_{\alpha i}[\psi, \mathbf{r}_i] \tag{21}$$

$$= \frac{g_\alpha}{\sqrt{4\pi}} \int \{\hat{B}_i, \psi\tau^*_{\alpha i}\hat{L}_i\psi\}\, d\tau_1 \dots d\tau_{i-1}\, d\tau_{i+1} \dots d\tau_A,$$

$$\{\hat{B}_i, \psi^*\tau_{\alpha i}\hat{L}_i\psi\} \equiv \sum_\beta \hat{B}_{\beta i}\psi^*\tau_{\alpha i}\hat{L}_{\beta i}\psi. \tag{22}$$

Elementary calculation, using Eqs. (9), (10), (12), (13), (16), (22), yield

$$\overline{H} = \frac{1}{2}\sum_{\alpha\vec{\varkappa}} \hbar\omega_{\vec{\varkappa}} - \frac{\hbar^2}{2m}\sum_{i=1}^{A}\int \psi^*\Delta_i\psi\, d\mathbf{r} \tag{23}$$

$$- 2\pi \sum_{\alpha=1}^{3} \iint \eta_\alpha[\psi, \mathbf{r}]\, \eta_\alpha[\psi, \mathbf{r}']$$

$$\times \frac{\exp\{-\mu|\mathbf{r} - \mathbf{r}'|\}}{|\mathbf{r} - \mathbf{r}'|}\, d\tau\, d\tau';$$

Furthermore, let

$$\psi(\mathbf{r}_1 \dots \mathbf{r}_A) = k^{3A/2} f(k\mathbf{r}_1, \dots, k\mathbf{r}_A), \tag{24}$$

where $f(\mathbf{r}_1 \dots \mathbf{r}_A)$ is a certain fixed normalized admissible function. It is easy to see that if f is normalized, ψ and $\Psi(r,q)$ are also normalized for any positive constant k. Simple interchange of the variables under the integral sign results in

$$\sum_{i=1}^{A} \int \psi^*\Delta_i\psi\, dr = k^2 \sum_{i=1}^{A} \int f^*\Delta_i f\, dr, \tag{25}$$

$$\eta_\alpha[\psi, \mathbf{r}] = k^{3-n-m}\eta_\alpha[f, k\mathbf{r}]. \tag{26}$$

The last equation results from Eqs. (14) and (15). In (25) and (26) f is a function of $\mathbf{r}_i$ rather than of $k\mathbf{r}_i$.

Let us expand the last term of Eq. (23) in positive and negative powers of k; this is done most simply by expanding the exponential function under the integral sign in a series and taking the quantities $k\mathbf{r}$ and $k\mathbf{r}'$ as new integration variables. As a result, the expansion term having the highest power of k will be

$$- k^{1-2n-2m} 2\pi \sum_\alpha \iint \frac{\eta_\alpha[f, \mathbf{r}]\, \eta_\alpha[f, \mathbf{r}']}{|\mathbf{r} - \mathbf{r}'|}\, d\tau\, d\tau'. \tag{27}$$

Here the function under the integral sign no longer contains k. It is easy to see that the term (27) is always negative. At sufficiently large values of k this is the governing term of the expansion.

The next to the last term of (23) is always positive and is proportional to k^2, as can be seen from (25). Therefore if

$$1 + 2n + 2m < 0, \tag{28}$$

and k increases in (23), the (27) becomes the dominant term, and $\overline{H} \to -\infty$. As k increases, $\Psi(r,q)$ continues to remain an admissible function, and inequality (17) should be observed. Consequently, the system has no ground state with a finite energy W_0.

If the inequality sign is reversed in (28), then as k increases, $\overline{H} \to +\infty$, W_0 can be finite, and consequently the existence of stationary state is not excluded. However, there is no reason in this case for insisting on a continuous existence of stationary states, for it is not known whether the absolute minimum of $\overline{H}$ will be finite after we forego the particular form of the wave function (18) and turn to its more general expressions.

The first term in equation (23) is the zero order energy of the meson field and can be disregarded in the discussion.

A) Pseudo-Vector Interaction between Nucleons and Meson Field

In this case the operator $\hat{H}'_i$ has the following form

$$\hat{H}_i' = -\sqrt{4\pi} \sum_{\alpha=1}^{3} g_\alpha \tau_{\alpha i} (\sigma_i, \nabla_i \varphi_\alpha), \tag{29}$$

where σ_i is the nucleon spin operator. Comparing this expression with (11) we see that

$$\hat{A}_{\beta i} = \partial/\partial x_{\beta i}, \ \hat{L}_{\beta i} = \sigma_{\beta i}, \ \beta = 1, 2, 3. \tag{30}$$

Consequently, according to definition (13), we get

$$\hat{B}_{\beta i} = -\partial/\partial x_{\beta i}. \tag{31}$$

The operators $\hat{B}_{\beta i}$ and $\hat{L}_{\beta i}$ actually have the homogeneity properties (14) and (15), whereby $n = -1$ and $m = 0$. Thus, condition (28) is satisfied, and consequently the system has no stationary states.

B) Scalar Interaction of Nucleons with Meson Field

In this case the operator $\hat{H}_i'$ has the following form

$$\hat{H}_i' = -\sqrt{4\pi} \sum_{\alpha=1}^{3} g_\alpha \tau_{\alpha i} \varphi_\alpha (\mathbf{r}_i). \tag{32}$$

Comparing this expression with (11) we see that

$$\hat{A}_i = 1, \ \hat{L}_i = 1. \tag{33}$$

Hence $\hat{B}_i = 1$, $n = 0$, $m = 0$, and consequently the inequality in (28) is reversed. Thus the existence of stationary states of the system is not excluded.

The two examples considered above show how simple it is to apply the general criterion (28) to specific variants of meson dynamics. In case of a mixture of meson fields with different forms of the operator $\hat{H}_i'$ and unequal μ, the results obtained above are generalized in a trivial manner: Instead of equation (23) we get

$$\overline{H} = \frac{1}{2} \sum_{\alpha \vec{\varkappa} p} \hbar \omega_{\vec{\varkappa} p} - \frac{\hbar^2}{2m} \sum_{l=1}^{A} \int \psi^* \Delta_l \psi dr - 2\pi \sum_{\alpha, p} \iint \eta_{\alpha p} [\psi, \mathbf{r}] \, \eta_{\alpha p} [\psi, \mathbf{r}'] \times \frac{\exp\{-\mu_p |\mathbf{r} - \mathbf{r}'|\}}{|\mathbf{r} - \mathbf{r}'|} d\tau d\tau'. \tag{34}$$

Here the index p runs over the different types of meson fields. All the integrals in the last term of equation (34) are positive, and it is therefore impossible for components with different values of p to cancel each other. Consequently if inequality (28) is valid for at least one of the meson fields, the system has no stationary states; no addition of any other meson fields can remedy the situation.

In connection with this it is appropriate to mention the work by Moller and Rosenfeld[3] and by Schwinger[4]*, in which a mixture of pseudo-scalar and vector meson fields is considered. When each field is taken individually, no stationary states are obtained for the deuteron problem; but stationary states are obtained when mixtures of these fields are taken in a definite ratio. Actually this does not contradict the results of our work, for these authors obtained a finite energy for the deuteron only after using a quasi-static potential for the nucleon interaction and discarding known infinite self-energies of the nucleons in the meson field. By neglecting these terms, these authors obtained system energies that are totally unsuitable as eigenvalues of operator (16).

---

[3] C. Moller and L. Rosenfeld, Kgl. Danske Vil. Sels. Math. fys. Medd. 17, 8 (1940).

[4] J. Schwinger, Phys. Rev. 67, 339 (1945)

* *Translator's note.*- This reference is actually to a paper by Ning Hu, not by Schwinger.

Translated by J. G. Adashko
243

SOVIET PHYSICS JETP VOLUME 2, NUMBER 3 MAY, 1956

Electromagnetic Properties of a Finely Stratified Medium

S. M. RYTOV
P. N. Lebedev Physical Institute, Academy of Sciences, USSR

(Submitted to JETP editor June [illegible], 1954)
J. Exper. Theoret. Phys. USSR **29**, 605-616 (November, 1955)

Media composed of alternate layers of two isotropic materials, when the layers are sufficiently thin, behave on the average with relation to an electromagnetic field as if they were homogeneous but anisotropic (uniaxial crystal). The effective permeability tensors ϵ and μ of such a crystal are obtained, and limiting values are derived for thin layers as functions of the parameters of their materials, and of the frequency. Losses in a finely stratified medium are considered, and also boundary conditions at its surface.

INTRODUCTION

THE propagation of waves in media with a periodic laminated structure has often been considered, but attention has been directed primarily at the case in which the structural period d is comparable with the wavelength[1,2]. The case $d \ll \lambda$ was studied by Tamm and Ginzburg[3] in the application to a laminated core, composed of alternate layers of a dielectric and a metal (iron), on the assumption of a quite strongly developed skin effect in the metal. Levin[4] discussed in detail the propagation of an electromagnetic wave in the direction perpendicular to the layers of the periodic structure, without absorption. His method of calculation and his results for the case of long waves will be used below.

Recently the electrodynamics of stratified media, composed of alternate layers of a metal and a dielectric, have again attracted attention in connection with the following application. It has been found that in a transmission line filled with such a stratified medium, with proper arrangement of the layers and choice of the phase velocity of the wave, there is a possibility of decreasing the losses accompanying the propagation[5]. In the work cited, the calculation was done for the simplest case of a line formed of two conducting planes, the space between which is uniformly or partially filled with the stratified medium. The calculation was carried out both with and without allowance for the thickness of the elementary layers. The amount of the loss, calculated for a coaxial line with the stratified medium, was found to be in satisfactory agreement with experiment[6]. In addition, a detailed theoretical analysis was carried out for this type of transmission line[7,8]*.

In a study of the electromagnetic properties of stratified media, I obtained in 1949 the results reported below. (These results are partly contained in Sec. 3 of a work[10] published later, where they were obtained by another method.)

The subject to be considered is the "macroscopic" electromagnetic properties of a medium that consists of alternate layers of arbitrary homogeneous materials. We suppose that there are alternate plane layers of two substances with complex permeabilities ϵ_1, μ_1 (layer thickness a) and ϵ_2, μ_2 (layer thickness b). We are interested in the field averaged over the period $d = a + b$ of such a stratified structure. The introduction of this average field evidently has significance only under the condition that, along any arbitrary direction of propagation, its change in a distance of order d is sufficiently small. Quantitatively, this condition can be formulated thus:

$$kd\,|n| \ll 1, \tag{1}$$

where $k = \omega/c = 2\pi/\lambda$, and n is the effective index of refraction of the medium, different for different

---

[1] Rayleigh, Phil. Mag. **24**, 145 (1887); Sci. Pap. III, p. 1

[2] L. Brillouin, *Wave propagation in periodic structures*, McGraw-Hill (1946), Sec. 44.

[3] I. E. Tamm and V. L. Ginzburg, Izv. Akad. Nauk SSSR, Ser. Fiz. **7**, 30 (1943).

[4] M. L. Levin, J. Tech. Phys. USSR **18**, 1399 (1948).

[5] A. M. Clogston, Proc. IRE **39**, 767 (1951); Bell Syst. Tech. J. **30**, 491 (1951).

* References 5 and 7 are reviewed in *Uspekhi fizicheskikh nauk*[9], but regrettably without mention of reference 3--work done considerably earlier, and based on considerations similar to those enunciated by Academician N. D. Papaleksia with reference to a quasi-stationary system (a laminated core, the dimensions of which are small in comparison with the wavelength in the surrounding space).

[6] H. S. Black, C. O. Mallinckrodt and S. P. Morgan, Proc. IRE **40**, 902 (1952).

[7] S. P. Morgan, Bell Syst. Tech. J. **31**, 883, 1121 (1952).

[8] E. F. Vaage, Bell Syst. Tech. J. **32**, 695 (1953).

[9] Usp. Fiz. Nauk **49**, 325 (1953).

[10] T. Sakurai, J. Phys. Soc. Japan **5**, 389 (1950).

directions of propagation and for different polarizations. As is shown below, for sufficiently long waves the effective properties of the medium are especially simple. That is, the inhomogeneous isotropic medium under consideration then behaves, with respect to the average field, like a homogeneous but anisotropic medium, i.e., the effective permeabilities ϵ^e, μ^e are singly degenerate tensors. This limiting transition to sufficiently small d/λ is analogous to the transition from x-rays to ultraviolet and longer waves in the case of crystals. The possibility of artificially constructing anisotropic materials of the indicated type and of varying their electromagnetic properties is likely to be of greater interest for "optical" centimeter waves than is their application merely to the decrease of losses in transmission lines.

From the symmetry of the problem, it is clearly sufficient to consider three cases of wave propagation: propagation in a direction parallel to the layers, for two polarizations (with either the electric or the magnetic vector parallel to the layers), and propagation in a direction perpendicular to the layers.

We take the z axis of a rectangular coordinate system perpendicular to the layers. The intensities of the true (quasi-microscopic) field in the material of the layers we will represent with $\mathbf{e}$ and $\mathbf{h}$, the average over a period d, by a line above.

PROPAGATION ALONG THE x AXIS; e DIRECTED ALONG THE y AXIS

In this case we have the following equation for the nonvanishing components $e_y = e$, h_x, and h_z of the quasi-microscopic field (Fig. 1):

$$\frac{\partial e}{\partial z} = ik\mu h_x, \qquad \frac{\partial e}{\partial x} = -ik\mu h_z, \quad \frac{\partial h_x}{\partial z} - \frac{\partial h_z}{\partial x} = ik\varepsilon e, \tag{2}$$

where the permeabilities ϵ, μ are periodic functions of z, taking alternately the values ϵ_1, μ_1 and ϵ_2, μ_2. We seek a solution, periodic in z with period d, in the form

$$e = U(z)\,e^{-iknx}, \qquad h_x = V(z)\,e^{-iknx}, \qquad h_z = W(z)\,e^{-iknx}. \tag{3}$$

Substitution in Eq. (2) gives

$$\frac{dU}{dz} = ik\mu W, \qquad nU = \mu W, \qquad \frac{dV}{dz} + iknW = ik\varepsilon U. \tag{4}$$

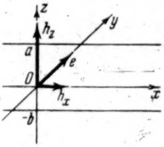

FIG. 1.

If ϵ and μ were continuous functions of z, then it would be possible immediately to apply to the ordinary Eq. (4), in the case of small d in which we are interested, the theorem of Fatou[11] on the approximate solution of an equation with rapidly oscillating periodic coefficients. Since in our problem the conditions of Fatou's theorem are not satisfied, and also to avoid premature commitment to the case of small d, we will start from the exact solution of Eqs. (4):

$$U = A\cos\alpha_1 z + B\sin\alpha_1 z, \qquad z \subset a,$$

$$V = -\frac{\alpha_1}{ik\mu_1}(A\sin\alpha_1 z - B\cos\alpha_1 z),$$

$$\alpha_1 = k\sqrt{n_1^2 - n^2}, \tag{5}$$

$$W = \frac{n}{\mu_1}(A\cos\alpha_1 z + B\sin\alpha_1 z), \qquad n_1^2 = \varepsilon_1\mu_1,$$

$$U = C\cos\alpha_2 z + D\sin\alpha_2 z, \qquad z \subset b,$$

$$V = -\frac{\alpha_2}{ik\mu_2}(C\sin\alpha_2 z - D\cos\alpha_2 z),$$

$$\alpha_2 = k\sqrt{n_2^2 - n^2},$$

$$W = \frac{n}{\mu_2}(C\cos\alpha_2 z + D\sin\alpha_2 z), \qquad n_2^2 = \varepsilon_2\mu_2.$$

On this solution must be imposed four conditions of continuity and periodicity of e and h_x (i.e., U and V) with respect to z:

$$U(+0) = U(-0), \qquad U(a-0) = U(-b+0), \tag{6}$$

$$V(+0) = V(-0), \qquad V(a-0) = V(-b+0).$$

On substituting Eq. (5) in Eq. (6), we get for A, B, C and D the four homogeneous equations

$$C = A, \qquad C\cos\alpha_2 b - D\sin\alpha_2 b = A\cos\alpha_1 a + B\sin\alpha_1 a, \tag{7}$$

$$D = \varkappa B, \qquad C\sin\alpha_2 b + D\cos\alpha_2 b = -\varkappa(A\sin\alpha_1 a - B\cos\alpha_1 a),$$

where

$$\varkappa = \mu_2\alpha_1/\mu_1\alpha_2. \tag{8}$$

---

[11] P. Fatou, Bull. de la Soc. math. de France 57, 98 (1928); L. Boltzmann, Wiss. Abh. I, 43 (1909).

On equating to zero the determinant of the system of equations (7), we get the following dispersion equation, determining n as a function of k:

$$(1+\varkappa^2)\sin\alpha_1 a\sin\alpha_2 b + 2\varkappa(1-\cos\alpha_1 a\cos\alpha_2 b)=0. \tag{9}$$

By solving this equation for κ, it is not difficult to reduce it to the following combination of two equations:

$$\frac{\operatorname{tg}\frac{\alpha_2 b}{2}}{\operatorname{tg}\frac{\alpha_1 a}{2}}=\begin{cases}-\varkappa,\\ -1/\varkappa.\end{cases} \tag{10}$$

With the aid of (5) we compute the mean values, over the period d, of U, V and W. If in addition we use the values of the ratios $A{:}B{:}C{:}D$ from (7), and the expression (8), we get the following expressions for the ratios of $\overline{U}$ and $\overline{V}$ to $\overline{W}$:

$$\frac{\overline{U}}{\overline{W}}=\frac{\overline{e}}{\overline{h}_z}=\frac{\mu_1\alpha_2^2-\mu_2\alpha_1^2}{n(\alpha_2^2-\alpha_1^2)}, \tag{11}$$

$$\frac{\overline{V}}{\overline{W}}=\frac{\overline{h}_x}{\overline{h}_z}=\frac{(1/\mu_1)-(1/\mu_2)}{k^2[(1/\alpha_1^2)-(1/\alpha_2^2)]}P,$$

where

$$P=\frac{U(a-0)-U(+0)}{V(a-0)-V(+0)} \tag{12}$$

$$=-\frac{ik\mu_1}{\alpha_1}\frac{1}{\operatorname{tg}(\alpha_2 b/2)}\frac{\varkappa\operatorname{tg}(\alpha_1 a/2)+\operatorname{tg}(\alpha_2 b/2)}{\varkappa\operatorname{tg}(\alpha_2 b/2)+\operatorname{tg}(\alpha_1 a/2)}.$$

According to Eq. (10), P is either zero [if the roots of the top equation (10) are taken for n] or infinite (for the roots of the botton equation).

In the first case the structure of the quasi-microscopic field is this: e and h_z are distributed in each layer symmetrically about its middle, i.e., they are even functions of $z - a/2$ in layer I and of $z + b/2$ in layer II. The longitudinal component h_x, however, is odd, so that the mean field is a transverse wave ($\overline{h}_x = 0$) with intensities $\overline{e}$ and $\overline{h}_z$.

In the second case the picture is the direct opposite: h_x is even, e and h_z odd with respect to the middles of the layers; consequently, the mean field has only the component $\overline{h}_x$. It is easy to see, however, that this case is not compatible with the condition of slow change of the mean field over distances of order d. For the space between the middles of the two layers, e.g., between $-b/2$ and $a/2$, can be regarded as bounded by perfectly conducting planes, since on them $e = h_z = 0$. But in such cracks of thickness $d/2$, for arbitrary permeabilities ϵ_1, μ_1 and ϵ_2, μ_2 of the "packings" between the perfectly conducting walls, the whole wave with $\lambda > d/2$ will be extinguished in the x direction in distances at most of order $d/2\pi$. Thus for the mean field in a stratum of the medium, the second case never satisfies condition (1) and therefore is of no interest.

In the first case, in order that the mean field intensities $E_y = \overline{U}e^{-iknx}$ and $H_z = \overline{W}e^{-iknx}$ may satisfy Maxwell's equations

$$\frac{\partial E_y}{\partial x}=-ik\mu^e H_z,\quad \frac{\partial H_z}{\partial x}=-ik\varepsilon^e E_y, \tag{13}$$

it is necessary to define the effective permeabilities ϵ^e and μ^e by the equations

$$n=\sqrt{\varepsilon^e\mu^e},\ \frac{E_y}{H_z}=\sqrt{\frac{\mu^e}{\varepsilon^e}}=\frac{\overline{U}}{\overline{W}}.$$

Hence, using (11), we get

$$\varepsilon^e=n^2\frac{\alpha_2^2-\alpha_1^2}{\mu_1\alpha_2^2-\mu_2\alpha_1^2},\quad \mu^e=\frac{\mu_1\alpha_2^2-\mu_2\alpha_1^2}{\alpha_2^2-\alpha_1^2}, \tag{14}$$

where n is the root of the upper equation (10), i.e., of the equation

$$\frac{\alpha_2}{\mu_2}\operatorname{tg}\frac{\alpha_2 b}{2}=-\frac{\alpha_1}{\mu_1}\operatorname{tg}\frac{\alpha_1 a}{2}. \tag{15}$$

PROPAGATION ALONG THE x AXIS; **h** DIRECTED ALONG THE y AXIS

The equations for the quasi-microscopic field, which in this case has components e_x, e_z and $h_y = h$ (Fig. 2), are as follows:

$$\frac{\partial h}{\partial z}=-ik\varepsilon e_x,\quad \frac{\partial h}{\partial x}=-ik\varepsilon e_z,$$

$$\frac{\partial e_x}{\partial z}-\frac{\partial e_z}{\partial x}=-ik\mu h,$$

and the conditions of continuity and periodicity at the boundaries between the layers are imposed on h and e_x. Evidently all the formulas relating to the present case can be obtained directly from the formulas of the preceding paragraph by changing **h**, **e**, ϵ, μ to **e**, -**h**, μ, ϵ, respectively. Here also there are two possible structures of the quasi-microscopic field. One of these does not give a mean field satisfying condition (1), since the corresponding microfield is rapidly extinguished in equivalent slots between the middles of the layers. Here these middle planes can be regarded as surfaces of an ideal magnet, for on them $h = e_z = 0$. The other structure of the microfield leads to a mean field that forms a transverse wave with intensities $E_z = \overline{e}_z$ and $H_y = \overline{h}$. This mean field satisfies Maxwell's equations:

$$\frac{\partial H_y}{\partial x} = ik\varepsilon^e E_z, \quad \frac{\partial E_z}{\partial x} = ik\mu^e H_y, \tag{16}$$

where ϵ^e and μ^e are given by the formulas

$$\varepsilon^e = \frac{\varepsilon_1\alpha_2^2 - \varepsilon_2\alpha_1^2}{\alpha_2^2 - \alpha_1^2}, \quad \mu^e = n^2 \frac{\alpha_2^2 - \alpha_1^2}{\varepsilon_1\alpha_2^2 - \varepsilon_2\alpha_1^2}, \tag{17}$$

obtained from (14) by the change indicated above. Eq. (15), correspondingly changed, determines the value of n:

$$\frac{\alpha_2}{\varepsilon_2}\,\mathrm{tg}\,\frac{\alpha_2 b}{2} = -\frac{\alpha_1}{\varepsilon_1}\,\mathrm{tg}\,\frac{\alpha_1 a}{2}. \tag{18}$$

The transcendental equations (15) and (18) in the general case do not permit expression of n in explicit form in terms of the parameters of the problem. Therefore, condition (1), for the slowness of change of the mean field, is also incapable of exhibition in a more explicit form. It must be emphasized, however, that in the two cases considered (propagation along the layers) condition (1) does not necessarily imply that the changes of the quasi-microscopic field across the thickness of the layers are small. The correctness of Eqs. (14), (15) and (17), (18) is by no means connected with this last, more severe condition. To clarify this remark, we apply these formulas to the case considered in reference 3, in which layers of iron (thickness a, $\epsilon_1 = -i4\pi\sigma/\omega$, $n_1^2 = -2i/k^2\delta^2$, where σ is the conductivity and δ is the skin depth) alternate with layers of an ideal dielectric (thickness b, $\mu_2 = 1$, $\epsilon_2 = n_2^2$).

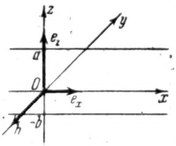

FIG. 2.

If the vector **e** is parallel to the layers [formulas (14) and (15)], then propagation along the layers is impossible, i.e., the microfield, and consequently also the mean field, dies out along x in a distance of order d. For, taking into account that a and $b \gg \delta$, and assuming in advance that $|n| \ll |n_1|$, we have

$$\frac{\alpha_1 a}{2} = \frac{ka}{2}\sqrt{n_1^2 - n^2} \approx \frac{ka}{2}n_1 = \frac{a}{\delta}\sqrt{-\frac{i}{2}},$$

so that

$$\mathrm{tg}\,\frac{\alpha_1 a}{2} \approx -i. \tag{19}$$

Then from (15)

$$\mathrm{tg}\,\frac{\alpha_2 b}{2} \approx \frac{\sqrt{2i}}{\mu_1\alpha_2\delta},$$

from which it is clear that $\alpha_2 b$ differs from π by a quantity of order $\mu_1\delta/b$. Neglecting this correction, we set $\alpha_2 b = \pi$, i.e.,

$$\alpha_2 = k\sqrt{n_2^2 - n^2} = \pi / b,$$

and since $n_2^2 = \epsilon_2 \ll \pi^2/k^2b^2$,

$$n \approx -i\pi / kb.$$

Thus the propagation factor has the form $\exp\{-iknx\} = \exp\{-\pi x/b\}$, and condition (1) is not satisfied.

If, however, the vector **h** is parallel to the layers [formulas (17) and (18)], then, using (19), we get from (18)

$$\mathrm{tg}\,\frac{\alpha_2 b}{2} \approx -\frac{k^2\varepsilon_2\mu_1\delta}{\alpha_2\sqrt{2i}},$$

from which it is evident that $|\alpha_2 b|$ is very small. Therefore, replacing the tangent by its argument, we find

$$\alpha_2^2 = k^2(\varepsilon_2 - n^2) = -\frac{2k^2\varepsilon_2\mu_1\delta}{b\sqrt{2i}},$$

whence

$$n^2 \approx \varepsilon_2\left(1 + \frac{2\mu_1\delta}{b\sqrt{2i}}\right).$$

That is, the mean index of refraction is close to the index of refraction of the dielectric layers, and the extinction of the mean field in the x direction proceeds very slowly (over distances of order $2b/\mu_1\sqrt{\epsilon_2}\,k\delta$), despite the rapid change of the microfield over the thickness of the layers ($\delta \ll a$). Using the expression already written for α_2^2 and n^2 and the expression $\alpha_1^2 = -2i/\delta^2$, we get from (17)

$$\varepsilon^e = \varepsilon_2\left(1 + \frac{2\delta}{b\sqrt{2i}}\right), \quad \mu^e = \frac{\mu_1 + (1+i)(b/2\delta)}{1 + (1+i)(b/2\delta)}.$$

This expression for the effective magnetic permeability agrees with that obtained in reference 3 [Eq. (14)].

We now derive formulas that hold in the case of sufficiently long waves, for which $|\alpha_1 a|$ and $|\alpha_2 b| \ll 1$. Replacing the tangents by their arguments in (15) and (18), we get from (15) and (14)

$$n = \sqrt{\varepsilon^e \mu^e}, \quad \varepsilon^e = \bar{\varepsilon}, \quad \mu^e = \tilde{\mu}, \tag{20}$$

where

$$\bar{\varepsilon} = \frac{a\varepsilon_1 + b\varepsilon_2}{a+b}, \quad \frac{1}{\tilde{\mu}} = \overline{\frac{1}{\mu}} = \frac{(a/\mu_1) + (b/\mu_2)}{a+b}, \tag{21}$$

and from (18) and (17):

$$n = \sqrt{\varepsilon^e \mu^e}, \quad \varepsilon^e = \tilde{\varepsilon}, \quad \mu^e = \bar{\mu}, \tag{22}$$

where

$$\frac{1}{\tilde{\varepsilon}} = \overline{\frac{1}{\varepsilon}} = \frac{(a/\varepsilon_1) + (b/\varepsilon_2)}{a+b}, \quad \bar{\mu} = \frac{a\mu_1 + b\mu_2}{a+b}. \tag{23}$$

A more precise evaluation--with account taken of cubic terms in the expansion of the tangents in (15) and (18)--shows that the correction terms in the effective permeabilities are of order $k^2 d^2$. For example, the expressions for ϵ^e and μ^e in the case of **e** parallel to the layers, with the indicated correction, are

$$\varepsilon^e = \bar{\varepsilon}\left[1 + \frac{k^2 a^2 b^2}{12 d^2} \frac{\bar{\mu}\tilde{\mu}}{\mu_1 \mu_2}(n_1^2 - n_2^2)\frac{\varepsilon_1 - \varepsilon_2}{\bar{\varepsilon}}\right], \tag{24}$$

$$\mu^e = \tilde{\mu}\left[1 + \frac{k^2 a^2 b^2}{12 d^2} \frac{\bar{\mu}\tilde{\mu}^2}{\mu_1^2 \mu_2^2}(n_1^2 - n_2^2)(\mu_1 - \mu_2)\right].$$

Replacement of ϵ and μ by μ and ϵ in (24) gives the expressions for ϵ^e and μ^e in the case in which the vector **h** is parallel to the layers.

Formulas (24) are valid provided the correction terms are small; the latter, unlike condition (1), contain differences of parameters describing properties of the layers. Consequently, if the parameters of one of the materials are not vastly different from the parameters of the other, then the applicability of (24) will be subject to less stringent limitations than that of condition (1). A different situation may be encountered in those cases in which the parameters of the two materials are significantly different (in absolute value), as is the case in the example considered of a laminated iron core. Here formulas (24) and analogous formulas for the other polarization will be valid only provided

$$a^2 \ll 6\delta^2,$$

that is, when there is sufficiently small change of the microfield over the thickness of the iron sheets.

PROPAGATION ALONG THE z AXIS

The microfield $e_x = e$, $h_y = h$ (Fig. 3) satisfies the equations

$$\frac{de}{dz} = -ik\mu h, \quad \frac{dh}{dz} = -ik\varepsilon e. \tag{25}$$

With continuous $\epsilon(z)$ and $\mu(z)$, it would be possible to conclude at once, on the basis of Fatou's theorem[11], that for $d \to 0$ the solution of Eqs. (25) would approach the solution of the same equations with average permeabilities $\bar{\epsilon}$ and $\bar{\mu}$*. A rigorous solution shows that this result remains valid also in the case under consideration of discontinuous ϵ and μ. Nevertheless, since we shall be interested in the magnitude of the correction to $\bar{\epsilon}$ and $\bar{\mu}$ in the effective ϵ^e and μ^e, here also we shall carry out an exact elementary calculation, following a method introduced by Levin[4].

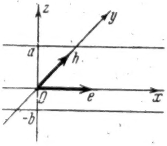

FIG. 3.

According to a theorem of Floquet[12], the solution of Eq. (25) has the form

$$e = U(z)\,e^{-iknz}, \qquad h = V(z)\,e^{-iknz}, \tag{26}$$

where U and V are periodic functions of z with period d. If we integrate Eqs. (25) directly for each of the layers and compare the results with (26), we get

---

* We notice that, on elimination of h (or e) from (25), we get for e (or h) an equation of second order; applied to it, Fatou's theorem gives for the mean index of refraction the value $n^2 = \overline{\epsilon\mu}$, while from (25) it follows that $n^2 = \bar{\epsilon}\bar{\mu}$. This discrepancy is due to the fact that the transformation to a second-order equation is tied up with a differentiation of one of the equations (25); and the derivative of the approximate solution is not equal to the limit for $d \to 0$ of the derivative of the exact solution. Therefore, for getting an approximate e and h, the transformation to a second-order equation is not permissible.

[12] G. Floquet, Ann. École Norm. 12, 47 (1883); Whittaker and Watson, *Modern Analysis* (4th ed., Cambridge, 1940), p. 412.

$$
\begin{aligned}
U &= e^{iknz}\left(Ae^{i\alpha_1 z} + Be^{-i\alpha_1 z}\right), & z &\subset a,\\
V &= -\frac{\alpha_1}{k\mu_1} e^{iknz}\left(Ae^{i\alpha_1 z} - Be^{-i\alpha_1 z}\right), & \alpha_1 &= kn_1 = k\sqrt{\varepsilon_1\mu_1},\\
U &= e^{iknz}\left(Ce^{i\alpha_2 z} + De^{-i\alpha_2 z}\right), & z &\subset b,\\
V &= -\frac{\alpha_2}{k\mu_2} e^{iknz}\left(Ce^{i\alpha_2 z} - De^{-i\alpha_2 z}\right), & \alpha_2 &= kn_2 = k\sqrt{\varepsilon_2\mu_2}.
\end{aligned}
\tag{27}
$$

Imposing on U and V the conditions of continuity and periodicity, which here also take the form (6), we get four homogeneous equations for the constants of integration:

$$
\begin{aligned}
C + D &= A + B,\\
e^{-iknb}\left(Ce^{-i\alpha_2 b} + De^{i\alpha_2 b}\right) &= e^{ikna}\left(Ae^{i\alpha_1 a} + Be^{-i\alpha_1 a}\right),\\
C - D &= \varkappa(A - B),\\
e^{-iknb}\left(Ce^{-i\alpha_2 b} - De^{i\alpha_2 b}\right) &= \varkappa e^{ikna}\left(Ae^{i\alpha_1 a} - Be^{-i\alpha_1 a}\right),
\end{aligned}
\tag{28}
$$

where

$$
\varkappa = \frac{\alpha_1\mu_2}{\alpha_2\mu_1} = \sqrt{\frac{\varepsilon_1\mu_2}{\varepsilon_2\mu_1}}. \tag{29}
$$

Setting the determinant of the system (28) equal to zero gives the dispersion equation, which determines n:

$$
\cos knd = \cos\alpha_1 a \cos\alpha_2 b - \frac{1+\varkappa^2}{2\varkappa}\sin\alpha_1 a \sin\alpha_2 b. \tag{30}
$$

In contrast to the two cases considered earlier, now, when the propagation occurs in the direction perpendicular to the layers, slow change of the mean field is possible only on condition that the microfield also changes only slightly over the thickness of the layers. In other words, condition (1) can be realized only when the waves are so long that $|\alpha_1 a|$ and $|\alpha_2 b| \ll 1$. If, on this assumption, we keep terms of no higher than the first order in k in calculating the mean values over a period, we get for the ratio of $\overline{U}$ to $\overline{V}$.

$$
\frac{\overline{U}}{\overline{V}} = \frac{\overline{e}}{\overline{h}} = \sqrt{\frac{\bar{\bar{\mu}}}{\bar{\bar{\varepsilon}}}}\left[1 + \frac{ikab}{4d}\,\frac{\mu_1\varepsilon_2 - \mu_2\varepsilon_1}{\sqrt{\bar{\bar{\varepsilon}}\bar{\bar{\mu}}}}\right], \tag{31}
$$

where $\overline{\epsilon}$ and $\overline{\mu}$ have the same meaning as in (21) and (23). To the same degree of exactness, n is obtained from Eq. (30) in the form

$$
n = \sqrt{\bar{\bar{\varepsilon}}\bar{\bar{\mu}}}, \tag{32}
$$

that is, the correction to n is of second order in kd (cf. reference 4).

If we require that Maxwell's equations

$$
\frac{\partial E_x}{\partial z} = -ik\mu^e H_y, \quad \frac{\partial H_y}{\partial z} = -ik\varepsilon^e E_x, \tag{33}
$$

shall hold for the mean fields $E_x = \overline{e}$ and $H_y = \overline{h}$, we must determine ϵ^e and μ^e from the conditions

$$
n = \sqrt{\varepsilon^e\mu^e}, \quad \frac{E_x}{H_y} = \sqrt{\frac{\mu^e}{\varepsilon^e}} = \frac{\overline{U}}{\overline{V}},
$$

whence

$$
\varepsilon^e = n\overline{V}/\overline{U}, \qquad \mu^e = n\overline{U}/\overline{V}.
$$

Substituting here (31) and (32), we get

$$
\begin{aligned}
\varepsilon^e &= \bar{\varepsilon}\left[1 - \frac{ikab}{4d}\,\frac{\mu_1\varepsilon_2 - \mu_2\varepsilon_1}{\sqrt{\bar{\bar{\varepsilon}}\bar{\bar{\mu}}}}\right],\\
\mu^e &= \bar{\mu}\left[1 + \frac{ikab}{4d}\,\frac{\mu_1\varepsilon_2 - \mu_2\varepsilon_1}{\sqrt{\bar{\bar{\varepsilon}}\bar{\bar{\mu}}}}\right].
\end{aligned}
\tag{34}
$$

The validity of Fatou's theorem is evident from this: with diminution of kd we arrive at the simple mean of the coefficients in Eqs. (25), i.e.,

$$
\varepsilon^e = \bar{\varepsilon}, \qquad \mu^e = \bar{\mu}. \tag{35}
$$

THE CASE OF LONG WAVES

Let kd be so small that the correction terms can be neglected both in (24) and in (34). The corresponding conditions take the following form, if we introduce the notation

$$
\frac{\bar{\varepsilon}\tilde{\varepsilon}}{\varepsilon_1\varepsilon_2} = \frac{a\varepsilon_1 + b\varepsilon_2}{a\varepsilon_2 + b\varepsilon_1} = P, \qquad \frac{\bar{\mu}\tilde{\mu}}{\mu_1\mu_2} = \frac{a\mu_1 + b\mu_2}{a\mu_2 + b\mu_1} = Q,
$$

$$
kab/d = R. \tag{36}
$$

For propagation along the layers with *e* parallel to the layers:

$$\frac{R^2}{12}\left|Q\,(n_1^2-n_2^2)\,\frac{\varepsilon_1-\varepsilon_2}{\bar{\varepsilon}}\right|\ll 1, \qquad (37a)$$

$$\frac{R^2}{12}\left|Q^2\,(n_1^2-n_2^2)\,\frac{\mu_1-\mu_2}{\bar{\mu}}\right|\ll 1 \,.$$

For propagation along the layers with *h* parallel to the layers:

$$\frac{R^2}{12}\left|P^2\,(n_1^2-n_2^2)\,\frac{\varepsilon_1-\varepsilon_2}{\bar{\varepsilon}}\right|\ll 1, \qquad (37b)$$

$$\frac{R^2}{12}\left|P\,(n_1^2-n_2^2)\,\frac{\mu_1-\mu_2}{\bar{\mu}}\right|\ll 1.$$

For propagation perpendicular to the layers:

$$\frac{R}{4}\left|\frac{\mu_1\varepsilon_2-\mu_2\varepsilon_1}{\sqrt{\bar{\varepsilon}\bar{\mu}}}\right|\ll 1. \qquad (37c)$$

If, in particular, $a = b = d/2$, then $P = Q = 1$, $R = kd/4$, and conditions (37 a, b, c) take the quite simple form

$$\frac{k^2d^2}{96}\left|(n_1^2-n_2^2)\,\frac{\varepsilon_1-\varepsilon_2}{\varepsilon_1+\varepsilon_2}\right|\ll 1, \qquad \frac{k^2d^2}{96}\left|(n_1^2-n_2^2)\,\frac{\mu_1-\mu_2}{\mu_1+\mu_2}\right|\ll 1, \qquad (38)$$

$$\frac{kd}{8}\left|\frac{\mu_1\varepsilon_2-\mu_2\varepsilon_1}{\sqrt{(\varepsilon_1+\varepsilon_2)(\mu_1+\mu_2)}}\right|\ll 1.$$

In this special case it is particularly clear that satisfaction of these inequalities still does not imply satisfaction of condition (1), which for the directions of propagation and of polarization considered takes the form:

$$kd\left|\sqrt{\frac{\mu_1\mu_2(\varepsilon_1+\varepsilon_2)}{\mu_1+\mu_2}}\right|\ll 1, \qquad (39)$$

$$kd\left|\sqrt{\frac{\varepsilon_2\varepsilon_2(\mu_1+\mu_2)}{\varepsilon_1+\varepsilon_2}}\right|\ll 1,$$

$$\frac{kd}{2}\left|\sqrt{(\varepsilon_1+\varepsilon_2)(\mu_1+\mu_2)}\right|\ll 1.$$

Considering conditions (37 a, b, c) satisfied and gathering together Eqs. (13), (16), (20), (22), (33) and (35), we get

$$\frac{\partial E_y}{\partial x}=-ik\tilde{\mu}H_z, \qquad \frac{\partial H_z}{\partial x}=-ik\bar{\varepsilon}E_y,$$

$$\frac{\partial H_y}{\partial x}=ik\tilde{\varepsilon}E_z, \qquad \frac{\partial E_z}{\partial x}=ik\bar{\mu}H_y,$$

$$\frac{\partial E_x}{\partial z}=-ik\bar{\mu}H_y, \qquad \frac{\partial H_y}{\partial z}=-ik\bar{\varepsilon}E_x.$$

It is not difficult to see that these equations belong to the general system of Maxwellian equations for a medium whose permeabilities are described by singly degenerate tensors with coincident principal axes and with principal values

$$\varepsilon_1^e=\varepsilon_2^e=\bar{\varepsilon}=\frac{a\varepsilon_1+b\varepsilon_2}{a+b}, \qquad \varepsilon_3^e=\tilde{\varepsilon}=\frac{\varepsilon_1\varepsilon_2(a+b)}{a\varepsilon_2+b\varepsilon_1},$$

$$\mu_1^e=\mu_2^e=\bar{\mu}=\frac{a\mu_1+b\mu_2}{a+b}, \qquad \mu_3^e=\tilde{\mu}=\frac{\mu_1\mu_2(a+b)}{a\mu_2+b\mu_1}. \qquad (40)$$

Thus in its "optical" range, the medium under consideration has the properties of a uniaxial crystal with optic axis perpendicular to the layers, and with normal surface consisting (for real ϵ_1, μ_1, ϵ_2, μ_2) of two ellipsoids of revolution (Fig. 4).

From the expressions (40) it is clear that, depending on the relations between the layer thicknesses *a* and *b* and the absolute values of the permeabilities, there are possible very different combinations of values of the effective permeabilities and, correspondingly, different degrees of anisotropy, dichroism, etc.

We shall express ϵ and μ in terms of the real permeabilities ϵ', μ' and the tangents of the loss angles

$$\varepsilon_k=\varepsilon_k'(1-i\,\mathrm{tg}\,\delta_k), \quad \mu_k=\mu_k'(1-i\,\mathrm{tg}\,\gamma_k) \quad (k=1,2),$$

$$\bar{\varepsilon}=\bar{\varepsilon}'\,(1-i\,\mathrm{tg}\,\bar{\delta}), \quad \bar{\mu}=\bar{\mu}'\,(1-i\,\mathrm{tg}\,\bar{\gamma}), \qquad (41)$$

$$\tilde{\varepsilon}=\tilde{\varepsilon}'\,(1-i\,\mathrm{tg}\,\tilde{\delta}), \quad \tilde{\mu}=\tilde{\mu}'\,(1-i\,\mathrm{tg}\,\tilde{\gamma}).$$

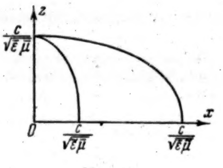

z
$\frac{c}{\sqrt{\bar{\varepsilon}\bar{\mu}}}$
x
0
$\frac{c}{\sqrt{\tilde{\varepsilon}\bar{\mu}}}$
$\frac{c}{\sqrt{\bar{\varepsilon}\bar{\mu}}}$

FIG. 4.

Neglecting squares and products of the tangents of the loss angles, we get from (40) and (41)

$$\bar{\varepsilon}' = \frac{a\varepsilon_1' + t\varepsilon_2'}{a+\beta}, \quad \operatorname{tg}\bar{\delta} = \frac{a\varepsilon_1' \operatorname{tg}\delta_1 + b\varepsilon_2' \operatorname{tg}\delta_2}{a\varepsilon_1' + b\varepsilon_2'}, \qquad (42)$$

$$\tilde{\varepsilon}' = \frac{\varepsilon_1' \varepsilon_2' (a+b)}{a\varepsilon_2' + l\varepsilon_1'}, \quad \operatorname{tg}\tilde{\delta} = \frac{a\varepsilon_2' \operatorname{tg}\delta_1 + b\varepsilon_1' \operatorname{tg}\delta_2}{a\varepsilon_2' + b\varepsilon_1'}$$

and analogous formulas for the magnetic quantities.

Figure 5 illustrates the behavior of $\bar{\epsilon}'$ and $\tilde{\epsilon}'$ as functions of a. On the graph is indicated the value corresponding to the maximum value of the difference $\bar{\epsilon}' - \tilde{\epsilon}'$, and this latter value itself is given. In Fig. 6 the dependence on a is shown for $\operatorname{tg}\bar{\delta}$ and $\operatorname{tg}\tilde{\delta}$, on the assumption $\epsilon_1' > \epsilon_2'$, for the cases $\operatorname{tg}\delta_2 > \operatorname{tg}\delta_1$ (solid curve) and $\operatorname{tg}\delta_2 < \operatorname{tg}\delta_1$ (dotted curve).

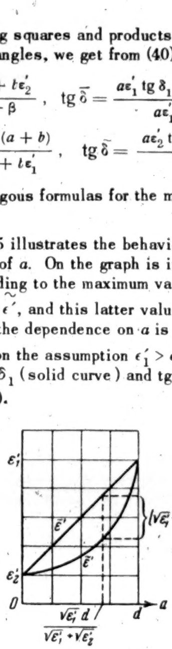

FIG. 5.

To the same degree of approximation as in formulas (42), the following expressions are obtained for the principal indexes of refraction, which we write in the usual form $\sqrt{\epsilon^e \mu^e} = n(1-i\kappa)$. With propagation along the optic axis (the z axis),

$$n = \sqrt{\bar{\varepsilon}'\bar{\mu}'}, \quad \varkappa = \frac{\operatorname{tg}\bar{\delta} + \operatorname{tg}\bar{\gamma}}{2}. \qquad (43a)$$

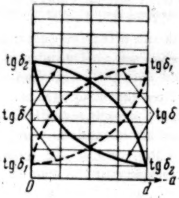

FIG. 6.

With propagation perpendicular to the optic axis: for the ordinary ray (**E** parallel to the layers),

$$n = \sqrt{\tilde{\varepsilon}'\bar{\mu}'}, \quad \varkappa = {}^1/_2(\operatorname{tg}\bar{\delta} + \operatorname{tg}\tilde{\gamma}); \qquad (43b)$$

for the extraordinary ray (**E** perpendicular to the layers),

$$n = \sqrt{\tilde{\varepsilon}'\bar{\mu}'}, \quad \varkappa = {}^1/_2(\operatorname{tg}\tilde{\delta} + \operatorname{tg}\bar{\gamma}). \qquad (43c)$$

For illustration we give a numerical example. We suppose that layers of a ceramic or titanate alternate with layers of paraffin. For wavelength $\lambda = 6$ cm we have

Titanate: $\epsilon_1' = 200$; $\operatorname{tg}\delta_1 = 0.006$;

Paraffin: $\epsilon_2' = 2.25$; $\operatorname{tg}\delta_2 = 0.0002$.

Let $a = b = d/2$*. Then the third (most stringent) of the conditions (38) gives

$$kd \ll 0.58, \text{ i.e., } d \ll 0.55 \text{ cm}.$$

Thus when $d = 1$ mm, formula (40) may be considered valid. From (42) we get

$$\bar{\varepsilon}' = 101, \quad \operatorname{tg}\bar{\delta} = 0.006,$$
$$\tilde{\varepsilon}' = 4.5, \quad \operatorname{tg}\tilde{\delta} = 0.0026.$$

From this it follows that for the ordinary wave the index of refraction (uniform in all directions for a magnetically isotropic medium) is $n = 10$, and $\kappa = 0.003$; i.e., the ordinary wave decays by a factor e in a distance $1/k\kappa n = 32$ cm. For the extraordinary wave, the second principal index of refraction is $n = 2.1$, and $\kappa = 0.0013$, which gives $1/k\kappa n = 347$ cm.

---

* The maximum anisotropy would correspond to $a = 0.87\,d$.

Obviously, in the range of values of the parameters in which Maxwell's equations hold for the mean field, with the effective permeabilities (21) and (23), the losses per unit volume of the medium can be calculated with the usual formula, derived directly from the averaged equations. But if conditions (37 a, b, c) are not satisfied, then the relations between means and mean squares become complicated, and the value of the losses can be found only by averaging of the true expressions for the heat generated, as is done in particular in reference 3. Equations (5) and (27) for the amplitudes of the quasi-microscopic fields make possible the carrying through of this type of calculation.

BOUNDARY CONDITIONS

When conditions (37) are satisfied, the stratified medium obeys Maxwell's equations with the tensor permeabilities ϵ^e and μ^e [cf. Eq. (40)]. In this case the boundary conditions, on a surface arbitrarily oriented with respect to the optic axis, can be obtained from Maxwell's equations themselves by the usual passage to a limit; they consist, as always, in continuity of the tangential components of the intensities **E** and **H** and of the normal components of the inductions **D** and **B**. If we represent by subscripts *e* and *i* the external and internal mean fields, and by **n** the unit vector normal to the boundary surface, we get

$$[\mathbf{n}, \mathbf{E}_e] = [\mathbf{n}, \mathbf{E}_i], \quad [\mathbf{n}, \mathbf{H}_e] = [\mathbf{n}, \mathbf{H}_i],$$
$$(\mathbf{n}, \mathbf{D}_e) = (\mathbf{n}, \mathbf{D}_i), \quad (\mathbf{n}, \mathbf{B}_e) = (\mathbf{n}, \mathbf{B}_i),$$

where $\mathbf{D}_i$ and $\mathbf{B}_i$ are related to $\mathbf{E}_i$ and $\mathbf{H}_i$ by the tensors ϵ^e and μ^e:

$$\mathbf{D}_i = \varepsilon^e \mathbf{E}_i, \quad \mathbf{B}_i = \mu^e \mathbf{H}_i.$$

In connection with these conditions, the following doubt may arise. The fields $\mathbf{E}_i$ and $\mathbf{H}_i$ inside the medium were obtained by averaging not all solutions of the equation for the microfield, but only those that lead to a transverse wave. The basis for rejecting the other solutions [for example, those corresponding to the lower Eq. (10)], for **e** parallel to the layers, was that they decay rapidly, in distances of the order of a period of the structure. But in the problem of boundary conditions, when theorems about flux or circulation are applied to a surface or contour arbitrarily close to the boundary surface, the argument mentioned loses its force, and there is no justification for asserting in advance that these decaying fields will not enter into the boundary conditions. That they actually do not enter can be shown as follows.

Any component of induction or of intensity of the microfield, either on the outside or on the inside face of the boundary, must be approximately periodic along the boundary, with the period of the structure on it. Let the boundary be a plane containing the y axis and inclined to a layer at angle φ (Fig. 7). Then along the boundary, i.e., along the η axis, the period will be equal to $d' = d/\sin\varphi$. Thus the component of induction or intensity under consideration, for example e_y, can be expanded in a Fourier series in coordinate η with period d'; the coefficients also vary as functions of η, but slowly - with a period $\gg\lambda$:

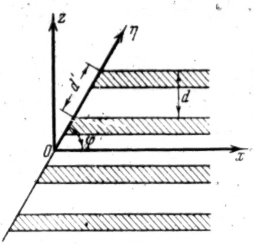

FIG. 7.

$$e_y = a_0 + a_1 \cos\frac{2\pi\eta}{d'} + \ldots + b_1 \sin\frac{2\pi\eta}{d'} + \ldots$$

If d' is small, not only in comparison with λ, but also in comparison with the shortest wavelength in the medium, i.e.,

$$d' = \frac{d}{\sin\varphi} \ll \frac{\lambda}{|n|_{\max}}, \quad \text{or} \quad kd\,|n|_{\max} \ll \sin\varphi, \tag{45}$$

then averaging over the period d' gives

$$\overline{e}_y = E_y = a_0 + O\left(\frac{d'}{\lambda}\right),$$

that is, upon such averaging of the boundary conditions for the microfield, all rapidly oscillating terms practically drop out. However, decaying fields are excited in the medium, thanks to these same rapidly oscillating terms in the resolution of the field on the boundary. In the outside region this is immediately obvious, since there we have an ordinary homogeneous medium. As for the inside region, if condition (37) is satisfied it likewise behaves like a homogeneous (though anisotropic) medium; and for $d' < \lambda/|n|_{\max}$ the boundary field, oscillating with period d', creates decaying waves in it also.

This reasoning and condition (45) show, together with this, that the case of small φ is actually peculiar. In this case, i.e., when $kd|n|_{\max} \geq \sin\varphi$, the periodic structure on the boundary represents a coarse "grating", giving not only decaying waves, but diffracted waves that propagate (in the reflected field outside the medium, such waves appear only when $kd \geq \sin\varphi$). As φ decreases, the angles of diffraction, counted from the maxima of order zero (which correspond to regular reflection and refraction), will decrease; and in the limit for $\varphi = 0$ (boundary parallel to a layer), such secondary waves will again not exist. Thus the averaged boundary conditions (44) are useful when condition (45) is satisfied, i.e, when the cut is not too oblique. Practically, such oblique cuts are of scarcely any interest.

I take this occasion to thank Academician M. A. Leontovich for the interest he showed in this work, and for discussion of a number of problems.

Translated by W. F. Brown, Jr.
244

SOVIET PHYSICS JETP VOLUME 2, NUMBER 3 MAY, 1956

Fock Self-Consistent Field for the Boron Atom in the Two-Configuration Approximation

I. I. GLEMBOTSKII, V. V. KIBARTAS AND A. P. IUTSIS
Physico-Technical Institute, Academy of Sciences (Lithuanian) SSR
Vilna State University

(Submitted to JETP editor July 12, 1954)
J. Exper. Theoret. Phys. USSR **29**, 617-621 (November, 1955)

Solutions are presented of the ordinary Fock equations for the ground configuration of the neutral boron atom, and of the Hartree equation, supplemented by configuration interaction terms, for the function $P(2p|r)$ of the configuration $1s^2 2p^3$, whose effect is included in the two-configuration approximation $1s^2 2s^2 2p - 1s^2 2p^3$. Values are also given for the total energy as determined in both the one-configuration and two-configuration approximations. The total potential function and the radial probability distribution are tabulated.

1. INTRODUCTION

REFERENCE 1 showed that the solution of the Fock self-consistent field equations is practically feasible in the two-configuration approximation[2]. Further study of the problem[3] led to the conclusion that if, instead of solving the exact Fock equations in the two-configuration approximation, one uses solutions of the corresponding simplified Fock equations, the result is hardly changed while the computational labor is reduced considerably. This simplification consists in solving the ordinary Fock equations for the configuration under investigation and, in addition to this, solving the Hartree equations supplemented by configuration terms for those radial wave functions of the perturbing configuration whose Fock equations contain configuration terms. In the present paper, we take advantage of this simplification in applying the Fock self-consistent field method in the two-configuration approximation to the ground configuration of the neutral boron atom.

In applying the many-configuration approximation to the ground configuration of the boron atom, the two-configuration approximation $1s^2 2s^2 2p - 1s^2 2p^3$ is of paramount importance. Therefore, in addition to solving the ordinary Fock equations for the ground configuration, one should also solve the Hartree equation, supplemented by configuration terms, for the function $P(2p|r)$ of the perturbing configuration $1s^2 2p^3$. The solutions of these equations and the corresponding values of the total energy are presented in the next section. In Section 3 we shall attempt to determine the effect of the two-configuration approximation on the total potential of the system and on the radial probability distribution of the electrons.

2. SOLUTIONS AND ENERGY VALUES

The ordinary Fock equations for the ground configuration of the boron atom have the following form:

$$\left[\frac{d^2}{dr^2} + \frac{2Z - 2Y_0(1s, 1s|r) - 4Y_0(2s, 2s|r) - 2Y_0(2p, 2p|r)}{r} - \varepsilon_{1s,1s}\right] P(1s|r) + \left[\frac{2Y_0(1s, 2s|r)}{r} - \varepsilon_{1s,2s}\right] P(2s|r) + \frac{1}{3}\frac{Y_1(1s, 2p|r)}{r} P(2p|r) = 0, \tag{2.1 a}$$

$$\left[\frac{d^2}{dr^2} + \frac{2Z - 4Y_0(1s, 1s|r) - 2Y_0(2s, 2s|r) - 2Y_0(2p, 2p|r)}{r} - \varepsilon_{2s,2s}\right] P(2s|r) + \left[\frac{2Y_0(1s, 2s|r)}{r} - \varepsilon_{1s,2s}\right] P(1s|r) + \frac{1}{3}\frac{Y_1(2s, 2p|r)}{r} P(2p|r) = 0, \tag{2.1 b}$$

$$\left[\frac{d^2}{dr^2} + \frac{2Z - 4Y_0(1s, 1s|r) - 4Y_0(2s, 2s|r)}{r} - \frac{2}{r^2} - \varepsilon_{2p,2p}\right] P(2p|r) + \frac{2}{3}\frac{Y_1(1s, 2p|r)}{r} P(1s|r) + \frac{2}{3}\frac{Y_1(2s, 2p|r)}{r} P(2s|r) = 0. \tag{2.1 c}$$

The Hartree equation, supplemented by configuration terms, for the function $P(2p|r)$ of the perturbing configuration $1s^2 2p^3$ of the two-configuration approximation is:

---

[1] V. V. Kibartas and A. P. Iutsis, J. Exper. Theoret. Phys. USSR **25**, 264 (1953)

[2] A. P. Iutsis, J. Exper. Theoret. Phys. USSR **23**, 129 (1952).

[3] A. P. Iutsis, V. V. Kibartas and I. I. Glembotskii, J. Exper. Theoret. Phys. USSR **27**, 425 (1954)

$$\left[\frac{d^2}{dr^2}+\frac{2Z-4Y_0(1s,\,1s\,|\,r)-4Y_0(2p,\,2p\,|\,r)}{r}-\frac{2}{r^2}-\varepsilon_{(2p,\,2p)_{22}}\right]P_2(2p\,|\,r) \tag{2.2}$$

$$-\frac{4\sqrt{2}}{9a_{12}}\,\frac{Y_1(2s,\,2p\,|\,r)_{12}}{r}\,P_1(2s\,|\,r)\,N(2p,\,2p)_{12}=0.$$

TABLE I

Normalized Radial Wave Functions of the Self-consistent Fock Field for the Ground Configuration of the Neutral Boron Atom

r	$P(1s\|r)$	$P(2s\|r)$	$P(2p\|r)$	$P_2(2p\|r)$	r	$P(1s\|r)$	$P(2s\|r)$	$P(2p\|r)$	$P_2(2p\|r)$
0.00	0.0000	0.0000	0.0000	0.0000	1.20	0.1054	−0.6808	0.6068	0.6625
0.01	0.1982	0.0400	0.0003	0.0003	1.25	0.0884	−0.6958	0.6156	0.6742
0.02	0.3771	0.0 60	0.0012	0.0011	1.30	0.0741	−0.7078	0.6230	0.6839
0.03	0.5382	0.1084	0.0027	0.0024	1.35	0.0620	−0.7170	0.6290	0.6918
0.04	0.6831	0.1374	0.0048	0.0042	1.40	0.0519	−0.7236	0.6337	0.6978
0.05	0.8127	0.1631	0.0073	0.0065	1.45	0.0434	−0.7277	0.6372	0.7020
0.06	0.9283	0.1858	0.0102	0.0091	1.50	0.0363	−0.7297	0.6395	0.7046
0.07	1.0311	0.2058	0.0136	0.0120	1.55	0.0303	−0.7297	0.6407	0.7056
0.08	1.1220	0.2231	0.0173	0.0154	1.6	0.0254	−0.7279	0.6410	0.7051
0.09	1.2020	0.2379	0.0214	0.0191	1.7	0.0177	−0.7196	0.6387	0.7000
0.10	1.2720	0.2505	0.0258	0.0231	1.8	0.0124	−0.7061	0.6332	0.6901
0.11	1.3328	0.2610	0.0305	0.0273	1.9	0.0087	−0.6884	0.6251	0.6761
0.12	1.3851	0.2695	0.0355	0.0318	2.0	0.0061	−0.6676	0.6146	0.6587
0.13	1.4297	0.2762	0.0407	0.0366	2.1	0.0042	−0.6443	0.6021	0.6386
0.14	1.4672	0.2811	0.0462	0.0416	2.2	0.0030	−0.6193	0.5882	0.6164
0.15	1.4982	0.2844	0.0519	0.0468	2.3	0.0021	−0.5932	0.5730	0.5925
0.16	1.5232	0.2863	0.0578	0.0522	2.4	0.0015	−0.5664	0.5567	0.5675
0.17	1.5427	0.2868	0.0639	0.0578	2.5	0.0010	−0.5393	0.5398	0.5418
0.18	1.5572	0.2859	0.0 01	0.0636	2.6	0.0007	−0.5122	0.5223	0.5156
0.19	1.5672	0.2839	0.0765	0.0695	2.7	0.0005	−0.4854	0.5044	0.4893
0.20	1.5730	0.2808	0.0830	0.0756	2.8	0.0003	−0.4590	0.4863	0.4633
0.22	1.5738	0.2715	0.0963	0.0881	3.0	0.0002	−0.4084	0.4499	0.4124
0.24	1.5622	0.2588	0.1101	0.1011	3.2	0.0001	−0.3611	0.4140	0.3643
0.26	1.5404	0.2430	0.1242	0.1145	3.4		−0.3176	0.3792	0.3196
0.28	1.5105	0.2246	0.1385	0.1283	3.6		−0.2782	0.3460	0.2787
0.30	1.4741	0.2041	0.1530	0.1424	3.8		−0.2427	0.3146	0.2418
0.32	1.4326	0.1818	0.1676	0.1567	4.0		−0.2109	0.2850	0.2089
0.34	1.3873	0.1581	0.1822	0.1712	4.2		−0.1828	0.2575	0.1798
0.36	1.3391	0.1331	0.1969	0.1859	4.4		−0.1580	0.2321	0.1542
0.38	1.2889	0.1071	0.2116	0.2008	4.6		−0.1362	0.2087	0.1317
0.40	1.2375	0.0805	0.2262	0.2157	4.8		−0.1172	0.1872	0.1121
0.42	1.1854	0.0532	0.2408	0.2306	5.0		−0.1006	0.1676	0.0952
0.44	1.1332	0.0256	0.2552	0.2456	5.2		−0.0862	0.1499	0.0809
0.46	1.0813	−0.0022	0.2694	0.2606	5.4		−0.0738	0.1338	0.0686
0.48	1.0300	−0.0301	0.2835	0.2755	5.6		−0.0631	0.1192	0.0580
0.50	0.9796	−0.0580	0.2974	0.2904	5.8		−0.0538	0.1061	0.0489
0.52	0.9304	−0.0857	0.3111	0.3052	6.0		−0.0459	0.0942	0.0412
0.54	0.8825	−0.1132	0.3245	0.3199	6.5		−0.0307	0.0698	0.0268
0.56	0.8360	−0.1404	0.3377	0.3345	7.0		−0.0204	0.0514	0.0172
0.58	0.7911	−0.1673	0.3507	0.3490	7.5		−0.0136	0.0377	0.0111
0.60	0.7478	−0.1937	0.3634	0.3633	8.0		−0.0092	0.0275	0.0072
0.65	0.6470	−0.2574	0.3940	0.3981	8.5		−0.0061	0.0200	0.0047
0.70	0.5569	−0.3173	0.4228	0.4316	9.0		−0.0040	0.0146	0.0030
0.75	0.4771	−0.3731	0.4497	0.4635	9.5		−0.0027	0.0107	0.0019
0.80	0.4073	−0.4246	0.4746	0.4937	10		−0.0018	0.0078	0.0013
0.85	0.3467	−0.4715	0.4976	0.5220	11		−0.0008	0.0042	0.0005
0.90	0.2943	−0.5139	0.5187	0.5484	12		−0.0004	0.0023	0.0002
0.95	0.2491	−0.5519	0.5379	0.5727	13		−0.0002	0.0012	0.0001
1.00	0.2104	−0.5856	0.5552	0.5948	14		−0.0001	0.0007	
1.05	0.1774	−0.6151	0.5707	0.6149	15			0.0004	
1.10	0.1493	−0.6407	0.5844	0.6329	16			0.0002	
1.15	0.1255	−0.6625	0.5964	0.6488	17			0.0001	

In Eqs. (2.1) and (2.2), Z denotes the nuclear charge, $\epsilon_{nl,n\bar{l}}$ are Lagrange multipliers. The function $Y_k(nl, n\bar{l}\,|\,r)$ is defined as usual. When necessary, indices are attached to this function to indicate the number of the configuration to which the corresponding wave function refers. Since, in our approximation, the function $P(1s\,|\,r)$ is the same in both configurations, the function $Y_0(1s, 1s\,|\,r)$ in Eq. (2.2) is the same as in Eq. (2.1). In (2.2), $P(2p\,|\,r)$ refers to the perturbing configuration except in the case of the quantity $N(2p, 2p)_{12}$ defined in Eq. (3.1) of reference 2. Here one of the functions $P(2p|r)$ refers to the basic configuration (index 1), while the second refers to the perturbing configuration (index 2). The supplementary indices on the Lagrange multiplier in Eq. (2.2) indicate that it refers to configuration 2. The absolute value of the constant a_{12} gives the weight of configuration 2 relative to configuration 1.

In solving Eq. (2.1), we used as initial trial functions the corresponding solutions of the Hartree equation, given in reference 4. The solution was carried up to self-consistency index $\eta = 0.0025$ (cf. Eq. (2.8) of reference 5). To solve Eq. (2.2), the initial function $P_2(2p\,|r)$ was constructed using a hydrogen-like analytic wave function obtained with the aid of the results of references 6 and 7. For the starting value of a_{12} we took the value obtained using analytic wave functions[7], where the constants were determined in the one-configuration approximation. The solution of Eq. (2.2) was carried to a self-consistency index of 0.0050 for $P_2(2p\,|\,r)$ and 0.002 for a_{12}. The normalized solutions are given in Table I. We should point out that the solution of Eq. (2.1) was carried out on the assumption that $\epsilon_{1s,2s} = 0$. The orthogonality of the functions $P(2s|r)$ and $P(1s|r)$ was achieved by direct orthogonalization after each successive solution.

The values of the Lagrange multipliers, the

TABLE II

Values of the Lagrange Multipliers, Radial Integrals, and Energy, for the Ground Configuration of the Boron Atom (in Atomic Units)

$\varepsilon_{1s,\ 1s} = 15.386$	$G_0(1s,\ 2s) = 0{,}0385$
$\varepsilon_{2s,\ 2s} = 0.9903$	$G_1(1s,\ 2p) = 0{,}0430$
$\varepsilon_{2p,\ 2p} = 0.6182$	$G_1(2s,\ 2p) = 0.2728$
$\varepsilon_{(2p,\ 2p)_{22}} = 1.1452$	$F_0(2p,\ 2p)_{22} = 0.4646$
$F_0(1s,\ 1s) = 2.9325$	$F_0(1s,\ 2p)_{22} = 0.6388$
$F_0(2s,\ 2s) = 0.4602$	$G_1(1s,\ 2p)_{22} = 0.0420$
$F_0(1s,\ 2s) = 0{,}6485$	$G_1(2s,\ 2p)_{12} = 0.2978$
$F_0(1s,\ 2p) = 0.5994$	$N(2p,\ 2p)_{12} = 0.9894$
$F_0(2s,\ 2p) = 0.4370$	

	a	b
E_{11}	— 24.562	— 24.562
E_{22}	— 24.045	— 24.003
E_{12}	+ 0.129	+ 0.139
ΔE	— 0.030	— 0.033
a_{12}	— 0.233	— 0.238
E	— 24.592	— 24.595
$E_{\mathbf{exp}}$	— 24.658	

Footnote.- a) on the assumption that $P_2(2p\,|\,r) = P(2p|\,r)$; b) using $P_2(2p\,|r)$ as determined in the two-configuration approximation.

---

[4] G. K. Tsiunaitis and A. P. Iutsis, J. Exper. Theoret. Phys. USSR **28**, 452 (1955); Soviet Phys. **1**, 358 (1955).

[5] A. P. Iutsis and G. K. Tsiunaitis, J. Exper. Theoret. Phys. USSR **23**, 512 (1952).

[6] V. I. Kavetskis and A. P. Iutsis, J. Exper. Theoret. Phys. USSR **25**, 257 (1953).

[7] A. B. Bolotin and A. P. Iutsis, J. Exper. Theoret. Phys. USSR **24**, 537 (1953).

radial integrals, the constant a_{12} and the energy are given in Table II, in which the experimental energy value is also included.

3. TOTAL POTENTIAL FUNCTION AND RADIAL PROBABILITY DISTRIBUTION

In quantum-mechanical computations, the function

$$T(A_i|r) = 2\Big[Z - \sum_{nl} c_{nl} Y_0(nl, nl\,|\,r)\Big]. \qquad (3.1)$$

plays an important role. Here A_i denotes the term A of the configuration i of an atom whose atomic number is Z; c_{nl} is the number of electrons in the nl shell.

The function $T(A_i|r)$, divided by $2r$, represents the potential of the total system. We shall call this function the total potential function.

It is not difficult to show that the total potential function for the term A of the configuration i, can be represented, in the many-configuration approximation, in the form:

$$T(A^i\,|\,r) = \frac{1}{\sum\limits_j a_{ij}^2} \sum_j a_{ij}^2\, T(A_j\,|\,r). \qquad (3.2)$$

In particular, in the two-configuration approximation $1s^2 2s^2 2p - 1s^2 2p^3$, where $P(1s\,|\,r)$ is the same for both configurations, the total potential function for the configuration $1s^2 2s^2 2p$ is:

$$T(r) = 2\Big\{Z - 2Y_0(1s, 1s\,|\,r) \qquad (3.3)$$

$$- \frac{1}{1 + a_{12}^2}\,[2Y_0(2s, 2s\,|\,r)_{11} + Y_0(2p, 2p\,|\,r)_{11}$$

$$+ 3a_{12}^2 Y_0(2p, 2p\,|\,r)_{22}]\Big\}.$$

The subscripts on $Y_0(1s, 1s\,|\,r)$ have been omitted for the reason just mentioned.

In the one-configuration approximation, we have the following expression for the radial probability distribution:

$$W(A_i\,|\,r) = \sum_{nl} c_{nl} P^2(nl\,|\,r). \qquad (3.4)$$

To obtain the corresponding expression in the many-configuration approximation, we must replace T by W in (3.2). We obtain the following expression for the radial distribution of the configuration

TABLE III

Total Potential Function and Radial Distribution for the Ground Configuration of the Boron Atom

r	$T(r)$	$10^3\delta T$	$W(r)$	$10^3\delta W$	r	$T(r)$	$10^3\delta T$	$W(r)$	$10^3\delta W$
0.00	10.000	0	0.000	0	1.0	2.549	−6	1.086	+4
0.02	9.547	0	0.295	−1	1.1	2.273	−7	1.209	+3
0.04	9.106	0	0.969	−2	1.2	2.019	−7	1.319	+2
0.06	8.684	0	1.789	−3	1.3	1.787	−7	1.402	+1
0.08	8.286	0	2.612	−5	1.4	1.577	−6	1.455	+1
0.10	7.914	+1	3.355	−7	1.5	1.388	−5	1.477	+1
0.12	7.569	+1	3.976	−8	1.6	1.218	−5	1.473	+1
0.14	7.249	+1	4.457	−9	1.8	0.931	−5	1.400	+2
0.16	6.955	+1	4.799	−9	2.0	0.707	−5	1.271	+2
0.18	6.685	0	5.010	−8	2.2	0.533	−5	1.114	+1
0.20	6.437	0	5.105	−8	2.4	0.400	−5	0.952	0
0.24	6.001	0	5.021	−6	2.6	0.300	−4	0.797	0
0.28	5.631	−1	4.679	−4	2.8	0.224	−4	0.657	−1
0.32	5.316	−1	4.198	−1	3.2	0.125	−2	0.430	−2
0.36	5.043	−2	3.662	+1	3.6	0.069	−2	0.272	−2
0.40	4.802	−2	3.131	+4	4.0	0.038	−1	0.168	−2
0.44	4.587	−3	2.641	+6	4.4	0.022	0	0.102	−2
0.48	4.392	−4	2.212	+8	4.8	0.013	0	0.061	−1
0.52	4.211	−4	1.852	+9	5.2	0.007	0	0.036	−1
0.56	4.041	−5	1.561	+9	5.6	0.004	0	0.022	0
0.6	3.881	−5	1.336	+10	6	0.002_5	0	0.013	0
0.7	3.509	−6	1.010	+10	7	0.000_9	0	0.003	0
0.8	3.166	−6	0.926	+8	8	0.000_4	0	0.001	0
0.9	2.847	−6	0.976	+6	9	0.000_2	0		

Footnote.- The values of T and W are given in the two-configuration approximation. Also given are the differences between the two-configuration and one-configuration values, multiplied by 1000.

$1s^22s^22p$ in the two-configuration approximation $1s^22s^22p - 1s^22p^3$:

$$W(r) = 2P^2(1s\,|\,r) + \frac{1}{1+a_{12}^2}\,[2P_1^2(2s\,|\,r) + P_1^2(2p\,|\,r) + 3a_{12}^2P_2^2(2p\,|\,r)]. \quad (3.5)$$

The values of T and W are given in Table III. In the table, the steps in r are twice the interval used in the calculations. Interpolation can easily be done if necessary. This is especially true for the total potential function, which is frequently used in computations.

4. CONCLUSIONS

From the results presented in Table II, we see that the two configuration approximation improves the theoretical energy value by 0.033 atomic units. Changing from one electron wave functions, determined in the one-configuration approximation, to functions determined in the two-configuration approximation is associated with an improvement of the result by 0.003 at.u., compared with 0.011 at.u. for the case of the neutral beryllium atom[1]. Investigation of this question shows that, for beryllium, the configuration $2s^22p^3$ would also give a much smaller effect than the $2s^22p^2$ configuration[8].

From Table III we see that the values of the total potential function T and the radial probability distribution W, as determined in the two-configuration approximation, differ from their values in the one-configuration approximation by less, in absolute value, than 0.007 and 0.010 respectively. The sign of this difference shows that the two-configuration approximation gives smaller screening of the nuclear charge in the neighborhood of the nucleus, and larger screening far away from it, as compared with the results obtained in the one-configuration approximation.

---

[8] V. V. Kibartas, V. I. Kavetskis and A. P. Iutsis, J. Exper. Theoret. Phys. USSR **29**, 623 (1955); Soviet Phys. **2**, 481 (1956).

Translated by M. Hamermesh
245

SOVIET PHYSICS JETP VOLUME 2, NUMBER 3 MAY, 1956

Fock Self-Consistent Field in the Three-Configuration Approximation for the Beryllium Atom

V. V. KIBARTAS, V. I. KAVETSKIS AND A. P. IUTSIS
Vilna State University and Vilna State Teachers' Institute

(Submitted to JETP editor July 12, 1954)
J. Exper. Theoret. Phys. USSR **29**, 623-628 (November, 1955)

The problem of the practical application of the Fock self-consistent field method in the many-configuration approximation is examined. The three-configuration approximation $1s^22s^2 - 1s^22p^2 - 2s^22p^2$ is applied to the ground configuration of the neutral beryllium atom. Values of the total potential function and the radial probability distribution are given.

1. INTRODUCTION

THE Fock self-consistent field method[1] was extended to the many-configuration approximation in reference 2. It was shown[3] that the solution of the Fock equations in the two-configuration approximation is practically feasible. It was later shown[4] that the solutions of the Fock equations in the two-configuration approximation can, without noticeable loss of accuracy, be replaced by solutions of simplified Fock equations in the two-configuration approximation. Computations by this simplified method were carried out for the ground configurations of Be, B^+, C^{++}[4], and B [5].

The fact that going over from the one-configuration to the two-configuration approximation involves relatively little additional computational labor points to the possibility of practical extension of the method to the case where a greater number of configurations are taken into account. The present paper is devoted to this question. We solve the problem by a method similar to one previously applied[6], in which analytic wave functions were used. Calculations are carried out for the ground configuration of the neutral beryllium atom.

Previous work[6] shows that in the case of the three-configuration approximation $1s^22s^2 - 1s^22p^2 - 1s^23d^2$, the last configuration gives a negligible effect. This configuration was therefore neglected in references 3 and 4, and the two-configuration approximation $1s^22s^2 - 1s^22p^2$ applied. Further study of the question shows that, for the ground configuration of atoms of the type of Be, when one uses one-electron wave functions determined in the many-configuration-approximation, one should use the three-configuration approximation $1s^22s^2 - 1s^22p^2 - 2s^22p^2$ for more accurate calculations. So, as a specific example of the application of the Fock self-consistent field method in the many-configuration approximation, we have in the present paper applied the last-mentioned three-configuration approximation for the case of the Be atom.

2. GENERAL CONSIDERATION OF THE PROBLEM

As in reference 6, the configuration under investigation will be denoted by the subscript 1. We shall assume that the many-configuration approximation reduces, for practical purposes, to the m - configuration approximation. Formulas (2.1) - (2.8) of reference 6 are unaltered, so that to avoid repetition we shall not give them here.

In order to apply the Fock method for finding one-electron wave functions, we construct the expression:

$$E' = \frac{1}{\sum_{i=1}^{m} a_{1i}^2}\left[\sum_{i=1}^{m} a_{1i}^2 E'_{ii} + 2\sum_{k>i=1}^{m} a_{1i}\, a_{1k} E'_{ik}\right], \quad (2.1)$$

where

$$E'_{ik} = E_{ik} + \sum_{nl,\, n'l} (1 + \delta_{ik}\delta_{nn'} - \delta_{nn'}) \quad (2.2)$$

$$\times\; a_{1i}\, a_{1k}\, \varepsilon_{(nl,\,n'l)_{ik}} N(nl,\, n'l)_{ik}.$$

Here δ_{ij} is the Kronecker delta, $\epsilon_{(nl,n'l)_{ik}}$ are

---

[1] V. A. Fock, Z. Physik. **61**, 126 (1930).

[2] A. P. Iutsis, J. Exper. Theoret. Phys. USSR **23**, 129 (1952).

[3] V. V. Kibartas and A. P. Iutsis, J. Exper. Theoret. Phys. USSR **25**, 264 (1953).

[4] A. P. Iutsis, V. V. Kibartas and I. I. Glembotskii, J. Exper. Theoret. Phys. USSR **27**, 425 (1954).

[5] I. I. Glembotski, V. V. Kibartas and A. P. Iutsis, J. Exper. Theoret. Phys. USSR **29**, 617 (1955); Soviet Phys. **2**, 476 (1956).

[6] V. I. Kavetskis and A. P. Iutsis, J. Exper. Theoret. Phys. USSR **25**, 257 (1953).

Lagrange multipliers, $N(nl, n'l)_{ik}$ is defined by expression (2.8) of reference 6, and the summation extends over all nl and $n'l$ (including $n' = n$) for given i and k.

We shall assume that the E_{ik} are expressed in terms of radial integrals. Then the Fock equations in the many-configuration approximation take on the following quite general form:

$$\frac{\partial E'_{11}}{\partial P_1(nl\,|\,r)} + 2\sum_{i=2}^{m} a_{1i}\frac{\partial E'_{1i}}{\partial P_1(nl\,|\,r)} = 0 \qquad (2.3a)$$

for all nl of the configuration under investigation, and

$$\frac{\partial E'_{kk}}{\partial P_k(nl\,|\,r)} + 2\sum_{k\neq j=1}^{m} \frac{a_{1j}}{a_{1k}}\frac{\partial E'_{kj}}{\partial P_k(nl\,|\,r)} = 0 \qquad (2.3b)$$

for all nl of the perturbing configurations ($k = 2,3,\dots m$).

The first term in Eq. (2.3) is just the left-hand side of the usual Fock equations (in the one-configuration approximation), while the remaining terms are configuration terms. We should point out that configuration terms appear in the equations of only those $P(nl\,|\,r)$ which are contained in at least one of the $E_{ij} (i \neq j = 1,2,\dots m)$. The remaining equations are just the corresponding ordinary Fock equations.

We consider the case where the perturbing configurations differ from the fundamental configuration in a pair of (nl)'s. Then the symbolic derivative of E'_{ik} for $k \neq i$ is an exchange term multiplied by the factor $N(nl,n'l)_{ik} \leq 1$. Since $a_{1i} < 1$ for all i, the configuration terms in Eq. (2.3a) are insignificant compared to the exchange terms and can be neglected. On the other hand, in those equations (2.3b) in which configuration terms appear, the term in the sum for $j = 1$ is dominant, since it contains the factor $1/a_{ik}$ (note that $a_{11} = 1$). The other terms are less important. We can therefore neglect them relative to the dominant term. Under these conditions, the equations (2.3b) break up into equations for the separate two-configuration approximations $1 - k$ (for $k = 2,3,\dots m$). In this simplified form of the Fock self-consistent field method in the many-configuration approximation, we use solutions of the ordinary Fock equations as one-electron wave functions for the fundamental configuration, and solutions of the Fock equations in the various two-configuration approximations as one-electron wave functions for the perturbing configurations. In these separate two-configuration approximations, we can make the further simplification, as proposed in reference 4 and applied in references 4 and 3: the exchange terms are neglected compared to configuration terms in the Fock equations for the wave functions of the perturbing configurations.

For those wave functions of the perturbing configuration whose Fock equations do not contain configuration terms, the corresponding one-electron wave functions of the fundamental configuration are used. Thus, in practical application of the Fock self-consistent field in the many-configuration approximation, in addition to solving the ordinary Fock equations for the fundamental configuration, it is sufficient to solve the simplified two-configuration Fock equations for those wave functions of the perturbing configurations which appear in the expressions for the nondiagonal matrix elements of the energy, which couple the fundamental configuration with the corresponding perturbing configurations.

3. PRACTICAL APPLICATION OF THE METHOD

Let us apply the self-consistent Fock field in the three-configuration approximation $1s^2 2s^2 - 1s^2 2p^2 - 2s^2 2p^2$ (abbreviated 1 - 2 - 3) to the ground configuration of the beryllium atom. In this case, the nondiagonal matrix elements of the energy are:

$$E_{12} = -\frac{1}{\sqrt{3}} G_1(2s, 2p)_{12} N^2(1s, 1s)_{12}, \qquad (3.1)$$

$$E_{13} = -\frac{1}{\sqrt{3}} G_1(1s, 2p)_{13} N^2(2s, 2s)_{13}, \qquad (3.2)$$

$$E_{23} = G_0(1s, 2s)_{23} N^2(2p, 2p)_{23}. \qquad (3.3)$$

We assume that

$$P_2(1s\,|\,r) = P_1(1s\,|\,r) = P(1s\,|\,r), \qquad (3.4a)$$

$$P_3(2s\,|\,r) = P_1(2s\,|\,r) = P(2s\,|\,r). \qquad (3.4b)$$

Here the indices attached to a function denote the configuration to which the corresponding radial wave function refers. Functions without indices are those of the fundamental configuration, determined in the one-configuration approximation. In view of Eq. (3.4), we have

$$N(1s, 1s)_{12} = N(2s, 2s)_{13} = 1. \qquad (3.5)$$

We have the following simplified two-configuration equations for determining the functions $P_2(2p\,|\,r)$ and $P_3(2p\,|\,r)$:

$$\left[\frac{d^2}{dr^2}+\frac{2Z-4Y_0(1s,1s\,|\,r)-2Y_0(2p,2p\,|\,r)_{22}-0,8Y_2(2p,2p\,|\,r)_{22}}{r}-\frac{2}{r^2}\right.$$
$$\left.-\,\varepsilon_{(2p,\,2p)_{22}}\right]P_2(2p\,|\,r)+\frac{1}{a_{12}}\frac{2}{\sqrt{3}}\frac{Y_1(2s,2p\,|\,r)_{12}}{r}P(2s\,|\,r)=0, \tag{3.6a}$$

$$\left[\frac{d^2}{dr^2}+\frac{2Z-4Y_0(2s,2s\,|\,r)-2Y_0(2p,2p\,|\,r)_{33}-0,8Y_2(2p,2p\,|\,r)_{33}}{r}-\frac{2}{r^2}\right.$$
$$\left.-\,\varepsilon_{(2p,\,2p)_{33}}\right]P_3(2p\,|\,r)+\frac{1}{a_{13}}\frac{2}{\sqrt{3}}\frac{Y_1(1s,2p\,|\,r)_{13}}{r}P(1s\,|\,r)=0. \tag{3.6b}$$

The values of the functions $P(1s\,|r)$ and $P(2s|r)$ are given in reference 3. For the function $P_2(2p|r)$ we use the corresponding function, given in reference 3, which is a solution of the unsimplified equation in the two-configuration approximation. The solution of Eq. (3.6b) is given in Table I. An analytic wave function was used for starting the solution of this equation. The solution was carried to self-consistency index 0.0050 for $P_3(2p|r)$ and 0.0005 for a_{13}.

TABLE I

Normalized Radial Wave Function $P(2p|r)$ of the Perturbing Configuration $2s^2 2p^2$ of the Two-Configuration Approximation $1s^2 2s^2$ - $2s^2 2p^2$

r	$P(2p\|r)$	r	$P(2p\|r)$	r	$P(2p\|r)$
0.00	0.0000	0.30	1.4396	1.10	0.2093
0.01	0.0051	0.32	1.4761	1.15	0.1727
0.02	0.0201	0.34	1.4993	1.20	0.1422
0.03	0.0441	0.36	1.5104	1.25	0.1168
0.04	0.0764	0.38	1.5103	1.30	0.0957
0.05	0.1161	0.40	1.5003	1.35	0.0783
0.06	0.1623	0.42	1.4815	1.40	0.0640
0.07	0.2142	0.44	1.4551	1.45	0.0522
0.08	0.2708	0.46	1.4222	1.50	0.0426
0.09	0.3313	0.48	1.3840	1.55	0.0347
0.10	0.3949	0.50	1.3414		
0.11	0.4606	0.52	1.2953	1.6	0.0283
0.12	0.5279	0.54	1.2467	1.7	0.0187
0.13	0.5959	0.56	1.1961	1.8	0.0124
0.14	0.6640	0.58	1.1443	1.9	0.0083
0.15	0.7316			2.0	0.0055
		0.60	1.0919	2.1	0.0037
0.16	0.7981	0.65	0.9612	2.2	0.0024
0.17	0.8631	0.70	0.8357	2.3	0.0016
0.18	0.9261	0.75	0.7191	2.4	0.0011
0.19	0.9868	0.80	0.6133	2.5	0.0007
0.20	1.0447	0.85	0.5193	2.6	0.0005
0.22	1.1516	0.90	0.4370	2.7	0.0003
0.24	1.2452	0.95	0.3658	2.8	0.0002
0.26	1.3246	1.00	0.3049		
0.28	1.3893	1.05	0.2530	3.0	0.0001

The values of the Lagrange multipliers, radial integrals and energy are given in Table II. To obtain the value of the energy in the three-configuration approximation, we also made use of the data of Table 2 of reference 3.

4. TOTAL POTENTIAL FUNCTION AND RADIAL PROBABILITY DISTRIBUTION

The total potential function[4] has the following form in the three-configuration approximation $1s^2 2s^2$ - $1s^2 2p^2$ - $2s^2 2p^2$:

$$T(r)=2\left\{Z-\frac{1}{1+a_{12}^2+a_{13}^2}\left[2(1+a_{12}^2)\,Y_0(1s,1s\,|\,r)\right.\right.$$
$$\left.\left.+\,2(1+a_{13}^2)\,Y_0(2s,2s\,|\,r)+2a_{12}^2Y_0(2p,2p\,|\,r)_{22}+2a_{13}^2Y_0(2p,2p\,|\,r)_{33}\right]\right\}. \tag{4.1}$$

TABLE II

Values of Radial Integrals and Energy (in atomic units)

$\varepsilon(2p,\ 2p)_{33} = 33{,}936$
$F_0(2p,\ 2p)_{33} = 2{,}0060$
$F_2(2p,\ 2r)_{33} = 1{,}0012$
$F_0(2s,\ 2p)_{33} = 0.4752$
$G_1(2s,\ 2p)_{33} = 0{,}0168$

$G_1(1s,\ 2p)_{13} = 1{,}2570$
$N(2p,\ 2p)_{23} = 0{,}1837$
$E_{33} = +9.197$
$E_{13} = -0{,}726$
$E_{23} = 0{,}001$

	a	b
ΔE	$-0{,}022$	$-0{,}065$
a_{13}	$+0.030$	$+0.030$
a_{12}	$+0.33$	$+0.31_5$
E_{theor}		-14.642
E_{exp}		-14.666

Footnote.- a) two-configuration approximation $1s^22s^2$ - $2s^22p^2$; b) three-configuration approximation $1s^22s^2$ - $1s^22p^2$ - $2s^22p^2$.

TABLE III

Total Potential Function and Radial Probability Distribution

r	$T(r)$	$10^3\delta T$	W	$10^3\delta W$	r	$T(r)$	$10^3\delta T$	W	$10^3\delta W$
0.00	8.000	0	0.000	0	1.0	2.205	−8	0.514	+10
0.02	7.665	0	0.151	−1	1.1	2.033	−8	0.487	+ 8
0.04	7.337	+1	0.516	−2	1.2	1.869	−8	0.506	+ 7
0.06	7.018	+1	0.991	−3	1.3	1.714	−8	0.547	+ 5
0.08	6.712	+1	1.504	−5	1.4	1.568	−8	0.599	+ 4
0.10	6.421	+1	2.010	−6	1.5	1.430	−8	0.651	+ 2
0.12	6.146	+1	2.476	−8	1.6	1.300	−8	0.698	+ 2
0.14	5.887	+1	2.886	−9	1.8	1.067	−8	0.765	+ 1
0.16	5.645	+1	3.230	−10	2.0	0.868	−7	0.792	+ 1
0.18	5.420	+1	3.507	−11	2.2	0.700	−7	0.784	+ 1
0.20	5.209	+1	3.712	−12	2.4	0.561	−7	0.748	+ 1
0.24	4.833	0	3.945	−10	2.6	0.447	−6	0.693	+ 1
0.28	4.509	0	3.969	−8	2.8	0.355	−5	0.628	+ 1
0.32	4.231	−1	3.841	−6	3.2	0.219	−5	0.488	0
0.36	3.992	−1	3.608	−3	3.6	0.134	−3	0.358	− 2
0.40	3.784	−2	3.312	0	4.0	0.081	−3	0.253	− 3
0.44	3.603	−3	2.984	+2	4.4	0.049	−1	0.173	− 3
0.48	3.443	−4	2.650	+4	4.8	0.029	−1	0.116	− 2
0.52	3.301	−4	2.325	+6	5.2	0.017	−1	0.076	− 2
0.56	3.174	−5	2.021	+8	5.6	0.010	0	0.049	− 2
0.6	3.059	−5	1.745	+10	6	0.006	0	0.031	− 1
0.7	2.806	−6	1.189	+11	7	0.002_2	0	0.010	0
0.8	2.588	−7	0.824	+11	8	0.000_4	0	0.003	0
0.9	2.388	−8	0.614	+12	9			0.001	0

Footnote.- The values of T and W are given in the three-configuration approximation $1s^22s^2$ - $1s^22p^2$ - $2s^22p^2$. Also given are the differences (three-config. value minus one-config. value) multiplied by 1000.

For the radial distribution we find:

$$W(r) = \frac{1}{1 + a_{12}^2 + a_{13}^2} [2(1 + a_{12}^2) P^2(1s \mid r) + 2(1 + a_{13}^2) P^2(2s \mid r) + 2a_{12}^2 P_2^2(2p \mid r) + 2a_{13}^2 P_3^2(2p \mid r)]. \quad (4.2)$$

Equation (3.4) was used in getting Eqs. (4.1) and (4.2).

The values of T and W are presented in Table III. The intervals in the table have been doubled for the same reason that applied to the corresponding table of reference 5.

5. CONCLUSIONS

Comparison of Table I of the present paper with Table I of reference 3 shows that the function $P(2p|r)$ for the perturbing configuration $2s^2 2p^2$ deviates from the function $P(2p|r)$ for the perturbing configuration $1s^2 2p^2$, approaching the function $P(1s|r)$. This results from the smallness of a_{13} in (3.6b). This unusual behavior of the $P(2p|r)$ function when calculated in the two-configuration approximation is the reason why the energy correction caused by the perturbing configuration $2s^2 2p^2$ is significant, whereas it is negligible if we use one-electron wave functions determined in the one-configuration approximation.

From Table II we see that the three-configuration approximation $1s^2 2s^2$ - $1s^2 2p^2$ - $2s^2 2p^2$ gives a correction to the energy of 0.064 atomic units. The energy value calculated in the three-configuration approximation deviates from the experimental value by only 0.024 atomic units.

Table III shows that the absolute magnitudes of the differences between the values of the total potential function T and the probability distribution W determined in the three-configuration approximation and their values as given by the one-configuration approximation are no greater than 0.008 and 0.012 respectively. Most of the change is due to the perturbing configuration $1s^2 2p^2$, while the configuration $2s^2 2p^2$, because of the smallness of a_{13}, has a negligible effect on these quantities.

Translated by M. Hamermesh

SOVIET PHYSICS JETP VOLUME 2, NUMBER 3 MAY, 1956

Determination of Longitudinal Relaxation Times for Magnetic Resonance of Atomic Nuclei in an Intense High-Frequency Magnetic Field

S. D. GVOZDOVER AND N. M. IEVSKAIA
Moscow State University

(Submitted to JETP editor June 18, 1954)
J. Exper. Theoret. Phys. USSR 29, 637-644 (November, 1955)

Two methods for determining the longitudinal relaxation time T_1 are treated. The methods are based on the use of the inversion of the dispersion signals observed in an intense high-frequency magnetic field during a change in the constant field and on the change in the time interval which precedes the inversion point. In order to verify the methods, an evaluation of the effect of the intermediate region which connects the resonance region and the region of free relaxation was carried out. Relationships are obtained which allow the determination of the longitudinal relaxation time. In order to confirm the methods experimentally, the dependence of the longitudinal relaxation time on the concentration of paramagnetic ions was measured in aqueous solutions of cupric sulfate and ferric nitrate.

1. INTRODUCTION

IN the present work methods are explained for the determination of the longitudinal relaxation time T_1 in the case of magnetic resonance of atomic nuclei in an intense high-frequency magnetic field accompanied by periodic modulation of the constant magnetic field. By an intense high-frequency magnetic field is meant a field under the application of which the magnetization vector **M** undergoes a strong perturbation and becomes inverted.

The theory of magnetic resonance for the case of an intense high-frequency magnetic field is given in reference 1, where it is shown that if the conditions

$$\Delta t \ll T_1,\quad T_2 \ll T_1,\quad T_2 \ll T \qquad (1)$$

(where Δt is the duration of the signals being observed, T_1 and T_2 are the longitudinal and transverse relaxation times, respectively, and T is the period of the modulation) are fulfilled, then the complete process of passage through resonance under modulation may be divided into two regions: the region of resonance, in which the magnetization vector **M** undergoes a strong perturbation and becomes inverted, and the region of free relaxation of the magnetization vector **M** to its statistical magnitude $\mathbf{M}_0$.

Let us introduce the dimensionless parameters

$$\nu = \frac{1}{\omega_m T_1},\quad \mu = \frac{1}{\omega_m T_2},\quad k = \frac{H_m}{H_1}, \qquad (2)$$

and the dimensionless time

$$x = \omega_m t, \qquad (3)$$

where ω_m is the frequency of the modulating magnetic field, H_m is the amplitude of the modulating magnetic field and H_1 is half the amplitude of the high-frequency magnetic field.

As is shown in reference 1, a change in the longitudinal component of the magnetization $M_z(x)$ in the region of resonance is characterized by a magnitude of the coefficient of inversion R, defined as the ratio of the maximum magnitude of the longitudinal component of magnetization at the time of leaving the region of resonance $[M_z(x_2)]$ to the maximum magnitude of the longitudinal component of magnetization at the beginning of the resonance region $[M_z(x_1)]$

$$R = \frac{M_z(x_2)}{M_z(x_1)} \qquad (4)$$

The magnitude of the coefficient of inversion R depends on the parameter k, that is, on the ratio of the amplitudes of the modulating and the high-frequency fields, and may take on values lying between the limits[2]

$$-1 \leqslant R \leqslant 0. \qquad (5)$$

The absolute value of the coefficient of inversion increases with decreasing k. In the region of free relaxation the longitudinal component on the magnetization $M_z(x)$ satisfies the relationship

---

[1] S. D. Gvozdover and A. A. Magazanik, J. Exper. Theoret. Phys. USSR 20, 705 (1950).

[2] S. D. Gvozdover and N. M. Pomerantsev, Vestn. Moscow State Univ. 9, 79 (1953).

$$M_z(x) = M_0 - [M_0 - M_z(x_2)]\, e^{-\nu(x-x_2)}, \qquad (6)$$

where $M_z(x_2)$ is the magnitude of M_z on leaving the region of resonance ($x > x_2$).

The magnitude of the dispersion signal u observed during resonance is proportional to the value of the longitudinal component of the magnetization M_z at entrance into the region of resonance[1].

On sinusoidal modulation of the magnetic field, resonance regions occur twice during each modulation period. If the signals are observed on the screen of an oscilloscope, then, with an elliptical sweep pattern synchronized with the modulating magnetic field, two signals separated from each other appear on the screen. If we change the spacing between signals, changing the constant magnetic field, then the amplitudes of the second signal become unique probes, with the aid of which we may obtain the curve of the variation of M_z in the region of free relaxation.

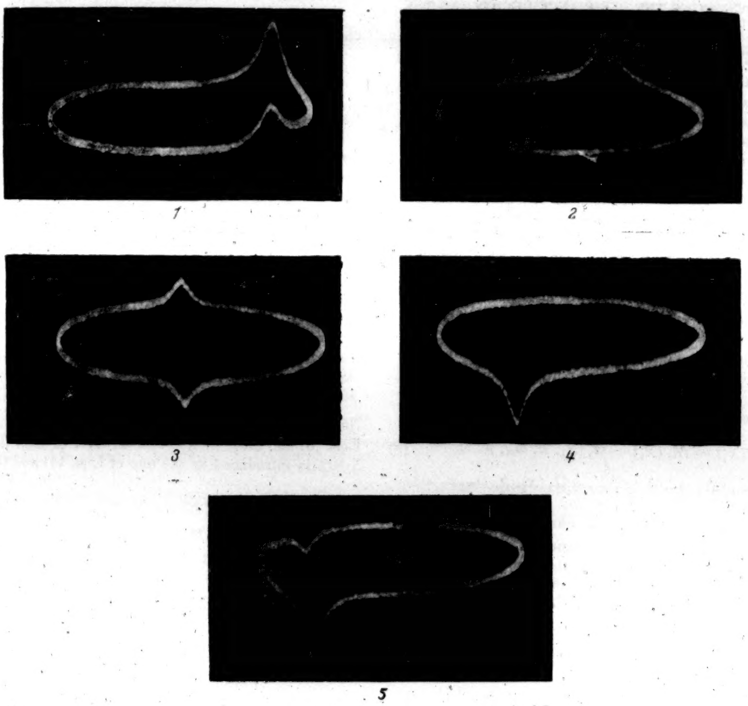

1

2

3

4

5

FIG. 1. Change in magnitude and sense of the dispersion signals during a gradual change in the constant magnetic field. The oscillograms were obtained with a 0.01 M solution of $Fe(NO_3)_3$ under the conditions: modulation frequency 50 cps, amplitude of the modulating magnetic field 19 oersteds, half amplitude of the high-frequency magnetic field 1 oersted.

In Fig. 1 are shown typical oscillograms, illustrating the change of magnitude and sense of the dispersion signals on change of the constant magnetic field. Oscillograms *2* and *4* (Fig. 1) correspond to the case in which the second probing resonance field occurs just at the instant when M_z passes through zero during free relaxation to its statistical magnitude. At this instant, called the instant of inversion, the probing signal is not observed.

2. THE EFFECT OF THE INTERMEDIATE REGION CONNECTING THE RESONANCE REGION AND THE REGION OF FREE RELAXATION

The idea that $M_z\,(x)$ completes, for each period of the modulation, a closed cycle consisting of two exponential sections obeying Eq.(6) and two resonance regions joining them and obeying Eq. (4) is, of course, an approximation. Actually, during the approach to the resonance region and during the leaving of it, an intermediate region exists, in which the behavior of $M_z\,(x)$ is more complicated. As a consequence of the presence of the transitional intermediate field, the values of $M_z(x)$ at points x_1 and x_2 are somewhat diminished in comparison with what they would have been if M_z had merely conformed to an exponential growth up to the instant x_1. Let us evaluate the error which arises in such an approximate treatment. We shall designate by $M_z(x)$ the values which M_z actually has at points x_1 and x_2 and by $M_z'(x)$ the values which it would have had if resonance conditions had occurred instantaneously:

$$M_z(x_1) = M_z'(x_1) - \Omega_1(x_1, k, \omega_m, \mu, \nu), \qquad (7)$$

$$|M_z(x_2)| = |M_z'(x_2)| - |\Omega_2(x_2, k, \omega_m, \mu, \nu)|.$$

The functions Ω_1 and Ω_2 characterize a decrease in the magnitude of the signal as a result of the beginning of the action of the resonance conditions. For the coefficient of inversion R, we obtain, on taking account of Eq. (7), the expression

$$|R| = \left|\frac{M_z(x_2)}{M_z(x_1)}\right| \qquad (8)$$

$$= |R'|\left[1 + \frac{\Omega_1}{M_z'(x_1)} - \left|\frac{\Omega_2}{M_z'(x_2)}\right|\right],$$

where $R' = M_z'(x_2)/M_z'(x_1)$.

Under the conditions

$$\frac{\Omega_1}{M_z'(x_1)} \ll 1, \quad \left|\frac{\Omega_2}{M_z'(x_2)}\right| \ll 1 \qquad (9)$$

it follows from Eq. (8) that

$$R = R'.$$

In the intermediate region Eq. (6) takes the form

$$M_z(x) = M_0' - [M_0' - M_z(x_2)] \qquad (10)$$

$$\times e^{-\nu(x-x_2)} + (|\Omega_2| - \Omega),$$

where $M_0' = M_0 - |\Omega_2|$ and $\Omega \leq \Omega_1$ characterize the decrease in the signal at an arbitrary point x.

Equation (10) is analogous to Eq. (6) with changed coefficients. If

$$\frac{\Omega_1}{M_0} \ll 1, \quad \left|\frac{\Omega_2}{M_0}\right| \ll 1, \qquad (11)$$

then Eqs. (10) and (6) coincide.

Conditions (9) and (11) allow us to estimate the error which arises on the employment of Eqs. (4) and (6), not taking into account the intermediate region. For example, under the conditions

$$\nu = 0.1, \quad \mu = 1, \quad k = 10, \quad \omega_m = 314,$$

an estimate of the values of $M_z\,(x)$ and $M_z'(x)$ gives

$$\frac{\Omega_1(x_1)}{M_0} < 0.02, \qquad \frac{\Omega_1(x_1)}{M_z'(x_1)} < 0.2, \qquad (12)$$

$$\left|\frac{\Omega_2(x_2)}{M_0}\right| < 0.02, \qquad \left|\frac{\Omega_2(x_2)}{M_z'(x_2)}\right| < 0.2.$$

Noting that the difference $(\Omega_1 - |\Omega_2|)$ occurs in Eqs. (8) and (10), we see that an error of less than 5-10% is introduced by the use of Eqs. (4) and (6).

3. DETERMINATION OF T_1 BY THE INVERSION METHOD

Let us introduce the width of the signal into the expressions given in reference 1 for the magnitude of the dispersion signals arising during a closed cycle of the modulation.

We use the designations

$$m(x) = M_z(x)/M_0'; \qquad (13)$$

$$m(x_{1,1}) = m_{11}, \quad m(x_{2,1}) = m_{21}$$

$$m(x_{1,2}) = m_{12}, \quad m(x_{2,2}) = m_{22}, \qquad (14)$$

where the first index denotes the instant of entering and leaving the resonance region, and the second indicates the number of the resonance region. If the resonance region is sufficiently narrow, then the instants of time at which M_z attains its extreme values are near the instants of time for which $u_x/u_{max} = \frac{1}{2}$. Consequently, we shall take the distance between the points of half amplitude of the dispersion signal $u(x)$ as the width of the signal Δ. We denote by η the interval of time between signals from maximum to maximum. With these designations,

$$x_{12} - x_{21} = \eta - \Delta, \qquad x_{11} - x_{22} = 2\pi - \eta - \Delta. \tag{15}$$

Then, from Eqs. (8), (10), (13) and (15), neglecting the terms (12), we obtain

$$m_{11} = \frac{1 - Re^{-\nu(2\pi-2\Delta)} - (1-R)\,e^{-\nu(2\pi-\eta-\Delta)}}{1 - R^2 e^{-\nu(2\pi-2\Delta)}}, \tag{16}$$

$$m_{12} = \frac{1 - Re^{-\nu(2\pi-2\Delta)} - (1-R)\,e^{-\nu(\eta-\Delta)}}{1 - R^2 e^{-\nu(2\pi-2\Delta)}},$$

where m_{11} determines the amplitude of the upper signal and m_{12} the amplitude of the lower signal.

As follows from Eq. (16), the magnitude of the signal depends on the distance η between signals and on the width of the signal Δ. Moreover, the magnitude of the signals depends on the coefficient of inversion R and on the ratio of the longitudinal relaxation time T_1 to the modulation period T.

Expressions for the magnitude of the signals have also been obtained in reference 3. However, the relations introduced in this work are written on the supposition that $R = 1$, and no account is taken in them of the width of the signal. This, as follows from Eq. (16), results in a rough approximation. In those cases where the inversion of the signals arising gives a sufficiently great portion of the exponential [for which it is necessary to use a modulation frequency such that T/T_1 will be greater than unity and at the same time will fulfill condition (1)], it is possible to use it for the determination of the longitudinal relaxation time T_1. An indication of the possibility of employing such a method was given in reference 1.

Both formulas (16), corresponding to the upper and lower signals, can be put into the form

$$m = P - |Q|\,e^{-\nu y}, \tag{17}$$

where

$$P = \frac{1 - Re^{-\nu(2\pi-2\Delta)}}{1 - R^2 e^{-\nu(2\pi-2\Delta)}}, \tag{18}$$

$$Q = -\frac{1-R}{1 - R^2 e^{-\nu(2\pi-2\Delta)}},$$

and y corresponds to the time elapsed from the end of the preceding signal to the beginning of the following one, which is equal to

$y = x_{11} - x_{22} = 2\pi - \eta - \Delta$ for the upper signal, (19)

$y = x_{12} - x_{21} = \eta - \Delta$ for the lower signal, respectively.

As has already been stated above, the amplitude of the signal u arising is proportional to m, that is,

$$u = Nm = N[P - |Q|\,e^{-\nu y}], \tag{20}$$

where N is a coefficient which is constant for a given substance and definite experimental conditions. In order to determine T_1 it is necessary, according to (20), to know P and Q, which, in their turn, are functions of T_1, and also R, the magnitude of which is unknown.

We consider two neighboring signals (either two upper or two lower)

$$u_i = N[P - |Q|\,e^{-\nu y_i}], \qquad u_{i+1} = N[P - |Q|\,e^{-\nu y_{i+1}}]. \tag{21}$$

Taking the difference of their amplitudes and then taking its logarithm, we obtain

$$\ln(u_{i+1} - u_i) = \ln N|Q| - \nu y_i + \ln[1 - e^{-\nu(y_{i+1}-y_i)}]. \tag{22}$$

Under the condition that $\nu(y_{i+1} - y_i) < 0.1$, we may take

$$e^{-\nu(y_{i+1}-y_i)} = 1 - \nu(y_{i+1} - y_i). \tag{23}$$

Putting (23) into (22) and introducing the symbols:

$$\alpha_i = \ln\,(u_{i+1} - u_i) - \ln(y_{i+1} - y_i), \qquad \beta = \ln N|Q|\,\nu, \tag{24}$$

we obtain

$$\alpha_i = \beta - \nu y. \tag{25}$$

Equation (25) is the equation of a straight line,

---

[3] L. E. Drain, Proc. Phys. Soc. (London) A62, 301 (1949).

the ordinates and the abscissas of which are determined by experiment; it is necessary to find the slope of the straight line.

Using the method of least squares[4] for the determination of $\nu = 1/\omega_m T_1$, we obtain

$$T_1 = \frac{1}{\omega_m} \frac{n\sum_{l=1}^{n}(y_l)^2 - \left(\sum_{l=1}^{n} y_l\right)^2}{\sum_{l=1}^{n}\alpha_l \sum_{l=1}^{n} y_l - n\sum_{l=1}^{n}\alpha_l y_l}. \tag{26}$$

It is assumed that in Eq. (26) we have n points; consequently, in accordance with (24), $n + 1$ signals.

In a practical application of this method to oscillograms such as those introduced in Fig. 1, the position, width and amplitude of the signals are measured. The amplitudes of the signals u are measured during a superposition on the oscillogram-with-signal of the oscillogram ellipse without signals, taken when the longitudinal magnetic field H_z does not reach the resonance value. Knowing the modulation frequency ω_m and taking into consideration that the sweep of the oscillogram, as also of the modulation field, is sinusoidal, we may determine y.

An experimental verification of the methods showed that repeated determinations of T_1 for one and the same sample according to Eq. (26), under conditions where the values of u and y were of an exactitude of 5-10%, give an error in the determination of T_1 of the order of 10-20%.

4. DETERMINATION OF T_1 BY THE METHOD OF THE INVERSION POINT

An expression for the coefficient of inversion R can be obtained from Eq. (16). At the inversion point $m_{12} = 0$ and

$$R = \frac{1 - e^{\nu(\eta_0 - \Delta)}}{1 - e^{-\nu(2\pi - \eta_0 - \Delta)}}, \tag{27}$$

whence $\eta_0 - \Delta$, the distance from the end of the upper signal to the inversion point of the lower signal, is equal to

$$\eta_0 - \Delta = \frac{1}{\nu}\ln\left(\frac{1 - R}{1 - Re^{-\nu(2\pi - 2\Delta)}}\right). \tag{28}$$

The inversion point of the upper signal is located at the same distance from the lower signal (see oscillograms 2 and 4 of Fig. 1). The dependence of $\dfrac{\eta_0 - \Delta}{2\pi} = \dfrac{\tau_0 - \delta}{T}$ on R and $\nu\, 2\pi = \dfrac{T}{T_1}$ is given in Fig. 2 (τ_0 and δ have the dimension of time and are equal, respectively, to $\dfrac{\eta_0}{\omega_m}$ and $\dfrac{\Delta}{\omega_m}$). As follows from Fig. 2, the distance to the inversion point depends, for constant modulation period, on the value of the longitudinal relaxation time T_1 and on the magnitude of the coefficient of inversion. It follows from Eq. (27) that if T_1 is found and the values of η_0 and Δ are known—the magnitudes being determined experimentally, then we may find the coefficient of inversion R, and, conversely, if the magnitude of R is known, then T_1 may be determined from Eq. (27). The absolute value of the coefficient of inversion R, as is shown in reference 2, must increase with dedreasing $k = H_m/H_1$. If the values of T and T_1 are constant, then, as follows from Fig. 2, the distance to the point of inversion must increase on increase in $|R|$.

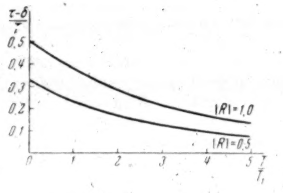

FIG. 2. Dependence of the position of the inversion point on the ratio of the modulation period to the longitudinal relaxation time (T/T_1) for $|R| = 1$ and $|R| = 0.5$.

In order to explain the behavior of R in its dependence on k, the dependence of the distance to the inversion point η_0 on the magnitude of the ratio V_{L1}/I_m, proportional to $1/k$, was taken (V_{L1} is the amplitude of the voltage at the generator coil, proportional to H_1, I_m is the current through the modulation coils, proportional to H_m[5]). The dependence of η_0 and $\eta_0 - \Delta$ on V_{L1}/I_m, taken in a 0.064 M solution of $CuSO_4$, is represented in Fig. 3. Experiment shows that for an increase in H_1, with constant H_m and ω_m, beginning from a certain value of H_1 (in Fig. 3, for $V_{L1}/I_m > 40$), $\eta_0 - \Delta$ is of constant magnitude, to within an accuracy of a few percent.

It follows from Eq. (27) that for constant ν (that is, for constant ω_m and T_1) the magnitude of $\eta_0 - \Delta$ can be constant only for constant R. As k decreases, $|R|$ must increase accordingly, but it is

---

[4] K. P. Iakolev, *Mathematical Treatment of Experimental Results*, GITTL, 1950.

[5] S. D. Gvozdover and N. M. Ievskaia, J. Exper. Theoret. Phys. USSR 25, 435 (1953).

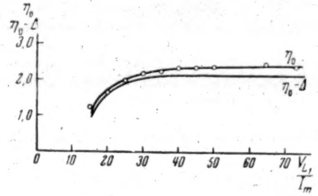

FIG. 3. Dependence of the distance to the inversion point η_0 and $(\eta_0-\Delta)$ on the ratio of the high-frequency voltage at the generator coil to the modulation current. This ratio is proportional to $1/k$.

practically unchanged; consequently, $|R|$ is near unity, and the following method may be proposed for the evaluation of T_1.

We introduce the notation

$$z_1 = \nu(2\pi - \eta_0 - \Delta), \quad z_2 = \nu(\eta_0 - \Delta). \quad (29)$$

Then Eq. (27) takes the form

$$R = \frac{1 - e^{z_2}}{1 - e^{-z_1}}. \quad (30)$$

If the ratio

$$\frac{z_2}{z_1} = \frac{\eta_0 - \Delta}{2\pi - \eta_0 - \Delta}, \quad (31)$$

which is determined experimentally, is known, then, knowing a magnitude, for example, of z_2, which fulfills Eq. (30) for a given R, and with the assigned z_2/z_1, we can determine T_1 from Eq. (29). For the purpose of such an evaluation,

TABLE I

z_2	$\left(\frac{z_2}{z_1}\right)_{R=-1}$	$\left(\frac{z_2}{z_1}\right)_{R=-0.9}$	z_2	$\left(\frac{z_2}{z_1}\right)_{R=-1}$	$\left(\frac{z_2}{z_1}\right)_{R=-0.9}$
0.01	1.00	0.91	0.36	0.64	0.55
0.02	0.98	0.87	0.37	0.62	0.54
0.03	0.97	0.86	0.38	0.61	0.53
0.04	0.96	0.85	0.39	0.60	0.52
0.05	0.95	0.84	0.40	0.59	0.50
0.06	0.94	0.84	0.41	0.58	0.49
0.07	0.93	0.83	0.42	0.57	0.48
0.08	0.92	0.83	0.43	0.56	0.47
0.09	0.91	0.82	0.44	0.55	0.46
0.10	0.90	0.81	0.45	0.54	0.45
0.11	0.89	0.80	0.46	0.52	0.44
0.12	0.88	0.79	0.47	0.51	0.43
0.13	0.87	0.78	0.48	0.50	0.42
0.14	0.86	0.77	0.49	0.49	0.40
0.15	0.85	0.76	0.50	0.48	0.39
0.16	0.84	0.75	0.51	0.47	0.38
0.17	0.83	0.74	0.52	0.45	0.37
0.18	0.82	0.73	0.53	0.44	0.35
0.19	0.81	0.72	0.54	0.43	0.34
0.20	0.80	0.71	0.55	0.42	0.33
0.21	0.79	0.70	0.56	0.40	0.31
0.22	0.78	0.69	0.57	0.39	0.30
0.23	0.77	0.68	0.58	0.38	0.28
0.24	0.76	0.67	0.59	0.36	0.26
0.25	0.75	0.66	0.60	0.35	0.24
0.26	0.74	0.65	0.61	0.33	0.22
0.27	0.73	0.64	0.62	0.32	0.20
0.28	0.72	0.63	0.63	0.30	0.17
0.29	0.71	0.62	0.64	0.28	0.12
0.30	0.70	0.61	0.65	0.26	
0.31	0.69	0.60	0.66	0.24	
0.32	0.68	0.59	0.67	0.22	
0.33	0.67	0.58	0.68	0.19	
0.34	0.66	0.57	0.69	0.14	
0.35	0.65	0.56			

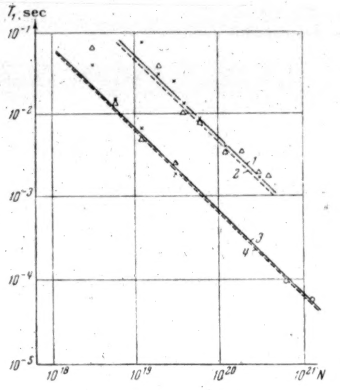

FIG. 4. Dependence of the longitudinal relaxation time T_1 on the concentration of paramagnetic ions N for water solutions of $CuSO_4$ and $Fe(NO_3)_3$. The following symbols are used in the figure: Δ for measurements by the method of inversion, × for measurements by the method of the inversion point, O for measurements by the form of the signal: *1* is T_1 for Cu^{++} ions, *2* is T_1 for the same ions according to reference 8, *3* is T_1 for Fe^{+++} ions, *4* is T_1 for the same ions according to reference 8.

tables of values of z_2 satisfying Eq. (30) for $R = -1$ and $R = -0.9$ have been composed (Table I). We may analogously draw up a similar table satisfying any chosen R.

An anlaysis of expression (30) shows that an evaluation of T_1 for $R = -1$ gives the minimum possible value

$$(T_1)_{R=-1} < (T_1)_R, \qquad (32)$$

and that for $z_2/z_1 < 0.4$ $(T_1)_{R=-1}$ differs from $(T_1)_{R=-0.9}$ by not more than 12%. A determination of $(T_1)_{R=-1}$ under the conditions that η_0 and Δ are determined only with an accuracy of up to 5% gives a maximum error of 10%. Thus, if conditions are created under which the distance to the inversion point remains practically unchanged, then a determination of T_1 from Eqs. (30), (29) and the Table will give an error of not more than 20%.

The method proposed is quite simple and permits a rapid determination of the longitudinal relaxation time T_1 with an accuracy not less than the accuracy given by other methods. An essential advantage of the method, as of every method employing periodic modulation of the constant magnetic field, is the possibility of working in an unstabilized magnetic field, which possibility considerably simplifies the setup for the measurement of the longitudinal relaxation time.

5. EXPERIMENTAL VERIFICATION OF THE METHODS

As a test, in a special arrangement[5], of the methods described, values of the longitudinal relaxation time T_1 were measured for water solutions of various concentrations of cupric sulfate, $CuSO_4$, and ferric nitrate, $Fe(NO_3)_3$.

The obtained dependence of T_1 on the concentration of paramagnetic ions Cu^{++} and Fe^{+++} in the solution is given in Fig. 4 (curves *1* and *3*). The values of T_1 for 2*M* and 1*M* solutions of ferric nitrate were determined with the aid of the solution for the form of the signal in an intense high-frequency magnetic field in the case of short relaxation times[6]. From Fig. 4 it is clear that the dependence of T_1 on the concentration of paramagnetic ions is represented by a straight line making an angle of 45° with the axis of abscissa ; whence it follows that the magnitude of the longitudinal relaxation time T_1 is inversely proportional to the concentration of paramagnetic ions. The deviation from the law of inverse proportionality for small concentrations may be explained by inaccuracy in the preparation of the solutions. As a consequence of the fact that the solutions were prepared by means of successive dilutions, the percentage content of Cu^{++} and Fe^{+++} ions at small concentrations was somewhat reduced as a result of hydrolysis, and this led to the apparent increase in T_1.

A comparison of the results of the measurement of T_1 by the method of inversion and by the method of the inversion point shows that the values of T_1 coincide within the limits of the error of the measurement and, moreover, coincide, within the limits of the error, with the results given in the literature[7,8] (see Fig. 4, curves *2* and *4*). This confirms the correctness of the methods we have treated.

---

[6] F. Bloch, Phys. Rev. 70, 460 (1946).

[7] N. Bloembergen, E. M. Purcell and R. V. Pound, Phys. Rev. 73, 679 (1948).

[8] N. Bloembergen, *Nuclear Magnetic Relaxation*, The Hague, 1948.

Translated by M. G.Gibbons
248

SOVIET PHYSICS JETP VOLUME 2, NUMBER 3 MAY, 1956

Fission of Uranium by Slow π^- Mesons, Fast Neutrons and γ-Rays of Energies Up to 250 mev

G. E. BELOVITSKII, T. A. ROMANOVA, L. V. SOUKHOV AND I. M. FRANK
P. N. Lebedev Physical Institute, Academy of Sciences, USSR

(Submitted to JETP editor March 9, 1955)
J. Exper. Theoret. Phys. USSR **29**, 537-550 (November, 1955)

The fission of uranium by slow π^- mesons, fast neutrons and high energy γ-rays has been studied by use of thick photographic plates. It has been found that there is a high probability that the uranium nucleus will undergo fission when it captures a π^- meson. This probability is close to 0.5. At high energies of excitation, fission is often accompanied by the emission of charged particles--protons and α-particles. We have determined the energy distribution and angular distribution of these particles. The mechanism of the fission of uranium at high excitation energies is discussed on the basis of these observations.

IT is known that slow negative π^- mesons, just like slow neutrons, are easily captured by nuclei. It is natural to expect that such mesons should induce the fission of uranium and other heavy elements with high probability. However, since the energy liberated upon capture of a meson is many times larger than upon capture of a slow neutron (6-8 mev) the interaction leading to fission might have quite different characteristics. In part, it might be expected that it would, at least in some respects, be comparable to fission induced by particles of high energies (fast neutrons, etc.).

In order to establish and study the fission of uranium by π^- mesons, the technique of thick-layered photographic plates in which uranyl acetate had been introduced was used. The very first experiments, carried out at the start of 1950, showed that the fission of uranium took place with π^- mesons and established some characteristics of this process. This phenomenon was then studied in more detail during 1950*.

A characteristic of fission induced by slow mesons is the presence, in considerable probability, of protons of energies above 10 mev accompanying fission (of the order of once in every 6-7 fissions).

The fission of uranium by π^- mesons was established and studied independently in the work of Ivanova and Perfilov[4] with results in agreement with ours.

The fission of uranium by π^- mesons has also been the subject of work by Al-Salam[5] and John and Fry[6]. Among twenty-two cases of fission, Al-Salam observed three cases of the emission of fast particles. The author merely states that these particles might be α-particles or protons. In the work of John and Fry, there was observed one such case which the authors regard as an exchange proton, even though its energy is about 7 mev.

Earlier, using various methods, the fission of uranium by neutrons and γ-rays of energies up to 100 mev had been extensively studied. It was established that in addition to fission into two fragments, there occurs fission into three particles in 1-2% of the events. In thermal neutron induced fission, the third particle is an α-particle appearing in two groups of ranges: short range α-particles in a yield of $\sim 1\%$ and long range α-particles with a yield of $\sim 0.3\%$[7]. When fission is induced by neutrons of up to 10 mev the yield of long range particles is somewhat smaller[8]. Fast protons have not been observed previously*.

Thus the frequent presence of fast protons as third particles characterizes the fission of uranium with slow π^- mesons and distinguishes it from earlier examples of fission. It is natural to assume that this characteristic is connected with the large energy of excitation produced in the nucleus by capture of π^- mesons. In order to investigate this hypothesis further, there were carried out in 1951-1952 experiments on the fission of uranium by neutrons having energy of 460 mev and by γ-rays up to 250 mev. (At that time there were no data on the cross section for fission by photons of energy above 100 mev.)*

---

* Preliminary results were communicated by us in the report for April 1950[1]. The complete results were presented in our reports for June 1950 and March 1951[2].

[1] G. E. Belovitskii, L. V. Soukhov, T. A. Romanova and I. M. Frank, Report Phys. Inst., Acad. Sci. USSR, April 1950.

[2] G. E. Belovitskii, L. V. Soukhov, T. A. Romanova and I. M. Frank, Report Phys. Inst., Acad. Sci. USSR, June 1950 and March 1951.

[4] N. S. Ivanova and N. A. Perfilov, J. Exper. Theoret. Phys. USSR **28**, 732 (1955).

* In the work of Hill[9] of the fission of U^{235} by slow neutrons, there has been observed the emission of protons of low energies. However, the yield of these is insignificantly 0.02%.

[5] S. G. Al-Salam, Phys. Rev. **84**, 254 (1951).

[6] W. John and W. T. Fry, Phys. Rev. **91**, 1234 (1953).

[7] Tsien San-Tsiang et al, J. Phys. et Radium **8**, 165 200 (1947).

[8] E. W. Titterton, Phys. Rev. **83**, 673 (1953).

[9] D. L. Hill, Phys. Rev. **87**, 1049 (1952).

The results of these studies agree with each other and make possible some conclusions about the characteristics of fission of very highly excited nuclei. The results of our work[1,2,10,11] during 1950-1952 are presented in this article. A short summary has been published already as a letter[12].

1. EXPERIMENTAL PART

In this work we used photographic plates having an emulsion thickness of $100\,\mu$. The plates were sensitive to protons of energy up to 30 mev. In order to increase the efficiency of observing fission events a technique was worked out for introducing uranium salts into the emulsion in large amounts, evenly distributed throughout. To do this the plates were first kept in water at 25° C for 30 min and then in a 2.5-10% solution of uranyl nitrate for 30 min at the same temperature. Experiments showed that the preliminary soaking in water increased the amount of uranium absorbed by the emulsion by a factor of 4 and at the same time induced an even distribution throughout the thickness of the plate. After treatment, the plates were dried in an air stream for 30 min. They were then irradiated and immediately developed. It was established that extensive washing of the plates before development did not wash out the uranium significantly. The presence of uranium in the emulsion not only decreases the sensitivity of the photographic plates and speeds up the disappearance of latent images produced by charged particles but increases the difficulty of subsequent development as a result of contraction and lowering of the pH of the emulsion.

For these reasons the presence of large amounts of uranium necessitated a new method of development. A two solution method was used. The plates were first treated in base (a 3% solution of Na_2CO_3) and then were developed in the following solution: para-amino-phenol--4 gm, anhydrous sulphite--50 gm, H_2O--to make 1000 cm^3.

The preliminary treatment with base corrects the pH of the uranium containing emulsion and accelerates its expansion. This makes it easier for the developer to penetrate into the depths of the emulsion. The result is a more even development, since the depletion of the developer as a result of penetration into the interior of the emulsion is compensated by the higher local concentration of base.

In the final experiments the following development procedure was used:

1) Treatment in base: 30 min at 18° C;
2) Treatment in the developer: 30 min at 18° C;
3) Stop-bath: 15 min (a 2% solution of acetic acid) at 15° C;
4) Distilled water washing: 15 min;
5) Fixing: 1½-2 hrs;
6) Final washing: 1½-2 hrs;
7) Drying.

The search for mesons stopping in emulsion and for fission fragments was carried out with a binocular microscope, objective of 60 × (P· A = 1.0), ocular of 7 × and magnification of 1.5 × (total magnification 630 ×). The measurement of the range of the fragments and the grain counting was made with an objective of 90 × (P· A = 1.3) and with an ocular of 15 ×, giving an overall magnification of about 2000 ×.

The irradiations of the photographic plates with slow π^- mesons and with neutrons of maximum energy equal to 180 and 460 mev were carried out at the synchrocyclotron of the Institute for Nuclear Problems of the Academy of Sciences.

The slow π^- mesons were produced in a lead target 2 mm thick by 560 mev α-particles. They were deflected by the magnetic field of the cyclotron, passed through absorbers which slowed them down and impinged on the photographic plates. These were introduced into the vacuum chamber of the cyclotron in a sealed casette on a special probe. The irradiation time was 5-15 min.

The neutrons used for these experiments were produced either in a bombardment of Cu with 560 mev α-particles or by a bombardment of Be with 180 mev and 460 mev protons.

As was shown in the work of Djelepov and

---

* The results of these studies were given in our report for Dec. 1952[10]. This work also used photographic techniques. These are described in the report for June 1952[11].

[10] G. E. Belovitskii, L. V. Soukhov and I. M. Frank, Report Phys. Inst., Acad. Sci. USSR, Dec. 1952.

[11] T. A. Romanov, and G. E. Belovitskii, Report Phys. Inst., Acad. Sci. USSR, June 1951.

[12] G. E. Belovitskii, T. A. Romanov, L. V. Soukhov and I. M. Frank, J. Exper. Theoret. Phys. USSR **28**, 729 (1955); Soviet Phys. 1, 581 (1955).

Kazarinov[13], the bombardment of targets with monoergic protons produces neutrons with a distribution in energies. The maximum in the spectrum of neutrons is at a lower energy than the energy of the original particles. For protons of 180 mev this maximum lies 20-30 mev lower; for 460 mev protons it lies 80-100 mev lower. Thus the most probable neutron energies in the two cases are 150 and aprproximately 380 mev. A more complete description of the energy spectrum of the neutrons (for energies less than 100 mev) has been given[14], where it is shown that more than 50% of the neutrons have energies less than 100 mev, being formed by evaporation processes from excited Be and Cu nulcei. In the rest of this paper such neutrons with a broad energy spectrum will be called 150 mev neutrons and 380 mev neutrons.

For comparison, we also investigated the fission of uranium with 14 mev neutrons. These experiments were carried out at a high voltage set. In most cases the photographic plates were oriented horizontally relative to the neutron beam. In the irradiations with fast neutrons the photographic plates were protected from slow neutrons by cadmium sheets 1 mm thick.

The irradiations with γ-rays were carried out at maximum γ-ray energies of 30, 80 and 250 mev. In most cases the plates were oriented perpendicular to the γ-ray beam. These irradiations were carried out with the synchrotron of the Lebedev Institute of Physics of the Academy of Sciences.

2. THE INTERACTION OF π^- MESONS WITH URANIUM NUCLEI

Of the more than 3000 π^- mesons ending in the emulsion there were 96 observed cases of π^- mesons producing fission in uranium. For comparison, among 634 π^- mesons ending in emulsions that had not been impregnated with uranyl acetate there was not found a single case of uranium fission. Among the 96 fissions, 81 had only 2 fragments; a third particle was emitted in the other 15 cases.

In the fission of uranium by π^- mesons into two fragments the two particles, as a rule, go off in opposite directions. Figure 1 shows microphotographs of typical fission events induced in uranium by π^- mesons (microphotographs *1-4*). The presence of the π^- meson track usually makes it possible to determine the point where the fission occurred and thus to determine the separate ranges of the two fragments. These fragment ranges were measured with an accuracy no better than 5%.

In Fig. 2 are presented the distribution in total ranges of the two fragments (only including those cases where a recoil nucleus with a range greater than 1-2 was not observed) for 45 cases of π^- meson induced fission of uranium; in Fig. 3 are shown the distributions of ranges of the light and heavy fragments. For comparison in Fig, 2 there is shown the distribution of total ranges of both fragments from 243 cases of uranium fission induced by the neutron background. The larger scatter in the ranges of fragments in the case of meson fission as compared to neutron fission is probably connected with the lower accuracy of measurement, since in the case of neutron fission only those cases were picked which lay in the plane of the emulsion. For comparison there is also presented in Fig. 3 the distribution in ranges of the light and heavy fragments from the thermal neutron fission of U^{235}. This was taken from a report in 1949 by Bøggild[15]. The ranges in air were converted into ranges in emulsion using a relative stopping power factor of 1680.

It is seen from Figs. 2 and 3 that there is no significant change in the ranges of fragments of fission induced by π^- mesons from those arising from neutron fission. It is also seen that π^- meson induced fission proceeds in a more symmetrical fashion than does neutron induced fission.

Among the 96 cases of fission induced by π^- mesons we saw 15 cases accompanied by a third charged particle. Microphotographs of such instances are presented in Fig. 4 (*5-8*). In such fissions the fragment ranges stay the same as in fissions not accompanied by a third particle.

These cases have the following characteristics:

In one case the fission is accompanied by the emission of a long range α-particle. Its full range in emulsion is equal to 105 μ, leading to an energy of 14 mev. The angles between it and the heavy and light fragments are 98 and 82°, respectively.

In one case there was emitted a highly ionizing particle with a range of only 2.5 μ. If it is assumed that this is an α-particle, its energy is equal to 0.8 mev. This particle was likewise emitted at an angle of 90° with respect to both fragments. In 13

---

[13] V. P. Djelepov and Y. M. Kazarinov, Dokl. Akad. Nauk SSSR **99**, 939 (1954).

[14] J. Cassels et al, Phil. Mag. **42**, 215 (1951).

[15] J. K. Boggild et al, Phys. Rev. **76**, 988 (1949).

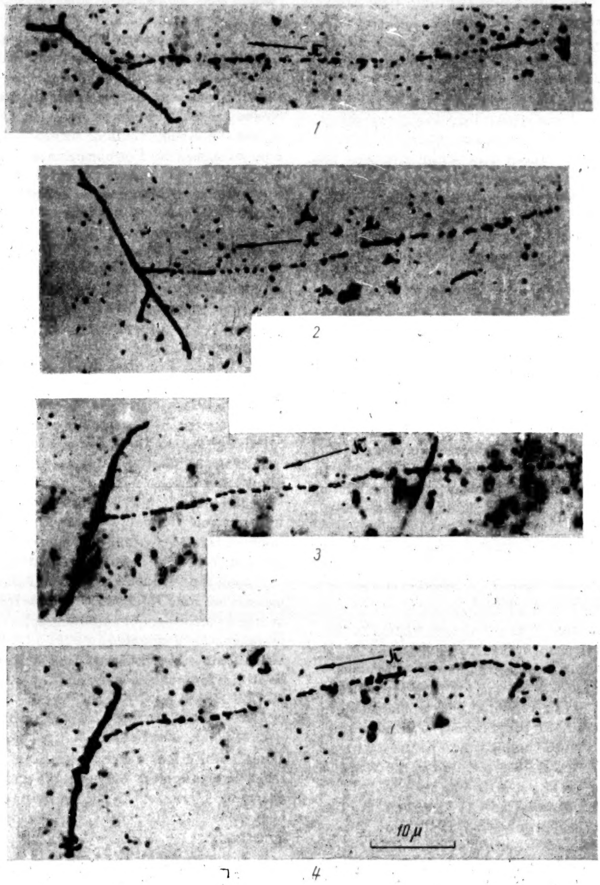

FIG. 1. The Fission of uranium by π^- mesons into two fragments; microphotographs *1-4*.

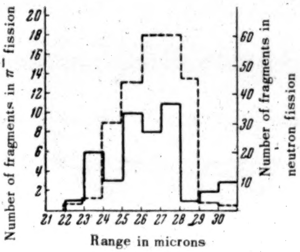

FIG. 2. The distribution in total ranges of the fragments from uranium fission induced by π^- mesons and by neutrons; solid line--fragments from π^- mesons fission; dashed line--fragments from slow neutron fission.

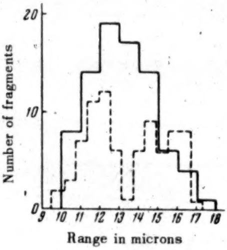

FIG. 3. The distribution in ranges of the light and heavy fragments in the π^- fission and slow neutron fission of uranium; solid line--fragments in π^- fission; dashed line--fragments from slow neutron fission.

cases of fission the third particle emitted is singly charged. Since none of these stopped in the emulsion, a definite mass assignment could not be made. However, since these particles are singly charged, as was established from the observed ionization (grain density along the track), it is natural to assume that most of these are protons. However, it cannot be excluded that among them were some deuterons or tritons. Using the curve of grain density as a function of range of π^- mesons, it was possible to calculate the ranges of these particles from their measured grain densities and from this their energies on the assumption that the particles were protons. This range spectrum is pictured in Fig. 5. (If it is assumed that the particles emitted are α-particles, then their energy must be 16 times the energy of protons producing a track with the same grain density. This would lead to energies in the range 170-450 mev, which are impossible from conservation of energy considerations.)

In view of the possible large fluctuations in grain density, this evaluation of the energy of the particles has an accuracy only to within 20%.

The small number of cases studied makes it impossible to make definite statements about the angular distribution of these particles relative to the direction of motion of the fission fragments. In the observed cases, considering equal solid angles, there were emitted 5 particles between 0 and 48°, 3 particles between 48 and 70° and 5 particles between 70 and 90°. On the basis of these numbers it can be said that there is no strong preference for angles close to 90° such as is observed in the case of α-particles emitted in neutron induced fission.

3. THE PROBABILITY OF URANIUM FISSION BY π^- MESONS

In order to determine the probability of fission of uranium by mesons it is necessary to compare the number of expected captures of π^- mesons by uranium nuclei with the number of observed cases of fission.

The number of uranium nuclei that were incorporated into the emulsion was determined by counting α-particles from the natural radioactivity of uranium. In this measurement a correction was made for the α-particles that left the emulsion. In addition, proper account was taken of the fact that the emulsion is not sensitive all of the time (equal to 3 hours) between the start of the soaking in uranyl acetate until the final state of development.

The amount of uranium in the emulsion turned out to be 0.106 gm/cm^3 of dry emulsion (0.028×10^{22} nuclei/cm^3) and was established with 10% accuracy. From this data and from the atomic constitution of the emulsion it was found that 11% of the π^- mesons stopping in the gelatine would be captured by a uranium nucleus.

The calculation was made under the following assumptions:

1) The emulsion is a heterogeneous mixture--a suspension of AgBr crystals in gelatine.

2) The uranium is completely adsorbed on the gelatine;

3) The fraction of π^- mesons stopping in the

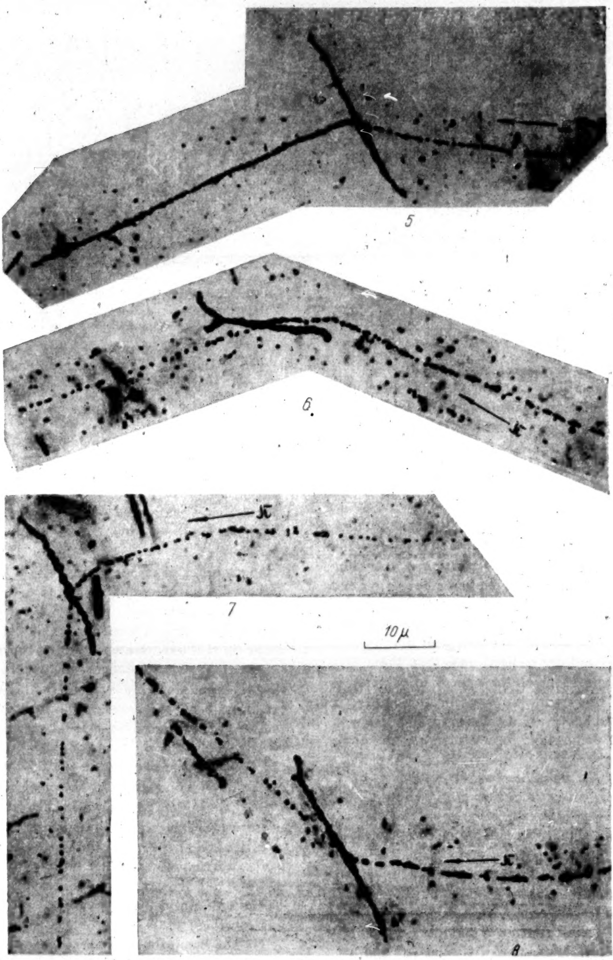

FIG. 4. The fission of uranium by π^- mesons into two fragments accompanied by fast charged particles; microphotograph 5 -- a 14 mev α-particle is emitted; microphotograph 6 -- an $\sim$ 12 mev proton is emitted; microphotograph 7 -- an $\sim$ 18 mev proton is emitted; and microphotograph 8 — a 20 mev proton is emitted.

AgBr and in the gelatine is proportional to the stopping powers of these substances[16];

4) The probability of capture of a π^- meson that stops in the gelatine by the different elements present (C, N, O, U) is proportional to the nuclear charge Z.

This same method for calculating the probability of capture of mesons by uranium was used by John and Fry[6].

Systematic scanning found 1983 π^- mesons stopping in the emulsion. Of these, 72 π^- mesons produced uranium fission (the μ^- contamination in the π^- meson beam was 5%). If one assumes that the efficiency of observing the stopped mesons is about 0.7, then 5.7 percent of the π^- mesons produce fission. This leads to a probability of 0.5 that a π^- meson that has been captured by a uranium nucleus will produce fission.

If the assumptions used in the calculation of the probability of a uranium nucleus capturing a meson are correct, then 50% of the time that a π^- meson is captured by such a nucleus it induces fission. The probabilities of fission found by other workers[4-6] in the same way lie in the regions 0.2-0.4. Since the accuracy of these measurements is not large it is not possible to say that they disagree significantly from each other. If, in contrast to the assumptions made above, the emulsion is regarded as a homogeneous medium and it is assumed that the π^- mesons are captured by the component nuclei with a probability proportional to their charge, then the probability that the π^- meson will produce fission after being captured by a uranium nucleus comes out close to unity.

In view of the inaccuracy of the measurements and the ambiguity of the calculation of the capture probability of mesons by uranium, it is necessary to conclude merely that a significant fraction of the π^- mesons captured by uranium induce fission. It should be mentioned that in this work it was not found possible to establish definitely other types of uranium fission into two or more fragments under the influence of π^- mesons. This was due to the fact that in all this work only those cases of fission were selected in which the two fragments were directed in opposite or almost opposite directions (in the range ±10°). Other possible types of fission were hard to identify since control plates, not loaded with uranyl acetate, showed similarly appearing cases. Microphotographs of several of the more certain cases of fission of uranium by π^- mesons into 3 or 4 fragments are presented in Fig. 6 (*9-11*). In microphotographs *9* and *10* the tracks have been produced by multiply charged particles. One of the tracks in the microphotograph *10* might be a recoil nucleus. In order to satisfy conservation of momentum it is necessary to assume the emission of several neutrons.

In addition to fission into 3 or 4 fragments there are possible spallation processes involving the emission of 2-3 multiply charged particles, leaving at angles much smaller than 180°, and charged particles with $Z \leq 2$. A microphotograph of such a case is presented in Fig. 6 (*11*).

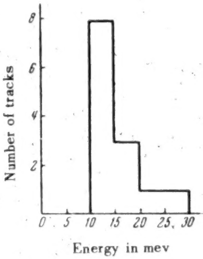

FIG. 5. The energy spectrum of protons accompanying uranium fission induced by π^- mesons.

4. THE FISSION OF URANIUM BY FAST NEUTRONS

There were found 309 fission events in the plates irradiated in the 380 mev neutron beam. In 67 of these the fission was accompanied by the emission of one or more long range charged particles. Twenty-one out of these 67 cases involved the emission of two extra particles; four of them had three; and in two instances there were four extra particles*. Thus with neutrons of this energy the probability of such complex fission events is 1:5.

In photographs irradiated by 150 mev neutrons there were found 389 uranium fission events. Of these 25 were accompanied by a third long range particle. Here the probability of such processes is 1:16.

In the case of photographic plates irradiated with 14 mev neutrons there were found 1917 fission events. Among these there was not a single case of a fission accompanied by a long range alpha

---

[16] A. Bonettie and G. Tomasini, Nuovo Cim. 8, 693 (1951).

* In Fig. 7 are shown microphotographs of such fission events (microphotographs *12-18*).

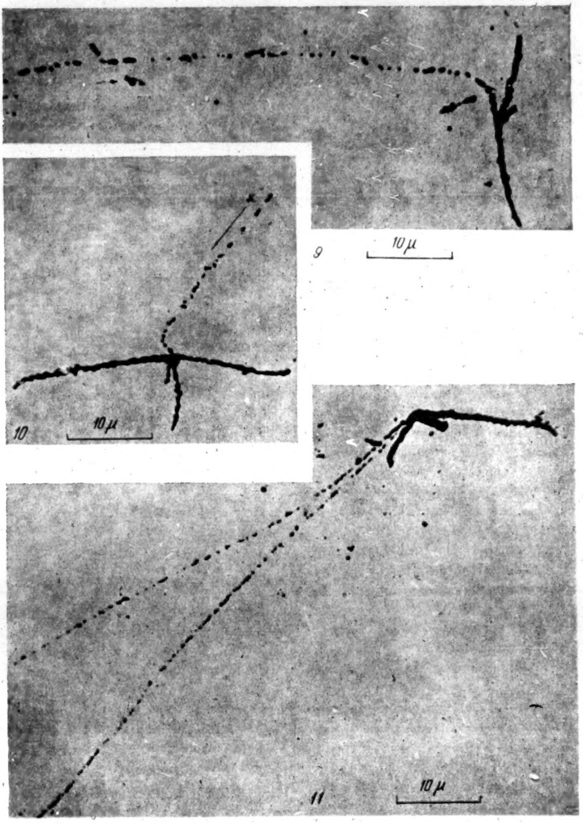

FIG. 6. Probable cases of uranium fission induced by π^- mesons. Microphotograph *9*--fission into three fragments; microphotograph *10*--fission into three or four fragments; microphotograph *11*--division into three fragments accompanied by the emission of a fast charged particle.

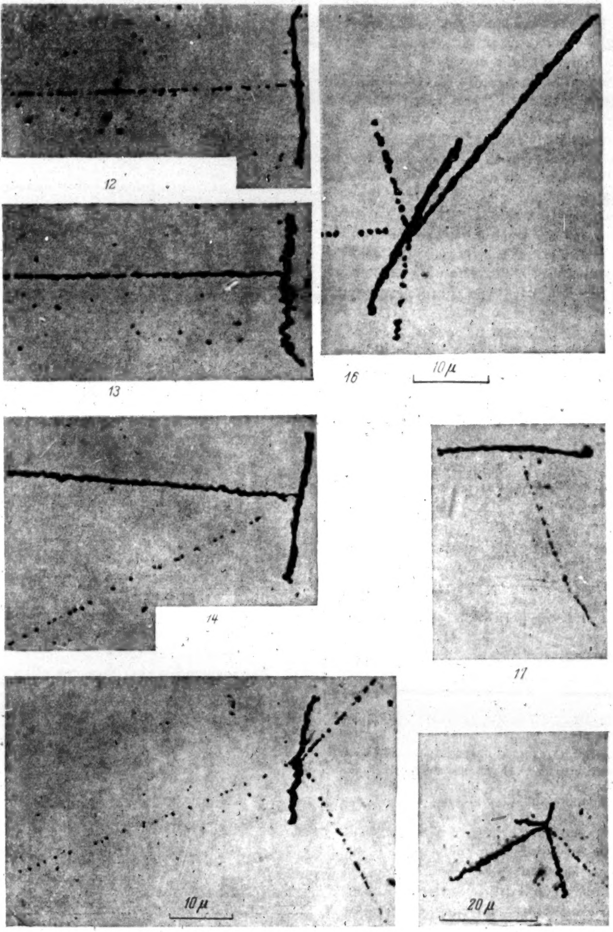

12 13 16 14 17 15 18

FIG. 7. Cases of the fission of uranium by 150 and 380 mev neutrons accompanied by the emission of fast charged particles. Microphotograph *12*--a 14 mev proton is emitted: microphotograph *13*-- an 18 mev α-particle is emitted; microphotograph *14*--two particles, 16 mev α-particle and a 23 mev proton, are emitted; microphotograph *15*-- three particles, 23, 23 and 14.5 mev protons, are emitted; microphotograph *16*-- four particles, 7, 15 and 30 mev protons, and an ~ 14 mev α-particle, are emitted; microphotograph *17*-- a 1.7 mev proton is emitted; microphotograph *18*-- a probable case of fission into four fragments accompanied by the emission of a fast charged particle.

particle. Thus the production of long range protons and alpha particles in the case of 14 mev neutron fission must be a very rare event.

A comparison of the results of these experiments with neutrons of three different energies clearly shows that the probability of the uranium fission being accompanied by a third long range particle rises with the energy of the incoming neutron and that such fission events are definitely caused by high energy neutrons.

In cases where it was possible we measured the total ranges and the separate ranges of the light and heavy fragments of the fission accompanied by a long range particle. The site of the fission event was assumed to be the point of emission of the fast particle accompanying the fission. The average total range turned out to be the same as the range of fragments from fission caused by low energy neutrons.

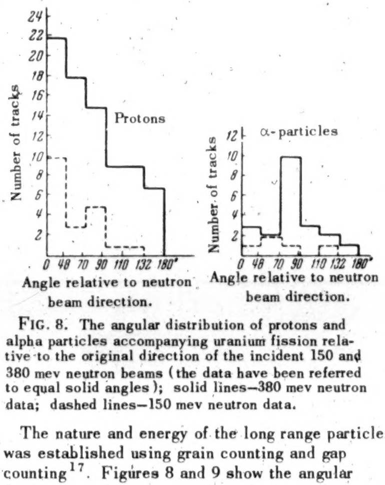

FIG. 8. The angular distribution of protons and alpha particles accompanying uranium fission relative to the original direction of the incident 150 and 380 mev neutron beams (the data have been referred to equal solid angles); solid lines—380 mev neutron data; dashed lines—150 mev neutron data.

The nature and energy of the long range particles was established using grain counting and gap counting[17]. Figures 8 and 9 show the angular distribution of these particles relative to the direction of the incident neutrons and relative to the plane perpendicular to the fission fragment direction. The data are presented in equal solid angles. It is seen from Fig. 8 that most of the protons come off at angles less that 90° relative to the neutron direction. It is seen from Fig. 9 that the protons are emitted essentially isotropically relative to the fission fragment directions.

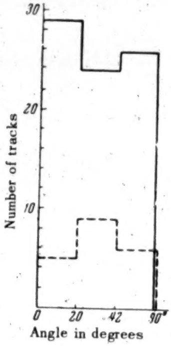

FIG. 9. Distribution of angles (relative to a plane normal to the fission fragment direction) of protons accompanying the 150 and 380 mev neutron fission of uranium (the data have been referred to equal solid angles); solid lines—380 mev neutron data; dashed lines--150 mev neutron data.

In contrast, α-particles apparently have a strong angular preference. Thus out of a total of 27 α-particles, 16 had angles less than 20° relative to a plane normal to the fission fragment trajectories (see below, Fig. 14).

The energy of the singly charged particles, on the assumption that they are all protons (it is

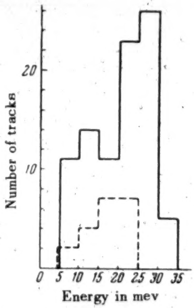

FIG. 10. Energy spectrum of the protons accompanying the fission of uranium by 150 and 380 mev neutrons; solid lines--380 mev neutron data; dashed lines—150 mev neutron data.

---

[17] P. E. Hodgson, Phil. Mag. 41, 725 (1951).

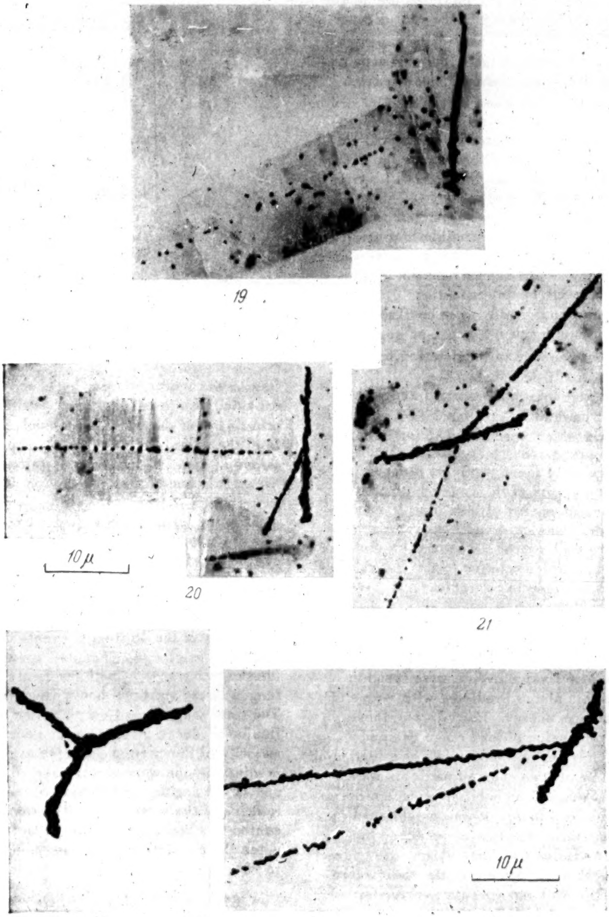

FIG. 11. Cases of uranium fission (induced by γ-rays having energies up to 250 mev) accompanied by the emission of fast charged particles: microphotograph *19* -- a 9.5 mev proton is emitted; microphotograph *20* -- a 13 mev proton and a 35 mev α-particle are emitted; microphotograph *21* -- a 9.7 mev proton and a 24 mev α-particle are emitted; microphotograph *22* -- a 10 mev proton and a 36 mev α-particle are emitted; microphotograph *23* -- a probable fission event into three fragments.

possible that some of these particles are deuterons or tritons), lies mainly in the energy range 10-30 mev (Fig. 10). The energy range of the α-particles lies in the range 14-25 mev. Actually, the range of the protons accompanying the fast neutron fission of uranium might extend to values even higher than 30 mev but because of the limited sensitivity of the photographic plates to such protons these would not be observed. For some of the protons the energy turned out to be lower than the potential barrier of uranium (about 10 mev).

Since the majority of these particles did not stop in the emulsion, it is possible that some of the protons included in Fig. 10 in the energy interval 5-10 mev came to be there because of inaccuracies in the energy determination. However, the emission of such particles is confirmed by other experiments carried out with photographic plates of lower sensitivity (registering protons of energies up to 10-15 mev).

In such photographic plates irradiated with 140 mev neutrons there were found 3293 cases of fission, among which were 33 involving the emission of a long range charged particle. A considerable number of these particles stopped in the emulsion. A majority of them turned out to be protons having an energy of less than 10 mev. In particular, there was observed a proton with an energy as low as 1.7 mev*. The angular distribution of these particles relative to the fragments turned out to be close to isotropic.

5. THE INTERACTION OF HIGH ENERGY γ-RAYS WITH URANIUM NUCLEI

A total of 2066 fission events were found in the photographic plates irradiated with γ-rays of 250 mev maximum energy. Forty-five of these involved the emission of long range charged particles. Thirty-seven were cases of emission of only one; in eight, two charged particles were emitted**. Thus, the probability of such processes is at least one in 46. It was established in control experiments that fission produced by background particles (secondary neutrons) contributed less that 0.2 percent to the observed result. These control experiments were performed by irradiating plates outside the γ-ray beam.

In photographic plates irradiated with γ-rays of 80 mev maximum energy there were found 614 fission events, 3 of them being accompanied by the emission of a third long range particle. Thus the probability of the emission of such a particle here is of the order of one in 200. In experiments with γ-rays of up to 30 mev there were found 717 fission events. In one of these there was a long range α-particle.

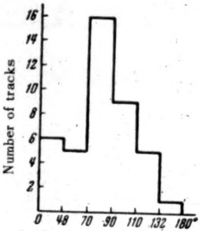

Angle relative to the γ-ray beam direction.

FIG. 12. The angular distribution of the protons accompanying uranium fission relative to the incident 250 mev maximum energy γ-ray beam direction. (The data have been referred to equal solid angles.)

Thus the emission of a singly charged particle was not observed. Apparently, at energies of excitation of about 20 mev, close to that produced in the interaction of 14 mev neutrons with uranium, the emission of charged particles has a very low probability.

In those of the 45 fission events accompanied by charged particles we measured where it was possible the total range of both fragments and the ranges of the light and heavy fragments separately. The total range turned out to be the same as in fission produced by low energy neutrons. The majority of the emitted particles accompanying uranium fission were singly charged. Figure 12 shows the angular distribution of these particles relative to the γ-ray beam. The results are presented in equal solid angles. The figure indicates the characteristic maximum at angles close to 90°.

Figure 13 shows the distribution of angles between the singly charged particle and the plane normal to the motion of the fragments. It is seen that this distribution is close to isotropic. On the other hand, α-particles show an asymmetric angular distribution: of eleven cases, six show an angle less than 20° relative to the plane normal to the fragment direction (Fig. 14). Figure 15 shows the energy spectrum of the

---

* A microphotograph of this case is shown in Fig. 7. Microphotograph 17.

** Microphotographs and microdrawings of such fission events are presented in Fig. 11, microphotographs 19-22.

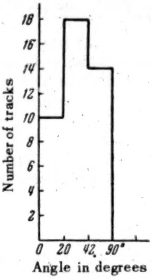

FIG. 13. The distribution of angles (relative to the plane perpendicular to the fragment directions) of the protons emitted in the fission of uranium by γ-rays having energies up to 250 mev. (The data have been referred to equal solid angles.)

singly charged particles. This spectrum (assuming all the particles are protons) extends from 6 to 25 mev. The α-particle spectrum extends from 18 to 35 mev.

These results on the fission of uranium by high energy γ-rays makes it possible to conclude that the effective cross section for uranium fission with γ-rays higher in energy that 100 mev is not negligible, as it appears to be in the energy interval 30-100 mev[18]. It is obvious that the significant increase in the fraction of fissions accompanied by a third particle when the γ-ray spectrum is extended to 250 mev indicates that the γ-rays above 100 mev are contributing appreciably to the events being studied. Similar results were obtained by Bannik and Ivanov[19].

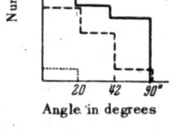

FIG. 14. The distribution of angles (relative to the plane normal to the fragment direction) of the α-particles emitted in the fission of uranium by slow π^- mesons, fast neutrons and γ-rays having energies up to 250 mev; solid line — α-particles from neutron fission; dashed line — α-particles from γ-ray fission; dotted line— α-particle from π^- fission.

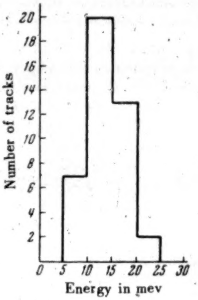

FIG. 15. Energy spectrum of the protons emitted in the fission of uranium by γ-rays of 250 mev maximum energy.

The formation of stars when γ-rays of energy higher than 80 mev impinge on the nuclei of emulsion has been studied by Wexler, Pissarev and Lebedev[20] and likewise by Kikuchi[21]. There it has been shown that the cross section for star formation of the nuclei in photographic emulsions increases 3-4 fold in the γ-ray energy interval 80-250 mev. This is in excellent qualitative agreement with our results on the increase in fission events accompanied by long range particles (produced by high energy γ-rays). This would be hard to explain without assuming that the fission cross section rises in this energy interval. Our result has also been confirmed by the recently published work in which the cross section for uranium fission by γ-rays has been determined as a function of energy from 125 to 300 mev[22].

---

[18] G. C. Baldwin and G. S. Kleiber, Phys. Rev. 71, 3 (1947).

[19] B. P. Bannik and Y. C. Ivanov, Report Phys. Inst., Acad. Sci. USSR, 1953.

[20] V. I. Veksler, C. V. Lebedev and V. E. Pissarev, Report Phys. Inst., Acad. Sci. USSR, 1952.

[21] S. Kikuchi, Phys. Rev. 81, 1061 (1951).

[22] J. Gindler and K. B. Duffield, Phys. Rev. 94, 759 (1954).

6. DISCUSSION OF RESULTS

It is seen from Fig. 2 that the ranges of the fission fragments in the case of π^- fission have the same magnitudes as the ranges of fission fragments produced by moderate energy neutrons. The average total ranges of the fragments in π^- meson fission and in neutron induced fission are 26 and 27 microns, respectively, and thus the same within experimental error. A similar result was obtained from measurements on the total ranges of fragments from fast neutron (150 and 380 mev) fission, and in fission produced by γ-rays of energies up to 250 mev. This result is in good agreement with the recently published data on the ranges of fission fragments produced by the interaction of 335 mev protons with uranium [23]

The distribution and ranges of light and heavy fragments in π^- induced fission when compared with that from slow neutron fission (Fig. 3) indicates that π^- induced fission is more symmetrical. The same result was found for fission induced by fast neutrons and by high energy γ-rays, and agrees with recently published data in the literature[24,25].

If it is assumed that in π^- induced uranium fission the nucleus divides in the usual way into two equal fragments, then the total kinetic energy available for the fragments should be equal to about 160 mev. If to this is added a significant part of the energy available upon capture of a π^- meson, for example, 50 to 100 mev, then the total kinetic energy of the fragments would be 200 to 250 mev. This would produce fragments with ranges of 30 and 33 microns. The observed range (Fig. 2) as a rule did not exceed 29 microns, and ranges greater than 31 microns have not been observed at all. Such long ranges must have a low abundance.

From this we conclude that the energy brought into the uranium nucleus by the π^- meson is not transformed into kinetic energies of fission fragments, but produces other processes*.

Since this originally available energy is used only in small portion for the emission of charged particles, it is natural to assume that the main part is carried off by neutrons. This energy can be transferred to separate nucleons ejected instantaneously from the nucleus, but might also be used to excite the nucleus as a whole. It is known[26] that the average energy of excitation of AgBr nuclei when they capture π^- mesons is approximately 100 mev. The excitation energy remaining in the uranium nucleus could be of the same magnitude. Evaporation theory, developed in published work[27], should be applicable at such energies of excitation of the uranium nucleus.

On the basis of this work, we found that the uranium nucleus, after capturing a π^- meson, can evaporate, on the average, about 10 neutrons before it undergoes fission. These neutrons should have average kinetic energies of 2-3 mev. Approximately the same number of neutrons should be emitted from similarly excited uranium nuclei when they are irradiated with fast neutrons and high energy gamma rays. A similar conclusion was reached by Gol'danskii, Taroumov and Pen'kin[28], and from work on the average number of neutrons emitted by a lead nucleus upon capture by a slow π^- meson[29]. There is somewhat greater interest in the mechanism of the emission of the long range charged particles accompanying fission. The energy spectrum of these particles and their angular distribution is significant in this regard. The energy spectra of the fast, singly charged particles accompanying the fission of uranium by π^- mesons, fast neutrons and high energy γ-rays, are presented in Figs. 5, 10 and 15. Because of the limited sensitivity of photographic plates for high energy protons, these spectra are presented only for energies less than 30 mev and thus represent significantly distorted versions of the true energy spectra of these particles*.

The observed difference in shape of the spectra of protons produced by π^- mesons and γ-rays from that produced by fast neutrons does not appear significant in view of the small number of events observed. At the same time this difference may be connected with a difference in the type of interaction. When π^- mesons or gamma quanta are absorbed the interaction is with at least two nucleons; a fast neutron on the other hand can interact with a single nucleon in a nucleus. The secondary nucleons produced will have various energies and thus affect the shape of the energy spectrum. It has already been pointed out that these spectra have a small number of particles having energies less than 10 mev. It is hard to say what fraction of all protons have such energies. Using the data of Bernardini[30] to get the fraction of particles that we did not observe, leads to a value of 5% of all protons with energies less than 10 mev. It is still not clear what the mechanism can be for producing such particles with energies less than the coulomb barrier. It is possible that the uranium nucleus, having emitted 10 neutrons, is so proton rich that the proton binding energy is decreased enough to increase the probability of its emission. It can also be assumed that some of these particles are emitted not from the uranium nucleus but from excited fission fragments which have a smaller coulomb barrier.

---

* This same conclusion was deduced earlier for fission produced by fast neutrons[3].

[3] J. Jungerman and S. Wright, Phys. Rev. 76, 1112 (1949).

[23] E. Douthett and D. Templeton, Phys. Rev. **94**, 128 (1954).

[24] M. Lindner and R. Osborne, Phys. Rev. **94**, 1323 (1954).

[25] R. Schmitt and N. Sugarman, Phys. Rev. **95**, 1260 (1954).

* From published work by G. Bernardini[30] in which the energy spectra of protons emitted in the interaction of 400 mev protons with the nuclei of photographic emulsions has been determined, it follows that the particles we did not observe (having energies greater than 30 mev) represent 50% of all particles.

[26] M. G. K. Menon et al, Phil. Mag. **41**, 583 (1950).

[27] K. J. La Couteur, Proc. Phys. Soc. (London) 63A, 259 (1950).

[28] V. I. Gol'danskii, E. Z. Taroumov and V. C. Pen'kin, Dokl. Akad. Nauk SSSR **101**, 1027 (1955).

[29] V. Cocconi-Tongiorgi and D. Edwards, Phys. Rev. **88**, 145 (1952).

[30] G. Bernardini et al, Phys. Rev. **85**, 826 (1952); **88**, 1017 (1952).

The α-particles accompanying fission show the characteristic asymmetry in relation to the direction of motion of the fragments. The majority of them are given off in directions close to 90° relative to the fission fragment direction. This conclusion is supported by Fig. 14, in which are presented data on the angular distribution of α-particles emitted in the π^- fission of uranium, fast neutron fission and fission by gamma rays having energies up to 250 mev. It is well known that the α-particles accompanying fission induced by low energy neutrons come out at angles less than 30° relative to the plane normal to the fission fragment motion[7,31]. This angular distribution is determined by the α-particles being emitted in the actual fission process. Since they are affected by the coulomb fields of both fragments they must move in a direction close to 90° relative to the fragment direction. It is reasonable to assume that a considerable fraction of the α-particles that we observed are likewise emitted during the actual fission process.

The angular distribution of fast protons relative to the fission fragment direction is close to isotropic in the fission of uranium by mesons, fast neutrons (Fig. 9) and γ-rays (Fig. 13). From this it appears that the majority of the protons are not emitted in the fission act. The angular distribution of these particles relative to the neutron beam direction (Fig. 8) shows a well-defined preference for the beam direction. Out of 99 particles observed in fission induced by neutrons having energies up to 150 and 380 mev, 75 make an angle less than 90° relative to the incident beam direction and only 27 come out at angles greater than 90°.

When fission is induced by the photons of high energy, the accompanying singly charged particles show a characteristic preference for angles close to 90° relative to the incident beam direction. Such an angular distribution points to the majority of these particles being emitted before the fission act. If these particles were emitted by the uranium nucleus as part of the evaporation process, their angular distribution might be expected to be close to isotropic. Their observed anisotropy indicates that a significant fraction of them are recoil nucleons produced either as a result of the first interaction, or as a result of the development of the nuclear cascade produced by the incident neutron or γ-quantum inside the nucleus. Since it is hard to imagine that in π^- induced fission there should exist a different mechanism of production of charged particles, we believe that this process also occurs in the meson situation.

It follows from the experiments with fast neutrons and γ-rays that the probability of emission of charged particles and their number per fission event increases as the energy brought into the nucleus is increased. In this connection it should be kept in mind that this experiment did not detect the emission of protons having energies greater than 30 mev, nor did it detect fast neutrons which may have accompanied fission. Moreover, the incident neutrons contained more than 50% of neutrons having energies significantly smaller than 100 mev. These, although effective in producing fission, are relatively ineffective as regards the process being investigated. For these reasons the true probability for the emission of fast particles increases with energy at a faster rate than we have observed. Taking into account these factors we conclude that practically every case of fission of uranium induced by 300 mev neutrons has associated with it an emitted fast nucleon.

In conclusion it should be pointed out again that in these investigations of the fission of

---

[31] L. Marshall, Phys. Rev. 75, 1339 (1949).

uranium by π^- mesons, fast neutrons and high energy γ-quanta there were selected only fission events in which the fragments came out in opposite or almost opposite directions. We thus do not exclude the possibility that other types of fission, into 2-3, or more fragments, might occur in the interaction of π^- mesons with uranium nuclei. These experiments were not designed to characterize such events. For example, in Fig. 7 there is presented a microphotograph (*18*) of a possible fission of uranium into 4 fragments and accompanied by the emission of a fast charged particle. This was produced by neutrons having an energy of up to 150 mev. In Fig. 11 (*23*) there is presented a probable uranium fission event produced by γ-rays of up to 250 mev energy. This fission is into 3 heavy fragments.

CONCLUSIONS

1. It has been established that different types of particles--slow π^- mesons, high energy γ-rays and fast neutrons--effectively induced fission in the uranium nucleus. The data on the fission of uranium by π^- mesons indicate that, in a significant number of cases (approximately 50%), a meson captured by the uranium nucleus will induce it to undergo fission.

The experiments indicate that photons having energy greater than 100 mev have a significant probability of inducing uranium fission.

2. The ranges of the fragments from uranium fission induced in different ways (π^- mesons, 150-380 mev neutrons, γ-rays with energy up to 250 mev) have the same magnitudes as the ranges of the fragments in the slow neutron fission of uranium. From this it follows that the energy brought in by these different particles is not transformed into kinetic energy of the fragments but is used in other processes. The distribution in fission product ranges indicates that the fission of uranium at high energies of excitation is more symmetrical than is the slow neutron fission of this nucleus.

3. The fission of uranium by slow negative π^- mesons, 150-380 mev neutrons and γ-rays having energies up to 250 mev, is accompanied by the emission of singly charged particles, probably protons. Most of these particles have energies greater than 10 mev and are emitted either as a result of a direct collision or as a result of the cascade process started by the incident particle in the uranium nucleus. Besides the protons there are emitted long range α-particles which, in contrast to the protons, are frequently produced in the act of fission. The frequency of emission of the protons and α-particles increases as the energy of excitation of the uranium nucleus is increased. At energies of excitation of 100-200 mev, star formation preceding fission is observed.

4. The fission of uranium at high energies of excitation is quite frequently accompanied by the emission of fast protons and α-particles. However, the charged particles carry off only an insignificant fraction of the energy brought in by the incident particle. The main part of this energy brought into the nucleus by π^- mesons, fast neutrons and high energy γ-rays must be used up in the emission of neutrons of various energies. A large fraction of the neutrons must be emitted before fission.

In conclusion, we consider it a pleasant duty to express gratitude to M. G. Meshcheriakov, V. P. Djelepov and F. P. Grigoriev for help in carrying out the experiments with the π^- mesons and fast neutrons; to V. I .Veksler and Y. C. Ivanov for help in the experiments with high energy γ-rays; and likewise to A. N. Kouznetsov, Y. N. Lizounov and I. L. Nesmelov who carried out the main labor of the plate scanning.

Translated by A. Turkevich
238

SOVIET PHYSICS JETP VOLUME 2, NUMBER 3 MAY, 1956

The Theory of Strong Coupling for Meson Fields I

B. T. Geilikman
Moscow State Teachers' Institute

(Submitted to JETP editor June 17, 1954)
J. Exper. Theoret. Phys. USSR **29**, 417-429 (October, 1955)

Scalar and pseudoscalar meson fields which interact with infinitely heavy extended nucleons are considered in the strong coupling approximation. A theory of excitation is developed in the reciprocal coupling constant of the nucleons with the meson field.

A series of experimental facts and, in particular, the scattering of π-mesons by protons bear witness to the inapplicability of the theory of excitation (weak coupling) for the description of the interaction of the meson field with nucleons. In view of this, considerable interest attaches to the study of another limiting case for the meson field – that of strong coupling, i.e., expansion not in direct, but in reciprocal powers of the coupling constant of the nucleons with the meson field $g^2/\hbar c$.

In a series of published works, the meson field interacting with nucleons in the approximation of strong coupling has been studied. In the present paper I and in the following paper II, the nucleons are assumed to be extended and to be infinitely heavy, and the nucleonic vacuum is not considered. In a third paper, a field interacting with moving, extended nucleons of finite mass will be considered, and an attempt will be made to set up a relativistic theory with account taken of the nucleonic vacuum. The extension of the nucleon (smeared out interaction) is introduced temporarily. After passing to renormalization, the "radius" a of the nucleon must be equated to zero. In certain cases (nonguage coupling) such a transition to $a = 0$ can be made even before renormalization (see II).

1. We consider first the meson field corresponding to a spin of zero which interacts with a single quiescent, infinitely massive, extended nucleon. The Hamiltonian in this case has the form[1-3]:

$$H = \frac{1}{2}\int \sum_{\alpha=1}^{3} \left(\Pi_\alpha^2 + c^2 (\nabla\Phi_\alpha)^2 + c^2\varkappa^2\Phi_\alpha^2 - 2\sqrt{4\pi}\, g c O_\alpha \Phi_\alpha\right) d\mathbf{r}, \tag{1}$$

$$[\Pi_\alpha(\mathbf{r}), \Phi_\beta(\mathbf{r}')] = -i\hbar\delta_{\alpha\beta}\delta(\mathbf{r}-\mathbf{r}'); \quad [\Pi_\alpha(\mathbf{r}), \Pi_\beta(\mathbf{r}')] = [\Phi_\alpha(\mathbf{r}), \Phi_\beta(\mathbf{r}')] = 0.$$

Here $O_\alpha = \tau_\alpha U(\mathbf{r}-\mathbf{r}_1)$ for the scalar field and $O_\alpha = (\tau_\alpha/\varkappa)(\vec{\sigma}, \nabla U(\mathbf{r}-\mathbf{r}_1))$ for the pseudoscalar field; in the case of a neutral field, α has only a single value and τ_α must be replaced by unity. $\tau_1 = \tau_x$; $\tau_2 = \tau_y$; $\tau_3 = \gamma_1 + \gamma_2\tau_z$; $\varkappa = \mu c/\hbar$. $U(\mathbf{r}-\mathbf{r}_1)$ is the source function; $\int U(\mathbf{r})\, r d\mathbf{r} \approx a$ is the "radius" of the nucleon; $a \ll \varkappa^{-1}$. In the transition to a point source, $U(\mathbf{r}-\mathbf{r}_1) \to \delta(\mathbf{r}-\mathbf{r}_1)$.

For $U(\mathbf{r}-\mathbf{r}_1)$, we can choose the formally covariant expression (four-dimensional representation; see reference 4):

$$U(\mathbf{r}-\mathbf{r}_1) = \int_{\infty}^{\infty} F\left((\mathbf{r}-\mathbf{r}_1)^2 - c^2(t-t_1)^2\right) dt_1,$$

where F is some function of the invariant $(\mathbf{r}-\mathbf{r}_1)^2 - c^2(t-t_1)^2$.

From the Hamiltonian (1) we obtain the field equation:

$$\Box\Phi_\alpha - \varkappa^2\Phi_\alpha = -(g/c)\sqrt{4\pi}\, O_\alpha.$$

We expand Π_α and Φ_α in plane waves:

---

[1] G. Wentzel, Helv. Phys. Acta **13**, 269 (1940); **14**, 633 (1941).

[2] W. Pauli and S. Dancoff, Phys. Rev. **62**, 85 (1942).

[3] R. Server and S. Dancoff, Phys. Rev. **63**, 143 (1943).

[4] H. Mc Manus, Proc. Roy. Soc. (London) **195A**, 323 (1948).

$$\Pi_\alpha = \sum p_{k\alpha} e^{i(\mathbf{k},\mathbf{r})}/\sqrt{V}; \quad \Phi_\alpha = \sum q_{k\alpha} e^{i(\mathbf{k},\mathbf{r})}/\sqrt{V}.$$

Then, from Eq. (1) we obtain

$$H = \frac{1}{2}\sum_{k,\alpha}(p^{*}_{k\alpha}p_{k\alpha} + \omega_k^2 q^{*}_{k\alpha}q_{k\alpha} - gcO_{\alpha k}q_{k\alpha}); \quad (2)$$

$$\omega_k^2 = c^2(\varkappa^2 + k^2);$$

$$O_{\alpha k} = \frac{2\sqrt{4\pi}}{\sqrt{V}}\int e^{i(\mathbf{k},\mathbf{r})}O_\alpha(\mathbf{r})\,d\mathbf{r};$$

For $g = 0$ the positions of equilibrium $q^0_{k\alpha}$ of the field are equal to zero; for $g \neq 0$, the $q^0_{k\alpha}$ differ from zero, thanks to an energy of interaction of the meson field linear relative to $q_{k\alpha}$. We can find $q^0_{k\alpha}$ by minimizing the potential energy of the oscillators of the field with respect to $q_{k\alpha}$. In the case of a neutral scalar field, when $O_{\alpha k}$ is a number, $q^0_{k\alpha}$ is determined from the equation:

$$\omega_k^2 q_{k\alpha} - (gc/2)\,O_{\alpha k} = 0.$$

In the general case $O_{\alpha k}$ and, consequently, the potential energy V_f of the meson field are spin operators (by spin we imply both ordinary and isotopic spin):

$$V_f = {}^1\!/_2 \sum_{k,\alpha}(\omega_k^2 q^{*}_{k\alpha}q_{k\alpha} - gc\, q_{k\alpha}O_{\alpha k}).$$

Therefore, in order to find the equilibrium positions $q^0_{k\alpha}$ in this case, we must first diagonalize V_f in the spin variable and then minimize the eigenvalues $V_{f\lambda}$ with respect to $q_{k\alpha}$. Here the $q^0_{k\alpha}$ will in general be different for each of the four spin states λ. Inasmuch as the $q^0_{k\alpha}$ are evidently proportional to g, as in the case of a neutral scalar field, the potential energy of the equilibrium position will be proportional to g^2. If we now take into account the kinetic energy of the meson field, $T_f = \frac{1}{2}\sum_{k,\alpha} p^{*}_{k\alpha}p_{k\alpha}$, and consider vibrations about the position of equilibrium $q^0_{k\alpha}$ for each of the spin states, then the energy of vibration will be determined by the usual expression: $\Sigma(n_{k\alpha} + {}^1\!/_2)\hbar\omega_k$. Then the energy of vibration is proportional to g^0. For the neutral scalar field, when O_α is not an operator, preliminary separation of the potential energy and minimization of it represents a rigorous operation which leads to the same results as in the well-known canonical transformation , which diagonalizes the Hamiltonian [Eq. (1)][5]. In the general case, when O_α is a spin operator, initial neglect of the kinetic energy T_f and diagonalization of the single potential energy V_f according to the spin variables is sensible only if T_f is significantly less than V_f for $q_{k\alpha} = q^0_{k\alpha}$, i.e., as follows from the estimates made above, if $g^2/\hbar c$ is sufficiently large. For a sufficiently large value of $g^2/\hbar c$ (a more precise criterion for the applicability of the expansion for different variants of coupling will be determined later), the scheme of reasoning mentioned above can be assumed on the basis of the simple method of diagonalization of the total Hamiltonian (1) or (2). We first neglect the kinetic energy of the meson field T_f in the Hamiltonian; we then diagonalize the remaining potential energy in the spin variables and find the eigenfunctions which depend on the spin variables, and the eigenvalues. The eigenfunctions and eigenvalues, like the parameters, depend on the $q_{k\alpha}$. If we minimize the eigenvalues with respect to q for each of the spin states, we find the positions of equilibrium of the oscillators. In the following approximation, it is possible to take into account the kinetic energy neglected earlier and consider the vibrations of the oscillators about the known equilibrium positions. In contrast to the neutral scalar field, the potential energy of the vibrations, in view of the operator character of $O_{\alpha k}$, apart from terms quadratic in $q_{k\alpha} - q^0_{k\alpha}$ (which are proportional to g^0), will contain anharmonic terms which are proportional to g^{-2}, g^{-4}, etc. For practical calculations it is more convenient to consider the Hamiltonian (1) directly, not expanding Π_α and Φ_α in plane waves, as was done in Eq. (2).

The suggested method of solution of the Schrödinger equation is similar to the method which is employed in the theory of molecules. In the Hamiltonian which contains the coordinates of the electrons $\mathbf{r}_i$ and of the nucleus $\mathbf{R}_i$:

---

[5] G. Wentzel, *Quantum Theory in Wave Fields*, p. 61.

$$H = \sum_i \frac{p_i^2}{2m} + \sum_i \frac{P_i^2}{2M} + V(\mathbf{r}_i, \mathbf{R}_i)$$

$$\equiv T_e(\mathbf{p}_i) + Tn(\mathbf{P}_i) + V(\mathbf{r}_i, \mathbf{R}_i),$$

we first neglect the kinetic energy of the nucleus, which is proportional to a small parameter m/M (in our case we discard the kinetic energy of the meson field), and the remaining Hamiltonian is diagonalized in terms of the electronic variables (in our case, in the spin variables). For each electronic state the energy is minimized with respect to the coordinates of the nucleus (in our case, with respect to the coordinates of the oscillator field). In the next approximation, the kinetic energy of the nucleus is taken into account and, for each electronic state m, the vibrations of the nucleus about its known equilibrium position and the rotation of the molecule as a whole are considered.

In the theory of molecules two variants of this method are applied. In the first case we select as the unperturbed Hamiltonian $H^0 = T_e + V(\mathbf{r}_i, \mathbf{R}_i)$ for arbitrary values of the variables $\mathbf{R}_i$, and as the perturbation H', the kinetic energy of the nucleus T_n[6,7]. Here the ψ function of zeroth approximation $\psi_m^0(\mathbf{r}_i, \mathbf{R}_i)$ depends not only on $\mathbf{r}_i$ but also on $\mathbf{R}_i$, the eigenvalues $E_m^0(\mathbf{R}_i)$ also depend on the $\mathbf{R}_i$. The total Ψ function of the system is sought in the form of an expansion in the functions of zero approximation $\psi_m^0(\mathbf{r}_i, \mathbf{R}_i)$:

$$\Psi_l(\mathbf{r}_i, \mathbf{R}_i) = \sum_m \chi_{lm}(\mathbf{R}_i)\, \psi_m^0(\mathbf{r}_i, \mathbf{R}_i);$$

$$\chi_{lm} = \chi_l^0 \delta_{lm} + \chi'_{lm};$$

As always in the theory of perturbation, it is assumed that $\chi'_{lm} \ll \chi_l^0$. Substituting $\Psi_l(\mathbf{r}_i, \mathbf{R}_i)$ in the equation $(H^0 + H')\,\Psi = E\Psi$, we must take it into account that the momenta of the nuclei, $\mathbf{P}_i$, do not commute with the $\mathbf{R}_i$ which enter into $\psi_m^0(\mathbf{r}_i, \mathbf{R}_i)$. However, in actuality, the nuclei in the molecule contain vibrations close to the minimum energy $E_l^0(\mathbf{R}_i)$ which plays the role of potential energy for the nucleus. Therefore, $E_l^0(\mathbf{R}_i)$ and $\psi_l^0(\mathbf{r}_i, \mathbf{R}_i)$ must be expanded in series of $\mathbf{R}_i - \mathbf{R}_{li}^0$ ($\mathbf{R}_{li}^0$ is the value of $\mathbf{R}_i$ which corresponds to minimum E_l^0) and limit ourselves to the first two or three terms of the series.

In view of this, we must go by a different path in the consideration of the bound states of the nuclei in the molecule; initially, we choose as the unperturbed Hamiltonian $H^0 = T_e + V(\mathbf{r}_i, \mathbf{R}_{li})$ where the $\mathbf{R}_{li}$ are fixed values of $\mathbf{R}_i$, which must subsequently be so chosen that they correspond to the minimum potential energy of the nuclei (reference 7, Sec. 3). The perturbation in this case is evidently

$$H' = Tn + V(\mathbf{r}_i, \mathbf{R}_i) - V(\mathbf{r}_i, \mathbf{R}_{li}).$$

We seek a Ψ function of the system in the form

$$\Psi_l(\mathbf{r}_i, \mathbf{R}_i) = \sum_m \chi_{lm}(\mathbf{R}_i)\, \psi_m^0(\mathbf{r}_i, \mathbf{R}_i).$$

It was shown by Born and Oppenheimer[7] that the $\mathbf{R}_{li}$ are determined from the equation

$$\int \psi_l^{0*}(\mathbf{r}_i, \mathbf{R}_{li}) \left[\frac{\partial V}{\partial \mathbf{R}_i}(\mathbf{r}_i, \mathbf{R}_i)\right]_{\mathbf{R}_i = \mathbf{R}_{li}} \psi_l^0(\mathbf{r}_i, \mathbf{R}_{li}) \prod_i d\mathbf{r}_i \tag{4}$$

$$= \left|\frac{\partial V}{\partial \mathbf{R}_{li}}\right|_{ll} = 0,$$

which represents the condition of solvability for the ψ function of first approximation. The condition (4) corresponds to the minimum potential energy of the nuclei in the lth state.

2. Two variants are also possible in the case of the meson field which interacts with the nucleon.

In the first variant:

$$H^0 = \frac{c^2}{2} \int \sum_\alpha \Big[(\nabla\Phi_\alpha)^2 + \varkappa^2\Phi_\alpha^2$$

$$- 2\sqrt{4\pi}\frac{g}{c} O_\alpha \Phi_\alpha\Big] d\mathbf{r}$$

$$H' = {}^1\!/_2 \int \sum_\alpha \Pi_\alpha^{2]} d\mathbf{r};$$

---

[6] W. Pauli, *General Principles of Wave Mechanics.*

[7] M. Born and R. Oppenheimer, Ann. d. Physik **84**, 457 (1927).

we find the ψ function of zeroth approximation, which depends on the variable of ordinary and isotopic spin s, from the equation $H^0\psi^0_\lambda(s, \Phi_\alpha) = E^0_\lambda(\Phi_\alpha)\infty\, \psi^0_\lambda(s, \Phi_\alpha)$. In this case it is expedient to construct Φ_α (and Π_α) from plane waves. The functionals ψ^0_λ and E^0_λ depend on the Φ_α as parameters.

We seek the Ψ function of the system in the form:

$$\Psi_\lambda = \sum_u \chi_{\lambda\mu}(\Phi_\alpha)\,\psi^0_\mu(s, \Phi_\alpha). \tag{5}$$

In the case of a charged pseudoscalar field, $\mu = 1, \ldots, 4$; for a charged scalar and neutral pseudoscalar field, $\mu = 1, 2$. If the eigenvalues E^0_λ are degenerate, than, in seeking the correct functions of zeroth approximation, i.e., $\chi_{\lambda\mu}$, the secular equation must be solved. This case will be considered in III.

If all the E^0_λ for a given Φ_α are not degenerate, it is immediately possible to assume that $\chi_{\lambda\mu} = \chi^0_\lambda\delta_{\lambda\mu} + \chi'_{\lambda\mu}$; $\chi'_{\lambda\mu} \ll \chi^0_\lambda$. Then, substituting (5) in (1) and multiplying by ψ^{0*}_μ we get, for $\mu = \lambda$:

$$|H'\chi^0_\lambda|_{\lambda\lambda} + \sum |H'\chi'_{\lambda\nu}|_{\lambda\nu} = (E_\lambda - E^0_\lambda)\,\chi^0_\lambda, \tag{6}$$

and for $\mu \neq \lambda$,

$$|H'\chi^0_\lambda|_{\mu\lambda} + \sum_\nu |H'\chi'_{\lambda\nu}|_{\mu\nu} = (E_\lambda - E^0_\mu)\,\chi'_{\lambda\mu}. \tag{7}$$

Here $|H'\chi'|_{\mu\nu} = (\psi^{0*}_\mu, H'\chi_{\lambda\nu}\psi^0_\nu)$ are the matrix elements for the spin functions ψ^0_μ. The H' acts on the parameter Φ_α which enters into ψ^0_μ. Limiting ourselves to terms of first order in H', we get from Eq. (7) an expression for $\chi'_{\lambda\mu}(\lambda \neq \mu)$:

$$\chi'_{\lambda\mu} = (E^0_\lambda - E^0_u)^{-1}\,|H'\chi^0_\lambda|_{\mu\lambda} \tag{8}$$

and substituting Eq. (8) in Eq. (6), the equation for χ^0_λ ($\chi'_{\lambda\lambda}$ can be set equal to zero; see Landau and Lifshitz[8]):

$$\begin{aligned} &|H'\chi^0_\lambda|_{\lambda\lambda} \\ &+ \sum_{\nu\neq\lambda} \{H'(E^0_\lambda - E^0_\nu)^{-1}\,|H'\chi^0_\lambda|_{\nu\lambda}\}_{\lambda\nu} + E^0_\lambda\chi^0_\lambda \equiv H_\lambda\chi^0_\lambda \\ &\equiv \int \widetilde{H}_\lambda\, d\mathbf{r}\,\chi^0_\lambda = E_\lambda\chi^0_\lambda. \end{aligned} \tag{9}$$

In the Hamiltonian H_λ we must set $\Phi_\alpha = \varphi^0_\alpha + \varphi_\alpha$. If φ^0_α is determined from the condition of the variation minimum of H_λ (analogous to the condition $\partial E^0_l/\partial \mathrm{R}_i = 0$ in the theory of molecules):

$$\frac{\delta H_\lambda}{\delta\varphi^0_\alpha} = \frac{\partial\widetilde{H}}{\partial\varphi^0_\alpha} - \sum_h^3 \frac{\partial}{\partial x_h}\left(\frac{\partial\widetilde{H}_\lambda}{\partial(\partial\varphi^0_\alpha/\partial x_p)}\right) = 0,$$

then the terms $H^{(1)}_\lambda$, linear in φ_α, will be absent in the functional expansion of $\widetilde{H}_\lambda$ in powers of φ_α:

$$\widetilde{H}_\lambda = \widetilde{H}^0_\lambda + \widetilde{H}^{(1)}_\lambda + H^{(2)}_\lambda + \cdots$$

It is not difficult to show that $\widetilde{H}_\lambda$ from the beginning contains only quadratic terms in Π_α.

Concrete calculations according to the first method are usually rather difficult in the case of the meson field. Computations according to the second variant, which we shall consider in more detail[9], are much simpler.

In this case we immediately assume $\Phi_\alpha = \varphi^0_{\alpha\lambda} + \varphi_\alpha$. The field $\varphi^0_{\alpha\lambda}$ will be determined precisely later. In view of the fact that $\varphi^0_{\alpha\lambda}$ is not an operator, the commutator relations for φ_α and Π_α have the same form as for Φ_α and Π_α:

$$[\Pi_\alpha(\mathbf{r}), \varphi_\beta(\mathbf{r}')] = -i\hbar\delta_{\alpha\beta}\delta(\mathbf{r} - \mathbf{r}')$$

The unperturbed Hamiltonian is

$$\begin{aligned} H^0 = \frac{c^2}{2}\int\sum_\alpha^3 \Big[&(\nabla\varphi^0_{\alpha\lambda})^2 \\ &+ \varkappa^2(\varphi^0_{\alpha\lambda})^2 - 2\sqrt{4\pi}\,\frac{g}{c}\,O_\alpha\varphi^0_{\alpha\lambda}\Big]\,d\mathbf{r}, \end{aligned}$$

---

[8] L. D. Landau and E. M. Lifshitz, *Quantum Mechanics*, I, GITTL, 1948, pp. 162, 182, 498.

[9] B. Geilikman, Dokl. Akad. Nauk SSSR **90**, 359 (1953).

with the perturbation

$$H' = H - H^0 = H^{(1)} + H^{(2)};$$

$$H^{(1)} = c^2 \int \sum_\alpha \left[(\varkappa^2 - \Delta)\, \varphi^0_{\alpha\lambda} - \frac{g}{c}\sqrt{4\pi} O_\alpha \right] \varphi_\alpha d\mathbf{r}; \tag{10}$$

$$H^{(2)} = {}^1/_2 \int \sum_\alpha \left(\Pi^2_\alpha + c^2 \varphi_\alpha (\varkappa^2 - \Delta)\, \varphi_\alpha \right) d\mathbf{r};$$

$H^{(1)}$ is first order in φ_α, $H^{(2)}$ is second order.

The eigenfunctions of the zeroth approximation, which depend on the variable s, satisfy the Schrödinger equation:

$$H^0 \psi^0_{\lambda\mu} (s, \varphi^0_{\alpha\lambda}) = E^0_{\lambda\mu} \psi^0_{\lambda\mu} (s, \varphi^0_{\alpha\lambda}). \tag{11}$$

We seek the complete Ψ function of the system in the form:

$$\Psi_\lambda (s, \varphi_\alpha) = \sum_\mu \chi_{\lambda\mu} (\varphi_\alpha)\, \psi^0_\mu (s, \varphi^0_{\alpha\lambda}) \qquad (\psi^0_\mu \equiv \psi^0_{\lambda\mu}),$$

where we write $\Psi_\lambda (\chi_{\lambda\mu})$ and the eigenvalue E_λ in the absence of degeneracy for $E^0_{\lambda\lambda} (E^0_{\lambda\lambda} \neq E^0_{\lambda\mu}$ for $\mu \neq \lambda$) in the form of series in the expansion parameter:

$$\Psi_\lambda = \Psi^0_\lambda + \Psi^{(1)}_\lambda + \Psi^{(2)}_\lambda + \cdots;$$

$$\chi_{\lambda\mu} = \chi^0_\lambda \delta_{\lambda\mu} + \chi^{(1)}_{\lambda\mu} + \chi^{(2)}_{\lambda\mu} + \cdots;$$

$$E_\lambda = E^0_\lambda + E^{(1)}_\lambda + E^{(2)}_\lambda + \cdots; \qquad E^0_\lambda \equiv E^0_{\lambda\lambda}.$$

We then get for $\Psi^{(1)}_\lambda$, according to perturbation theory,

$$(H^0 - E^0_\lambda)\, \Psi^{(1)}_\lambda = (E^{(1)}_\lambda - H^{(1)})\, \Psi^0_\lambda;$$

$$\Psi^0_\lambda = \chi^0_\lambda \psi^0_\lambda (s).$$

This equation has a solution if the right side is orthogonal (over spin coordinates) to $\psi^0_\lambda(s)$, i.e.,

$$(H^{(1)}_{\lambda\lambda} - E^{(1)}_\lambda)\, \chi^0_\lambda = 0;$$

Here

$$H^{(1)}_{\lambda\lambda} = (\psi^{0*}_\lambda, H^{(1)} \psi^0_\lambda)/(\psi^{0*}_\lambda, \psi^0_\lambda);$$

since $E^{(1)}_\lambda$ does not depend on the φ_α, this is possible for $\chi^0_\lambda \neq 0$ only under the condition $H^{(1)}_{\lambda\lambda} = 0$, i.e., as is evident from Eq. (10),

$$(\Delta - \varkappa^2)\, \varphi^0_{\alpha\lambda} = -\frac{g}{c}\sqrt{4\pi}\, |O_\alpha (\mathbf{r})|_{\lambda\lambda}; \tag{12}$$

$$|O_\alpha|_{\lambda\lambda} = (\psi^{0*}_\lambda, O_\alpha \psi^0_\lambda) / (\psi^{0*}_\lambda, \psi^0_\lambda).$$

Equation (12) is equivalent to the condition $\delta H_\lambda / \delta \varphi^0_\alpha = 0$ in the first variant. It also follows from the requirement of a minimum $\delta E^0_\lambda = 0$ for the energy $E^0_\lambda = (\psi^{0*}, H^0 \psi^0)/(\psi^{0*}, \psi^0)$ (see reference 9). For such a choice of $\varphi^0_{\alpha\lambda}$,

$$H^{(1)} = gc\sqrt{4\pi} \int \sum_\alpha (|O_\alpha|_{\lambda\lambda} - O_\alpha)\, \varphi_\alpha\, d\mathbf{r}.$$

The solution of Eq. (12) has the form

$$\varphi^0_\alpha = \frac{g}{c\sqrt{4\pi}} \int G(\mathbf{r}, \mathbf{r}')\, |O_\alpha (\mathbf{r}')|_{\lambda\lambda}\, d\mathbf{r}'; \tag{13}$$

$$G(\mathbf{r}, \mathbf{r}') = \frac{e^{-\varkappa|\mathbf{r}-\mathbf{r}'|}}{|\mathbf{r} - \mathbf{r}'|}.$$

We substitute Eq. (13) in Eq. (11):

$$\left\{ \frac{g^2}{2} \int \sum_\alpha [|O_\alpha (\mathbf{r})|_{\lambda\lambda} - 2 O_\alpha (\mathbf{r})]\, |O_\alpha(\mathbf{r}')|_{\lambda\lambda} \right. \tag{14}$$

$$\left. \times\, G(\mathbf{r}, \mathbf{r}')\, d\mathbf{r}\, d\mathbf{r}' \right\} \psi^0_\mu = E^0_\mu \psi^0_\mu.$$

Equation (14) represents formally a nonlinear system of four algebraic equations for the four components of ψ^0_μ (in the case of a charged pseudoscalar field). However, the system is in reality easily solved in the following way[10]. We replace the mean values of the spin operators τ_α and $\tau_\alpha \sigma_k$ by undetermined numerical parameters: $|\tau_\alpha|_{\lambda\lambda} = \eta_\alpha$; $|\tau_\alpha \sigma_k|_{\lambda\lambda} = \xi_{\alpha k}$. Then the system is linear and can be solved without difficulty. The eigenfunctions and eigenvalues depend on these parameters. Evidently the numerical values of the parameters $\xi_{\alpha k}(\eta_\alpha)$ can be found from the equations:

---

[10] B. Geilikman, Dokl. Akad. Nauk SSSR **91**, 39 (1953).

$$\xi_{\alpha k} = (\psi^{0*}_{\lambda\lambda}(s, \xi_{\alpha k}), \tau_\alpha \sigma_k \psi^0_{\lambda\lambda}(s, \xi_{\alpha k})); \qquad (15)$$

$$\eta_\alpha = (\psi^{0*}_{\lambda\lambda}(s, \eta_\alpha), \tau_\alpha \psi^0_{\lambda\lambda}(s, \eta_\alpha)) \qquad (\psi^{0*}, \psi^0) = 1.$$

It is simplest to find $\xi_{\alpha k}$ and η_α by comparing the expression for the eigenvalue $E^0_{\lambda\lambda}$ which is obtained by the solution of the system (14), in which $|\tau_\alpha \sigma_k|$ and $|\tau_\alpha|_{\lambda\lambda}$ are replaced by the parameters $\xi_{\alpha k}$ and η_α, with the general expression for $E^0_{\lambda\lambda}$:

$$E^0_{\lambda\lambda} = |\, H^0_\lambda |_{\lambda\lambda}$$

$$= -(g^2/2) \int \sum_\alpha |\, O_\alpha(\mathbf{r}) |_{\lambda\lambda} |\, O_\alpha |\, (\mathbf{r}') |_{\lambda\lambda}$$

$$\times \quad G(\mathbf{r}, \mathbf{r}')\, d\mathbf{r}\, d\mathbf{r}'.$$

Usually, as is easy to show, the equations (15) are equivalent to the conditions of a minimum $E^0_{\lambda\lambda}$ with respect to $\xi_{\alpha k}(\eta_\alpha)$. Evidently, in the case of the pseudoscalar field, $E^0_{\lambda\mu} \sim g^2/a^3 \varkappa^2$ and in the case of the scalar field, $E^0_{\lambda\mu} \sim g^2/a$ (see II[11]). The eigenfunctions of the Hamiltonian $H^0 = H^0_\lambda$ in which are substituted the parameters $\xi^\lambda_{\alpha k}(\eta^\lambda_\alpha)$ found from Eq. (15), form a complete orthogonal set. Here it is essential that for each state λ the sets of numbers $\xi^\lambda_{\alpha k}(\eta^\lambda_\alpha)$ (and consequently the field $\varphi^0_{\alpha\lambda}$) are different, as was shown in reference 11. We assume that for the given Hamiltonian H^0_λ the eigenvalues $E^0_{\lambda\lambda}$ are not degenerate, although there can be similar $E^0_{\lambda\lambda}$ among the different λ ($E^0_{\lambda\lambda} = E^0_{\lambda'\lambda'}$), as is the actual case (see reference 11). The generalization to the case of the presence of degeneracy will be considered in III.

We now substitute the expression for the complete ψ function in the Schrödinger equation with the total Hamiltonian (1) $H = H^0_\lambda + H'$. It is appropritae here, as in the first variant, to write down the equations for $\chi^{(1)}_{\lambda\mu}, \chi^{(2)}_{\lambda\mu}$ etc., separately, and to obtain one equation for $\chi'_{\lambda\mu} = \chi^{(1)}_{\lambda\mu} + \chi^{(2)}_{\lambda\mu} + \ldots$ in first, second, etc., approximations. Multiplying the Schrodinger equation by ψ^{0*}_μ we get for $\lambda = \mu$

$$H'_{\lambda\lambda}\chi^0_\lambda + \sum_\nu H'_{\lambda\nu}\chi'_{\lambda\nu} = E'_\lambda(\chi^0_\lambda + \chi'_{\lambda\lambda}) \qquad (16)$$

and for $\lambda \neq \mu$

$$H'_{\mu\lambda}\chi^0_\lambda + \sum_\nu H'_{\mu\nu}\chi'_{\lambda\nu} = (E^0_\lambda - E^0_{\lambda\mu} + E'_\lambda)\,\chi'_{\lambda\mu}; \qquad (17)$$

$$H'_{\mu\nu} = (\psi^{0*}_\mu H' \psi^0_\nu);$$

$$E'_\lambda = E_\lambda - E^0_\lambda = E^{(1)}_\lambda + E^{(2)}_\lambda + \ldots$$

Now, assuming that $\chi'_{\lambda\mu} \ll \chi^0_\lambda$ we find $\chi'_{\lambda\mu}$ from Eq. (17)(by the method of successive approximations) with accuracy to terms of second order in φ_α:

$$\chi'_{\lambda\mu} = \Big\{ H'_{\mu\lambda}(E^0_\lambda - E^0_{\lambda\mu} + E'_\lambda)^{-1} \qquad (18)$$

$$+ \sum_{\nu \neq \lambda} H^{(1)}_{\mu\nu} H^{(1)}_{\nu\lambda} (E^0_\lambda - E^0_{\lambda\nu})^{-1} (E^0_\lambda - E^0_{\lambda\mu})^{-1} \Big\} \chi^0_\lambda;$$

substituting Eq. (18) in (16), we find the equation χ^0_λ with accuracy to terms of third order in φ_α (we assume $\chi'_{\lambda\lambda}$ equal to zero):

$$(H_{\lambda 2} + H'_{\lambda 3} + H'_{\lambda 3})\,\chi^0_\lambda = E'_\lambda \chi^0_\lambda, \qquad (19)$$

$$H_{\lambda 2} = H'_{\lambda\lambda} + \sum_{\mu \neq \lambda} H^{(1)}_{\lambda\mu} H^{(1)}_{\mu\lambda} (E^0_\lambda - E^0_{\lambda\nu})^{-1}$$

$$= {}^1\!/_2 \int \sum_\alpha^3 (\Pi^2_\alpha + c^2(\nabla\varphi_\alpha)^2 + c^2\varkappa^2\varphi^2_\alpha)\, d\mathbf{r}$$

$$+ c^2 \int \sum_{\alpha,\beta}^{3,3} K_{\alpha\beta}(\mathbf{r}, \mathbf{r}')\, \varphi_\alpha(\mathbf{r})\, \varphi_\beta(\mathbf{r}')\, d\mathbf{r}\, d\mathbf{r}';$$

---

[11] B. Geilikmann, J. Exper. Theoret.. Phys. USSR 29, 430 (1955).

$$K_{\alpha\beta}(\mathbf{r},\mathbf{r}') = 4\pi g^2 \sum_{\mu\neq\lambda} \frac{|O_\alpha(\mathbf{r})|_{\lambda\mu}\,|O_\beta(\mathbf{r}')|_{\mu\lambda}}{E^0_\lambda - E^0_{\lambda\mu}};$$

$$H'_{\lambda 3} = \sum_{\mu\neq\lambda} H^{(1)}_{\lambda\mu} H^{(1)}_{\mu\lambda} [(E^0_\lambda - E^0_{\lambda\mu} + E'_\lambda)^{-1}$$

$$- (E^0_\lambda - E^0_{\lambda\mu})^{-1}];$$

$$H''_{\lambda 3} = \sum_{\mu\neq\lambda}\sum_{\nu\neq\lambda} H^{(1)}_{\lambda\mu} H^{(1)}_{\mu\nu} H^{(1)}_{\nu\lambda} (E^0_\lambda - E^0_{\lambda\mu})^{-1} (E^0_\lambda - E^0_{\lambda\nu})^{-1};$$

$$H^{(2)}_{\mu\nu} = H^{(2)}\delta_{\mu\nu}.$$

It is essential that $H^{(1)}_{\lambda\lambda} = 0$, whereupon the smallest terms in Eq. (10) are second order in φ_α.

3. At first we neglect in Eq. (19) the terms $H'_{\lambda 3}$ and $H''_{\lambda 3}$. By a variation of the Hamiltonian or with the aid of the quantum Poisson brackets, $\left(\dot{\varphi}_\alpha = \frac{i}{\hbar}[H_{\lambda 2}, \varphi_\alpha]\,;\dot{\Pi}_\alpha = \frac{i}{\hbar}[H_{\lambda 2}, \Pi_\alpha]\right)$, it is possible to obtain the equation of the field:

$$\Box\varphi_\alpha - \varkappa^2\varphi_\alpha = \int \sum_\beta \widetilde{K}_{\alpha\beta}(\mathbf{r},\mathbf{r}')\,\varphi_\beta(\mathbf{r}')\,d\mathbf{r}':$$

$$\widetilde{K}_{\alpha\beta} = K_{\alpha\beta}(\mathbf{r},\mathbf{r}') + K_{\beta\alpha}(\mathbf{r}',\mathbf{r});$$

if we set $\varphi_\alpha(\mathbf{r},t) = \varphi_\alpha(\mathbf{r})e^{-i\epsilon t/\hbar}$, then

$$(\varkappa^2 - \Delta)\,\varphi_{\alpha k} + \int \sum_\beta \widetilde{K}_{\alpha\beta}(\mathbf{r},\mathbf{r}')\,\varphi_{\beta k}(\mathbf{r}')\,d\mathbf{r}' \tag{20}$$

$$= \frac{\omega_k^2}{c^2}\varphi_{\alpha k};$$

$$\varepsilon_k = \hbar\omega_k.$$

Each solution of the system (20) can be represented in the form of a three component function $\varphi_k^\rho = \{\varphi_{k1}^\rho, \varphi_{k2}^\rho, \varphi_{k3}^\rho\}$. For a given quantum number k, which characterizes the motion of the meson in the space coordinates, $\rho = 1, 2, 3$. The eigenfunctions of Eq. (20), φ_k^ρ, form a complete orthogonal set: $\int (\varphi_k^{\rho *}, \varphi_{k'}^{\rho'})\,d\mathbf{r} = \delta_{\rho\rho'}\delta_{kk'}$, ω_k^2/c^2 are the eigenvalues of Eq. (20).

We expand Π and φ in the functions φ_k^ρ:

$$\varphi = \{\varphi_1, \varphi_2, \varphi_3\} = \sum_{k,\rho} q_{k,\rho}\varphi_k^\rho;\quad \Pi = \sum_{k,\rho} p_{k\rho}\varphi_k^\rho$$

and substitute in the equation $H_{\lambda 2}\chi^0_\lambda = E_{\lambda 2}\chi^0_\lambda$. Taking into account Eq. (20) we obtain

$$\tfrac{1}{2}\sum_{k,\rho}(p^*_{k\rho}p_{k\rho} + \omega_k^2 q^*_{k\rho}q_{k\rho})\,\chi^0_\lambda(q_{k\rho}) \tag{21}$$

$$= E_{\lambda 2}\chi^0_\lambda(q_{k\rho});$$

$$E_{\lambda 2} = \sum_{k,\rho}(n_{k\rho} + \tfrac{1}{2})\,\hbar\omega_k.$$

Equation (21) corresponds to a set of mutually noninteracting meson oscillators. The eigenfunctions φ_k^ρ of Eq. (20) thus describe the motion of the meson which interacts with the nucleon. The energy of interaction

$$(\hbar^2/2\mu)\int \widetilde{K}_{\alpha\beta}(\mathbf{r},\mathbf{r}')\ldots,$$

is of zeroth order relative to g, since $E^0_\lambda - E^0_{\lambda\mu} \sim g^2$. As $a \to 0$, the interaction undergoes transition to point interaction.

We consider first the solution of Eq. (20) for $\omega \geq c\varkappa$ ($\epsilon \geq \mu c^2$; free motion of the meson). In this case we get from Eq. (20)

$$\varphi_\alpha = a_\alpha e^{i(\mathbf{k},\mathbf{r})} - \sum_{\beta\mu}\int [L'_{\alpha\mu}(\mathbf{r})|O_\beta(\mathbf{r}')|_{\mu\lambda} \tag{22}$$

$$+ L''_{\alpha\mu}(\mathbf{r})|O_\beta(\mathbf{r}')|_{\lambda\mu}]\,\varphi_\beta(\mathbf{r}')\,d\mathbf{r}'.$$

Here

$$k^2 = \frac{\omega_k^2}{c^2} - \varkappa^2;\quad L'_{\alpha\mu}(\mathbf{r})$$

$$= g^2(E^0_\lambda - E^0_{\lambda\mu})^{-1}\int \frac{e^{ik|\mathbf{r}-\mathbf{r}'|}}{|\mathbf{r}-\mathbf{r}'|}\,|O_\alpha(\mathbf{r}')|_{\lambda\mu}\,d\mathbf{r}',$$

$$L''_{\alpha\mu}(\mathbf{r})$$

$$= g^2(E^0_\lambda - E^0_{\lambda\mu})^{-1}\int \frac{e^{ik|\mathbf{r}-\mathbf{r}'|}}{|\mathbf{r}-\mathbf{r}'|}\,|O_\alpha(\mathbf{r}')|_{\mu\lambda}\,d\mathbf{r}'.$$

The solution of the system of integral equations (22) with degenerate nuclei can easily be found[12]

$$\varphi_\alpha = a_\alpha e^{i(\mathbf{k},\mathbf{r})} + \sum_{\mu,\beta} \left(c'_{\alpha\beta\mu}(\mathbf{k})\, L'_{\alpha\mu}(\mathbf{r}) + c''_{\alpha\beta\mu}(\mathbf{k})\, L''_{\alpha\mu}(\mathbf{r})\right). \tag{23}$$

We get a set of equations for the coefficients $c'_{\alpha\beta\mu}$ and $c''_{\alpha\beta\mu}$ by substituting Eq. (23) in Eq. (22):

$$\begin{gathered} c_{\alpha\beta\mu} + \sum_{\nu,\gamma}\Big[c'_{\beta\gamma\nu}\int |O_\beta(\mathbf{r})|_{\mu\lambda} L'_{\beta\nu}(\mathbf{r})\,d\mathbf{r} + c''_{\beta\gamma\nu}\int |O_\beta|_{\mu\lambda} L''_{\beta\nu}\,d\mathbf{r}\Big] \\ + a_\beta\int |O_\beta|_{\mu\lambda} e^{i(\mathbf{k},\mathbf{r})}\,d\mathbf{r} = 0; \\ c''_{\alpha\beta\mu} + \sum_{\nu,\gamma}\Big[c'_{\beta\gamma\nu}\int |O_\beta|_{\lambda\mu} L'_{\beta\nu}\,d\mathbf{r} \\ + c''_{\beta\gamma\nu}\int |O_\beta|_{\lambda\mu} L''_{\beta\nu}\,d\mathbf{r}\Big] + a_\beta\int |O_\beta|_{\lambda\mu} e^{i(\mathbf{k},\mathbf{r})}\,d\mathbf{r} = 0. \end{gathered} \tag{24}$$

Equation (20) can also have solutions which correspond to the coupled state of the meson ($\epsilon < \mu c^2$). For example, for a scalar, nonrelativistic meson, for $\lambda = 1$, Eq. (20) has the form (we have assumed that $E_1^0 - E_{12}^0 = \gamma g^2/a$):

$$\begin{gathered} -\frac{\hbar^2}{2\mu}\Delta\varphi_\alpha + \frac{4\pi\hbar^2 a}{\mu\gamma}\sum_{\beta=1}^{3}\left(|\tau_\beta|_{12}|\tau_\alpha|_{21} + |\tau_\alpha|_{12}|\tau_\beta|_{21}\right) U(\mathbf{r}-\mathbf{r}_1)\int U(\mathbf{r}')\,\varphi_\beta(\mathbf{r}')\,d\mathbf{r}' \\ = \varepsilon'\varphi_\alpha; \quad \varepsilon' = \varepsilon - \mu c^2 \ll \mu c^2. \end{gathered}$$

In the limit as $a \to 0$;

$$-\frac{\hbar^2}{2\mu}\Delta\varphi_\alpha + \frac{4\pi\hbar^2}{\mu\gamma}\sum_{\beta}\left(|\tau_\beta|_{12}|\tau_\alpha|_{21} + |\tau_\alpha|_{12}|\tau_\beta|_{21}\right)\lim_{a\to 0} aU(\mathbf{r}-\mathbf{r}_1)\,\varphi_\beta(\mathbf{r}) = \varepsilon'\varphi_\alpha.$$

Negative levels are not possible if the interaction is not attractive, and in the case of attraction also if $U_0 \ll \hbar^2/\mu a^2$ (U_0 is the depth of the potential well)[8]. If this condition is not satisfied, coupled states of the mesons are possible. These states correspond to so-called isobars. The function of the coupled s-state for $r > a$ has the form $e^{-\alpha r}/r$; $\alpha = \sqrt{2\mu|\epsilon'|}/\hbar$. The energy of the coupled state, as well as the energy of the free state, is of zeroth order in g.

We consider the terms $H'_{\lambda 3}$ and $H''_{\lambda 3}$. The terms in $H'_{\lambda 3}$ quadratic in φ can easily be computed. The Hamiltonian $H_{\lambda 2} + H'_{\lambda 3}$ is decomposed into a sum of the Hamiltonians of the oscillators if we decompose II and φ in the eigenfunctions $\tilde{\varphi}_k^\rho$ of Eq. (20). Here, however, the quantities $E_\lambda^0 - E_{\lambda\mu}^0$ are replaced by the quantities $E_\lambda^0 - E_{\lambda\mu}^0 + E_{\lambda 2}(n_{k\rho})$ [with numbers $n_{k\rho}$ which are defined by the zero approximation, i.e., by Eq. (21)]. In such a substitution, only the frequencies ω_i of the discrete spectrum ($h\omega_i < \mu c^2$) are changed. For $\epsilon \geqslant \mu c^2$, the functions $\tilde{\varphi}_k^\rho$ have the form of Eq. (23), but in the expression for $L'_{\alpha\mu}$ and $L''_{\alpha\mu}$ (in Eqs. (23) and (24), we now have $E_\lambda^0 - E_{\lambda\mu}^0 + E_{\lambda 2}(n_{k\rho})$ instead of $E_\lambda^0 - E_{\lambda\mu}^0$. The values $L'_{\alpha\mu}(\mathbf{r})$ and $L''_{\alpha\mu}(\mathbf{r})$ represent diverging waves; actually, as $r \to \infty$, $L_{\alpha\mu} \sim f(\theta)\, e^{ikr}/r$. It is therefore easy to find the scattering cross sections of the meson by the nucleon, φ_k^ρ, from the expression (23), for $d\sigma$. If we assume, in the factor $E_\lambda^0 - E_{\lambda\mu}^0 + E_{\lambda 2}$ which enters into Eq. (23), $n_{k\rho} = 1$, $n_{k'\rho'} = 0$; $k' \neq k$, $\rho' \neq \rho$, we obtain the amplitude of the scattering of the meson in the state ρ (in the actual scattering problem the initial and final ψ functions of the state are linear combinations of functions with different $\rho = 1, 2, 3$; the degenerecy for different λ must also be considered, see below):

---

[12] V. I. Smirnov, *Course in Higher Mathematics* **4**, GITTL, 1951, p. 50.

$$f_{\alpha\rho}(\vartheta) = \frac{1}{k}\sum_{\beta,\mu}\frac{\Gamma^{\rho}_{\alpha\beta\mu}}{\varepsilon(k) - (E^0_{\lambda\mu} - E^0_{\lambda})}; \tag{25}$$

$$\Gamma^{\rho}_{\alpha\beta\mu} = kg^2\frac{1}{a^{\rho}_{\alpha}}\Big[c'_{\alpha\beta\mu}(\mathbf{k})\int e^{-i(\mathbf{k}',\mathbf{r})}\,|O_{\alpha}(\mathbf{r})|_{\lambda\mu}d\mathbf{r}'$$

$$+ c''_{\alpha\beta\mu}(\mathbf{k})\int e^{-i(\mathbf{k}',\mathbf{r})}\,|O_{\alpha}(\mathbf{r})|_{\mu\lambda}\,d\mathbf{r}\Big];$$

$$\mathbf{k}' = k\mathbf{r}/r.$$

Damping has been introduced in Eq. (25) in the usual fashion (see reference 8). It is essential that the quantities $E^0_{\lambda} - E^0_{\lambda\mu}$ which enter into Eq. (25) as well as the eigenvalue of the energy of the nucleon be of the order g^2.

The term $H''_{\lambda 3}$, cubical in φ_{α}, defines the interaction of the mesons (in addition to the analogous interaction between the nucleonic vacuum); it forms a correction to the energy of order g^{-2} (in the same way as the term of fourth order in $\varphi - H_{\lambda 4}$).

Thus in the order g^2 (zeroth approximation) we obtain the classical field φ^0_{α} (pseudomeson) and the eigenvalue of the energy of the nucleon; in order g^0 (first approximation) – the second quantized field--real mesons which do not interact among themselves, free and in a bound state (isobars), and in order g^{-2} (second approximation) – the anharmonicity of the field of real mesons (and corrections to the eigenvalue of the energy of the nucleon).

Knowing the field $\Phi_{\alpha} = \varphi^0_{\alpha} + \varphi_{\alpha}$ we can find the magnetic moment of the nucleon **M** in the state λ in the absence of mesons (see reference 2):

$$\mathbf{M}_{\lambda} = \frac{e\hbar}{4mc}(\vec{\sigma}_{\lambda\lambda} + \{\tau_z\vec{\sigma}\}_{\lambda\lambda}) + \frac{ec}{2\hbar}\int[\mathbf{r},\mathbf{S}]\,d\mathbf{r};$$

for the pseudoscalar field

$$\mathbf{S} = \varphi_{2\lambda}\nabla\varphi_{1\lambda} - \varphi_{1\lambda}\nabla\varphi_{2\lambda}$$

$$-2(g\sqrt{\pi}/\varkappa c)(\varphi_{2\lambda}\{\tau_1\vec{\sigma}\}_{\lambda\lambda} - \varphi_{1\lambda}\{\tau_2\vec{\sigma}\}_{\lambda\lambda})\,U(\mathbf{r}-\mathbf{r}_1).$$

In the zeroth approximation $\Phi_{\alpha} \approx \varphi^0_{\alpha}$ and in accord with Eq. (13)

$$\mathbf{M}_{\lambda} = \frac{e\hbar}{4mc}(\vec{\sigma}_{\lambda\lambda} + \{\tau_z\vec{\sigma}\}_{\lambda\lambda}) \tag{26}$$

$$+ \left(\frac{g^2\alpha}{\hbar c}\right)\left(\frac{e}{\varkappa^2 a}\right)[\{\tau_2\vec{\sigma}\}_{\lambda\lambda}, \{\tau_1\vec{\sigma}\}_{\lambda\lambda}];$$

$$\alpha = -a\int d\mathbf{r}\,d\mathbf{r}'\,x\frac{\partial}{\partial x}\left(\frac{1}{|\mathbf{r}-\mathbf{r}'|}\right)U(\mathbf{r}')\Big[U(\mathbf{r})$$

$$+\frac{1}{4\pi}\int\frac{U(\mathbf{r}'')\,d\mathbf{r}''}{|\mathbf{r}-\mathbf{r}''|^3}\Big]; \quad \alpha \sim 1.$$

The calculated field φ_{α} gives the corrections of order g^0.

4. Let us consider the conditions of applicability of our theories. We have assumed that

$\chi'_{\lambda\mu} \ll \chi^0_{\lambda}$; $H' \ll H^0(\varphi_{\alpha} \ll \varphi^0_{\alpha})$. In the absence of mesons, $\varphi^2_{\mathrm{av}} \sim \frac{\omega^3_{\mathrm{max}}}{c^3}(q^2_k)_{\mathrm{av}} \sim \frac{\hbar}{ca^2}(\omega_{\mathrm{max}} \sim \frac{c}{a})$,

and $(\varphi^0)_{\mathrm{av}} \sim \frac{g}{ca}$; $(\varphi^0)_{\mathrm{ps}} \sim \frac{g}{c\varkappa a^2}$; therefore $H^{(1)} \ll H^0$ and $\chi'_{\lambda\mu} \ll \chi^0_{\lambda}$($H^{(2)}$ does not in general have nondiagonal matrix elements), if $g^2/\hbar c \gg 1$ in the case of a scalar field, and $g^2/\hbar c \gg \varkappa^2 a^2$ in the case of a pseudoscalar field.

In the presence of mesons the conditions below ought to be satisfied: $\Sigma n_{k\rho}\hbar\omega_k \ll g^2/a$ (scalar field) and $\Sigma n_{k\rho}\hbar\omega_k \ll g^2/\varkappa^2 a^3$ (pseudoscalar field).

In the method just set forth, use is made of a system of spin functions $\psi^0_{\lambda\mu}$ and eigenvalues $E^0_{\lambda\mu}$ for each state, more precisely, one system ψ^0_{μ} and E^0_{μ}, but with different numerical values of the parameters $\xi^{\lambda}_{\alpha k}$ (η^{λ}_{α}).

It was shown in reference 11 that in the case of a symmetric field all $E^0_{\lambda\lambda}$ are equal: $E^0_{\lambda'\lambda'} = E^0_{\lambda\lambda'}$. It is easy to see that this degeneracy cannot change the energy spectra found above.

For simplicity, let us consider a scalar field, and let us assume that for each λ the energy and the Ψ function $\Psi_{\lambda} = \sum_{\mu}\chi_{\lambda\mu}\psi^0_{\lambda\mu}(s)$ have been to terms of order g^{-2}.

If we have two Ψ functions Ψ_1 and Ψ_2 with similar energies, then we can assume that the correct Ψ function of the system has the form $\Psi = c_1\Psi_1 + c_2\Psi_2$. This problem is similar to the problem of the particle which can move in two potential wells located at a certain distance from each other. If the ψ functions for the motion of the particle in each well are known, the symmetric ψ function is a linear combination of these functions[13].

Substituting $\psi = c_1\Psi_1 + c_2\Psi_2$ in the Schröndinger equation, we get the secular equation for c_1 and c_2:

$$(V_{11}+\varepsilon)c_1 + (S\varepsilon + V_{12})c_2 = 0;$$

$$(S^*\varepsilon + V_{21})c_1 + (V_{22}+\varepsilon)c_2 = 0,$$

where

$$\begin{gathered} V_{11} = -\int (\Psi_1^*, (H-H_1)\Psi_1)\,d\tau; \\ V_{22} = E_1 - E_2 - \int (\Psi_2^*, (H-H_2)\Psi_2)\,d\tau; \\ V_{12} = S(E_1-E_2) - \int (\Psi_1^*, (H-H_2)\Psi_2)\,d\tau; \\ V_{21} = -\int (\Psi_2^*, (H-H_1)\Psi_1)\,d\tau; \\ \varepsilon = E - E_1;\ d\tau = \prod_{h,\rho} dq_{h\rho}^{(1)} = \prod_{h,\rho} dq_{h\rho}^{(2)}; \\ S = \int (\Psi_1^*, \Psi_2)\,d\tau; \end{gathered} \tag{27}$$

$$\Phi - \varphi_\lambda^0 = \sum_{k,\rho} q_{k\rho}^{(\lambda)}\,\varphi_{k\lambda}^{\rho},$$

whence $H_1\Psi_1 = E_1\Psi_1$ and $H_2\Psi_2 = E_2\Psi_2$.

Inasmuch as we have assumed that E_1 and E_2 have been computed with accuracy $\sim g^{-2}$, then $V_{11} \sim g^{-4}$, and $V_{22} = E_1 - E_2 + O(g^{-4})$. We estimate $S_1 V_{21}$ and V_{12}:

$$S = \sum_{\mu,\nu} (\psi_{1\mu}^{0*}, \psi_{2\nu}^{0}) \int \chi_{1\mu}^* \chi_{2\nu}\,d\tau;\quad \chi_\lambda^0 = \prod_{k,\rho} F_{n_{k\rho}}(q_{k\rho}^{\lambda});$$

$F_{n_{k\rho}}$ is the Hermite polynomial. It follows from Eq. (27) that

$$q_{k\rho}^{(2)} = \int \Big(\varphi_1^0 - \varphi_2^0 + \sum_{k',\rho'} q_{k'\rho'}^{(1)}\varphi_{k'1}^{\rho'}\Big)\varphi_{k2}^{\rho *}\,d\mathbf{r};$$

It was shown in reference 11 that $\varphi_{\alpha k\lambda}^{\rho} = \varphi_{\alpha k\lambda}\delta_{\rho\alpha}$ and $\varphi_{\alpha k1} = \varphi_{\alpha k2}$; then $q_{\alpha k}^{(2)} = q_{\alpha k}^{0} + q_{\alpha k}^{(1)}$; $q_{\alpha k}^{0} = 0$ for $\alpha = 1.2$; $q_{3k}^{0} = \dfrac{g}{2c\sqrt{\pi}\sqrt{\pi^2}}\,\dfrac{1}{k^2+\varkappa^2}$; $S \approx \sqrt{\dfrac{\hbar c}{g^2}}\,e^{-(g^2/\hbar c)\ln(\varkappa a)^{-1}}$ and $V_{21} \approx \dfrac{g\sqrt{\hbar c}}{a}\,e^{-(g^2/\hbar c)\ln(\varkappa a)^{-1}}$; for the pseudo-scalar field $S \approx \dfrac{\varkappa a\sqrt{\hbar c}}{g}\,e^{-g^2/(\hbar c\varkappa^2 a^2)}$,

$$\varepsilon = \frac{1}{2(1-|S|^2)}\Big[V_{11} + V_{22} - V_{12}S^* - V_{21}S \mp \sqrt{(V_{11}+V_{22}-V_{12}S^*-V_{21}S)^2 + 4(1-|S|^2)(V_{12}V_{21}-V_{11}V_{22})}\Big] \tag{28}$$

for $V_{12} = V_{21} = S = 0$ the correction ϵ to E_1 is the same as for the nonsymmetrized function Ψ_χ. This correction, connected with V_{21}, V_{12}, S, i.e., with the symmetrization of the function ψ_χ is, according to Eq. (28), of the order of $e^{-g^2/\hbar c}\,(e^{-g^2/(\hbar c\varkappa^2 a^2)})$ and in view of this is negligible.

If we do not consider ϵ but the Ψ function of the system, then it is evident that, in the absence of degeneracy, for different λ we can use linear combinations of the functions χ_λ.

The results we have obtained are quite intelligible, since in the decomposition in a complete orthogonal set of functions $\psi_{\lambda\mu}^0$ the effect of the field corresponding to other λ was automatically considered (but with power, not exponential accuracy).

The same results are obtained if symmetrization of the functions of zeroth approximation is carried out initially: $\psi^0(s) = \Sigma c_\lambda \psi_{\lambda\lambda}^0$, but the computations in this case are much more complicated.

The theory is easily generalized to the case of several nucleons which interact with the meson field[10, 14]. The Hamiltonian for n nucleons has the form

$$H = \frac{1}{2}\int \sum_\alpha \Big(\Pi_\alpha^2 + c^2(\nabla\Phi_\alpha)^2 + c^2\varkappa^2\Phi_\alpha^2 - 2\sqrt{4\pi}\,gc\sum_i^n O_\alpha(\mathbf{r}-\mathbf{r}_i)\,\Phi_\alpha\Big)\,d\mathbf{r}. \tag{29}$$

---

[13] P. Gombas, *The Problem of Many Particles*, IIL, 1952, p. 219.

[14] B. Geilikman, Dokl. Akad. Nauk SSSR **90**, 991 (1953).

As the Hamiltonian of zeroth approximation we choose

$$H^0 = \frac{c^2}{2}\int \sum_{\alpha}\Big[(\nabla\varphi_\alpha^0)^2 + \varkappa^2(\varphi_\alpha^0)^2 - 2\sqrt{4\pi}\, gc \sum_{i}^{n} O_{\alpha i}\,\varphi_\alpha^0\Big] d\mathbf{r},$$

in which the φ_α^0 satisfy the equation

$$(\varkappa^2 - \Delta)\,\varphi_\alpha^0 = \frac{g}{c}\sqrt{4\pi}\sum_{i}^{n} |O_{\alpha i}|_{\lambda\lambda}.$$

Then

$$H^0 = \frac{g^2}{2}\int \sum_{\alpha,i,j}^{3,n,n} [\,|O_{\alpha i}(\mathbf{r})|_{\lambda\lambda} - 2O_{\alpha i}(\mathbf{r})]\,|O_{\alpha j}(\mathbf{r}')|_{\lambda\lambda} \times G(\mathbf{r},\mathbf{r}')\,d\mathbf{r}\,d\mathbf{r}', \tag{30}$$

and the perturbation has the form $H' = H^{(1)} + H^{(2)}$;

$$H^{(1)} = gc\sqrt{4\pi}\int \sum_{\alpha,i} \varphi_\alpha(\,|O_{\alpha i}|_{\lambda\lambda} - O_{\alpha i})\,d\mathbf{r};$$

$$H^{(2)} = \frac{1}{2}\int \sum_{\alpha} (\Pi_\alpha^2 + c^2\varphi_\alpha(\varkappa^2 - \Delta)\,\varphi_\alpha)\,d\mathbf{r}.$$

The equation for $\chi'_{\lambda\mu}$ and the equation for χ_λ^0 have the same form as in the case of a single nucleon – Eqs. (18) and (19), except that $K_{\alpha\beta}$ is now determined by the expression

$$K_{\alpha\beta} = 4\pi g^2 \sum_{\mu\neq\lambda}\sum_{i,j}^{n,n} |O_{\alpha i}(\mathbf{r})|_{\lambda\mu}\,|O_{\beta j}(\mathbf{r}')|_{\mu\lambda}\,(E_\lambda^0 - E_{\lambda\mu}^0)^{-1}.$$

The equation for φ_k^ρ coincides with Eq. (20), but with the new expression for $K_{\alpha\beta}$. The more general expression for the energy in the zeroth approximation has the form

$$E_\lambda^0 = H_{\lambda\lambda}^0 = -\frac{g^2}{2}\int \sum_{\alpha,i,j} |O_{\alpha i}(\mathbf{r})|_{\lambda\lambda}\,|O_{\alpha j}(\mathbf{r}')|_{\lambda\lambda}\, G(\mathbf{r},\mathbf{r}')\,d\mathbf{r}\,d\mathbf{r}',$$

Here E_λ^0 is the self-energy and the energy of interaction of the nucleons. If all $|\mathbf{r}_i - \mathbf{r}_j| \gg a$:

$$(E_\lambda^0)_{sc} = -\frac{g^2}{2}\sum_{i\neq j,\alpha} |\tau_{\alpha i}|_{\lambda\lambda}\,|\tau_{\alpha j}|_{\lambda\lambda}\,\frac{e^{-\varkappa|\mathbf{r}_i - \mathbf{r}_j|}}{|\mathbf{r}_i - \mathbf{r}_j|} + \text{const};$$

$$(E_\lambda^0)_{ps} = -\frac{g^2}{2\varkappa^2}\sum_{i\neq j,\alpha} (\{\tau_{\alpha i}\vec{\sigma}\}_{\lambda\lambda},\ \nabla_i)\,(\{\tau_{\alpha j}\vec{\sigma}\}_{\lambda\lambda},\ \nabla_j)\,\frac{e^{-\varkappa|\mathbf{r}_i - \mathbf{r}_j|}}{|\mathbf{r}_i - \mathbf{r}_j|} + \text{const}.$$

As is known, in the case of weak coupling, the self-energy and the energy interaction of the nucleons in the second approximation in the theory of perturbations appear as the diagonal matrix element of the spin operator V[5]:

$$V = -\frac{g^2}{2}\lim_{a\to 0}\int \sum_{\alpha,i,j} O_{\alpha i}(\mathbf{r})\,O_{\alpha j}(\mathbf{r}')\,\frac{e^{-\varkappa|\mathbf{r}-\mathbf{r}'|}}{|\mathbf{r}-\mathbf{r}'|}\,d\mathbf{r}\,d\mathbf{r}'. \tag{31}$$

In the presence of strong coupling, $O_{\alpha i}(\mathbf{r})O_{\alpha j}(\mathbf{r}')$ appears in Eq. (31) in place of $O_{\alpha i}(\mathbf{r})|\,O_{\alpha j}(\mathbf{r}')\,|_{\lambda\lambda}$, and $|\,O_{\alpha i}(\mathbf{r})O_{\alpha j}(\mathbf{r}')\,|_{\lambda\lambda}$ appears in $V_{\lambda\lambda}$, not $|O_{\alpha i}(\mathbf{r})|_{\lambda\lambda}|O_{\alpha j}(\mathbf{r}')\,|_{\lambda\lambda}$, as in E_λ^0.

Translated by R. T. Beyer
221

SOVIET PHYSICS JETP VOLUME 2, NUMBER 3 MAY, 1956

Study of the Structure of the Surface of a Liquid by the Method of Reflection of Light

V. A. Kizel'
Uzbek State University

(Submitted to JETP editor July 2, 1954)
J. Exper. Theoret. Phys. USSR **29**, 658-668 (November, 1955)

Measurements were carried out on the elliptical polarization of light reflected from the surface of a liquid with incidence at Brewster's angle, for 60 liquids. The dependence of the effect on temperature was studied and its relation to the characteristics of a near-oriented arrangement is shown. A modification in the structure of the surface in the neighborhood of the freezing point was revealed, also a connection of this phenomenon with supercooling.

THE works[1-4] have demonstrated the possibility of studying the surface structure of a liquid by means of the effect which arises upon reflection of light by this surface--elliptical polarization of the reflected beam when the incident beam is linearly polarized. The results obtained are of great interest for the theory of a liquid; however, for their complete theoretical interpretation, an increase is necessary of the experimental material which is entirely insufficient up to now. In the present work, the results of investigations carried out along this line are reported.

1. THE EXPOSED SURFACE OF A NONABSORBING LIQUID

A description of the method, apparatus and experimental procedure is given in reference 1.

The results of our measurements are presented in Tables I-IV; for comparison, some data from earlier works are included. The characteristics of the optical anisotropy are taken from references 5 and 6 without recalculation, and some improvements in the precision are made according to references 7 and 8.

The measurements were performed at 15-18° C, unless another temperature is indicated. The values marked with the sign $\sim$ are given tentatively (see below). The limits of variation of the quantity (everywhere in the text the values given are for $\rho' = \rho \times 10^5$) are from 220 to 30; for the overwhelming majority of liquids, the values lie within narrower limits--from $\sim$ 180 to 80.

We made measurements of the coefficient of ellipticity ρ for 60 liquids; from earlier works data can be obtained for about another 30. On the basis of such material, it is already possible to look for relations of the effect with various parameters of the liquids investigated.

Let us consider Table I. Here there is a clearly expressed regularity--ρ increases with increase in the number of carbon atoms. The growth at the beginning of the series is very rapid, slowing down further along, and ρ tends to a definite limit. For the acids and the alcohols, this course is seen distinctly; for the ethers, the limit is apparently not yet completely attained. The limits for the acids and the alcohols are practically the same; the values of the limits for the ketones and the ethers are close.

The observed dependence does not permit one to relate ρ directly to the length of the molecular chain, which is known to increase linearly, nor with the anisotropy which is essentially different, for instance, for acids and alcohols. On analyzing the data for the various substituents (Tables II and III, likewise Table IV), one is forced to note that no direct correlation can be seen between ρ and the parameters that have been introduced; in particular, large ρ's do not at all tally with a large anisotropy.

Relations with the size and shape of molecules are apparently eliminated, for instance, for CCl_4, palmitic acid ($C_{16}H_{32}O_2$) and ethyl cinnamate

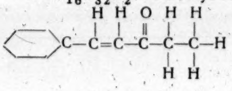

---

[1] V. A. Kizel', J. Exper. Theoret. Phys. USSR **26**, 228 (1954).

[2] C. Bouhet, Ann. de Phys. **15**, 5 (1931).

[3] C. V. Raman and L. A. Ramdas, Phil. Mag. 3, 220 (1927).

[4] D. V. Sivukhin, J. Exper. Theoret. Phys. USSR 21, 76 (1951).

[5] J. Cabannes, *La Diffusion Moleculaire de la Lumiere*, Paris, 1929.

[6] Bhagavantam, *Scattering of Light*, Calcutta, 1940.

[7] H. Stuart, in Landolt-Bornstein's Phys. Chem Tab., 1951.

[8] M. F. Vuks, J. Exper. Theoret. Phys. USSR **24**, 351 (1953); M. F. Vuks and I. I. Bilenko, J. Exper. Theoret. Phys. USSR **23**, 105 (1952)

TABLE I

Homologous Series

Liquid	Coefficient of Ellipticity $\rho \times 10^5$	Optical Anisotropy $\delta^2 \times 10^3$		Surface Tension σ 18°	Thermal Coefficient of Free Energy k
		Vapor	Liquid		
Hydrocarbons					
Pentane	70	11.0	3.1		
Hexane	~ 62	12.7	2.8		
n. Octane	92	12.5	2.2	27.2	
Isooctane	90	10.1	1.8		
Alcohols					
Methyl	46	17.5	3.5	22.7	0.67
Ethyl	~ 95	7.6	2.6	22.6	0.94
n. Propyl	90	10.1	1.9	22.6	1.11
Isopropyl	99	11.0	1.1	21.0	1.05
n. Butyl	103	14.5	1.6	24.4	1.36
n. Amyl	102	11.0	1.5	25.7	1.35
Isoamyl	100	9.3	—	24.4	1.35
Octyl[2]	102	—	—	27.7	—
Acids					
Formic	34	35.9	47.0	37.8	0.57
Acetic	91	24.1	25.1	28.0	1.3
Propionic[2]	96	23.2	20.1	26.7	1.53
Butyric	~ 90	17.1	16.5	27.1	1.63
Caproic	~ 108	—	—	—	—
Pelargonic[2]	102	—	—	—	—
Palmitic (110°)	~ 106	—	—	—	—
Ketones					
Methylmethylketone[2]	81	14.3	11.3	23.3	1.57
Methylethylketone	130	28.8		24	1.89
Methylpropylketone	122	17.1		24.3	1.73
Ethers					
Diethyl (0°)	108	22	3.7	19.2	1.9
Dibutyl	125			23.4	
Diisoamyl	140				

TABLE II

Substitutions for Methane and Ethane

Liquid	Substitute	Coefficient of Ellipticity $\rho \times 10^5$	Optical Anisotropy $\delta^2 \times 10^3$ Vapor	Optical Anisotropy $\delta^2 \times 10^3$ Liquid	Surface Tension σ_{18°	Thermal Coefficient of Free Energy k
Formic Acid	O, OH	34	35.9	47	37.8	0.57
Nitromethane	NO_2	35	—	—	37.7	1.14
Methyl Alcohol	OH	46	17.5	3.5	22.7	0.67
Carbon Tetrachloride	Cl, Cl, Cl, Cl	107	0 – 1.7	1.6	26.3	1.95
Chloroform	Cl, Cl, Cl	129	11.0	9.4	27.5	2.06
Bromoform	Br, Br, Br	130	25.0	9.5	51 (20°)	
Methyl Iodide	I	137				
Dibromomethane	Br, Br	200				
Diiodomethane	I, I	221				
Ethylene Glycol	OH, OH	79			46.0	1.04
Acetic Acid	O, OH	91	24.1	25.1	28.0	1.30
Ethyl Alcohol	OH	95	7.6	2.6	22.6	0.94
Ethyl Acetate	O, OC_2H_5	99	18.8	7.4	24.0	2.23
Tetrabromoethane	Br, Br, Br, Br	103			49.0	2.51
Ethyl Bromide	Br	123	19.7	13.9		
Ethyl Iodide	I	129			28.4	1.65
Dibromoethane	Br, Br	159	32.2	29.5	38.0	2.14
Dichloroethane	Cl, Cl	178	29.5	14 - 18	32.0	2.17
Ethylenediamine	NH_2, NH_2	180				

ρ's were obtained equal to 107, 102 and 114, respectively[2]. The influence of double bonds is likewise imperceptible. Thus, for propyl (C_3H_7OH) and allyl (C_3H_5OH) alcohol we have values for ρ' of 90 and 110, respectively[3]; the values for pentane and amylene, for oleic acid and the saturated acids are close. Evidently, there is no effect of the compactness of the molecular structure, as well.

With respect to the effect of various functional groups, one can make discrete observations; thus, for example, the substitution of H by CH_3 produces almost no change in ρ. Substitution of one halide by another usually changes ρ a little; apparently, introduction of NO_2 reduces ρ while NH_2 increases it; however, all of these observations are qualitative. There is also no connection with the magnitude of the dipole moment, as comparison has shown. No direct correlation between the values of ρ and of δ^2_{liq} can be recorded. One can say the same about the relation with the crystal structure of a given substance. Thus, for cyclohexanol, which crystallizes in the isotropic cubic system, and for water, which has an isotropic tetrahedral coordination of molecules, the values of ρ' are 132 and 40, respectively, while for paradichlorobenzene and napthalene, which are highly anisotropic in crystal form (monoclinic system), the values of ρ' are 105 and 110, respectively.

Theory indicates that the effect of ellipticity is determined not by the individual properties of the molecules and not by the properties of the liquid, as such, but by the fact of a difference of the surface layers from the deeper lying material, and the magnitude of the effect, schematically speaking, depends on the degree of the difference. If one proceeds from the concept of a surface (which is prevalent in the literature) as a layer (with a more or less well-ordered orientation) of molecules strictly on the surface of the liquid, with a coated layer of mobile, freely rotating adsorbed molecules of vapor (of the more recent works, cf. reference 9), then one can suppose that both of these layers contribute their share in the creation of the ellipticity. With such a model, the value of ρ must naturally depend on many parameters. For homologous series, where all the parameters vary regularly from one term to another, the value of ρ

---

[9] A. Wyllie, Proc. Roy. Soc. (London) **197**, 383 (1949).

TABLE III

Substitutions for Benzene

Liquid	Substitute	Coefficient of Ellipticity $\rho \times 10^5$	Optical Anisotropy $\delta^2 \times 10^3$		Surface Tension σ_{18°	Thermal Coefficient of Free Energy k	Total Surface Energy U *
			Vapor	Liquid			
Benzene		135	37.5	18.0	29.1	2.73	70.26
Phenol (100°)	OH	~ 80	30.4	18.5	36.5	1.70	
Benzaldehyde	CHO	87			38.8	2.17	
Para-Dichlorobenzene (100°)	Cl, Cl	~ 90	67.8		-----	-----	71.45
Para-Dibromobenzene (120°)	Br, Br	~ 92		55.8	-----	-----	-----
Nitrobenzene	NO_2	101	54.7		42.9	2.23	81.70
Ortho-Nitrotoluene	CH_3NO_2	109	46.1				
Toluene	CH_3	114	37.7	20.4	28.5	2.13	65.53
Benzyl Chloride	CH_2Cl	114	41.4				
Ortho-Nitrochlorobenzene . .	Cl, NO_2	~ 116					
Anisole[2]	OCH_3	118		14.5	35.2	2.0	
Bromobenzene	Br	120	42.3	31.7	37.5	2.33	71.48
Benzyl Alcohol	CH_2OH	122					
Mesitylene	CH_3, CH_3, CH_3	134			28.5	2.40	
Ortho-Xylene	CH_3, CH_3	137	44	21.6	30.5	2.20	
Chlorobenzene	Cl	138	43.3	30.6	33.7	2.79	71.01
Aniline	NH_2	186	54.7	21.6	43.4	1.57	82.40

* S. Sugden, Trans. Farad. Soc. **22**, 486 (1926)

also changes regularly; for the substituents, where the changes of the various parameters can proceed sometimes in the same direction and sometimes in opposite directions for different substances, the dependencies are masked.

The complex dependence of ρ on temperature established below, which is essentially different for different liquids, confirms these deliberations.

2. MEASUREMENTS FOR THE SURFACE OF A LIQUID IN VACUUM

Spherical, thin-walled (~ 0.4 — 0.6 mm) glass ampoules, 80 mm in diameter, were filled with the investigated liquids by distillation under vacuum. After the filling, the ampoules were disconnected from the distillation apparatus and the pumping was continued for some time while the liquids boiled; then the ampoules were also disconnected from the pump. The level of the liquid in the disconnected ampoule passed through its center. The measurements were carried out on the earlier setup; the point of reflection was fixed in the center of the surface and in this way the beams went through the glass normally (the aperture of the beam was 12′). Such an arrangement led to a minimum of error arising from reflections from the glass. The glass of the ampoules was examined initially, for freedom of double refraction in the interval 0° — 220° C. The quality of the glass of the ampoules was likewise checked according to the quality of the image of a cross-hairs given by transmitted beams; ampoules in which a somewhat distorted image was obtained were rejected.

Control experiments were carried out with separated ampoules which had contained a little liquid, to determine the effect of a layer of vapor molecules adsorbed on the glass; such an effect was not detected.

The outside surface of the ampoule was very carefully cleaned immediately before a measurement. Brewster's angle was determined for a given temperature *in situ* by phase difference (the principal angle determined practically[1] coinciding with Brewster's angle). In this way, difficulties in the measurement of the index of refraction at various temperatures and pressures were avoided, and also errors which can be caused by a slight nonparallelism of the walls of the ampoules and the like. After each series of 10 twofold measurements, Brewster's angles was determined anew; for each liquid, 3 — 5 such series were made.

The results of several measurements are given

TABLE IV

Liquid	Coefficient of Ellipticity $\rho \times 10^5$	Optical Anisotropy $\delta^2 \times 10^3$		Surface Tension $\sigma_{18°}$	Thermal Coefficient of Free Energy k
		Vapor	Liquid		
Heterocyclic Compounds					
Pyridine	177	42.4		35.8	2.30
Quinoline[2]	125	72.5		44.8	1.92
Dioxane	107	9.4		35.7	2.31
Furfuryl Alcohol	71				
Other Compounds					
Stannic Chloride	~ 125	0			
Napthalene (100°)	~ 110	72.5	55	30.3	2.29
α-Chloronapthalene	128				
α-Bromonapthalene	139			44.6	
Cyclohexanol (30°)	~ 132	12	2.5		
Benzyl Ether	102				2.63

in Table V. As is seen, for all liquids the values of ρ are somewhat less than with an exposed surface. This can be explained by the influence of several factors (most likely operating together). It is known that the least impurity strongly increases the value of ρ. Such impurities even arise on an ideally pre-cleaned surface after its contact with the atmosphere; the latter was demonstrated both by the investigations of ellipticity and by the methods of luminescent analysis (see, for instance, the review in reference 10). There is no doubt that with the procedure described, the surface is cleaner than an exposed surface periodically cleaned by scraping off the top adulterated layer, which is the method used by all authors, including ourselves. This also reduces the values of ρ.

On the other hand, the character of the adjoining medium is far from indifferent to the condition of the surface, which can vary with a change in the total pressure and in the partial pressure of the vapor of the investigated substance.

It should be mentioned that in a layer of the order of 0.1 — 0.5 mm in depth from the exposed surface of a liquid, there exists a temperature jump of the order of 1 — 4°. This circumstance, shown, for example, in reference 11, was established also for our specific conditions---of an exposed surface---by measurements carried out in our laboratory by A. F. Stepanov*. All such type measurements were carried out with thermocouples 0.03 — 0.05 mm in diameter, which averaged the temperature over a relatively thick layer; the true jump in the surface layers might be even larger. Inasmuch as the true temperature of the surface layer is lower when it is exposed than when it is in equilibrium with the vapor, the value of ρ is correspondingly larger, since it increases with cooling (see below).

Leaving asided these considerations, we emphasize the chief result---the overwhelming part of the effect survives even under vacuum. This demonstrates without a doubt that its origin lies not in contaminations of the surface or in chemical processes on it, but in its structure.

3. DEPENDENCE OF THE COEFFICIENT OF ELLIPTICITY ON TEMPERATURE

The ampoules described in Sec. 2 were placed in an oil thermostat (Fig. 1). To eliminate the infiltration of cold air into the thermostat, a stream of hot air could be produced along the outer walls by means of the coils C_1 and C_2 with adjustable heating. Fluctuations of the temperature of the liquid did not exceed ±0.1°. The inside of the thermostat was charged with fine blackened

---

[10] V. A. Kizel' and M. N. Rakhmatov, Uch. Zap. Tomsk State Univ. 1, 4 (1954).

[11] W. Prüger, Z. Physik 115, 202 (1940).

* Ready for press.

TABLE V

Liquid	$\rho_{\text{vac}} \times 10^5$	$\dfrac{\rho_{\text{vac}}}{\rho_{\text{atm}}}$
Dichloroethane	147	0.83
Dibromoethane	135	0.85
Pyridine	151	0.85
Acetic Acid	81	0.88
Chlorobenzene	123	0.89
Cyclohexanol (28°)	138	0.89
Dibromomethane	180	0.90
Bromoform	120	0.92
Benzene	127	0.94
Nitrobenzene	97	0.96
CCl_4	105	0.98
$SnCl_4$	123	------
Average		0.91

aluminum filings into which the ampoule was sunk; this assured uniform heating up and completely eliminated convection currents (in the presence of which measurements are impossible). The thermostat was provided with adjusting screws and shock absorbers.

Before measurements, the liquid was held at the assigned temperature for ½ — 1 hour. For each temperature, 3 — 5 series of 10 double measurements were made; Brewster's angle was determined as described above. The results of the measurements are given in Figs. 2 and 3.

It is evident that the described method gives the variation of $\rho = \rho(p, T)$. It is difficult to doubt that the chief cause of the variation of ρ is the variation in temperature and that the effect of pressure is small. The vapor pressure for the majority of the liquids, even at the maximum temperatures, lies within the range of ~ 1 atm, and in this way the variation of ρ lies within a 10% range (Sec. 2). The pressure reaches large values only for CCl_4 (~ 5 atm), benzene and dichlorethane (~ 2 atm); however, no noticeable peculiarities are seen in the course of these curves. If, on the basis of the considerations of Sec. 2, one supposes that a decrease in pressure reduces ρ, then one might assume that an increase in p raises it. Then the curves $\rho = \rho(T)$ should fall somewhat more steeply, i.e., the dependence on T should become sharper.

The method employed eliminates errors introduced by the procedure of cleaning the surface. Let us consider the feasibility of some others.

1. The determination of Brewster's angle was carried out to a precision of 0.5′; even over this interval ρ changes somewhat, as we showed in reference 1; probably this is the chief source of random errors. The presence of the surfaces of glass can increase the scattered light somewhat and reduce the contrast range of the stripes of the compensator; this does not give systematic errors, however.

2. The variation with pressure and temperature of the properties of the layer of vapors adsorbed on the inner walls of the ampoule can hardly be

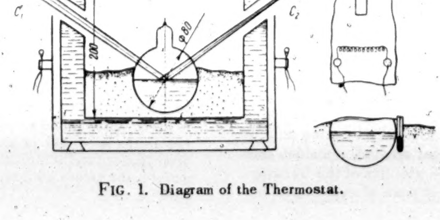

FIG. 1. Diagram of the Thermostat.

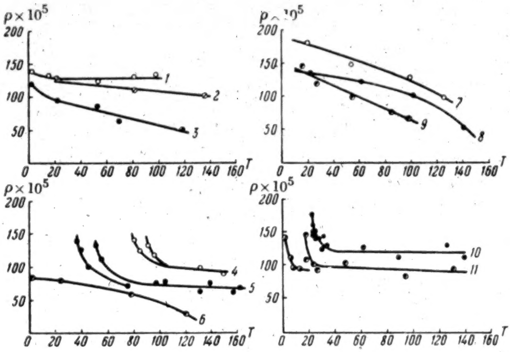

FIG. 2. Temperature dependence of ellipticity. *1*-benzene, *2*-chlorobenzene, *3*-nitrobenzene, *4*-napthalene, *5*-phenol, *6*-acetic acid, *7*-dibromomethane, *8*-dibromoethane, *9*-dichloroethane, *10*-cyclohexanol, *11*-benzophenone.

noticed, for the ~~rays pass~~ normally, and the effects of the thin layers act on the polarization only in the vicinity (±20′ – 30′) of Brewster's angle[1]

3. One cannot categorically maintain that the advent of double-refraction in the glass of the ampoules at large pressures (~ 5 atm) is not possible, but this could be somewhat marked only for CCl_4, where it is difficult to infer this effect, judging by the course of the curve.

What has been stated permits us to believe that the chief errors of the method are random, not systematic, and that the trend of the phenomenon is accurately shown. However, as is seen from Figs. 2 and 3, the error in the course of the curves can amount to 5 — 6% on the average.

From the data obtained it is possible to make a series of very substantial deductions. The chief of these is that, without a doubt, a significant dependence of the effect on temperature was established.

In the majority of liquids, the freezing point of which lies in the interval studied, a sudden drop is clearly visible in the vicinity of the freezing point and a considerably more sloped course beyond it*.

We discuss the phenomena in the neighborhood of the freezing point in Sec. 4; here we consider the shape of the curves somewhat removed from the freezing point.

The liquids studied can be divided into three groups. In the first, the dependence on temperature in the range under consideration is absent. (cyclohexanol, CCl_4, bromoform); in the second it is hardly noticeable or weak (benzene, paradichlorobenzene, bensophenone, orthochloronitrobenzene, chlorobenzene, napthalene, phenol). Finally, the third is characterized by a sudden drop (nitrobenzene, acetic acid, dibromoethane, dichloroethane, dibromomethane, pyridine). The first group

---

* We note here that those rough data which are entered in Tables III and IV were calculated by means of this curve. For $SnCl_4$ it was assumed that on going over to an exposed surface, ρ changes in the same manner as for CCl_4; for the remaining substances, values of ρ were taken in the sloping part of the curves (evidently, more appropriate for comparison with the other liquids) and it was assumed that for an exposed surface, the values are larger by 10%, according to Table V.

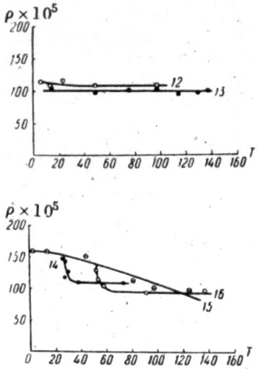

FIG. 3. Temperature Dependence of Ellipticity.
12 - bromoform, *13* - CCl_4, *14* - orthochloronitrobenzene, *15* - pyridine, *16* - paradichlorobenzene.

TABLE VI

Curve No. in Figs. 2 & 3	Liquid	Crystal		$\gamma_{eff} = f(T)$	γ^2_{eff}/γ^2
		System	Optical Anisotropy		
	1st Group				
10	Cyclohexanol	Cubic	Weak		0.2
12	Bromoform	Hexagonal	”	slowly rising	0.38
13	CCl_4	Cubic	”		0.27^5
	2nd Group				
1	Benzene		”	Rising	0.61
5	Phenol		”	”	0.61
4	Napthalene	Monoclinic	Strong	No Change	0.76
16	Para-Dichlorobenzene	”	”	”	0.77
2	Chlorobenzene			Slowly rising	0.84
	3rd Group				
9	Dichloroethane				0.62 - 1.06*
8	Dibromoethane				0.92
6	Acetic Acid		”	Decreasing	1.24
3	Nitrobenzene		”	rapidly falling	1.54
15	Pyridine				

---

* Measured in our laboratory.

can be characterized rather clearly: these are substances with small effective anisotropy of the liquid, and have crystals weakly optically anisotropic. In the second group are substances with values of effective anisotropy of the liquid ranging from large (napthalene, benzophenone) to moderate (benzene). The anisotropy of the crystals is likewise varied---from large (napthalene, paradichlorobenzene) to moderate (benzene, phenol). For nitrobenzene and acetic acid of the third group, both large values of δ^2_{liq} and considerable crystal anisotropy are characteristic[8,12]. A comparison with the course of the temperature dependence of the effective anisotropy of the liquids permits one to delineate the second and third groups. From Table VI, in which the 5th and 6th columns are derived from reference 8 ($\gamma^2 = \delta^2 9 \alpha^2$, where α is the mean polarizability), it is seen that for substances of the second group there is an increase or an invariance of the effective anisotropy, but for those of the third, a drop in it.

Especially characteristic is the ratio $\gamma^2_{\mathrm{eff}}/\gamma^2 = \delta^2_{\mathrm{liq}}/\delta^2$; it is very small for the first group, for the second group it is less than 1 and for the third > 1 or very near to it. For chlorobenzene this ratio is somewhat larger than for the rest of the substances of the second group, and the drop of the curve is a bit steeper. Data on the anisotropy of cyclohexanol is lacking, but if one proceeds from analogies with the aliphatic alcohols, on the one hand, and with the small change of anisotropy on going from benzene to phenol, on the other, and takes into account that for cyclohexanol and cyclohexane Δ_{liq} is 0.12 and 0.08, respectively, one can assume values for it, tentatively, a little larger than for cyclohexane (for which $\gamma^2_{\mathrm{eff}}/\gamma^2 = 0.16$, cf. reference 8); this was also done in Tables IV and VI. For pyridine there are no values of γ, and the ratio $\Delta_{\mathrm{liq}}/\Delta_{\mathrm{vap}}$, measured by us, equals 13.6, i.e., the anisotropy of the liquid is large (in benzene this ratio if 9), and the drop of the curve is rapid.

Recently, a series of weighty arguments have been put forward in favor of the idea that the difference of the anisotropy of the molecules from the effective anisotropy of the liquid is a result of the existence of a near-oriented arrangement in the latter[12]; the effective anisotropy is regarded as a guage of the anisotropy of near order in the liquid, and the ratio $\gamma^2_{\mathrm{eff}}/\gamma$ as a measure of the character and extent of the near-oriented arrangement[8]. In the work of reference 13 this ratio is related to the "correlating parameter" of Ansel'm[12].

As is seen, this ratio also determines the thermal course of ρ in the region considered. On the basis of what has been said, one can suppose that the presence of ellipticity is brought about by two factors. One of these is undoubtedly connected with differences in the oriented arrangement on the surface of the liquid, and in its thickness. Its effect increases with an increase in $\gamma^2_{\mathrm{eff}}/\gamma^2$; for liquids with large values of this ratio and with large anisotropy of near order, the chief role is played by just this factor, since at higher temperatures where the oriented arrangement is broken up, ρ falls off to very small values in these liquids. The other factor is not connected with the temperature or with an oriented arrangement (cf. Sec. 4); for certain liquids with small anisotropy of near order it evidently plays the main role. For most of the liquids, both of these factors probably act together.

4. PROCESSES NEAR THE FREEZING POINT

The sharp deflection of the curves, in approaching the freezing point is very interesting. In greater or lesser degree it is observable in all liquids which have their freezing point within the temperature interval studied.

Benzene and nitrobenzene were supercooled to ~ -4 or -5°, acetic acid to -10°. Our method did not permit measurements to be made for $T < 2°$ C, but for the first two liquids the beginning of the rise of the curves is nevertheless seen. Only in bromoform was the rise not detected; probably, this is explained by the fact that the curve is very steep for it, and our preparations scarcely allowed supercooling. Instead, they crystallized at approximately 6° with the least variation of temperature, so that the rise could not be detected.

That the phenomenon is functionally related to changes of structure during "preparations" for solidification, is shown especially clearly by effects which arise during supercooling. It is known that the process of supercooling depends on the previous history of a liquid; this is reflected in our curves. Thus, for example, our preparation of benzophenone melted in open air at ~ 40°. After melting it in an evacuated ampoule, measurements were performed; it was cooled to ~ 17.2°, when it began to crystallize, and then heated to

---

[12] M. F. Vuks, Uspekhi Fiz. Nauk 61, 393 (1953); A. I. Ansel'm, J. Exper. Theoret. Phys. USSR 17, 489 (1947).

[13] V. I. Elfimov, Dissertation, Leningrad State Univ., 1954.

140° (right-hand curve). Further measurements were carried out during cooling and the left-hand curve was obtained (at 0° the liquid still had not solidified).

An analogous procedure was carried out for napthalene and phenol; the latter was melted in the thermostat heated to 55°, and measurements were conducted during heating (curve on right). Measurement during cooling gave the left-hand curve. In all cases, the sloping parts of the curves agree within the limits of our accuracy. From these examples it is seen that the bend of the curves comes right after the freezing point.

Cyclohexanol permitted only an insignificant supercooling, orthochloronitrobenzene likewise; therefore, the curves were reduced to a few "settings" with intermediate heating, and the described phenomena left a mark only in the scatter of the points.

In the curves in the region considered, within the limits of our accuracy of measurement and with the available material, it is hard to notice the difference between substances with different effective anisotropy of the liquid or with different crystal lattices, and also differences in the behavior of the three groups noted. The difference in the curves for liquids disposed to strong supercooling (for example, benzophenone) and indisposed (for example, orthochloronitrobenzene)[14], apparently reduces only to a different slope of the curve (which also depends on the previous history).

The facts we stated lead to the idea that in the immediate vicinity of the freezing point the changes in the structure of the surface and stratum of the liquid accelerate sharply. The mechanism of this process, as far as can be judged, is not exactly like that which prevails away from the freezing point.

Other facts can be pointed out which illustrate the likelihood of such differences (cf. also reference 15). Thus, it is noted in reference 8 that the approach to the melting point and supercooling have no special effect with respect to the intensity and depolarization of light scattered in the volume. On the other hand, for the surface layers of liquids (of the saturated acids) the appearance of anisotropy over an interval of 1-4° from the melting point was found[16] (though also not for a free surface, but for a boundary with glass, which can introduce an orienting effect[17]). Thus the hypothesis seems possible that the observed phenomena are brought about by changes in the structure, namely, in the surface. To detail the mechanism of these changes is difficult at present.

It should be kept in mind that the presence in a liquid of the slightest impurities (which are difficult to determine chemically) can, generally speaking, act on its structure (which was shown already in Stuart's early works). It is likely that this applies to the structure of the surface in even greater degree. A special synthesis of the compounds is desirable here, although the good agreement of some of our data from Tables I-III with reference 2 also indicates the reproducibility of the data with the use of the usual compounds with proper purification.

In conclusion, it can be said that the present work, being in many respects still exploratory, demonstrates with certainty the great complexity of processes on the surface of a liquid, and also indicates the possibility of obtaining information about them which yields to interpretation by means of our method.

A. F. Stepanov, G. D. Pridatko and A. N. Mirumiants participated in making the measurements, and we express our appreciation to them. We likewise express deep thanks to the director of the chair for organic chemistry at S.A.G.U., Prof. I. P. Tsukervanik for the compounds kindly given to us.

---

[14] V. I. Danilov, Izv. Akad. Nauk SSSR, Ser. Fiz. **9**, 16 (1941).

[15] H. S. Green, *The Molecular Theory of Fluids*, Amsterdam, 1952.

[16] A. M. Taylor and A. King, Opt. Soc. Amer. **23**, 308 (1933).

[17] B. V. Deriagin, Uspekhi Fiz. Nauk **51**, 393 (1953).

Translated by R. L. Eisner
251

SOVIET PHYSICS JETP VOLUME 2, NUMBER 3 MAY, 1956

Absorption Spectrum of Excess Silver in the Low Temperature and High Temperature Modifications of Silver Iodide

P. N. KOKHANENKO AND L. V. GRIGORUK
Siberian Physico-Technical Institute of the Tomsk State University

(Submitted to JETP editor July 8, 1954)
J. Exper. Theoret. Phys. USSR **29**, 676-679 (November, 1955)

It is demonstrated that maxima at 4290 and 3340 Å in the absorption spectrum of AgI, which are due to atoms or ions of excess silver, disappear when the AgI is transformed into the high temperature modification, and reappear during the reverse transformation into the low temperature modification. The presence of excess silver increases the transition temperature of one modification of AgI into the other by 5-15° C.

THE connection between the absorption spectra of atoms or ions of excess metals distributed in sublimated films of the haloid salts and the type of lattice typical of the salt has been previously demonstrated[1,2]. It was thought interesting to determine how the absorption of the excess metal in any particular polymorphous substance would change when the substance was transformed from one modification to another. In this instance, the change in the lattice structure of the basic substance will take place under conditions of unvarying concentration and distribution of the diffused particles of excess metal.

A convenient object for investigation is silver iodide with a stoichiometric excess of silver. The excess silver (atoms or ions) in the absorption spectrum of sublimated AgI films produces sharp and strong maxima at 4290 and 3340 Å. The transformation of the low temperature modification of AgI into the high temperature modification takes place at a relatively low temperature, i.e, at 145.8° C. These modifications, as is well known, are enantiotropic, and when cooled to less than 145.8° C the high temperature modification retransforms into the low temperature modification. The low temperature modification of AgI has a lattice of the wurtzite type. In the high temperature modification only the the iodine lattice remains solid (cubic volume-centered), while the ions of silver distribute themselves statistically among all the positions possible to them, moving freely within the iodine lattice.

Sublimated AgI films with an adequate content of excess silver were obtained by the Shalimova[3] method of vacuum sublimation. The quartz test-glass with flat walls, on one of which the salt film was deposited, was placed in a special oven, and the absorption spectra were photographed at various film temperatures, using transmitted light. A hydrogen gas tube was used as the light source. The temperature of that portion of the wall of the test glass on which the illuminated portion of the salt film was located was measured with the aid of a thermocouple. The absorption spectra were recorded at intervals of 15-20° C while the films were being heated from room temperature to 170-180° C, and while they were being re-cooled to room temperature. Before each recording, the required temperature of the film was determined, and the film was maintained at this temperature for thirty minutes. The spectra were photographed by means of a quartz spectrograph having low dispersion. In all, 11 sublimated AgI films were prepared and investigated. In the spectra of several of the films, the excess silver maximum at 3340 Å was poorly delineated, and the spectra of such films were investigated photometrically only in the region of the intensive maximum at 4290 Å. For this reason the data given below refer only to that portion of the spectrum in which the maximum at 4290 Å occurs, which was intensive in the spectra of all the investigated films. In those cases in which the maximum at 3340 Å was clearly defined, as measurements demonstrated, its behavior with change in temperature of the film and transformation of one modification into the other differs in no way from the behavior of the maximum at 4290 Å.

Upon increasing the temperature of the AgI films, the change in the absorption spectrum proceeds in two directions. On the one hand, the excess silver absorption maximum is continuously displaced in the direction of the long waves, becomes broader, and the height of the maximum is reduced. On the other hand, the general level of absorption is at first reduced, and beginning at 120-130° C, again becomes stronger. The excess

---

[1] K. V. Shalimova, *Photoluminescence of sublimated phosphors*, Avtoreferat, Inst. of Phys., Acad. Sci., Moscow, 1952.

[2] P. N. Kokhanenko and V. D. Gol'tsov, Dokl. Akad. Nauk SSSR **85**, 543 (1952); P. N. Kokhanenko, J. Exper. Theoret. Phys. USSR **26**, 120 (1954).

[3] K. V. Shalimova and A. V. Byelkina, J. Exper. Theoret. Phys. USSR **21**, 326 (1951).

silver absorption band, despite a certain amount of indefiniteness, remains adequately intensive and clear up to the point of transition of the AgI from the low temperature to the high temperature modification. Upon transformation of the AgI into the high temperature modification, the excess silver absorption band disappears and no other new bands appear in the investigated portion of the spectrum. The transition temperature, judging from the spectra, is different for different samples, and lies between 150 and 160° C, i.e., is 5-15° C higher than the transition temperature of one modification into the other in the case of the pure AgI salt (145.8° C). The disappearance of the band itself takes place over a temperature interval of 10-15° C. When the films are cooled below the transition temperature, the excess silver absorption band reappears at the same point and with the same intensity. The selective reflection from the short wave side of the band is somewhat intensified. Figure 1 presents the absorption curves for one of the AgI samples. The broken curve *1* shows the absorption at room temperature before heating of the film; curve *2* is the lowermost absorption curve, corresponding to 127° C. To assure clarity of the sketch, not all of the intermediate curves are drawn. Upon further heating, the general level of absorption again increases and the absorption curves rise above curve *2*. Curve *3* is the absorption curve at 146° C; the excess silver absorption maximum is clearly defined on the curve. Curve *4* is recorded at a 10° higher level, at 156°; the maximum has disappeared and only an insignificant bulge is noticeable in its place. Curve *5* shows the absorption at 170°; there is not a trace of a maximum on the curve. Curve *6* shows the absorption at room temperature after solidification of the film; an intense excess silver maximum has again appeared on the curve, which is somewhat less symmetrical as a result of the intensification of the selective reflection from the short wave end of the band.

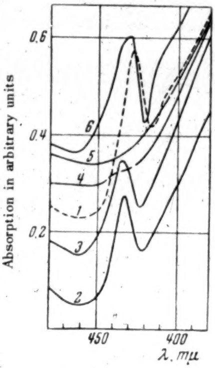

FIG. 1

Analogous results were also obtained with other specimens. A somewhat different course of change in absorption was observed in only one of the samples, the absorption curves of which are presented in Fig. 2. The intermediate curves are not shown, in order to preserve the clarity of the figure. The broken curve *1* represents the absorption at room temperature prior to heating the film. In addition to the excess silver absorption maximum, there is a broad, vague maximum at 5000 Å, attributable, probably, to colloidal particles of excess silver. Curve *2* is the lowermost absorption curve, corresponding to 131° C. Curve *3* represents the absorption at 140° C; the excess silver absorption maximum on this curve is sufficiently intensive and sharply delineated. The next curve *4* was obtained at 153° C. Increasing the temperature by 13° resulted in the complete disappearance of the maximum. Moreover, in contrast to the other specimens, the absorption in the region of the colloid particle absorption maximum was sharply intensified and the absorption in the ultraviolet portion of the spectrum was weakened (short wave portions of the absorption curves are not shown in the figure). Apparently, during the transformation of the specimen in question, which already contains colloidal silver, from the low temperature to the high temperature modification, a portion of the ions (or atoms) of excess silver diffused in the lattice are forced out, and transformed into colloidal particles. Upon further increase in temperature, the intensification of absorption in the long wave region and decrease of absorption in the ultraviolet region of the spectrum continues, as may be seen from curve *5*, recorded at 160°. Upon cooling the film to room temperature, the initial absorption spectrum was not re-established (curve *6*). The intensive absorption maximum of the colloidal particles was retained, but instead of the absorption band at 4290 Å, a faint reflection band appeared. The appearance in the absorption spectra, recorded with transmitted light, of selective reflection bands of excess metals only, had already been noted by us for the chemically related substance CuI[2].

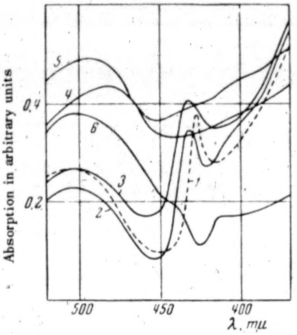

FIG. 2

The results obtained make it possible to draw the following conclusions.

1. During the transformation of the low temperature modification of AgI into the high temperature modification, the absorption bands of excess silver (atoms or ions) disappear, and during the reverse transformation they again reappear. The fact that the excess atoms or ions of silver do not produce any maxima at all in the absorption spectrum of the high temperature modification in the investigated region can be explained by the fact that this modification of AgI has only one fixed lattice---the iodine lattice. Since the silver lattice melts apart and the silver ions intermingle freely, then there is no reason to suppose that the ions (or atoms) of excess silver can occupy any sort of definite, regular position in the crystal, and therefore there is no reason, either, to expect structural absorption of light. The very fact of the disappearance of the excess silver absorption maxima during the transformation of AgI into the high temperature modification, which does not possess a silver lattice, testifies that the particles of excess metal must dispose themselves in the lattice of the basic substance according to some definite order in order to produce individual maxima in the absorption spectrum.

2. Judging on the basis of the absorption spectra, the presence of excess silver increases the transition temperature for the transformation of the low temperature modification of AgI into the high temperature modification by 5-15° C. A certain disparity in the transition temperatures of the various specimens is apparently connected with a difference in the concentration of the excess silver. Upon transformation of AgI into the high temperature modification, a reduction in volume of approximately 10% takes place[4]. One is led to believe that the presence of a large excess of silver distributed throughout the lattice in the form of atoms or ions interferes with this reduction and delays the reconstruction of the lattice. The fact that the disappearance of the excess silver absorption band in the spectrum of each individual specimen does not take place at a strictly defined temperature, but over an interval of 10-15°, is apparently connected with the complicated structure of the sublimated films. Small, individual crystals of AgI contain a different excess of silver and undergo structural transformation at different temperatures.

---

[4] V. D. Kuznyetsov, *Crystals and crystallization*, Moscow, 1953, p. 280.

Translated by A. Gertner
253

SOVIET PHYSICS JETP VOLUME 2, NUMBER 3 MAY, 1956

Two Electrode High-Frequency Discharge at Pressures from 100 mm Hg to Atmospheric

G. S. SOLNTSEV AND M. M. DMITRIEVA
Moscow State University

(Submitted to JETP editor July 12, 1954)
J. Exper. Theoret. Phys. USSR **29**, 651-657 (November, 1955)

Two electrode discharges were investigated in air, nitrogen and argon, in pressures from 100 mm Hg up to atmospheric, and for frequencies of 35-36 mc. The intensity of the longitudinal electric field in the canal of a discharge was measured. Separate measurements were carried out at 1.5 mc. The experimental results are discussed.

THERE has been very little recent work aimed at clarifying the study of two electrode high-frequency discharges at low and atmospheric pressures. The structure of such discharges, the distribution of voltage among the different parts, and the electrical parameters have not been investigated. Isolated works[1-3] have paid principal attention to the measurement of the ignition potential, which characterizes the condition for onset of the discharge. Of these works, only the first was carried out in the shortwave region, the others being made with centimeter waves. However, the study of a steady, stationary discharge at short radio wavelengths presents some interest.

The purpose of the present research was the investigation of the structure of high-frequency twoelectrode discharge in air at atmospheric pressure, and also the measurement of the field intensity in the canal of the discharge in air, nitrogen, and argon at pressures from 100 mm Hg up to atmospheric.

1. HIGH-FREQUENCY DISCHARGE AT ATMOSPHERIC PRESSURE

A generator of high-frequency electromagnetic waves of conventional design was used to produce the discharge. The power supplied to the generator was 1.5-2 kilowatt, the frequency was 35-36 mc. The resonant circuit for the discharge was coupled inductively to the plate circuit of the generator and therefore did not have a high dc voltage.

The investigation of the discharge included measurement of the ignition potential for various distances between the electrodes. The discharge was simultaneously photographed. This permitted estimates of the sizes of the different portions of the discharge. Electrodes in the form of two iron spheres were placed one above the other in order to preserve the geometrically correct form of the discharge. The discharge was produced vertically, so that the convection currents of the heated gas did not distort its shape. The distance between the spheres was measured by means of a micrometer screw. The electrodes were made of sufficiently large diameter (33 mm) to avoid their being strongly heated.

One could follow the appearance of new portions of the discharge upon increase of the distance between the electrodes. A discharge with bright layers α in front of the electrodes was produced at $l = 0.2$ mm. Beginning at a separation of 0.6 mm, there appeared a new part β—narrower and not so bright—at the near-electrode layers (Fig. 1). Upon further increase of the separation to 1.4-1.7 mm, the canal of the discharge appeared. The diameter of the canal was 0.8-0.9 mm. The canal was surrounded by a corona, which is not visible on the photographs because of its low intensity.

The canal is the principal current carrying portion of the discharge. Observations of the transition from one electrode (jet) to two electrode discharge confirm this fact. Figure 2 shows a two electrode discharge which is produced from a one electrode discharge by the insertion of a metallic conductor. The canal discharge transferred to this conductor, which served as the second electrode. The less brightly illuminated region of the discharge, which surrounds the canal in the form of a corona, is left extended in the vertical direction by the convective flow of the heated gas, and takes an insignificant part in the transport of current in the two electrode discharge which is formed.

Beginning at a separation of 1.4-1.7 mm, i.e., at separations corresponding to the onset of the canal discharge, the potential increases almost linearly with increase in separation between the electrodes. Upon further increase in the separation,

---

[1] S. Githens, Phys. Rev. **57**, 822 (1940).

[2] McDonald and S. Brown, Phys. Rev. **76**, 1634 (1949).

[3] D. Q. Posin, Phys. Rev. **73**, 496 (1948).

the length of the discharge increases due to extension of the canal. This allows us to draw a conclusion as to the field intensity in the canal*.

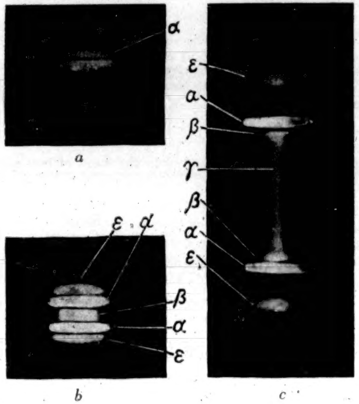

FIG. 1. Structure of a two electron discharge in air for different electrode separations. ∝, β, γ = different parts of the discharges, ϵ = flashing at the electrodes, occa- by the reflection of the discharge on them; *a:* $l = 0.3$ mm, *b:* $l = 1.3$ mm, *c:* $l = 5.6$ mm.

The magnitude of the field intensity in a discharge exposed to open air amounts to about 260 eff. volts/cm, which greatly exceeds the field intensity in the ordinary dc case. There is a total potential of 300 eff. volts in the near-electrode part of the discharge. The power in the electromagnetic vibrations in the discharge circuit changes with a change in the filament voltage of the generator tube. For different filament voltages, the magnitude of the field intensity changes in the range 250-300 eff. volts/cm. Figure 3 shows the dependence of the ignition potential on the electrode separation.

FIG. 2. Transition of a jet discharge into a two electrode discharge.

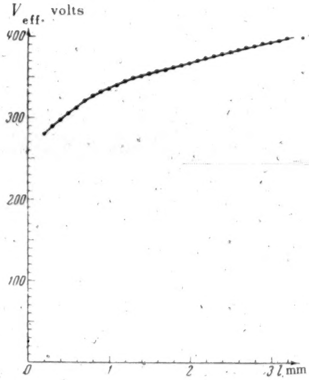

FIG. 3. Dependence of the ignition potential on the electrode separations. Air: f = 35-36 mc.

All the above data on the external form and dependence of the ignition potential on the length of the high-frequency discharge applies to a discharge at 35-36 mc. The radiofrequency generator had limited power, which did not permit a study of the discharge in a wide range of rf power in the secondary circuit, in which the discharge occurred.

---

* It should be noted that this method of determining the field intensity in the canal of a discharge is evidently the only possible one. It does not appear possible to apply probe measurements in the given pressure range (and at such high frequencies) to the measurement of the field intensity of the radiofrequency field. Optical measurements on line splitting (Stark effect) also fail to give decisive results, since the relatively small magnitude of the field intensity would lead to insignificant line splitting, and the detection of these latter would require extraordinarily high resolving power on the part of the spectral apparatus.

To obtain a radiofrequency discharge at a frequency of 1.5 mc, a generator with two tubes GK-3000 was employed. This arrangement provided far more power than the generator employed at 35-36 mc. This generator made it possible to obtain the discharge under conditions of a much greater range of rf power in the circuit. Variation in the rf power in the circuit was produced by variation of the filament voltage of the generator tubes. The external form of the discharge depended essentially on this power. The external form of the discharge is shown in Fig. 4 at a frequency of 1.5 mc for different values of the rf power W in the secondary circuit. If this power is not large (W_1), then the external form of the discharge differs but little from the discharge at 35 mc. The difference lies only in the dimensions of the brightness below the near-electrode layer. These are larger at 35 mc than at 1.5 mc (Fig. 4*a*). For higher rf power in the secondary (W_2), an increase is observed in the size of all portions of the discharge, with a broadening of the canal at its middle (Fig. 4*b*). For still higher rf power (W_3), the external form of the discharge is shown in Fig. 4*c*. The significant broadening of the canal and the increased intensity of all parts of the discharge are noteworthy features. The discharge is not stationary, and over long periods of time, a scorching of the electrodes is observed.

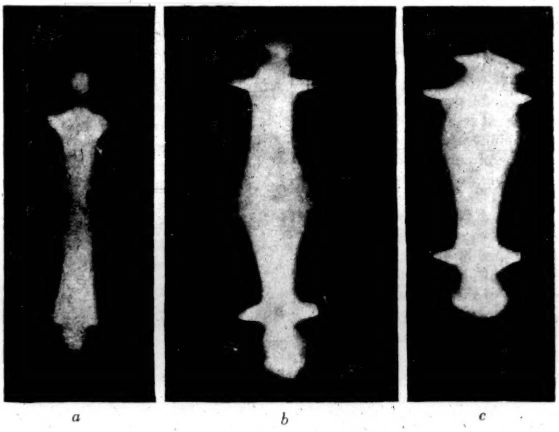

FIG. 4. Two electrode high-frequency discharge at 1.5 mc and atmospheric pressure for different powers W of the electromagnetic signal in the circuit. a = power W_1 in circuit; b = power W_2 in circuit; c = power W_3 in circuit ($W_1 < W_2 < W_3$).

The dependence of the potential at the electrodes on the distance between them, for various output powers of the generator, is shown in Fig. 5. Under all circumstances, the potential increases with increase in separation. Measurement of the longitudinal field intensity in the canal of the discharge was possible only in the case of a low power discharge, when broadening of the canal did not take place (Fig. 5, curve *a*). In this case the value of the field intensity amounted to 850 eff. volts/cm. For higher powers (Fig. 5, curves *b*, *c*), it was not possible to draw any conclusions as to the field intensity in the canal, since the canal itself had a clearly demonstrated inhomogeneity of structure along its length.

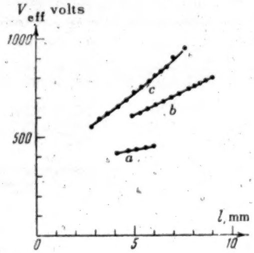

FIG. 5. Dependence of the ignition potential on the electrode separations (air; $f = 1.5$ mc) for different powers W of the electromagnetic signal. a = power W_1 in circuit, b = power W_2 in circuit, c = power W_3 in circuit ($W_1 < W_2 > W_3$).

2. RADIOFREQUENCY DISCHARGE AT LOWER PRESSURES (100-760 mm Hg) IN AIR, NITROGEN AND ARGON

A special tube was necessary for the investigation of the discharge at reduced pressures. It had metallic (telescoping) sections, which permitted a smooth moving of one electrode relative to the other and the accurate measurement of the distance between them.

The upper electrode E (Fig. 6) was rigidly clamped to the rod C, one end of which was a rectangular parallelopiped of square cross section, while the other was a spiral thread with a pitch of 0.7 mm. Upon rotation of the inner section S_2 by means of the shaft P, the end of the rod with the thread screwed into or out of the section S_2. The rod C itself, which was held by the controls N, could not rotate. As a consequence, rotation of the section S_2 led to a forward motion of the rod, and therefore to forward motion of the electrode also. The second electrode was not movable. The distance between the electrodes was determined by the number of turns of the screw. The electrodes were made of copper in the form of spheres of diameter 30 mm. The tube, which had double walls, and the sections, were cooled with oil, which was driven under pressure successively through the lower section, the tube and the upper section by means of a rotary pump.

The dependence of the ignition voltage of the discharge on the length of the discharge gap was investigated for various pressures in air, nitrogen (impurity 0.6% oxygen) and argon (impurity 0.27% nitrogen; 0.1% oxygen) (Figs. 7, 8, 9).

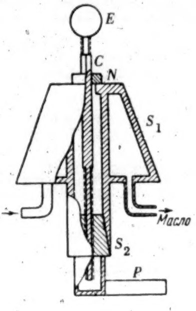

FIG. 6. Section with movable electrode; E = electrode, S_1 = principal section, which is inserted into discharge tube, S_2 = section for movement of the electrode, C = threaded rod, N = control, P = shaft.

Before the beginning of a series of measurements at some pressure, a definite value of the potential across the discharge gap in the absence of a discharge was established for a fixed distance between the electrodes (3.5 mm). This potential (650 eff. volts) served as a parameter for measurements at different pressures. It bears a well-defined relation with the magnitude of the capacitive current which flows across the discharge gap in the absence of discharge. We thus de-

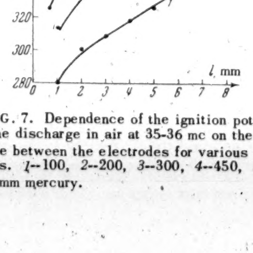

FIG. 7. Dependence of the ignition potential of the discharge in air at 35-36 mc on the distance between the electrodes for various pressures. 1--100, 2--200, 3--300, 4--450, 5--760 mm mercury.

termined the load in voltamperes which the discharge gap represents (in the absence of discharge). This parameter characterized, in known amount, the regime of the rf signal in the circuit, i.e., the source of energy which feeds the discharge under investigation.

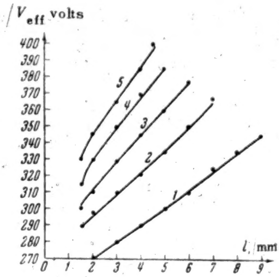

FIG. 8. Dependence of the ignition potential of the discharge in nitrogen at 35-36 mc on the distance between the electrodes for various pressures. *1*--100, *2*--200, *3*--300, *4*--500, *5*--760 mm mercury.

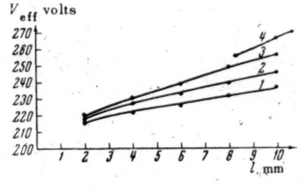

FIG. 9. Dependence of the ignition potential of the discharge in argon at 35-36 mc on distance between the electrodes for various pressures. *1*--760, *2*--100, *3*--300, *4*--400 mm mercury.

The field intensity in the canal of the discharge was determined from the dependence of the ignition potential on the distance between the electrodes for a fixed pressure. As a control, another group of measurements was performed (the dependence of the ignition potential on the pressure was investigated for different fixed distances between the electrodes), from which it was also possible to determine the intensity of the field.

The data for the field intensity in the canal of the radiofrequency discharge (frequency of the field, 35-36 mc) are shown in Fig. 10 for air, nitrogen and argon under different pressures. The potential found in the near-electrode regions of the discharge amounts to several hundred volts, which confirms the presence of strong electric fields in these parts of the discharge, and is in agreement with the presence in the near-electrode layer of spectral lines which correspond to high excitation potentials. This potential has its largest value for the air discharge, and its least for argon. For all three gases the ignition potential increased upon increase in pressure.

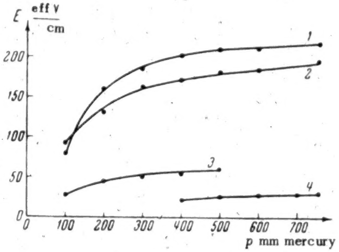

FIG. 10. Dependence of the field strength in the canal of the discharge on the pressure. *1*--air, *2*--nitrogen, *3*--argon, *4*--argon (filamented discharge); $f = 35\text{-}36$ mc.

The external form and structure of the discharges in air and nitrogen for pressures of 100-200 mm Hg are very similar, and are characterized by the presence of a red, sharply bounded canal and bluish near-electrode layers. Upon increase in pressure, the lateral dimensions of all parts of the discharge decrease and a corona appears around the canal in the air discharge. The brightness of the illumination of this corona increases with increase in pressure. Excitation of the corona is connected with the formation of an oxide layer.

The discharge in argon at pressures of 100-500 mm Hg has a diffuse yellowish-blue wide canal and a bluish near-electrode layer. At pressures of 300-760 mm Hg, there takes place a feathering or filamentation of the discharge, which is accompanied by the formation of a very bright bluish-white canal (Fig. 11). In the pressure range from 300 to 500 mm Hg in argon, both filamented and unfilamented discharges could exist. Filamentation of the discharge takes place upon increase in the length of the discharge for constant pressure, or upon increase in the pressure for constant length of discharge. The current density in the filamentation increases more than sixfold. As is evident from Fig. 10, the field intensity in this case is decreased by a factor greater than two.

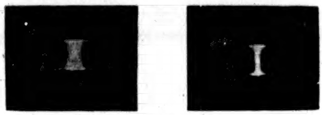

FIG. 11. Discharge in argon: *a*: unfilamented discharge, $p = 200$ mm mercury; *b*: filamented discharge, $p = 300$ mm mercury.

3. DISCUSSION OF THE RESULTS

The experimental results indicate that the field intensity in the canal of a high-frequency discharge changes, for a given range of pressure, upon change in pressure, so that the energy received by the electron in its free path remains constant. This is one of the conditions of similarity which applies both for dc discharge and rf discharge:

$$E/N = C, \tag{1}$$

where E is the field intensity, N the density of the neutral gas, C a constant for a given gas.

The dependence $E = E(p)$ for argon (curves *3*, *4*, Fig. 10) is close to linear. Deviations from linearity are connected with the dependence of the gas density on its temperature:

$$N = p/kT, \tag{2}$$

where p is the pressure of the gas, T the temperature and k Boltzmann's constant.

It follows from Eqs. (1) and (2) that

$$E = Cp/kT, \tag{3a}$$

$$\partial E/\partial p = C/kT. \tag{3b}$$

According to Eq. (3b), the increase in the temperature of the gas, which is observed upon increase in pressure, ought to produce a decrease in $\partial E/\partial p$, i.e., the slope of the tangent in the graph.

In the filamentation of the discharge in argon, there takes place a sharp increase of the current density in the canal. This effect is accompanied by an increase in the temperature of the gas in the filaments of the discharge. In correspondence with Eqs. (3a) and (3b), the magnitude of the field intensity in this case must decrease at fixed pressure. Likewise, the slope of the tangent to the curve $E = E(p)$ must also decrease. Curves *3* and *4* (Fig. 10) show that this is actually the case.

For frequencies which correspond to the very short wavelength of radio waves, and for pressures at which the experiment was conducted, Eq. (1) is equally valid for rf and dc discharge. Actually, under these conditions, the frequency of collision of the electron with the particles of the gas is significantly higher than the frequency of the field; in other words, the electron moves from one collision to another in a slowly changing, "almost constant" field. Diffusion of the electrons along the canal of the discharge does not have to be taken into account, since the canal represents a homogeneous plasma (uniformity of brightness, constancy of longitudinal field intensity).

The law of the change of the field intensity with pressure for discharges in air and nitrogen differs from that for argon (see curves *1* and *2*, Fig. 10).

As was shown by the measurements (carried out by Khokhlov[4]) of the temperature of the gas T in the canal of a two electrode discharge, the dependence of the temperature on pressure has the same form as the dependence of the field intensity on pressure. For pressures of 100-200 mm Hg, E as well as T increases rapidly with pressure; for much higher pressures the increase of E occurs much more slowly (T also hardly changes with further increase in pressure). It follows from this that the rapid increase of E in the canal of the discharge which is open to air is connected with the intensive dissociation of H_2O, with the remaining particles of air, and with the formation of NO which absorbs part of the energy communicated to the electric field by the electron.

The curve $E = E(p)$ for nitrogen is much more sloping. This can explain the fact that in the canal of a nitrogen discharge, a number of processes are missing which take place in air and which prevent the electron from gathering sufficient energy for ionization. Both in air and in nitrogen, part of the energy supplied to the discharge is consumed in the excitation of vibrational and rotational levels of the molecules. These processes do not take place in argon; as a consequence, the field intensity necessary for maintaining the discharge in this gas is less than for nitrogen and air.

---

[4] M. Z. Khokhlov, Dissertation, Moscow State Univ., 1954.

Processes connected with losses of energy in the discharge require and increase in the field intensity for their compensation. This explains the deviation of the dependence of $E = E(p)$ for discharges in air and nitrogen from the path of this dependence for discharge in argon. In the latter, condition (1) is satisfied, and an increase in the field intensity is dependent only on the necessity of compensating the decrease in the free path length of the electron.

The high (of the order of hundredsof volts/cm) value of the field intensity is dependent on the fact that, because of the limited supply of energy of electromagnetic vibrations in the oscillatory circuit, the discharge in its regime corresponds to a glow discharge of high pressure with comparatively small current density (hundreds of milliamperes).

CONCLUSIONS

1. It is established that the field intensity in the canal of a high-frequency discharge increases upon increase in pressure from 100 mm Hg to atmospheric in the range 75-220 eff. V/cm (air), 90-200 eff. volts/cm (nitrogen), which corresponds to a regime of glow discharge of high pressure.

2. For pressures above 300 mm Hg there takes place a filamenting of the canal of the discharge in argon. Here the current density increases severalfold, both for increase in the length of the discharge (pressure fixed) or for increase in the pressure (fixed length of discharge). In the pressure range 300-500 mm Hg, both filamented and unfilamented discharges could take place.

3. The field intensity in the canal of the discharge in argon for pressures from 100 to 500 mm Hg amounts to 25-60 eff. volts/cm. In the pressure range 400-760 mm Hg (filamented discharge) the field intensity has the value 20-30 eff. volts/cm.

4. Increase in the field intensity with pressure is determined by the necessity of compensating, first the decrease in the free path length of the electron, second, the losses of energy at the express of the processes of dissociation and chemical reactions, and also the excitation of vibrational and rotational levels of molecules and the loss of free electrons at the expense of the formation of negative ions.

In conclusion, we consider it our duty to express our gratitude to Prof. N. A. Kaptsov for his valuable advice during the work and for his criticisms of the present research.

Translated by R. T. Beyer
250

SOVIET PHYSICS JETP VOLUME 2, NUMBER 3 MAY, 1956

Asymptotic Behavior of Electromagnetic Vacuum-Polarization in the Presence of Meson Interactions

V. B. BERESTETSKII

(Submitted to JETP editor June 23, 1954)
J. Exper. Theoret. Phys. USSR 29, 585-598 (November, 1955)

It is proved that when $e^2 \ll g^2 \ll 1$ the asymptotic form of the photon propagation function is the same as in the case $g^2 = 0$.

1. INTRODUCTION

1. LANDAU, Abrikosov and Khalatnikov[1] found the asymptotic form of the photon propagation function (Green's function) $D^{F'}_{\alpha\beta}$. If this function is written in the transverse gauge

$$\frac{i}{2} D^{F'}_{\alpha\beta}(k) \equiv D_{\alpha\beta}(k) = \frac{1}{k^2}\left(\delta_{\alpha\beta} - \frac{k_\alpha k_\beta}{k^2}\right)\tilde{d}_t,$$

then as proved in reference 1,

$$\tilde{d}_t^{-1} = 1 - {}^4/_3\, \varepsilon y, \qquad (1)$$

with

$$y = \ln\frac{k^2}{m^2}; \quad \varepsilon = \frac{e^2}{(4\pi)^2} = \frac{1}{4\pi}\frac{1}{137}$$

Equation (1) takes into account only the interaction between a photon and the electron-positron vacuum. Landau[1] already observed that it must be supplemented with terms corresponding to other types of charged particle. In addition it is necessary to take account of the nonelectrodynamic interactions of these particles. Since we have at present no way to handle strong interactions, it is not, strictly speaking, possible to evaluate the effects of mesons and nucleons. It seems nevertheless interesting to consider these effects, assuming that the meson-nucleon coupling constant g is large compared with the electric charge but still small compared with 1,

$$e^2 \ll g^2 \ll 1.$$

Then we may use the method of reference 1 to derive asymptotic expressions.

We shall show that, in spite of the stronger nonelectromagnetic interaction, the particles give the same contribution to the photon propagation function as if the interaction were absent, i.e., the asymptotic form of $D_{\alpha\beta}$ is independent of g. With the assumptions we have made, the nonelectromagnetic interaction does not produce a "form-factor" which changes the interaction of the particles with the Maxwell field.

2. When $e^2 \ll g^2$, we may expect that the nucleon propagation function $S^{F'} = (2/i)G$, the meson function $\Delta^{F'} = (2/i)\Delta$, and the vertex function Γ_5 of the pseudoscalar meson-nucleon interaction, may be determined without considering electromagnetic interactions. The asymptotic expressions for these functions were found by Abrikosov, Galanin and Khalatnikov[2], and by Galanin, Ioffe and Pomeranchuk[3]. They are as follows*

$$\begin{gathered} G(p) = \frac{i\hat{p}}{p^2}\, b(x); \\ \Delta(p) = \frac{1}{p^2}\, c(x), \\ \Gamma_5(p;\, 0) = \Gamma_5(0;\, p) = \Gamma_5(p;\, p) = \gamma_5\, a(x), \end{gathered} \qquad (2)$$

with $x = \ln(p^2/m^2)$. Explicit expressions for $a(x)$, $b(x)$ and $c(x)$ are given in references 2 and 3, but are not needed here.

The calculations can be done in two different ways. One may operate with unrenormalized functions d_t, a, b, c etc. and then renormalize the final expressions[1,2]. Or one may renormalize the starting equations[3] and then operate only with renormalized functions (we denote these by $\tilde{d}_t$, $\tilde{b}$ etc). It is easy to show that the two methods are equivalent, since the transition from unrenormalized to renormalized functions can be made at any stage of the calculation.

We shall use the first method since it is more convenient. In the divergent integrals we cut off the range of the logarithmic variable x with an upper limit L which will disappear from the results after renormalization. The renormalized quantities are defined by the requirement that for $x = 0$ they become equal to the corresponding free-particle propagation functions, i.e., the normalized functions $\tilde{b}(x)$, $\tilde{d}_t(x)$ etc. are equal to unity at $x = 0$. Thus

---

[1] L. D. Landau, A. A. Abrikosov and I. M. Khalatnikov, Dokl. Akad. Nauk SSSR 95, 497, 1177 (1954)

* We use the following notations: $p^2 = \mathbf{p}^2 - p_0^2$; $\hat{p} = \sum_{\alpha=1}^{4} \gamma_\alpha p_\alpha$; $\gamma_j = -i\beta\alpha_j$ for $j = 1, 2, 3$; $\gamma_4 = \beta$, $\gamma_5 = \gamma_1\gamma_2\gamma_3\gamma_4\, (\gamma_5^2 = 1)$; $\Gamma_5(p;\, k) \equiv \Gamma_5(p,\, p-k;\, k)$ with p the nucleon and k the meson momentum. We use Heaviside units for e and g and set $\hbar = c = 1$.

[2] A. A. Abrikosov, A. D. Galanin and I. M. Khalatnikov, Dokl. Akad. Nauk SSSR 97, 793 (1954).

[3] A. D. Galanin, B. L. Ioffe and I. Ia. Pomeranchuk, J. Exper. Theoret. Phys. USSR 29, 51 (1955); Soviet Phys. 2, 37 (1956).

$$\tilde{d}_t(x) = \frac{d_t(x)}{d_t(0)}; \tag{3}$$

$$\tilde{a}(x) = \frac{a(x)}{a(0)};\ \tilde{b}(x) = \frac{b(x)}{b(0)};\tilde{c}(x) = \frac{c(x)}{c(0)} \tag{3a}$$

The renormalization of electric charge and of the meson-nucleon coupling constant are defined as follows:

$$e_1^2 d_t(0) = e^2; \tag{4}$$

$$g_1^2 a^2(0)\, b^2(0)\, c(0) = g^2, \tag{4a}$$

where e_1 and g_1 are the unrenormalized, e and g the renormalized constants$^+$.

2. INTERACTION WITH NEUTRAL MESONS

1. We consider protons interacting with the Maxwell field A_α and with a neutral meson field φ. In the Lagrangian of the system the interactions are represented by the following terms (the meson interaction being pseudoscalar)

$$U_1 = ig_1 \bar{\psi} \gamma_5 \psi \varphi, \qquad U_2 = ie_1 \bar{\psi} \gamma_\alpha \psi A_\alpha.$$

The electromagnetic polarization of the proton vacuum is represented by the graph shown in Fig. 1. The wiggly lines denote the propagation of photons, the continuous lines denote protons. The propagation of the protons here includes the meson-proton interaction. The ordinary vertex denotes a matrix γ_α; the "blob" vertex denotes a function Γ_β, the vertex function describing the interaction of a proton with the Maxwell field in the presence of the meson interaction. The vacuum-polarization tensor $P_{\alpha\beta}$ corresponding to Fig. 1 has the following form**

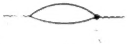

FIG. 1

$$P_{\alpha\beta}(k) = \frac{ie_1^2}{(2\pi)^4} \int \mathrm{Sp}\, \gamma_\alpha G(p) \Gamma_\beta(p;\ k) G(p-k)\, d^4k. \tag{5}$$

The function $G(p)$ has the form (2), while Γ_β is determined by the integral equation

$$\Gamma_\beta(p;\ k) = \gamma_\beta + \frac{ig_1^2}{(2\pi)^4} \int \Gamma_5(p;\ p-q) \times G(q) \Gamma_\beta(q;\ k) G(q-k) \times \Gamma_5(q-k;\ q-p) \Delta(p-q)\, d^4q. \tag{6}$$

Eq. (6) is represented graphically in Fig. 2. The dotted line denotes a meson$^+$, and the vertices with dotted lines incident denote the vertex function Γ_5. Eq. (6) is valid for $g^2 x < 1$. We assume also $e^2 x \ll 1$, i.e., perturbation theory is valid for the electromagnetic interaction.

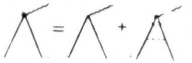

FIG. 2

Since the integral in Eq. (5) diverges for large p, we separate the integrand into terms of various orders in (k/p). Then $G(p-k)$ and $\Gamma_\beta(p,k)$ take the form

$$G(p-k) = G(p) + G^{(1)}(p,\ k) + G^{(2)}(p,\ k),$$
$$\Gamma_\beta(p;\ k) = \Gamma_\beta^{(0)}(p) + \Gamma_\beta^{(1)}(p;\ k) + \Gamma_\beta^{(2)}(p,\ k). \tag{7}$$

According to Eq. (2)

$$\begin{aligned} G(p) &= ib(x)(\hat{p}/p^2), \\ G^{(1)}(p,\ k) &= ib(x)(\hat{p}\hat{k}\hat{p}/p^4), \\ G^{(2)}(p,\ k) &= ib(x)(\hat{p}\hat{k}p\hat{k}\hat{p}/p^6). \end{aligned} \tag{8}$$

We may write for $\Gamma_\beta^{(0)}$

$$\Gamma_\beta^{(0)} = \gamma_\beta \xi(x), \tag{9}$$

+Eq. (3), (3a), (4), (4a) coincide with the usual renormalization conditions of Dyson[4]. Because of the introduction of the cutoff L, the renormalization constants Z_1, Z_2, Z_3 here become functions of L. In electrodynamics $Z_3(L) = d_t(0)$; $Z_1 = Z_2 = 1$. In meson theory $Z_3(L) = c(0)$; $Z_2(L) = b(0)$; $Z_1^{-1}(L) = a(0)$.

[4] F. J. Dyson, Phys. Rev. 75, 1736 (1949).

** $P_{\alpha\beta}$ is defined in such a way that the Dyson-Schwinger equation for the photon Green's function $D_{\alpha\beta}$ takes the form $(-\Box + P)D = 1$.

+Equation (6) is obtained from Fig. 2 by first writing down the scattering matrix by the ordinary rules of perturbation theory, going as far as third-order terms, and then substituting Γ_5 for γ_5, $(2/i)G$ for S^F, and $(2/i)\Delta$ for Δ^F.

while $\Gamma^{(1)}_\beta$ and $\Gamma^{(2)}_\beta$ consist of slowly varying functions of $x = \ln(p^2/m^2)$ and $y = \ln(k^2/m^2)$, multiplied by (k/p) and by $(k/p)^2$ respectively. The structure of these functions will be discussed in detail later. Substituting Eq. (7) into (5) we obtain

$$P_{\alpha\beta}(k) = \frac{ie_1^2}{(2\pi)^4}\int \gamma_\alpha G(p)\,[\Gamma^{(0)}_\beta(p)\,G(p) + \Gamma^{(0)}_\beta(p)\,G^{(1)}(p,\, k) + \Gamma^{(1)}_\beta(p,\, k)\,G(p) + \Gamma^{(1)}_\beta(p,\, k)\,G^{(1)}(p,\, k) + \Gamma^{(0)}_\beta(p)\,G^{(2)}(p,\, k) + \Gamma^{(2)}_\beta(p,\, k)\,G(p) + \ldots]\, d^4p.$$

Here the first (quadratically divergent) term is independent of k and must be removed by the usual appeal to gauge-invariance. The next two terms contain odd powers of the vector p_α and therefore vanish after integration$^+$. The remaining terms are logarithmically divergent. The higher terms in the expansion in powers of (k/p), which are here omitted, would give convergent integrals and therefore are negligible in the asymptotic region.

2. We observe that $\Gamma^{(0)}_\sigma(p) = \Gamma_\sigma(p;\,0)$ can be immediately fixed by Ward's identity[5], which states that

$$\Gamma_\sigma(p;\ 0) = i\,\frac{\partial G^{-1}(p)}{\partial p_\sigma}.$$

With Eq. (2) this gives

$$\Gamma^{(0)}_\sigma(p) = \frac{1}{b(x)}\,\gamma_\sigma$$

or by comparison with Eq. (9)

$$\xi(x) = 1/b(x). \tag{10}$$

However, we shall also derive equations which determine ξ directly from Eq. (6), since this is necessary for the later work.

We substitue Eqs. (7), (8), (9) into (6). This gives three equations, of degrees zero, one and two in k. The zero-order equation is

$$\gamma_\sigma\xi(x) = \gamma_\sigma + \frac{ig_1^2}{(2\pi)^4}\int \Gamma_5(p;\ p-q)\,b(z)\,\frac{i\hat{q}}{q^2} \times \xi(z)\,\gamma_\sigma\,b(z)\,\frac{i\hat{q}}{q^2}\,\Gamma_5(q-k;\ q-p) \times \Delta(p-q)\,d^4q \qquad \left(z = \ln\frac{q^2}{m^2}\right)$$

The last integral diverges logarithmically at large q, hence we may neglect k^2 and p^2 in it in comparison with q^2, and set the lower limit of integration at $q^2 = p^2 (k^2 \ll p^2)$. Then using Eq. (2) we obtain

$$\xi(x)\,\gamma_\sigma = \gamma_\sigma + \frac{iq_1^2}{(2\pi)^4} \times \int_{q^2>p^2} a^2(z)\,b^2(z)\,c(z)\,\xi(z)\,\gamma_5\,\frac{i\hat{q}}{q^2}\,\gamma_\sigma\,\frac{i\hat{q}}{q^2}\,\gamma_5\,\frac{d^4q}{q^2}. \tag{11}$$

The integrand of Eq. (11) may be simplified. Since γ_5 anticommutes with $\hat{q}$ and γ_σ,

$$\gamma_5\, i\hat{q}\gamma_\sigma i\hat{q}\gamma_5 = \hat{q}\gamma_\sigma\hat{q}.$$

By rotating the q_4 axis through an angle $\pi/2$ in the complex plane (see reference 1), we bring the integral into a euclidean space in which the averaging over angles is simple and gives

$$\overline{q_\alpha q_\beta} = {}^1/_4\, q^2\delta_{\alpha\beta},$$

i.e.

$$\overline{\hat{q}\gamma_\sigma\hat{q}} = {}^1/_4\, q^2\gamma_\alpha\gamma_\sigma\gamma_\alpha = -{}^1/_2\, q^2\gamma_\sigma.$$

Then we write for the volume-element

$$d^4q = i\pi^2 q^4\,dz \qquad \left(z = \ln\frac{q^2}{m^2}\right), \tag{12}$$

and Eq. (9) takes the form

$$\xi(x) = 1 + \frac{\lambda_1}{2}\int_x^L a^2(z)\,b^2(z)\,c(z)\,\xi(z)\,dz, \tag{13}$$

with

$$\lambda_1 = g_1^2/(4\pi)^2.$$

3. The equation of first degree in k obtained from (6) is the following

---

$^+$ These terms depend linearly on k_α, and it is clear that the tensor $P_{\alpha\beta}$ cannot be a linear function of k_α.

[5] J. C. Ward, Phys. Rev. **78**, 182 (1950); A. Salam, Phys. Rev. **79**, 910 (1950); N. M. Kroll and M. A. Ruderman, Phys. Rev. **93**, 233 (1954).

$$\Gamma_\sigma^{(1)}(p,\ k) = \frac{ig_1^2}{(2\pi)^4}\int \Gamma_5(p;\ p-q)\, b(z)\, \frac{i\hat{q}}{q^2}\Big[\xi(z)\,\gamma_\sigma\, b(z)\,\frac{i\hat{q}\,\hat{k}\,\hat{q}}{q^4}$$
$$+\,\Gamma_\sigma^{(1)}(q,\ k)\, b(z)\,\frac{i\hat{q}}{q^2}\Big]\Gamma_5(q-k;\ q-p)\,\Delta(p-q)\, d^4q.$$

This integral converges for $q^2 \gg p^2$. The important range of integration is $k^2 < q^2 < p^2$ (the situation is exactly the same as in reference 1 when $k^2 \ll p^2$). Hence in the integrand we may neglect k and q compared with p. Then using Eq. (2) we find

$$\Gamma_\sigma^{(1)}(p,\ k) - \frac{ig_1^2}{(2\pi)^4}\,\frac{a^2(x)\,c(x)}{p^2}\int\limits_{k^2<q^2<p^2} b^2(z)\,\gamma_5\,\frac{i\hat{q}}{q^2}\,\Gamma_\sigma^{(1)}(q,\ k)\,\frac{i\hat{q}}{q^2}\,\gamma_5\, d^4q$$
$$= \frac{ig_1^2}{(2\pi)^4}\,\frac{a^2(x)\,c(x)}{p^2}\int\limits_{k^2<q^2<p^2} b^2(z)\,\xi(z)\,\gamma_5\,\frac{i\hat{q}}{q^2}\,\gamma_\sigma\,\frac{i\hat{q}\,\hat{k}\,\check{q}}{q^4}\,\gamma_5\, d^4q.$$

The inhomogeneous term on the right of this linear integral equation contains an odd power of q in the integrand and therefore vanishes. So the equation is homogeneous and implies[++]

$$\Gamma_\sigma^{(1)}(p,\ k) = 0. \tag{14}$$

4. The equation of second degree in k obtained from Eq. (6) takes the following form after using Eqs. (14), (8) and (9):

$$\Gamma_\sigma^{(2)}(p,\ k) = \frac{ig_1^2}{(2\pi)^4}\int \Gamma_5(p;\ p-q)\, b(z)\,\frac{i\hat{q}}{q^2}\Big[\xi(z)\,\gamma_\sigma b(z)\,\frac{i\hat{q}\,\hat{k}\,\hat{q}\,\hat{k}\,\hat{q}}{q^6}$$
$$+\,\Gamma_\sigma^{(2)}(q,\ k)\, b(z)\,\frac{i\hat{q}}{q^2}\Big]\Gamma_5(q-k;\ q-p)\,\Delta(p-q)\, d^4q.$$

In this integral the important range is again $k^2 < q^2 < p^2$ Hence using (2) we obtain

$$\Gamma_\sigma^{(2)}(p,\ k) - \frac{ig_1^2}{(2\pi)^4}\,\frac{a^2(x)\,c(x)}{p^2}\int\limits_{k^2<q^2<p^2} b^2(z)\,\gamma_5\,\frac{i\hat{q}}{q^2}\,\Gamma_\sigma^{(2)}(q,\ k)\,\frac{i\hat{q}}{q^2}\,\gamma_5\, d^4q$$
$$= \frac{ig_1^2}{(2\pi)^4}\,\frac{a^2(x)\,c(x)}{p^2}\int\limits_{k^2<q^2<p^2} b^2(z)\,\xi(z)\,\gamma_5\,\frac{i\hat{q}}{q^2}\,\gamma_\sigma\,\frac{i\hat{q}\,\hat{k}\,\hat{q}\,\hat{k}\,\hat{q}}{q^6}\,\gamma_5\, d^4q. \tag{15}$$

We evaluate the right side Eq. (15). First we remove the matrix γ_5 as before

$$\gamma_5 i\hat{q}\gamma_\sigma i\hat{q}\,\hat{k}\hat{q}\hat{k}\,\hat{q}\,\gamma_5 = \hat{q}\gamma_\sigma\hat{q}\,\hat{k}\hat{q}\hat{k}\,\hat{q}.$$

Next an averaging over angles gives*

$$\overline{q_\alpha q_\beta q_\gamma q_\delta} \doteq Bq^4\,(\delta_{\alpha\beta}\delta_{\gamma\delta} + \delta_{\alpha\gamma}\delta_{\beta\delta} + \delta_{\alpha\delta}\delta_{\beta\gamma}), \tag{16}$$
$$B = {}^1/_{24}$$

and therefore

$$\overline{\hat{q}\gamma_\sigma\,\hat{q}\,\hat{k}\,\hat{q}\,\hat{k}\,\hat{q}} = {}^1/_3\, q^4\,(k^2\gamma_\sigma - \hat{k}k_\sigma).$$

Substituting this into Eq. (15), we reduce the right side to the form

$$-\frac{\lambda_1}{3}\,\frac{k^2\gamma_\sigma - \hat{k}\,k_\sigma}{p^2}\,a^2(x)\,c(x)\int_y^x b^2(z)\,\xi(z)\,dz. \tag{17}$$

From Eq. (17) it is clear that we should look for a solution $\Gamma_\sigma^{(2)}(p,k)$ of the form

$$\Gamma_\sigma^{(2)}(p,\ k) = \frac{1}{3}\,\frac{k^2\gamma_\sigma - \hat{k}\,k_\sigma}{p^2}\, s(x,\ y) \tag{18}$$
$$\left(x = \ln\frac{p^2}{m^2};\quad y = \ln\frac{k^2}{m^2}\right)$$

Substituting Eq. (18) into (15) and using the same arguments which we applied in the derivation of Eq. (17), we find

---

[++] In the equation for $\Gamma_\sigma^{(1)}$ there are terms of order k/p^2 but none of order k/p, and the higher terms in the development of Γ_5 and Δ also give extra powers of $(1/p)$. From this it is obvious that the first-order term is absent in the expansion of Γ_σ in powers of (k/p).

* The form of Eq. (16) follows from considerations of symmetry. The value of B is easily obtained as follows. Since $\overline{q_1^4} = q^4 3B$; $\overline{q_1^2 q_2^2} = \overline{q_1^2 q_3^2} = \overline{q_1^2 q_4^2} = Bq^4$, we have $\overline{q_1^2 q^2} = 6Bq^4$. But $\overline{q_1^2} = \frac{1}{4}q^2$, hence $B = 1/24$.

$$s(x,\ y) = -\frac{\lambda_1}{2}a^2(x)\,c\,(x)\int\limits_y^x b^2(z)\,[\xi(z) - s(z,\ y)]\,dz. \tag{19}$$

5. We substitute Eqs. (7), (8), (9), (14) and (18) into the expression (6) for the polarization tensor, carry out the angular integrations, and introduce logarithmic variables. The result is

$$P_{\alpha\beta}(k) = {}^4/_3\,\varepsilon_1\,(k^2\delta_{\alpha\beta} - k_\alpha k_\beta)\int\limits_y^L b^2(x)\,[\xi(x) - s(x,\ y)]\,dx,$$

with

$$\varepsilon_1 = e_1^2/(4\pi)^2$$

or alternatively[+]

$$d_t^{-1}(y) = 1 + {}^4/_3\,\varepsilon_1\int\limits_y^L b^2(x)\,[\xi(x) - s(x,\ y)]\,dx. \tag{20}$$

Comparing Eqs. (20) and (19), we see that the function $d_t^{-1}(y)$ is simply related to $s(x,y)$. If we write

$$s(x,\ y) = -\frac{\lambda_1}{2}a^2(x)\,c(x)\,q(x,\ y), \tag{21}$$

then

$$d_t^{-1}(y) = 1 + {}^4/_3\,\varepsilon_1\,q(L,\ y). \tag{22}$$

By Eqs. (21) and (19), the function $q(x,\ y)$ satisfies the equation

$$q(x,\ y) = \int\limits_y^x b^2(z)\left[\xi(z) + \frac{\lambda_1}{2}a^2(z)\,c(z)\,q(z,\ y)\right]dz. \tag{23}$$

The integral equation (23) can be transformed into a differential equation by differentiating it with respect to x. This gives

$$\frac{\partial q(x,\ y)}{\partial x} = b^2(x)\left[\xi(x) + \frac{\lambda_1}{2}a^2(x)\,c(x)\,q(x,\ y)\right], \tag{24}$$

with the initial condition

$$q(x,\ x) = 0. \tag{24a}$$

We combine Eq. (24) with the differential equation for $\xi(x)$ obtained by differentiating Eq. (13),

$$\frac{d\xi(x)}{dx} = -\frac{\lambda_1}{2}a^2(x)\,b^2(x)\,c(x)\,\xi(x), \tag{25}$$

with the boundary condition

$$\xi(L) = 1. \tag{25a}$$

We multiply Eq. (24) by $\xi(x)$, Eq. (25) by $q(x,\ y)$, and add. The result is

$$\frac{\partial}{\partial x}[\xi(x)\,q(x,\ y)] = b^2(x)\,\xi^2(x)$$

and hence by Ward's identity (10)

$$\frac{\partial}{\partial x}[\xi(x)\,q(x,\ y)] = 1. \tag{26}$$

The constant λ_1 does not occur in this equation. Using the boundary condition (24a), we obtain from Eq. (26)

$$\xi(x)\,q(x,y) = x - y. \tag{27}$$

The boundary condition (25a) now gives

$$q(L,y) = L - y$$

and hence by Eq. (22)

$$d_t^{-1} = 1 + {}^4/_2\,\varepsilon_1(L - y). \tag{28}$$

After renormalizing by the rules described in references 3 and 4, Eq. (28) is transformed into Eq. (1), and this completes the proof of the assertion made at the beginning of this paper.

6. The results which have been obtained can be extended to the case of interaction with a scalar neutral field. In this case the interaction operator takes the form $U_1 = g_1\bar{\psi}\psi\,\varphi$, i.e. it differs from the pseudoscalar interaction by changing $i\gamma_5$ into 1. But we have seen that the matrices γ_5 appeared in our equations in pairs, separated by an odd number of matrices γ_α. Therefore

$$i\gamma_5(\ldots)\,i\gamma_5 = 1\,(\ldots),$$

i.e., the equations for both cases are identical.

The same is true for the asymptotic forms of the

[+] We observe that if at this point we carry out the renormalization according to Eqs. (3), (3a), (4), (4a), then Eq. (20) and (10) give

$$\tilde{d}_t^{-1}(y) = 1 + {}^4/_3\,\varepsilon Z_1'\left\{\int\limits_y^L b^2(x)[\tilde{\xi}(x) - \tilde{s}(x,\ y)]\,dx - \int\limits_0^L \tilde{b}^2(x)\,[\xi(x) - \tilde{s}(x,0)]\,dx\right\},$$

with

$$b(x) = b(0)\,\tilde{b}(x);\ \ \xi(x) = \xi(0)\,\tilde{\xi}(x);\ \ s(x,\ y) = \xi(0)\,\tilde{s}(x,\ y);$$

$$Z_1' = \frac{1}{\xi(0)} = \tilde{\xi}(L) = Z_2 = b(0)$$

Compare the analogous expressions in reference 3.

functions $a(x)$, $b(x)$ and $c(x)$ obtained in references 2 and 3. They also remain unchanged for a scalar field. In general, the difference between scalar and pseudoscalar fields cannot appear in effects for which the nucleon mass is negligible. This follows from the fact that there exists only one type of Dirac particle with $m = 0$, whereas with finite m there are two types of particles with different parity properties.

3. INTERACTION WITH A SYMMETRIC MESON FIELD

1. In the case of a symmetric meson field, the interaction operators are U_1 between nucleon and meson, U_2 between nucleon and photon, and U_3 between meson and photon, as follows:

$$\begin{aligned} U_1 &= ig_1\bar{\psi}\gamma_5\tau_j\psi\varphi_j, \\ U_2 &= ie_1\bar{\psi}\gamma_\sigma\frac{1-\tau_3}{2}\psi A_\sigma, \\ U_3 &= ie_1\varphi_j T_{3,jk}\frac{\partial}{\partial x_\alpha}\varphi_k A_\alpha. \end{aligned} \tag{29}$$

Here τ_j is the isotopic spin operator for the nucleon (a Pauli matrix), φ_j is the meson field (a vector in 3-dimensional isotopic space), and T_i is the isotopic spin operator for the meson,

$$T_{i,jk} = -ie_{ijk}$$

where e_{ijk} is the unit antisymmetric tensor.

As before we assume $e_1^2 \ll g_1^2$ and suppose that the nucleon and meson propagation functions and the meson-nucleon vertex function depend only on the interaction U_1. They have the same form (2) as in the case of the neutral field, but with different functions $a(x)$, $b(x)$ and $c(x)$ (see references 2 and 3). We keep the same notations for these functions, since we do not use their explicit forms. But the vertex functions of the nucleon-photon and meson-photon interactions must be investigated afresh. Denoting them by Γ_σ and V_σ respectively, we may write the vacuum-polarization tensor in the following general form

$$\begin{aligned} &P_{\alpha\beta}(k) \\ &= \frac{ie_1^2}{(2\pi)^4}\int \mathrm{Sp}\,\gamma_\alpha\frac{1-\tau_3}{2}G(p)\Gamma_\beta(p;k)G(p-k)\,d^4p \\ &- \frac{ie_1^2}{(2\pi)^4}\int \mathrm{Sp}\,i(2p_\alpha-k_\alpha)T_3\Delta(p)V_\beta\Delta(p-k)\,d^4p. \end{aligned} \tag{30}$$

The first term in Eq. (30) comes from nucleons (Fig. 1), the second from mesons (Fig. 3).

FIG. 3

The minus sign in the second term is connected with the Bose statistics of the mesons. The operations Sp act both on the Dirac matrices (in the first term) and on the isotopic spin matrices (in both terms). The factor $i(2p_\alpha - k_\alpha)$ is the Fourier transform of the operator $(\partial/\partial x_\alpha)$.

The vertex parts Γ_σ and V_σ satisfy integral equations which are represented graphically* in Figs. 4 and 5. As before, the wiggly lines denote photons,

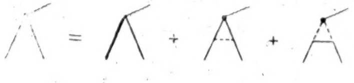

FIG. 4

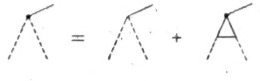

FIG. 5

the dotted lines mesons, and the continuous lines nucleons. The "blob" vertices denote functions Γ_σ or V_σ, the vertices without a photon line denote $\Gamma_5\tau_\alpha$, and the ordinary vertices with a photon line denote $-\frac{1-\tau_3}{2}\gamma_\sigma$ or $i(2p_\sigma - k_\sigma)T_3$.

The graphs of Fig. 4 produce the equation

$$\begin{aligned} \Gamma_\sigma(p;k) = \gamma_\sigma &+ \frac{ig_1^2}{(2\pi)^4}\int \tau_j\Gamma_5(p;p-q) \\ &\times G(q)\Gamma_\sigma(q;k)G(q-k) \\ &\times \Gamma_5(q-k;\, q-p)\tau_j\Delta(p-q)\,d^4q \\ &+ \frac{ig_1^2}{(2\pi)^4}\int \Gamma_5(p;l)G(p-l)\Gamma_5 \\ &\times (p-l;\, k-l)\Delta(l)\tau_j V_{\sigma,jk}\tau_k\Delta(l-k)\,d^4l, \end{aligned} \tag{31}$$

---

* In Figs. 4 and 5 we retain those graphs which in perturbation theory (i.e. when the equations are solved by iteration) give terms with asymptotic behavior $(g_1^2)^n L^n$, and we drop (considering g_1^2 to be small) those graphs which lead to asymptotic behavior $(g_1^2)^n L^m$ with $n > m$. But the graph of Fig. 5 actually belongs to the latter class. Graphs containing squares of nucleon lines (which are unrenormalizable by the usual methods) do not need to be considered in this problem.

and those of Fig. 5 produce the equation

$$V_{\sigma,jk}(q;k) = i(2q_\sigma - k_\sigma)T_{3,jk} + \frac{ig_1^2}{(2\pi)^4}\int \mathrm{Sp}\, G(f)\Gamma_\sigma(f;k)G(f-k) \times [\Gamma_5(f-k;q-k)G(f-k)\Gamma_5(f-q)\tau_j\tau_k - \Gamma_5(f-k;-q)G \times (f-k+q)\Gamma_5(f-k+q;q)\tau_k\tau_j]\, d^4f. \tag{32}$$

In Eq. (32) the two terms of the integrand correspond to the two directions in which the triangular loop in Fig. 5 can be described. In the case of neutral mesons, the expression corresponding to this closed loop vanishes because of the conservation of charge-parity (Furry's theorem), since a neutral spin-zero meson has even charge-parity. Hence it is clear that the isotopic spin dependence of the vertex-function V_σ must be given by

$$V_\sigma = T_3 Z_\sigma, \tag{33}$$

where Z_σ does not involve isotopic spin matrices. The vertex function V_σ will be written in the form

$$\Gamma_\sigma = {}^1\!/_2(X_\sigma - \tau_3 Y_\sigma), \tag{34}$$

where X_σ and Y_σ contain no isotopic spin matrices.

Substituting Eqs. (33) and (34) into (31) and (32) and using the relations

$$\tau_j\tau_j = 3;\ \tau_j\tau_3\tau_j = -\tau_3;$$
$$\tau_j T_3 \tau_j = 2\tau_3;$$
$$\mathrm{Sp}\,\tau_j\tau_k = 2\delta_{jk};\ \mathrm{Sp}\,T_3\tau_j\tau_k = -2T_{3,jk},$$

we eliminate the isotopic spin variables and obtain equations for X_σ, Y_σ and Z_σ:

$$X_\sigma(p,k) = \gamma_\sigma + \frac{3ig_1^2}{(2\pi)^4}\int \Gamma_5(p;p-q)G(q)X_\sigma(p,k) \times G(q-k)\Gamma_5(q-k;\ q-p)\Delta(p-q)\,d^4q; \tag{35}$$

$$Y_\sigma(p,k) = \gamma_\sigma - \frac{ig_1^2}{(2\pi)^4}\int \Gamma_5(p;p-q)G(q)Y_\sigma(q,k)G(q-k) \times \Gamma_5(q-k;\ q-p)\Delta(p-q)\,d^4q + 4i\frac{g_1^2}{(2\pi)^4}\int \Gamma_5(p;l)G(p-l)\Gamma_5(p-l;k-l) \times \Delta(l)Z_\sigma(l,k)\Delta(l-k)\,d^4l; \tag{36}$$

$$Z_\sigma(q,k) = i(2q_\sigma - k_\sigma) - \frac{ig_1^2}{(2\pi)^4}\int \mathrm{Sp}\, G(f)Y_\sigma(f,k)G(f-k) \times [\Gamma_5(f-k;q-k)G(f-k) \times \Gamma_5(f-q;-q) - \Gamma_5(f-k;-q) \times G(f-k+q)\Gamma_5(f-k+q;q)]\,d^4f. \tag{37}$$

This system separates into Eq. (35) determining X_σ, and the simultaneous Eqs. (36) and (37) determining Y_σ and Z_σ.

2. Eq. (35) differs from Eq. (6) only by a numerical coefficient, and can be solved by precisely the same method. Expanding X_σ by powers of k

$$X_\sigma(p,k) = X_\sigma^{(0)}(p) + X_\sigma^{(1)}(p,k) + X_\sigma^{(2)}(p,k),$$

we obtain

$$X_\sigma^{(0)} = \xi(x)\gamma_\sigma;\ \xi(x) = \frac{1}{b(x)}\left(x = \ln\frac{p^2}{m^2}\right), \quad X_\sigma^{(1)} = 0, \tag{38}$$

$$X_\sigma^{(2)} = \frac{k^2\gamma_\sigma - \hat{k}k_\sigma}{p^2}s(x,y) = -\lambda a^2(x)c(x)q(x,y),$$

where $\xi(x)$ and $q(x,y)$ satisfy

$$\xi(x) = {}^3\!/_2\lambda_1\int_x^L a^2(z)b^2(z)c(z)\xi(z)\,dz + 1,$$
$$q(x,y) = \int_y^x b^2(z)[\xi(z) + {}^3\!/_2\lambda_1 a^2(z)c(z)q(z,y)]\,dz. \tag{39}$$

Transforming Eq. (37) into a differential equation, and using Ward's identity, we obtain the analog of Eq. (26)

$$\frac{\partial}{\partial x}[\xi(x)q(x,y)] = 1,$$
$$\xi(x)q(x,y) = x - y. \tag{40}$$

3. We determine Y_σ and Z_σ in a similar way by first expanding them in powers of k,

$$Y_\sigma = Y_\sigma^{(0)} + Y_\sigma^{(1)} + Y_\sigma^{(2)},$$
$$Z_\sigma = Z_\sigma^{(0)} + Z_\sigma^{(1)} + Z_\sigma^{(2)}, \tag{41}$$

By virtue of Ward's identity and Eq. (2), $Y_\sigma^{(0)}$ and $Z_\sigma^{(0)}$ are given by

$$Y_\sigma^{(0)} = i\frac{\partial G^{-1}(p)}{\partial p_\sigma} = \eta(x)\gamma_\sigma; \tag{42}$$

$$\eta(x) = \xi(x) = 1 / b(x); \tag{42a}$$

$$Z_\sigma^{(1)} = i \frac{\partial \Delta^{-1}(p)}{\partial p_\sigma} = 2 i p_\sigma \zeta(x); \tag{43}$$

$$\zeta(x) = 1 / c(x). \tag{43a}$$

The structure of the quantities $Y_\sigma^{(1)}$, $Y_\sigma^{(2)}$, $Z_\sigma^{(1)}$ $Z_\sigma^{(2)}$ can be determined (as in Section 2) by an explicit calculation of the inhomogeneous terms in the equations which are obtained by substituting Eq. (41) into (36) and (37). When this is done, the factor $Y_\sigma(f,k)\,G(f-k)$ in the integrand of Eq. (37) must be expanded as far as terms of order k^2/p^2. In the first integral of Eq. (36) the product $Y_\sigma(q, k)\,G(q-k)$ must be expanded to order (k^2/q^2); in the second integral the factors $Z_\sigma(l-k)\,\Delta(l-k)$ must be expanded to order (k^2/l^2) and the factor $G(p-l)$ to order (l/p). The last remark is connected with the fact that if we retained only $G^{(0)}(p-l) = G(p) \sim (1/p)$, we should obtain an integrand proportional to an odd power of the vector l_σ and the integral would vanish. Unlike the nucleon vertex operator Γ_σ, the meson vertex operator V_σ depends linearly on l_σ in the zero-order approximation. The next term in the expansion is $G^{(1)}(p,l) \sim (l/p^2)$ and leads to a logarithmic integral $[\int \ldots d^4l / l^4]$ with a coefficient proportional to (k^2/p^2). When this program is carried through, we obtain

$$Z_\sigma^{(1)}(p, k) = -ik_\sigma,$$

$$Y_\sigma^{(1)}(p, k) = \frac{\hat{p}\, k_\sigma}{p^2} r(x, y);$$

$$Y_\sigma^{(2)}(p, k) = \frac{k^2}{p^2}\gamma_\sigma u_1(x, y) + \frac{k^2\, \hat{p}\gamma_\sigma \hat{p}}{p^4} v_1(x, y) + \frac{\hat{k}\, k_\sigma}{p^2} u_2(x, y) + \frac{\hat{p}\,\hat{k}\,\hat{p}\, k_\sigma}{p^4} v_2(x, y); \tag{44}$$

$$Z_\sigma^{(2)}(p, k) = \frac{ik^2 p_\sigma}{p^2} w_1(x, y) + \frac{i(kp)\, k_\sigma}{p^2} w_2(x, y), \tag{45}$$

where we have separated the factors which depend only on the logarithmic variables $x = \ln(p^2/m^2)$ and $y = \ln(k^2/m^2)$.

We notice that $Z_\sigma^{(1)}$ and $Y_\sigma^{(1)}$ contain only longitudinal components (proportional to k_σ). The expressions for $Y_\sigma^{(2)}$ and $Z_\sigma^{(2)}$ also contain some purely longitudinal terms (those involving the functions u_2, v_2, and w_2). We can save time by ignoring the longitudinal terms completely. After substitution into Eq. (30), these terms give longitudinal components of the polarization tensor $P_{\alpha\beta}$. But this tensor satisfies the transversality condition $P_{\alpha\beta}k_\alpha = 0$. Therefore these terms must either vanish or else cancel each other out exactly.

We thus neglect $Z_\sigma^{(1)}$ and $Y_\sigma^{(1)}$, and project the expressions (44) and (45) for $Y_\sigma^{(2)}$ and $Z_\sigma^{(2)}$ onto an arbitrary transverse vector e_σ with $e_\sigma k_\sigma = 0$. Then the substitution into Eqs. (36) and (37) gives the following equations relating terms of second order in k:

$$\begin{aligned} u_1 &= \frac{\lambda_1}{3} a^2(x)\, c(x)\, q_1(x, y), \\ v_1 &= \frac{2}{3} \lambda_1 a^2(x)\, b(x)\, q_2(x, y), \\ w_1 &= -\frac{8}{3} \lambda_1 a^2(x)\, b(x)\, q_1(x, y), \end{aligned} \tag{46}$$

where q_1 and q_2 satisfy the equations

$$\begin{aligned} &q_1(x, y) \\ &= \int_x^x b^2(z) \Big[\eta(z) - \frac{\lambda_1}{2} a^2(z)\, c(z) (q_1(z, y) \\ &+ 2\lambda_1 a^2(z)\, b(z)\, q_2(z, p)\big] dz, \\ &q_2(x, y) \\ &= \int_x^x c^2(z) [\zeta(z) + 4\lambda_1 a^2(z)\, c(z)\, q_1(z, y)]\, dz. \end{aligned} \tag{47}$$

The zero-order equations are the following

$$\begin{aligned} \eta(x) &= 1 - \frac{\lambda_1}{2} \int_x^L a^2(z)\, b^2(z)\, c(z)\, \eta(z)\, dz \\ &+ 2\lambda_1 \int_x^L a^2(z)\, b(z)\, c^3(z)\, \zeta(z)\, dz, \\ \zeta(x) &= 4\lambda_1 \int_x^L a^2(z)\, b^3(z)\, \eta(z)\, dz. \end{aligned} \tag{48}$$

Eqs. (47) and (48) may be easily transformed into a system of differential equations

$$\begin{aligned} &\frac{\partial}{\partial x} [\eta(x)\, q_1(x, y)] = b^2(x)\, \eta^2(x) \\ &- 2\lambda_1 a^2(x)\, b^2(x)\, c(x) [\eta(x)\, q_1(x, y) \\ &- \zeta(x)\, q_2(x, y)], \\ &\frac{\partial}{\partial x} [\zeta(x)\, q_2(x, y)] = c^2(x)\, \zeta(x) \\ &+ 4\lambda_1 a^2(x)\, b^2(x)\, c(x) [\eta(x)\, q_1(x, y) \\ &- \zeta(x)\, q_2(x, y)] \end{aligned} \tag{49}$$

with the boundary conditions

$$q_1(xx) = q_2(xx) = 0, \qquad \eta(L) = \zeta(L) = 1. \tag{49a}$$

Since by Eq. (42)

$$b(x)\eta(x) = c(x)\zeta(x) = 1,$$

we may subtract the second Eq. (49) from the first, and with the notations

$$\eta q_1 - \zeta q_2 = R; \; 6\lambda_1 a^2 b^2 c = f,$$

we obtain $\dfrac{\partial R(x, v)}{\partial x} = -f(x) R(x, y),$

which gives

$$R(x, y) = A(y) \exp\left\{-\int^{x} f(z)\, dz\right\}.$$

But the boundary condition $R(x, x) = 0$ implies $A(x) = 0$, i.e. $R(x, y) = 0$ or

$$\eta(x) q_1(x, y) = \zeta(x) q_2(x, y). \tag{50}$$

Substituting Eq. (50) into (49), we obtain

$$\frac{\partial}{\partial x}[\eta(x) q_1(x, y)] = \frac{\partial}{\partial x}[\zeta(x) q_2(x, y)] = 1,$$

and with the boundary conditions this implies

$$\eta(x) q_1(x, y) = \zeta(x) q_2(x, y) = x - y. \tag{51}$$

4. We now return to the vacuum-polarization tensor. First of all, substituting Eqs. (33) and (34) into (30), we have

$$P_{\alpha\beta}(k) = \frac{ie_1^2}{(2\pi)^4}\left\{\frac{1}{2}\int \operatorname{Sp} \gamma_\alpha G(p)\,[X_\beta(p, k) + Y_\beta(p, k)]\, G(p-k)\, d^4p - 2\int i(2p_\alpha - k_\alpha)\,\Delta(p)\, Z_\beta(p, k)\,\Delta(p-k)\, d^4p\right\}. \tag{52}$$

Since the tensor $P_{\alpha\beta}$ is transverse, it may be written in the form

$$P_{\alpha\beta} = (\delta_{\alpha\beta} k^2 - k_\alpha k_\beta)\,\Pi. \tag{53}$$

To determine II, it is enough to substitute into Eq. (52) instead of the vectors X_β, Y_β and Z_β the transverse components

$$X = X_\beta e_\beta; \; Y = Y_\beta e_\beta; \; Z = Z_\beta e_\beta$$
$$(e_\beta k_\beta = 0; \quad e_\beta e_\beta = 1).$$

For $G(p - k)$ we substitute the expansion (7), (8), and similarly for $\Delta(p - k)$. From Eq. (2) it follows that

$$\Delta^{(0)}(p, k) = \Delta(p) = c(x)/p^2,$$
$$\Delta^{(2)}(p, k) = \frac{c(x)}{p^2}\left[\frac{4(pk)^2}{p^4} - \frac{k^2}{p^2}\right].$$

For X_σ, Y_σ and Z_σ we use Eqs. (38), (42), (43), (44) and (45). Making the transformation to Euclidean space and integrating over angles, we obtain

$$\Pi(y) = {}^2/_3\,\varepsilon_1 \int_y^L \{b^2(x)\,[\xi(x) + \eta(x) - {}^3/_2\, s(x, y) - {}^3/_2\, u_1(x, y) + 3v_1(x, y)] + c^2(x)\,[\zeta(x) - {}^3/_2\, w_1(x, y)]\}\, dx \tag{54}$$

or using also Eqs. (39), (46) and (47)

$$\Pi(y) = {}^2/_3\,\varepsilon_1 \{q(L, y) + q_1(L, y) + q_2(L, y)\}. \tag{55}$$

But Eqs. (40) and (51) give

$$q(L, y) = q_1(L, y) = q_2(L, y) = L - y,$$

i.e.,

$$\Pi(y) = 2\varepsilon_1 (L - y).$$

Therefore

$$d_t^{-1}(y) = 1 + \Pi(y) = 1 + 2\varepsilon_1 (L - y). \tag{56}$$

After renormalization[+] by means of Eqs. (3) and (4), we obtain

$$\tilde{d}_t^{-1}(y) = 1 - 2\varepsilon y. \tag{57}$$

We see that the renormalized expression for the vacuum polarization

$$\tilde{\Pi}(y) = -2\varepsilon y \tag{58}$$

is independent of the meson coupling constant λ. $\tilde{\Pi}(y)$ is simply the sum of the proton polarization $\frac{4}{3}\epsilon y$ and the meson polarization $-\frac{2}{3}\epsilon y$ which are obtained from perturbation theory[6] in the limit when $y \gg 1$ and $\epsilon y \ll 1$.

4. CONCLUDING REMARKS

1. The result we have obtained, that the photon propagation function is independent of meson interactions for $e^2 \ll g^2 \ll 1$, is closely connected with the renormalizability of the theory with scalar coupling. The property of renormalizability already implies a strong restriction on the possible

---

[+] Since $\epsilon y \ll 1$, we have $d_t^{-1} = 1 - \partial_t$.

[6] R. P. Feynman, Phys. Rev. 76, 769 (1949).

behavior of the propagation functions. Consider first the purely electrodynamic problem. The function $d_t(y)$ depends parametrically on ϵ_1 and L

$$d_t(y) = f_1(y; \varepsilon_1, L).$$

The renormalizability means that after the transformations (3) and (4) the function $d_t(y)$ becomes independent of L. From the form of the original equations defining d_t (see reference 1), it is easy to see that y, ϵ_1 and L can occur in the solution only in the combination $\epsilon_1(L - y)$. In fact, the equations contain ϵ_1 linearly in front of the integral signs, and the limits of integration are L and y. Hence, after introducing the new variable $t = \epsilon_1(L - y)$, the equations no longer contain parameters in the coefficients or in the limits of integration. Thus

$$d_t^{-1}(y) = f[\varepsilon_1(L - y)].$$

By Eqs. (3) and (4), the function

$$\tilde{d}_t(y) = \frac{f[\varepsilon_1(L - y)]}{f(\varepsilon_1 L)}$$

with

$$\varepsilon_1 - \varepsilon f(\varepsilon_1 L) = 0$$

is independent of L. This is possible if f is a linear function

$$f(z) = 1 + \varkappa z, \tag{59}$$

in agreement with the result of reference 1 (actually $\varkappa = 4/3$).

Similarly, in the purely mesonic problem the solutions can depend on the parameters $\lambda_1 L$ only in the combination $\lambda_1(L - y)$. Consider the function

$$\begin{aligned} \theta^{-1}(x) &= a^2(x)\, b^2(x)\, c(x) \\ &= F^{-1}[\lambda_1(L - y)]. \end{aligned} \tag{60}$$

By Eqs. (4) and (4a), the renormalized function

$$\tilde{\theta}(x) = \frac{F[\lambda_1(L - x)]}{F(\lambda_1 L)}$$

with

$$\lambda_1 - \lambda F(\lambda_1 L) = 0$$

is independent of L, which is possible if F is a linear function

$$F(z) = 1 + \nu z. \tag{61}$$

This agrees with the results of references 2, 3, both for neutral and symmetric meson fields (in the latter case $\nu = 5$).

2. In our problem d_t contains three parameters ϵ_1, λ_1 and L. Since we use perturbation theory with respect to ϵ_1, the function d_t has the following structure:

$$d_t^{-1}(y) = 1 + \varepsilon_1 \int_y^L \varphi[\lambda_1(L - y); \tag{62}$$

$$\lambda_1(L - x)]\, dx = 1 + \frac{\varepsilon_1}{\lambda_1}\Phi[\lambda_1(L - y)].$$

We renormalize the charge by Eqs. (4) and (62),

$$\varepsilon_1 = \frac{\varepsilon}{1 + \frac{\varepsilon}{\lambda_1}\Phi(\lambda_1 L)}$$

and the meson-nucleon coupling constant by Eqs. (4a), (60) and (61)

$$\lambda_1 = \lambda\theta(x) = \lambda F(\lambda_1 L);\ \lambda_1 = \frac{\lambda}{1 - \nu\lambda L}.$$

then the function $\tilde{d}_t^{-1}(y)$, renormalized according to Eq. (3), takes the form

$$\begin{aligned} \tilde{d}_t^{-1} &= \frac{1 + \frac{\varepsilon_1}{\lambda_1}\Phi[\lambda_1(L - y)]}{1 + \frac{\varepsilon_1}{\lambda_1}\Phi(\lambda_1 L)} \\ &= 1 + \frac{\varepsilon(1 - \nu\lambda L)}{\lambda}\left\{\Phi\left[\frac{\lambda(L - y)}{1 - \nu\lambda L}\right] - \Phi\left(\frac{\lambda L}{1 - \nu\lambda L}\right)\right\}. \end{aligned} \tag{63}$$

Eq. (63) is independent of L only when $\Phi(z)$ is a linear function of z. But in that case, it is easy to see that $\tilde{d}_t$ is also independent of λ.

In conclusion I express my deep gratitude to I. Ia. Pomeranchuk for many interesting comments, and to B. L. Ioffe and I. M. Shmushkevich for their interest in this work and for critical remarks.

Translated by F. J. Dyson
242

SOVIET PHYSICS JETP VOLUME 2, NUMBER 3 MAY, 1956

The Photographic Action of Ionizing Particles. I.

THE FORM OF THE BLACKENING CURVE FOR PHOTOGRAPHIC FILM EXPOSED TO RADIATION

A. L. KARTUZHANSKII
Leningrad, USSR

(Submitted to JETP editor June 15, 1954)
J. Exper. Theoret. Phys. USSR **29**, 516-528 (October, 1955)

The form of the curve expressing the blackening density of an irradiated photographic film is investigated as a function of the exposure. The data obtained for films of various sensitivity and various types of radiation, as well as the data concerning the effect of supplementary exposure, are used to determine the degree of dispersion of the latent image.

INTRODUCTION

AT the present time there is in the literature a great amount of data concerning the type of dependence between the photographic blackening and the intensity of a beam of ionizing particles. These data cover the action of particles of various types and various energies. However, usually the purpose of obtaining such data was purely utilitarian and, hence, practically no attempts were made to connect the results obtained with the theory of the formation of a latent image due to the action of these particles.

It should be stated that for the case of the photographic action of light, the interpretation of the shape of the blackening curve, in particular, the portion near the origin, has yielded important results[1]. In particular, the curves expressing the optical density of blackening, D, (above the fog) as a function of the exposure, H, i.e., the product of the intensity of radiation and the exposure time*, can have various forms depending on the values of the radiation intensity and the exposure time at which the given curve was obtained. Generally speaking, two types of curves are possible (Fig. 1). The curve of the first type (I) is characteristic for small amounts of irradiation and long exposure times. The curve shows that, under these conditions, large centers of latent image are formed in the emulsion crystals, thus yielding developable crystals. The curve of the second type (II) is characteristic of strong irradiation and short exposure times. These conditions point to the formation of extremely small centers – the so-called subcenters which, in spite of being thermally stable, do not contribute to the developability unless something is added to these latent centers by additional exposure or in some other way. Thus, for the case of the photographic action of light, the analysis of the blackening curves permits us to establish the degree of dispersion of the latent image[2], i.e., its distribution among separate centers. At the same time, the data concerning the dimensions of the centers (even if they are comparable) formed under different conditions may serve as a means of understanding the mechanism of formation of the latent image.

For the case of photgraphic action of ionizing particles, no such analysis is available. However, numerous facts indicate that the degree of dispersion of the latent image created by these particles can vary to a great degree, depending upon the ionizing properties of the particles and the sensitivity of the photographic film[3]. Data which is available in the literature on the blackening curves obtained by particle irradiation point to the fact that they can be evaluated by analogy with Fig. 1. Thus, for α- particles of natural origin, the experimental curves can be very easily described by the equation $D = D_0(1 - e^{-kH})$ which can be obtained theoretically[4] merely by assuming that every crystal which comes into contact with the α- particles can be developed, i.e., it acquires a sufficiently large center of latent image. Therefore, it can be expected that in this case the blackening curve will be of type I. From the equation of the curve, its slope will be a maximum at

---

* This relation differs from that widely used in the photographic literature, which expresses a dependence between the blackening density and the logarithm of the exposure, and which is represented graphically by the so-called characteristic curve.

[1] P. C. Burton and W. F. Berg, Photograph. J. 86B, 2 (1946).

[2] P. V. Meiklar, Uspekhi Fiz. Nauk **38**, 43 (1949).

[3] A. L. Kartuzhanskii, Uspekhi Fiz. Nauk **52**, 341 (1954).

[4] S. Kinoshita, Proc. Roy. Soc. (London) **83A**, 432 (1910).

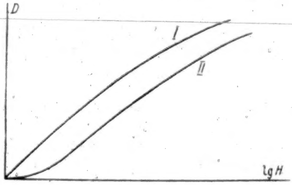

FIG. 1. *I* - the curve characteristic for small intensities and long exposure times; *II* - the curve characteristic for high intensities and short exposure times.

the origin. For protons, which possess smaller ionizing power and form smaller latent image centers, the blackening curves differ considerably from type I, and approach type II[5]. If electrons are used for irradiation, the form of the portion of the curve close to the origin, which is characteristic of the curve of type II, can be observed with an even greater degree of clarity. This becomes more noticeable as the energy of the particles is increased and the sensitivity of the photographic film is decreased[6].

It was deemed necessary to conduct a systematic study of the forms of the blackening curves of various photographic films exposed to irradiation by various ionizing particles, and to correlate the data obtained in this manner with the general scheme of the formation of the latent image under the action of the particles. By comparing these data to the analogous data for the case of light, it is possible to estimate the degree of similarity of the photographic actions of the light and the particles. A study of this kind had also some practical interest for us in connection with the development of a method of quantitative β - radiography from the blackening data[7]. We have not considered the case of high density blackening for which a certain analogy with the action of light has recently been discovered[8].

EXPERIMENTAL METHOD

The following radioactive isotopes were used as particle sources: Po^{210}, possessing monochromatic α - radiation with the energy 5.3 mev; C^{14}, possessing β - radiation with a maximum energy of 0.155 mev, i.e., with a comparatively high ionizing power; P^{32}, possessing β - radiation with a maximum energy of 1.7 mev, i.e., consisting chiefly of particles with the minimum ionizing power, or very close to it. In a number of the other experiments an electron microscope with an accelerating potential of 50 kv was used.

A number of photographic films of widely differing sensitivity were used in the experiments: positive plates of the Plant No. 2 GUKPP, electron sensitive plates of the same manufacturer, and also films of high concentration designed especially for the detection of ionizing particles. To obtain a scale of blackening, each plate was exposed for different times, i.e., blackening for different exposure times was produced on different portions from the same source. This was achieved by displacing the plates (laterally) with respect to the source. The same exposure method was used in the case of the electronmicroscope. The sources used possessed a sufficiently high activity (of the order of 10 - 100 μc on a cm^2 of surface), which permitted us to use exposure times of not more than 20-30 minutes.

The developing process was done in a metol-hydroquinone developer, ID-19, diluted with distilled water in the ratio of 1:2, at a constant temperature (20 ± 0.5) °C, and stirred with a soft rubber brush. If, in a given experiment, it was necessary to compare several plates, they were developed concurrently. Developing time amounted to 20 minutes for the highly concentrated thick films and 8 minutes for the positive plates and the electron sensitive plates. Upon the determination of the developing process, the highly concentrated films were placed in a 1% solution of acetic acid for 10 minutes, after which they were fixed and washed in the usual manner. All other films were rinsed in flowing water and then immediately submerged in the fixing solution.

The measurement of the blackening density was performed on the photoelectric microphotometer MF-2. The weak blackening was of greatest interest to us as it gave the initial portion of the blackening curve.

As the relative error in measuring these blackenings is rather large, each blackening was measured a number of times. Moreover, the results of several experiments were completely eliminated because of the inhomogeneity of the observed blackening. Essential precautions and critical evaluation of the results insured the measurements of small blackening densities with the error ΔD of not more than 0.01. For blackenings induced by

---

[5] P. Brix, Z. Physik. **126**, 35 (1949).

[6] N. Digby, K. Firth and R. J. Hercock, J. Photograph. Sci. **1**, 194 (1953).

[7] I. L. Finagin, A. L. Kartuzhanskii and B. P. Soltitskii, Zh. Tekhn. Fiz. **25**, 1276 (1955).

[8] K. S. Bogomolov and V. N. Zharkov, Dokl. Akad. Nauk **92**, 1161 (1953).

α - particles in the highly concentrated films, it was possible to increase the precision of measurements of small densities by counting the number of tracks appearing on a unit area of the film and subsequently correlating this number with the optical blackening density of the same area in accordance with a specially constructed scale. The tracks were counted with the aid of a binocular microscope, MBE - 1, equipped with a 90 power immersion objective and 15 power eyepiece. Initially it was thought that the method of counting the tracks could also be applied to blackenings induced by β - particles; however, the lack of monochromaticity of the radiation of the β sources and the fact that the tracks varied in their appearance and lengths, and also because of the density of grains in these tracks, led to inexact results. The error in this case exceeded all the incidental errors incurred in the direct measurements of blackening densities.

All blackening densities in the curves shown below are given after the fog density has been subtracted.

In certain experiments the films, after being irradiated with particles, were subjected to additional exposures by light of varying spectral distribution. The plate was placed in a special plate holder into the opening of which a corresponding colored light filter and also a neutral light filter were inserted. A 300 watt projection lamp was used as a source; the filament of the lamp was placed parallel to the plate. We found that for a plate of dimensions 3 × 4 cm, and a distance between plate and lamp of 15 cm, the variation in uniformity of illumination at various points of the plate did not exceed 5%.

EXPERIMENTAL RESULTS

In Fig. 2, the blackening curves are shown that were obtained by the irradiation of six photographic films with α-particles from the Po^{210} source. The parts of these curves close to the origin are plotted to a larger scale in the insert. Among the four highly concentrated films designated *A*, *B*, *C*, and *D*, the film *A* is the least sensitive. The traces of the α - particles on this film consist merely of several points and are very difficult to distinguish, while the blackening is very slight even for exposures several times longer than those used for other films.

From the study of Fig. 2, it can be seen that the blackening curves for all films except *A* pass through the origin of coordinates and have maximum slope at that point. Although the use of the criterion of Fig. 1 has not been rigorously substantiated, these curves should undoubtedly testify to the formation of sufficiently large latent image centers in every emulsion crystal impinged upon by an α - particle in any of the films. This is also known from other data[3]. The blackening curve of the film *A*, unlike all the other curves and in contrast to the data concerning the action of α - particles quoted in the literature, does not pass through the coordinate system origin. Its first

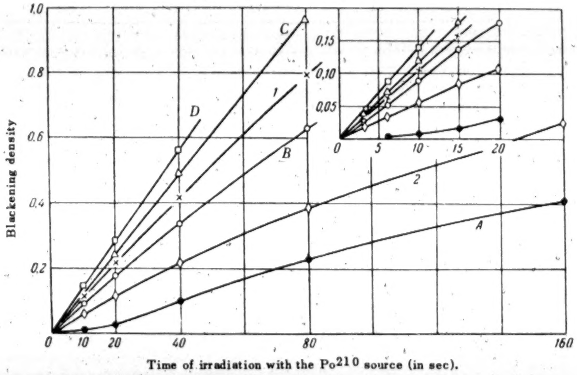

FIG. 2. *1* - the electron sensitive plates; *2* - positive plates, *A*, *B*, *C*, *D*, highly concentrated films

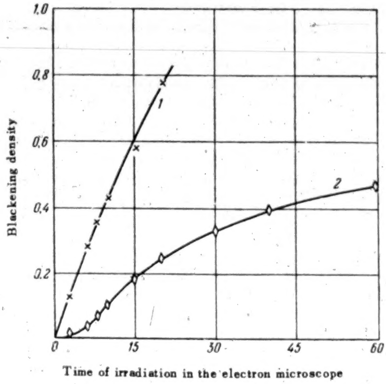

FIG. 3. *1* - electron sensitive plates; *2* - positive plates

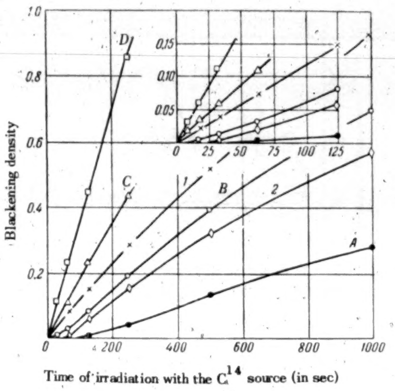

FIG. 4. *1* - electron sensitive plates; *2* - positive plates, *A*, *B*, *C*, *D* - highly concentrated films.

derivative does not have a maximum at the beginning of the curve and it is not a monotonic function as it is the case with all other curves. Since the sensitivity of the film *A* is quite small, relatively few of its crystals impinged upon by α - particles become developable, i.e., acquire latent image centers which are capable of effecting development. This is easily seen from the character of the α - traces in this film. If this is the reason for the behavior of the film *A*, then we are justified in relating the form of the initial portion of the blackening curve with the dimensions of the silver centers in the emulsion crystals (as we have related them for the case of light in Fig. 1), and also with the sensitivity of the film.

In Fig. 3, the blackening curves are given for the electrosensitive and positive plates subjected to the irradiation of 50 kv electrons in the electron microscope. In Fig. 4, the blackening curves are given for all six films for irradiation by C^{14} source. As for the β - spectrum of C^{14}, the maximum energy amounts to 155 kev, and the mean energy is, as usual, smaller by a factor of 3. The results given in Figs. 3 and 4 agree quite well as should have been expected.

The data shown in these diagrams show, in good agreement with data of Fig. 2, that highly sensitive films in whose emulsion crystals large latent image centers are formed, are characterized by blackening curves possessing maximum slope at the origin. The films of small sensitivity, where the emulsion crystals are not in position to make effective use of the conduction electrons, which are formed by the passing of an ionizing particle, are characterized by curves analogous with curve II in Fig. 1. A substantially new fact that is apparent in Figs. 3 and 4, as compared with Fig. 2, is that now among films possessing curves of type II, there are besides the film *A*, also the positive plates and film *B*, the purpose and the sensitivity of which are limited to the recording of α - particles of natural origin. In this fashion, by going to particles with a smaller ionizing power, a further differentiation of the photographic films under investigation takes place (according to their sensitivities). This difference becomes immediately apparent from a study of the form of the initial portions of the blackening curves of these films.

The blackening curves for five of the films (film *A* is excluded because of its insufficient sensitivity) obtained by irradiation from a P^{32} source are shown in Fig. 5. The mean energy of the β - radiation spectrum of this isotope amounts to some 0.7 mev; hence, a considerable portion of the active radiation consists either of particles of minimum ionizing ability, or of particles whose ionizing ability differs from the minimum by a relatively small factor (1.5 - 2.0 times). Under these conditions, a sufficient sensitivity, corresponding to the maximum slope of the blackening curve at the coordinate origin, is evident only in the case of the film *G*, designed for the detection of relativistic particles. The film *B*, intended for the detection of nonrelativistic particles of considerable energies, is found to be

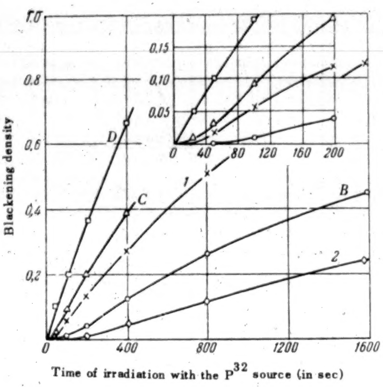

FIG. 5. *1* - electron sensitive plates; *2* - positive plates, *A*, *B*, *C*, *D* - highly concentrated films.

insufficiently sensitive for the detection of the above radiation; the same statement can be made concerning the electron sensitive plates, intended for irradiation in an electron microscope or some similar device, i.e., for irradiation by electrons possessing energies of less than 100 kev. The above conclusions are in full agreement with the shapes of the curves shown in Fig. 5.

From the data presented in Figs. 2 - 5, it is possible to establish a correspondence between the shapes of the initial portions of the blackening curves and the dimensions of the latent image centers in the emulsion crystals. At the same time, we know the dimensions of these centers to be dependent on the relationship between the ionizing capabilities of the impinging particles and the sensitivity of the film. It should be noted that the interpretation of the present experimental data is analogous to that proposed for the case of light, and that no auxiliary concepts have been invoked.

Some of the data available in the literature[9-11] indicate that the sensitivity of a film irradiated by particles can be increased by subjecting the film to a supplementary exposure to light of low intensity; some additional build-up of the latent image centers created through the action of the particles is thus effected. This method had been employed previously[1] to intensify the latent image centers formed by exposure to light. It was found in that case that an intensification took place only if the latent image was highly dispersed, and the blackening curve prior to the secondary exposure to light was of type II (Fig. 1); the secondary exposure then resulted in a type I blackening curve. The experiments described below are designed to demonstrate an analogous change in the shapes of the blackening curves of films first irradiated by particles and then exposed to light.

In making use of secondary exposure, a number of things must be taken into account. Mainly, it should be noted that in thick and highly concentrated layers, the scattering and the absorption of light are so high that the depth of penetration of the secondary exposure effects can be made comparable with that of the particles only by the use of radiation of sufficiently long wavelength. On the other hand, the action of long wave radiation, as contrasted to that of short wave radiation, is to destroy, rather than to build up the latent image (Herschel effect). This fact makes very difficult the selection of the spectral composition of radiation to be used for secondary exposure. It should be mentioned that in the case of thin films of normal concentrations - electron sensitive and positive plates - the use of short wave radiation is permissible; in fact, any wavelength up to the beginning of the ultraviolet region may be employed. It is also essential to select the exposure time correctly; it must be so chosen as to obtain the minimum possible background density due to the supplementary exposure, together with the greatest possible intensification.

An account of the experiments performed is now in order. Among the films subjected to irradiation by α- particles, the film *A* appeared to be the most interesting, because of the properties noted in Fig. 2. In this particular film the length of the α- particle tracks did not exceed 20 μ (in other films where individual tracks could be distinguished, their length was found to be some 25-27μ), and the spectral composition of the light used for the secondary exposure could be varied widely, practically throughout the entire visible range. Figure 6 shows the blackening curves corresponding to secondary irradiation through the ZhS-18 filter, which transmits light with $\lambda > 490$ mμ; the penetration depth in this case amounts to some 20 μ. Similarly, Fig. 7 shows analogous curves corresponding to irradiation through the KS-14 filter ($\lambda > 620$ mμ), with penetration depth of some 35-40 μ. Finally, in Fig. 7 similar curves are shown for the case of irradiation through the KS-19 filter ($\lambda > 700$ mμ), with the penetration depth up to

---

[9] E. Schopper, S. Magun and W. Braun, Z. Naturforsch. **6a**, 338 (1951).

[10] S. G. Grenishin, Zh. Tekhn. Fiz. **22**, 33 (1952).

[11] K. Zuber. Nature **170**, 669 (1952).

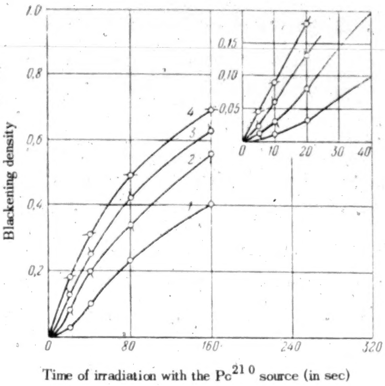

FIG. 6. *1* - no supplementary exposure to light; *2* - supplementary exposure time 3 sec; *3* - supplementary exposure time 6 sec; *4* - supplementary exposure time 12 sec.

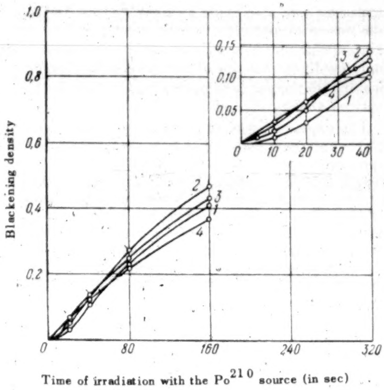

FIG. 8. *1* - no supplementary exposure to light; *2* - supplementary exposure time 30 sec; *3* - supplementary exposure time 100 sec; *4* - supplementary exposure time 300 sec.

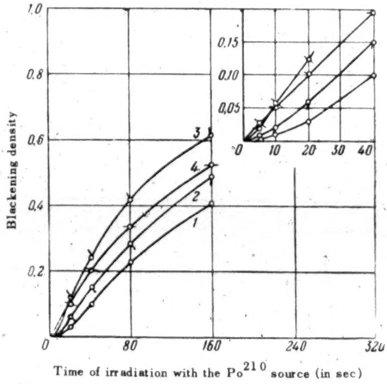

FIG. 7. *1* - no supplementary exposure to light; *2* - supplementary exposure time 15 sec; *3* - supplementary exposure time 50 sec; *4* - Supplementary exposure time 150 sec.

50 mμ. In accordance with convention, the blackening density data for these curves are given after the substraction of the background densities due to the secondary exposure, and of the fog.

A study of Figs. 6-8 permits us to arrive at definite conclusions. First of all, the action of the supplementary exposure brings about not only an increase in blackening, but also a change in the form of the initial portion of the blackening curve; specifically, a gradual transition from type I to type II is observed. It follows that an increase in blackening is connected with an increase in the developability which is brought about by the build-up of the already existing latent image centers. The formation of new centers due to the action of light is excluded from consideration by the act of subtraction of the background density from all blackening densities of regions irradiated by particles. Hence, the curves of Figs. 6-8 demonstrate only the effect of the supplementary exposure on the previously formed centers.

We must also take note of the fact that there exists a definite relationship between the effects of the supplementary exposure and the spectral composition of light used for this purpose. It is found, for example, that the comparatively short wave radiation, transmitted by the ZhS-18 filter, produces an inhomogeneous increase in all blackening densities. On the other hand, the radiation of longer wavelengths transmitted by the KS-14 and KS-19 filters causes the heavy blackenings to disappear, because of the Herschel effect, if the exposure time is sufficiently long; at the same time weak blackenings are intensified. Until the present time, the dual action of the long wave radiation, dependent upon the blackening density, was known mainly for the case when the first exposure was also made by light[12,13]. As far as the action of particles is concerned, the intensification was observed only in one investigation[9] and only for linear density of the developed crystals making up the particle tracks, rather than for the optical density of continuous blackening.

The explanation of the dual action of the supplementary exposure given in the reference can be applied in our case. It is known that long wavelength light is absorbed both by the latent image centers, resulting in their decrease in size, and by the silver halide, effecting the formation of the photolytic silver which subsequently builds up the available centers. The predominance of either of the competing processes depends on the degree of light absorption by both types of absorbinn centers. In the case of small blackenings, where the latent image is not abundant, the absorption by the silver halide matrix predominates and hence the centers are built up.

In the case of heavy blackenings, the predominant process is the absorption by the latent image centers; hence a decrease in size results.

In the group consisting of the emulsion *A*, *B*, *C*, and *D*, the particle sensitivity and the light sensitivity vary identically; hence, under similar conditions of irradiation by particles, the formation and the build-up of centers must predominate over the dissolution in the case of the film *B* to a greater degree than in the case of *A*, for the film *C* to a greater degree than for *B*, etc. This can be directly seen from the results of the experiments with the film *B*, which were conducted analogously to those described above for the film *A*.

For the case of film *B* , Fig. 9a (exposure with the KS-14 filter) and Fig. 9b (exposure with the KS-19 filter) show no noticeable intensification of the latent image and consequently no change of the initial portion of the curve. This is in good agreement with the previously proposed explanation since, as it was mentioned above, the film *B* is sufficiently sensitive to α-particles. At the same time, the Herschel effect in the film *B* can only be observed when the filter KS-19 is used and generally is weaker than for the film *A*. This can be explained by the fact that in the more sensitive film, under the action of exactly the same radiation, the formation or the build-up of latent image centers predominates in resolution for heavy blackening and in the long wavelength portion of the spectrum over that for the less sensitive film.

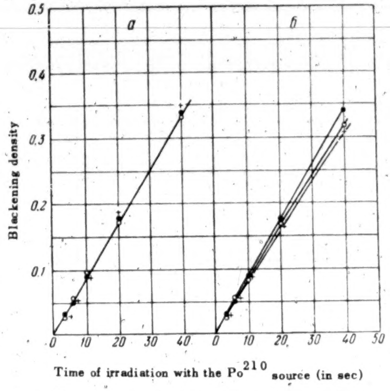

FIG. 9. *a*: ● - no supplementary exposure to light; O - supplementary exposure time 15 sec; + - supplementary exposure time 75 sec; *b*: ● - no supplementary exposure to light; O - supplementary exposure time 100 sec; + - supplementary exposure time 300 sec.

A number of experiments were conducted in which the primary exposure was made with β-particles from the C^{14} source. It can be seen that in a specially prepared cross section the depth of penetration of these particles in the highly concentrated films amounts to some 40 μ; this excludes the possibility of using filters with the short wave length cut off greater than that of KS-14. Curves obtained for irradiation by the C^{14} source and a supplementary exposure to light are shown in Fig. 10; the KS-19 filter was used in the case of the films *C* and *D* and the KS-14 filter for the films *A* and *B*. It can easily be seen that in the films *A*, *B*, and *C* some intensification is apparent, whereas there is none at all in the film *D*. If the unexpected appearance of the intensification phenomenon in the film *B* , which is highly sensitive to the β-radiation, is temporarily disregarded (this irregularity will be explained later), then the obtained results are in full agreement with the proposed explanation of the action of supplementary exposure.

It should also be noted that in Fig. 10 (unlike Figs. 8 and 9) the supplementary exposure in the case of the films *A* and *B* did not produce a full intensification, i.e., the disappearance of the inflection in the initial portion of the blackening curve was not observed even for exposures which produced background densities of 1.5 - 2.0. This indicates a definite difference in the degree of dispersion of the latent images produced by the α- and the β-particles. These films of normal concentrations (positive and electron sensitive plates) were also subjected to the consecutive

---

[12] P. V. Meiklar, Zh. Fiz. Khim. 19, 441 (1945).

[13] Iu. N. Gorokhovskii and S. A. Shestakov, Zh. Fiz. Khim. 11, 356 (1938).

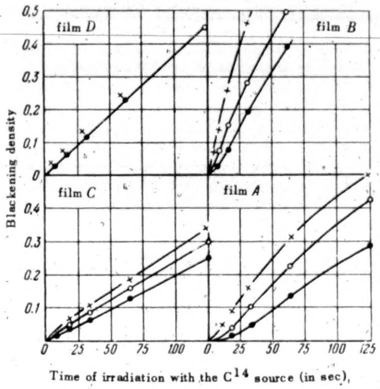

FIG. 10. Film *A*: ● - no supplementary exposure to light; O - supplementary exposure time 100 sec; + - supplementary exposure time 300 sec; Film *B*: ● - no supplementary exposure to light; O - supplementary exposure time 50 sec; + - supplementary exposure time 150 sec. Film *C*: ● - no supplementary exposure to light; O - supplementary exposure time 20 sec; + - supplementary exposure time 60 sec. Film *D*: ● -no supplementary exposure to light; O - supplementary exposure time 12 sec; + - supplementary exposure time 40 sec.

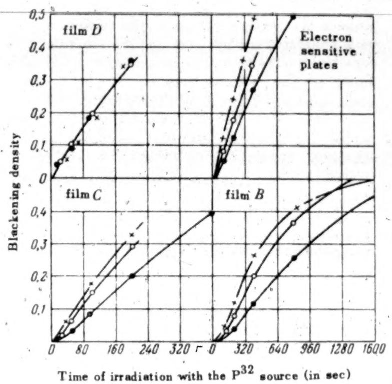

FIG. 11. Film *B*: ● - no supplementary exposure to light; O - supplementary exposure time 300 sec; + - supplementary exposure time 1000 sec. Film *C* : ● - no supplementary exposure to light; O - supplementary exposure time 20 sec; + - supplementary exposure time 60 sec. Film *D*: ● - no supplementary exposure to light; O - supplementary exposure time 12 sec; + - supplementary exposure time 40 sec. Electron sensitive plates: ● - no supplementary exposure to light; O - supplementary exposure time 50 sec; + - supplementary exposure time 150 sec.

action of the β - radiation from C^{14} and the supplementary exposure to light. Here it was possible to use radiation of shorter wavelength for the supplementary exposure; for example, the 365 mμ mercury line, and the 436 mμ mercury line which were separated by means of the UFS-3 filter and a colored gelatin filter, respectively. Although in this case the conditions of exposure could thus be varied to a greater extent than for other films, the results obtained did not yield any new information as compared with the results given above, although they verified these completely.

We would like to present some data from a series of experiments in which the primary exposure was performed by β - particles from a P^{32} source. It should be noted that according to calculations the β-radiation from a P^{32} source is capable of penetrating the emulsion layers to a depth in excess of 1 mm; in any case, this radiation penetrated through all of the films investigated. Films *A* and *B* each had an emulsion thickness of 50μ, the films *C* and *D* – a thickness of 100μ. The two latter films were exposed on both sides with the aid of the KS-19 filter; since the radiation transmitted by this filter penetrates to the depth of nearly 50μ, this practice permitted us to extend the action of the supplementary exposure to all emulsion crystals, on the surface as well as in the depth of the film. For thinner films the problem was correspondingly simpler.

The blackening curves obtained from these experiments for the films *B*, *C*, and *D* and for the electron sensitive plates are shown in Fig. 11. The absence of any intensification in the case of film *D* and its presence in all other films should be considered quite normal.

The differences in the degree of dispersion of the latent image created by the action of various particles and in various films are obvious from the data given here. However, it should be remembered that any particle, even one with a comparatively high ionizing capability, invariably forms a highly dispersed latent image – the degree of dispersion never being less than in the case of light; thus, the experiments described above reflect only very small differences in the degree of the image dispersion. The correctness of this assertion can be seen from the following experiment. It is known[1] that a brief exposure to light of high intensity also creates a highly dispersed latent image, which can be intensified by a subsequent exposure to light of small intensity. This process creates large latent image centers. We have subjected the positive and the electron sensitive plates to a uniform exposure of 8 μsec duration. The radiation was supplied by a flash lamp; the UFS-3 and neutral gray filters were used. Conditions were so adjusted that a uniform blackening density of approximately 0.5 was obtained. Instead of subjecting the plates so treated to a secondary exposure to light, we superimposed the usual blackening pattern of the Po^{210} α-source. The intensification effect was not observed in any of the cases, i.e., the α-particles did not produce the effect obtained with the radiation capable of creating coarsely dispersed latent images. At the same time, the reverse order of exposures produced a marked intensification in some cases.

The following modification of the experiment described above is of interest. Instead of using the flash lamp the uniform blackening of the plates was produced by irradiation in the electron microscope. In this case the subsequent irradiation by α-particles gave a distinct intensification, i.e., the resulting blackening density was always greater than the sum of the blackening densities formed by each of the separate exposures. No such effect was observed when the exposures were performed in the reverse order. The obtained results can be understood if one assumes that an intensification will take place only in the case where the radiation used for the primary exposure creates a latent image of a higher degree of dispersion than that used for the secondary one; this statement applies to light as well as to particles. It follows that no particles, ever those of high ionizing power, even form centers larger than those due to exposure to light, even if the latter is highly concentrated and of very short duration.

These data also supply the answer to the question proposed recently by Biberman and Kovner[14] concerning the possibility of build-up of centers created by the action of particles of smaller ionizing power by the subsequent action of particles of higher ionizing power. As these authors consider such an experiment as a conclusive proof of the formation of a highly dispersed latent image due to the action of particles and the possibility of its subsequent build-up, the proposed hypothesis is also supported from this point of view.

CONCLUSIONS

1. The dependence of the blackening density, D, on the exposure, H, has been investigated for six different photographic films irradiated by α- and β-particles of various energies.

2. It has been shown that the shape of the initial portion of the curve, $D = f(H)$ is a characteristic of the degree of dispersion of the latent image.

3. It has been established that the degree of dispersion increases as the energies of the ionizing particles and the sensitivity of the film are decreased.

4. A subsequent exposure to light serves to change the degree of dispersion of the latent image formed by the ionizing particles in a regular fashion; both the build-up and the dissolution (Hershel effect) of the latent image are observed.

5. The latent images due to the action of light and of particles were found to be qualitatively the same for all particles and films.

---

[14] L. M. Biberman and I. A. Kovner, J. Exper. Theoret. Phys. USSR 26, 234 (1954).

Translated by G. Makhov
234

SOVIET PHYSICS JETP VOLUME 2, NUMBER 3 MAY, 1956

The Question of the Possibility of Measuring the Temperature of the Column of a Jet Discharge Using the 3064 Å Hydroxyl Band

M. Z. KHOLKOV
Moscow State University

(Submitted to JETP editor July 13, 1954)
J. Exper. Theoret. Phys. USSR **29**, 645-650 (November, 1955)

It is shown that measurements of the temperature of the column of a jet discharge at pressures greater than 100 mm Hg using the 3064 Å hydroxyl band yield the temperature of the neutral gas. This is connected with the predominant role of thermal dissociation of water at the pressures indicated as compared with dissociation due to the action of fast electrons with simultaneous excitation of the hydroxyl which is formed.

ONE of the difficulties in using molecular bands to determine the temperature of a neutral gas in an electric discharge lies in the fact that the distribution of molecules by rotational states corresponding to the temperature of the neutral gas can be stated a priori only for stable molecules. In this case, because of the "duplicating" property of the collisions between an electron and the molecules[1], the distribution over rotational levels for the upper electronic state is similar to the distribution for the ground state where it is determined by the temperature of the neutral gas. Hence, using molecular spectra it is possible to determine the temperature of the neutral gas in non-isothermal states; under the same conditions the relative intensity of the atomic lines yields only the excitation temperature. In the case of the nitrogen molecule, which is of interest in what follows, this method has been verified experimentally by comparison with independent temperature measurements performed with thermocouples[2,3].

Once the applicability of the method is established, the temperature, as is well known, can be determined by starting with the relation:

$$\ln \frac{I}{i\nu^4} = C + \frac{B}{kT} J(J+1), \qquad (1)$$

where I is the intensity of the spectral line at a frequency ν corresponding to a transition characterized by a rotational quantum number J (the upper electronic state) and transition probability i, B is the rotational constant, T is the absolute temperature and C is a constant.

In the case of the unstable molecules which are formed in the same discharge, there is at hand experimental evidence giving examples both of a deviation from the distribution given in Eq. (1) as well as the maintenance of a particular type of distribution for which the obtained temperature values cannot possibly coincide with the temperature of the neutral gas under these conditions. Thus, for example, Hori[4] has observed a case (for a discharge between carbon electrodes at 4 mm Hg, using the molecules CO and CN) in which there was observed a Boltzmann distribution over the rotational levels but with sharply differentiated temperatures (1600 °K and 5200 °K respectively). What has been stated applies also in the hydroxyl case. Moreover there has been observed for this molecule a case of two intensity maxima in the Q_1-branch of the 3064 Å band[5]. One of these can be interpreted as the temperature, but the other arises as a result of the dissociation of water under the action of electronic collisions with simultaneous excitation of the hydroxyl which is formed under these conditions[6]. In this reaction part of the activation energy can be converted to rotational energy and thus can disturb the temperature distribution of the molecules over rotational states.

Cristesku and Grigorovici[7] have employed the hydroxyl method using the 3064 Å band in a study of a jet discharge at atmospheric pressure (62.5 and 84.5 mc). At various points of the column of the discharge a Boltzmann distribution of the molecules over rotational states was observed with temperatures ranging from 3600 °K to 4180 °K which the authors interpreted as the temperature of the neutral gas. However, substantial doubts as to the validity of these results have been raised in the work of Mochalov, Nikiforov and Bogonostsev[8], and up to the present time the temperature of the column of a jet discharge has remained an open question. An attempt to verify the hydroxyl method by a comparison with the spectral-line reversal method undertaken in reference 7 is not conclusive, since the reversal method is valid only under isothermal conditions, and these cannot possibly be assumed to apply in the column of a jet discharge (Saha calculations for a discharge in air are too crude because of the arbitrary choice of the effective ionization potential).

---

[1] A. D. Sakharov, Izv. Akad. Nauk SSSR, Ser. Fiz. **12**, 229 (1948).

[2] W. Wijk, Z. Physik **59**, 313 (1930).

[3] O. S. Duffendack and Kuang Tseng Chao, Phys. Rev. **56**, 176 (1939)

[4] T. Hori, Proc. Phys. Math. Soc. Japan **25**, 595 (1943).

[5] E. Lyman, Phys. Rev. **53**, 379 (1938).

[6] V. H. Kondrat'ev, *Free Hydroxyl*, State Inst. Tech. (1939).

[7] G. Critesku and R. Grigorovici, Bul. Soc. Roum. Phys. **42**, 78 (1941).

Attempts to verify the applicability of the hydroxyl method in other types of discharges have also been unsuccessful. In an investigation of the arc between copper electrodes at atmospheric pressure in air, Mikhalevskii and Prokof' eva[9] compared the temperature obtained by the hydroxyl method with the temperature determined from the intensity of iron lines. As stated above, however, in non-isothermal situations one can only discuss the excitation temperature of the iron lines in question.

Considerable interest attaches to the spectroscopic investigation of a jet discharge at reduced pressures because in this case conditions are realized which make feasible the verification of thehydroxyl method; namely, the appearance of bands due to stable molecules which are suitable for temperature measurements.

EXPERIMENT AND DISCUSSION

The experimental arrangement is essentially the same as that in reference 10. The operating frequency of the oscillator was 32-33 mc. The discharge tube and the electrodes were oil-cooled; this provided the possibility of prolonged photography under stable temperature conditions of the spectrum of the jet discharge. With the exception of the last two copper lines at rather high discharge powers, lines due to the metals in the electrode were not present in the discharge spectrum.

An ISP-22 spectroscope having a three-lens system for slit illumination was used. The slit width was 0.015 mm and the height of the intermediate-image diaphragm was 2 mm. With this choice of diaphragm the exposure was never greater than 2-3 hours. The mercury lines at 3132 Å and 3342 Å, which lie close to the portion of the discharge spectrum being studied, were used as intensity reference marks.

At atmospheric pressure the most intense band in the spectrum of the jet discharge in air is the 3064 Å band. With a reduction in pressure, starting at approximately 400 mm Hg the 2nd positive nitrogen system becomes quite strong (Fig. 2). The most suitable for the temperature determination is the (0,0) band at 3371 Å. The 3064 Å hydroxyl band partly overlaps the 2nd positive system (2,0) but the lines which are not overlapped remain sufficiently clear to permit a simultaneous temperature determination with the hydroxyl.

Assuming that at temperatures ranging from 2000 °K to 3500 °K the intensity of the lines of the Q_1-branch falls off rapidly with an increase in K, the most suitable branch for the temperature measurements is the P_1-branch, and this was used for the principal measurements. Lines for K equal to 4, 5, 8, 14, 16, 17, 18, and 19 were used. Separate measurements using the Q_1-branch yielded values which did not differ from the values measured using the P_1-branch by more than 1-2% which is within the limits of accuracy of this method. In those cases for which the intensity of the bands was not great enough, certain other lines of the 3064 Å band were used. The value of the intensity factor for the 3064 Å band was taken from references 6, 9. Missing values were calculated according to Earls[11]*.

In making the measurements with the 3371 Å nitrogen band, following Cristesku and Grigorovici, we used the value of i associated with the $^1\Pi - {}^1\Pi$ transition because in working with the ISP – 22 with $j > 28$ the branches $P_{1,2,3}$ of the $^3\Pi - {}^3\Pi$ transition run together and practically form one branch of the $^1\Pi - {}^1\Pi$ transition.

---

[8] K. N. Mochalov, A. Ia. Nikiforov and A. S. Bogonostsev, J. Exper. Theoret. Phys. USSR **20**, 474 (1950).

[9] V. D. Mikhalevskii and V. V. Prokof'eva, J. Exper. Theoret. Phys. USSR **20**, 7 (1950).

[10] G. S. Solntsev, M. E. Khokhlov and E. A. Rodina, J. Exper. Theoret. Phys. USSR **22**, 406 (1952).

* We may note that the use of the Hill-Van Vleck limit formulas, particularly by Cristesku and Grigorovici, leads to a temperature which is somewhat high (200 ° for a measured temperature of 4000°K and 50° for 2000 °K). In the work of Cristesku and Grigorovici this error was accidentally compensated by another: That due to the neglect of the ν^4 factor, which in the case of the P_1-branch leads a value which is too low by 250° for a measured temperature of 4000 °K and 65 ° for 2000 °K.

[11] L. T. Earls, Phys. Rev. **48**, 423 (1935).

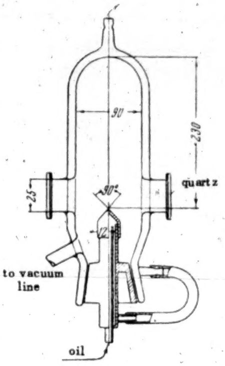

FIG. 1. Diagram of the apparatus (dimensions in mm)

After substitution of the calculated values of the constants, Eq. (1) assumes the form: for the 3064 Å band

$$0.00945\,\lg\frac{I}{i\nu^4} = C - \frac{K(K+1)}{T} \tag{2}$$

for the 3371 Å band

$$0.89\cdot\lg\frac{i}{i\nu^4} = C - \frac{J(J+1)}{T} \tag{3}$$

(J is the value of the total angular momentum including the electron spins, and K is the value exclusive of the electronic spin).

In Fig. 3 are shown plots of Eqs. (2) and (3) for the column of the jet discharge. Also shown are cases in which lines of the four branches ($P_{1,2}Q_{1,2}$) of the 3064 Å band were used.

We now consider the effect of self-absorption. Self-absorption, as is well known, is most important for the strongest lines of the band and this leads to a characteristic departure of the points from the line $\frac{I}{i\nu^4} = C + \frac{B}{kT} J(J+1)$ for the central portion[12]. In the present case this departure was not observed. Because of the freedom from self-absorption it is possible to reduce the estimate of the optical thickness $\tau = k_0 l$ for the strongest lines of the bands in question. The estimate was made on the basis of a pressure of 200 mm Hg and a temperature of 3000 °K. At this temperature the most intense lines are those of the P_1 - branch of the 3064 Å band with $K = 7$ and the P - branch of the 3371 Å band with $J = 25$. Under these conditions the concentration of water molecules is $\sim 10^{16}\,\mathrm{cm}^{-3}$ and the degree of thermal dissociation of the water is $\sim 10^{-1} - 10^{-2}$. Then the population of the level characterized by $K = 7$, $N_7 = 0.8\times10^{-2}$ is $N_{\mathrm{OH}} \sim 8\times10^{13}\,\mathrm{cm}^{-3}$. According to Kondrat'ev, k_0/N may be taken as $6.85\times10^{-16}\,\mathrm{cm}^{-1}$ (for 300 °K). Coverting to $T = 3000\,°\mathrm{K}$ ($k_0/N \sim 1/\sqrt{T}$) gives $k_0/N \sim 2\times10^{-16}\,\mathrm{cm}^{-1}$. From these data we find in any case that τ is less than 1.6×10^{-2} since l is less than 1 cm.

In nitrogen it is necessary to take account of the fact that the lower level of the $C^3\Pi_u - C^3\Pi_g$ has an excitation potential of 7.5 ev, whence it follows that the equilibrium concentration of nitrogen molecules in the $C^3\Pi_g$ state is approximately $5\times10^5\,\mathrm{cm}^{-3}$, $N_{25} = 27\times10^{-2} N_{C^3\Pi_g}$. The lifetime of the upper state is $\sim 10^{-8}$ sec and the Doppler width of the line is ~ 0.015 Å, thus $k_0/N \sim 10^{-12}\,\mathrm{cm}^{-1}$ and $\tau < 10^{-8}$ so that for $\tau \sim 1$ concentrations of nitrogen in the $C^3\Pi_g$ state exceeding equilibrium by a factor of 10^8 would be required and this is not very probable.

In the table are shown the results of measurements of the temperature at various pressures for those cases in which it was possible to carry out simultaneous measurements with nitrogen (T_{N_2}) and the hydroxyl (T_{OH}).

In view of the fact that the shape of the jet discharge varies markedly with changes in the power and the pressure, for definiteness all measurements were made in the part of the column close to the electrodes (point A, Fig. 4). The height of the flame h_1 (Fig. 4) was taken as a parameter with p = const.

From the present data it is apparent that for pressures above 100 mm Hg the temperatures as measured with the hydroxyl and with nitrogen are in agreement within the limits of the accuracy of the method (5%) and consequently that the temperature as measured with the hydroxyl yields the temperature of the neutral gas. At lower pressures the temperature measured by the hydroxyl method exceeds significantly the temperature of the neutral gas as determined with nitrogen. We may note that in certain pressure cases the temperature determination is not unique (Fig. 5).

---

[12] W. Lochte-Holtgreven and H. Maecker, Z. Physik 105, 1 (1937).

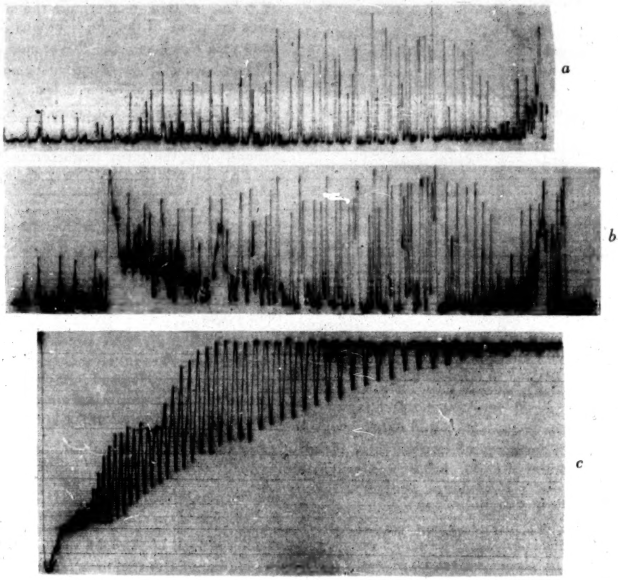

FIG. 2. Microphotograms** of the spectrum of the column of the jet discharge: *a*) 3064 Å band at atmospheric pressure; *b*) 3064 Å band at 100 mm Hg overlapped by the (2,0) band of the 2nd positive system of nitrogen; *c*) 3371 Å band of the 2nd positive system of nitrogen at 150 mm Hg.

From the given data it is also apparent that for pressures less than 150 mm Hg there occurs a rapid reduction in the temperature of the discharge.

It would seem that the disagreement between the rotational temperature for the hydroxyl and for nitrogen for $p < 100$ mm Hg is a direct indication of the nonisothermal conditions in the plasma of the column of the jet discharge at these pressures. However, the agreement of these temperatures at higher pressures is still not a sufficient basis for the converse conclusion. The fact that the hydroxyl method gives the correct values of the temperature of the neutral gas in the discharge can be explained by the fact that for $p > 100$ mm Hg the temperature in the jet discharge is sufficiently high for strong thermal dissociation of water. The molecules obtained under these conditions do not have surplus rotational energy. On going over to pressures < 100 mm Hg, however, along with the reduction of the temperature of the discharge there is an increase in the strength of the hydroxyl formation process which takes place by virtue of collisions between water molecules, and fast electrons with simultaneous excitation of anomalously high rotational levels.

Thus the possibility of applying the hydroxyl method under the conditions which obtain in the column of a jet discharge depends on the existence of a sufficiently high temperature, not lower than approximately 2500 °K. Experimentally this has

---

** The author is indebted to the director of the Crimean Astrophysics Observatory Acad. Sci. USSR for permission to use the self-recording microphotometer of the observatory.

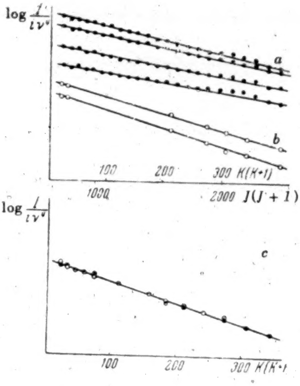

FIG. 3. *a*) *P*-branch of the 3371 Å band (100 mm); P_1 - branch of the 3064 Å band (210 mm); *c*) 3064 Å band (210 mm); ● P_1 - branch; O Q_1 - branch; ● Q_2-branch; ⊗ P_2- branch.

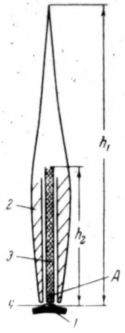

FIG. 4. Structure of the jet discharge: *1* - electrode; *2*- outer shell of the discharge; *3*- column of the discharge; *4* - electrode layer.

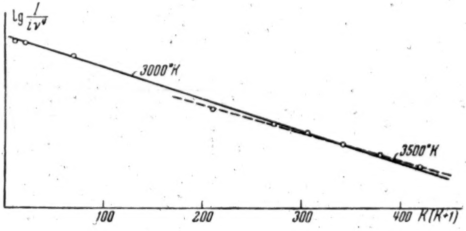

FIG. 5

been shown to hold up to a pressure of 316 mm Hg; but since there is no reason to expect that the temperature of the discharge is reduced to any significant degree upon a further increase of the pressure, these results should apply up to atmospheric pressure and beyond. Hence, the results of a temperature measurement in a jet discharge by the hydroxyl method and, in particular, those obtained by Cristesku and Grigorovici should be valid. The effect of a reduction of the temperature because of the concentration of the hydroxyl in the cooler peripheral parts of the discharge as noted by Mikhalevskii and Prokof'eva is considerably smaller in the present case presumably because of the lower source temperature; this makes it reasonable to suppose that the maximum hydroxyl concentration will be along the axis of the column of the discharge. Another basis for this conclusion is the agreement of the temperatures obtained with nitrogen and with the hydroxyl at pressures below 316 mm Hg. At

TABLE

p, mm Hg	h_1, mm	T_{OH} °K	T_{N_2} °K	$\lvert T_{OH} - T_{N_2}\rvert$
316	50	3610	3510	100
	70	3580	3620	40
	100	3640	3700	60
	150	3640	3570	70
210	50	3480	3410	70
	65	3690	3630	30
	70	3700	3520	180
	85	3570	3520	50
	180	3690	3630	60
	220	3670	3750	80
150	35	3140	3070	70
	50	3260	3250	10
	60	3220	3340	120
	80	3510	3400	110
	90	3480	3510	30
100	45	2370	2310	60
	55	2360	2670	190
	70	2820	2880	60
	85	3020	3100	20
66	40	2160	1970	190
	45	2530	1880	650
	60	2720	2100	620
	70	2980	2200	780
30	50	2300	2080	220
	70	2620	2290	330
	100	3010	2250	760

atmospheric pressure, where according to Cristesku and Grigorovici the temperature of the discharge reaches 4000 °K, this question apparently requires further study.

In conclusion we wish to take this opportunity to express our gratitude to Prof. N. A. Kaptsov for continued interest in the present work.

Translated by H. Lashinsky
249

SOVIET PHYSICS JETP VOLUME 2, NUMBER 3 MAY, 1956

Dielectric Losses in Ionic Dielectrics in Strong Electric Fields

L. E. GUREVICH AND V. N. GRIBOV

(Submitted to JETP editor February 22, 1954)
J. Exper. Theoret. Phys. USSR **29**, 629-636 (November, 1955)

Skanavi[1] introduced a representation for dielectrics containing ions which may be found in two neighboring positions of equilibrium in the crystalline lattice, and investigated the losses due to transitions of these ions between the two positions of equilibrium, in weak electric fields. In the present article, dielectric losses due to the same mechanism in strong fields are investigated. Three limiting cases are considered. The results of the calculations are summarized in formulas (33)-(34), (35)-(38), and (44)-(45).

1. GENERAL STATEMENTS

LET the probability of transition of an ion from the first position of equilibrium to the second, or the reverse, per unit time, be $\nu \exp(-U/kT)^2$. In the presence of an electric field, the energy barrier U changes. Expanding U in a series of powers of the field E, we may write

$$U' = U \mp pE, \qquad (1)$$

where the two signs refer to transitions of the ion in opposite directions. If $n_1 = n - \Delta n$, $n_2 = n + \Delta n$ are the number of ions in the two positions of equilibrium, per unit volume, then

$$\frac{\partial n_1}{\partial t} = -\frac{\partial n_2}{\partial t} = -n_1 \nu \exp\left\{-\frac{U - pE}{kT}\right\} + n_2 \nu \exp\left\{-\frac{U + pE}{kT}\right\}, \qquad (2)$$

and the dipole moment per unit volume is

$$P = (n_2 - n_1)\, p' = 2p'\Delta n, \qquad (3)$$

where $p' \approx p$ has the dimensions of a dipole moment, and an order of magnitude of 10^{-18}. By virtue of Eq. (2), P satisfies the equation

$$\frac{\partial P}{\partial t} = \frac{\overline{P} - P}{\tau}; \qquad (4)$$

where

$$\overline{P} = np' \tanh\frac{pE}{kT} \equiv P_0 \tanh\frac{pE}{kT}, \qquad (5)$$

and

$$\tau^{-1} = 2\nu e^{-U/kT} \cosh\frac{pE}{kT} \equiv \tau_0^{-1} \cosh\frac{pE}{kT}. \qquad (6)$$

Introducing the new variable

$$\vartheta = \int_0^t \tau^{-1}(x)\, dx, \qquad (7)$$

we obtain the solution of Eq. (4) in the form

$$P(\vartheta) = e^{-\vartheta} \int e^{\vartheta'}\, \overline{P}(\vartheta')\, d\vartheta' \qquad (8)$$

Let

$$E = E_0 \sin \omega t, \qquad (9)$$

and

$$pE_0 / kT = \alpha, \quad \omega t = x, \quad \omega\tau_0 = \beta. \qquad (10)$$

In order to obtain the losses in the stationary state, we exclude the influence of the instant of application of the field by assuming it to have occurred at $t = -\infty$. Then Eq. (8) gives

$$P(x) = \frac{P_0}{\beta} e^{-\vartheta(x)} \int_{-\infty}^{x} e^{\vartheta(y)} \sinh(\alpha \sin y)\, dy, \qquad (11)$$

where

$$\vartheta(x) = \frac{1}{\beta} \int_0^x \cosh(\alpha \sin y)\, dy. \qquad (12)$$

Hence, it is evident that the dipole moment depends on the two parameters α and β, Eq. (10) determining the dependence of the losses on the field E and the frequency ω.

As a consequence of the periodicity of the field the energy lost during the period T_0 is

$$q = \int_0^{T_0} E\, dP = \int_0^{2\pi} E \frac{dP}{dx}\, dx = -\int_0^{2\pi} P \frac{dE}{dx}\, dx.$$

Consequently, the losses per unit time are

$$Q = -\frac{\omega}{2\pi} E_0 \int_0^{2\pi} \cos x \cdot P(x)\, dx. \qquad (13)$$

---

[1] G. I. Skanavi, *Physics of Dielectrics*, GITTL, 1949

[2] Ia. I. Frenkel, *Kinetic Theory of Liquids*, Oxford, 1946; p 22.

In the future we will make use of the relation

$$\vartheta(x+n\pi)=\vartheta(x)+\vartheta(n\pi), \tag{14}$$

from which, according to Eq. (11), it follows that

$$P(x+n\pi) = \frac{P_0}{\beta}e^{-\vartheta(x)-\vartheta(n\pi)}\int\limits_{-\infty}^{x+n\pi}e^{\vartheta(y)}\sinh(\alpha\sin y)\,dy = (-1)^n P(x). \tag{15}$$

2. LOSSES AT LOW FREQUENCIES

The methods for calculating $P(x)$ are somewhat different for $\beta \lesssim 1$ and for $\beta \gg 1$, i.e., for low and for high frequencies. In the first case, it is convenient to transform Eq. (11) for $P(x)$ on the basis of Eq. (12) for $\theta(x)$:

$$P=\frac{P_0}{\beta}e^{-\vartheta(x)}\int\limits_{-\infty}^{x}e^{-\vartheta(y)}\{\cosh(\alpha\sin y) - e^{-\alpha\sin y}\}\,dy = P_0\Big[1-\frac{1}{\beta}e^{-\vartheta(x)}\int\limits_{-\infty}^{x}e^{\vartheta(y)-\alpha\sin y}dy\Big] \equiv P_0(1-J), \tag{16}$$

whence, in virtue of Eq. (16), the losses are

$$Q=\frac{\omega}{\pi}E_0P_0\int\limits_0^{\pi}\cos xJ(x)\,dx\equiv Q_1+Q_2, \tag{17}$$

$$Q_1=\frac{\omega}{\pi}E_0P_0\int\limits_0^{\pi/2}\cos xJ(x)\,dx;$$

$$Q_2=\frac{\omega}{\pi}E_0P_0\int\limits_{\pi/2}^{\pi}\cos xJ(x)\,dx,$$

where

$$J(x) = \frac{1}{\beta}\int\limits_{-\infty}^{x}\exp[-\{\vartheta(x)-\vartheta(y)+\alpha\sin y\}]\,dy \tag{18}$$

$$=\frac{1}{\beta}\int\limits_{-\infty}^{0}\exp[-\{\vartheta(x)-\vartheta(x+y) + \alpha\sin(x+y)\}]\,dy=\frac{1}{\beta}\int\limits_0^{\infty}\exp\Big[-\Big\{\alpha\sin(x-y) + \frac{1}{\beta}\int\limits_0^{y}\cosh[\alpha\sin(x-z)]\,dz\Big\}\Big]dy.$$

When $\alpha \gg 1$, the integral in the braces, rapidly increasing with an increase of y, has primary importance. Therefore, for the calculation of J, the essential region is $y \ll 1$, and hence, $z \ll 1$. Expanding $\sin(x-y)$ and $\sin(x-z)$ in a series of powers of y and z, and limiting the series to the first powers, we are able to perform the integration. Considering, on the basis of Eq. (15), the first half of a period ($\sin x > 0$), denoting

$$\alpha\cdot\sin y=\xi;\quad \alpha\beta\cos x=\eta \tag{19}$$

and introducing the variable

$$\tau=\alpha\cdot|\cos x|\cdot y,$$

we obtain:

if $0<\omega t<\pi/2$ or $\eta>0$, (20

$$J=J_1=\frac{1}{\eta}\exp\Big\{-\frac{1}{\eta}\sinh\xi-\xi\Big\}\int\limits_0^{\infty}\exp\Big\{-\frac{1}{\eta}\sinh(\tau-\xi)+\tau\Big\}\,d\tau,$$

and if $\pi/2<\omega t<\pi$ or $\eta<0$,

$$J=J_2=-\frac{1}{\eta}\exp\Big\{-\frac{1}{\eta}\sinh\xi-\xi\Big\}\int\limits_0^{\infty}\exp\Big\{\frac{1}{\eta}\sinh(\tau+\xi)-\tau\Big\}\,d\tau.$$

It is easy to verify that when $\xi = 0$ the sum of the two expressions is equal to two, which corresponds [by Eq. (17)] to the condition

$$P(0)+P(\pi)=0, \tag{21}$$

when $x = \pi/2$ both expressions tend toward zero exponentially, so that the region of values of $x \approx \pi/2$ is nonessential, and in the future we exclude it from consideration.

In order to evaluate the conditions of applicability of the expansions in powers of y and z, which led to Eq. (20), it is necessary to perform the expansion in Eq. (18) up to the second order of the small quantities, and to determine the conditions under which the additional terms are insignificant in the essential region. In this way we arrive at the conditions:

for $\alpha = pE_0/kT \gg 1$

$$\operatorname{arc\,sinh}^3\alpha\omega\tau_0\gg\alpha^2, \tag{22}$$

and for $\alpha \lesssim 1$

$$\beta^2 = (\omega\tau_0)^2 \gg 1. \tag{23}$$

3. CALCULATION OF POLARIZATION LOSSES

Let us denote the integrals J_1 and J_2 in Eq. (20) by

$$J = \frac{1}{|\eta|} \exp\left\{\mp \frac{1}{\eta} \sinh\xi - \xi\right\} \times \int_0^\infty \exp\left\{-\frac{1}{|\eta|} \sinh(\tau \mp \xi) \pm \tau\right\} d\tau. \tag{24}$$

They are calculated simply when $|\eta| = \alpha\beta\,|\cos x| \gg\ll 1$.

Let us consider first the case $|\eta| \gg 1$ or

$$\alpha\beta = \frac{pE_0}{kT}\,\omega\tau_0 \gg 1, \tag{25}$$

which is possible only when the conditions of Eq. (22) are fulfilled.

Let us denote

$$\rho = \operatorname{arc\,sinh} |\eta| \approx \ln 2\,|\eta|, \qquad z = \tau - \rho \mp \xi. \tag{26}$$

Then the expression in the exponent in Eq. (24) becomes

$$-\xi - \frac{1}{|\eta|}\sinh(\tau \mp \xi) \pm \tau = -\frac{\sinh(z+\rho)}{\sinh\rho} \pm (z+\rho) = -\sinh z \coth\rho - \cosh z \quad \pm(z+\rho).$$

But when $|\eta| \gg 1$, $\coth\rho \approx 1$, and we get

$$e^{-z} \pm (z+\rho),$$

Therefore

$$J = \frac{1}{|\eta|} \exp\left\{\mp \frac{1}{|\eta|} \sinh\xi\right\} \times \int_{-\xi-\rho}^{\infty} \exp\{-(e^z \mp z) \pm \rho\}\, dz.$$

Letting $e^z = t$, we get

$$J_1 = 2\exp\left\{-\frac{1}{|\eta|}\sinh\xi\right\} \int_{e^{-(\xi+\rho)}}^{\infty} e^{-t}\,dt = 2\exp\left(-\frac{1}{|\eta|}\left\{\sinh\xi + \frac{1}{2}e^{-\xi}\right\}\right) = 2\exp\left(-\frac{1}{2|\eta|}e^{\xi}\right),$$

$$J_2 = \frac{1}{2\eta^2}\exp\left\{\frac{1}{|\eta|}\sinh\xi\right\} \times \int_{\xi-\rho}^{\infty} \exp\{-e^z - z\}\,dz. \tag{27}$$

Letting $e^z = t$, we get

$$J_2 = -\frac{1}{2\eta^2}\exp\left\{\frac{1}{|\eta|}\sinh\xi\right\} \int_{e^{\xi-\rho}}^{\infty} e^{-t}\,\frac{dt}{t^2} = \frac{1}{|\eta|}\exp\left\{\frac{1}{|\eta|}\sinh\xi - \xi\right\}\exp\left[-(e^{\xi-\rho})\right] + O,$$

where O is a term of the order $\frac{1}{\eta^2}\ln|\eta|$. Disregarding the additional term, we have

$$J_2 = \frac{1}{|\eta|}\exp\left\{-\frac{1}{2|\eta|}e^{-\xi} + \xi\right\}.$$

Finally, disregarding the first of the quantities which are added in the square brackets, we find

$$J_2 = \frac{1}{|\eta|}e^{-\xi}. \tag{28}$$

Formulas (27) and (28) are unvalid only in the neighborhood of $x = \frac{\pi}{2}$, but in this case the integrals J_1 and J_2 tend toward zero exponentially. Finally, we have for $|\eta| \gg 1$:

$$P = P_0\left[1 - 2\exp\left(-\frac{1}{2|\eta|}e^{\xi}\right)\right], \quad \eta > 0, \qquad P = P_0\left[1 - \frac{1}{|\eta|}e^{-\xi}\right], \quad \eta < 0. \tag{29}$$

Let us proceed now to the case $|\eta| \ll 1$, i.e.,

$$\alpha\beta = \frac{pE_0}{kT}\,\omega\tau_0 \ll 1, \tag{30}$$

which corresponds to the low frequencies, $\omega\tau_0 \ll 1$. In this case, in the expression for J, Eq. (24), only small values of τ contribute essentially. Expanding $\sinh(\tau \pm \xi)$ in a series of powers of τ and integrating, we get

$$J = \frac{1}{\cosh\xi}e^{-\xi}\left(1 \pm \frac{|\eta|}{\cosh\xi}\right)$$

$$= \frac{1}{\cosh\xi}e^{-\xi}\left(1 + \frac{\alpha\beta\cos x}{\cosh\xi}\right), \quad (31)$$

$$P(x) = P_0\left\{1 - \left(\frac{1}{\cosh\xi} + \frac{\alpha\beta\cos x}{\cosh^2\xi}\right)e^{-\xi}\right\}. \quad (32)$$

Now let us determine the magnitude of the losses. When $|\eta| \gg 1$ Eq. (29) decreases exponentially with an increase of $\xi \doteq \alpha\sin x$; therefore only small values of x are essential, and we may write $\eta = \alpha\beta\cos x \approx \alpha\beta$. Introducing the variable $\sin x = t$, we get

$$Q = Q_1 + Q_2 = \frac{\omega}{\pi}E_0P_0$$

$$\times \left\{\int_0^1 2\exp\left(-\frac{1}{2\alpha\beta}e^{\alpha t}\right)dt - \frac{1}{\alpha\beta}\int_0^1 e^{-\alpha t}dt\right\}.$$

After some simple transformations, taking into account $e^{\alpha} \gg 1$, we get

$$Q = \frac{\omega}{\alpha\pi}E_0P_0\left\{-2\mathrm{Ei}\left[-\frac{1}{2\alpha\beta}\right] - \frac{1}{\alpha\beta}\right\}.$$

Since, for $x \ll 1$,

$$\mathrm{Ei}[-x] = \ln\gamma x,$$

where $\gamma = e^C = 1.78$ (C is Euler's constant), then

$$Q = \frac{\omega}{\alpha\pi}E_0P_0\left\{2\ln\frac{2\alpha\beta}{\gamma} - \frac{1}{\alpha\beta}\right\}.$$

Returning to the original variables, we get (still disregarding the second term)

$$Q = 2\frac{\omega kTn}{\pi}\frac{p'}{p}\ln\left(1.122\frac{pE_0}{kT}\omega\tau_0\right), \quad (33)$$

under the conditions:

$$\frac{pE_0}{kT} > 1, \quad \frac{pE_0}{kT}\omega\tau_0 > 1,$$

$$\operatorname{arc\,sinh}\frac{pE_0}{kT}\omega\tau_0 < \left(\frac{nE_0}{kT}\right)^2. \quad (34)$$

In the opposite limiting case $|\eta| \ll 1$, the first term in Eq. (31) when multiplied by $\cos x$ in accordance with Eq. (17) and integrated from zero to π gives zero. This leaves only the second term:

$$Q = \alpha\beta\frac{\omega}{\pi}E_0P_0\int_0^{\pi}\frac{\cos^2 x}{\cosh^2\xi}e^{-\xi}dx \quad (35)$$

$$= \frac{2}{\pi}n\frac{p'pE_0^2}{kT}\omega^2\tau_0 f\left(\frac{pE_0}{kT}\right),$$

where

$$f(\alpha) = \int_0^1 \frac{e^{-\alpha x}}{\cosh^2\alpha x}\sqrt{1-x^2}\,dx. \quad (36)$$

The function $f(\alpha)$ decreases monotonically with increasing α

$$f(\alpha) = \frac{\pi}{4} - \frac{\alpha}{3} \qquad \text{when } \alpha < 1,$$

$$f(\alpha) = \frac{1}{\alpha}\left(\frac{\pi}{2} - 1\right) \quad \text{when } \alpha > 1. \quad (37)$$

Eqs. (35)-(37) are valid under the conditions:

$$(pE_0/kT)\,\omega\tau_0 < 1, \quad \omega\tau_0 < 1. \quad (38)$$

4. LOSSES AT HIGH FREQUENCIES

We now return to Eqs. (11) and (12).

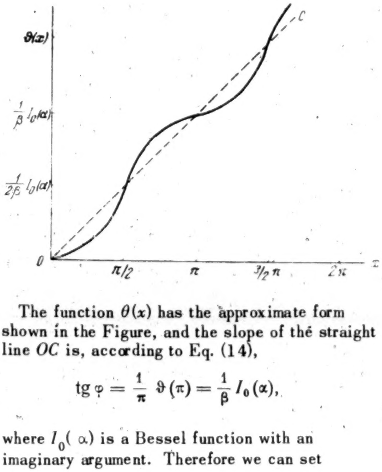

The function $\theta(x)$ has the approximate form shown in the Figure, and the slope of the straight line OC is, according to Eq. (14),

$$\operatorname{tg}\varphi = \frac{1}{\pi}\vartheta(\pi) = \frac{1}{\beta}I_0(\alpha),$$

where $I_0(\alpha)$ is a Bessel function with an imaginary argument. Therefore we can set

$$\vartheta(x) = \frac{1}{\beta}I_0(\alpha)x + \psi(x), \quad (39)$$

where

$$\psi(x) = \frac{1}{\beta}\int_0^x\{\cosh(\alpha\sin y)$$

$$- I_0(\alpha)\}dy \leqslant \frac{1}{\beta}I_0(\alpha) \quad (40)$$

and has a period of π. We set

$$\frac{1}{\pi}\vartheta(\pi) = \frac{I_0(\alpha)}{\omega\tau_0} \ll 1, \quad (41)$$

substitute Eq. (39) into Eq. (11) and expand in a series of powers of ψ. Taking into account the inequalities (40) and (41), we have

$$P(x) = \frac{P_0}{\beta}\exp\left\{-\frac{1}{\beta}I_0(\alpha)\,x\right\}$$

$$\times\left[\int_{-\infty}^{x}\exp\left\{\frac{1}{\beta}I_0(\alpha)\,y\right\}\sinh(\alpha\sin y)\,dy\right.$$

$$-\psi(x)\int_{\infty}^{x}\exp\left\{\frac{1}{\beta}I_0(\alpha)\,y\right\}\sinh(\alpha\sin y)\,dy \qquad (42)$$

$$\left.+\int_{\infty}^{x}\exp\left\{\frac{1}{\beta}I_0(\alpha)\,y\right\}\psi(y)\sinh(\alpha\sin y)\,dy\right]$$

$$\equiv P_1 + P_2 + P_3.$$

We develop $\psi(xq)$ and sinh $(\alpha\sin y)$ in Fourier series:

$$\psi(x) = \sum_{n=1}^{\infty} a_n \sin 2nx,$$

$$\sinh(\alpha\sin y) = \sum_{k=0}^{\infty} b_{2k+1}\sin(2k+1)\,y,$$

where $a_n = \frac{1}{\pi}(-1)^n\frac{1}{\beta}I_{2n}(\alpha)$, $b_{2k+1} = 2(-1)^k I_{2k+1}(\alpha)$,

since both functions are odd. Then the losses are equal to

$$Q = -\frac{\omega E_0}{2\pi}\int_{-\pi}^{\pi}P(x)\cos x\,dx \qquad (43)$$

$$= Q_1 + Q_2 + Q_3,$$

corresponding to the three parts of Eq. (42).

After some simple calculations we get

$$Q_1 = E_0P_0\omega\,\frac{(1/\beta)\,I_1(\alpha)}{1+(I_0^2(\alpha)/\beta^2)},$$

$$Q_2 = \frac{E_0P_0\omega}{\pi^2}\,\frac{I_0(\alpha)}{\beta^3}\sum_{k=1}^{\infty}I_2\;(\alpha)\,I_{2k+1}(\alpha)\,\frac{1}{(I_0^2(\alpha)/\beta^2)+(2k+1)^2},$$

$$Q_3 = \frac{E_0P_0\omega}{\pi^2}\,\frac{I_0(\alpha)}{\beta^3}\sum_{k=1}^{\infty}\frac{I_{2k}(\alpha)}{k}\,(I_{2k+1}(\alpha)+I_{2k+1}(\alpha))\,\frac{1}{(I_0^2(\alpha)/\beta^2)+(2k+1)^2}.$$

Since the small parameter in the expansion whose square we are neglecting is $\frac{1}{\beta}I_0(\alpha)$, then to our approximation,

$$Q_1 + Q_2 + Q_3 = E_0P_0\omega\cdot\frac{1}{\beta}I_1(\alpha),$$

and consequently

$$Q = \frac{E_0P_0}{\tau_0}\,I_1\left(\frac{pE_0}{kT}\right), \qquad (44)$$

under the condition

$$\frac{I_0^2(pE_0/kT)}{\omega^2\tau_0^2} \ll 1. \qquad (45)$$

From Eqs. (35) and (44) we see that, just as in the case of a weak field[1], the losses increase with frequency at low frequencies and are independent of frequency at high frequencies.

Translated by D. Lieberman and M. Mestchersky
247

Letters to the Editor

Interaction of Nucleons through a Pseudoscalar Meson Field

A. A. RUKHADZE
P. N. Lebedev Physical Institute,
Academy of Sciences, USSR

(Submitted to JETP editor February 9, 1955)
J. Exper. Theoret. Phys. USSR **29**, 709-711 (November, 1955)

IN 1945 Tamm[1] (see also reference 2) suggested a quantum mechanical method for investigating relativistic problems in particle interactions. A covariant formulation of Tamm's method was later given by Cini[3].

We have applied Tamm's method to the problem of the interaction of nucleons through a pseudoscalar meson field. In the first Tamm approximation for pseudoscalar coupling, the integral equation for a two nucleon system is obtained from the Hamiltonian:

$$H(x) = -\frac{if}{2}[\bar{\psi}_\alpha(x),\ \psi_\beta(x)](\gamma_5\tau_i)^i_{\beta\alpha}\varphi_i(x), \tag{1}$$

and for pseudovector coupling, from the Hamiltonian:

$$H(x) = \overset{i}{\underset{\mu}{j}}(x)\frac{\partial\varphi_i(x)}{\partial x_\mu} + (j_\mu n_\mu)^2, \tag{2}$$

where

$$\overset{i}{\underset{\mu}{j}}(x) = -\frac{ig}{2}\overline{[\psi}_\alpha(x),\ \psi_\beta(x)](\gamma_5\gamma_\mu\tau i)_{\beta\alpha}. \tag{3}$$

In the first Tamm approximation the following probability amplitudes are taken different from zero:

$$\langle\Psi_0^*|\psi_\alpha^+\psi_\beta^+|\Psi(\sigma)\rangle$$

$$= A^\sigma_{\alpha\beta}(x_1,\ x_2) \text{ (amplitude sought)}$$

$${}_0\langle\psi_\alpha^+\psi_\beta^+\varphi_i^+|\Psi(\sigma)\rangle \quad \text{and} \quad {}_0\langle\bar{\psi}_\alpha^+\psi_\beta^+\psi_\gamma^+\psi_\delta^+\varphi_i^+|\Psi(\sigma)\rangle$$

The equations are investigated by the following renormalization program: All divergent terms in the equation due to unobservable vacuum fluctuations ("vacuum diagrams") are removed. The divergent terms remaining in the equations correspond to self-energies of the nucleons, and are written as

$$-\frac{3ig^2}{4}\int_{-\infty}^{\sigma}dx_1\int_{-\infty}^{\sigma_1}dx_2\{S^+(x''-x_1) \tag{3'}$$

$$\times N(x_2-x_1)A^{\sigma_2}(x_2,\ x')$$

$$-S^+(x'-x_1)N(x_2-x_1)A^{\sigma_2}(x_2,\ x'')$$

$$+S^+(x''-x_2)N(x_1-x_2)A^{\sigma_2}(x_1,\ x')$$

$$-S^+(x'-x_2)N(x_1-x_2)A^{\sigma_2}(x_1,\ x'')\}.$$

For pseudoscalar coupling,

$$N(x_2-x_1) \equiv \gamma_5 S_F(x_2-x_1)\gamma_5\Delta_F(x_2-x_1) \tag{4}$$

$$\equiv -\frac{4}{(2\pi)^8}\int I_1(p)\,e^{ip(x_2-x_1)}\,dp$$

$$= -\frac{4}{(2\pi)^8}\int dp\,e^{ip(x_2-x_1)}\int\frac{\gamma_5(\mathrm{p}-\mathrm{k}+m)\gamma_5 dk}{[(p-k)^2-m^2](k^2-\mu^2)}$$

For pseudovector coupling,

$$N(x_2-x_1) \tag{5}$$

$$\equiv \gamma_5\gamma_\mu S_F(x_2-x_1)\gamma_5\gamma_\nu\frac{\partial^2\Delta_F(x_2-x_1)}{\partial x_{1\mu}\partial x_{2\nu}} + m\Delta^{(1)}(0)$$

$$= -\frac{4}{(2\pi)^8}\int e^{ip(x_2-x_1)}I_2(p)\,dp + m\Delta^{(1)}(0).$$

The quantity $I(p)$ can be written in the form

$$I(p) = I(m) + \sum_{n=1}^{N}(p-m)^n A_n - I_c(p) \tag{6}$$

and therefore

$$N(x_2-x_1) = B_0\delta(x_2-x_1) \tag{7}$$

$$+\sum_{n=1}^{N}B_n\int e^{ip(x_2-x_1)}(p-m)^n dp + N_c(x_2-x_1)$$

(for pseudoscalar coupling $N = 1$, for pseudovector coupling $N = 3$).

The introduction of terms B_0 into the equations for a two nucleon system is prevented by mass renormalization, and terms which contain B_n are rejected. As a result of this, we can make the following substitution in Eq. (3)

$$N(x) \to N_c(x),$$

where

$$N_{\mathbf{r}}(x)=\frac{-1}{(8\pi^4)^2}\int e^{ipx}I_{1,2c}(p)\,dp. \tag{8}$$

In the momentum representation, the equation for a two nucleon system in the center of mass takes the following form

$$(2E-W)A^{rs}(k,j)=[\cdots]-g^2F(E)A^{rs}(k,J), \tag{9}$$

where [. . .] denotes the terms corresponding to the noncovariant Tamm theory[2].

The last terms of Eq. (9) arise by separating finite parts from the divergent terms of the equation;

$$F(E)\sim\int\frac{(E-m)I_c(p_4\gamma_4-\mathbf{k}\vec{\gamma})}{(3E-W-p_4)(E-W+p_4)}\,dp_4. \tag{10}$$

The denominator in Eq. (10) is obtained from the finite limits of integration with respect to time in the divergent terms of Eq. (3). Asymptotically, for large values of p_4, $l_{1c}(p)\sim p_4$(pseudoscalar coupling), $l_{2c}\sim p_4^3$ (pseudoscalar coupling). Therefore, for pseudovector coupling, the integral (10) diverges, and accordingly, the integral equation (9) is not free of divergences. Thus the proposed renormalization program does not lead to a definite result for pseudovector coupling. We note that in perturbation theory, divergences of this type do not arise, thanks to the infinite limits of integration with respect to time.

$F(E)$ is finite for pseudoscalar coupling.

We thus find for pseudoscalar coupling a) for large k, i.e., for small distances between particles, $F(E)\to 0$, and accordingly the form of the interaction does not differ from the results of reference 2; b) for small k, i.e., for large distances between particles,

$$F(E)=\frac{k^2}{m}\varphi(\gamma),$$

where

$$\varphi(\gamma)=\frac{3f^2}{4\pi(2\pi)^3}\times\int_0^1 dx\,\frac{[\gamma x^2-(x-1)^2][2\gamma x-(\gamma+1)x^2-x+2]x}{\sqrt{(1-\gamma)x^4+(\gamma-2)x^2+x}\,[\gamma x+(x-1)^2]}; \tag{11}$$

$\gamma\equiv\mu^2/m^2$. For small values of γ, $\varphi(\gamma)>0$, in particular for $\gamma=1/36$, $\varphi(\gamma)>0$.

It therefore follows that the computation of renormalized terms in the equations for a two nucleon system with pseudoscalar coupling is equivalent to a decrease in the nucleon mass

$$m^*=m/1+\varphi(\gamma). \tag{12}$$

After this analysis was completed, there appeared an article[4] in which it was shown that higher Tamm approximations in the equations of a two nucleon system with pseudoscalar coupling lead to divergences similar to those described above for the pseudovector coupling. This shows that the proposed renormalization program in principle does not remove divergence difficulties which arise for the pseudoscalar as well as for the pseudovector coupling.

In conclusion, I wish to take this occasion to express my gratitude to V. B. Silin for suggesting this problem and for his constant help during the analysis.

---

[1] I. E. Tamm, J. of Phys. USSR **5**, 1 (1945).

[2] I. E. Tamm, V. P. Silin and V. Ia. Feinberg, J. Exper. Theoret. Phys. USSR **24**, 3 (1953).

[3] M. Cini, Nuovo Cimento **10**, 526, 614 (1953).

[4] H. Lehman, Z. Naturforsch **8a**, 579 (1953).

Translated by M. A. Melkanoff
265

The Connection between the Distribution of a Quasi-monochromatic Stationary Process and the Distribution of Its Envelope

S. M. RYTOV
P. N. Lebedev Physical Institute
Academy of Sciences, USSR

(Submitted to JETP editor July 23, 1955)
J. Exper. Theoret. Phys. USSR **29**, 702-703
(November, 1955)

BLANC-Lapierre and coworkers[1] have recently shown that if one knows the characteristic function $f_\xi(u)$ of a quasi-monochromatic stationary random process $\xi(t)=A\cos(\omega_0t-\theta)$ (A and θ are functions of t, slowly varying compared to $\cos\omega_0t$) then the probability distribution $W_A(A)$ of the envelope $A(t)$ can be obtained using the Hankel transform:

$$\frac{w_A(A)}{A}=\int_0^\infty f_\xi(u)\,J_0(Au)\,u\,du, \tag{1}$$

where J_0 is the zero order Bessel function. From this it follows that if ξ is distributed normally, then A follows the Rayleigh distribution.

Hence, knowing $f_\xi(u)$, one can use the Fourier transform to obtain the distribution of ξ:

$$w_\xi(\xi) = \frac{1}{2\pi}\int_{-\infty}^{+\infty} f_\xi(u)e^{-iu\xi}du\,, \tag{2}$$

while the Hankel transform gives the distribution of the amplitude A. This elegant result is based on the following conditions: 1) A and θ are independent and 2) θ is distributed uniformly in the interval $(0, 2\pi)$. It is not difficult to show that both these are necessary conditions for $\xi(t)$ to be stationary, taking the two-dimensional distribution $w(A, \theta)$ to be stationary. The latter must have the form $w(A, \theta)\,dA\,d\theta = w_A(A)\,dA\,d\theta/2\pi$ or else the process $\xi(t)$ will not be stationary.

In the present note I should like to show that (1) and (2) can be used to derive a formula which gives $w_\xi(\xi)$ directly in terms of $w_A(A)$. Indeed, according to (1) we have

$$f_\xi(u) = \int_0^\infty w_A(A)J_0(Au)\,dA.$$

In conjunction with (2) this gives

$$w_\xi(\xi) = \int_0^\infty w_A(A)\,dA\,\frac{1}{2\pi}\int_{-\infty}^{+\infty} J_0(Au)e^{-i\xi u}du\,.$$

The inner integral is $1/\pi\sqrt{A^2-\xi^2}$ when $A \geq |\xi|$ and zero for $A < |\xi|$[2], so that

$$w_\xi(\xi) = \frac{1}{\pi}\int_{|\xi|}^{\infty}\frac{w_A(A)\,dA}{\sqrt{A^2-\xi^2}}, \tag{3}$$

or, introducing the new variable of integration x, $A = |\xi|\,\mathrm{ch}\,x$

$$w_\xi(\xi) = \frac{1}{\pi}\int_0^\infty w_A(|\xi|\cosh x)\,dx \tag{4}$$

It is easy to verify that the Rayleigh distribution for A:

$$w_A(A) = \frac{A}{\sigma^2}e^{-A^2/\sigma^2}$$

implies by formula (4), the normal distribution for ξ with mean square $\overline{\xi^2} = \sigma^2$. If the amplitude is fixed, i.e., $w_A(A) = \delta(A - A_0)$ then from (3) it follows that

$$w_\xi(\xi) = \begin{cases} 1/\pi\sqrt{A_0^2-\xi^2} & (|\xi| \leqslant A_0), \\ 0 & (|\xi| > A_0). \end{cases}$$

The uniform distribution for A, i.e., $w_A(A) = 1/A_0$ for $A \leq A_0$ and $w_A(A) = 0$ for $A > A_0$ gives, according to (4)

$$w_\xi(\xi) = \begin{cases} \dfrac{1}{2\pi A_0}\ln\left(\dfrac{A_0+\sqrt{A_0^2-\xi^2}}{A_0-\sqrt{A_0^2-\xi^2}}\right) & (|\xi| \leqslant A_0) \\ 0 & (|\xi| > A_0). \end{cases}$$

The exponential distribution $w_A(A) = \alpha e^{-\alpha A}$ for the amplitude A leads to a Macdonald function of zero order for the distribution of ξ.

$$w_\xi(\xi) = \frac{\alpha}{\pi}\int_0^\infty e^{-\alpha|\xi|\cosh x}dx = \frac{\alpha}{\pi}K_0(\alpha\xi).$$

---

[1] A. Blanc-Lapierre, M. Savelli and A. Tortrat, Ann. Telécomm. **9**, 237 (1954).

[2] I. M. Ryzhik and I. S. Gradshtein, *Tables of Integrals, sums, series and products*, Moscow, Leningrad, 1951, p. 268 .

Translated by R. Krotkov
260

The Fermi-Yang Hypothesis

S. S. Filippov
Institute of Nuclear Problems
Academy of Sciences of the USSR

(Submitted to JETP editor December 18, 1954)
J. Exper. Theoret. Phys. USSR **29**, 707-708
(November, 1955)

According to the Fermi-Yang hypothesis a π-meson is considered as a composite particle consisting of a proton and an anti-neutron in a bound state. In the work of Fermi and Yang[1] the interaction between a nucleon and an anti-nucleon is approximated by a potential well whose width is equal to the nuclear Compton wavelength, $r_0 = \hbar/Mc$, and whose depth is determined by the requirement that the lowest energy eigenvalue of the system equals the meson rest energy $E = \mu c^2$. With this condition they obtain the value $V_0 = 26.5\ Mc^2$ for the depth of the well in the formation of the ${}^1S_0$ proton-anti-neutron system.

In recent years, a series of particles have been discovered with mass intermediate between that of nucleons and π-mesons. Such a family of particles may also be considered from the point of view of the Fermi-Yang hypothesis, i.e., as nucleon-anti-nucleon systems in bound states. It is interesting to compare the value of the interaction potential obtained in this case with the enormously strong potential obtained by Fermi and Yang by considering the π-meson as a composite particle.

Fermi and Yang have considered the problem in the two particle approximation. The Schrödinger equation for the proton-anti-neutron system is as follows:

$$[-c\hbar i(\vec{\alpha}_P - \vec{\alpha}_A)\vec{\nabla} \qquad (1)$$

$$+ Mc^2(\beta_P + \beta_A) - V(r)(1 - \vec{\alpha}_A\vec{\alpha}_P)]\,\psi = E\psi,$$

where ψ is a 16-components wave function, r is the relative coordinate and the indices P and A refer to the proton and the anti-neutron. Given an interaction potential $V(r)$ in the form of a well of width r_0 and depth V_0, the continuity condition on the logarithmic derivative of the wave function at $r = r_0$ gives[2] for the state ${}^1S_0$:

$$k \operatorname{ctg} k_{r_0} = -k_0, \qquad (2)$$

where

$$k^2 = \frac{E(8V_0^2 - 2V_0E + 4M^2c^4 - E^2)}{4(\hbar c)^2(2V_0 - E)}, \qquad (3)$$

$$k_0^2 = \frac{4M^2c^4 - E^2}{4(\hbar c)^2} \qquad (4)$$

The value of the potential depth V_0 can be found from Eq. (2) for various stipulated values of $E = \mu c^2$ and $r_0 = \hbar c/\kappa$ (κ is the rest mass of the composite particle; if it is assumed that the Fermi-Yang force arises from quanta exchange, then the parameter κ corresponds to their rest energy). The value of V_0 is given in the Table below for various values of E and κ. All quantities are given in units of Mc^2. For π-mesons $\mu \approx 0.15\,M$ (i.e., $E \approx 0.15$) and with $r_0 = \hbar/Mc$ ($\kappa = 1$) we have the value obtained by Fermi and Yang $V_0 \approx 26.5$; for τ-, κ-, χ-particles for $r_0 = 2\hbar/Mc$ ($\kappa = 0.5$), $V_0 \approx 2.2$, i.e., about 2 bev. The maximum possible value of the masses $\mu = E/c^2$ of the constructed particles diminishes with increasing value of r_0.

$\varkappa = 1.2$		$\varkappa = 1.0$		$\varkappa = 0.8$		$\varkappa = 0.6$		$\varkappa = 0.4$		$\varkappa = 0.2$	
E	V_0	E	V_0	E	V_0	E	V_0	E	V_0	E	V_0
0.15	37.7	0.13	30.5	0.09	31.5	0.12	14.4	0.11	7.8	0.12	2.0
0.72	7.3	0.46	8.7	0.37	7.4	0.83	1.1	0.54	1.2		
1.09	4.5	0.81	4.6	0.96	2.3						
1.25	3.7	1.26	2.4	1.14	1.3						
1.54	2.5	1.43	1.5								
1.66	1.9										

The present calculation was suggested by Prof. Ia. P. Terletskii.

---

[1] E. Fermi and C. N. Yang, Phys. Rev. 76, 1739 (1949).

[2] L. D. Landau and E. M. Lifshitz, *Quantum Mechanics*, vol. 1, p. 140, GTTI, 1948.

Translated by M. A. Melkanoff

On the Development by Means of Leaders of the Process of Breakdown of Liquids

(Reply to the Remarks of G. A. Vorob'ev)

I. E. BALYGIN

J. Exper. Theoret. Phys. USSR 29, 708-709
(November, 1955)

IN one of the 1954[1] issues of JETP there were published some remarks by G. A. Vorob'ev on my article[2] which dealt with the question of pre-breakdown currents in liquids. These remarks referred to my conclusion that in the absence of a limitation on the discharge current the breakdown of liquids takes place by a single avalanche process without a leader stage. In the above remarks this conclusion was questioned, and it was asserted that, independently of such limitations, the breakdown process must always be of the leader type. In support of his views G. A. Vorob'ev quoted an American article[3] in which, however, something quite to the contrary is stated.

It should be noted that in my article the absence of a leader stage was mentioned in the sense that the development of the breakdown process takes place gradually, without interruptions in time. For such relatively small interelectrode gaps as a few centimeters it appeared to me useful to speak of an avalanche stage which then goes over into streamer stage. In the case of an uninterrupted development of the process a streamer, or streamers traveling in opposite directions, short the electrodes, the principal discharge is formed and the breakdown ends in the formation of a highly conducting bridge. I used the concept of the leader stage in those cases when the process of the development of the breakdown was discontinuous in time.

In my opinion it is shown sufficiently clearly in reference 2 and more particularly in reference 4 that specifically in the absence of resistors *R* to limit the current, the breakdown of certain liquid dielectrics takes place without a leader stage in the sense indicated above.

In investigating the pre-breakdown processes in liquids one could come to the conclusion[2] that the development of the breakdown process in some cases takes place unexpectedly or suddenly. The breakdown begins to form progressively without an appreciable increase in current right up to the moment of the "collapse" of voltage. The process itself of the formation of breakdown naturally takes a certain length of time. This time has been determined by me in certain cases[4].

In what circumstances then does a discontinuous development of the breakdown or a leader process occur? On the basis of experimental data described in references 2 and 4 it is possible to assert that when the current in the discharge channel is limited, the temperature of the latter does not rise sufficiently so that the intense thermal ionization and photoionization can make the discharge channel of the first leader highly conducting. There are reasons to believe that this process of formation of a highly conducting bridge (broadening of the channel) grows in a cumulative fashion under favorable circumstances. As the degree of ionization increases, the current flowing through the channel also increases. The temperature of the latter increases in the meantime, and consequently the intensity of thermal ionization and photoionization increases, the broadening of the channel increases still further, etc. Of course it is also necessary to take into account here the processes which oppose the development of the breakdown, such as the capture by the molecules of the liquid of the electrons in the streamer, recombination, excitation of electrons in atoms and molecules of the liquid, radiation, heat being conducted away, collisions of the second kind, etc. When the discharge current is limited, the broadening of the channel must cease at a certain stage, and these opposing processes assume a dominant influence: the discharge stops.

It should be noted that, as experiments have shown, during the statistical delay time, sometimes even without the inclusion of a limiting resistor, the progressive development of the discharge is suppressed by the opposing processes in the stage of formation of avalanches or even of small streamers. However, this takes place only in the case when the applied voltage is somewhat lower than the breakdown value. Therefore such processes should not be confused with the progressive development of the breakdown.

---

[1] G. A. Vorob'ev, J. Exper. Theoret. Phys. USSR **27**, 764 (1954)

[2] I. E. Balygin, J. Exper. Theoret. Phys. USSR **25**, 736 (1953).

[3] T. W. Liao, J. G. Anderson, Trans. AIEE **72**, 641 (1953).

[4] I. F. Balygin, J. Exper. Theoret. Phys. USSR **24**, 338 (1954).

Translated by G. M. Volkoff
264

Photoelectric Recording of Spectra of Combination (Raman) Scattering of Powdery Materials

IA. S. BABOVICH AND V. M. PIVOVAROV

(Submitted to JETP editor March 1, 1955)
J. Exper. Theoret. Phys. USSR **29**, 696-697
(November, 1955)

IN the solution of a number of applied problems, and also in the investigation of certain basic problems, such as the question of the influence of the aggregate state on the character of the spectrum of combination (Raman) scattering, one frequently deals with powdered material. Digressing from the specific method (amply described in the literature[1-3]) for obtaining the spectra from similar objects, we note that there is no indication in any of the well-known reference works that photoelectric recording of the spectra has been applied. A photographic plate has always served as the energy detector. However, a direct comparison with the photographic plate shows the advantages of the photoelectric detector, particularly in its superior presentation of weak lines in a continuous background[4,5], so that the expediency of using the photoelectric method of recording should not require comment.

The results of the experiments on photoelectric recording of spectra from certain powdery materials--napthalene and a series of nitro derivatives of benzene—are given in this letter. The method of diffuse reflection was used to obtain the spectra[3]. Recording of the spectra was obtained by the photoelectric arrangement described earlier[5]. The spectra were excited by a specially prepared, high power, low pressure mercury lamp. Such a lamp, being practically free from a continuous background spectrum, considerably simplified the solution of the problem undertaken.

The lamp was constructed of molybdenum glass in the form of a spiral with three loops (inner diameter about 100 mm). Water cooled liquid mercury served as the cathode. An auxiliary mercury anode was located near the cathode. The operating anode was a molybdenum tube. The lamp was fed from a 120 volt constant current circuit. Ignition was produced by a high voltage pulse (10-11 kv) after a preliminary heating by an electric oven in the presence of the arc cathode--auxiliary anode. The operating current of the lamp was 15-25 amp. Under these conditions, the potential drop across the lamp was approximately 70-100 volts. The lamp was installed in an illuminator, which was evacuated by a procedure in which cold phenamine was blown through it. It was coated with magnesium oxide to increase the light yield.

The first experiments showed that, in spite of a strong reflection of light from the faces of the crystals of the substance and from the vessel of tapered conical glass, the continuous background spectrum was very weak. It was not necessary to insert a background absorbing filter in the primary beam; it was necessary only to use a filter which absorbed the short wavelength radiation. A vessel with an aqueous solution of potassium ferricyanide (red, molarity approximately 0.003 in a layer 8 mm thick) was inserted in the secondary beam just in front of the inlet slit of the monochromator in order to weaken the exciting line $\lambda = 4358$ Å; a blue glass filter BG-25 (located in the same position) was used to attenuate the long wave portion of the spectrum. Our particular monochromator, constructed on the principle of

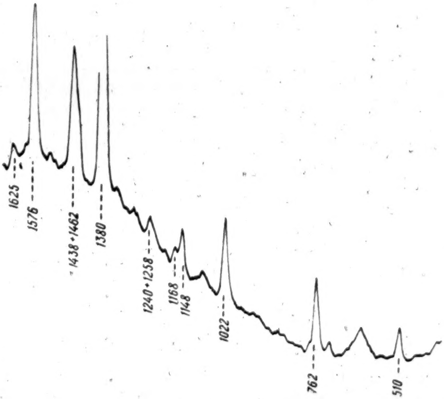

FIG. 1. Spectrum of combination scattering of powdery naphthalene. Voltage source FEU, 910 volts. The width of inlet and outlet slits was 0.2 mm. Frequencies (in cm^{-1}) are shown for certain lines of combination scattering.

the diffraction grating, made the use of the latter filter necessary; we demonstrated that false lines (ghosts) appear in the spectrum as a result of intense green and orange lines of the mercury lamp falling on the light apparatus. Although the intensity of the ghosts made up only 0.002-0.003% of the intensity of the basic lines, nevertheless, they appeared and interfered with the measurement, because of the very great sensitivity of our apparatus. In the course of thus weakening the undesirable radiations by means of filters, the useful radiation was also attenuated, by about a factor of five. However, this did not prevent the obtaining of a complete, high quality record.

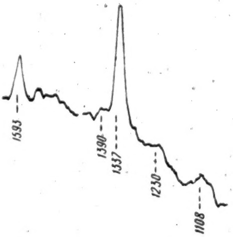

FIG. 2. Spectrum of combination scattering of powdery paranitrotoluene. Supply voltage FEU, 910 volts. Width of inlet slit, 0.7 mm, outlet slit, 0.2 mm. Frequencies (in cm^{-1}) are shown for certain lines of combination scattering.

For illustration, we have reproduced in Figs. 1 and 2 the records of the spectra of naphthalene and paranitrotoluene, excited by the blue line of mercury, $\lambda = 4358$ Å. The second substance, being finely crystalline and slightly transparent, absorbed the exciting line rather strongly, and made it difficult to obtain a spectrum. Comparison of a series of such records shows excellent reproducibility. The intensity distribution over the spectrum is altered, however, a consequence of the use of filters.

We have thus shown the possibility of the direct recording of the spectra of combination scattering from powdery materials. It would be appropriate in any further investigation of powdery materials to use a dual monochromator for the purpose of increasing the luminosity of the apparatus and for obtaining spectra with undistorted intensity distribution.

---

[1] K. Kol'raush, *Spectra of Combination Scattering*, IIL, 1952.

[2] G. S. Landsberg and F. S. Baryshanskaia, Izv. Akad. Nauk SSSR, Ser. Fiz. **10**, 509 (1946).

[3] Ia. S. Bobovich and M. M. Pakhomova, Dokl. Akad. Nauk SSSR **92**, 947 (1953).

[4] M. M. Sushchinskii, J. Exper. Theoret. Phys. USSR **20**, 304 (1950).

[5] Ia. S. Bobovich and D. B. Gurevich, J. Exper. Theoret. Phys. USSR **27**, 318 (1954).

Translated by J. M. Coogan
256

Meson Corrections in the Theory of Beta Decay

S. S. GERSHTEIN AND IA. B. ZEL'DOVICH

(Submitted to JETP editor June 8, 1955)
J. Exper. Theoret. Phys. USSR 29, 698-699
(November, 1955)

IN a recent note, Finkelstein and Moszkowski[1] discuss the effect of strong coupling between nucleons and pions on the beta decay of nucleons.

Using the language of Feynman diagrams these authors[1] consider, in addition to the fundamental process (Fig. 1 *a*), another process involving the virtual emission of one π^0 meson (Fig. 1 *b*). The calculation is carried out on the basis of the hypotheses under which Chew[2] discusses nuclear forces and the creation and scattering of mesons, and Friedman[3] discusses the anomalous magnetic moment of the nucleon: the nucleon is assumed to be infinitely heavy, and integrals over the momenta of virtual mesons are cut off at a specified value $p_{\max}$. From comparison with experiment it is found that $p_{\max}$ is close to Mc. A system with charge symmetry is considered so that the operator τ_3 enters into the expression for the coupling of nucleons to π^0.

Our notation will be very similar to that of Sachs[4]. Let P_1 be the probability that there is a virtual π^0 meson around the nucleon, compared with the probability that the nucleon is "bare", i.e., has no mesons around it*. The beta-decay coupling constants of a bare nucleon are denoted

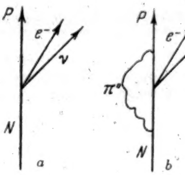

FIG. 1

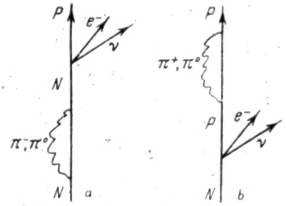

FIG. 2

by g_F' (Fermi interaction with S and V interaction types) and g_T' (Gamow-Teller interaction with T and A interaction types). In the case of a real nucleon surrounded by a meson cloud, the same constants as obtained experimentally are denoted by g_F and g_T, and the ratio g_T^2/g_F^2 equals R; from experiment[5] $R = 1.75$, i.e., $R > 1$. The results of Finkelstein and Moszkowski[1] then appear as follows:

$$g_F = g_F'(1 - P_1);\ g_T = g_T'\left(1 + \frac{1}{3}P_1\right),$$

$$\frac{g_T'}{g_F'} = \frac{1 - P_1}{1 + \frac{1}{3}P_1}\ \frac{g_T}{g_F} = \frac{1 - P_1}{1 + \frac{1}{3}P_1}\cdot\sqrt{R} \simeq 1.$$

While agreeing with their principal conclusion, which is that $g_T'/g_F' \cong 1$, we wish to make a few comments regarding the calculation.

1) The calculation does not follow for renormalization of the nucleon wave function as a result of the possibility of creating virtual mesons. By Feynman's[6] method renormalization is represented as an added self-energy contribution at the free ends of the diagrams (Figs. 2*a* and 2*b*). In these diagrams it is necessary to consider not only neutral but also charged pions (a charged meson in the vertex part of Fig. 1*b* obviously gives a vanishing result). It is easily seen that on the basis of the hypotheses which were adopted by Finkelstein and Moszowski, and taking renormalization into account, the correct result is

$$g_F = g_F'\frac{1 - P_1}{1 + 3P_1};\ g_T = g_T'\frac{1 + {}^1/_3 P_1}{1 + 3P_1}.$$

Thus the correction does not affect the ratio g_T'/g_F'. However, the correction may be significant when comparing the absolute value of $g_\beta = g_F' = g_T'$ with the coupling constant $g\mu$ that determines the probability of $\mu^\pm = e^\pm + 2\nu$ decay; Finkelstein and Moszkowski[1] had this comparison in mind. A numerical result in accordance with both the latter authors and Chew[2] is that $1 + 3P_1 = 1.7$.

2) Finkelstein and Moszkowski[1] do not consider the possibility of beta conversion of mesons, i.e., processes such as $\pi^\pm = \pi^0 + e^\pm + \nu$, which may be represented by diagrams like Fig. 3.

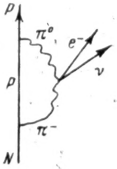

FIG. 3.

If the probability of $\pi^\pm \rightarrow \pi^0$ beta decay is the same as for mirror nuclei, the contribution from the process represented by the diagram of Fig. 3 is of the same order as the meson correction in diagram 1*b*; the absence of experimental indication of the $\pi^\pm = \pi^0 + e^\pm + \nu$ process does not contradict the hypothesis, since as a result of strong competition from $\pi^\pm = \mu^\pm + \nu$ decay, the former process may occur in only the small fraction 10^{-7} of the decays of free charged pions**.

The question of the beta decay of pions has been thoroughly examined by one of the authors of the present note[7]. It was shown that the S and T beta-interaction types do not give beta decay of a pion in the approximation to which the theory of isotopic invariance is valid. Thus the possibility of neglecting diagrams such as Fig. 3, as is done by Finkelstein and Moszkowski[1], is actually associated with the representation of the Fermi beta interaction by the scalar S rather than by the vector type V, which is in accordance with the latest experimental findings[8].

It is of no practical significance but only of theoretical interest that in the case of the vector interaction type V we should expect the equality

$$g_{\mathrm{F}\,(V)} \equiv g'_{\mathrm{F}\,(V)}$$

to any order of the meson-nucleon coupling constant, taking nucleon recoil into account and allowing also for interaction of the nucleon with the electromagnetic field, etc. This result might be forseen by analogy with Ward's identity for the interaction of a charged particle with the electromagnetic field; in this case virtual processes involving particles (self-energy and vertex parts) do not lead to charge renormalization of the particle.

3) We have calculated the meson corrections by invariant perturbation theory, using pseudoscalar coupling between pion and nucleon (coupling constant g).

In the expression for the self-energy and vertex parts a convergence factor $C(k^2)$ was introduced, where k is the momentum 4-vector of a virtual meson:

$$\sum = \int \tau_i \gamma_5 (\hat{p} - \hat{k} - m)^{-1} \gamma_5 \tau_i (k^2 - \mu^2)^{-1} C(k^2)\, d^4k,$$

$$\Gamma_0 = \int \tau_i \gamma_5 (\hat{p} - \hat{k} - m)^{-1} \tau_+ \hat{O} (\hat{p} - \hat{k} - m)^{-1} \gamma_5 \tau_i (k^2 - \mu^2)^{-1} C(k^2)\, d^4k,$$

$$C(k^2) = \lambda^2 / (\lambda^2 - k^2).$$

In addition to integration over momentum space (d^4k), a summation was carried out over the index i of meson isotopic spin. The beta process operator was represented as the product of the operator τ_+ which transforms a neutron into a proton, and the operator $\hat{O}$ which consists of the γ matrix ($\hat{O} = 1$ for S; $\hat{O} = \gamma_i \gamma_k$ for the T interaction type).

The meson mass renormalization term was calculated from Σ in the usual way: m is the mass of the nucleon, μ is the mass of the meson, and terms of the order of μ/m are neglected. Taking renormalization of the wave functions into account, the result becomes

$$g_{\mathrm{F}\,(S)} = g'_{\mathrm{F}\,(S)} \left[1 - \frac{g^2}{32\pi^2} \left(5 \ln\left(\frac{\lambda^2}{m^2}\right) - \frac{1}{2}\right)\right],$$

$$g_{\mathrm{GT}\,(T)} = g'_{\mathrm{GT}\,(T)} \left[1 - \frac{g^2}{32\pi^2} \left(3 \ln\left(\frac{\lambda^2}{m^2}\right) + \frac{1}{2}\right)\right].$$

For small g and large λ a relativistic calculation also gives a decrease of $g'_{\mathrm{GT}}/g'_{\mathrm{F}}$ compared with $g_{\mathrm{GT}}/g_{\mathrm{F}}$.

In the present state of the theory of interactions of pions with nucleons one cannot give preference to a relativistic perturbation theory calculation over the calculations of Finkelstein and Moszkowski[1], who employ coupling constants derived from experimental data.

---

* In the notation of Finkelstein and Moszkowski[1], $P_1 = 3\delta$.

** In the case of virtual mesons (Fig. 3) $\pi \rightarrow \mu + \nu$ decay is obviously forbidden by energy considerations.

---

[1] R. J. Finkelstein and S. A. Moszkowski, Phys. Rev. **95**, 1695 (1954).

[2] G. G. Chew, Phys. Rev. **95**, 285, 1669 (1954).

[3] M. H. Friedman, Phys. Rev. **97**, 1123 (1955).

[4] R. G. Sachs, Phys. Rev. **87**, 1100 (1952).

[5] R. Gerhart, Phys. Rev. **95**, 288 (1954).

[6] R. P. Feynman, Symposium on *Recent Developments in Quantum Electrodymanics*, 1954.

[7] Ia. B. Zel'dovich, Dokl. Akad. Nauk SSSR **97**, 421 (1954).

[8] W. P. Alford and D. R. Hamilton, Phys. Rev. **95**, 1351 (1954).

Translated by I. Emin
257

Electrical After-Effects in Rochelle Salt

K. N. KARMEN
Shakhtin State Teachers' Institute

(Submitted to JETP editor November 6, 1954)
J. Exper. Theoret. Phys. USSR **29**, 533 (October, 1955)

A decrease of residual charge resulting from an increase in the duration of charging of samples of Rochelle salt has been reported[1]. A similar decrease of residual charge in the presence of a number of sequential electrical impulses has been observed by other investigators[2,3]. As is known[4], Rochelle salt, besides this phenomenon of fatigue, also has inherent unipolarity, which results in the asymmetrical polarization P_a relative to the forward and reverse polarization. This asymmetry P_a has been investigated[5] as a necessary consequence of the existence of large regions of spontaneous polarization. However, considering the question of fatigue and unipolarity, Kosman and Sozina[6] arrive at the conclusion that in reality there exists no distinction between fatigue and unipolarity, and that both are dependent on a shut-off layer, arising as a result of the action of polarization on the specimen.

Markedly contradictory opinions concerning the nature of unipolarity stimulated us to investigate in more detail the after effects produced by means of continuous action of electrical polarization on the specimen.

The experiment was carried out using the arrangement, dimensions of specimens, and assembly of electrodes which has been reported previously[7]. The method used in the present work consisted of a superposition onto the specimen of short electrical impulses in the forward and reverse directions. In the intervals between two consecutive impulses the specimen remained undisturbed. The condition of the specimen was determined by the charge or discharge of a quantity of electricity Q, which was determined by means of a galvanometer. Typical curves, characteristic of the initial condition, are presented in Fig. 1 *a*. It is established that the majority of investigated specimens have, for one of the directions of polarization and with a voltage

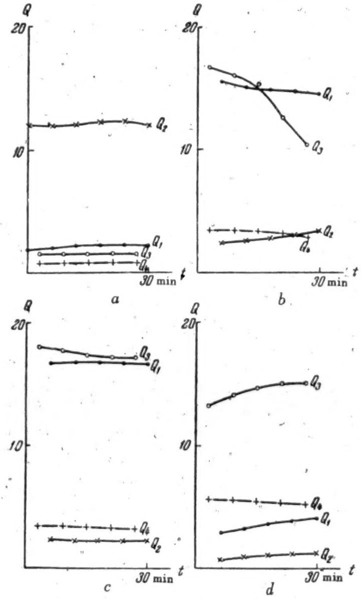

a *b* *c* *d*

FIG. 1. The dependence of the charge-discharge quantities of electricity on the duration of action of the polarization. Q_1 and Q_2 are the charge-discharge quantities of electricity produced by superposition of impulses in the forward direction. Q_3 and Q_4 are the same quantities with impulses in the reverse direction. $E = 75$ volts/cm; $T = 18\,^{\circ}\mathrm{C}$. ($Q$ is in units of 5.4×10^{-8} coulomb). The duration of the interval between two impulses in three minutes. *a*- is the initial condition; *b* - is after the action of polarization 48 times; *c* - is after 70 times; and *d* - is after the action of polarization 172 times.

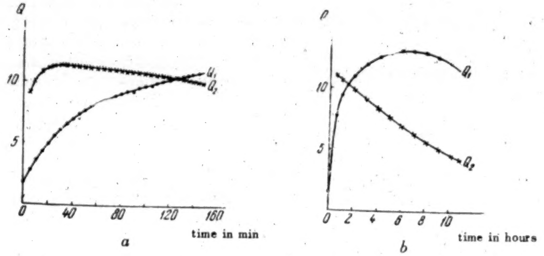

FIG. 2. Dependence of the charge-discharge quantities of electricity Q_1 and Q_2 on the increase of number of superimposed pulses with $E = 75$ volts/cm and $T = 18°C$. (Q is in units of 5.4×10^{-8} coulombs). Duration of interval between pulses is 10 seconds. At *a* the duration of each pulse is 5 minutes. At *b* the duration of each pulse is 1 hour.

of 50 to 100 volts/cm, residues in discharging which considerably surpass the residues in charging.

Fig. 2 shows the change of charge-discharge residues with an increase of number of impulses, according to the sign and magnitude of the electrical impulses. As is apparent from the adduced facts, the average rate of establishing polarizations and depolarizations changes over wide ranges in its dependence on the duration of action of the polarizing force. The smallest rate of establishing polarization results in a practically final value in no more than 5 minutes. Complete discharge is initially provided by isolating the sample for ten seconds, even in the case of the largest variation of accumulated charge produced from preceding impulses. This complete discharge results in an initial increase of the rate of establishing polarization. Subsequently, the rate of establishing polarization and depolarization decreases until the sample practically does not discharge, even with greater intervals of isolation. In this case superposition of sequential pulses of the opposite sign in fact produces overcharging. The result is that after the uninterrupted continuous action of the applied potential difference, the overcharging is able in turn to cause considerable delayed action.

The investigations showed that considerable unipolarity is inherent on most of the specimens and that this unipolarity is a permanent characteristic. However, prolonged action of electrical polarization is able to alter the unipolarity considerably, in particular to cause its disappearance. The disappearance of unipolarity indicates a transition from an "inherent" condition, in which the sample exists predominantly in one direction of spontaneous polarization, to a condition in which the forward and reverse directions of spontaneous polarization are equally likely. The maximum change of condition shows itself by a change of the predominant orientation of domains into opposition. The mechanisms of the processes, taking place in the samples over such a long interval of time, still remain insufficiently explained.

---

[1] J. Valasek, Phys. Rev. **24**, 560 (1924).

[2] G. Oplatke, Physik. Z. **34**, 296 (1933).

[3] M. S. Kosman, J. Exper. Theoret. Phys. USSR **19**, 899 (1949).

[4] I. V. Kurchatov, *Rochelle-Electricity*, 1933.

[5] W. G. Cady, *Piezoelectricity* (Mc Graw-Hill Book Company, Inc., New York, 1946).

[6] M. S. Kosman and A. N. Sozina, J. Exper. Theoret. Phys. USSR **20**, 1116 (1950).

[7] K. N. Karmen, J. Exper. Theoret. Phys. USSR **26**, 370 (1954).

Translated by L. A. D'Asaro
236

Formation of a μ-Meson Pair in Positron Annihilation

V. B. BERESTETSKII AND I. IA. POMERANCHUK
Academy of Sciences, USSR

(Submitted to JETP editor September 29, 1955)
J. Exper. Theoret. Phys. USSR **29**, 864
(December, 1955)

IF there is no specific interaction peculiar to μ-mesons more essential than the electro-

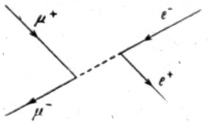

magnetic, then experimental investigation of electrodynamic processes with participation of μ-mesons can give significant information about the limits of applicability of contemporary field theory and the nature of physical laws near these limits, since the Compton wavelength of the μ-meson is comparable with those dimensions near which one can expect fundamental modifications in space-time concepts[1]. The transformation of an electron-positron pair into a pair of μ-mesons can serve as one such process. The minimum energy E_n required of the positron for the formation of such a pair by collision with an electron at rest is given by $E_n = (2\mu/m)\mu c^2 \approx 4 \times 10^{10}$ ev(μ = μ-meson mass, m = electron mass) This process, as well as two-quantum annihilation, appears to be a second-order process in the sense of perturbation theory. The effective cross section σ is expressed in the following form:

$$\sigma = \frac{\pi}{6}\frac{e^4}{mc^2E}\left(1+\frac{E_n}{2E}\right)\left(1-\frac{E_n}{E}\right)^{1/2}. \qquad (1)$$

Near the threshold of the reaction ($E - E_n \ll E_n$)

$$\sigma = (\pi/8)(e^2/\mu c^2)^2[1-(E_n/E)]^{1/2}.$$

For $E \gg E_n$

$$\sigma = (\pi/12)(e^2/\mu c^2)^2(E_n/E).$$

The maximum cross section (for $E \approx 1.7\, E_n$) per atom is given by

$$\sigma_{\max} \approx Z(\pi/6)e^4/mc^2E$$

$$= Z(\pi/12)(e^2/\mu c^2)^2 \approx 5Z \cdot 10^{-31}\ \mathrm{cm}^2$$

It is approximately 70 times smaller than the cross section for two-photon annihilation σ_γ for such energies:

$$\sigma_\gamma = Z(\pi e^4/mc^2E)\ln(2E/mc^2)$$

$$\approx \pi Z(e^2/\mu c^2)^2\ln(4\mu^2/m^2).$$

The information referred to above would be contained in any deviation of experimental data from Eq. (1).

---

[1] I. Ia. Pomeranchuk, Dokl. Akad. Nauk SSSR **103**, 1005; **104**, 51 (1955).

Translated by H. Royden
282

Relaxation Processes in the Interaction of Nuclear Magnetic Moments with an Oscillator Loop

N. M. POMERANTSEV
Moscow State University

(Submitted to JETP editor April 4, 1955)
J. Exper. Theoret. Phys. USSR **29**, 375-376 (September, 1955)

DURING experiments on the magnetic resonance of atomic nuclei, a sample material is usually placed in the coil of an oscillator loop which is in a magnetic field[1,2]. The precession at resonance of the vector of the total magnetic moment induces an electromotive force in the coil of the oscillator loop.

Bloembergen and Purcell[3] considered the fact that the dissipation of energy which takes place in the oscillator loop will, independent of other factors, contribute to the attenuation of this precession. They also considered the interactions of the total magnetic moment vector with the oscillator loop for the case of free Larmor precession, and also for the case in which the loop is placed in a constant magnetic field and fed with high frequency voltage of constant amplitude. However, in practice, the magnetic field does not remain constant, but is modulated in most cases by an alternating field of audio frequency. In this case an oscillation of the amplitude of the precession of the total magnetic momentum vector takes place and changes the form of the signals in such a way that they have the form of damping oscillating functions[4]. Solutions obtained in reference 3 cannot answer the question of how the form of the signals is influenced by the interaction of the system of nuclear magnetic moments with the oscillator loop when the longitudinal component of the magnetic field is modulated.

The question of the interaction of the nuclear magnetic moments with the oscillator loop when the loop is connected to an automatic oscillating system, was considered by the author in reference 5. It has been proven theoretically and experimentally that in this case the amplitude of the oscillations of the generator is modulated by the signal $v(t)$, and the frequency by the signal $u(t)$. These signals are the solution of Bloch's equation[1]. Also, experimentally and theoretically it has been shown that, depending on the parameter α, which determines the stability of the system, there takes place more or less strong cutting off of the upper frequencies of the signal $v(t)$. In the case of relatively stable systems (large α) the signal $v(t)$ is sent through practically without distortion.

The results of this work are easily applied in the case when the oscillating loop is fed from an external generator. The initial system of equations will be as follows

$$\frac{d^2V}{dt^2} + \omega^2 V = \omega^2 E \cos(\omega_0 t - \psi) - \frac{\omega}{Q}\frac{dV}{dt} - A\frac{dM_x}{dt},$$

$$\frac{dW}{dt} + \left[\frac{1}{T_2} + i\gamma H_z\right] W - i\gamma B M_z \frac{dV}{dt} = 0,$$

where E, ω_0 and ψ are the amplitude, frequency and phase of oscillation of the generator, Q is the quality of the loop. For the meaning of the other symbols see reference 5. Applying the method used in reference 5, we obtain for the voltage of the oscillator loop the following:

$$V = \rho \cos(\omega t - \varphi),$$

where

$$\rho = EQ + \rho', \quad \varphi = \psi + \frac{\pi}{2} + \varphi',$$

$$\rho' = {}^1\!/_4\, \omega\gamma ABEQ \int_{-\infty}^{t} v(\eta) \exp\left\{\frac{\omega}{2Q}(\eta - t)\right\} d\eta,$$

$$\varphi' = {}^1\!/_4\, \omega\gamma AB \int_{-\infty}^{t} u(\eta)\, d\eta.$$

The above expressions show that when the magnetic field is changed rapidly, additional distortions of the signal $v(t)$ appear. These distortions take form in cutting off the upper frequencies of $v(t)$. They are substantial for small frequencies and for large values of the Q of the oscillator loop.

---

[1] F. Bloch, Phys. Rev. **70**, 460 (1946).

[2] C. D. Gvosdover and A. A. Magazanik, J. Exper. Theoret. Phys. USSR **20**, 705 (1950).

[3] N. Bloembergen and E. M. Purcell, Phys. Rev. **95**, 8 (1954).

[4] K. V. Vladimirskii, Dokl. Akad. Nauk SSSR **58**, 1625 (1947).

[5] N. M. Pomerantsev, Vestnik Moscow State Univ. 2, 47 (1955).

Translated by M. Polonsky
208

CONTENTS

JOURNAL OF TECHNICAL PHYSICS, USSR VOLUME 25, NO. 14 1955

Photo Conduction of HgI_2 under the Action of Visible Light . . . . D. V. Chepur 2411
On the Combined Crystallization of Hexagonal CdSe with ZnSe, InAs and In_2Se_3 . . . . N. A. Goriunova, V. A. Kotovich snd V. A. Frank-Kamenetskii 2419
To the Electric Conduction of Copper Oxide . . . . A. I. Andrievskii, V. I. Voloshchenko and M. T. Mishchenko 2422
Electric Conduction of Solid Ionic-atom-valent Substances, VI . . . . R. L. Miuller 2428
Electric Conduction of Solid Ionic-atom-valent Substances, VII . . . . R. L. Miuller 2440
Electric Conduction of Aluminum and Zinc Oxides at High Temperatures . . P. T. Oreshkin 2447
Application of a Hydrophobic Earth to Eliminate Frosty Swelling of Ground Water . . . . . . D. I. Sel'kin 2451
Experimental Determination of the Heat Conduction Coefficient of 94 Percent (by Volume) Ethyl Alcohol in the -75 - + 200° C Temperature Range . . . . N. V. Tsederberg and D. L. Timrot 2458
Secondary Emission under the Action of Positive Potassium Ions Differing as to Charge . . . . . . I. P. Flaks 2463
Electron Emission under the Action of Positive Zinc, Mercury, Thallium and Lead Ions Differing as to Charge . . . . I. P. Flaks 2467
Effect of Adsorption of Dipole Barium Oxide Molecules on the Photo-electron Emission of an Antimony-Caesium Cathode . . . . V. M. Gavriliuk 2469
Electron-Optic Investigation of Compound Photo-cathodes . . . . L. N. Bykovskaia and Iu. M. Kushnir 2477
Investigation of the Stretching of Polymers in Polarized Infra-red Light . . . . V. N. Nikitin, M. V. Vol'kenshtein and B. Z. Volchek 2486
To the Theory of Self-oscillations in a Reverberating Klystron . . . . R. V. Khokhlov 2492
Trajectory of Thermal Jets in the Air Layer Close to the Earth . . . . . . V. F. Dunskii 2501
Application of the Thermal and Mass-exchange Differential Equation System to the Contact Drier Process . . . . M. I. Makovozov 2511
On the Interaction of Coupled Electromagnetic Resonators with a Beam of Charged Particles . . . . A. I. Akhiezer and Ia. B. Fainberg 2516
On the Radiation of Charged Particles Moving Through Coupled Resonators . . . . A. I. Akhiezer, G. A. Liubarskii and Ia. B. Fainberg 2526
Low-clearance Beta Spectrometer . . . . S. A. Baranov and R. M. Polevoi 2535
Stigmator for an Electron Microscope . . . . P. A. Stoianov 2537
Photo-electro-optic Dynamometer . . . . G. A. Dubov and V. R. Regel' 2542
On Certain Anti-symmetric Magnetic Fields with Double Focussing, I . . Iu. V. Vandakurov 2545
Electronograph of Simplified Construction . . . . M. A. Rumsh 2556

Letters and Brief Communications

Investigation of High-speed Processes Using Inertial Pick-offs . . . . A. M. Bonch-Bruevich and Ia. A. Imas 2565
Determination of Hydrogen in Certain Metals by the Method of Isotopic Equalization . . . . A. N. Zaidel' and A. A. Petrov 2571
Author Index to Vol. 25 2574
Index to Vol. 25 2587

DOKLADY AKADEMII NAUK SSSR VOLUME 105, NO. 1 1955

MECHANICS

Mechanisms to Generate 'Poder' of Conical Sections . . . . . Acad. I. I. Artobolevskii 38

ELASTICITY THEORY

On Certain Direct Methods in the Nonlinear Theory of Shallow Shells . . I. I. Vorovich 42

PHYSICS

Influence of Small Impurities on the Galvano-magnetic Properties of Bismuth . . . . N. E. Alekseevskii, N. B. Brandt and T. I. Kostina 46

Luminescence Yield of a System with Three Energy Levels . . . . V. V. Antonov-Romanovskii, B. I. Stepanov, M. V. Fok and A. P. Khapaliuk 50

Investigation of the Widths of Combined Lines Depending on the Aggregate State of the Substance . . . . P. A. Bazhulin and A. V. Rakov 54

Dependence of the Gamma and Photo-luminescence Yield of NaI-Tl Crystals on the Concentration of Thallium . . . . L. M. Beliaev, M. D. Galanin, Z. L. Morgenshtern and Z. A. Chizhikova 57

On a Possible Interpretation of the Oscillatory Spectra of Simple Silicate Glass . . . . Ia. S. Bobovich, O. P. Gipin and T. P. Tulub 61

On the Asymptotic Form of the Electron Green's Function . . . . L. P. Gor'kov 65

Excited Nucleon States . . . . I. I. Gurevich 69

Phase Analysis of Proton Scattering by Protons . . . . A. Zimin 73

Quantum Kinetic Equations for Multiple Scattering . . . . A. Migdal 77

On the Character of the Variation of the Electric Conduction for a Jump-shaped Deformation of the Metallic Single Crystals . . . . V. N. Rozhanskii, Iu. B. Goriunov and E. D. Shchukin 80

GEOPHYSICS

Structure of the Earth's Core in the North Tien-Shen Region according to the Data of the Depth of Seismic Probing . . G. A. Gamburtsev⁺, P. S. Veitsman and Iu. V. Tulina 83

On the Experimental Study of the Mechanism of Primary Wind Wave Generation . . . . E. G. Nikiforov 87

BIOPHYSICS

On the Relation of the Characteristics of Vision to the Quantum Fluctuations of Light . . . . E. S. Ratner 90

⁺deceased

DOKLADY AKADEMII NAUK SSSR VOLUME 105, NO. 2 1955

MECHANICS

On Nonlinear Oscillations in Systems with Varying Parameters . . . V. O. Kononenko 229

MATHEMATICAL PHYSICS

Quantum Kinetic Equation for Pair Collisions . . . . A. B. Migdal and N. M. Polievktov-Nikoladze 233

PHYSICS

Observations of Generation and Disintegration of Unstable Particles in an Emulsion Chamber . . . . V. V. Alpers, R. I. Gerasimova, I. I. Gurevich, A. P. Mishakova and L. V. Surkova 236

On Light Scattering Near a Point of Phase Transition of the Second Kind . . . . V. L. Ginzburg 240

On the Theory of the Intermediate State of Superconductors . . . I. E. Dzialoshinskii 244

Dispersion of the Speed of Sound in Carbon Bisulfide . . . . V. A. Molchanov and I. L. Fabelinskii 248

Spectral Dependence of the Photo-luminescence Yield of Alkali-halides Activated by Thallium . . . . Z. L. Morgenshtern 250

On the Fine Structure of a Deformation Jump of Zinc Single Crystals . . . . V. N. Rozhanskii and Iu. V. Goriunov 253

GEOPHYSICS

Equation of Turbulent Diffusion . . . . A. S. Monin 256

Motion of the Earth's Axis and Variation of Angular Velocity of the Earth Caused by Erosion . . . . I. F. Monin 260

TECHNICAL PHYSICS

Chromium Diffusion in Solid Solutions Based on Nickel . P. L. Gruzin and G. B. Fedorov 264

On the Nature of Annealing the Brittleness of Steel . . . . A. I. Rizol', L. G. Sakvarelidze and L. M. Utevskii 268

ELECTROTECHNICS

Generalization of a Theorem of Variation and Compensation for n-Parameter Electric Loops . . . . N. A. Brazm 271

DOKLADY AKADEMII NAUK SSSR VOLUME 105, NO. 3 1955

MATHEMATICAL PHYSICS

On the Determination of the Particle Potential through Its S-function . . . M. G. Krein 433

On the Determination of the Position of the Boundary Separating the Phases in a Two-phase Heat-conducting Medium for Its Steady Thermal State . . . . L. I. Rubinshtein 437

Distribution Functions with Time Correlation in the Statistical Mechanics of Classic Systems . . . . V. V. Tolmachev 439

PHYSICS

Compensation Theory of the Space Charge of Ion Beams in the Steady Region . . . . V. S. Anastasevich 442

On Determination of the Boundaries of Applicability of Quantum Electrodynamics by Means of Measurements of the Electron Magnetic Moment . . . . G. M. Gandel'man and Ia. B. Zel'dovich 445

On the Effect of Surface-active Media on the Jump-form Deformation of Single-crystal Zinc . . . . V. N. Rozhanskii, Iu. V. Goriunov and Acad. P. A. Rebinder 448

On the Spin and Parity of the τ-Meson . . . . . . I. I. Gurevich and A. P. Mishakova 451

Liquid-vapor Phase Diagram of a System of Helium Isotopes (He^3 - He^4) . . . . B. N. Esel'son and N. G. Berezniak 454

Charge Over-normalization without Perturbation Theory . . N. M. Polievktov-Nikoladze 458

On the Over-normalized, Meson Charge Becoming Zero in Pseudoscalar Theory with Pseudoscalar Coupling . . . . I. Pomeranchuk 461

On the Theory of Total Reflection . . . . F. I. Fedorov 465

Investigation of Embryonic Magnetic Reversal in Silicon Iron Crystals . . . . Ia. S. Shur and V. R. Abel's 469

TECHNICAL PHYSICS

New Tables of Supporting Values of Enthalpy and the Specific Volume of Water Vapor . . . . V. A. Kirillin, A. E. Sheindlin and E. E. Shpil rain 472

Heaving of the Fluid Surface under the Action of Ultrasonics . . . . M. Kornfel'd and N. Molokhova 476

Continuous Resistance of Vinyl Plastic for Various Forms of the Stress State . . . . Iu. I. Iagn and I. I. Tseloval'nikov 478

CRYSTALLOGRAPHY

Theory of Structural Amplitude Coupling . . . . A. I. Kitaigorodskii 482

DOKLADY AKADEMII NAUK SSSR VOLUME 105, NO. 4 1955

MECHANICS

On Oscillations in Nonlinear Systems with Many Degrees of Freedom . . . . V. O. Kononenko 664

HYDRAULICS

New Understanding of the Principles of Siphon Operation . . . . . N. G. Malishevskii 668

ELASTICITY

Radial Oscillations of a Hollow Sphere with a Singular Series of Elastic After-effects . . . . M. I. Rozovskii 672

ASTRONOMY

Investigation of the Brightness of the Sky in the Region around 1 μ during the Solar Eclipse of June 30, 1954 . . . . S. F. Rodionov and E. D. Sholokhova 676

PHYSICS

On the Question of the Energy of Electron Affinity of Halogen Atoms . . . . I. N. Bakulina and N. I. Ionov 680

Surface Resistance of Tin in the Superconducting State at a 7.3×10^{10} cps Frequency . . . . P. A. Bezuglyi, A. A. Galkin and G. Ia. Levin 683

Lee Type Model in Quantum Electrodynamics . Acad. N. N. Bogoliubov and D. V. Shirkov 685

Adiabatic Approximation in Green's Function Theory . . . . . . V. L. Bonch-Bruevich 689

Angular Distribution of Fragments in Uranium 238 Splitting by Neutrons of Various Energies . . . . A. A. Varfolomeev, A. S. Romantseva and V. M. Kutukova 693

Investigation of Broadening of Line of Anisotropic Light Scattering for Fluids and the Determination of Relaxation Times . . . . M. F. Vuks and V. L. Litvinov 696
On Reabsorption of Luminescence in Fine Layers . . . . M. D. Galanin 700
On the Green's Function for the Photon . . . . N. M. Polievktov-Nikoladze 703
Reflection of Ferromagnetic 'Domenov' by Electron-Optic Methods . . . . G. V. Spivak, N. G. Kanavina, I. S. Sbitnikov and T. N. Dombrovskaia 706

TECHNICAL PHYSICS

Transfer Characteristics of Semiconductor Triodes . . . . E. I. Adirovich and V. G. Kolotinlova 709
On Luminescence and Light Absorption by a Diamond . . . . G. O. Gomon 713

DOKLADY AKADEMII NAUK SSSR VOLUME 105, NO. 5 1955

MECHANICS

On the Dynamic Computation of Solid Bracing of Side Slopes of Hydro-technical Construction Subject to Impact by Broken Waves . . . . F. F. Molero 916

ELASTICITY

Radial Deformation of a Hollow Sphere with Anisotropy and Elastic After-effects . . . . M. I. Rozovskii 920

ASTRONOMY

Polarimetric Investigation of M8 and M20 Nebulae and the Stars Adjoining Them . . . . V. A. Dombrovskii 924
Certain Remarks on the Radiation of the Variable BD 67°922 . . . . . L. V. Mirzoian 928
On the Question of the Lithium, Beryllium and Deuterium Content in the Solar Atmosphere . . . . I. S. Shklovskii 931

PHYSICS

On the Theory of Atomic Magnetic Moments in Ferromagnetics . . . . . . N. S. Akulov 935
On the Question of Renormalization in Mesodynamics . . . . A. M. Brodskii 939
Fine Structure of the Basic X-ray K Spectrum Absorption of Titanium in Certain Dielectric Materials . . . . E. E. Vainshtein, I. B. Staryi and M. N. Bril' 943
Formation of π Meson Pairs by Gamma Quanta and the Retarding Radiation of π Mesons by Nuclei . . . . Iu. A. Vdovin 947
Effective Potential of π Meson-Nucleon Interaction . . . . V. R. Velibekov and V. A. Meshcheriakov 951
Obtaining Negative Ions by Overcharging . . . . V. M. Dukel'skii 955
Spectra of Combined Scattering of Low-molecular Polysiloxanes . . . . Ia. M. Slobodin, Ia. E. Shmuliakovskii and K. A. Rzhendzinskaia 958
On the Theory of Dirac Particle Scattering Taking Damping into Account . . . . A. A. Sokolov and B. K. Kerimov 961
Magnetic Contrast in an Electron Mirror and Observation of Ferromagnetic 'Caking' . . . . G. V. Spivak, I. N. Prilezhaeva and V. K. Azovtsev 965
On the Theory of X-ray Scattering by Macroscopic Isotropic Bodies . . . . V. N. Filipovich and E. A. Porai-Koshits 968
Two-charge Renormalization Group in Pseudoscalar Meson Theory . . . D. V. Shirkov 972

TECHNICAL PHYSICS

Use of CdS Photoresistance in Combination with Phosphors as Gamma-ray Detector of Cobalt-60 . . . . S. D. Margolin and I. G. Fakidov 976

CRYSTALLOGRAPHY

On Strong and Weak Statistical Relations Between Structural Amplitude Signs . . . . Acad. N. V. Belov and N. I. Golovastikov 978

DOKLADY AKADEMII NAUK SSSR VOLUME 105, NO. 6 1955

MECHANICS

On the Estimate and Increase of the Strength of Bodies from Isotropic Inhomogeneous Material . . . . Ia. B. Fridman and N. B. Sobolev 1166
Motion of Fine Solid Particles in a Free Air Stream . . . . A. P. Chernov 1170

HYDRAULICS

On Determining the Pressure Function in Inhomogeneous Oil Deposit Strata . . . . . . G. S. Salekhov 1174

ELASTICITY

Solution of the Three-dimensional Problem of Elasticity for a Wedge with Displacements Assigned on the Boundaries . . . . . . Ia. S. Ufliand 1177
On Bending of a Circular Plate Partially Supported and Partially Free on the Contour . . . . . . D. I. Sherman 1180

ASTRONOMY

Variation of Solar Rotation because of Substances under the Action of the Poynting-Robertson Effect Falling on it . . . . . . V. S. Safronov 1184

PHYSICS

On Electric Conduction and Self-difussion Coefficients of Cations in Silver Iodide . . . . . . V. I. Baranovskii, B. G. Lur'e and A. N. Murin 1188
Difference of the Mass of Elementary Particles . A. Brodskii, D. Ivanenko and N. Korst 1192
On Certain Laws in the Structure of the Basic X-ray K Band Absorption of Atoms in Crystals of Alkali-halides . . . E. E. Vainshtein, R. L. Barinskii and K. I. Narbutt 1196
Electric Resistance and Its Variation in a Strong Magnetic Field for Iron-nicla Alloys in the Low (14-90°) Temperature Range . . . . . . E. Kondorskii and I. Ozhigov 1200
Nuclear Interaction of π Mesons in Copper . . . . . . N. M. Kocharian, G. S, Saakian, M. T. Aivasian, Z. A. Kirakosian and A. S. Aleksanian 1204
On the Question of Determining the Relative Phosphorescence Yield and Intensity of Organo-luminofors . . . . . . B. Ia. Sveshnikov 1208
Centers of Capture and Kinetic After-exposure of Ammonium Halide Phosphors . . . . . . L. Ia. Uibo and I. V. Iaek 1212

GEOPHYSICS

On the Dynamics of Steady Currents in an Inhomogeneous Sea . . . . . P. S. Lineikin 1215
Lightness of the Crepuscular Sky in the 1 Micron Region . . . . . . E. D. Sholokhova and M. S. Frish 1218

BIOPHYSICS

Early Variation in the Bone Marrow and Blood of Exposed Humans Uncovered Using a Luminescent Microscope . . . . . . M. N. Meisel' and V. A. Sondak 1221

TECHNICAL PHYSICS

On Crystalline Structure and Nature of ω-phase in Titanium-Chromium Alloys . . . . . . Iu. A. Bagariatskii, G. I. Nosova and T. V. Tagunova 1225
Supersaturation and Condensation in a Turbulent Flow between two Damp Surfaces of Non-identical Temperatures . . . . . . S. S. Dukhin 1229
Study of the Mechanism of the Growth of Tempering Brittleness of Steel in the Electron Microscope . . . . . . N. V. Kazakova and N. V. Koroleva 1233
On the Correspondence between the Variation of the Dissociation Elasticity and the Electric Resistance of Cobalt Arsenide . . . . . . M. I. Kochnev 1236
On the Dislocation Theory of the Fatigue of Metals . . . . . . I. A. Oding 1238
Influence of Pressure on the Transformation of Austenite into Martensite . . . . . . A. I. Stregulin and N. P. Chuprakova 1241

ELECTRIC ENGINEERING

Computation of the Parameters of a System of a Triple Cascade Electric-machine Control by Weakening the Motor Current (Taking into Account the Time Constants of the Exciter and the Amplifier) . . . . . . N. P. Kunitskii 1244

CRYSTALLOGRAPHY

On the Stability of Doublet Fixations of Methylene Blue and Benzidine in Clayey Minerals . . . . . . N. E. Vedeneeva 1248

CONTENTS – *continued*

Russian Reference

Letters to the Editor:

Interaction of Nucleons through a Pseudoscalar Meson Field . A. A. Rukhadze 570 29, 709
The Connection between the Distribution of a Quasi-monochromatic Stationary Process and the Distribution of Its Envelope . . . . S. M. Rytov 571 29, 702
The Fermi-Yang Hypothesis . . . . S. S. Filippov 572 29, 707
On the Development by Means of Leaders of the Process of Breakdown of Liquids . . . . I. E. Balygin 573 29, 708
Photoelectric Recording of Spectra of Combination (Raman) Scattering of Powdery Materials . . . . Ia. S. Babovich and V. M. Pivovarov 574 29, 696
Meson Corrections in the Theory of Beta Decay . . . . S. S. Gershtein and Ia. B. Zel'dovich 576 29, 698
Electrical After-effects in Rochelle Salt . . . . K. N. Karmen 578 29, 533
Formation of a μ-Meson Pair in Positron Annihilation . . . . V. B. Berestetskii and I. Ia. Pomeranchuk 580 29, 864
Relaxation Processes in the Interaction of Nuclear Magnetic Moments with an Oscillator Loop . . . . N. M. Pomerantsev 581 29, 375
Table of Contents, Journal of Technical Physics, USSR, Volume 25, No. 14 . . . 583
Tables of Contents, Doklady Akademii Nauk SSSR, Volume 105, Nos. 1-6 583

SOVIET PHYSICS JETP VOLUME 2, NUMBER 3 MAY, 1956

CONTENTS

			Russian Reference
Temperature Dependence of the Elastic Constants of Monocrystals of Sodium Chloride and Silver Chloride	A. V. Stepanov and I. M. Eidus	377	29, 669
The Theory of the Hall Effect in Ionic Semiconcuctors	M. I. Klinger	383	29, 439
The Double-Configurational Approximation in the Case of Carbon-like Atoms	A. B. Bolotin, I. B. Levinson and L. I. Levin	391	29, 449
Investigation of the Isotopic Constitution of Lithium	K. Ordzhonikidze and V. Shiuttse	396	29, 479
An Investigation of the Isotopic Constitution of Boron	V. Shiuttse	402	29, 486
The Behavior of Helium II in the Neighborhood of a Heat Radiating Surface	E. L. Andronikashvili and G. G. Mirskai	406	29, 490
Secondary Electron Emission in Thin Layers of Be II	I. M. Bronshtein and T. A. Smorodina	410	29, 495
Secondary Electron Emission in Thin Layers of Silver	I. M. Bronshtein and T. A. Smorodin	414	29, 500
Direct Measurement of the Total Light of Rapidly Decaying Processes of Luminescence	N. A. Tolstoi and I. A. Litvinenko	420	29, 507
Observation of Electroconductive Convection in Electrolytes	G. A. Ostroumov	428	29, 529
Fission of Heavy Nuclei by Slow π^- Mesons	N. A. Perfilov and N. S. Ivanova	433	29, 551
On the Correlation Method for the Determination of the Absolute Yield of Nuclear Reactions	V. I. Gol'danskii and M. I. Podgoretskii	441	29, 559
Theory of Strong Coupling for Meson Fields. III	B. T. Geilikman	451	29, 572
Existence of Quantum Stationary States of Point Nucleons Which Interact with the Meson Field	S. I. Pekar	462	29, 599
Electromagnetic Properties of a Finely Stratified Medium	S. M. Rytov	466	29, 605
Fock Self-consistent Field for the Boron Atom in the Two-configuration Approximation	I. I. Glembotskii, V. V. Kibartas and A. P. Iutsis	476	29, 617
Fock Self-consistent Field in the Three-configuration Approximation for the Beryllium Atom	V. V. Kibartas, V. I. Kavetskis and I. P. Iutsis	481	29, 623
Determination of Longitudinal Relaxation Times for Magnetic Resonance of Atomic Nuclei in an Intense High-frequency Magnetic Field	S. D. Gvozdover and N. M. Ievskaia	486	29, 637
Fission of Uranium by Slow π^- Mesons, Fast Neutrons and γ-Rays of Energies up to 250 mev	G. E. Belovitskii, T. A. Romanova L. V. Soukhov and I. M. Frank	493	29, 537
The Theory of Strong Coupling for Meson Fields. I	B. T. Geilikman	509	29, 417
Study of the Structure of the Surface of a Liquid by the Method of Reflection of Light	V. A. Kizel'	520	29, 658
Absorption Spectrum of Excess Silver in the Low Temperature and High Temperature Modifications of Silver Iodide	P. N. Kokhanenko and L. V. Grigoruk	530	29, 676
Two Electrode High-Frequency Discharge at Pressures from 100 mm Hg to Atmospheric	G. S. Solntsev and M. M. Dmitrieva	533	29, 651
Asymptotic Behavior of Electromagnetic Vacuum-Polarization in the Presence of Meson Interactions	V. B. Berestetskii	540	29, 585
The Photographic Action of Ionizing Particles. I	A. L. Kartuzhanskii	550	29, 516
The Question of the Possibility of Measuring the Temperature of the Column of a Jet Discharge Using the 3064 Å Hydroxyl Band	M. Z. Kholkov	559	29, 645
Dielectric Losses in Ionic Dielectrics in Strong Electric Fields	L. E. Gurevich and V. N. Gribov	565	29, 629

(Contents continued on inside back cover)